# GASTROINTESTINAL IMMUNITY AND CROSSTALK WITH INTERNAL ORGANS IN FISH

EDITED BY: Nan Wu, Carmen G. Feijoo, Wei-Dan Jiang, Rune Waagbø and Min Wan

PUBLISHED IN: Frontiers in Immunology

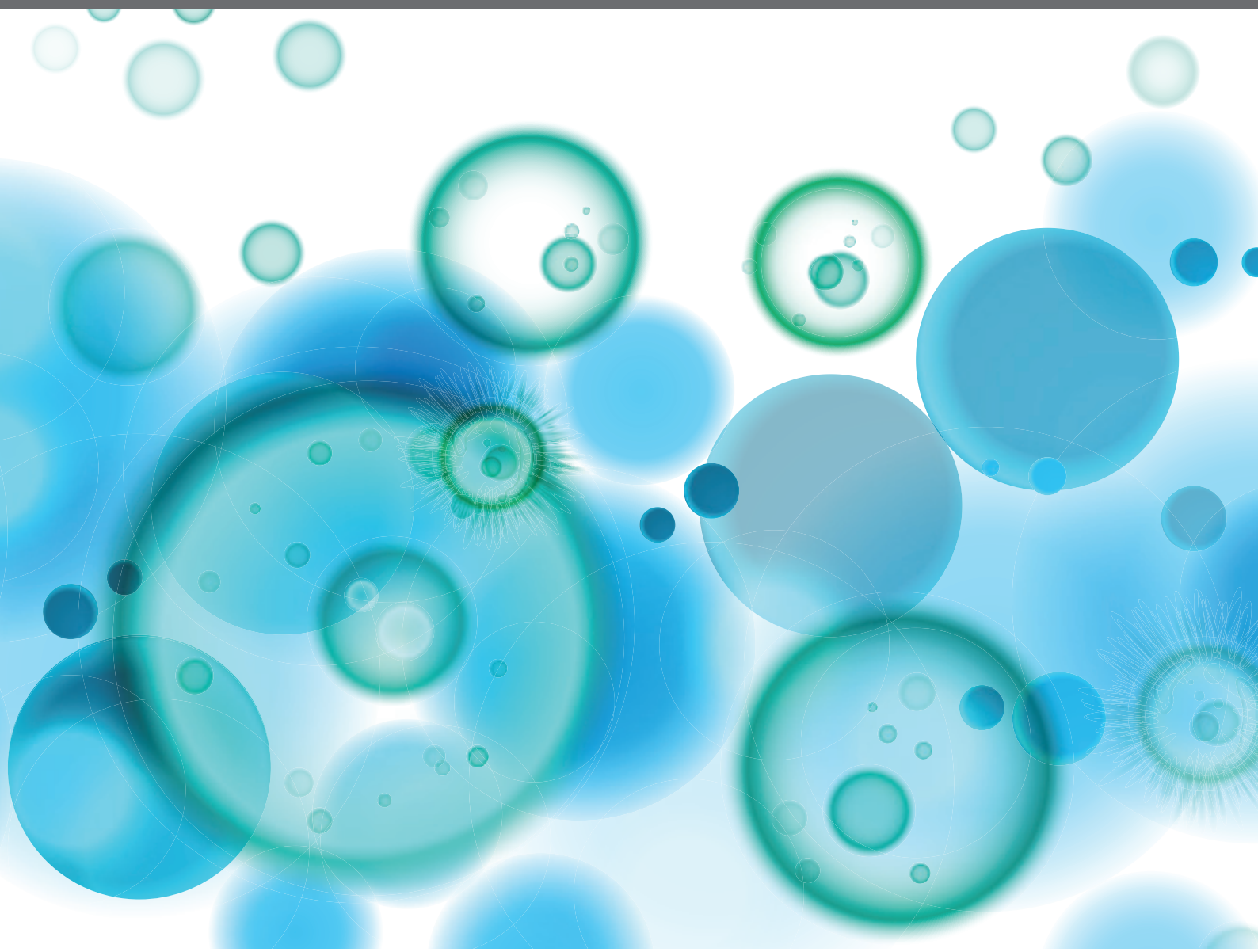

frontiers Research Topics

# frontiers



ISSN 1664-8714
ISBN 978-2-88971-686-9
DOI 10.3389/978-2-88971-686-9

## About Frontiers

Frontiers is more than just an open-access publisher of scholarly articles: it is a pioneering approach to the world of academia, radically improving the way scholarly research is managed. The grand vision of Frontiers is a world where all people have an equal opportunity to seek, share and generate knowledge. Frontiers provides immediate and permanent online open access to all its publications, but this alone is not enough to realize our grand goals.

## Frontiers Journal Series

The Frontiers Journal Series is a multi-tier and interdisciplinary set of open-access, online journals, promising a paradigm shift from the current review, selection and dissemination processes in academic publishing. All Frontiers journals are driven by researchers for researchers; therefore, they constitute a service to the scholarly community. At the same time, the Frontiers Journal Series operates on a revolutionary invention, the tiered publishing system, initially addressing specific communities of scholars, and gradually climbing up to broader public understanding, thus serving the interests of the lay society, too.

## Dedication to Quality

Each Frontiers article is a landmark of the highest quality, thanks to genuinely collaborative interactions between authors and review editors, who include some of the world's best academicians. Research must be certified by peers before entering a stream of knowledge that may eventually reach the public - and shape society; therefore, Frontiers only applies the most rigorous and unbiased reviews.
Frontiers revolutionizes research publishing by freely delivering the most outstanding research, evaluated with no bias from both the academic and social point of view. By applying the most advanced information technologies, Frontiers is catapulting scholarly publishing into a new generation.

## What are Frontiers Research Topics?

Frontiers Research Topics are very popular trademarks of the Frontiers Journals Series: they are collections of at least ten articles, all centered on a particular subject. With their unique mix of varied contributions from Original Research to Review Articles, Frontiers Research Topics unify the most influential researchers, the latest key findings and historical advances in a hot research area! Find out more on how to host your own Frontiers Research Topic or contribute to one as an author by contacting the Frontiers Editorial Office: frontiersin.org/about/contact

# GASTROINTESTINAL IMMUNITY AND CROSSTALK WITH INTERNAL ORGANS IN FISH

Topic Editors:
**Nan Wu,** Chinese Academy of Sciences, China
**Carmen G. Feijoo,** Andres Bello University, Chile
**Wei-Dan Jiang,** Sichuan Agricultural University, China
**Rune Waagbø,** Norwegian Institute of Marine Research (IMR), Norway
**Min Wan,** Ocean University of China, China

**Citation:** Wu, N., Feijoo, C. G., Jiang, W.-D., Waagbø, R., Wan, M., eds. (2021). Gastrointestinal Immunity and Crosstalk With Internal Organs in Fish. Lausanne: Frontiers Media SA. doi: 10.3389/978-2-88971-686-9

# Table of Contents

frontiers in Immunology

EDITORIAL
published: 28 September 2021
doi: 10.3389/fimmu.2021.734538

# Editorial: Gastrointestinal Immunity and Crosstalk With Internal Organs in Fish

*Nan Wu[1]*, Rune Waagbø[2], Min Wan[3], Carmen G. Feijoo[4] and Wei-Dan Jiang[5]*

*[1] Institute of Hydrobiology, Chinese Academy of Sciences, Wuhan, China, [2] Department of Biological Sciences, Institute of Marine Research/University of Bergen, Bergen, Norway, [3] Department of Aquaculture, College of Fisheries, Ocean University of China, Qingdao, China, [4] Facultad de Ciencias de la Vida, Universidad Andres Bello, Santiago, Chile, [5] Animal Nutrition Institute, Sichuan Agricultural University, Ya'an, China*

**Keywords: teleost fish, gastrointestinal immunity, crosstalk, foodborne inflammation, pathogen, vaccine**

## Editorial on the Research Topic

## Gastrointestinal Immunity and Crosstalk With Internal Organs in Fish

Recently, fish mucosal immunity has gradually become a hot spot in the basic study of aquaculture disease control. Mucosae is not only the physical barrier that separate teleost fish body from the environment, but it is armed with a complex network of cellular and humoral factors of innate and adaptive immunity, which work in coordination to protect them from infection or inflammation in a pathogen rich aquatic environment. Fish intestinal mucosal system is involved in the disease-control of water pathogens, as well as the induction of oral tolerance to dietary antigens and microbiota. To do so, the different immune cells that form part of the gut associated lymphocyte tissue (GALT) are distributed in the intestinal epithelial layers (IEL) and lamina propria (LP), and from there detect innocuous and harmful antigens as well as interact with the mucosal microflora.

Cytokines, chemokines and antibodies that reach blood circulation after immune response has been triggered in the gut, could stimulate other organs, such as liver, spleen and kidney. Although the local mucosal immune response could repress the infection process to a certain extent, the systemic and mucosal innate and adaptive immune cells or molecular components activated in the gut upon stimulation, will still interact with other internal organs.

It is our pleasure to present the Research Topics of gastrointestinal immunity in fish to the readers. The present journal issue is focused on fish gastrointestinal immunity and crosstalk with internal organs and collects 13 articles, including a review article and twelve original research articles from a total of 93 authors. The contributions cover research on fish gastrointestinal immune response resulted after food, pathogens, or vaccination stimulation. Also, the effects of the crosstalk between gut and other organs have been revealed from innate and adaptive point of view.

Foodborne intestinal inflammation is a major health and welfare issue that need to be considered when using plant-derived components as ingredients for fish diets, especially for carnivorous fishes. In Atlantic salmon, an intestinal transcriptomic analysis revealed that the presence of soybean meal in the diet altered the transmembrane transporter- and channel- activities and upregulated inflammation-associated genes. This coincided with an increase in different type of immune cell, especially lymphocytes in the soybean meal-fed group (Kiron et al.). To clarify the dominant anti-nutrient factor, a study on intestinal immunity after salmon feeding with marine- or plant-derived protein and lipid, showed that mucin and antimicrobial peptides were the most affected in the latter case (Sørensen et al.). As a major anti-nutritional factor, soybean-derived glycinin cause typical foodborne enteritis in grouper, while the addition of sodium butyrate decreased the inflammation by blocking MHC II-PI3K/mTOR signaling (Yin et al.).

OPEN ACCESS

***Edited and reviewed by:***
*Miki Nakao,*
*Kyushu University, Japan*

****Correspondence:***
*Nan Wu*
*wunan@ihb.ac.cn*

***Specialty section:***
*This article was submitted to Comparative Immunology, a section of the journal Frontiers in Immunology*

***Received:*** *01 July 2021*
***Accepted:*** *13 September 2021*
***Published:*** *28 September 2021*

***Citation:***
*Wu N, Waagbø R, Wan M, Feijoo CG and Jiang W-D (2021) Editorial: Gastrointestinal Immunity and Crosstalk With Internal Organs in Fish. Front. Immunol. 12:734538. doi: 10.3389/fimmu.2021.734538*

The intestinal barrier is often challenged during pathogen invasions. Both bacteria and virus induce intestinal immune response, activating several cytokine signaling pathways. Grass carp (*Ctenopharyngodon idella*) IL22 was reported to play a pro-inflammatory role in both intestinal mucosal and systemic immunity, and $IL22^+$ cells were found to be induced during a bacterial challenge with *Flavobacterium columnare* (Yang et al.). On the other hand, after grass carp challenge with grass carp reovirus (GCRV), the progression of intestinal disorder paralleled a sharply increased gene expression of protein phosphatase PP1 (PPP1R3G) in both intestine and head kidney, indicating that fish intestine could be a frontline of innate immune response (Hu et al.). In addition, for subtle regulating of fish gastrointestinal immune gene expression, non-coding RNA regulatory networks were revealed by transcriptomic analysis. At post-transcriptional level, both lncRNA-miRNA-mRNA and ceRNA networks played a regulatory role in the intestine upon *Edwardsiella tarda* infection of marine fish, such as black rockfish (*Sebastes schlegilii*) and olive flounder (*Paralichthys olivaceus*) (Cao et al., Xiu et al.).

To control disastrous infection of pathogens at the frontline, mucosal vaccines are currently being explored as an effective tool, along with the recent achievement in fish mucosal immunology. Oral administration of a vaccine formulated with LamB antigen, obtained from duckweed (*Wolffia globosa*), was used to generate antibodies to prevent Vibriosis infection in zebrafish (*Danio rerio*) (Heenatigala et al.). Another paper demonstrated that an immersion vaccine induced highest IgM level in the intestine compared to gill and skin tissues in carp (*Carassius auratus*) and grouper (*Epinephelus coioides*) (Gong et al.). During mucosal immunization, B cell responses, evidenced as changes in immunoglobulins (IgM, IgT and IgD) levels, as well as T cell responses reflected by increased CD8 and CD4 level (Munoz-Atienza et al.), were analyzed in mucosal and non-mucosal immune organs. Yet, different effects were detected depending on the administration routes used, including oral and nasal vaccination, anal intubation and immersion vaccination in fish (Munoz-Atienza et al.).

Regarding the crosstalk between gut and other organs in fish gastrointestinal immunity, the papers included in this issue showed the participation of the liver, kidney and spleen. During *Vibrio harveyi* infection, the gut-liver axis was affected, since intestinal inflammation and dysbacteriosis were observed concomitantly with the appearance of hepatic nodules, besides the typical symptoms in the heart and kidney (Deng et al.). Head kidney macrophages of Atlantic salmon fed with a fish meal and fish oil diet, showed the highest phagocytic activity compared to fish fed with diets based on plant-derived protein and lipid (Sørensen et al.). Meanwhile, short chain fatty acids (SCFAs), which are products of microbial fermentation of dietary fiber in the gut, promoted bacterial clearance by head kidney macrophages in turbot (*Scophthalmus maximus* L.) (Zhang et al.). On the other hand, a fish meal and fish oil diet, as well as a fish meal and rapeseed oil diet induced the presence of the highest amount of lymphocytes in head kidney of Atlantic salmon (Heenatigala et al.). During immersion vaccination in carp and grouper, the existence of a hindgut-liver-spleen immune synergy was proposed based on immunoglobulin gene expressions (Gong et al.).

Overall, advances in the research of gastrointestinal immunity and its associated inter-organ crosstalk included in this issue provide novel and central data to improve our understanding of mucosal immune barrier function in teleost fish. New insights related to intestinal mucosal immune regulation are key aspects when designing better diets formulations and new mucosal vaccines, as well as genetically facilitated infection control and prevention. Eventually, deepening knowledge of the regulation of intestinal immune homeostasis will enhance fish health and further guarantee an efficient growth performance in a long-term perspective.

We hope and expect the aquaculture research community will find this collection of articles within the gastrointestinal immunity topic informative and inspiring. As editors, we would like to thank the authors for their interesting contributions, as well as express our gratitude to all referees for their careful evaluation of the papers. Many thanks to all the colleagues who responded to this call, but whose interests could not be accommodated within the confines of this research topic. Finally, we extend our sincere appreciation to *Frontiers in Immunology* for supporting this exciting Research Topic

## AUTHOR CONTRIBUTIONS

NW prepared the draft editorial. RW, MW, CF, and W-DJ revised the manuscript. All authors contributed to the article and approved the submitted version.

## FUNDING

This work was funded by the grant from National Natural Science Foundation of China (31872592) to NW.

## ACKNOWLEDGMENTS

As editors of this Special issue on the Research Topic Gastrointestinal Immunity and Crosstalk with Internal Organs in Fish. We would like to thank the authors for their interesting contributions, as well as express our gratitude to all referees for their careful evaluation of the papers. Finally, we extend our sincere appreciation to Frontiers in Immunology for supporting this exciting Research Topic.

**Conflict of Interest:** The authors declare that the research was conducted in the absence of any commercial or financial relationships that could be construed as a potential conflict of interest.

**Publisher's Note:** All claims expressed in this article are solely those of the authors and do not necessarily represent those of their affiliated organizations, or those of the publisher, the editors and the reviewers. Any product that may be evaluated in this article, or claim that may be made by its manufacturer, is not guaranteed or endorsed by the publisher.

frontiers in Immunology

ORIGINAL RESEARCH
published: 20 August 2020
doi: 10.3389/fimmu.2020.01857

# Expression of LamB Vaccine Antigen in *Wolffia globosa* (Duck Weed) Against Fish Vibriosis

*P. P. M. Heenatigala*[1,2,3†], *Zuoliang Sun*[1,2†], *Jingjing Yang*[1,2], *Xuyao Zhao*[1,2] and *Hongwei Hou*[1,2*]

[1] University of Chinese Academy of Sciences, Beijing, China, [2] The State Key Laboratory of Freshwater Ecology and Biotechnology, The Key Laboratory of Aquatic Biodiversity and Conservation of Chinese Academy of Sciences, Institute of Hydrobiology, Chinese Academy of Sciences, Wuhan, China, [3] Inland Aquatic Resources and Aquaculture Division (IARAD), National Aquatic Resources Research and Development Agency (NARA), Colombo, Sri Lanka

Vibriosis is a commonly found bacterial disease identified among fish and shellfish cultured in saline waters. A multitude of *Vibrio* species have been identified as the causative agents. LamB, a member of outer membrane protein (OMPs) family of these bacteria is conserved among all *Vibrio* species and has been identified as an efficient vaccine candidate against vibriosis. Rootless duckweed (*Wolffia*) is a tiny, edible aquatic plant possessing characteristics suitable for the utilization as a bioreactor. Thus, we attempted to express a protective edible vaccine antigen against fish vibriosis in nuclear-transformed *Wolffia*. We amplified *LamB* gene from virulent *Vibrio alginolyticus* and it was modified to maximize the protein expression level and translocate the protein to the endoplasmic reticulum (ER) in plants. It was cloned into binary vector pMYC under the control of CaMV 35S promoter and introduced into *Wolffia globosa* by *Agrobacterium*-mediated transformation. Integration and expression of the *LamB* gene was confirmed by genomic PCR and RT-PCR. Western blot analysis revealed accumulation of the LamB protein in 8 transgenic lines. The cross-protective property of transgenic *Wolffia* was evaluated by orally vaccinating zebrafish through feeding fresh transgenic *Wolffia* and subsequently challenging with virulent *V. alginolyticus*. High relative percent survival (RPS) of the vaccinated fish (63.3%) confirmed that fish immunized with transgenic *Wolffia* were well-protected from *Vibrio* infection. These findings suggest that *Wolffia* expressed LamB could serve as an edible plant-based candidate vaccine model for fish vibriosis and feasibility of utilizing *Wolffia* as bioreactor to produce edible vaccines.

**Keywords: vibriosis, *Wolffia globosa*, LamB, edible vaccine, recombinant protein, oral immunization**

OPEN ACCESS

***Edited by:***
*Wei-Dan Jiang,*
*Sichuan Agricultural University, China*

***Reviewed by:***
*Qihui Yang,*
*Guangdong Ocean University, China*
*Yishan Lu,*
*Guangdong Ocean University, China*

***Correspondence:**
*Hongwei Hou*
*houhw@ihb.ac.cn*

*[†] These authors have contributed equally to this work*

***Specialty section:***
*This article was submitted to Comparative Immunology, a section of the journal Frontiers in Immunology*

***Received:*** *06 April 2020*
***Accepted:*** *10 July 2020*
***Published:*** *20 August 2020*

***Citation:***
*Heenatigala PPM, Sun Z, Yang J, Zhao X and Hou H (2020) Expression of LamB Vaccine Antigen in Wolffia globosa (Duck Weed) Against Fish Vibriosis. Front. Immunol. 11:1857. doi: 10.3389/fimmu.2020.01857*

## INTRODUCTION

Vibriosis is a serious disease commonly identified among fish and shellfish aquaculture and has become a major limiting factor in the aquaculture industry worldwide. A group of Gram-negative bacteria inhabiting in saline waters belonging to the genus *Vibrio* has been identified as the causative agent (1). Massive (mis) use of antibacterials to control vibriosis has resulted in severe environmental as well as health concerns (2). Thus, development of vaccination strategies against vibriosis will be an effective solution for the management of vibriosis in aquaculture. Most

vaccines currently used (especially for viral diseases) come from lab cultured pathogens through attenuation or inactivation, bringing potential risk of residual pathogenic activity. In this regard, recombinant proteins expressed in plant bioreactors are safer and more reliable, as they contain specific components of pathogens with the immunological properties of the original pathogen but not its pathogenic properties (3, 4).

Among fish vaccine delivery techniques, oral routes (oral immunization) would be an attractive alternative, as it is simple, cheap, and ideal for mass administration to fish of all sizes without causing a stress. However, oral immunization is a multifaceted process, depending on multiple cellular and molecular mechanisms. As teleost, fish lack Peyer's patches and antigen-transporting M cells, which are important to initiate the gut immune responses but their second segment of the gut has been identified as the main site of antigen uptake (5, 6). For that, many lymphoid cells and macrophages are diffusely present between the epithelial cells and in the lamina propria enterocytes of the hind gut (6, 7). Thus, as teleost fish intestine can easily be exploited for oral vaccination strategies.

Oral vaccination of fish has become less effective due to digestive degradations of antigens in the acidic environment of the foregut, before it reaches the immune responsive areas of the hind gut (8). Thus, while developing edible vaccines, special concern should be given to protect antigen from the harsh gastric environment to ensure antigen uptake in the second gut segment of fish. Protective antigens expressed in transgenic plants are the ideal solution for such issues. Thick, rigid cell walls of the plants encapsulate the antigenic proteins, thus protecting them well from the acidic environment of the stomach. They act as vehicles to orally deliver protective antigens (9) to get through the acidic environment of the foregut without intestinal degradation. Thus, the antigen can reach the second gut in the intestine safely in sufficient quantities and successful oral vaccination can be achieved.

Outer membrane proteins (OMPs) are unique components reside in the outer membrane of Gram-negative bacteria and responsible for maintaining the integrity and selective permeability of the bacterial outer membrane (10). As they are being localized at the bacterial cell surfaces, OMPs of Gram-negative bacteria could be efficiently recognized as foreign substances by immunological defense systems of hosts. Thus, OMPs of Gram-negative bacteria have been identified as highly immunogenic components due to their exposed epitopes as well as being conserved in nature (11). LamB proteins are a family of OMPs identified in vibrios and Lun et al. (12) has reported that it can be used as a broad cross-protective vaccine candidate against vibriosis.

*Wolffia,* the rootless duckweed is the smallest member of the duckweed family as well as in the plant kingdom (13). Due to its prominent asexual propagation, rootless characteristics and extremely reduced size, it has become an attractive, highly efficient bio-manufacturing platform for foreign protein production and makes it a more suitable candidate for submerged cultivation in bio-fermenters (14). Thus, high biomass of genetically homogeneous *Wolffia* populations can be easily obtained within the compact environment on artificial media. As it is an edible plant, the proteins in transgenic *Wolffia* can be directly consumed without extraction and/or purification of the active constituent. This is one of the main advantages identified in this system and makes *Wolffia* a more attractive member among the duckweed family, especially in edible vaccine research.

Lack of an efficient gene transformation protocol for *Wolffia* has limited the utilization of this valuable plant as a bio-manufacturing platform. To fulfill this gap in our previous work, we developed an efficient gene transformation protocol for *W. globosa*, the *Wolffia* species available in China (15). As the second step, here we focused on exploring the feasibility to express an edible protective vaccine antigen LamB for fish vibriosis in *W. globosa*.

# MATERIALS AND METHODS

## Amplification of Gene of Interest

LamB outer membrane protein of *Vibrio* bacteria was selected as the antigenic protein to express in *W. globosa*. The pathogenic *Vibrio alginolyticus* ECGY0608 (kindly given by Professor Ai-hua Li, Institute of Hydrobiology, Chinese Academy of Sciences) isolated from diseased fish was used to amplify the *LamB* gene. Genomic DNA of *V. alginolyticus* was extracted from overnight cultures in the TSA medium with a TIANamp Bacteria DNA kit (Cat.—DP 302, Tian GEN Biotech Beijin Co. LTD) according to the manufacturer's protocol. DNA extracts obtained were used as templates to amplify the *LamB* gene using degenerate primers. The primer sequences were lamB-f: 5-ATG AAA AAA GTA AGT SNY ATT GCA G-3 and LamB-r: 5-TTA CCA CCA AGC TTC NRC TTG-3 (12). PCR was carried out in a thermal cycler (Eppendorff, USA) with the following set up: Initial denaturation for 5 min at 95°C, Then 30 cycles were run with conditions: 95°C for 30 s, 48°C for 45 s, and 72°C for 1 min and final cycle of 72°C for 7 min. The PCR product was analyzed by electrophoresis on a 1.2% agarose gel, and purified with Easy Pure PCR purification kit (TRANS Gen Biotech). The amplified DNA fragment was cloned into the pGEM-T-Easy vector (Promega) and sequenced (http://www.tsingke.net).

## Database Searching and Bioinformatics Analysis

The identities of the nucleotide sequences were determined by comparing with known sequences in GenBank using the respective BLAST program available at NCBI (http://www.ncbi.nlm.nih.gov/).

## Designing and Construction of Plant Transformation Vector for *Agrobacterium*-Mediated Transformation of *W. globosa*

The *LamB* gene obtained was further modified to achieve higher protein expression, accumulation, and isolation. To enhance *Agrobacterium tumefaciens*-mediated stable gene expression in *W. globosa*, we designed the construct to express ER targeted LamB fusion protein under the control of cauliflower mosaic virus (CaMV) 35S promoter, a tCUP translational enhancer,

**TABLE 1 |** Primers used to modify *LamB* gene.

| Primers | Sequence (5′- 3′) | Annealing temperature (°C) |
|---|---|---|
| tCUP Pst2 (F) | TGCACTGCAGAATACTAGCCTATT | 55.6 |
| Prb1 NocI (R) | TTACTTTTTTCATCCATGGGGCAGGGGAAG | |
| Lamb Modi (F) | CTTCCCGTGCCCCATGGATGAAAAAAG TAA | 56 |
| Lamb Corr (R) | TTCTTCAGAGATCAGTTTCTGTTCGTC GACCCACCAAG | |
| Lamb Modi (F) | CTTCCCGTGCCCCATGGATGAAAAAAGTAA | 57 |
| Lamb Modi (R) | CGCGGATCCGAGCTCATCCTTCAGA TCTTCTTCAGA | |
| Overlap F—a | TGCACTGCAGAATACTAGCCTATTTTATTTCAA | 58.7 |
| Overlap R—a | CGCGGATCCGAGCTCAT | |

PR1b signal peptide, and the nopaline synthase (nos) terminator in the plant expression vector pMYC.

Thus, tobacco cryptic constitutive promoter (tCUP) enhancer and pathogenesis-related protein 1b (PR1b) signal peptide were synthesized (http://www.tsingke.net) and spliced together with the 5′ end of the *LamB* sequence by overlap extension (16). MYC protein tag and KDEL retention signal peptide was incorporated to the 3′ end of *LamB* by newly designed primers. Specific restriction sites (*Pst1/Ncol1/Sal1/BamHI*) were designed from the cloned nucleotide sequence to amplify the encoding sequence for the mature LamB protein, and incorporated into the PCR during *LamB* gene modification. Primer sequences used to modify the *LamB* gene are shown in **Table 1**. Schematic representation of the expression cassette (modified *LamB* gene) is shown in **Figure 1**. It was sub-cloned into the pGEM-T-Easy vector (Promega) and the modifications were confirmed by sequencing (http://www.tsingke.net).

Then the LamB expression cassette was cut out from the pGEM-T-Easy between cut sites *Pst1* and *BamHI* and using the same sites, cloned into pMYC binary vector under the control of the CaMV 35S promoter. Thus, the gene was located downstream from the 35S cauliflower mosaic virus promoter (CaMV35S) and upstream of the nopaline synthase 3′ UTR (NOSt) to give the binary vector pMYC-*LamB*. We confirmed the successful insertion of the LamB expression cassette into the binary vector pMYC-*LamB* by restriction enzyme digestion and sequencing (http://www.tsingke.net). The resulting binary vector pMYC-LamB was used for LamB protein expression in *W. globosa*, following its *Agrobacterium*-mediated transformation (15).

Thus, the construct (pMYC-*LamB*) was mobilized into the commercially available disarmed *Agrobacterium* strain EHA105 (http://www.transgen.com.cn/) by heat shock according to the manufacture's protocol and used for the transformation of *W. globosa*.

## Tissue Culture and *Agrobacterium*-Mediated Transformation of *W. globosa*

*W. globosa* fronds were collected from Wuhan Botanical Garden (RDSC Clone *W. globosa* 5563), Chinese Academy of Sciences (CAS) (30.54° N and 114.42° E) at the city of Wuhan, Hubei province, China. Aseptic populations of *W. globosa* single clones were obtained in solid SH medium (17) with 2% sucrose and 0.6% agar and used as explants in this study. *W. globosa* clusters were induced by culturing explants in cluster induction medium for 4 months (18). Clusters obtained were used for the transformation experiments.

*Agrobacterium*-mediated nuclear transformation was performed as previously described (15). Briefly, *W. globosa* clusters were mixed with glass beads and bacterial suspension of *A. tumefaciens* (EHA105 harboring the pMYC-*LamB* construct) and subjected to vigorous shaking for 30 min to injure the clusters. Subsequently, these were blotted onto sterile filter paper, and co-cultivated for 72 h on antibiotic-free liquid SH medium. Then clusters were subjected to 2 week resting period and finally for 1 month selection. Plant selectable marker used in the construct was Hyg-R. Thus, Hygromycin B (Hyg) was used as the selection agent at the concentration of 5.0 $mgl^{-1}$ to select transgenic explants as well as to obtain pure transgenic lines. All steps of transformation experiments were carried out at 25 ± 1°C under the white light of 85 μmol $m^{-2}$ $s^{-1}$, 16: 8 h light: dark photoperiod.

## Genomic Analysis of Transgene Integration

To confirm gene integration within the plant genome we first performed a PCR assay. Total genomic DNA from the putative transgenic and wild-type *W. globosa* explants was extracted using a plant genome extraction kit, NuClean PlantGen DNA Kit (CWBIO, China) (http://www.cwbiotech.com.cn/) according to the manufacture's protocol. Genomic DNA obtained was used as the template to amplify the modified *LamB* gene integrated. PCR analysis of putatively transgenic plants was performed using PCR primers, Overlap F—a and Overlap R—a (**Table 1**). Overlap PCR primers amplify a 1,548-bp fragment comprising the sequence of modified *Lam B* gene.

## RT-PCR Detection of the *LamB* Gene Integrated

Total RNA from wild and transformed *W. globosa* was extracted using the Trizol reagent (Invitrogen). cDNA was synthesized with 2 μg of total RNA using a Prime Script RT reagent Kit (Takara) according to the manufacture's protocol. RT-PCR for *LamB* was conducted with newly designed *LamB* gene specific primers (*LamB*-RT-F: 5′-GTTTCTTTCGCTTGGGTTCG-3′, *LamB*-RT-R: 5′-CATTACGCCGTTTTTCGCAT-3′). An *Actin* gene was used as the internal control. *Actin* gene was amplified using two degenerate primers, ActF: 5′-GTGYTKGAYTCTGGTGATGGT GT-3′ and ActR: 5′-ACCTTRATCTTCATGCTGCTSGG-3′ (15).

## Immunoblot Detection of LamB Protein in Transgenic *W. globosa*

Total soluble protein was extracted from transgenic and wild type *Wolffia* fronds. The fronds were ground in liquid nitrogen to a fine powder. 0.5 g powder was re-suspended in 4 volumes of extraction buffer [50 mM Tris–HCl, pH 8.0, 10 mM EDTA, pH 8.0, 10% (v/v) glycerol, 1% (w/v) SDS, 30 mM 2-mercaptoethanol, 4 μg/ml aprotinin, and 4 μg/ml leupeptin]. Total proteins were

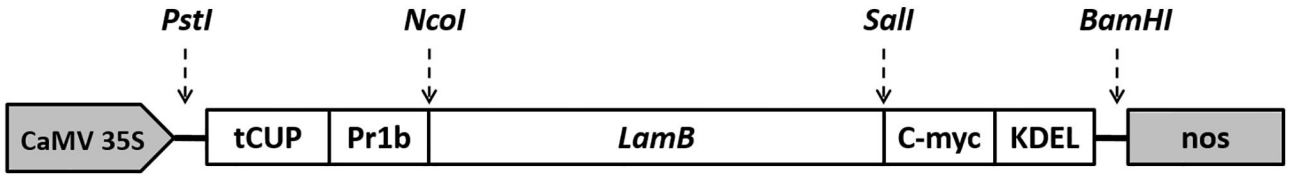


**FIGURE 1 |** Schematic representation of T-DNA region of the expression vector (pMYC-*LamB*) construct used for *W. globosa* transformation. Transgene expression fragment (*LamB*) was placed under the control of the cauliflower mosaic virus 35S promoter, tCUP, translational enhancer from the tobacco cryptic upstream promoter; Pr1b, tobacco pathogenesis related 1b protein secretary signal peptide; C-myc, detection/purification tag; KDEL, endoplasmic reticulum retrieval tetrapeptide; nos, nopaline synthase transcription terminator.

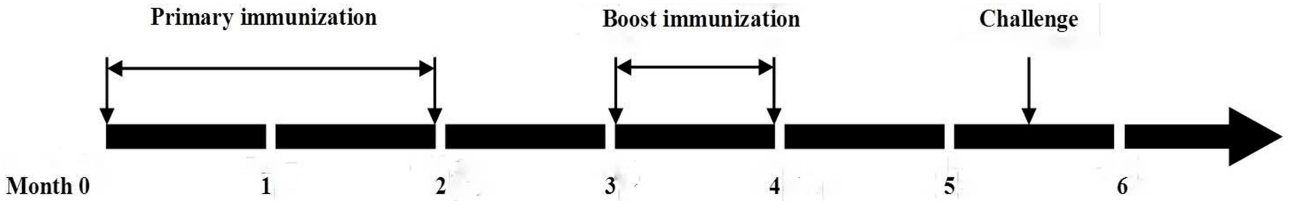


**FIGURE 2 |** Design of oral immunization assay of zebrafish.

extracted for 20 min at 4°C and then centrifuged at 14,000× g for 10 min at 4°C. Supernatant was taken for further analysis. Protein extracts were quantified with the help of BCA protein assay kit (Beyotime, China, Cat. P0012) according to the manufacturer's instructions.

Protein extracts were subjected to fully automated capillary electrophoresis (CE) based Western blot assay to identify the recombinant LamB protein in transgenic *Wolffia*. Automated Western blot was performed by the Peggy Sue instrument, Protein Simple (Santa Clara, CA, USA). Biotinylated molecular weight ladder, streptavidin-HRP, DTT, fluorescent standards, luminol-S, peroxide, sample buffer, stacking matrix, separation matrix, running buffers, wash buffer, and the HRP-conjugated secondary antibody, were used according to the manufacture's protocol. Mouse anti-myc (QW–bio, China) was used as the primary antibody. "Virtual blot" electrophoretic images were generated using Compass Software (ProteinSimple). The kit also provides capillaries, antibody diluents, and sample loading plates.

## Fish Immunization

Healthy and *V. alginolyticus* infection-free four months old wild type zebrafish (AB strain) obtained from single parental stock were purchased from a fish farm/Institute of Hydrobiology (Wuhan, China) (mean weight 0.4 g; length 2–3 cm) and acclimatized for 2 months prior to experiments. During acclimatization, fish were kept in tanks with running water. Water temperature was ∼28°C and fish were reared at 12:12 h light: dark cycle. Fish were fed twice a day with commercial feed and wild type *W. globosa*. The animal studies were approved by the Animal Care and Use Committee of the Institute of Hydrobiology, Chinese Academy of Sciences (approval ID Keshuizhuan Y73Z061).

## Oral Vaccination and Sampling

From the acclimatized fish, 270 apparently healthy (no clinical signs) individuals were randomly divided into three groups at a density of 30 fish/tank. A description of oral immunization and challenge infection is shown in **Figure 2**. The fresh biomass of wild type and transgenic *W. globosa* were used for the vaccination experiment. The fish in group 1 were fed with commercial feed twice a day during the experimental period and it was used as the control group. The fish in group 3 were immunized (primary immunization) by feeding with transgenic *W. globosa* and commercial feed twice a day for the period of 2 months. Then booster vaccination was performed for another month after 1 month interval of primary immunization. The fish in group 2 were fed with wild type untransformed *W. globosa* and commercial feed according to the schedule described in **Figure 2**. Oral vaccination experiments were performed in biological triplicates. Blood was collected from vaccinated and unvaccinated fish (from five fish at each time) at 5, 6, 7, 8, 9, and 10 weeks after booster vaccination. Blood (5 μl/fish) was collected from the caudal vein of fish by placing a capillary tube through the caudal fin cut. The blood was allowed to clot by keeping at room temperature for 2 h and then at 4°C overnight. Serum was collected after centrifugation at 750 × g for 10 min and was stored at −80°C for ELISA.

## Experimental Challenge and Calculation of Relative Percent Survival (RPS)

Six weeks post-vaccination, 30 fish from each group (group 1, 2, and 3) were anesthetized by immersing in tricaine methane sulfonate (MS-222) solution and challenged by intraperitoneal inoculation with 10 μl of $3.25 \times 10^8$ cfu/ml cell suspension. Thirty fish were challenged by intraperitoneal inoculation with 10 μl PBS as control.

Bacterial suspension was prepared as follows: virulent *Vibrio alginolyticus* was cultured at 28°C in TSB medium for 18 h, harvested by centrifugation at 4,000 g for 10 min and washed with PBS three times. Bacteria were suspended in 0.01 M PBS (pH 7.4) and adjusted to the concentration of $3.25 \times 10^{10}$ cells/ml. In a preliminary assay, the median lethal dose ($LD_{50}$) was determined to be $6.5 \times 10^7$ CFU per fish. Fish from vaccinated and control groups were challenged using five times their lethal dose ($LD_{50}$) (12). Fish mortality was monitored daily for 14 days, and dead fish were removed on a daily basis. The relative percent survival (RPS) was calculated by the following formula: RPS = [1− (% mortality of vaccinated fish/% mortality of control fish)] × 100%.

## Indirect ELISA for Detection of Antigen-Specific Serum Antibody

To analyze the protein by a more sensitive method for the detection of immunogenic epitopes of expressed protein, antibody titer was determined from the immunized fish by sandwich ELISA. Briefly, the sera of zebrafish were serially diluted in carbonate/bicarbonate buffer, pH 7.4 (1:1, v/v) and added in triplicate to wells of the plates. The plates were incubated overnight at 4°C. The remaining binding sites were blocked 1 h at 37°C with PBS-TS. Then 100 µl purified LamB (0.5 µg/well) was added to the plates. After incubation at 37°C for 2 h and washing three times with PBS-T, rabbit anti-LamB sera (1:1000 diluted in PBS-TS) were added to the plates. The plates were incubated and washed as above. HRP conjugated with goat-anti rabbit IgG (1:1000 diluted in PBS-TS) was added and incubated for another 1 h at 37°C and was then reacted with o-Phenylenediamine (OPD) substrate (Beyotime) for 10 min. Finally, the reaction was blocked by 2M $H_2SO_4$, and the absorbance of each and every well was measured at 492 nm with the help of Bio-Rad iMark micro-plate reader. The student's *t*-test was used to conduct significant tests.

# RESULTS

## Amplification of Gene of Interest

From the genomic DNA of pathogenic *V. alginolyticus,* we successfully amplified the 1,200 bp full-length ORF of antigenic *LamB* gene. The deduced amino acid sequence of amplified gene consists of 447 amino acid residues. Gene was amplified using degenerate *LamB* primers as described by Lun et al. (12). According to Lun et al. (12), the annealing temperature of the PCR reaction was 58°C. However, though we were unable to amplify the *LamB* gene at this temperature, we were able to successfully amplify it at an annealing temperature of 48°C. The gene sequence was subjected to the homology search BLASTn in NCBI (http://www.ncbi.nlm.nih.gov/). Results showed 99% similarity with the *LamB* gene of *V. alginolyticus* (Accession no. EU625279). With this finding, the gene amplified was confirmed as the *LamB* gene of *V. alginolyticus* and it was used to construct the expression vector (pMYC-*LamB*) to transform antigenic *LamB* gene into *Wolffia* plant for antigenic protein expression trials.

## Molecular Characterization of Transgenic Plants

We obtained hygromycin-resistant transgenic *Wolffia* fronds after 7–8 weeks of cultivation on SH medium in the presence of 5.0 mg $l^{-1}$ hygromycin (Hyg). In total, 8 independent hygromycin-resistant transgenic *Wolffia* lines with *LamB* gene construct were identified and those were confirmed by PCR conducted with *LamB* gene specific primers (**Figure 3A**). To confirm that the *LamB* gene was correctly transcribed, the transgenic *Wolffia* were characterized in more detail by RT-PCR with *LamB* gene specific primers. PCR products of the expected size corresponding to the specific primers were detected in the transgenic *Wolffia*, whereas no amplified PCR product was detected in non-transformed wild-type *Wolffia* (**Figure 3B**). The

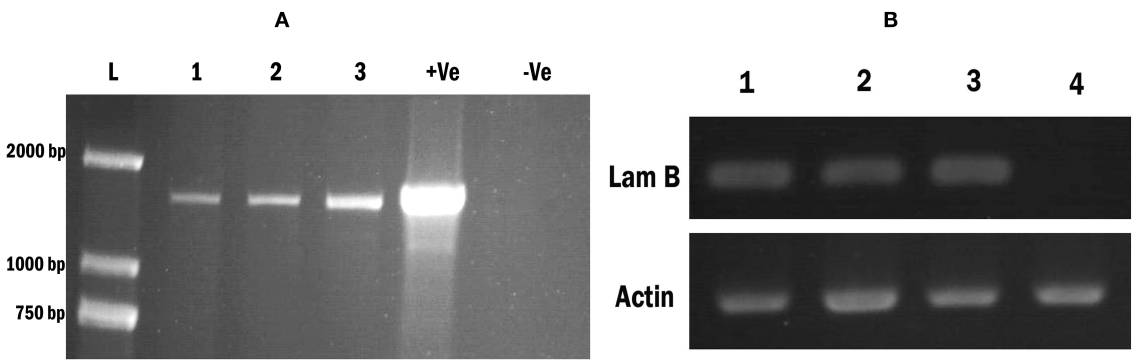


**FIGURE 3 |** Screening transgenic *Wolffia* and confirmation of the modified *LamB* gene integration. **(A)** PCR amplification of modified *LamB* gene from *Wolffia* transformant. L: 2,000 bp ladder, Lane 1–3: contained 3 independent *LamB* integrated *Wolffia* lines. Lane 4: (Marked as +ve) contains plasmid extract containing LamB construct and it was used as the positive control. Lane 5: (marked –ve) contains genomic DNA from wild plants. **(B)** RT-PCR for the *LamB* in *Wolffia* transformant. An *Actin* gene was used as the internal control. Lanes 1–3: Putative *Wolffia* transformants, Lanes 4: Wild type plants.

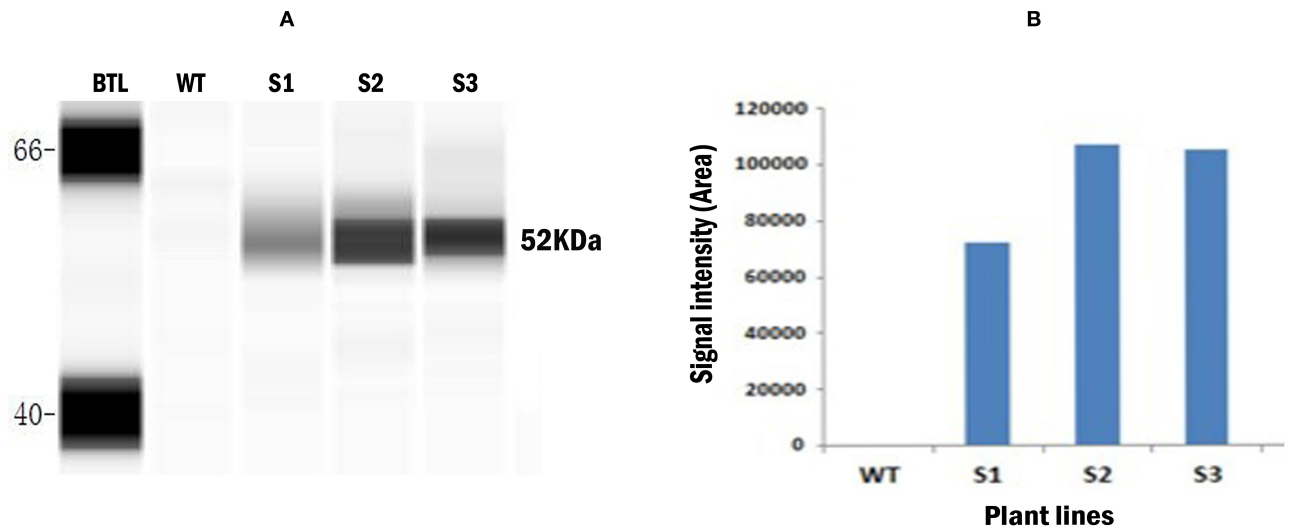


**FIGURE 4 |** Capillary electrophoresis (CE) based Western blot assay conducted for detection of recombinant *LamB* protein in protein extracts of transgenic *Wolffia*. **(A)** Gel-like image viewed from Western blot assay. Left to right: BTL: Biotinylated ladder WT: Un-transformed wild type plant, S1–S3: Transformed plants. Anti- c-myc mouse monoclonal antibody was used as a primary antibody and the HRP-conjugated mouse anti-mouse IgG antibody used as a secondary antibody. **(B)** Signal intensity (area) shown in Capillary electrophoresis (CE) based Western blot assay for detection of recombinant LamB protein in protein extracts from the fronds of wild type and transformed *Wolffia*. WT - Wild type *Wolffia*, S1–S3 transgenic *Wolffia* lines.

*Actin* gene was used as an internal control. All transgenic *Wolffia* lines we tested were positive for the LamB transcript (**Figure 3B**).

## Immunoblot Detection of LamB Protein in Transgenic *W. globosa*

CE based western blot assay was conducted with the total soluble protein extracted from the transgenic *Wolffia* to confirm the expression of recombinant *LamB* protein. Probing blots with mouse anti-myc primary antibody revealed full-length 52-kDa protein (**Figure 4A**). This product is consistent with the predicted size of fully intact recombinant LamB protein. The total soluble protein from wild-type plants did not show any band, indicating that mouse anti-myc antibody did not cross-react with any plant proteins in the crude extract. This confirmed the production of recombinant LamB antigenic protein in transformed *W. globosa*. The signal intensity (area) of CE based Western blot assay corresponding to the expression level of recombinant protein varied between three transgenic lines, indicating the different levels of protein expression in transgenic *Wolffia*. **Figure 4B** shows the different expression levels (signal intensity/area) obtained for three transgenic lines. The highest level of signals was detected in the S2 transgenic line and signal from S1 was comparatively weak according to the CE based western blot.

## Cross-Protective Analysis of LamB Recombinant Protein Produced in Transgenic *Wolffia*

Zebrafish were orally immunized with transgenic *Wolffia* and subsequently challenged with the pathogenic *V. alginolyticus* to evaluate the cross-protective potential of LamB recombinant protein produced in transgenic *Wolffia*. Fish mortality rate and sandwich ELISA were determined to evaluate the efficacy of this oral vaccine. Cumulative mortality of challenged zebrafish is shown in **Table 2**. Mortality rate of LamB vaccinated zebrafish was significantly lower compared to the control group ($P < 0.05$). The RPS of LamB vaccinated group was 63.3%. These results confirmed the protective capacity of LamB vaccinated zebrafish against *V. alginolyticus*. However, the antibodies against LamB protein in the sera of vaccinated fish were not detected by sandwich ELISA.

**TABLE 2 |** Cumulative mortality of challenged zebrafish after vaccination by *V. alginolyticus* ECGY0608.

| Groups | Feed details | Cumulative percent mortality (Dead fish/total fish) |
|---|---|---|
| 1 | Normal diet feed | 100% (30/30) |
| 2 | 50% normal diet + 50% wild type *Wolffia* | 93.3% (28/30) |
| 3 | 50% normal diet + 50% transgenic *Wolffia* | 36.7% (11/30) |

## DISCUSSION

Among members of the duckweed family, *Wolffia* has been identified as a valuable bioreactor for foreign protein production (19). Lack of an efficient gene transformation protocol has limited the utilization of this valuable plant as a bio-manufacturing

platform. To fulfill this gap in our previous work, we developed an efficient gene transformation protocol for *W. globosa*, the *Wolffia* species available in China (15). Use of antibiotics to control vibriosis in aquaculture causes serious health and environmental issues (20). Immunoprophylaxis would be a promising tool for effective control of this disease in a more effective and economical manner. Thus, as the second phase of our study, we attempted to demonstrate bioencapsulation of vaccinogenic outer membrane protein of vibrio in *Wolffia* for oral delivery against fish vibriosis.

With the morphological and functional differences investigated within the fish intestine, its second segment was identified as the main place of antigen uptake (5, 6). Studies conducted by Rombout et al. (21) and Firdaus (22) using fish with formalin killed *V. anguillarum* and feed-based adjuvant vaccine of *Streptococcus agalactiae* have proven that oral vaccination in fish could elicit certain levels of humoral and mucosal immunities following the development of gut-associated lymphoid tissue (GALT) (23). Thus, oral vaccines will be effective immune stimulators only if the antigenic substances reach the correct inductive sites in the fish gut. Accordingly, to achieve highly efficient edible vaccines, special techniques need to be developed to prevent antigenic substances from biodegradation in the proteolytic environment of the fish foregut till it reaches the local immune system.

Encapsulating vaccinogenic components in edible plants has become popular due to a number of advantages such as low production cost, direct administration by feeding without a needle and syringe and possible long-term storage without special storage facilities. Until now, many successful oral vaccines by expressing recombinant proteins in edible plants with higher expression level have been published for human diseases but for the fish diseases it is limited. In these studies, producing vaccine antigens in edible plants, including tomato, potato, lettuce, or rice has been identified as a viable approach for expressing mucosal vaccines (23–26). In particular, Shina et al. (27) has reported expression of a vaccinogenic recombinant major capsid protein (rMCP) of rock bream iridovirus in transgenic rice callus against iridovirus of fish. In this study oral immunization of Rock bream with rMCP in lyophilized rice callus powder has elicit the intestinal mucosal immunity for protection against iridovirus infection. This study suggests that oral administration of plant expressed vaccine antigen as a useful method to implement a vaccine program against fish diseases.

Recently duckweeds have been identified as a more efficient bio-manufacturing platform to express heterologous proteins. However few reports on utilizing duckweeds for protein expression can be seen (28–30) and *Lemna* was the commonly used species. Single attempt on utilizing *Wolffia* to express human granulocyte colony-stimulating factor (hG-CSF) by nuclear-transformation at the level of 0.002–0.2% has been reported (31). But expressing vaccine antigens has not been reported.

Outer membrane proteins (OMP) of gram negative bacteria are identified as a type of vaccine candidate and used to formulate vaccine against bacterial pathogens. OMPs of bacteria are being localized at the exteriors of the cell surface and are targets for bactericidal and protective antibodies (32, 33). Thus, we focused on LamB OMP of *Vibrio* to be expressed in *W. globosa*, which has already been identified as a broad cross protective vaccine antigen against fish vibriosis (12). We constructed LamB expression vector and introduced *LamB* gene into the nuclear genome of *Wolffia* as an alternative approach to prevent fish vibriosis.

Development of effective plant based edible vaccines deals with the level of foreign protein expressed in transgenic plants. Higher protein expression is necessary to induce protective immune responses of host via oral routes of delivery. Tobacco cryptic constitutive promoter (tCUP) is a translational enhancer sequence used for the expression vectors and it is being effective across a wide range of plant species, including monocots, dicots, or gymnosperms and a wide range of other organisms such as yeast (34). It can be combined with other promoters, such as CaMV 35S promoter, to elevate their activity further (34, 35). Thus, for our LamB expression construct, we used tCUP translational enhancer sequence to achieve higher expression of heterologous LamB protein in *Wolffia*. Moreover, signal peptides and endoplasmic reticulum (ER) retention signals are often used in expression vectors for correct compartmentalization and retention of the heterologous protein in plant ER (36–39). This minimizes the modifications happening to the glycoproteins in Golgi apparatus (40). Thus, we used PR1b signal peptide sequence and ER retention signal KDEL for our construct to direct and keep the homologous LamB protein in ER.

Finally using the pMYC-*LamB* construct and the *Agrobacterium*-mediated stable nuclear transformation protocol we developed, we successfully expressed the homologous *LamB* antigenic gene in *Wolffia*, and regeneration of transgenic *Wolffia* occurred at a satisfactory level. The PCR and transcription analysis conducted with the transgenic *Wolffia* indicated that the foreign genes have been transcribed correctly. All transgenic *Wolffia* lines were phenotypically indistinguishable from wild type control fronds. The development and growth rate of these transgenic *Wolffia* did not differ from the corresponding characteristics of the non-transformed control fronds. This indicates that the expression of the foreign protein has no effect on the growth and development of transgenic *Wolffia*. Thus, we successfully utilized this less/under exploited plant species, *W. globosa* as a novel vaccine expression platform to express the antigenic *LamB* against vibriosis. As an edible aquatic plant, this antigenic protein expressed transgenic *Wolffia* can be used to vaccinate the herbivorous fish through direct feeding without extraction and/or purification of the active constituent. To vaccinate the carnivorous fish, transgenic *Wolffia* can be fed with meat or commercial feeds.

The signal intensity (area) of CE based western blot assay corresponding to the expression level of recombinant LamB protein varied between three independent transgenic *Wolffia* lines. This indicates that the protein expression in the three transgenic lines is variable. This variation may be due to differences in the location/integration site of the newly

introduced gene, the copy number of the T-DNA integrated and/or T-DNA organization (41, 42), as well as epigenetic effects (43). However, in our study we were unable to quantify the LamB protein accumulation in transgenic *Wolffia* due to the unavailability of protein standards.

The biological activity of recombinant LamB protein was assessed through bacterial challenge followed with an immunological assay. According to our findings the protective capacity of recombinant LamB against pathogenic *V. alginolyticus* in immunized fish were significant. This result confirmed the protective capacity of recombinant LamB against *V. alginolyticus* in fish. Even though the challenge test clearly indicates the protective capacity of transgenic *Wolffia*, with the ELISA we were unable to detect the antibodies against LamB in the sera of vaccinated fish. Some identified reasons for this type of erroneous results are competitive inhibition of test antibodies by relevant antibodies present in animal serum, denaturation of enzymes conjugated to detection antibodies, change in antibody specificity due to antigenic drift, sampling time and condition of the fish (44, 45).

In conclusion, we have successfully expressed antigenic LamB outer membrane protein of *Vibrio* in transgenic *Wolffia* against fish vibriosis and the successful nuclear transformation of LamB fusion protein with their functional properties is further demonstrated. Confirmation on its immunogenic property needs to be verified further by immunological studies to accomplish its immunostimulant property. However, our study opens the way to utilize the smallest flowering plant, *Wolffia,* for the development of low cost, easily deliverable and effective subunit vaccines.

## DATA AVAILABILITY STATEMENT

All datasets generated for this study are included in the article/supplementary material.

## ETHICS STATEMENT

The animal study was reviewed and approved by Animal Care and Use Committee of the Institute of Hydrobiology, Chinese Academy of Sciences (approval ID Keshuizhuan Y73Z061).

## AUTHOR CONTRIBUTIONS

HH and PH planned and designed the research. PH, ZS, JY, and XZ performed experiments and data analysis. PH, ZS, and HH wrote the manuscript. All authors contributed to manuscript revision and read and approved the submitted version.

## FUNDING

This work was supported by National Key R & D Program (2018YFD0900801), the Major Project of Technology Innovation Program of Hubei, China (2017ABA135), Open Project of Guangdong Provincial Key Laboratory of Applied Botany, South China Botanical Garden, Chinese Academy of Sciences (AB2018020), and Hubei Province Postdoctoral Science Foundation.

## ACKNOWLEDGMENTS

The authors are thankful to the University of Chinese Academy of Sciences (UCAS) scholarship program.

## REFERENCES

1. Austin B, Austin DA. *Bacterial Fish Pathogens: Disease of Farmed and Wild Fish*. Chichester: Springer Praxis Publishing Ltd (2007). p. 61–150.
2. Heuer OE, Kruse H, Grave K, Collignon P, Karunasagar I, Angulo FJ. Human health consequences of use of antimicrobial agents in aquaculture. *Clin Infect Dis*. (2009) 49:1248–53. doi: 10.1086/605667
3. Marsian J, Lomonossoff GP. Molecular pharming - VLPs made in plants. *Curr Opin Biotech*. (2016) 37:201–6. doi: 10.1016/j.copbio.2015.12.007
4. Giddings G. Transgenic plants as protein factories. *Curr Opin Biotech.* (2001) 12:450–4. doi: 10.1016/S0958-1669(00)00244-5
5. Georgopoulou U, Sire MF, Vernier JM. Immunological demonstration of intestinal absorption and digestion of protein macromolecules in the trout (*Salmo gairdneri*). *Cell Tissue Res*. (1986) 245:387–95. doi: 10.1007/BF00213946
6. Rombout JHWM, Van den Berg AA, Van den Berg CTGA, Witte P, Egberts E. Immunological importance of the second gut segment of carp. III. systemic and/or mucosal immune responses after immunization with soluble or particulate antigen. *Fish Biol.* (1989) 36:179–86. doi: 10.1111/j.1095-8649.1989.tb02967.x
7. Georgopoulou U, Vernier JM. Local immunological response in the posterior intestinal segment of the rainbow trout after oral administration of macromolecules. *Dev Comp Immunol.* (1986) 10:529–37. doi: 10.1016/0145-305X(86)90174-6
8. Stefaan V, Frans O, Renaat K, Armand M. Mucosal response in African catfish after administration of *Vibrio anguillarum* $O_2$ antigens via different routes. *Fish Shellfish Immun.* (2005) 18:125–33. doi: 10.1016/j.fsi.2004.06.004
9. Rigano MM, Walmsley AM. Expression systems and developments in plant-made vaccines. *Immunol Cell Biol.* (2005) 83:271–7. doi: 10.1111/j.1440-1711.2005.01336.x
10. Nikaido H. Molecular basis of bacterial outer membrane permeability revisited. *Microbiol Mol Biol R.* (2003) 67:593–656. doi: 10.1128/MMBR.67.4.593-656.2003
11. Khushiramani R, Girisha SK, Karunasagar I, Karunasagar I. Cloning and expression of an outer membrane protein ompTS of *Aeromonas hydrophila* and study of immunogenicity in fish. *Protein Expr Purif.* (2007) 51:303–7. doi: 10.1016/j.pep.2006.07.021
12. Lun J, Xia C, Yuan C, Zhang Y, Zhong M, Huang T, et al. The outer membrane protein, LamB (maltoporin), is a versatile vaccine candidate among the Vibrio species. *Vaccine.* (2014) 32:809–15. doi: 10.1016/j.vaccine.2013.12.035
13. Landolt E. The family of Lemnaceae - a monographic study Vol 1. In: Landolt E, editor. *Veroffentlichungen des Geobotanischen Institutes der Eidgenossischen Technischen Hochschule*, Zurich: Geobotanical Institute of the ETH, Stiftung Rubel (1986).
14. Thompson BG. The maximization of the productivity of aquatic plants for use in controlled ecological life support systems (CELSS). *Acta Astronaut.* (1989) 19:269–73. doi: 10.1016/0094-5765(89)90039-8
15. Heenatigala PPM, Yang J, Bishopp A, Sun Z, Li G, Kumar S, et al. Development of efficient protocols for stable and transient gene transformation for *Wolffia Globosa* using Agrobacterium. *Front. Chem.* (2018) 6:227. doi: 10.3389/fchem.2018.00227
16. Horton RM, Hunt HD, Ho SN, Pullen JK, Pease LR. Engineering hybrid genes without the use of restriction enzymes: gene splicing by overlap extension. *Genes.* (1989) 77:61–8. doi: 10.1016/0378-1119(89)90359-4

17. Schenk RU, Hildebrandt AC. Medium and techniques for induction and growth of monocotyledonous and dicotyledonous plant cell cultures. *Can J Bot*. (1972) 50:199–204. doi: 10.1139/b72-026
18. Khvatkov P, Chernobrovkina M, Okuneva A, Shvedova A, Chaban I, Dolgov S. Callus induction and regeneration in *Wolffia arrhiza (L.)* Horkel ex Wimm. *Plant Cell Tis Org*. (2015) 120:263–73. doi: 10.1007/s11240-014-0603-4
19. Les DH, Crawford DJ, Landolt TE, Gabel JD, Kimball RT, Rettig JH. Phylogeny and systematics of lemnaceae, the duckweed family. *Syst Bot*. (2002) 27:221–40. doi: 10.1043/0363-6445-27.2.221
20. Subasinghe RP, Barg U, Tacon, A. Chemicals in asian aquaculture: need, usage, issues and challenges. In: *Proceeding of the Meeting on the Use of Chemicals in Aquaculture in Asia*. Tigbauna, Iloilo, Philippines. (1996). p. 1–7. Available online at: http://hdl.handle.net/10862/612
21. Rombout JW, Blok LJ, Lamers CH, Egbert E. Immunization of carp (*Cyprinus carpio*) with a *Vibrio anguillarum* bacterin: Indications for a common mucosal immune system. *Dev Comparative Immunol*. (1986) 10:341–51. doi: 10.1016/0145-305X(86)90024-8
22. Firdaus NM. *Immune responses to Streptococcus agalactiae in red tilapia, Oreochromis spp. following vaccination with non-adjuvanted and adjuvanted vaccine (FAV) incorporated feed pellets* (Masters thesis), Universiti Putra Malaysia, Serdang Seri Kembangan, Malaysia (2011). Available online at: http://psasir.upm.edu.my/id/eprint/77356.
23. Embregts CW, Forlenza M. Oral vaccination of fish: Lessons from humans and veterinary species. *Dev Comp Immunol*. (2016) 64:118–37. doi: 10.1016/j.dci.2016.03.024
24. Fernandez-San Millan A, Ortigosa SM, Hervas-Stubbs S, Corral-Martinez P, Segui-Simarro JM, Gaetan J, et al. Human papillomavirus L1 protein expressed in tobacco chloroplasts self-assembles into virus-like particles that are highly immunogenic. *Plant Biotechnol J*. (2008) 6:427–41. doi: 10.1111/j.1467-7652.2008.00338.x
25. Koya V, Moayeri M, Leppla SH, Daniell H. Plant-based vaccine: mice immunized with chloroplast-derived anthrax protective antigen survive anthrax lethal toxin challenge. *Infect Immun*. (2005) 73:8266–74. doi: 10.1128/IAI.73.12.8266-8274.2005
26. Scotti N, Alagna F, Ferraiolo E, Formisano G, Sannino L, Buonaguro L, et al. High-level expression of the HIV-1 Pr55gag polyprotein in transgenic tobacco chloroplasts. *Planta*. (2009) 229:1109–22. doi: 10.1007/s00425-009-0898-2
27. Shina YJ, Kwona TH, Seob JY, Kimb TJ. Oral immunization of fish against iridovirus infection using recombinant antigen produced from rice callus. *Vaccine*. (2013) 31:5210–5. doi: 10.1016/j.vaccine.2013.08.085
28. Ko SM, Sun HJ, Oh MJ, Song IJ, Kim MJ, Sin HS, et al. Expression of the protective antigen for PEDV in transgenic duckweed, *Lemna minor*. *Hortic Environ Biote*. (2011) 52:511–5. doi: 10.1007/s13580-011-0007-x
29. Firsov A, Tarasenko I, Mitiouchkina T, Ismailova N, Shaloiko L, Vainstein A, et al. High-yield expression of M2e peptide of avian influenza virus H5N1 in transgenic duckweed plants. *Mol Biotechnol*. (2015) 57:653–61. doi: 10.1007/s12033-015-9855-4
30. Firsov A, Tarasenko I, Mitiouchkina T, Shaloiko L, Kozlov O, Vinokurov L, et al. Expression and immunogenicity of M2e peptide of avian influenza virus H5N1 fused to ricin toxin B chain produced in duckweed plants. *Front Chem*. (2018) 6:22. doi: 10.3389/fchem.2018.00022
31. Khvatkov P, Firsov A, Shvedova A, Shaloiko L, Kozlov O, Chernobrovkina M, et al. Development of *Wolffia arrhiza* as a producer for recombinant human granulocyte colony-stimulating factor. *Front Chem*. (2018) 6:304. doi: 10.3389/fchem.2018.00304
32. Li H, Xiong XP, Peng B, Xu CX, Ye MZ, Yang TC, et al. Identification of broad cross-protective immunogens using heterogeneous antiserum-based immunoproteomic approach. *J Proteome Res*. (2009) 8:4342–9. doi: 10.1021/pr900439j
33. Li H, Ye MZ, Peng B, Wu HK, Xu CX, Xiong XP, et al. Immunoproteomic identification of polyvalent vaccine candidates from *Vibrio parahaemolyticus* outer membrane proteins. *J Proteome Res*. (2010) 9:2573–83. doi: 10.1021/pr1000219
34. Malik K, Wu K, Li XQ, Martin-Heller T, Hu M, Foster E, et al. A constitutive gene expression system derived from the tCUP cryptic promoter elements. *Theor Appl Genet*. (2002) 105:505–14. doi: 10.1007/s00122-002-0926-0
35. Tian L, Wu K, Levasseur C, Ouellet T, Foster E, Latoszek-Green M, et al. Activity of elements from the tobacco cryptic promoter, tCUP, in conifer tissues. *In Vitro Cell. Dev. Biol. Plant*. (2003) 39:193–202. doi: 10.1079/IVP2002365
36. Haq TA, Mason HS, Clements JD, Arntzen CJ. Oral immunization with a recombinant bacterial antigen produced in transgenic plants. *Science*. (1995) 268:714–6. doi: 10.1126/science.7732379
37. Tabe LM, Wardley-Richardson T, Ceriotti A, Aryan A, McNabb W, Moore A, et al. A biotechnological approach to improving the nutritive value of alfalfa. *J Anim Sci*. (1995) 73:2752–9. doi: 10.2527/1995.7392752x
38. Ko K, Tekoah Y, Rudd PM, Harvey DJ, Dwek RA, Spitsin S, et al. Function and glycosylation of plant-derived antiviral monoclonal antibody. *Proc Natl Acad Sci USA*. (2003) 100:8013–8. doi: 10.1073/pnas.0832472100
39. Park M, Kim SJ, Vitale A, Hwang I. Identification of the protein storage vacuole and protein targeting to the vacuole in leaf cells of three plant species. *Plant Physiol*. (2004) 134:625–39. doi: 10.1104/pp.103.030635
40. Fujiyama K, Misaki R, Sakai Y, Omasa T, Seki T. Change in glycosylation pattern with extension of endoplasmic reticulum retention signal sequence of mouse antibody produced by suspension-cultured tobacco BY2 cells. *J Biosci Bioeng*. (2009) 107:165–72. doi: 10.1016/j.jbiosc.2008.09.016
41. Breyne P, Gheysen G, Jacobs A, Van Montagu M, DePicker A. Effect of T-DNA configuration on transgene expression. *Mol Gen Genet*. (1992) 235:389–96. doi: 10.1007/BF00279385
42. Hobbs SLA, Warkentin TD, De Long CMO. Transgene copy number can be positively or negatively associated with transgene activity. *Plant Mol Biol*. (1993) 21:17–26. doi: 10.1007/BF00039614
43. Matzke AJ, Matzke MA. Position effects and epigenetic silencing of plant transgenes. *Curr Opin Plant Biol*. (1998) 1:142–8. doi: 10.1016/S1369-5266(98)80016-2
44. Schrijver RS, Kramps JA. Critical factors affecting the diagnostic reliability of enzyme-linked immunosorbent assay formats. *Rev Sci Tech Off Int Epiz*. (1998) 17:550–61. doi: 10.20506/rst.17.2.1117
45. Terato K, Do CT, Cutler D, Waritani T, Shionoya H. Preventing intense false positive and negative reactions attributed to the principle of ELISA to re-investigate antibody studies in autoimmune diseases. *J Immunol Methods*. (2014) 407:15–25. doi: 10.1016/j.jim.2014.03.013


**Conflict of Interest:** The authors declare that the research was conducted in the absence of any commercial or financial relationships that could be construed as a potential conflict of interest.

frontiers in Immunology

ORIGINAL RESEARCH
published: 06 October 2020
doi: 10.3389/fimmu.2020.586889

# Characterization of IL-22 Bioactivity and IL-22-Positive Cells in Grass Carp *Ctenopharyngodon idella*

*Yibin Yang*[1,2,3,4], *Junya Wang*[1,2,3], *Jiawen Xu*[1,2,3], *Qin Liu*[1,2,3], *Zixuan Wang*[1,2,3], *Xiaozhen Zhu*[1,2,3], *Xiaohui Ai*[4], *Qian Gao*[1,2,3], *Xinhua Chen*[5] *and Jun Zou*[1,2,3,6*]

[1] *Key Laboratory of Exploration and Utilization of Aquatic Genetic Resources, Ministry of Education, Shanghai Ocean University, Shanghai, China,* [2] *International Research Center for Marine Biosciences at Shanghai Ocean University, Ministry of Science and Technology, Shanghai, China,* [3] *National Demonstration Center for Experimental Fisheries Science Education, Shanghai Ocean University, Shanghai, China,* [4] *Yangtze River Fisheries Research Institute, Chinese Academy of Fishery Sciences, Wuhan, China,* [5] *Key Laboratory of Marine Biotechnology of Fujian Province, Institute of Oceanology, Fujian Agriculture and Forestry University, Fuzhou, China,* [6] *Laboratory for Marine Biology and Biotechnology, Qingdao National Laboratory for Marine Science and Technology, Qingdao, China*

OPEN ACCESS

***Edited by:***
*Min Wan,*
*Ocean University of China, China*

***Reviewed by:***
*Chao Li,*
*Qingdao Agricultural University, China*
*Yong-Hua Hu,*
*Chinese Academy of Tropical Agricultural Sciences, China*

****Correspondence:***
*Jun Zou*
*jzou@shou.edu.cn*

***Specialty section:***
*This article was submitted to Comparative Immunology, a section of the journal Frontiers in Immunology*

***Received:*** *24 July 2020*
***Accepted:*** *21 August 2020*
***Published:*** *06 October 2020*

***Citation:***
*Yang Y, Wang J, Xu J, Liu Q, Wang Z, Zhu X, Ai X, Gao Q, Chen X and Zou J (2020) Characterization of IL-22 Bioactivity and IL-22-Positive Cells in Grass Carp Ctenopharyngodon idella. Front. Immunol. 11:586889. doi: 10.3389/fimmu.2020.586889*

Interleukin (IL)-22 plays an important role in regulating inflammation and clearance of infectious pathogens. IL-22 homologs have been discovered in fish, but the functions and sources of IL-22 have not been fully characterized. In this study, an IL-22 homolog was identified in grass carp and its bioactivities were investigated. The grass carp IL-22 was constitutively expressed in tissues, with the highest expression detected in the gills and hindgut. It was upregulated in the spleen after infection with *Flavobacterium columnare* and grass carp reovirus and in the primary head kidney and spleen leukocytes stimulated with LPS and IL-34. Conversely, it was downregulated by Th2 cytokines such as IL-4/13B and IL-10. The recombinant IL-22 produced in bacteria showed a stimulatory effect on the expression of inflammatory cytokines and STAT3 in the primary head kidney leukocytes and CIK cells. Moreover, the IL-22-positive cells were found to be induced in the hindgut and head kidney 24 h after infection by *F. columnare*. Our data suggest that IL-22 plays an important role in regulating mucosal and systemic immunity against bacterial and viral infection.

**Keywords: interleukin 22, IL-22 producing cells, cytokine, bioactivity, grass carp**

## HIGHLIGHTS

- An IL-22 homolog was identified in grass carp.
- IL-22 is upregulated during infection of *Flavobacterium columnare* and grass carp reovirus.
- IL-22 is induced in primary leukocytes by IL-34 but downregulated by IL-4/13B and IL-10.
- IL-22 upregulates inflammatory cytokines and STAT3.
- The IL-22-positive cells are increased in number in the hindgut and head kidney after infection by *F. columnare*.

## INTRODUCTION

Interleukin (IL)-22 belongs to the IL-10 cytokine family and consists of 6 alpha helices. It is mainly produced by activated Th17 cells, natural killer (NK) cells, and innate lymphoid cells (ILCs) and acts upon a wide range of cell types such as T cells, macrophages, epithelial cells, stem cells, fibroblasts, and keratinocytes (1, 2). IL-22 acts to generate chemokines, inflammatory factors, and antimicrobial peptides (AMPs) (3, 4) and mediates mucosal defenses to subsequently limit bacterial replication and facilitate pathogen clearance by promoting the production and secretion of AMPs, by enhancing the phagocytic activities of innate cells, and by inhibiting the autophagous processes of target cells (5). Excessive levels of IL-22 can cause malfunctioning of the immune system, resulting in a failure to clear pathogens and in chronic inflammatory diseases such as psoriasis (6).

IL-22 binds to a heterodimeric receptor complex consisting of a high binding affinity chain (IL-22R1) and IL-10R2, which are also shared by IL-10, IL-19, IL-20, IL-24, and IL-26 (7). Cellular signaling of IL-22 mainly involves activation of Janus kinase/signal transducers together with the activators of the transcription (JAK/STAT) signaling pathway, the p38 pathway, the extracellular signal-regulated kinase/extracellular regulatory protein kinase pathway, and the JNK/SAPK pathway (8). The functions of IL-22 can be antagonized by use of a soluble IL-22 binding protein (IL-22BP) which shares high sequence homology with IL-22R1 and thus competes with IL-22R1 for the binding site in IL-22 (9, 10).

The IL-22 gene is present in all jawed vertebrates and is clustered with the IFN-γ gene in the genome. Across species, most IL-22 genes are organized into 6 exons and 5 introns. Exceptions include the IL-22 genes in haddock (*Melanogrammus aeglefinus*) and pufferfish (*Fugu rubripes*) which are comprised of 5 exons and 4 introns. Fish IL-22 proteins span 170–190 amino acids (aa) with a hydrophobic signal peptide of 25–30 aa and are structurally conserved. The crystal structure of zebrafish (*Danio rerio*) IL-22 has been assessed and determined to display a typical class II cytokine structure comprised of 6 α helices (11). Fish IL-22 has been found to be highly expressed in mucosal tissues such as the intestine and gills, and its production can be induced in response to proinflammatory stimuli such as LPS and cytokines (12–17). For example, LPS-based treatments of intestinal cells that were freshly isolated from Mandarin fish (*Siniperca chuatsi*) resulted in 10–20-fold increases in IL-22 transcription levels (17). Proinflammatory cytokines such as IL-1β and TNF-α are also potent inducers of IL-22 expression (18, 19). Further, it was found that IL-22 was markedly upregulated at mucosal sites in fish infected with gram-negative or gram-positive bacterial pathogens (15). Recently, IL-22-producing cells were characterized in rainbow trout (*Oncorhynchus mykiss*) and were found to reside in gill filaments and interbranchial lymphoid tissues, having accumulated thereafter the fish infected with *Aeromonas salmonicida* (20). That study demonstrated that IL-22 is a key regulator, which coordinates the immune responses against bacterial pathogens (20).

IL-22 bioactivity has been examined in several fish species, including Mandarin fish (17), pufferfish (21), zebrafish (13), rainbow trout (12), So-iuy mullet (*Liza haematocheila*) (22), turbot (*Scophthalmus maximus*) (14), Atlantic cod (*Gadus morhua*), and haddock (23). IL-22 has been shown to induce the expression of antimicrobial peptide genes including defensins, hepcidin, and LEAP-2 in the primary leukocytes isolated from the spleen and intestine tissues (12, 17). This suggests that IL-22 is essential for the initiation of anti-bacterial defenses in fish. As in mammals, the IL-22-activated antimicrobial responses in fish can be antagonized by the IL-22-binding protein (18). *In vivo* administration of recombinant IL-22 indeed enhanced protection of *L. haematocheila* against *Streptococcus dysgalactiae* and *of S. maximus* against *Aeromonas hydrophila* (14, 22). The studies highlight the central role and importance of IL-22 in the dynamics and mechanisms underlying antibacterial immunity.

In this study, an IL-22 homolog was identified in grass carp (*Ctenopharyngodon idella*, *Ci*) and expression analyzed in response to PAMPs, cytokines, and bacterial and viral infection. The biological activities of recombinant IL-22 were examined in the modulation of immune genes in different cell types. In addition, monoclonal antibodies were produced against the recombinant IL-22 and characterized for detecting the IL-22-producing cells.

## MATERIALS AND METHODS

### Fish

Grass carp (*Ctenopharyngodon idella*) (120 ± 10 g) were obtained from Binhai Base, Shanghai Ocean University, China. Fish were placed in tanks with aeration for at least 10 days before experimental procedures including intraperitoneal (i.p.) injection and tissue sampling. All experiments were conducted under the national regulations on use of laboratory animals of China and approved by the ethics committee of laboratory animals of Shanghai Ocean University (SHOU-DW-2019-003).

### Cloning and Identification of CiIL-22

Total RNA was extracted from spleen and kidney of healthy grass carp using the TRIzol Reagent (Invitrogen) according to the manufacturer's instructions. cDNA was synthesized using a PrimeScript Gamma II 1st-strand cDNA Synthesis Kit (Takara). The synthesized cDNA was stored at −20°C for gene cloning. The partial cDNA sequence of *Ci*IL-22 was obtained from the whole-genome database of grass carp (http://www.ncgr.ac.cn/grasscarp/) (24). A rapid amplification of cDNA ends PCR kit (Life Technology) was used to amplify the full-length sequence of *Ci*IL-22 using the specific gene primers in **Table 1**.

### Sequence Analysis of CiIL-22

The nucleotide sequence of *Ci*IL-22 was assembled and analyzed by DNAMAN 8.0. using ORFfinder listed on the NCBI website (https://www.ncbi.nlm.nih.gov/orfinder/). Protein and nucleic acid translation was performed by Primer Premier 5.0. BLASTN and BLASTP (http://www.ncbi.nlm.Nih.gov/BLAST/) were used to identify the homologous sequences. Homology of sequences was analyzed using the Cluster Omega (https://www.ebi.ac.uk/

**TABLE 1 |** Primers used in this study.

| Primers | Sequence (5′-3′) | Application |
|---|---|---|
| Fa | GCACATCTTGCATGCAGATGATC | 3′-RACE |
| Fb | GATCTGCACAGGCTCGCACAAG | 3′-RACE |
| Fc | TGCAGAACATGCGCAGGTCAAG | 3′-RACE |
| Ra | GTCTTCCTTCTGTGCATGTTCAG | 5′-RACE |
| Rb | TAGAGGTTGTTCCAGGTGACG | 5′-RACE |
| Rc | GGGGCGCGGGCGCATGAGGTGC | 5′-RACE |
| IL-22-F | CTCGTCTACGAGGAACATCAGTC | Verify the full length |
| IL-22-R | GCATGAAAGCACAGTTCCCATGCC | Verify the full length |
| IL-22-qF | CCGTACTGTAGCAACAGTGCAG | Real-time PCR |
| IL-22-qR | TCACATTCTTGCAGAGCAGGATTC | Real-time PCR |
| IL-34-qF | TCAACAGGGTATAAAGAGGGTT | Real-time PCR |
| IL-34-qR | ATCCAGTAATGACTTGGGTGTA | Real-time PCR |
| IL-6-qF | CAGCAGAATGGGGGAGTTATC | Real-time PCR |
| IL-6-qR | CTCGCAGAGTCTTGACATCCTT | Real-time PCR |
| IL-1β-qF | TCTCCTCGTCTGCTGGGTGT | Real-time PCR |
| IL-1β-qR | CAAGACCAGGTGAGGGGAAG | Real-time PCR |
| IL-8-qF | TCTACCCTCCTAGCCCTCACTG | Real-time PCR |
| IL-8-qR | TCATGGTGCTTTGTTGGCAAGGA | Real-time PCR |
| IL-10-qF | GCAACAGAACATCAATAGTCCTT | Real-time PCR |
| IL-10-qR | CACCCTTTTCCTTCATCTTTTCA | Real-time PCR |
| TGF-β1-qF | TTGGGACTTGTGCTCTAT | Real-time PCR |
| TGF-β1-qR | AGTTCTGCTGGGATGTTT | Real-time PCR |
| IL-21-qF | CCACCAACGATTTGAAGGACTGC | Real-time PCR |
| IL-21-qF | CTGGGCAACTTTTCCACAATGA | Real-time PCR |
| STAT3-F | GGCTCTATGGAATGAAGGGTA | Real-time PCR |
| STAT3-R | CAACTGACTGGATCTGGGTCT | Real-time PCR |
| EF-1α-qF | CAGCACAAACATGGGCTGGTTC | Real-time PCR |
| EF-1α-qR | ACGGGTACAGTTCCAATACCTCCA | Real-time PCR |
| UPM-Long | CTAATACGACTCACTATAGGGCAAGC AGTGGTATCAACGCAGAGT | 3′-RACE |
| UPM-Short | CTAATACGACTCACTATAGGGC | 3′-RACE |
| NUP | AAGCAGTGGTATCAACGCAGAGT | 3′-RACE |
| APG | CCAGACTCGTGGCTGATGCA GGGGGGGGGGGGGGGGG | 5′-RACE |
| AP | CCAGACTCGTGGCTGATGCA | 5′-RACE |
| T7 | TAATACGACTCACTATAGGG | Plasmid verification |
| T7-tet | GCTAGTTATTGCTCAGCGG | Plasmid verification |
| pcDNA3.1-F | CTAGAGAACCCACTGCTTAC | Plasmid verification |
| pcDNA3.1-R | TAGAAGGCACAGTCGAGG | Plasmid verification |

Tools/msa/clustalo/). Signal peptide was predicted using SignalP program (version 3.0) (http://www.cbs.dtu.dk/services/SignalP/), and multiple-sequence alignment was generated using GeneDoc software. A phylogenetic tree was constructed using the Neighbor Joining method and repeated for 10,000 times to obtain the bootstrap values.

## Tissue Expression Analysis of CiIL-22

Seven tissues including liver, spleen, head kidney, hindgut, skin, gill, and thymus were taken from six healthy grass carp. Total RNA was extracted using the TRIzol Reagent and reverse transcribed into cDNA using the premix 2 × Hifair™ II SuperMix plus Kit (Yeasen). The synthesized cDNA samples were stored at −20°C until use.

Quantitative real-time PCR (qPCR) was performed using the iTaq™ Universal SYBR® Green Supermix (Bio-Rad) and run on the LightCycler 96 Real Time PCR System (Roche) to analyze gene expression. The qPCR conditions are as follows: 1 cycle of 95°C for 30 s and 40 cycles of 95°C for 10 s, 60°C for 20 s, and 72°C for 20 s. A 10-fold dilution of plasmid DNA containing the target gene fragment was used to establish a standard curve for each gene to quantify the transcription levels. Elongation factor 1α (EF-1α) was used as an internal reference gene to normalize gene expression (25). The expression levels of each gene were calculated as arbitrary units which were normalized to that of EF-1α. Fold changes of expression were calculated by comparing the average expression levels of the experimental groups with that of corresponding control groups. The primers used for qPCR are described in **Table 1**.

## Bacterial Challenge

The *Flavobacterium columnare* G4 strain, provided by the State Key Laboratory of Freshwater Ecology and Biotechnology, Institute of Hydrobiology, Chinese Academy of Sciences (26), was used for the challenge experiment. Bacteria were cultured in Shieh medium at 28°C for 48 h with continuous shaking at 200 rpm/min to reach logarithmic growth phase, centrifuged at 4,200 × g for 4 min and resuspended in PBS buffer. Bacteria were adjusted to a concentration of $1 \times 10^7$ CFU/ml.

In the bacterial challenge experiment, 50 healthy grass carp were randomly divided into two groups, 25 fish in each group. Fish were injected intraperitoneally (i.p.) with 1 μl bacteria suspension ($1 \times 10^7$ CFU/ml) per gram body weight or the same volume of PBS. Spleen, thymus, hindgut, gill, and head kidney were collected at 24, 48, and 72 h after injection, and homogenized in the TRIzol reagent for total RNA extraction. Total RNA was reverse transcribed into cDNA for expression analysis.

## Viral Infection

Grass carp reovirus virus (GCRV) II was provided by the Institute of Virology, Chinese Academy of Sciences. In the infection experiment, 50 healthy grass carp were randomly divided into two groups, 25 fish in each group. Fish were i.p. injected with 200 μl GCRV solution (resuspended in DMEM, $1 \times 10^7$ $TCID_{50}$/ml) or 200 μl DMEM. Head kidney, thymus, gill, spleen, and hindgut were sampled at days 1, 3, 7, and 14 and homogenized in the TRIzol reagent for total RNA extraction and cDNA synthesis.

## Production and Purification of Recombinant CiIL-22 in Bacteria

The predicted mature peptide of *Ci*IL-22 (starting from was $M^{21}$) cloned into pET-21d (Invitrogen). The constructed plasmid was sequenced with T7 and T7-tet primers (**Table 1**) and transformed into *Escherichia coli* BL21 cells. The bacteria were induced with 1 mM IPTG to produce recombinant *Ci*IL-22 (r*Ci*IL-22) (27). r*Ci*IL-22 was expressed as inclusion bodies which were subject to denaturation, refolding, and purification using the Superdex

200 column (GE Healthcare). Purified r*Ci*IL-22 was analyzed by SDS-PAGE and concentration determined by the Bradford method. Protein was aliquoted and stored at −80°C.

## Modulation of CiIL-22 Expression in Head Kidney and Spleen Leukocytes and CIK Cells

Head kidney and spleen of grass carp were sampled for isolation of leukocytes as previously described (25, 28). Cells were counted and cultured in a 6-well plate at $10^6$ cells/well for 6 h. The cells were stimulated with different immune stimulants including poly(I:C) (50 μg/ml), PHA (10 μg/ml), and LPS (50 μg/ml), or cytokines including r*Ci*IL-2 (20 ng/ml), r*Ci*IL-4/13B (20 ng/ml), r*Ci*IL-10 (20 ng/ml), r*Ci*IL-34 (20 ng/ml), r*Ci*IFN-1 (20 ng/ml), or r*Ci*IFN-γrel (20 ng/ml). Poly(I:C), PHA and LPS were purchased from Sigma and recombinant cytokines purified in our laboratory. After stimulation, cells were collected for extraction of total RNA and gene expression analysis.

Head kidney leukocytes of grass carp were prepared by discontinuous density gradient centrifugation (25, 28). Isolated leukocytes were cultured on a 6-well plate for 6 h and stimulated with r*Ci*IL-22 for 12 h. The CIK cell line of grass carp was provided by the National Pathogen Collection Center for Aquatic Animals, Shanghai Ocean University. The CIK cells were seeded in 6-well plates and cultured for about 6 h and stimulated with r*Ci*IL-22. Total RNA was extracted from the cells for expression analysis of IL-1β, IL-6, IL-8, IL-10, IL-21, IL-22, IL-34, TGF-β1, and STAT3 by qPCR.

## Generation of CiIL-22 Monoclonal Antibody and Confocal Microscopy

The *Ci*IL-22 monoclonal antibody (mAb) was generated against the r*Ci*IL-22 by the Beijing Huada Protein Research and Development Center Co. Ltd. Western blotting was performed to verify the antibody specificity. Briefly, the r*Ci*IL-22 was separated by PAGE electrophoresis and transferred to the PVDF membrane using a semi-dry transfer method. The membrane was blocked with TBS buffer with 5% skimmed milk powder for 1 h and incubated with the primary antibody (diluted 1:1,000, v/v) with TBS containing 0.2% Tween 20 at room temperature for 1 h or at 4°C overnight. After washing with TBS-T (TBS containing 0.1% Tween 20) buffer for 3 × 5 min, the membrane was incubated with the goat anti-mouse IgG H & L (IRDye® 680RD, 1: 10,000 dilution, v/v, Odyssey) at room temperature for 1 h, washed with TBS-T (containing 0.1% Tween 20) buffer for 3 × 5 min, and photographed under the Odyssey CLx image system (Odyssey).

To validate the reactivity of mAbs with the r*Ci*IL-22 expressed in eukaryotic cells, the mature peptide of *Ci*IL-22 (starting from $M^{21}$) was synthesized and inserted into pcDNA3.1 (Genewiz). The pcDNA3.1-*Ci*IL-22 plasmid was transfected into HEK293T cells and cultured at 37°C in a $CO_2$ incubator for 48 h. The cells were lysed in RIPA buffer on ice for 10 min and used for Western blotting.

For confocal microscopy, the r*Ci*IL-22 mAb was labeled with FITC Fluor (HuaBio). Grass carp were infected with *F. columnare* as described above. Twenty-four hours post infection, the hindgut and kidney were fixed with 4% paraformaldehyde, dehydrated, and embedded (29), and cryo section was made. After antigen heat retrieval, the sections were incubated with *Ci*IL-22 monoclonal antibody overnight at 4°C, fully washed, and the nuclei were stained with DAPI (1 μg/ml, Beyotime Biotech, China). Fluorescent imaging was viewed on a confocal laser scanning microscope (Nikon, Japan) and analyzed with the NIS Elements Viewer Software (Nikon, Japan).

## Statistical Analysis

The qPCR data were analyzed using the SPSS package 20.0 (SPSS Inc., Chicago, IL, USA). One-way ANOVA and the LSD *post-hoc* test were used to determine the significance ($^*p < 0.05$ or $^{**}p < 0.01$) between treatment group and control group.

# RESULTS

## Sequence Identification of CiIL-22

The cDNA sequence of *Ci*IL-22 is 975 bp (NCBI accession number: MN643172) and contains an open reading frame (ORF) of 510 bp encoding a peptide of 169 aa (**Figure 1**). The *Ci*IL-22 gene consists of 5 exons and 4 introns and is located in the chromosomal locus containing IFN-γ and IL-26 (**Figure 1B**). Multiple-sequence alignment showed that the 4 cysteine residues forming 2 intramolecular disulfide bonds are conserved in fish (11) (**Figure 1A**). *Ci*IL-22 shares 21.2–54.1% sequence identity with known homologs (**Table 2**) and is placed in the IL-22 clade in the phylogenetic tree, supported by a branch bootstrap value of 96% (**Figure 1C**).

## Analysis of CiIL-22 Expression in Fish

The expression of *Ci*IL-22 was examined in different tissues of healthy fish. These included the head kidney, liver, spleen, hindgut, skin, gills, and thymus. The expression levels of *Ci*IL-22 varied considerably among the tissues, with hindgut and gills displaying the highest levels of expression (**Figure 2A**).

To evaluate the IL-22 response to bacterial infection, fish were i.p. injected with *F. columnare*. Upregulation of *Ci*IL-22 expression was observed in the hindgut at 48 and 72 h post infection (hpi), in the head kidney at 72 hpi, and in the spleen at 24 hpi (**Figure 2B**). In contrast, *Ci*IL-22 expression was downregulated in the thymus at 24, 48, and 72 h hpi and in the head kidney at 48 hpi. *Ci*IL-22 expression was also investigated in fish during a 14-day challenge trial after GCRV infection. Induced expression was detected in the gills and spleen at day 7 and in the hindgut and head kidney at day 14 (**Figure 2C**).

## Modulation of CiIL-22 Expression in Primary Cells

Leukocytes were isolated from the head kidney and spleen and simulated with various stimuli to examine IL-22 expression. **Figure 3** shows that *Ci*IL-22 expression was induced by LPS (50 μg/ml) in both tissues. PHA also decreased the expression of *Ci*IL-22 in the head kidney but had no effect in spleen leukocytes. 50 μg/ml of poly(I:C) had a stimulatory effect on the expression of *Ci*IL-22 in the spleen leukocytes at 48 h while it had an inhibitory effect in the head kidney leukocytes. PHA also

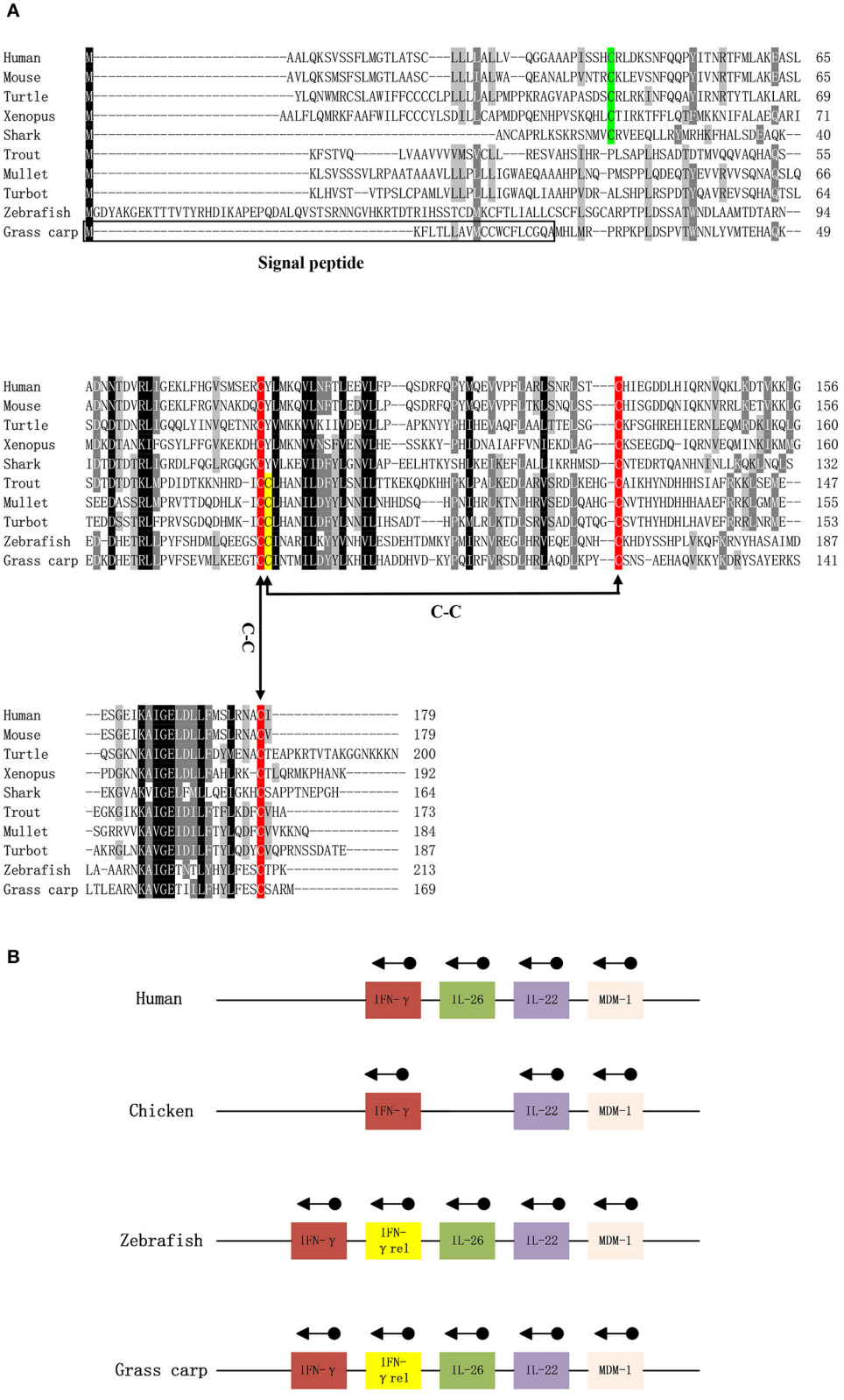


**FIGURE 1 |** Continued

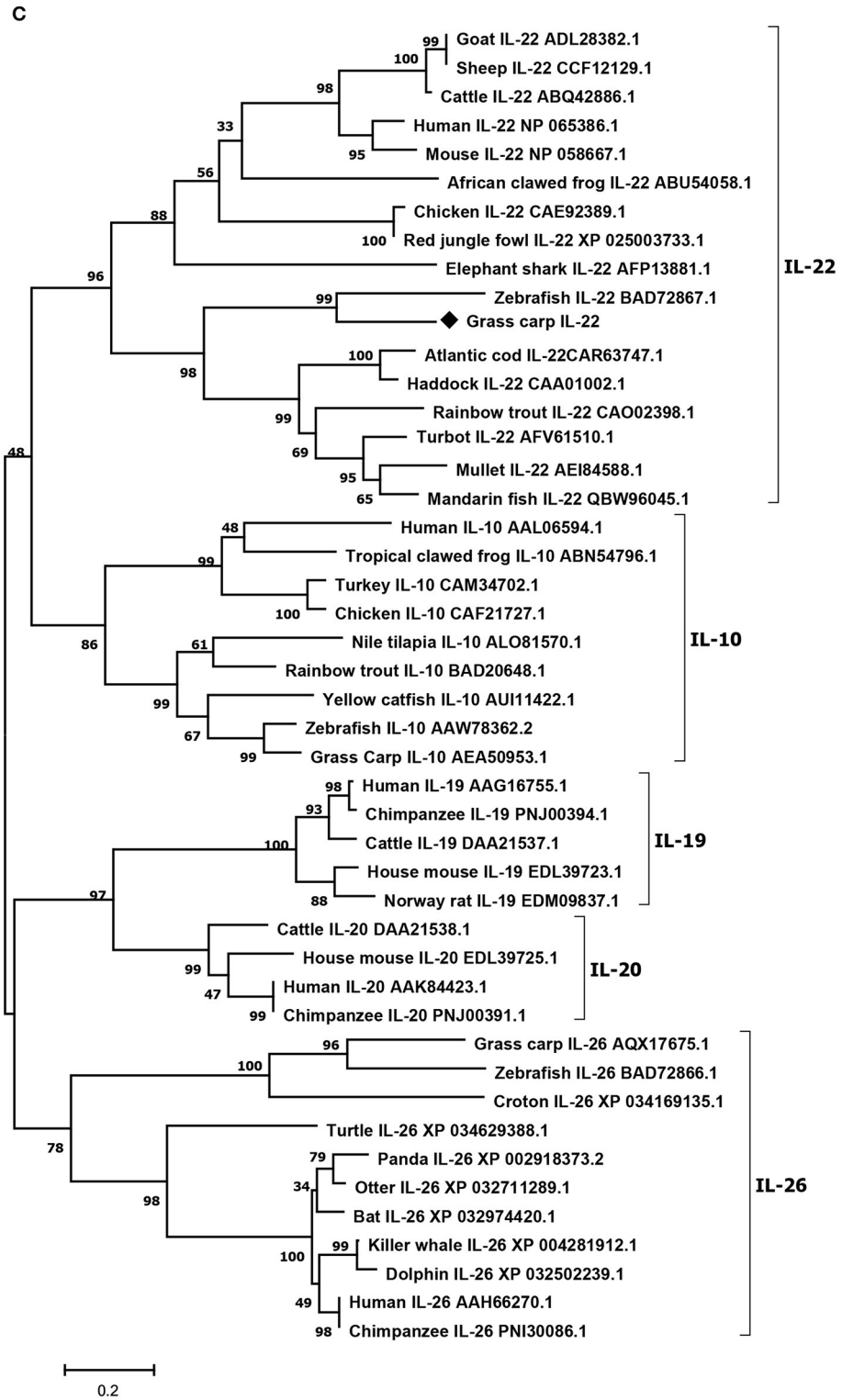


**FIGURE 1 |** Protein sequence alignment **(A)**, gene synteny **(B)**, and the phylogenetic tree **(C)** of *Ci*IL-22 and IL-10 family members. The predicted signal peptide is boxed, and putative disulfide bonds of *Ci*IL-22 are indicated. Arrows indicate gene transcription orientation. The tree was constructed using the Neighbor-Joining method within the MEGA program (Version 6.0). The JTT matrix-based model using the pair-wise deletion option was chosen. The percentages of bootstrap values (>70%) are shown next to the branches based on 10,000 bootstrap replications. Protein sequences of IL-10 family members including IL-10, IL-19, IL-20, IL-22, and IL-26 were obtained from the NCBI database. The *Ci*IL-22 is indicated by "♦".

**TABLE 2 |** Amino acid identities (%) of *Ci*IL-22 with other homologs.

| | 1 | 2 | 3 | 4 | 5 | 6 | 7 | 8 | 9 |
|---|---|---|---|---|---|---|---|---|---|
| 1. Human | | | | | | | | | |
| 2. Mouse | 77.65 | | | | | | | | |
| 3. Turtle | 45.51 | 42.13 | | | | | | | |
| 4. Frog | 32.20 | 32.77 | 37.37 | | | | | | |
| 5. Shark | 31.13 | 30.46 | 29.01 | 25.62 | | | | | |
| 6. Turbot | 20.13 | 18.87 | 16.47 | 15.98 | 17.93 | | | | |
| 7. Grass carp | 22.44 | 21.15 | 23.12 | 23.27 | 21.68 | 30.62 | | | |
| 8. Rainbow trout | 21.43 | 21.43 | 18.47 | 17.31 | 22.46 | 48.82 | 28.03 | | |
| 9. Zebrafish | 20.51 | 19.87 | 25.95 | 20.75 | 18.57 | 29.34 | 54.09 | 47.06 | |
| 10. Mullet | 17.39 | 16.77 | 16.27 | 14.37 | 18.44 | 59.89 | 30.00 | 24.22 | 26.63 |

decreased the expression of *Ci*IL-22 in the head kidney but had no effect in spleen leukocytes. To assess the effects of cytokines on the expression of *Ci*IL-22, primary head kidney leukocytes were incubated with 20 ng/ml of r*Ci*IL-2, r*Ci*IL-4/13B, r*Ci*IL-10, r*Ci*IL-34, r*Ci*IFN-1, or r*Ci*IFN-γrel for 12 h. *Ci*IL-22 was moderately upregulated by r*Ci*IL-2 and r*Ci*IL-34 but downregulated by r*Ci*IL-4/13B and r*Ci*IL-10 (**Figure 4**). r*Ci*IFN-1 and r*Ci*IFN-γrel had no effects on *Ci*IL-22 expression levels.

## Bioactivities of Recombinant CiIL-22 Protein

To evaluate the biological activity of *Ci*IL-22, the recombinant *Ci*IL-22 (r*Ci*IL-22) protein was produced in bacteria and purified using size exclusion chromatography (**Figure 6**). Modulation of inflammatory cytokines by r*Ci*IL-22 was analyzed in the primary head kidney leukocytes and CIK cells. As shown in **Figure 5**, the expression of IL-1β, IL-6, IL-8, IL-10, IL-22, and IL-34 was induced by 2 and 20 ng/ml of protein, while 200 ng/ml of protein had inhibitory effects. However, the mRNA levels of IL-21 and TGF-β1 were only increased after stimulation with 20 ng/ml of *Ci*IL-22. In contrast, the CIK cells responded differently to r*Ci*IL-22 stimulation (**Figure 5**). Induced expression was detected for IL-1β (at all 3 doses), IL-8 (at 200 ng/ml), IL-10 (2 ng/ml), and TGF-β1 (200 ng/ml), while IL-22 expression was suppressed.

## Localization of IL-22-Producing Cells

Monoclonal antibodies of *Ci*IL-22 were produced in mice using the purified r*Ci*IL-22 as an immunogen. Two positive clones were obtained, and their specificity was verified against the r*Ci*IL-22 using Western blotting. Clone GC3-22 was selected for further characterization using the cell lysate of HEK293 cells transfected with a plasmid expressing the mature peptide of *Ci*IL-22. As shown in **Figure 6**, a single protein of ∼17.4 kDa was detected, confirming the specificity of *Ci*IL-22 mAb with the recombinant protein expressed in eukaryotic cells. To localize the IL-22-producing cells in fish infected with *F. columnare*, the mAb (GC3-22) was labeled with the FITC Fluor for confocal microscopy. As shown in **Figure 7**, clustered IL-22-positive cells were detected in the inner wall of the hindgut but not in PBS-injected fish. In the head kidney, weak staining was seen in the region surrounding the renal tubules in PBS-injected fish but markedly intensified in infected fish. Moreover, the numbers of stained tubules in infected fish were increased significantly.

# DISCUSSION

In this study, an IL-22 homology was identified in grass carp. The IL-22 gene is present in all jawed vertebrates, mostly as a single gene. However, the IL-22 gene in polyploid fish exists as multiple copies and is clustered with the IFN-γ gene and IL-26 gene. This suggests that all these genes evolved from a common ancestor (12–15, 17, 22, 23). In teleost fish, this locus also contains an additional gene, termed IFN-γ rel, which has been duplicated from the IFN-γ gene (13, 30). The organization of the 5 exons and 4 introns separating the coding region of IL-22 also remains unaltered in all vertebrate species, including grass carp (**Figure 1B**) (23, 31). As for known IL-22 proteins, the translated *Ci*IL-22 protein was predicted to possess a signal peptide which can be cleaved to generate a mature peptide with a size comparable to IL-22s from other teleost fish species (13, 23). The *Ci*IL-22 of grass carp contained four cysteine (Cys) residues, three of which ($Cys^{73}$, $Cys^{118}$, and $Cys^{165}$) were conserved in vertebrates. The fourth cysteine residue (corresponding to $Cys^{74}$ in *Ci*IL-22) was aligned only within molecules derived from teleost fish (**Figure 1A**). Crystal structures of zebrafish IL-22 revealed that these four cysteines form 2 pairs of intramolecular disulfide bonds, namely $Cys^{73}$-$Cys^{165}$ and $Cys^{74}$-$Cys^{118}$. In humans, two disulfide bonds are also present (32). However, the positions of the cysteines forming the disulfide bonds in human IL-22 differ from the respective positions in fish IL-22. More specifically, the $Cys^{40}$ of human IL-22 pairs with $Cys^{122}$, and $Cys^{89}$ pairs with $Cys^{178}$. Intriguingly, the disulfide bonds seem to have little impact upon the overall protein topology of 6 α-helices (32).

IL-22 was constitutively expressed in most tissues with immune-related functions in healthy grass carp but was more highly expressed in the gills and hindgut (**Figure 2**). This observation is consistent with previous studies in which basal transcription was higher in mucosal tissues such as in the gills, pyloric cecae, and the intestine (12, 14, 17, 20, 23). These studies have suggested that IL-22 may mediate inflammation and facilitate the maintenance of homeostasis of the mucosal barrier in order to provide protection against pathogens. In a transgenic

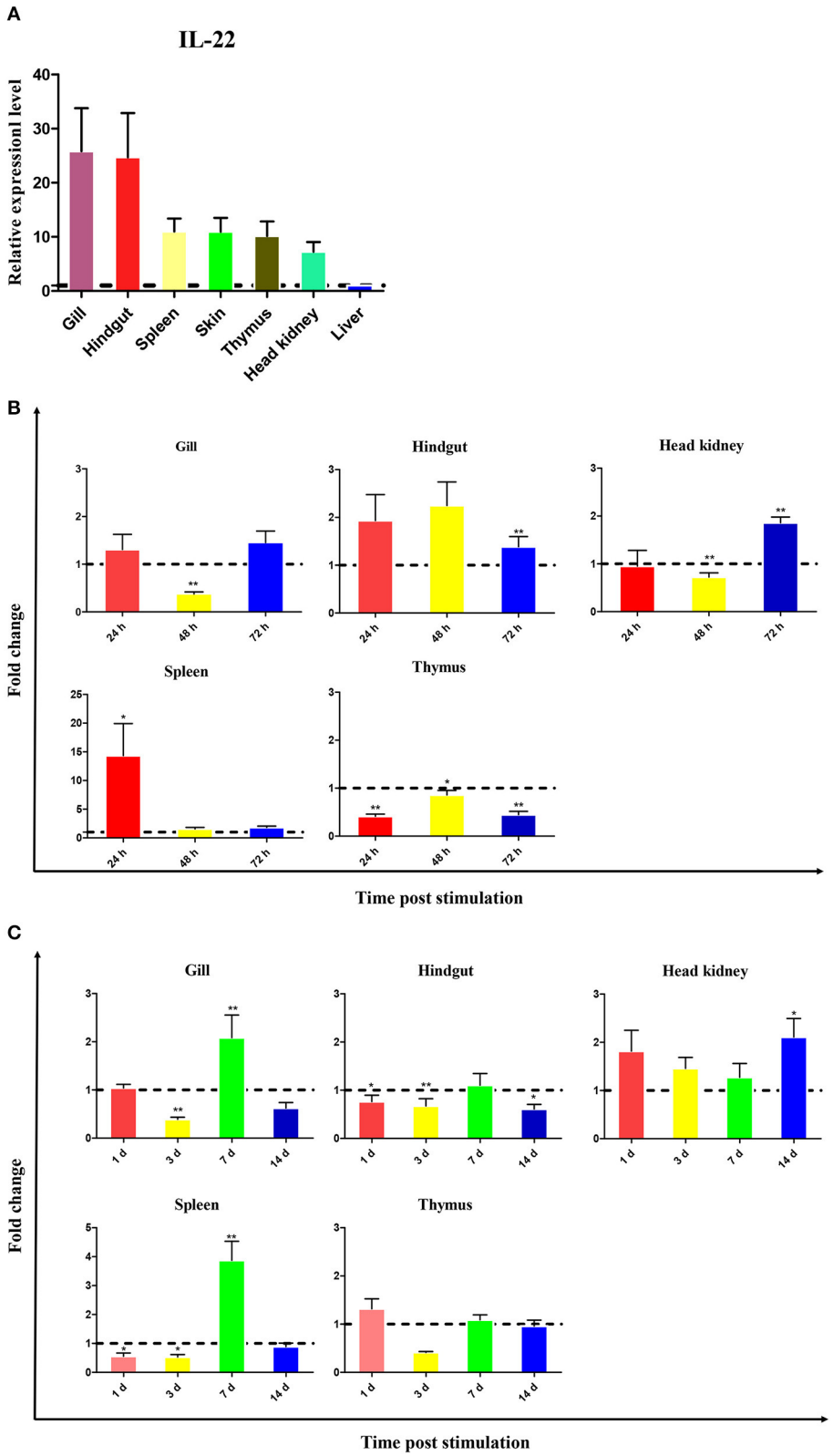


**FIGURE 2 |** Expression of *Ci*IL-22 in tissues of healthy fish **(A)** and fish infected with *F. columnare* **(B)** or GCRV **(C)**. The mRNA levels of *Ci*IL-22 were determined by qPCR. The relative expression levels of *Ci*IL-22 were expressed as arbitrary units that were normalized against the expression levels of EF-1α. Fold changes were calculated by comparing the average levels of gene expression of infected groups with those of corresponding control groups. Data are shown as mean + SEM ($n = 4$). $^{*}p < 0.05$ or $^{**}p < 0.01$ are considered significant.

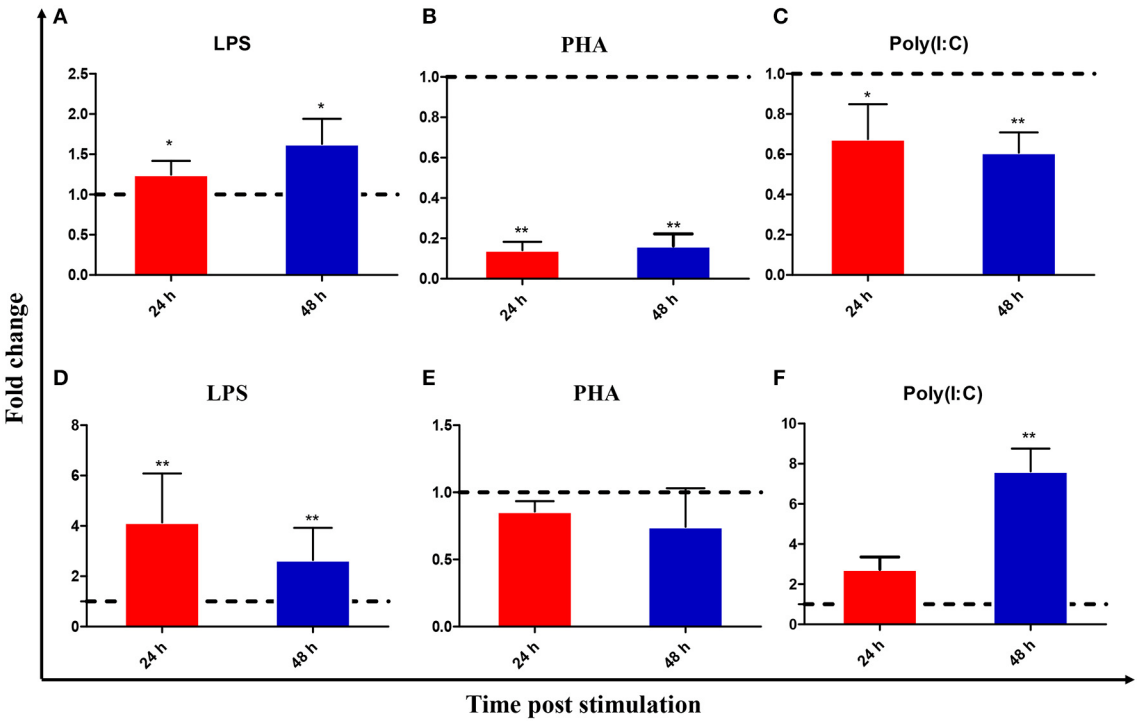


**FIGURE 3 |** Expression analysis of *Ci*IL-22 in the primary head kidney **(A–C)** and spleen **(D–F)** leukocytes, after stimulation with LPS, PHA, or poly(I:C). The cells were stimulated with LPS, PHA or poly(I:C) for 24 and 48 h and analyzed by qPCR. Data are shown as mean + SEM ($N = 4$). *$p < 0.05$ or **$p < 0.01$ are considered significant.

mouse-based modeling experiment, excessive expression of IL-22 resulted in both increased infiltration of macrophages into dermal layers and proliferation of keratinocytes, which caused subsequent thickening of the epidermis (33, 34). It has also been shown that IL-22 is involved in the inhibition of intestinal inflammation and tissue repair (3, 35, 36). For example, IL-22 promoted the healing intestinal trauma in assessments of acute intestinal injury (37) and also regulated intestinal flora under inflammation (38).

*In vitro* studies have indicated that *Ci*IL-22 is induced by LPS in primary leukocytes isolated from the head kidney and spleen (**Figure 3**). This is in line with previous studies where LPS was a robust inducer of IL-22 expression in cultured cells (8, 13–17). Furthermore, LPS is a known bacterial PAMP able to activate expression of inflammatory genes such as IL-1β, IL-8, IL-17A/F, and TNF-α in fishes (14, 39). Such actions are likely to be mediated by PRRs rather than TLR4, which is a known PRR in mammals, since the fish TLR4 homologs have much weaker binding affinities with LPS (40). However, the involvement of TLR4 as an associated PRR of LPS cannot be fully excluded. More recently, caspase 3 was identified as an intracellular PRR for recognizing LPS in mammals and is also present in fish (41). However, whether caspase 3 plays a role in LPS-induced IL-22 expression in fish remains to be investigated. Interestingly, IL-22 expression was inhibited at

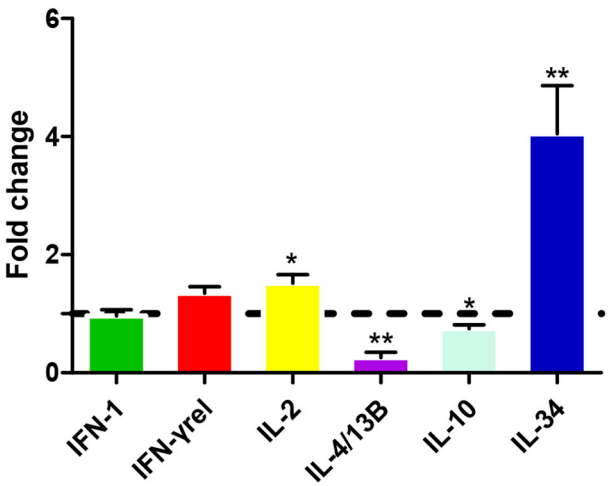


**FIGURE 4 |** Expression analysis of *Ci*IL-22 in primary head kidney leukocytes after stimulation with r*Ci*IFN-1, r*Ci*IFN-γrel, r*Ci*IL-2, r*Ci*IL-4/13B, r*Ci*IL-10, or r*Ci*IL-34. Head kidney macrophages were stimulated with r*Ci*IFN-1, r*Ci*IFN-γrel, r*Ci*IL-2, r*Ci*IL-4/13B, r*Ci*IL-10, or r*Ci*IL-34 for 12 h, and *Ci*IL-22 expression was analyzed using qPCR. The EF-1α gene was used as an internal control. Fold change was calculated by comparing the average levels of expression of stimulated cells with those of corresponding control groups. Data are shown as mean + SEM ($N = 4$). *$p < 0.05$ or **$p < 0.01$ is considered significant.

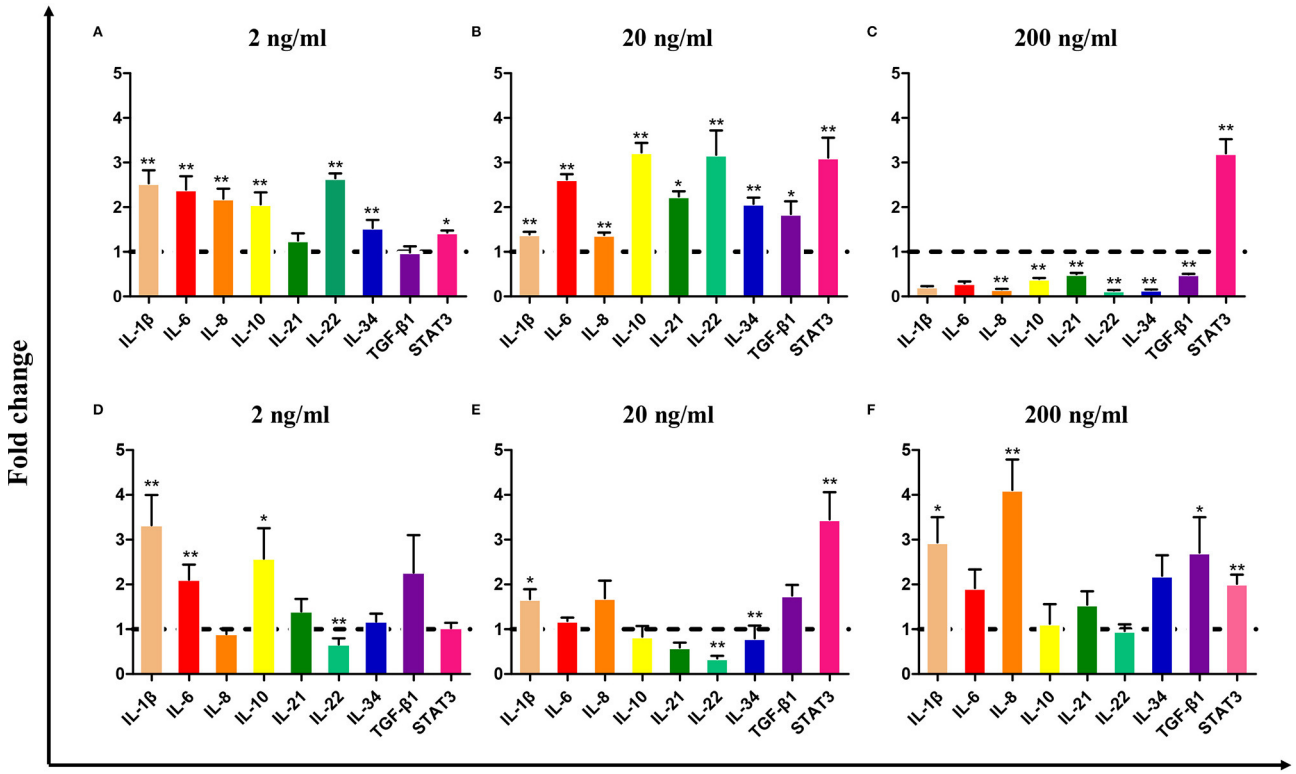


**FIGURE 5 |** The effects of bacteria-derived r*Ci*IL-22 on gene expression in the primary head kidney leukocytes **(A–C)** and CIK cells **(D–F)**. The primary head kidney leukocytes were prepared as described in the Materials and Methods and stimulated with r*Ci*IL-22 for 12 h. The mRNA expression of cytokines and STAT3 was analyzed by qPCR. Data are shown as mean + SEM ($N = 4$). *$p < 0.05$ or **$p < 0.01$ is considered significant.

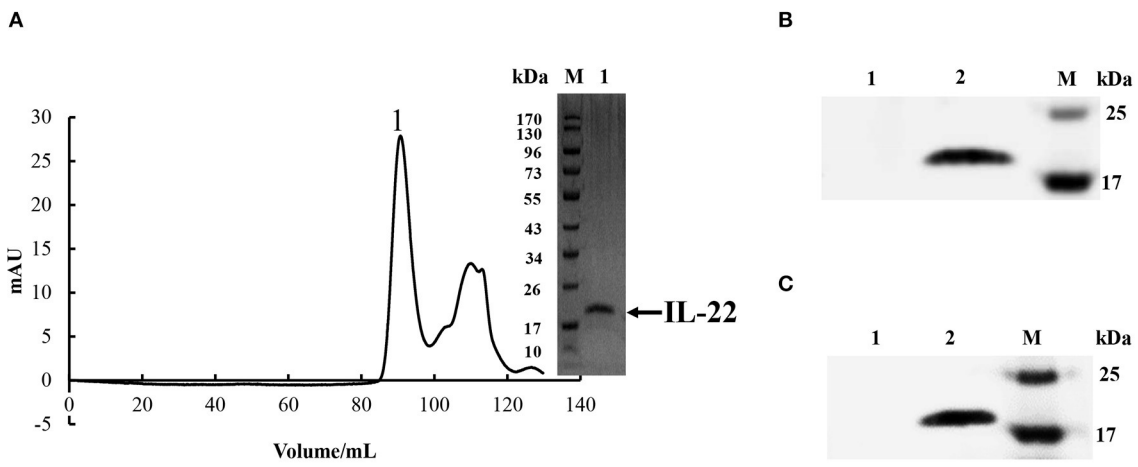


**FIGURE 6 | (A)** Purification of r*Ci*IL-22 in bacteria. r*Ci*IL-22 was expressed in *E. coli* BL21 cells as inclusion bodies, refolded, and purified by size exclusion chromatography. Fraction 1 was checked by SDS-PAGE. **(B)** Western blotting analysis of bacteria-derived recombinant *Ci*IL-22 using an IL-22 monoclonal antibody (GC3-22). Lane 1: protein buffer; lane 2: purified r*Ci*IL-22. **(C)** Western blotting analysis of recombinant *Ci*IL-22 expressed in HEK293 cells using mAb GC3-22. Lane 1, cell lysate of HEK293 cells transfected with pcDNA3.1; lane 2, cell lysate of HEK293 cells transfected with pcDNA3.1-*Ci*IL-22.

24 h and 48 h after stimulation by PHA (**Figure 3**). In turbot, IL-22 was upregulated in the primary leukocytes of the head kidney and spleen at 3 and 6 h post-stimulation with PHA, but this was not the case at 24 h (14). These studies suggest that induction of IL-22 expression by PHA appears to be swift and transient.

The effects of several cytokines on IL-22 expression were also examined. IL-22 expression was upregulated by IL-2 and IL-34

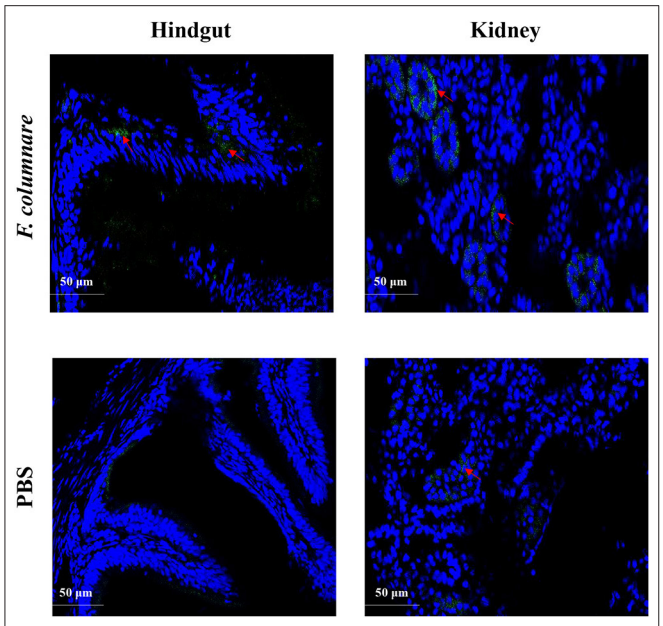


**FIGURE 7 |** Localization of IL-22-positive cells in the hindgut and kidney of grass carp. Fish were i.p. injected with 1 μl bacterial suspension ($1 \times 10^7$ CFU/ml) per gram body weight or an equal volume of PBS. Hindgut and kidney were fixed at 24 h after injection and subjected to confocal microscopic analysis using a mAb (GC3-22) against *Ci*IL-22.

in the primary head kidney leukocytes while it was inhibited by IL-4/13B and IL-10 (**Figure 4**). High amounts of IL-22 can be produced in lymphocytes involved in innate and adaptive immunity, including CD4 T cells, γδ T cells, NK cells, and innate lymphoid cells, and can be regulated by multiple factors (42, 43). Several cytokines such as IL-1β, IL-6, IL-23, and TGF-β1 are required for the development of Th17 cells which secrete IL-22 upon T cell receptor activation (42). IL-34 is known to regulate macrophage functions in mammals via the macrophage colony-stimulating receptor (MCSFR) (44). In our previous study, we demonstrated that recombinant IL-34 could upregulate the expression of proinflammatory cytokines such as IL-1β, IL-6, and IL-8 in enriched macrophage populations (25). In the present study, our data suggest that IL-22 may be produced by activated macrophages in fish and we consider that this warrants further investigation. The findings indicating the suppression of IL-22 expression by IL-4/13B and IL-10 in fish are also in agreement with past findings in mammals (42). These studies have indicated that Th2 cytokines play an inhibitory role in the regulation of Th17 responses in fish. However, observations of upregulation of IL-22 by IL-2 are also interesting. In the mammalian system, IL-2 together with IFN-γ promotes Th1 responses while antagonizing Th2 responses (45). The functions of fish IL-2 are still under debate, since fish seem to lack the highly affinitive binding private receptor equivalent to IL-2Rα (CD25) and rather facilitate binding to a private receptor shared by IL-15 (46).

The IL-22-mediated responses to bacterial infection have well been documented in fish. A number of studies have consistently shown that IL-22 can be upregulated at mRNA levels by gram-negative and gram-positive bacterial pathogens (13, 15–18). In a recent study, induction of the expression of the IL-22 protein was also observed in the gills of trout post-infection with *A. salmonicida* (21). In line with previous studies, it was not surprising that in our study mRNA expression of *Ci*IL-22 was induced in the spleen and hindgut of grass carp when they were infected with *F. columnare* (**Figure 2B**), which is a bacterial pathogen known to cause inflammation in fish (27, 28). In addition, our results indicate that the *Ci*IL-22 expression was increased in the tissues of fish infected with GCRV (**Figure 2C**). These findings suggest that *Ci*IL-22 is involved in the immune response to viral infection. In mice, the IL-22 secreted by conventional NK cells can reduce exacerbated inflammation caused by influenza virus infections and is required for the regeneration of damaged tracheal epithelial layers (47).

The biological effects of *Ci*IL-22 upon immune-related gene expression were evaluated in the primary head kidney leukocytes and CIK cells (a non-leukocyte cell line derived from grass carp kidney) (**Figure 5**). Our findings indicate that induction of a panel of cytokines including IL-1β, IL-6, IL-8, IL-10, IL-21, IL-22, IL-34, and TGF-β1 was pronounced in head kidney leukocytes but to a much lesser degree in CIK cells. These findings suggest that IL-22 may primarily target leukocytes. The differences may result from different numbers of IL-22 receptors expressed upon these cells. Interestingly, stimulatory effects were seen only in the leukocytes post-stimulation with low doses of IL-22 (2 and 20 ng/ml) while 200 ng/ml of IL-22 led to the inhibition of gene expression. Therefore, it is possible that the actions of IL-22 are dose dependent and could be regulated by a type of negative feedback. Moreover, the findings in the present study also imply that IL-22 elicits cellular responses through activation of STAT3-mediated signaling as STAT3 expression was upregulated by IL-22 in both the head kidney leukocytes and CIK cells (**Figure 5**). In mammals, STAT3 has been shown to be the central transcription factor mediating IL-22 signal transduction (48).

The mRNA levels of IL-22 expression have been relatively well-studied in fish (12, 14, 17, 20, 23). However, the cells secreting IL-22 have not been investigated until recently. Using monoclonal antibodies against synthesized peptides, Hu et al. (20) found that in trout, IL-22-producing cells were significantly increased in the gills and blood 24 h after i.p. infection with *A. salmonicida* and *Y. ruckeri*. Further, the IL-22$^+$ cells were confirmed as present in the gill lamellae and in the interbranchial region. The gill interbranchial region contains high numbers of T cells and is considered as a secondary lymphoid tissue in fish (49). Therefore, it is possible to speculate that the IL-22$^+$ cells therein are likely to be of lymphoid origin (20). Fish gut is also an important mucosal tissue and contains a diffuse gut-associated lymphoid tissue (GALT), although morphologically and functionally different from that in mammals (50). In the present study, the IL-22$^+$ cells were clearly detected in the inner wall of the hindgut of fish infected with *F. columnare* but were not detected in the hindgut of healthy fish (**Figure 7**). These findings indicate that the cells were involved in mounting antibacterial defenses in the gut. The IL-22$^+$ cells could be activated locally in the GALT or could have migrated from other sites as higher numbers of IL-22$^+$ cells were also found in the head kidney (**Figure 7**). In mammals, IL-22 is mainly secreted by activated Th17 cells and innate lymphoid cells (51).

In summary, an IL-22 homolog was identified in grass carp, an economically important aquaculture species in China. *In vitro* expression analyses revealed that it could be upregulated by LPS and cytokines such as IL-2 and IL-34 while it was inhibited by Th2 cytokines. Bacterial and viral infections resulted in increases in IL-22 expression in tissues. The recombinant IL-22 was effective in inducing the expression of a number of inflammatory cytokines and STAT3 in the primary head kidney leukocytes. Lastly, the IL-22-producing cells were located in the inner walls of the hindgut and in the tubules of the head kidney. This highlights the involvement of IL-22 in regulating mucosal and systemic immunity and its critical roles in the clearance of infectious pathogens.

## DATA AVAILABILITY STATEMENT

The datasets presented in this study can be found in online repositories. The names of the repository/repositories and accession number(s) can be found below: https://www.ncbi.nlm.nih.gov/genbank/, MN643172.

## ETHICS STATEMENT

The animal study was reviewed and approved by the ethics committee of laboratory animals of Shanghai Ocean University.

## AUTHOR CONTRIBUTIONS

JZ conceived and designed the study. YY performed most of the experiments. JW, JX, QL, ZW, and XZ assisted in protein preparation and analyses. XA, QG, and XC provided bioinformatics assistance and support. JZ and YY wrote the manuscript. All authors approved the manuscript.

## FUNDING

This work was supported by the Science and Technology Commission of Shanghai Municipality (Grant No. 19390743100), the National Natural Science Foundation of China (Grant No. U1605211), and Key Laboratory of Marine Biotechnology of Fujian Province (Grant No. 2020MB01).

## ACKNOWLEDGMENTS

The authors would like to thank Dr. Haixia Xie, Institute of Hydrobiology, Chinese Academy of Sciences, for providing *F. columnare*, and Dr. Qin Fang, Institute of Virology, Chinese Academy of Sciences, for providing GCRV.

## REFERENCES

1. Rutz S, Eidenschenk C, Ouyang W. IL-22, not simply a Th17 cytokine. *Immunol Rev.* (2013) 252:116–32. doi: 10.1111/imr.12027
2. Sabat R, Ouyang W, Wolk K. Therapeutic opportunities of the IL-22-IL-22R1 system. *Nat Rev Drug Discov.* (2014) 13:21–38. doi: 10.1038/nrd4176
3. Sugimoto K, Ogawa A, Mizoguchi E, Shimomura Y, Andoh A, Bhan AK, et al. IL-22 ameliorates intestinal inflammation in a mouse model of ulcerative colitis. *J Clin Invest.* (2008) 118:534–44. doi: 10.1172/JCI33194
4. Wolk K, Kunz S, Witte E, Friedrich M, Asadullah K, Sabat R. IL-22 increases the innate immunity of tissues. *Immunity.* (2004) 21:241–54. doi: 10.1016/j.immuni.2004.07.007
5. Liang SC, Tan XY, Luxenberg DP, Karim R, Dunussi-Joannopoulos K, Collins M, et al. Interleukin (IL)-22 and IL-17 are coexpressed by Th17 cells and cooperatively enhance expression of antimicrobial peptides. *J Exp Med.* (2006) 203:2271–9. doi: 10.1084/jem.20061308
6. Ouyang W. Distinct roles of IL-22 in human psoriasis and inflammatory bowel disease. *Cytokine Growth Factor Rev.* (2010) 21:435–41. doi: 10.1016/j.cytogfr.2010.10.007
7. Xie MH, Aggarwal S, Ho WH, Foster J, Zhang Z, Stinson J, et al. Interleukin (IL)-22, a novel human cytokine that signals through the interferon receptor-related proteins CRF2-4 and IL-22R. *J Biol Chem.* (2000) 275:31335–9. doi: 10.1074/jbc.M005304200
8. Murano T, Okamoto R, Ito G, Nakata T, Hibiya S, Shimizu H, et al. Hes1 promotes the IL-22-mediated antimicrobial response by enhancing STAT3-dependent transcription in human intestinal epithelial cells. *Biochem Biophys Res Commun.* (2014) 443:840–6. doi: 10.1016/j.bbrc.2013.12.061
9. Wolk K, Witte E, Hoffmann U, Doecke WD, Endesfelder S, Asadullah K, et al. IL-22 induces lipopolysaccharide-binding protein in hepatocytes: a potential systemic role of IL-22 in Crohn's disease. *J Immunol.* (2007) 178:5973–81. doi: 10.4049/jimmunol.178.9.5973
10. Jones BC, Logsdon NJ, Walter MR. Structure of IL-22 bound to its high-affinity IL-22R1 chain. *Structure.* (2008) 16:1333–44. doi: 10.1016/j.str.2008.06.005
11. Siupka P, Hamming OJ, Frétaud M, Luftalla G, Levraud JP, Hartmann R. The crystal structure of zebrafish IL-22 reveals an evolutionary, conserved structure highly similar to that of human IL-22. *Genes Immunity.* (2014) 15:293–302. doi: 10.1038/gene.2014.18
12. Monte MM, Zou J, Wang T, Carrington A, Secombes CJ. Cloning, expression analysis and bioactivity studies of rainbow trout (*Oncorhynchus mykiss*) interleukin-22. *Cytokine.* (2011) 55:62–73. doi: 10.1016/j.cyto.2011.03.015
13. Igawa D, Sakai M, Savan R. An unexpected discovery of two interferon gamma-like genes along with interleukin (IL)-22 and−26 from teleost: IL-22 and−26 genes have been described for the first time outside mammals. *Mol Immunol.* (2006) 43:999–1009. doi: 10.1016/j.molimm.2005.05.009
14. Costa MM, Pereiro P, Wang T, Secombes CJ, Figueras A, Novoa B. Characterization and gene expression analysis of the two main Th17 cytokines (IL-17A/F and IL-22) in turbot, *Scophthalmus maximus*. *Dev Comp Immunol.* (2012) 38:505–16. doi: 10.1016/j.dci.2012.09.002
15. Peng Y, Cai X, Zhang G, Wang J, Li Y, Wang Z, et al. Molecular characterization and expression of interleukin-10 and interleukin-22 in golden pompano (*Trachinotus ovatus*) in response to *Streptococcus agalactiae* stimulus. *Fish Shellfish Immunol.* (2017) 65:244–55. doi: 10.1016/j.fsi.2017.04.019
16. Jiang R, Zhang GR, Zhu DM, Shi ZC, Liao CL, Fan QX, et al. Molecular characterization and expression analysis of IL-22 and its two receptors genes in yellow catfish (*Pelteobagrus filvidraco*) in response to *Edwardsiella ictaluri* challenge. *Fish Shellfish Immunol.* (2018) 80:250–63. doi: 10.1016/j.fsi.2018.06.012
17. Huo HJ, Chen SN, Li L, Laghari ZA, Li N, Nie P. Functional characterization of interleukin (IL)-22 and its inhibitor, IL-22 binding protein (IL-22BP) in Mandarin fish, *Siniperca chuatsi*. *Dev Comp Immunol.* (2019) 97:88–97. doi: 10.1016/j.dci.2019.03.007
18. Veenstra KA, Wangkahart E, Wang T, Tubbs L, Ben Arous J, Secombes CJ. Rainbow trout (*Oncorhynchus mykiss*) adipose tissue undergoes major changes in immune gene expression following bacterial infection or stimulation with pro-inflammatory molecules. *Dev Comp Immunol.* (2018) 81:83–94. doi: 10.1016/j.dci.2017.11.001

19. Wangkahart E, Secombes CJ, Wang T. Dissecting the immune pathways stimulated following injection vaccination of rainbow trout (*Oncorhynchus mykiss*) against enteric redmouth disease (ERM). *Fish Shellfish Immunol.* (2019) 85:18–30. doi: 10.1016/j.fsi.2017.07.056
20. Hu Y, Carpio Y, Scott C, Alnabulsi A, Alnabulsi A, Wang T, et al. Induction of IL-22 protein and IL-22-producing cells in rainbow trout *Oncorhynchus mykiss*. *Dev Comp Immunol.* (2019) 101:103449. doi: 10.1016/j.dci.2019.103449
21. Zou J, Clark MS, Secombes CJ. Characterisation, expression and promoter analysis of an interleukin 10 homologue in the puffer fish, *Fugu rubripes*. *Immunogenetics.* (2003) 55:325–35. doi: 10.1007/s00251-003-0580-y
22. Qi Z, Zhang Q, Wang Z, Zhao W, Chen S, Gao Q. Molecular cloning, expression analysis and functional characterization of interleukin-22 in So-iny mullet, *Liza haematocheila*. *Mol Immunol.* (2015) 63:245–52. doi: 10.1016/j.molimm.2014.07.006
23. Corripio-Miyar Y, Zou J, Richmond H, Secombes CJ. Identification of interleukin-22 in gadoids and examination of its expression level in vaccinated fish. *Mol Immunol.* (2009) 46:2098–106. doi: 10.1016/j.molimm.2009.01.024
24. Wang Y, Lu Y, Zhang Y, Ning Z, Li Y, Zhao Q, et al. The draft genome of the grass carp (*Ctenopharyngodon idellus*) provides insights into its evolution and vegetarian adaptation. *Nat Genet.* (2015) 47:625–31. doi: 10.1038/ng.3280
25. Xue Y, Jiang X, Gao J, Li X, Xu J, Wang J, et al. Functional characterisation of interleukin 34 in grass carp *Ctenopharyngodon idella*. *Fish Shellfish Immunol.* (2019) 92:91–100. doi: 10.1016/j.fsi.2019.05.059
26. Xie HX, Nie P, Sun BJ. Characterization of two membrane-associated protease genes obtained from screening out-membrane protein genes of *Flavobacterium columnare* G4. *J Fish Dis.* (2004) 27:719–29. doi: 10.1111/j.1365-2761.2004.00596.x
27. Hamming OJ, Lutfalla G, Levraud JP, Hartmann R. Crystal structure of zebrafish interferons I and II reveals conservation of type I interferon structure in vertebrates. *J Virol.* (2011) 85:8181–7. doi: 10.1128/JVI.00521-11
28. Meng Z, Shao J, Xiang L. CpG oligodeoxynucleotides activate grass carp (*Ctenopharyngodon idellus*) macrophages. *Dev Comp Immunol.* (2003) 27:313–21. doi: 10.1016/S0145-305X(02)00104-0
29. Chen Y, Zhang L, Hong G, Huang C, Qian W, Bai T, et al. Probiotic mixtures with aerobic constituent promoted the recovery of multi-barriers in DSS-induced chronic colitis. *Life Sci.* (2020) 240:117089. doi: 10.1016/j.lfs.2019.117089
30. Zou J, Secombes CJ. The function of fish cytokines. *Biology.* (2016) 5:23. doi: 10.3390/biology5020023
31. Dumoutier L, Louahed J, Renauld JC. Cloning and characterization of IL-10-related T cell-derived inducible factor (IL-TIF), a novel cytokine structurally related to IL-10 and inducible by IL-9. *J Immunol.* (2000) 164:1814–9. doi: 10.4049/jimmunol.164.4.1814
32. de Moura PR, Watanabe L, Bleicher L, Colau D, Dumoutier L, Lemaire MM, et al. Crystal structure of a soluble decoy receptor IL-22BP bound to interleukin-22. *FEBS Lett.* (2009) 583:1072–7. doi: 10.1016/j.febslet.2009.03.006
33. Wolk K, Haugen HS, Xu W, Witte E, Waggie K, Anderson M, et al. IL-22 and IL-20 are key mediators of the epidermal alterations in psoriasis while IL-17 and IFN-gamma are not. *J Mol Med.* (2009) 87:523–36. doi: 10.1007/s00109-009-0457-0
34. Boniface K, Lecron JC, Bernard FX, Dagregorio G, Guillet G, Nau F, et al. Keratinocytes as targets for interleukin-10-related cytokines: a putative role in the pathogenesis of psoriasis. *Eur Cytokine Netw.* (2005) 16:309–19.
35. Li LJ, Gong C, Zhao MH, Feng BS. Role of interleukin-22 in inflammatory bowel disease. *World J Gastroenterol.* (2014) 20:18177–88. doi: 10.3748/wjg.v20.i48.18177
36. Mizoguchi A. Healing of intestinal inflammation by IL-22. *Inflamm Bowel Dis.* (2012) 18:1777–84. doi: 10.1002/ibd.22929
37. Mizoguchi A, Yano A, Himuro H, Ezaki Y, Sadanaga T, Mizoguchi E. Clinical importance of IL-22 cascade in IBD. *J Gastroenterol.* (2018) 53:465–74. doi: 10.1007/s00535-017-1401-7
38. Rubino SJ, Geddes K, Girardin SE. Innate IL-17 and IL-22 responses to enteric bacterial pathogens. *Trends Immunol.* (2012) 33:112–8. doi: 10.1016/j.it.2012.01.003
39. Monte MM, Wang T, Holland JW, Zou J, Secombes CJ. Cloning and characterization of rainbow trout interleukin-17A/F2 (IL-17A/F2) and IL-17 receptor A: expression during infection and bioactivity of recombinant IL-17A/F2. *Infect Immun.* (2013) 81:340–53. doi: 10.1128/IAI.00599-12
40. Sepulcre MP, Alcaraz-Pérez F, López-Muñoz A, Roca FJ, Meseguer J, Cayuela ML, et al. Evolution of lipopolysaccharide (LPS) recognition and signaling: fish TLR4 does not recognize LPS and negatively regulates NF-kappaB activation. *J Immunol.* (2009) 182:1836–45 doi: 10.4049/jimmunol.0801755
41. Reyes-Becerril M, Sanchez V, Delgado K, Guerra K, Velazquez E, Ascencio F, et al. Caspase−1,−3,−8 and antioxidant enzyme genes are key molecular effectors following *Vibrio parahaemolyticus* and *Aeromonas veronii* infection in fish leukocytes. *Immunobiology.* (2018) 223:562–76. doi: 10.1016/j.imbio.2018.07.002
42. Wolk K, Witte E, Witte K, Warszawska K, Sabat R. Biology of interleukin-22. *Semin Immunopathol.* (2010) 32:17–31. doi: 10.1007/s00281-009-0188-x
43. Zenewicz LA, Flavell RA. Recent advances in IL-22 biology. *Int Immunol.* (2011) 23:159–63. doi: 10.1093/intimm/dxr001
44. Liu H, Leo C, Chen X, Wong BR, Williams LT, Lin H, et al. The mechanism of shared but distinct CSF-1R signaling by the non-homologous cytokines IL-34 and CSF-1. *Biochim Biophys Acta.* (2012) 1824:938–45. doi: 10.1016/j.bbapap.2012.04.012
45. Harrington LE, Hatton RD, Mangan PR, Turner H, Murphy TL, Murphy KM, et al. Interleukin 17-producing CD4+ effector T cells develop via a lineage distinct from the T helper type 1 and 2 lineages. *Nat Immunol.* (2005) 6:1123–32. doi: 10.1038/ni1254
46. Secombes CJ, Wang T, Bird S. The interleukins of fish. *Dev Comp Immunol.* (2011) 35:1336–45. doi: 10.1016/j.dci.2011.05.001
47. Kumar P, Thakar MS, Ouyang W, Malarkannan S. IL-22 from conventional NK cells is epithelial regenerative and inflammation protective during influenza infection. *Mucosal Immunol.* (2013) 6:69–82. doi: 10.1038/mi.2012.49
48. Nagalakshmi ML, Rascle A, Zurawski S, Menon S, de Waal Malefyt R. Interleukin-22 activates STAT3 and induces IL-10 by colon epithelial cells. *Int Immunopharmacol.* (2004) 4:679–91. doi: 10.1016/j.intimp.2004.01.008
49. Koppang EO, Fischer U, Moore L, Tranulis MA, Dijkstra JM, Köllner B, et al. Salmonid T cells assemble in the thymus, spleen and in novel interbranchial lymphoid tissue. *J Anatomy.* (2010) 217:728–39. doi: 10.1111/j.1469-7580.2010.01305.x
50. Torrecillas S, Caballero MJ, Mompel D, Montero D, Zamorano MJ, Robaina L, et al. Disease resistance and response against *Vibrio anguillarum* intestinal infection in European seabass (*Dicentrarchus labrax*) fed low fish meal and fish oil diets. *Fish Shellf Immunol.* (2017) 67:302–11. doi: 10.1016/j.fsi.2017.06.022
51. Sano T, Huang W, Hall JA, Yang Y, Chen A, Gavzy SJ, et al. An IL-23R/IL-22 circuit regulates epithelial serum amyloid A to promote local effector Th17 responses. *Cell.* (2015) 163:381–93. doi: 10.1016/j.cell.2015.08.061


**Conflict of Interest:** The authors declare that the research was conducted in the absence of any commercial or financial relationships that could be construed as a potential conflict of interest.

frontiers in Immunology

ORIGINAL RESEARCH
published: 26 November 2020
doi: 10.3389/fimmu.2020.607754

# Gut–Liver Immune Response and Gut Microbiota Profiling Reveal the Pathogenic Mechanisms of *Vibrio harveyi* in Pearl Gentian Grouper (*Epinephelus lanceolatus* ♂ × *E. fuscoguttatus* ♀)

*Yiqin Deng*[1,2], *Yaqiu Zhang*[1,3], *Haoxiang Chen*[1,3], *Liwen Xu*[1], *Qian Wang*[1] *and Juan Feng*[1,2]*

[1] Key Laboratory of South China Sea Fishery Resources Exploitation and Utilization, Ministry of Agriculture and Rural Affairs, South China Sea Fisheries Research Institute, Chinese Academy of Fishery Sciences, Guangzhou, China, [2] Tropical Aquaculture Research and Development Centre, South China Sea Fisheries Research Institute, Chinese Academy of Fishery Sciences, Hainan, China, [3] College of Fisheries and Life Science, Shanghai Ocean University, Shanghai, China

OPEN ACCESS

**Edited by:**
Nan Wu,
Institute of Hydrobiology (CAS), China

**Reviewed by:**
Qingpi Yan,
Jimei University, China
Hongyu Liu,
Guangdong Ocean University, China

***Correspondence:**
Juan Feng
juanfeng@scsfri.ac.cn

**Specialty section:**
This article was submitted to Comparative Immunology, a section of the journal Frontiers in Immunology

**Received:** 18 September 2020
**Accepted:** 29 October 2020
**Published:** 26 November 2020

**Citation:**
Deng Y, Zhang Y, Chen H, Xu L, Wang Q and Feng J (2020) Gut–Liver Immune Response and Gut Microbiota Profiling Reveal the Pathogenic Mechanisms of Vibrio harveyi in Pearl Gentian Grouper (Epinephelus lanceolatus ♂ × E. fuscoguttatus ♀). Front. Immunol. 11:607754. doi: 10.3389/fimmu.2020.607754

*Vibrio harveyi* causes vibriosis in nearly 70% of grouper (*Epinephelus* sp.), seriously limiting grouper culture. As well as directly inhibiting pathogens, the gut microbiota plays critical roles in immune homeostasis and provides essential health benefits to its host. However, there is still little information about the variations in the immune response to *V. harveyi* infection and the gut microbiota of grouper. To understand the virulence mechanism of *V. harveyi* in the pearl gentian grouper, we investigated the variations in the pathological changes, immune responses, and gut bacterial communities of pearl gentian grouper after exposure to differently virulent *V. harveyi* strains. Obvious histopathological changes were detected in heart, kidney, and liver. In particular, nodules appeared and huge numbers of *V. harveyi* cells colonized the liver at 12 h postinfection (hpi) with highly virulent *V. harveyi*. Although no *V. harveyi* was detected in the gut, the infection simultaneously induced a gut-liver immune response. In particular, the expression of 8 genes associated with cellular immune processes, including genes encoding inflammatory cytokines and receptors, and pattern recognition proteins, was markedly induced by *V. harveyi* infection, especially with the highly virulent *V. harveyi* strain. *V. harveyi* infection also induced significant changes in gut bacterial community, in which *Vibrio* and *Photobacterium* increased but *Bradyrhizobium*, *Lactobacillus*, *Blautia*, and *Faecalibaculum* decreased in the group infected with the highly virulent strain, with accounting for 82.01% dissimilarity. Correspondingly, four bacterial functions related to bacterial pathogenesis were increased by infection with highly virulent *V. harveyi*, whereas functions involving metabolism and genetic information processing were reduced. These findings indicate that *V. harveyi* colonizes the liver and induces a gut-liver immune response that substantially disrupts the composition of and interspecies interactions in

the bacterial community in fish gut, thereby altering the gut-microbiota-mediated functions and inducing fish death.

**Keywords: *Vibrio harveyi*, pearl gentian grouper, immune response, gut microbiota, interplay, pathogenesis**

## INTRODUCTION

*Vibrio harveyi* is an opportunistic pathogen that causes fatal vibriosis in aquatic vertebrates and invertebrates, leading to significant morbidity and mortality among a diverse range of fish species worldwide (1–3). It is reported that *V. harveyi* causes vibriosis in nearly 70% of grouper (*Epinephelus* sp.), a commercially important fisheries species in China, with a yield of 183,127 tonnnes in 2019 (4). *V. harveyi* usually infects its host *via* the processes of adhesion, invasion, reproduction, and toxin release, ultimately leading to the host's death (5, 6). Although several virulence determinants have been identified in *V. harveyi*, including extracellular products, lipopolysaccharide, bacteriophages, and quorum-sensing factors, empirical evidence of the host-pathogenic process in response to infection is otherwise sparse.

The most frequent clinical signs of *V. harveyi*-infected fish include lethargy, anorexia, erratic swimming, deep dermal lesions, skin ulcer, and eye lesions (7–9). The visceral organs of affected fish become congested and inflamed, particularly the liver, spleen, and kidney, resulting into gastroenteritis, vasculitis, septicemia, etc. (10–12). Fish have many nonspecific and specific immune mechanisms to eliminate pathogens during their attachment, penetration, survival, and spread within the host, thus resisting bacterial diseases (13). The gut-liver immune system has gradually become recognized in mammals, and its dysregulation is associated with many gut and liver diseases (14). The gut-associated lymphoid tissue (GALT) is an important constituent of the mucosal immune system, and constitutes a local immune environment of both defensive and tolerance (15). The liver is a central immunological organ, and is continuously exposed circulating antigens and endotoxins from the gut microbiota (16). Because it is adjacent to the GALT, it contributes to immune surveillance (14). In fish, the gut-liver immunity of tilapias infected with *Streptococcus agalactiae* has been comprehensively investigated by Wu et al. (17), with integrated transcriptomic and proteomic studies. Those data suggest that the fish gut and liver collaborate immunologically, maintaining immunological homeostasis with specific strategies. However, the fish gut-liver immune system remains largely unknown, including in the grouper after *V. harveyi* infection, although both enteritis and liver-and-gallbladder syndrome frequently occur, and have become limitations to grouper aquaculture (18, 19).

More than one billion microorganisms, predominantly bacteria, colonize the gastrointestinal tract and establish a mutualistic relationship with fish (20). However, when the mutualistic relationship between the host and its microbiota is disrupted, the gut microbiota can cause or contribute to disease (21, 22), including vibriosis, furunculosis, enteric septicemia, and aeromoniasis in fish (23, 24). For example, the relative abundances of Proteobacteria, Fusobacteria, Bacteroidetes, and Firmicutes change in *Ctenopharyngodon idellus* after *Aeromonas hydrophila* challenge, leading to the deformation of the intestinal villi, redness and congestion at the injection site, and even the death of the fish (25). In addition to digesting and fermenting carbohydrates and producing vitamins, the gut microbiota plays critical roles in the development of the GALT, the activation of the gut immune responses, and the prevention of colonization by pathogens, thus resisting disease and maintaining the homeostasis of the gut (20, 26). For example, infection with *Salmonella* in mice induces the processing of pro-interleukin 1β (pro-IL1β) (27). The consumption of *Bifidobacterium* in mice increased the number of regulatory T cells, and attenuated the severity of intestinal disease after *Salmonella* infection (28). In turn, the gut immune responses that are induced by commensal populations regulate the composition of the microbiota (29). Therefore, the changes in the gut microbiota caused by *V. harveyi* infection play an important role in fish resistance to *V. harveyi* infection and warrant further study.

In the present study, the pearl gentian grouper (*Epinephelus lanceolatus* ♂ × *E. fuscoguttatus* ♀) was selected as the research object. A histopathological analysis, the expression of immune-related genes, and the structure and function of the intestinal microbial community of the pearl gentian grouper were investigated after infection with a high- or low-virulence strain of *V. harveyi*. This design allowed us: (i) to assess how the interspecies interactions and functions of the gut bacteria were altered during the exacerbation of disease in the grouper; (ii) to screen sensitive gut taxa, e.g., bioindicators that are closely associated with the progression of *V. harveyi* infection; (iii) to evaluate the associations among *V. harveyi* infection, the gut microbiota, and the immune responses of the grouper; and (iv) to provide a scientific basis for immunological or microbe-based therapies for *V. harveyi* disease in the pearl gentian grouper.

## MATERIALS AND METHODS

### Bacterial Strains and Growth Conditions

*V. harveyi* 345:pMMB207 containing the chloramphenicol resistant plasmid pMMB207 (30) was originated from the *V. harveyi* 345 strain which was previously isolated from a diseased pearl gentian grouper by our group (31). The chloramphenicol resistant was used as the selection marker for bacterial pathogen load analysis. *V. harveyi* 345:pMMB207 was shown to have a median lethal dose ($LD_{50}$) of $4.49 \times 10^4$ CFU $g^{-1}$ in pearl gentian (data not published). An *hfq* deletion mutant was constructed with two rounds of allelic exchange (32) (data not published). When a grouper was injected with a 100 μL of culture containing

7.5$LD_{50}$ (a final dosage of $3.37 \times 10^5$ CFU $g^{-1}$) wild-type strain *V. harveyi* 345:pMMB207, the mortality rate was 41.11% at 12 h postinjection (hpi), 83.33% at 24 hpi, 86.70% at 48 hpi, and 86.70% at 108 hpi, whereas when a grouper was injected with the same amount the *hfq*-deletion mutant strain *V. harveyi* 345Δ*hfq*:pMMB207, the cumulative mortality rate was 0.00% at 108 hpi (**Figure S1**). Therefore, we defined these two strains as high-virulence and low-virulence *V. harveyi*, respectively. They were cultured in Luria–Bertani (LB) broth with 2% additional NaCl (LBS) containing 34 μg $mL^{-1}$ chloramphenicol (Cm) at 28°C.

## Fish Infection

The pearl gentian groupers used for the infection assay were purchased from a local aquaculture farm in Shenzhen, China, and had a mean weight of 50 ± 2 g. The groupers were cultured in aerated recycled seawater at room temperature and fed twice daily (8:00 am and 4:00 pm) with No. C5 commercial feed (Guangdong, the group of Marine biological research and development co., LTD). After acclimation for 2 weeks, 135 vigorous fish were randomly divided into three groups (groups A, B, and C; 15 fish per tank in triplicate for each group) and stop feeding before 24 h of injection. The high-virulence (group A) and low-virulence (group B) *V. harveyi* strains were cultured on glass slants overnight and resuspended in 3 mL normal saline. The cells were diluted to an optical density at a wavelength of 600 nm ($OD_{600}$) of 1.85 with normal saline. The fish in groups A and B were injected intraperitoneally (i.p.) with 100 μL of the diluted high-virulence and low-virulence *V. harveyi* cultures (7.5$LD_{50}$ and a final dosage of $3.37 \times 10^5$ CFU $g^{-1}$), respectively, and the control fish (group C) were injected i.p. with 100 μL of normal saline. And there were no feedings after the injection.

## Sampling

For each time point, one fish was randomly selected from each tank and totally three fishes were selected for each group (including group A, group B, and group C) and, sampled and dissected at 12, 24, and 48 hpi. Liver samples (30–50 mg) were collected on ice at 12, 24, and 48 hpi for a pathogen load analysis. The brain, heart, liver, spleen, gills, kidneys, and gut of each fish were fixed in 10% buffered formalin at 12 hpi for histopathological examination. Liver and gut samples (50–100 mg each) were soaked in 1 mL of RNAstore Reagent (Tiangen, Beijing, China) at 12 hpi, before RNA extraction and quantitative PCR. The whole gut contents were collected in sterile tubes at 12 hpi and immediately stored at −80°C before DNA extraction and gut microbiotal analysis.

## Bacterial Pathogen Load Assay

The pathogen load of the liver by the two *V. harveyi* strains was determined based on the study of Whitaker et al. (33), with some modification. The livers were homogenized in 500 μL of normal saline and the homogenized samples were 10-fold serially diluted with normal saline, and coated onto LBS medium containing 34 μg/mL Cm. The plates were incubated at 28 °C overnight. The numbers of bacterial colonies were recorded for the pathogen load analysis.

## Histopathological Analysis

Samples were fixed in 10% buffered formalin for at least 24 h. The tissues were then dehydrated, embedded in paraffin, and cut into sections (4 μm thick) with a rotary microtome RM2135 (Leica, Wetzlar, Germany). The sections were stained with hematoxylin and eosin (HE) with standard techniques for histopathological evaluation. All sections were observed under an optical Leica DFC495microscope (Ernst Leitz, Wetzlar, Germany).

## Total RNA Extraction, cDNA Synthesis, and Gene Expression

All reagents were from Takara (Takara Bio Inc., Shiga, Japan). According to the instructions, total RNA was extracted from the liver and gut with RNAiso Plus. Reverse transcription (RT) was performed with PrimeScript™ RT Reagent Kit with gDNA Eraser. Quantitative PCR was used to analyze gene expression with TB Green™ Premix Ex Taq™ Π (Tli RnaseH Plus). Relative expression was calculated with the $2^{-\Delta\Delta CT}$ method (34), using the gene β-actin as the endogenous control, and was normalized to the values for the gut samples in control group C. The primers used in this study are listed in **Table S1**.

## Gut Microbiotal Composition and Function

The total genomic DNA of the fish gut contents was extracted with the cetyl trimethylammonium bromide (CTAB) method. A 16S rRNA library was generated, sequenced, and analyzed as previously described (35). The functional capacity of each microbiota was predicted from the 16S rRNA gene sequence data with the Tax4Fun software (36). The 16S rRNA sequences were screened against the SILVA database with a BLAST search to obtain the functional annotation information. The functional pathways were annotated with the Kyoto Encyclopedia of Genes and Genomes (KEGG) orthology groups (37) at levels 1, 2, and 3.

## Statistical Analysis

A Bray–Curtis distance matrix was constructed for the bacterial community and function analyses with preliminary one-way permutational multivariate analysis of variance (PERMANOVA) and a principal co-ordinates analysis (PCoA). PERMANOVA was used to examine the diversity of the bacterial communities and functions in the different groups ($p < 0.05$ was considered statistically significant). PCoA was used to investigate the succession of microbiotal assemblages through the different groups. A SIMPER analysis was used to identify the bacterial taxa driving the differences among the different groups. One-way ANOVA was used to examine the variations in gene expression and α-diversity. A *t* test was used to examine the variations in pathogen load and bacterial functions. Pearson's correlation analysis was performed to determine the relationships among and within the gut bacterial communities, the predicted functions, and the expression levels of immunity-related genes. All statistical analyses were performed with PRIMER v6 and PERMANOVA+ (38) or IBM SPSS Statistics 19.0 (39). The pathogen load, expression levels of immune-related genes, and the relative abundances of phyla, genera, and bacterial function were shown as means ± SEM.

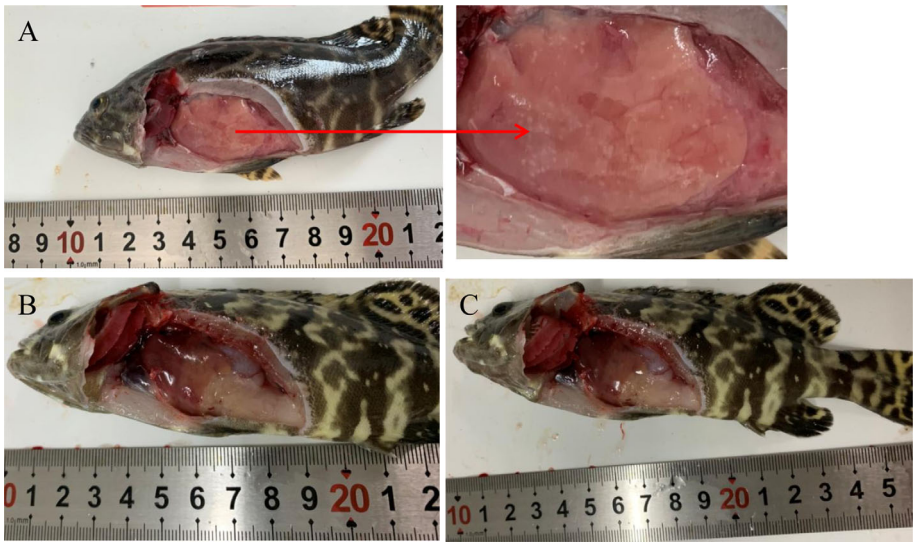


**FIGURE 1** | Pathological features of fish infected with high-virulence *V. harveyi* strain **(A)**, low-virulence *V. harveyi* strain **(B)**, or treated with normal saline **(C)**.

# RESULTS

## Comparative Pathogen Load and Histopathology of Groupers Infected With High- or Low-Virulence *V. harveyi* Strains

Nodules appeared in the liver at 12 hpi after injection with high-virulence *V. harveyi* (**Figure 1A**) but not with low-virulence *V. harveyi* or normal saline (**Figures 1B–C**). A pathogen load analysis indicated that the average bacterial pathogen load of the liver by high-virulence *V. harveyi* was 3.77- and 1.67-fold higher than that by low-virulence *V. harveyi* at 12 hpi and 24 hpi, respectively. Pathogen load with both *V. harveyi* strains increased at first and then decreased, reaching the highest value at 24 hpi. No *V. harveyi* was detected in the normal-saline-treated control group (**Figure 2**).

No obvious histopathological changes was seen in the brain, spleen, gill, or gut at 12 hpi (**Figures S2A–C, G–I, J–L** and **Figures 3G–I**). The hearts of the *V. harveyi*-infected fish had moderate bacterial myocarditis and little parenchymal infiltration by inflammatory cells (**Figures S2D, E**). The kidneys of the *V. harveyi*-infected fish showed hemorrhage in the renal interstitial tissues, associated with the dissolution of the tubules (**Figures S2M, N**). The most serious histopathological changes were seen in the liver. Vacuolar degeneration and karyorrhectic debris were present in the livers of the group A fish, accompanied by the dissolution of the pancreatic epithelial cells (**Figures 3A–C**). Venous blood vessel loss and connective tissue necrosis were present in the livers of the group B fish (**Figures 3D, E**). No histopathological changes were detected in the heart, kidney, or liver in the control group (**Figures S2F, O** and **Figure 3F**), and the histopathological damage was more serious in group A than in group B (**Figures S2** and **S3**).

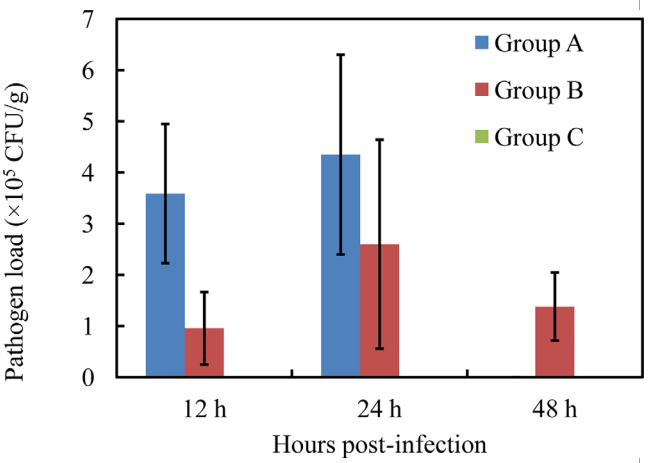


**FIGURE 2** | Liver pathogen load by high-virulence *V. harveyi* strain (Group A), low-virulence *V. harveyi* strain (Group B), and in normal-saline-treated fish (Group C). Values are means ± SEM (n = 3).

## Gut–Liver Immune Responses of Grouper to High-Virulence and Low-Virulence *V. harveyi* Strains

In the study of Wu et al. (17), 27 immune-related genes associated with nine different immune processes (**Table S1**) were selected to analyze the gut-liver immune response of the pearl gentian grouper to differently virulent *V. harveyi* strains. Gut advantage transcripts (the expression levels of gut and liver in control group were compared and the average expression altered more than 8-folds between these two control groups) encoded caspase (**Figure 4E**), the C-C motif receptor (CCR)

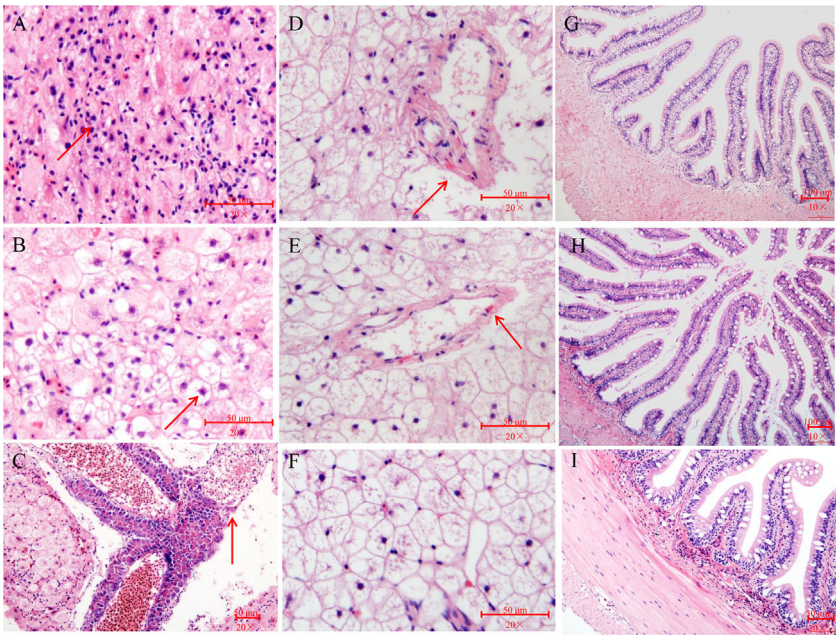


**FIGURE 3** | Histopathological changes in liver and gut of pearl gentian grouper after infection with *V. harveyi*. **(A–C)** Liver after infection with high-virulence *V. harveyi*. **(D** and **E)** Liver after infection with low-virulence *V. harveyi*. **(F)** Liver in fish treated with normal saline. **(G)** Gut after infection with high-virulence *V. harveyi*. **(H)** Gut after infection with low-virulence *V. harveyi*. **(I)** Gut in fish treated with normal saline. Arrows point to lesions.

(**Figure S3H**), C-reactive protein (CRR) (**Figure S3O**), and neuronal cell adhesion molecule (NCAM) (**Figure S3P**), whereas the liver advantage transcripts encoded C1q (**Figure 4A**), transferrin (**Figure 4F**), toll-like receptor (TLR) (Figure GL), and Kruppel-like factor (**Figure S3L**).

Although the expression of most genes were not significantly altered, the average expression of most genes varied strongly after injection with the *V. harveyi* strains (**Figure 4**). The gene encoding C1q (**Figure 4A**), which is involved in the immune process in the complement system, three genes encoding interferon (IFN)-induced proteins (**Figures 4B–D**), belonging to the immune process of inflammatory cytokines and receptors, two genes encoding caspase or transferrin and receptor (**Figures 4E, F**) and belonging to the immune process of other genes related to immune cell response, three genes encoding TLR, lectin, and nucleotide oligomerization domain (NOD) (**Figures 4G–I**), and belonging to the immune process of pattern recognition genes, one gene encoding ferritin (**Figure 4J**) and belonging to the immune process of acute phase reactions, and one gene encoding neutrophil cytosolic factor (NCF) (**Figure 4K**) belonging to the immune process of innate immune cells related, were upregulated in the gut and liver after injection with the high- or low-virulence *V. harveyi* strain. The expression of most of these genes tended to be higher after injection with the high-virulence *V. harveyi* strain than with the low-virulence *V. harveyi* strain.

## Distribution of Taxa in the Fish Gut

After splicing, quality control, and chimera filtration, a total of 576,940 effective reads were obtained, with an average of 64,104 ± 2,637 reads per sample (mean ± standard deviation) (**Table S2**). The unequal sequencing depths were rarified to 46,764 sequences per sample, resulting in 2,995 operational taxonomic units (OTUs) across all samples. The OTUs were aligned and annotated as 32 known phyla, 52 classes, 122 orders, 233 families, 586 genera, and 329 species. The 10 most abundant phyla were (in decreasing order) Proteobacteria, Firmicutes, Bacteroidetes, Actinobacteria, Acidobacteria, Verrucomicrobia, Gemmatimonadetes, unidentified_Bacteria, Chloroflexi, and Cyanobacteria, which accounted for 64.06, 22.04, 4.65, 3.34, 1.47, 0.98, 0.78, 0.78, 0.57, and 0.17% of the total microbial community, respectively, and together for 94.55–99.95% of the total bacteria (**Figure 5A**). At the genus level, the most abundant phylotypes were affiliated with *Vibrio*, *Photobacterium*, *Lactobacillus*, *Bradyrhizobium*, *Faecalibaculum*, *Blautia*, *Sphingomonas*, *Acidiphilium*, *Dubosiella*, and *Romboutsia*, belonging to Proteobacteria or Firmicutes, which accounted for 48.46, 5.07, 2.80, 2.52, 1.97, 1.89, 1.24, 1.06, 0.95, and 0.30% of the total microbial community, respectively, and together for 28.49–98.00% of the total bacteria (**Figure 5B**).

## Variations in Bacterial Diversity and Compositions Induced by *V. harveyi* Infection

The α-diversity of the bacterial communities tended to decrease in the order: group B > group C > group A (**Table S2**). PERMANOVA showed that the community compositions differed marginally significantly among the three groups (Pseudo-F = 1.4945, *P*-perm = 0.062). Furthermore, the

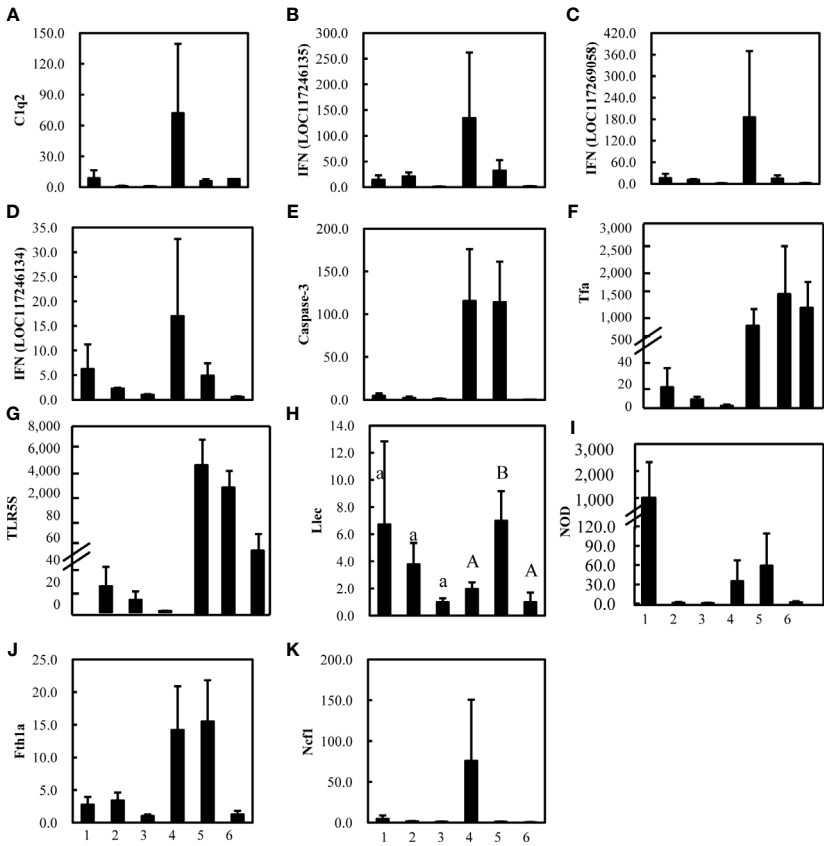


**FIGURE 4** | Expression levels of 11 **(A–K)** strongly altered immune-related genes in gut (1, 2, and 3) and liver (4, 5, and 6) of pearl gentian grouper after infection with high-virulence *V. harveyi* (1, 4), low-virulence *V. harveyi* (2, 5), or in fish treated with normal saline (3, 6). Expression was normalized to the expression in the gut of pearl gentian grouper treated with normal saline (3) and the ordinate is the normalized expression ratio. Except **Figure 4H** (Llec), no significantly differences were detected in other genes. Lowercase letters represent the results of one-way ANOVA of genes expression in gut (1, 2, and 3), and capital represent the results of one-way ANOVA of genes expression in liver (4, 5, and 6). Different letters **(A**, **B)** represent significant difference, and the same letters **(A)** represent no significant difference.

community dissimilarity of low-virulence-affected group B differed marginally significantly from that of the high-virulence-affected group A (Pseudo-F = 3.2601, P-perm = 0.099), although it was similar to that of the normal-saline-treated control group C (Pseudo-F = 0.9559, P-perm = 0.625). Axis 1 (PCO1) in the PCoA analysis separated high-virulence group A from low-virulence group B and control group C (identified as group B/C) (**Figure 6**). The first two axes (PCO1 and PCO2) explained 35.5% and 18.5% of the variation in composition, respectively (**Figure 6**).

Based on the PCoA results, a SIMPER analysis of the 10 most abundant genera was performed to compare group A and group B/C. The results indicated that *Vibrio*, *Photobacterium*, *Lactobacillus*, *Blautia*, *Bradyrhizobium*, and *Faecalibaculum* accounted for more than 80% (up to 82.01%) of the dissimilarity between the two groups (**Table 1**). The abundances of *Vibrio* and *Photobacterium* were 4.41- and 11.85-fold higher in high-virulence group A than in group B/C, respectively, whereas the abundances of *Bradyrhizobium*, *Lactobacillus*, *Blautia*, and *Faecalibaculum* were 11.56–144-fold lower in group A than in group B/C (**Table 1**).

## Functional Predictions and Differences Induced by *V. harveyi* Infection

In total, 387 KEGG pathways were predicted from the 16S rRNA OTU data with Tax4Fun. The 10 most abundant KEGG pathways at level 3 indicated that the gut microbiota was enriched with pathways associated with transporters, two component system, DNA repair and recombination proteins, transfer RNA biogenesis, purine metabolism, ABC transporters, pyrimidine metabolism, amino-acid-related enzymes, quorum sensing, and peptidases, belonging to the categories *environmental information processing*, *genetic information processing*, *metabolism*, and *cellular processes* (**Figure 7A**). Pearson's correlation analysis identified a significant positive association between community composition and function ($r$ = 0.611, $P$ = 0.001; **Figure 7B**).

A $t$ test indicated that 13 functions at KEGG level 3 with relative abundances of more than 1% differed significantly between group A and group B/C. In particular, seven of these functions were induced in high-virulence group A: biofilm formation-*Vibrio cholerae*, quorum sensing, bacterial secretion system, secretion system, nicotinate and nicotinamide

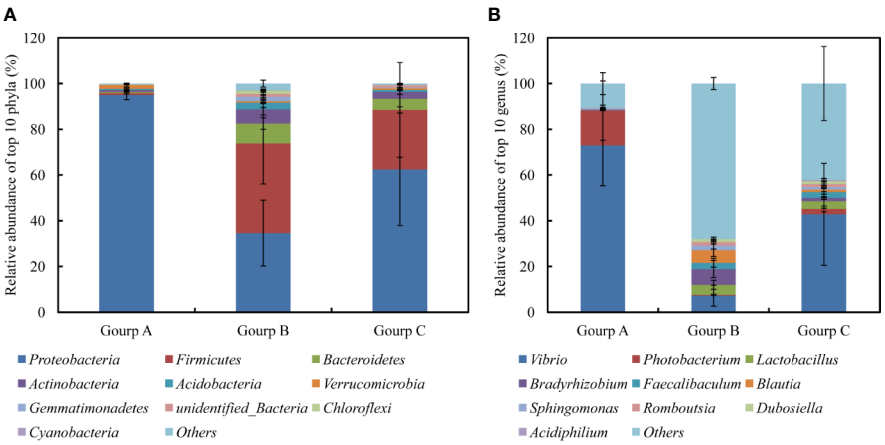


**FIGURE 5** | Relative abundances of 10 most abundant phyla **(A)** and genera **(B)**, averaged over each group. Values are means ± SEM (n = 3).

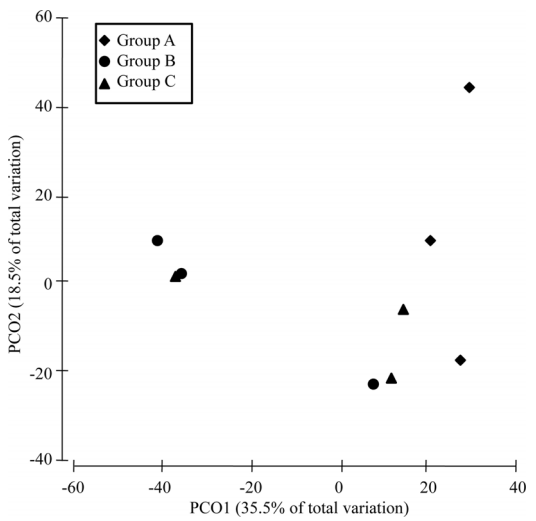


**FIGURE 6** | PCoA analysis of the dissimilarity (Bray–Curtis distances) in the intestinal bacterial community compositions of pearl gentian grouper after *V. harveyi* infection.

metabolism, ubiquinone and other terpenoid-quinone biosyntheses, and membrane and intracellular structural molecules. The other six pathways were reduced in high-virulence group A: base excision repair, nucleotide excision repair, ribosome, translation factors, streptomycin biosynthesis, and terpenoid backbone biosynthesis (**Figure 8**).

## Interactions Within and Among Gut Bacterial Communities, Predicted Functions in the Gut, and the Expression of Immune-Related Genes

Pearson's correlation coefficients indicated complex interrelationships within and among gut bacterial communities, the predicted functions in the gut, and the expression of immune-related genes (**Table S3**). There were strong negative relationships between *Vibrio* and *Lactobacillus* (r = −0.751, $P$ = 0.02), *Blautia* (r = −0.667, $P$ = 0.05), or *Faecalibaculum* (r = −0.668, $P$ = 0.049), and a positive relationship between *Lactobacillus* and *Faecalibaculum* (r = 0.984, $P$ = 0.000). Four of the six indicator taxa (*Vibrio, Lactobacillus*, *Blautia*, and *Faecalibaculum*) were closely associated with the 13 significantly changed functions There tended to be positive correlations between increased taxa and induced functions and between reduced taxa and reduced functions, but negative correlations between increased taxa and reduced functions and between reduced taxa and induced functions (**Table S3**).

The abundance of *Photobacterium* was significantly positively associated with the expression levels of two IFN-induced proteins (r = 0.891 and 0.975, $P$ = 0.001 and 0.001, respectively) and one caspases (r = 0.860, $P$ = 0.003, respectively). Furthermore, strong associations were comprehensive detected between different predicted functions and between various immune-related genes (**Table S3**).

# DISCUSSION

The pathogenic processes of *Vibrio* include its adhesion, infection, colonization, reproduction, and toxin release, by which it damages the cells and tissues of its hosts, interrupting and destroying the normal metabolism and functions of those hosts (5, 6). After *V. harveyi* challenge, the pathological features, bacterial pathogen load data, and histopathological analyses all indicated that *V. harveyi* colonized the grouper liver, inducing serious pathological changes, including vacuolar degeneration, the accumulation of karyorrhectic debris, pancreatic epithelial cell dissolution, venous blood vessel loss, and connective tissue necrosis. The liver is a central organ of the immune system (17). Several hundred thousand pathogens have been detected in the

**TABLE 1** | Dissimilarities in the total bacterial communities between group A and group B/C determined with a genera-level SIMPER analysis (data are square root transformed).

| Genera | Average abundance of group A | Average abundance of group B/C | Average Dissimilarity | Dissimilarity/Standard Deviation | Contribution (%) | Cumulative contribution (%) |
|---|---|---|---|---|---|---|
| *Vibrio* | 0.40 | 0.84 | 17.40 | 1.58 | 32.40 | 32.40 |
| *Photobacterium* | 0.09 | 0.31 | 8.35 | 1.06 | 15.54 | 47.94 |
| *Lactobacillus* | 0.17 | 0.02 | 5.29 | 1.37 | 9.86 | 57.80 |
| *Blautia* | 0.14 | 0.02 | 4.43 | 1.08 | 8.25 | 66.05 |
| *Bradyrhizobium* | 0.17 | 0.05 | 4.39 | 1.05 | 8.17 | 74.22 |
| *Faecalibaculum* | 0.12 | 0.01 | 4.18 | 1.05 | 7.79 | 82.01 |

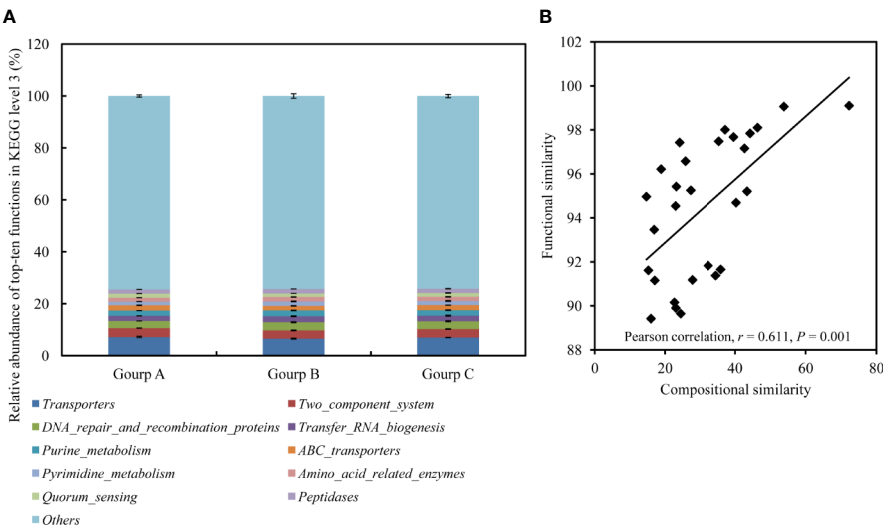


**FIGURE 7** | Relative abundances of 10 most abundant functions at KEGG level 3, averaged over each group **(A)**, and the correlations between compositional similarities and functional similarities **(B)**. Values are means ± SEM (n = 3).

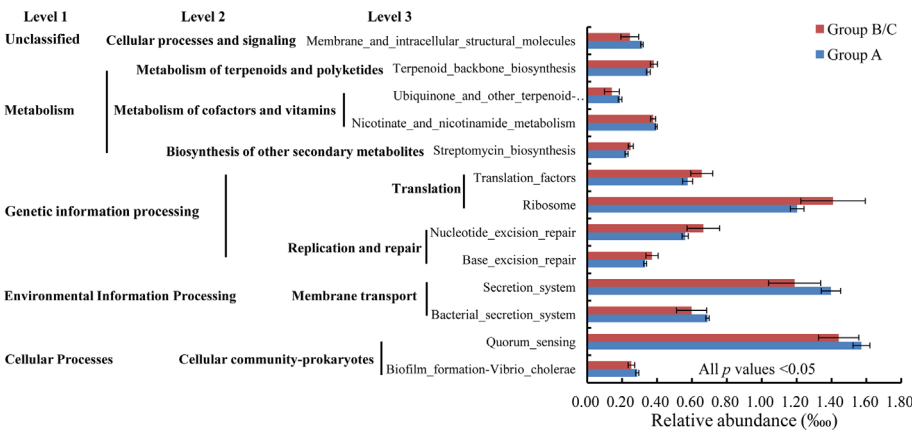


**FIGURE 8** | Relative abundances of bacterial functions with relative abundances > 1‰ that differed significantly between group A and group B/C.

liver, which suggests that *V. harveyi* may be easily adapt to the liver environment and proliferate (40). The number of high-virulence *V. harveyi* in the liver was much more than that of low-virulence *V. harveyi*, which may be related to the levels of the strains pathogenicity. Compared to the 12 hpi, the increase in the number of pathogens at 24 hpi might be due to the pathogen proliferating in the host, while the decrease in the number of pathogens at 48 hpi might be due to the host immune system

attacking the pathogen (40). In addition, no wild-type strain was detected in the liver at 48 hpi probably attribute to the stronger host immune response by injecting high-virulence *V. harveyi*. Here, the colonization of the liver by *V. harveyi* caused an immune response in the liver. In particular, the expression of immune-related genes was altered, including those encoding inflammatory cytokines and receptors (such as IFN-induced proteins), pattern recognition receptors (such as TLR and NOD), and other proteins related to immune cell response (caspase, transferrin, and the transferrin receptor), which are involved in inflammation, iron utilization, pathogen recognition and elimination, *etc.* The immune response caused by the high-virulence strain was stronger than that caused by the low-virulence strain. This is consistent with previous studies (41). IFNs are secreted by host cells, including macrophages, lymphocytes, natural killer cells and fibroblasts, in response to recognition of viral double-stranded RNA intermediates and relating to inflammation (42). Caspases are thought to play a pivotal role in biological phenomena such as cell death and inflammation (43). Transferrin and ferrin are responsible for iron acquisition, transport, and storage and important in the pathogenesis of disease (44). Pattern recognition receptors (TLRs, lectin, and NOD) play essential role in the recognization of specific patterns of microbial components, resulting in antigen elimination and activation of nonspecific inflammatory innate immunity of inflammation (29, 45). Therefore, *V. harveyi* infection attacked the central immune organ, the liver, probably causing an inflammatory response, iron limitation, and cellular apoptosis, resulting in pathological damage to the host and inducing an immune response.

The gut-liver immune system has been well studied in mammals and is gaining tremendous global attention in fish (17). The liver and gut are considered mutually responsive. A damaged gut can expose the liver directly to intestinal endotoxins, and the destruction of the normal liver physiology can cause intestinal dysfunction (46). The fish gut and liver may collaborate immunologically to maintain their homeostasis using strategies specific to both tissues. In this study, although there was no significant change in the intestinal pathology, the immune response in the gut was similar to that in the liver and was markedly induced by *V. harveyi* infection. The intestinal pathology changes during pathogen infection including intestinal mucosal necrosis, atrophy and abscission of intestinal villi, severe edema, congestion and inflammatory cells infiltration, which intuitively indicate the intestinal health (47, 48). For example, tilapia infected with different pathogenic *Streptococcus agalactiae* strains showed different pathology (47). At 3 day postinjection (dpi) infected with low pathogenic *S. agalactiae*, lamina propria were edema, while showed no histopathological changes at 7dpi and 14 dpi. In addition, at 3 dpi infected with high pathogenic *S. agalactiae*, lamina propria showed edema and congestion, and showed severe edema, congestion and inflammatory cells infiltration in lamina propria at 7 and 14 dpi (47). Therefore, the changes of intestinal pathology are related to bacterial virulence, infection time and even infection dosage. In this study, no obvious lesions happened in the intestinal probably attribute to insufficient infection time. However, the GALT, which is connected to the liver by bile and blood, forms a local immune environment for the purposes of both defense and tolerance, so the intestinal immune response is probably mediated by the gut-liver axis (17). The gut microbiota also plays critical roles in epithelial renewal and maturation, which in turn regulate immunological homeostasis, providing essential health benefits to its host. Compared with germ-free zebrafish, zebrafish which is conventionally raised exhibit a greater abundance of genes associated with epithelial proliferation and innate immune response (49). With a commensal microbiota, the germ-free zebrafish can robustly activate NF-kB and its target genes in intestinal and extra-intestinal tissues (50). Additionally, colonization of commensals in larvae stimulates neutrophils and activates pro-inflammatory genes through the TLR/MyD88 signaling pathway and phagocytes, thus enhance disease resistance in zebrafish (51). Additionally, the colonization of probiotics also active innate immune responses and protect fish against pathogens (52). Irianto & Austin (53) demonstrated that the humoral and cellular immunity was stimulated as the lysozyme activity and the number of erythrocytes, macrophages and lymphocytes were increased, after feeding rainbow trout with probiotics containing *Aeromonas hydrophila*, *Vibrio fluvialis*, *Carnobacterium* sp. and *Micrococcus luteus* for 2 weeks. However, pathogens infection is likely to cause intestinal immune stimulation and change intestinal microflora. For example, proinflammatory cytokines IL1β and tumor necrosis factor α (TNF-α), belonging to inflammatory cytokines and receptors, were activated in response to *V. anguillarum* infection in ayu (*Plecoglossus altivelis*), and the relative abundances of 16 taxa in the gut, including Clostridiales, changed consistently during infection (54). Therefore, the changes in the expression of immune-related genes in this study should induce changes in a variety of gut microbiota.

16S rRNA sequencing suggested that the gut microbial α-diversity was lower after infection with high-virulence *V. harveyi* than in the control group and after infection with low-virulence *V. harveyi*. Previous studies have shown that high gut microbial diversity is positively related to host health (55–57) and that the diversity of the gut bacteria decreases significantly during disease progression (58). A PCoA ordination biplot of the 16S rRNA data corroborated the notion that virulent *V. harveyi* infection modulated the total bacterial population of the gut microbiota in the pearl gentian grouper. Similar observations have also been reported for the gut bacteria of the zebrafish, insofar as the taxonomic annotations of the diseased zebrafish clustered together, whereas those of the healthy zebrafish were scattered (59). These findings imply that *V. harveyi* infection drives the gut bacterial community into a kind of diseased state, accompanied by reduced bacterial α-diversity. Highly virulent *V. harveyi* promoted the dysbiosis of the intestinal microorganisms and grouper disease, whereas the gut microbiota of the groupers infected with weakly virulent *V. harveyi* recovered to the state observed in the saline-treated normal control group. Commensal bacteria produce a series of enzymes to digest feed, and nutrients are absorbed into the blood vessels and lymphatic vessels

through the intestinal wall and then sent to all the body. In addition, commensals can protect the host by depriving invading pathogens of nutrients, secreting a range of antimicrobial substances and occupying the niche (60, 61). At the species level, no *V. harveyi* was detected in the gut microbiota, confirming that the intestinal immune response was probably caused by the gut-liver axis thus change the gut microbiota.

Our SIMPER analysis indicated that the six most abundant genera were the six most significantly different genera, accounting for more than 80.00% dissimilarity between the two groups defined by their significantly different mortalities (high-mortality group A and low-mortality group B/C). Highly virulent *V. harveyi* infection significantly increased the abundances of predominantly *Vibrio* and *Photobacterium*, whereas the abundances of *Lactobacillus*, *Blautia*, *Bradyrhizobium*, and *Faecalibaculum* decreased significantly. *Vibrio* and *Photobacterium* are well-known opportunistic pathogens associated with various diseases of marine animals, including vibriosis (62) and pasteurellosis (63). An overabundance of *Vibrio* spp. in the gut is reported to parallel disease progression in shrimp and crab (57, 64). *Photobacterium* species are pathogenic in a variety of marine animals, including fish, crustaceans, mollusks, and cetaceans (65, 66). *Lactobacillus*, *Blautia*, *Bradyrhizobium*, and *Faecalibaculum* are all well-known probiotics. *Lactobacillus* species are commensal inhabitants of the gastrointestinal tracts of animals and humans, with anti-pathogenic-bacteria properties and are used for the maintenance of healthy intestinal microflora (67, 68). *Blautia* is known to live in the gut and helps to assimilate nutrients (69). *Blautia hydrogenotrophica* contributes to the breakdown of indigestible components of the host's diet, predominantly plant materials such as terpenoids and polyketides (8). *Bradyrhizobium* and *Faecalibaculum* are important in nitrogen utilization by the host (70, 71), and in the prevention and treatment of metabolic syndrome, bowel disorders, and certain types of cancer (72–75). Highly virulent *V. harveyi* infection induced changes in these six taxa, indicating an increasing risk of disease in the host. Notably, a strong negative relationship was detected between *Vibrio* and *Lactobacillus*, *Blautia*, or *Faecalibaculum*, and a positive relationship was detected between *Lactobacillus* and *Faecalibaculum*. The abundance of *Photobacterium* was also significantly positively associated with the expression of IFN-induced proteins and caspase. Therefore, gut immunity was induced by the gut-liver axis, causing an imbalance in the interspecies interactions of the gut microbiota. The increase in potential pathogens and the reductions in probiotic bacteria could increase the competition for nutrients and niches in the gut, contributing to the occurrence and progression of disease. Changes in the relative abundances of these indicator bacteria could also be used to predict an increased risk of *V. harveyi* infection in the pearl gentian grouper. According to our preliminary results, the oral administration of live *Lactobacillus* cells in the groupers' diet for 5 days before their injection with the highly virulent *V. harveyi* strain reduced fish mortality after infection by 10% (**Figure S4**).

The physiological functions of the microbial community were also predicted, to further clarify the damage to the gut microbiota after *V. harveyi* infection. A significant positive correlation between bacterial compositional similarity and functional similarity was observed, indicating relatively low redundancy in the bacterial functions (76). In particular, the KEGG orthology groups induced in the high-mortality group, including biofilm formation–*Vibrio cholerae*, quorum sensing, bacterial secretion system, and secretion system, are related to bacterial pathogenesis (77, 78), and this finding was probably attributable to the increased amounts of pathogens present. The reduced metabolism and genetic information processing pathways could weaken the utilization of nutrients and cell functions, thus compromising fish survival and growth. Overall, both the dysbiosis of the intestinal bacterial communities and the disruption of their functions in the pearl gentian grouper caused by the immune changes that occurred during *V. harveyi* infection disturbed the physiological functions of the fish and exacerbated their disease.

In conclusion, this study demonstrated that *V. harveyi* infection induces pathological changes in the pearl gentian grouper. Although no *V. harveyi* was detected in the gut, the gut-liver axis caused parallel immune responses in the liver and gut. This in turn substantially disrupted the composition and functions of the gut bacterial community in the grouper, affecting its survival. Six infection-sensitive gut taxa are potential indicators of *V. harveyi* infection. These findings significantly improve our understanding of the interplay between the gut microbiota and the host immune responses from a microbial ecological perspective, while clarifying the virulence mechanism of *V. harveyi* in the pearl gentian grouper from the perspective of the host's response. In future work, we will focus on the following two aims: (i) to validate the ecological patterns in a natural infection process that simulates the complex "wild" ecosystem; and (ii) to identify the functions of the four probiotic taxa that were reduced in the group infected with highly virulent *V. harveyi* to establish microbe-based therapies for *V. harveyi* disease in the pearl gentian grouper.

## DATA AVAILABILITY STATEMENT

The datasets presented in this study can be found in online repositories. The names of the repository/repositories and accession number(s) can be found in the article/ **Supplementary Material**.

## ETHICS STATEMENT

The animal study was reviewed and approved by the Animal Care and Use Committee of the South China Sea Fisheries Research Institute, Chinese Academy of Fishery Sciences, Guangzhou, China.

## AUTHOR CONTRIBUTIONS

YD conceived the study, analyzed the data, and wrote the manuscript. YZ, HC, and QW performed the experiments. LX

critically revised the manuscript. JF contributed the reagents. All authors contributed to the article and approved the submitted version. All authors contributed to the article and approved the submitted version

## FUNDING

This work was supported by the National Natural Science Foundation of China (NSFC) (31902415), the Natural Science Fund of Guangdong (2018A030310695, 2019A1515011833), Hainan Provincial Natural Science Foundation of China (319QN336), the Central Public-interest Scientific Institution Basal Research Fund, South China Sea Fisheries Research Institute, CAFS (2019TS04), and the Central Public-interest Scientific Institution Basal Research Fund, CAFS (2019ZD0707).

## ACKNOWLEDGMENTS

We would like to thank International Science Editing (http://www.internationalscienceediting.com) for editing this manuscript.

## REFERENCES

1. Austin B, Zhang XH. *Vibrio harveyi*: a significant pathogen of marine vertebrates and invertebrates. *Lett Appl Microbiol* (2010) 43(2):119–24. doi: 10.1111/j.1472-765X.2006.01989.x
2. Won KM, Park SI. Pathogenicity of *Vibrio harveyi to* cultured marine fishes in Korea. *Aquaculture* (2008) 285(1-4):8–13. doi: 10.1016/j.aquaculture.2008.08.013
3. Lee KK, Liu PC, Chuang WH. Pathogenesis of gastroenteritis caused by *Vibrio carchariae* in cultured marine fish. *Mar Biotechnol* (2002) 4(3):267–77. doi: 10.1007/s10126-002-0018-9
4. Yu XJ, Xu L, Wu FX, Song DD, Gao HQ, Yu HS, et al. *Yearbook C.F.S.* Beijing: China Agriculture Press (2020).
5. Janda JM. Current perspectives on the epidemiology and pathogenesis of clinically significant *Vibrio* spp. *Khirurgiia* (1988) 1(11):114–8. doi: 10.1128/CMR.1.3.245
6. Mok KC. Vibrio harveyi quorum sensing: a coincidence detector for two autoinducers controls gene expression. *EMBO J* (2014) 22(4):870–81. doi: 10.1093/emboj/cdg085
7. Kraxberger-Beatty T, McGarey DJ, Grier HJ, Lim DV. *Vibrio harveyi*, an opportunistic pathogen of common snook, Centropomus undecimalis (Block), held in captivity. *J Fish Dis* (1990) 13:557–60. doi: 10.1111/j.1365-2761.1990.tb00819.x
8. Mohamad N, Mohammad Noor Amal Azmai Amal MNA, Yasin ISM, Zamri-Saad M, Sawabe T. Vibriosis in cultured marine fishes: a review. *Aquaculture* (2019) 512(2019):734289. doi: 10.1016/j.aquaculture.2019.734289
9. Alvarez, Austin B, Reyes. *Vibrio harveyi*: a pathogen of penaeid shrimps and fish in venezuela. *J Fish Dis* (2010) 21(4):313–6. doi: 10.1046/j.1365-2761.1998.00101.x
10. Colwell RR, Grimes DJ. Vibrio diseases of marine fish populations. *Helgolnder Meeresuntersuchungen* (1984) 37(1–4):265–87. doi: 10.1007/BF01989311
11. Grimes DJ, Colwell RR, Stemmler J, Hada H, Stoskopf M. Vibrio species as agents of elasmobranch disease. *Helgoland Marine Res* (1984) 37(1):309–15. doi: 10.1007/BF01989313
12. Zhang XH, He X, Austin B. *Vibrio harveyi*: a serious pathogen of fish and invertebrates in mariculture. *Mar Life Sci Tech* (2020) 2:231–45. doi: 10.1007/s42995-020-00037-z
13. Corbel MJ. The immune response in fish: a review. *J Fish Biol* (2006) 7(4):539–63. doi: 10.1111/j.1095-8649.1975.tb04630.x
14. Palak JT, David HA. Gut-liver immunity. *J Hepatol* (2016) 64(5):1187–9. doi: 10.1016/j.jhep.2015.12.002
15. Hakansson A, Molin G. Gut microbiota and inflammation. *Nutrients* (2011) 3 (6):637–82. doi: 10.3390/nu3060637
16. Heymann F, Tacke F. Immunology in the liver-from homeostasis to disease. *Nat Rev Gastro Hepat* (2016) 13:88–110. doi: 10.1038/nrgastro.2015.200
17. Wu N, Song YL, Wang B, Zhang XY, Jie X, Li Y, et al. Fish gut-liver immunity during homeostasis or inflammation revealed by integrative transcriptome and proteome studies. *Sci Rep* (2016) 6:36048. doi: 10.1038/srep36048
18. Cui LF, Yu XJ, Chen JY, Li Q, Zeng H, Yu WZ, et al. *2020 analysis of major aquatic animal diseases in China*. Beijing: China Agricultural Press (2020). (in Chinese).
19. Zhang W, Tan BP, Ye GL, Wang JX, Zhang HT. Identification of potential biomarkers for soybean meal-induced enteritis in juvenile pearl gentian grouper, *Epinephelus lanceolatus*♂ × *Epinephelus fuscoguttatus*♀. *Aquaculture* (2019) 512:734337. doi: 10.1016/j.aquaculture.2019.734337
20. Wu HJ, Wu E. The role of gut microbiota in immune homeostasis and autoimmunity. *Gut Microbes* (2012) 3(1):4–14. doi: 10.4161/gmic.19320
21. Xiong JB, Nie L, Chen J. Current understanding on the roles of gut microbiota in fish disease and immunity. *Zool Res* (2018) 40(1):1–7. doi: 10.24272/j.issn.2095-8137.2018.069
22. Ransom DP, Lannan CN, Rohovec JS, Fryer JL. Comparison of histopathology caused by *Vibrio anguillarum* and *Vibrio ordalii* in three species of Pacific salmon. *J Fish Dis* (1984) 7(2):107–15. doi: 10.1111/j.1365-2761.1984.tb00913.x
23. Chen Q, Yan Q, Wang K, Zhuang Z, Wang X. Portal of entry for pathogenic *Vibrio alginolyticus* into *Pseudosciaene crocea* and characteristic of bacterial adhesion to the mucus. *Dis Aquat Organ* (2008) 80(3):181–8. doi: 10.3354/dao01933
24. Shoemaker CA, Klesius PH. Protective immunity against enteric septicaemia in channel catfish, ictalurus punctatus (Rafinesque), following controlled exposure to *Edwardsiella ictaluri*. *J Fish Dis* (2010) 20(5):361–8. doi: 10.1046/j.1365-2761.1997.00310.x
25. Zheng WD, Cao HP, Yang XL. Grass carp (*Ctenopharyngodon idellus*) infected with multiple strains of *Aeromonas hydrophila*. *Afr J Microbiol Res* (2012) 6(21):4512–20. doi: 10.5897/AJMR11.1405

## SUPPLEMENTARY MATERIAL

The Supplementary Material for this article can be found online at: https://www.frontiersin.org/articles/10.3389/fimmu.2020.607754/full#supplementary-material

**SUPPLEMENTARY FIGURE 1 |** Cumulative mortality of pearl gentian grouper after intraperitoneal injection of *V. harveyi* 345:pMMB207 (Group A), *V. harveyi* 345Δ*hfq*:pMMB207 (Group B), and normal saline (Group C).

**SUPPLEMENTARY FIGURE 2 |** Histopathological changes in different organs of the pearl gentian grouper after infection with *V. harveyi*. Brain **(A)**, heart **(D)**, spleen **(G)**, gill **(J)**, and kidney **(M)** after infection with high-virulence *V. harveyi*. Brain **(B)**, heart **(E)**, spleen **(H)**, gill **(K)**, and kidney **(N)** after infection with low-virulence *V. harveyi*. Brain **(C)**, heart **(F)**, spleen **(I)**, gill **(L)**, and kidney **(O)** after treatment with normal saline. Arrows point to lesions.

**SUPPLEMENTARY FIGURE 3 |** Expression levels of another 16 (A–P) immune genes in the gut (1, 2, and 3) and liver (4, 5, 6) of the pearl gentian grouper after infection with high-virulence *V. harveyi* (1, 4), low-virulence *V. harveyi* (2, 5), or treatment with normal saline (3, 6). Expression was normalized to the expression in the grouper gut after treatment with normal saline (3) and the ordinate is the normalized expression ratio. One-way ANOVA indicated that no significantly differences were detected in the expression of genes.

**SUPPLEMENTARY FIGURE 4 |** Cumulative mortality of pearl gentian grouper after intraperitoneal injection of *V. harveyi*. 'With/without *Lactobacillus*' means that the fish were or were not administered live *Lactobacillus* cells orally in their diet for 5 days before injection.

26. Okubo H, Nakatsu Y, Sakoda H, Kushiyama A, Fujishiro M, Fukushima T, et al. Interactive roles of gut microbiota and gastrointestinal motility in the development of inflammatory disorders. *Inflamm. Cell Signal* (2015) 2(1). doi: 10.14800/ics.643
27. Man SM, Tourlomousis P, Hopkins L, Monie TP, Fitzgerald KA, Bryant CE. *Salmonella* infection induces recruitment of caspase-8 to the inflammasome to modulate il-1β production. *J Immuno* (2013) 191(10):5239–46. doi: 10.4049/jimmunol.1301581
28. Scully P, Macsharry J, O'Mahony D, Lyons A, O'Brien F, Murphy S, et al. Bifidobacterium infantis suppression of peyer's patch mip-1α and mip-1β secretion during salmonella infection correlates with increased local CD4 +CD25+ T cell numbers. *Cell Immunol* (2013) 281(2):134–40. doi: 10.3892/mmr.2019.10195
29. Gómez GD, Balcázar JL. A review on the interactions between gut microbiota and innate immunity of fish. *FEMS Immunol Med Microbiol* (2010) 52 (2):145–54. doi: 10.1111/j.1574-695X.2007.00343.x
30. Zhao Z, Liu JX, Deng YQ, Huang W, Ren CH, Call DR, et al. The *Vibrio alginolyticus* T3SS effectors, Val1686 and Val1680, induce cell rounding, apoptosis and lysis of fish epithelial cells. *Virulence* (2018) 9(1):318–30. doi: 10.1080/21505594.2017.1414134
31. Deng YQ, Xu HD, Su YL, Liu SL, Xu LW, Guo ZX, et al. Horizontal gene transfer contributes to virulence and antibiotic resistance of *Vibrio harveyi* 345 based on complete genome sequence analysis. *BMC Genomics* (2019a) 20 (1):761–79. doi: 10.21203/rs.2.13151/v1
32. Deng YQ, Feng J, Bei L, Su YL. Thermal shock-based Vibrio harveyi homologous recombinant gene knockout method. R.P.C State Intellectual Property Office (2017) R.P.C Patent Application No 201711295414.1 (in Chinese).
33. Whitaker WB, Parent MA, Boyd A, Richards GP, Boyd EF. The *Vibrio parahaemolyticus* ToxRS regulator is required for stress tolerance and colonization in a novel orogastric streptomycin-induced adult murine model. *Infect Immun* (2012) 80(5):1834–45. doi: 10.1128/IAI.06284-11
34. Livak KJ, Schmittgen TD. Analysis of relative gene expression data using real-time quantitative PCR and the $2^{-\Delta\Delta CT}$ Method. *Methods* (2001) 25(4):402–8. doi: 10.1006/meth.2001.1262
35. Deng YQ, Cheng CH, Xie JW, Liu SL, Ma HL, Feng J, et al. Coupled changes of bacterial community and function in the gut of mud crab (*Scylla Paramamosain*) in response to Baimang disease. *AMB Express* (2019b) 9 (1):18. doi: 10.1186/s13568-019-0745-1
36. Aßhauer KP, Wemheuer B, Daniel R, Meinicke P. Tax4Fun: predicting functional profiles from metagenomic 16S rRNA data. *Bioinformatics* (2015) 31(17):2882–4. doi: 10.1093/bioinformatics/btv287
37. Kanehisa M, Goto S, Sato Y, Furumichi M, Tanabe M. KEGG for integration and interpretation of large-scale molecular data sets. *Nucleic Acids Res* (2012) 40(D1):D109–14. doi: 10.1093/nar/gkr988
38. Clarke K, Gorley R. *PRIMER 6 v 6.1. 11 & PERMANOVA+ v 1.0. 1*. Plymouth, UK: PRIMER-E Ltd. (2008).
39. Costa M.D.G.F.A., Nunes M.M.D.J.C., Duarte JC, Pereira AMS. *IBM SPSS Statistics 19*. Revista De Enfermagem Referência Press (2012).
40. Luo G, Sun Y, Huang L, Su Y, Zhao L, Qin Y, et al. Time-resolved dual RNA-seq of tissue uncovers *Pseudomonas plecoglossicida* key virulence genes in host-pathogen interaction with *Epinephelus coioides*. *Environ Microbiol* (2020) 22(2):677–93. doi: 10.1111/1462-2920.14884
41. Zhang B, Luo G, Zhao L, Huang L, Qin Y, Su Y, et al. Integration of RNAi and RNA-seq uncovers the immune responses of *Epinephelus coioides* to L321_RS19110 gene of *Pseudomonas plecoglossicida*. *Fish Shellfish Immun* (2018) 81:121–9. doi: 10.1016/j.fsi.2018.06.051
42. Haller O, Kochs G, Weber F. The interferon response circuit: induction and suppression by pathogenic viruses. *Virology* (2006) 344:119–30. doi: 10.1016/j.virol.2005.09.024
43. Sakamaki K, Satou Y. Caspases: evolutionary aspects of their functions in vertebrates. *J Fish Biol* (2009) 74(4):727–53. doi: 10.1111/j.1095-8649.2009.02184.x
44. Ponka P, Beaumont CR, Richardson DR. Function and regulation of transferrin and ferritin. *Semin. Hematol* (1998) 35(1):35–54. doi: 10.1002/ejoc.201000409
45. Takeda K, Akira S. Tlr signaling pathways. *Semin Immunol* (2004) 16(1):3–9. doi: 10.1016/j.smim.2003.10.003
46. Visschers RGJ, Luyer MD, Schaap FG, Damink SWMO, Soeters PB. The gut-liver axis. *Curr Opin Clin Nutr Metab Care* (2013) 16(5):576–81. doi: 10.1097/MCO.0b013e32836410a4
47. Su YL, Feng J, Liu C, Li W, Xie YD, Li AX. Dynamic bacterial colonization and microscopic lesions in multiple organs of tilapia infected with low and high pathogenic *Streptococcus agalactiae* strains. *Aquaculture* (2017) 471:190–203. doi: 10.1016/j.aquaculture.2017.01.013
48. Li J, Norman YS. Pathogenicity of Vibrios in Fish: an Overview. *J Ocean Univ Qingdao* (2003) 2(2):117–28. doi: 10.1007/s11802-003-0039-7
49. Rawls JF, Samuel BS, Gordon JI. Gnotobiotic zebrafish reveal evolutionarily conserved responses to the gut microbiota. *Proc Natl Acad Sci USA* (2004) 101 (13):4596–601. doi: 10.1073/pnas.0400706101
50. Kanther M, Sun X, Mühlbauer M, Mackey LC, Flynn E, Bagnat M, et al. Microbial colonization induces dynamic temporal and spatial patterns of NF-kB activation in the zebrafish digestive tract. *Gastroenterology* (2011) 141 (1):197–207. doi: 10.1053/j.gastro.2011.03.042
51. Galindo-Villegas J, García-Moreno D, de Oliveira S, Meseguer J, Mulero V. Regulation of immunity and disease resistance by commensal microbes and chromatin modifications during zebrafish development. *Proc Natl Acad Sci USA* (2012) 109(39):E2605–14. doi: 10.1073/pnas.1209920109
52. Balcázar JL, De BI, Ruiz-Zarzuela I, Vendrell D, Calvo AC, Márquez I, et al. Changes in intestinal microbiota and humoral immune response following probiotic administration in brown trout (*salmo trutta*). *Brit J Nutr* (2007) 97 (3):522–7. doi: 10.1017/S0007114507432986
53. Irianto A, Austin B. Use of probiotics to control furunculosis in rainbow trout *Oncorhynchus mykiss* (Walbaum). *J Fish Dis* (2002) 25:333–42. doi: 10.1046/j.1365-2761.2002.00375.x
54. Nie L, Zhou QJ, Qiao Y, Chen J. Interplay between the gut microbiota and immune responses of ayu (*Plecoglossus altivelis*) during *Vibrio anguillarum* infection. *Fish Shellfish Immunol* (2017) 68:479–87. doi: 10.1016/j.fsi.2017.07.054
55. Lozupone CA, Stombaugh JI, Gordon JI, Jansson JK, Knight R. Diversity, stability and resilience of the human gut microbiota. *Nature* (2012) 489 (7415):220–30. doi: 10.1038/nature11550
56. Xiong J, Wang K, Wu JF, Lin L, Qian Q, Jie K, et al. Changes in intestinal bacterial communities are closely associated with shrimp disease severity. *Appl Microbiol Biotechnol* (2015) 99(16):6911–9. doi: 10.1007/s00253-015-6632-z
57. Dai WF, Yu WN, Zhang JJ, Zhu JY, Tao Z, Xiong JB. The gut eukaryotic microbiota influences the growth performance among cohabitating shrimp. *Appl Microbiol Biotechnol* (2017) 101:6447–57. doi: 10.1007/s00253-017-8388-0
58. Xiong J, Zhu J, Dai W, Dong C, Qiu Q, Li C. Integrating gut microbiota immaturity and disease-discriminatory taxa to diagnose the initiation and severity of shrimp disease. *Environ Microbiol* (2017) 19(4):1490–501. doi: 10.1111/1462-2920.13701
59. Yang HT, Zou SS, Zhai LJ, Wang Y, Zhang FM, An LG, et al. Pathogen invasion changes the intestinal microbiota composition and induces innate immune responses in the zebrafish intestine. *Fish Shellfish Immunol* (2017) 71:35–42. doi: 10.1016/j.fsi.2017.09.075 S1050464817305946.
60. de Bruijn I, Liu Y, Wiegertjes GF, Raaijmakers JM. Exploring fish microbial communities to mitigate emerging diseases in aquaculture. *FEMS Microbiol Ecol* (2017) 94(1):fix161. doi: 10.1093/femsec/fix161
61. Pérez T, Balcázar JL, Ruiz-Zarzuela I, Halaihel N, Vendrell D, de Blas I, et al. Host-microbiota interactions within the fish intestinal ecosystem. *Mucosal Immunol* (2010) 3(4):355–60. doi: 10.1038/mi.2010.12
62. Ina-Salwany MYI, Al-Saari N, Mohamad A, Mursidi FA, Mohd-Aris A, Amal MNA, et al. Vibriosis in fish: a review on disease development and prevention. *J Aquat Anim Health* (2019) 31(1):3–22. doi: 10.1002/aah.10045
63. Zorrilla I, Balebona MC, Mori·igo MA, Sarasquete C, Borrego JJ. Isolation and characterization of the causative agent of pasteurellosis, *Photobacterium damsela* ssp. piscicida, from sole, solea senegalensis (kaup). *J Fish Dis* (2010) 22(3):167–72. doi: 10.1046/j.1365-2761.1999.00157.x
64. Wang C. *Vibrio alginolyticus* infection induces coupled changes of bacterial community and metabolic phenotype in the gut of swimming crab. *Aquaculture* (2019) 499:251–9. doi: 10.1016/j.aquaculture.2018.09.031
65. Rivas AJ, Lemos ML, Osorio CR. *Photobacterium damselae* subsp. damselae, a bacterium pathogenic for marine animals and humans. *Front Microbiol* (2013) 4:283:283. doi: 10.3389/fmicb.2013.00283

66. Figge MJ, Cleenwerck I, van Uijen A, De Vos P, Huys G, Robertson L. *Photobacterium piscicola* sp. nov., isolated from marine fish and spoiled packed cod. *Syst Appl Microbiol* (2014) 37(5):329–35. doi: 10.1016/j.syapm.2014.05.003
67. Danziger L. Lactobacillus: a Review. *Clin Microbiol Newslett* (2008) 30(4):23–7. doi: 10.1016/j.clinmicnews.2008.01.006
68. Liu WS, Ren PF, He SX, Xu L, Yang YL, Gu ZM, et al. Comparison of adhesive gut bacteria composition, immunity, and disease resistance in juvenile hybrid tilapia fed two different Lactobacillus strains. *Fish Shellfish Immunol* (2013) 35 (1):54–62. doi: 10.1016/j.fsi.2013.04.010
69. Eren AM, Sogin ML, Morrison HG, Vineis JH, Fisher JC, Newton RJ, et al. A single genus in the gut microbiome reflects host preference and specificity. *Isme J* (2015) 9(1):90–100. doi: 10.1038/ismej.2014.97
70. Lodwig EM, Hosie AHF, Bourde`s A, Findlay K, Allaway D, Karunakaran R, et al. Amino-acid cycling drives nitrogen fixation in the legume-Rhizobium symbiosis. *Nature* (2003) 422:722–6. doi: 10.1038/nature01527
71. Breznak J. Nitrogen-fixing *Enterobacter agglomerans* isolated from guts of wood-eating termites. *Appl Environ Microbiol* (1977) 33(2):392–9. doi: 10.1002/jobm.3630181007
72. Guo ZG, Jun Y, Zhang J, Ward RE, Martin RJ, Lefever M, et al. Butyrate improves insulin sensitivity and increases energy expenditure in mice. *Diabetes* (2009) 58(7):1509–17. doi: 10.2337/db08-1637
73. Lin RS. Activation of the AMP activated protein kinase by short-chain fatty acids is the main mechanism underlying the beneficial effect of a high fiber diet on the metabolic syndrome. *Med Hypotheses* (2010) 74(1):123–6. doi: 10.1016/j.mehy.2009.07.022
74. Donohoe DR, Garge N, Zhang XX, Sun W, Connell TMO, Bunger MK, et al. The microbiome and butyrate regulate energy metabolism and autophagy in the mammalian colon. *Cell Metab* (2011) 13(5):520–6. doi: 10.1016/j.cmet.2011.02.018
75. den Besten G, van Eunen K, Groen AK, Venema K, Reijngoud DJ, Bakker BM. The role of short-chain fatty acids in the interplay between diet, gut microbiota, and host energy metabolism. *J Lipid Res* (2013) 54(9):2325–40. doi: 10.1194/jlr.R036012
76. Zhu JY, Dai WF, Qiu QF, Dong CM, Zhang JJ, Xiong JB. Contrasting ecological processes and functional compositions between intestinal bacterial community in healthy and diseased shrimp. *Microb Ecol* (2016) 72 (4):975–85. doi: 10.1007/s00248-016-0831-8
77. Hammer BK, Bassler BL. Quorum sensing controls biofilm formation in *Vibrio cholerae*. *Mol Microbiol* (2010) 50(5):101–4. doi: 10.1046/j.1365-2958.2003.03688.x
78. Miyata ST, Unterweger D, Rudko SP, Pukatzki S. Dual expression profile of type vi secretion system immunity genes protects pandemic *Vibrio cholerae*. *PloS Pathog* (2013) 9(12):e1003752. doi: 10.1371/journal.ppat.1003752

**Conflict of Interest:** The authors declare that the research was conducted in the absence of any commercial or financial relationships that could be construed as a potential conflict of interest.

frontiers in Immunology

ORIGINAL RESEARCH
published: 11 December 2020
doi: 10.3389/fimmu.2020.596514

# Intestinal Transcriptome Analysis Reveals Soy Derivative-Linked Changes in Atlantic Salmon

*Viswanath Kiron*[1]*, *Youngjin Park*[1], *Prabhugouda Siriyappagouder*[1], *Dalia Dahle*[1], *Ghana K. Vasanth*[1], *Jorge Dias*[2], *Jorge M. O. Fernandes*[1], *Mette Sørensen*[1] *and Viviane Verlhac Trichet*[3]*

[1] Faculty of Biosciences and Aquaculture, Nord University, Bodø, Norway, [2] SPAROS Lda., Olhão, Portugal, [3] DSM Nutritional Products, Global Innovation, Kaiseraugst, Switzerland

Intestinal inflammation in farmed fish is a non-infectious disease that deserves attention because it is a major issue linked to carnivorous fishes. The current norm is to formulate feeds based on plant-derived substances, and the ingredients that have antinutritional factors are known to cause intestinal inflammation in fishes such as Atlantic salmon. Hence, we studied inflammatory responses in the distal intestine of Atlantic salmon that received a feed rich in soybean derivatives, employing histology, transcriptomic and flow cytometry techniques. The fish fed on soy products had altered intestinal morphology as well as upregulated inflammation-associated genes and aberrated ion transport-linked genes. The enriched pathways for the upregulated genes were among others taurine and hypotaurine metabolism, drug metabolism—cytochrome P450 and steroid biosynthesis. The enriched gene ontology terms belonged to transmembrane transporter- and channel-activities. Furthermore, soybean products altered the immune cell counts; lymphocyte-like cell populations were significantly higher in the whole blood of fish fed soy products than those of control fish. Interestingly, the transcriptome of the head kidney did not reveal any differential gene expression, unlike the observations in the distal intestine. The present study demonstrated that soybean derivatives could evoke marked changes in intestinal transport mechanisms and metabolic pathways, and these responses are likely to have a significant impact on the intestine of Atlantic salmon. Hence, soybean-induced enteritis in Atlantic salmon is an ideal model to investigate the inflammatory responses at the cellular and molecular levels.

**Keywords: aquafeed, *Salmo salar*, soy saponin, intestinal inflammation, flow cytometry**

OPEN ACCESS

***Edited by:***
*Min Wan,*
*Ocean University of China, China*

***Reviewed by:***
*Javier Santander,*
*Memorial University of Newfoundland, Canada*
*M. Carla Piazzon,*
*Torre de la Sal Aquaculture Institute (IATS), Spain*

***Correspondence:**
*Viswanath Kiron*
*kiron.viswanath@nord.no*
*Viviane Verlhac Trichet*
*v.verlhac@me.com*

***Specialty section:***
*This article was submitted to Comparative Immunology, a section of the journal Frontiers in Immunology*

***Received:*** *19 August 2020*
***Accepted:*** *23 October 2020*
***Published:*** *11 December 2020*

***Citation:***
*Kiron V, Park Y, Siriyappagouder P, Dahle D, Vasanth GK, Dias J, Fernandes JMO, Sørensen M and Trichet VV (2020) Intestinal Transcriptome Analysis Reveals Soy Derivative-Linked Changes in Atlantic Salmon. Front. Immunol. 11:596514. doi: 10.3389/fimmu.2020.596514*

## INTRODUCTION

The quality of high-value farmed fishes such as Atlantic salmon (*Salmo salar*) depends to a great extent on the ingredients in their feeds. Furthermore, the increase in the demand for farmed salmon necessitates intensive farming and the adoption of sustainable feed ingredients. Awareness about sustainability and limited availability of finite marine sources has led to the replacement of fishmeal and fish oil in aquafeeds with plant derivatives. The current norm is to incorporate considerable

amounts of plant-derived components—proteins from pea, soybean, horse beans, oil from rapeseed, starch and gluten from wheat and maize gluten—in aquafeeds (1). However, carnivorous fishes are known to develop intestinal inflammation, *e.g.* when they consume high levels of terrestrial plant components such as the products from soybean. This undesirable health condition is mainly caused by antinutritional factors in soybean such as soyasaponin, $\beta$-conglycinin and glycinin (2–4).

Feeding fish with high levels of full-fat soybean products or low levels of the soybean meal with other legumes is known to not only affect their growth and nutrient utilization but also can disturb the integrity of the distal intestine. Plant-derived ingredients may shift the intestinal microbial community composition (5, 6), which in turn can affect the overall intestinal health, including immunity (7). Inflammation is the first sign of intolerance to dietary components, and fishes that develop the non-infectious disease will have widened lamina propria with many inflammatory cells, less absorptive vacuoles, and shortened brush border microvilli in their distal intestine (4). Fish with inflamed distal intestine will be characterized by poor nutrient digestibility and disturbances in transcellular water transport, especially when their feeds contain >30% soybean meal (8–10). Furthermore, the combination of soybean (even defatted meal) and other legumes can affect the metabolism and gut functions in Atlantic salmon; aberrations in epithelial barrier and major transcriptome changes are already reported (11–13). Studies that employed other fish species have also indicated the adverse effects of soybean meal or soy saponins on growth, nutrient utilization, antioxidant status, and intestinal morphology (14, 15). Thus, it is evident that plant-derived ingredients with antinutritional factors can affect the health of farmed fish, leading to undesirable fish welfare issues. Although the aforementioned studies have described soy-related inflammation in Atlantic salmon, it is imperative to further understand the molecular changes in the intestine of fish that develop intestinal inflammation. Identification of appropriate markers of inflammation would not only enable effective screening of new feed ingredients, but also enhance our understanding of the processes that are affected during inflammation in a lower vertebrate.

We employed a well-studied fish model, Atlantic salmon, to examine the dietary soy products-linked disturbances in the intestine. This study describes the changes in micromorphology, transcriptome of the distal intestine, and whole blood cells in the inflammation (SO) group compared to the control (CO) group. The novelty of the current study lies in the adoption of RNA-Seq to clearly delineate the molecular changes evoked during inflammation.

# MATERIALS AND METHODS

## Experimental Design

In this study, we examined the intestinal transcriptome of a carnivorous fish that developed inflammation. For this, Atlantic salmon post-smolts procured from a local commercial producer (Sundsfjord Smolt, Nygårdsjøen, Norway) were maintained at the Research Station of Nord University, Bodø, Norway, for 4 months. For the experiment, 120 fish (128.66 ± 13.29 g; mean ± SD) were randomly distributed to replicate tanks of the two study groups, *i.e.* CO and SO groups. During a 2-week acclimation period, all the fish were fed a commercial feed (Ewos AS, Bergen, Norway). The 800 L tanks were part of a flow-through seawater system at the Research Station. Water from a depth of 250 m in Saltenfjorden was pumped, filtered, and aerated, and then used for rearing the fish. The water flow rate was maintained at 1,000 L per h, and the average temperature and salinity of the rearing water were 7.6°C and 34 g $L^{-1}$, respectively. The dissolved oxygen saturation values, measured at the water outlet of the tanks was in the range 87–92%, and throughout the experimental period, we employed a 24-h light photoperiod.

The two feeds for the study were prepared as 3 mm extruded pellets by SPAROS Lda (Olhão, Portugal); a control feed for the CO group, and a soybean and soy saponin-containing feed for the SO group (**Supplementary Table 1**). The feeds contained only around 25% ingredients that were of marine origin; 15% fishmeal and 9.4–9.6% sardine oil. All other ingredients were from different plants: soybean, wheat, corn, and rapeseed. Although both the feeds contained soy protein concentrate and soy lecithin powder, only the SO feed contained soybean meal, soybean meal full fat and soy saponins (40% purity). The latter two ingredients were included in the SO feed to induce distal intestinal inflammation in the fish. These feeds were fed *ad libitum* to the respective fish groups, using automatic feeders (Arvo Tech, Huutokoshi, Finland). The feeders delivered the feeds twice a day, 08:00–09:00 and 14:00–15:00, and the daily feeding rate was 1.2% of the fish weight.

## Sampling

After 36 days of feeding, the fish were euthanized with an overdose (160 mg $L^{-1}$) of MS222 tricaine methanesulfonate (Argent Chemical Laboratories, Redmond, WA, USA) to collect the blood, distal intestine, and head kidney. The distal segment (DI) of the intestine was chosen as it is affected by dietary soy products. On the other hand, the head kidney (HK) was selected because it is a key organ involved in the systemic immune responses. First, 2 ml of whole blood (WB) was drawn from *vena caudalis* of fish (n = 10) using heparinized syringe and transferred to 15 ml centrifuge tubes containing 4 ml of culture medium (described later). Thereafter, the fish were dissected under aseptic conditions to collect the DI (after removing the contents) and HK samples (n = 6) which were then transferred to cryotubes, snap-frozen in liquid nitrogen and stored at −80°C. In addition, we had collected the DI samples on day 4 (n = 6); this sample was employed only to understand the histological changes at an early time point. The anterior most portion of the DI segment collected on day 36 was also used for the histology study. DI obtained on day 36 was used for the RNA-Seq and qPCR studies, and HK was employed for the RNA-Seq.

## Intestine Tissue Histomorphology

To understand the morphological changes in the distal intestine, samples of the segment were processed, and 5 µm sections of the tissues from the CO and SO groups were prepared as reported in

Vasanth et al. (16). Alcian Blue-Periodic Acid Schiff's reagent (AB-PAS, pH 1.0) (17) was used to stain the sections for mucins. Thereafter, the sections were viewed using a microscope (Olympus BX51, Olympus Europa GmbH, Hamburg, Germany) with a maximum magnification of 200×. The photomicrographs were captured employing a Camera (SC180, Olympus) and processed with the imaging software CellEntry (Soft Imaging System GmbH, Munster, Germany).

## Intestine/Head Kidney Transcriptome—RNA Isolation, Library Preparation, and Sequencing

To delineate the changes of the respective transcriptomes, total RNA was extracted from DI and HK samples following the QIAzol protocol (Qiagen, Hilden, Germany). RNA purity and quantity were determined using the NanoDrop 1000 (Thermo Fisher Scientific, Waltham, MA, USA). Furthermore, the integrity of the RNA isolated from the two organs was assessed using Agilent RNA screen tapes, following manufacturer's protocol, on the 2200 TapeStation system (Agilent Technologies, Santa Clara, CA, USA). Only samples with RIN > 7.5 were used for library preparation.

RNA sequencing libraries were prepared according to the protocols of Siriyappagouder et al. (18) by using NEBNext ultra II directional RNA library preparation kit with poly (A) mRNA magnetic isolation module (NEB #E7490; New England BioLabs®, Herts, UK). Briefly, 1 μg of total RNA was used as the starting material for the library preparation. The mRNA was enriched using oligo-dT magnetic beads and fragmented to ∼100–200 nt, prior to synthesis of the first and second cDNA strands. The resulting cDNA was purified and 3′ end repaired for adapter ligation. Further PCR enrichment (8 cycles) was performed, and PCR products were cleaned with AMPure XP beads (Beckman Coulter Inc., Brea, CA, USA) to ensure that the libraries were free from residual adapter dimers and unwanted (smaller) fragments. In total, 24 libraries were prepared (12 for DI and 12 for HK); there were six replicates per treatment group. Individual libraries were quantified, normalized and pooled at equimolar ratio and sequenced as single-end reads (75 bp) on an illumina NextSeq 500 sequencer (illumina, San Diego, CA, USA) with NextSeq 500/550 high output v2 reagents kit (illumina). Libraries from the DI and HK samples were sequenced separately by using two flow cells. The obtained raw sequencing data was deposited in the Sequence Read Archive, National Center for Biotechnology Information (NCBI) database under the accession number PRJNA640734.

## Intestine/Head Kidney Transcriptome—Data Processing and Statistical Analyses

Adapter sequences from the raw reads were removed using cutadapt (version 1.12) (19), employing the following parameters: -q 25, 20 –quality-base = 33 –trim-n -m 20. The quality of the clean reads was further assessed using FastQC (Andrews, 2010) and reads with quality <30 were removed. Reference genome of Atlantic salmon (assembly ICSASG_v2) and gene model annotation files were downloaded from NCBI to annotate the sequences. The software STAR (version 2.5.3a) was used to build the index, and cleaned reads were mapped to reference genome with default parameters.

We employed DESeq2 version 1.22.2, which uses shrinkage estimates for both dispersion and fold change to identify the differentially expressed genes (DEGs) (20). An organism database with Entrez geneID was prepared using AnnotationHub version 2.14.5 (21). Pathway enrichment and gene ontology (GO) over-representation of DEGs were assessed with clusterProfiler version 3.10.1 (22). Furthermore, the association of the enriched objects was delineated using the same package. Based on the report by Hong et al. (23), we performed separate enrichment analyses for up- and downregulated genes. The functions of the packages ggplot2 version 3.1.1 (24) and ggraph (25) were used to format the graphs.

## Intestine Transcriptome—Verifying the Expression of DEGs by Real-Time PCR

qPCR was performed to verify the mRNA levels of selected DEGs identified from the RNA-Seq study; here we employed the same samples that were used for the RNA-Seq study. Briefly, 1 μg of total RNA from each sample was reverse transcribed using the QuantiTect reverse transcription kit (Qiagen), according to the manufacturer's instructions. The obtained cDNA was further diluted 10 times with nuclease free water and used as PCR template. The PCR reactions were conducted using the SYBR green in LightCycler® 96 Real-Time PCR System (Roche Holding AG, Basel, Switzerland), following the method previously described by Vasanth et al. (16). The reactions were performed in duplicate on samples from six fish per group.

Primers for the selected genes were designed using the Primer-BLAST tool in NCBI. The primer secondary structures such as hairpin, repeats, self and cross dimer were accessed with NetPrimer (Premier Biosoft, Palo Alto, USA). The primers for the reference and target genes are given in **Table 1**. Using geNorm (26), a geometric normalization factor was computed for each of the samples based on the relative quantities of the two most stable genes (*rps29* and *ubi*) from among the set of four reference genes—elongation factor 1AB (*ef1ab*), ribosomal protein L13 (*rpl13*), ribosomal protein S29 (*rps29*), and ubiquitin (*ubi*). The expression levels of all the target genes were then calculated relative to the normalization factor.

## Cytological Studies—Cell Isolation and Culture

To further understand the feed-induced inflammatory responses, we examined the immune cell population in WB. The cell isolation and culture procedures for the WB samples have been described in Park et al. (27). Briefly, the collected WB was kept in 4 ml of ice-cold L-15 medium. To isolate the WB leucocytes (WBLs), we employed Percoll (Sigma-Aldrich, Oslo, Norway) 40%/60%. After centrifugation (500 × *g*, 30 min, 4°C), the cells that were separated at the interface of the Percoll gradients were carefully collected and washed twice with 4 ml of ice-cold L-15 by centrifugation (500 × *g*, 5 min, 4°C).

**TABLE 1** | Details of primers used for the qPCR verification study.

| Gene | Primer sequence | PCR efficiency (%) | Amplicon size (bp) | GenBank accession numbers |
|---|---|---|---|---|
| *anxa2* | CATTGCAGAAAGAATACAAAGGGG-**F** CCAGCGTGACAATACTGTG-**R** | 92.1 | 96 | XM_014161401.1 |
| *cath1b* | GTCCTCTGAAGAAAAATGGGAAAC-**F** GCATAGCATCTTCTGCCTC-**R** | 88.5 | 135 | NM_001123586.1 |
| *cath2* | CCGATTCTGGAGACTGGCAA-**F** TGTCCGAATCTTCTGAGTGC-**R** | 96.5 | 111 | NM_001123573.1 |
| *clcn1* | TCAGCAACAACAGTCTCT-**F** GCTGTGGATGGTGCTGTT-**R** | 93.0 | 82 | XM_014152555.1 |
| *clcn2* | CTCGGACACATCAGTAAG-**F** TGAGGGAGGTGGAGTCTAGC-**R** | 90.8 | 123 | XM_014184291.1 |
| *csad* | CGGTCTGGCTGACATAAT-**F** AGTTGACTCGTCCACCCTGA-**R** | 88.2 | 127 | NC_027317.1 |
| *gal3* | CGGAGCTACTAACAGATA-**F** GTTGGCTGGTTGGGTTGC-**R** | 90.1 | 127 | NM_001140833.1 |
| *gsto1* | GCTTCATGCCAAGGGGAT-**F** TCTCCAATGTCGGAACCAGG-**R** | 89.9 | 107 | NM_001141472.1 |
| *lysc2* | ATGAGAGCTGTTGTTGTTC-**F** AGACAGGCACACCCAGTT-**R** | 97.0 | 144 | XM_014145497.1 |
| *mta* | TGAATGCTCCAAAACTGG-**F** CCTGAGGCACACTTGCTG-**R** | 88.3 | 130 | NM_001123677.1 |
| *rbp2* | GACCTGCTACACCTGGACATC-**F** TCTCAACTGGCCTACCTG-**R** | 104.0 | 147 | NM_001146482.1 |
| *slc26a6* | TGGGCATGGAACACCTGA-**F** CACCAACTGTTAAACTCG-**R** | 91.1 | 124 | NC_027312.1 |
| *slc6a19* | ATGGAGGAGGAGCGTTTA-**F** CGATGCCAACACCTGTCAGA-**R** | 100.5 | 158 | NM_001141815.1 |
| *slc6a6* | GGTGTAATTCATTTCCGATGC-**F** CTCTTTCTGTGCCATGCTGC-**R** | 95.8 | 109 | XM_014134772.1 |
| *tnfrsf1b* | TCGGAGGTGTTATCGGAG-**F** CCTGGACCCTGTGAAGACTTT-**R** | 91.7 | 80 | XM_014133111.1 |
| Reference genes | | | | |
| *ef1ab* | TGCCCCTCCAGGATGTCTAC-**F** CACGGCCCACAGGTACTG-**R** | 94.5 | 59 | BG933853 |
| *rpl13* | CGCTCCAAGCTCATCCTCTTCCC-**F** CCATCTTGAGTTCCTCCTCAGTGC- **R** | 95.5 | 79 | BT048949.1 |
| *rps29* | GGGTCATCAGCAGCTCTATTGG-**F** AGTCCAGCTTAACAAAGCCGATG-**R** | 93.3 | 167 | BT043522.1 |
| *ubi* | AGCTGGCCCAGAAGTACAACTGTG-**F** CCACAAAAAGCACCAAGCCAAC-**R** | 94.9 | 162 | AB036060.1 |

*Annexin 2-like (anxa2), cathelicidin 1-B (cath1b), cathelicidin 2 (cath2), chloride channel protein 1-like (clcn1), chloride channel protein 2-like (clcn2), cysteine sulfinic acid decarboxylase-like (csad), galectin-3 (gal3), glutathione S-transferase omega-1(gsto1), lysozyme C II (lysc2), metallothionein A (mta), retinol binding protein II (rbp2), solute carrier family 26 member 6-like (slc26a6), solute carrier family 6 member 19 (slc6a19), solute carrier family 6 (neurotransmitter transporter, taurine) member 6 (slc6a6), and tumor necrosis factor receptor superfamily member 1B-like (tnfrsf1b).*

## Cytological Studies—Flow Cytometric Assay

ImageStream®X Mk II Imaging Flow Cytometer (Luminex Corporation, Austin, TX, USA) equipped with two argon-ion lasers (488 and 642 nm) and a side scatter laser (785 nm) was used for the flow cytometric assays. The acquired cell data was analyzed using IDEAS 6.1.822.0 software (Luminex Corporation). The protocols for the flow cytometric assays were previously described in Park et al. (27).

## WB Lymphocyte-Like Cell Population

To compare the percentage of lymphocyte-like cells of fish from the CO and SO groups, aliquots containing $1 \times 10^6$ cells of WBL in 50 µl PBS were prepared in 1.5 ml microcentrifuge tubes. Before every sample was run through the flow cytometer, 1 µl of propidium iodide (PI; 1 mg/ml, Sigma-Aldrich) was added to stain dead cells. Next, 1 mW 488 nm argon-ion laser and 0.47 mW 785 nm side scatter laser in the imaging flow cytometer were set to detect the dead cells (702/86 nm bandpass; Channel 5) and cell complexity (772/55 nm bandpass; Channel 6), respectively. Cell analyses were performed on 10,000 cells acquired at low speed (300 objects/s) and at a magnification of 40×. Dead cells were estimated as the percent of cells that were positive for PI (red fluorescent cells). After excluding the dead cells, viable cells were analyzed by generating brightfield (BF) area (size) *vs*. side scatter (SSC) intensity (complexity) dot plots. The settings of the cytometer were kept identical during the analysis of all the samples. We adopted a gating strategy based on our IFC protocols (27); using HK $IgM^+$ cells isolated by magnetic-activated cell sorting, lymphocyte localization (low BF area and low SSC intensity) was determined employing a BF area *vs*. SSC

intensity plot. In the present study, the percentages of cells in the lymphocyte localization gates were compared to determine the differences in the CO and SO groups.

## Data Handling and Statistical Analyses—Flow Cytometry and qPCR Studies

The data analyses were performed in RStudio. Normality of the qPCR and flow cytometry data was tested by Shapiro–Wilk Test, and the assumption of equal variance was checked by the Bartlett's Test. Unpaired Student's t-test was employed to compare the statistically significant difference between the two groups. Mann–Whitney U test was used for non-parametric data. The differences were considered significant at $p < 0.05$.

# RESULTS

## Soybean Products Induced Inflammation in the Distal Intestine of Atlantic Salmon

On the 4$^{th}$ day after the start of the trial, the DI of the SO group did not exhibit any characteristic morphological changes associated with inflammation (**Figure 1A**, **Supplementary Figure 1A**). However, at this time point, we could observe a reduction in absorptive vacuoles and more intraepithelial lymphocytes compared to those in the CO group. The morphological differences in the SO group were clearly discernible on the 36$^{th}$ day (**Figure 1B**, **Supplementary Figure 1B**); the SO group had fused villi, fewer supranuclear vacuoles, widened lamina propria, infiltration of inflammatory cells, and enlarged stratum compactum.

## Transcriptome of the Distal Intestine Revealed DEGs Induced by the Soybean Products

The transcriptomes of DI and HK were collected on day 36 when the fish intestine exhibited distinct features of inflammation. A total of over 563 million cleaned reads from 24 (12 from distal intestine and 12 from head kidney) samples were obtained after adapter trimming and quality filtering; of these over 435 million reads were mapped to Atlantic salmon transcriptome and genome. However, one biological replicate of the DI from the CO group was removed from the downstream analysis due to lower (22.83%) mapping percentage (**Supplementary Table 2**). An illustration of the bioinformatics pipeline is provided in **Supplementary Figure 2**.

The principal component analyses of the normalized counts pointed to the differential clustering of the CO and SO groups in the DI (**Figure 2A**), but not in the HK (**Figure 2B**). The dispersions of the gene expression data, as expected, decreased with increasing mean, and the MA (minus over average) plot revealed the differentially expressed genes after shrinking the dispersions and logarithmic fold changes (DI: **Supplementary Figures 3A, B**; HK: **Supplementary Figures 4A, B**). We identified 53 upregulated and 38 downregulated genes in the DI at a logarithmic fold change threshold of 0.75 and an adjusted p-value of 0.05 (**Figures 3A, B**; **Supplementary Figure 5**). However, DEGs were not detected in the case of HK ($p > 0.05$).

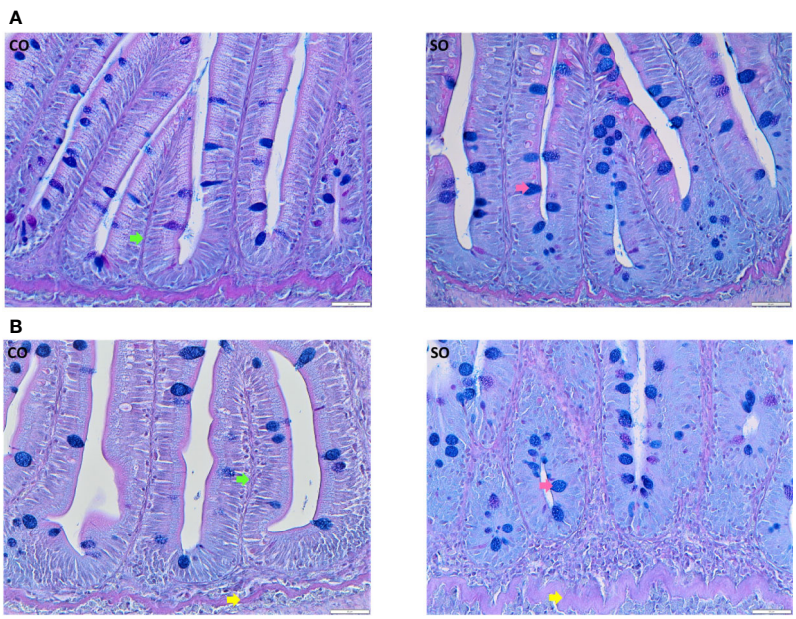


**FIGURE 1** | Photomicrographs of the distal intestine of Atlantic salmon from the CO and SO groups. **(A)** Inflammatory features are not visible in the SO group on day 4 after the start of the feeding trial. **(B)** Saponin-induced inflammatory characteristics are evident at day 36 of the trial. Control group—CO, and soy-derivatives fed group—SO. Pink arrow—goblet cells, green arrow: lamina propria, yellow arrow—stratum compactum. Scale bar: 50 µm.

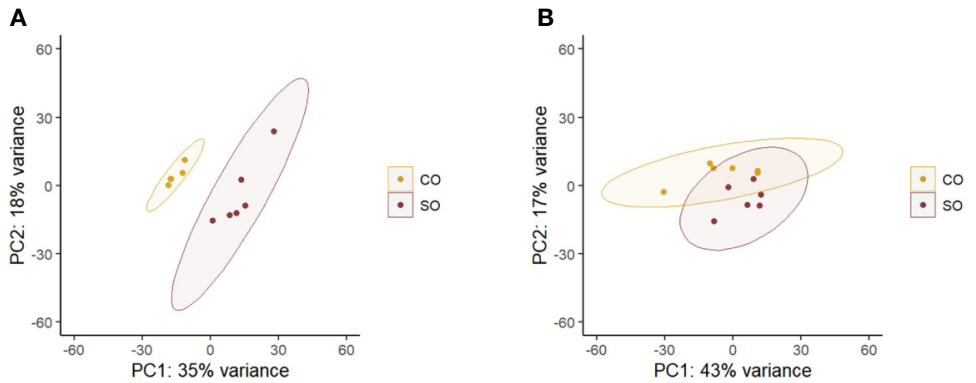


**FIGURE 2** | Principal component analysis plot shows the clustering of the CO and SO fish groups. **(A)** The distal intestine and **(B)** head kidney. Control group—CO, and soy-derivatives fed group—SO. Note that from the intestine data, one replicate was removed from the CO group because the reads did not yield a good mapping result.

The upregulated genes in the DI included inflammation-associated genes such as *cathelicidins*, *galectin*, *tumor necrosis factor receptor superfamily member 1B-like*, *lysozyme CII*, *annexin A2-like* (**Supplementary Tables 3**, **5**). Some solute carrier families were upregulated while others were downregulated in the SO group (**Supplementary Tables 4**, **5**). Genes connected to chloride channel proteins (*clcn1*, *clcn2*) were downregulated in the SO group. In addition, sodium-associated transporters were altered in the same group (*sodium/glucose co-transporter 1-like, slc5a1*, and *sodium- and chloride-dependent taurine transporter*, *slc6a6* were upregulated and *sodium-dependent neutral amino acid transporter B(0)AT1-like, slc6a19* and *potassium voltage-gated channel subfamily A regulatory beta subunit 2*, *kcnab2* were downregulated). Another anion exchanger, *solute carrier family 26 member 6*, *slc26a6* and the mitochondrial amino acid transporter, *slc25a48* were upregulated in the SO group.

The expression of 15 DEGs was verified by qPCR. The bar plots in **Supplementary Figure 6** show the mRNA levels of the selected genes. The mRNA levels correlated positively with the read counts from the RNA-Seq study (**Supplementary Figure 7**).

## Soybean Products Affected the Biological Pathways

The enriched pathways for the upregulated genes were taurine and hypotaurine metabolism, beta-alanine metabolism, pantothenate and coenzyme (CoA) biosynthesis, drug metabolism–cytochrome P450, drug metabolism–other enzymes, metabolism of xenobiotics by cytochrome P450, steroid biosynthesis, and glutathione metabolism (**Figure 4A**). All these enriched pathways had common genes; the exception was steroid biosynthesis (**Figure 4B**). The package clusterProfiler did not detect any enriched pathways for the downregulated genes. The enriched GO terms based on the upregulated genes were among others, oxidoreductase activity, some binding and lyase activities (**Figure 4C**). More GO terms based on the downregulated genes were enriched; many belonged to transmembrane transporter activity, channel activity and some binding activity (**Figure 4D**). For the upregulated genes, NADP, vitamins, pyridoxal phosphate, flavin adenine dinucleotide, and coenzyme binding were enriched (**Figure 4C**). On the other hand, for the downregulated genes, tetrapyrrole, iron ion, oxygen, heme, and amino acid binding were the enriched GO terms (**Figure 4D**).

## Soybean Products Induced Inflammation Was Marked by an Increase in WB Lymphocyte-Like Cells

To compare the percentage of WB lymphocyte-like cells from the CO and SO groups, WBL population was presented on a brightfield area (cell size) *vs* side scatter intensity (cell complexity) dot plot (**Figures 5A, B**). The gate for lymphocyte-like cells was determined based on salmon $IgM^+$ cell area, as previously described by Park et al. (27). From **Figure 5C**, it is evident that the SO group (77.64%) had higher percentage of WBL-like cells compared to the CO group (74.35%; $p < 0.05$).

# DISCUSSION

Diet-induced intestinal inflammation is a common clinical issue that has to be tackled by understanding the associated mechanisms because the disease has pervaded all classes of the global population. In humans, Crohn's disease and ulcerative colitis are inflammatory bowel diseases. These non-communicable diseases are assumed to be early adulthood diseases caused by genetic and environmental factors which disturb immunity and weaken epithelial barrier (28). Like humans, carnivorous farmed fish are prone to diet-linked allergies that can affect their growth (4, 8–10). Here we describe the soybean/soy saponin-induced inflammation primarily based on the changes in the transcriptome of the DI of Atlantic salmon. The results indicate the alteration of around 90 genes and disturbance of associated pathways and GO terms in the DI of fish. Furthermore, the differential counts of the immune cells also point to possible changes in the immune status of this fish group.

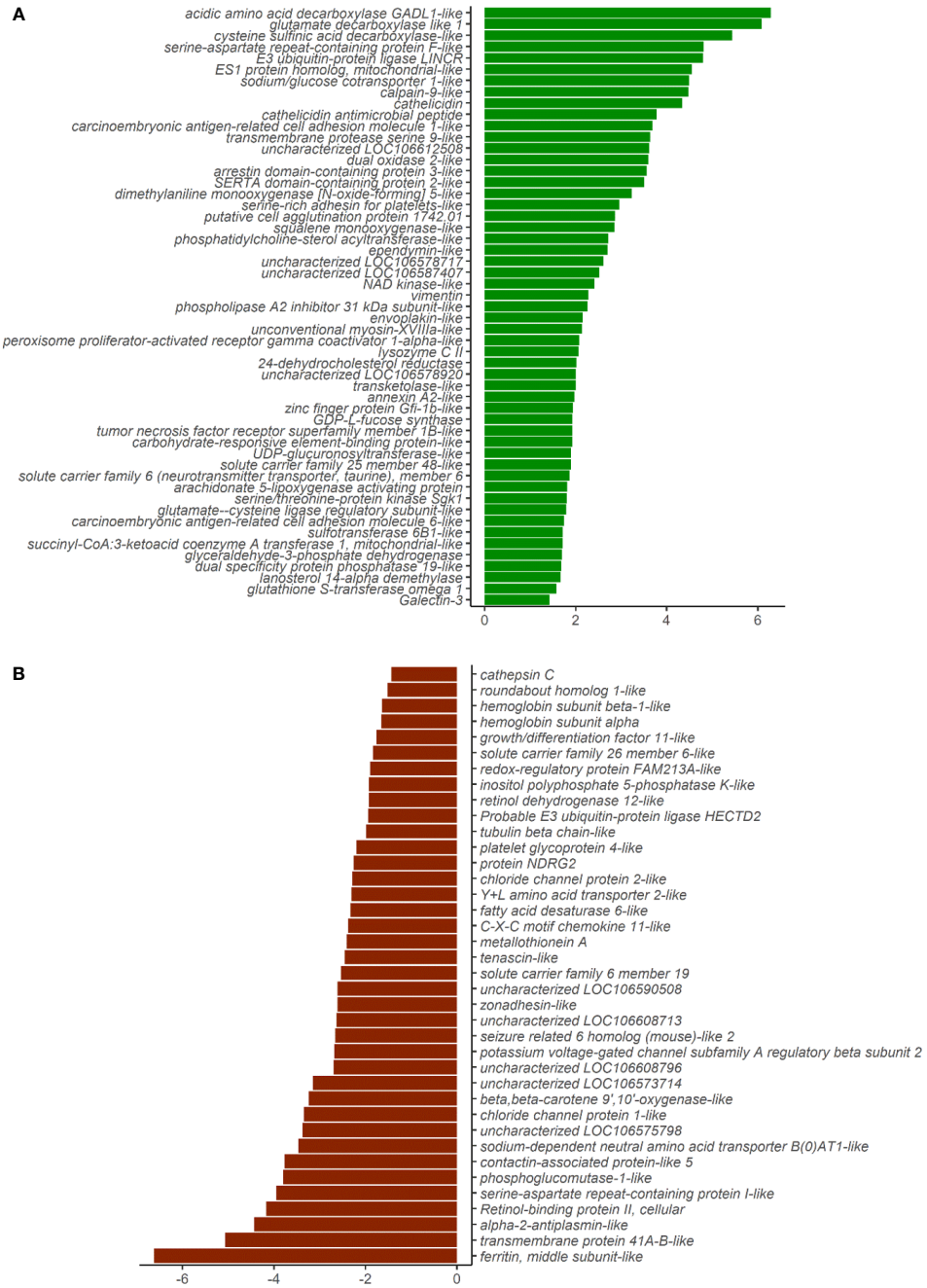


**FIGURE 3** | Plot showing the differentially expressed genes in the distal intestine of Atlantic salmon. **(A)** Fifty-three genes were upregulated in the SO group (green bars). **(B)** Thirty-eight genes were downregulated in the SO group (red bars). X-axis labels show the log2foldchange, and the y-axis shows the differentially expressed genes.

## High Fat Soybean Products and Soy Saponin Induced Inflammation in the Distal Intestine of Atlantic Salmon

Certain soybean products are known to cause inflammation in the intestine of carnivorous fishes (2, 4, 9, 12, 14). High levels of soybean meal in diets or the presence of antinutritional factors is reported to be the main reasons for the inflammatory condition (2, 10). Feeding even 10% of solvent extracted soybean meal or 25% defatted soybean meal can give rise to pathophysiological changes in Atlantic salmon (12, 29). Furthermore, the severity of inflammation in the DI of this fish is dependent on the content of the antinutritional factor (30). A study points out that the impact of soy saponin concentrate (of 69% purity) feeding for 53 days is relatively

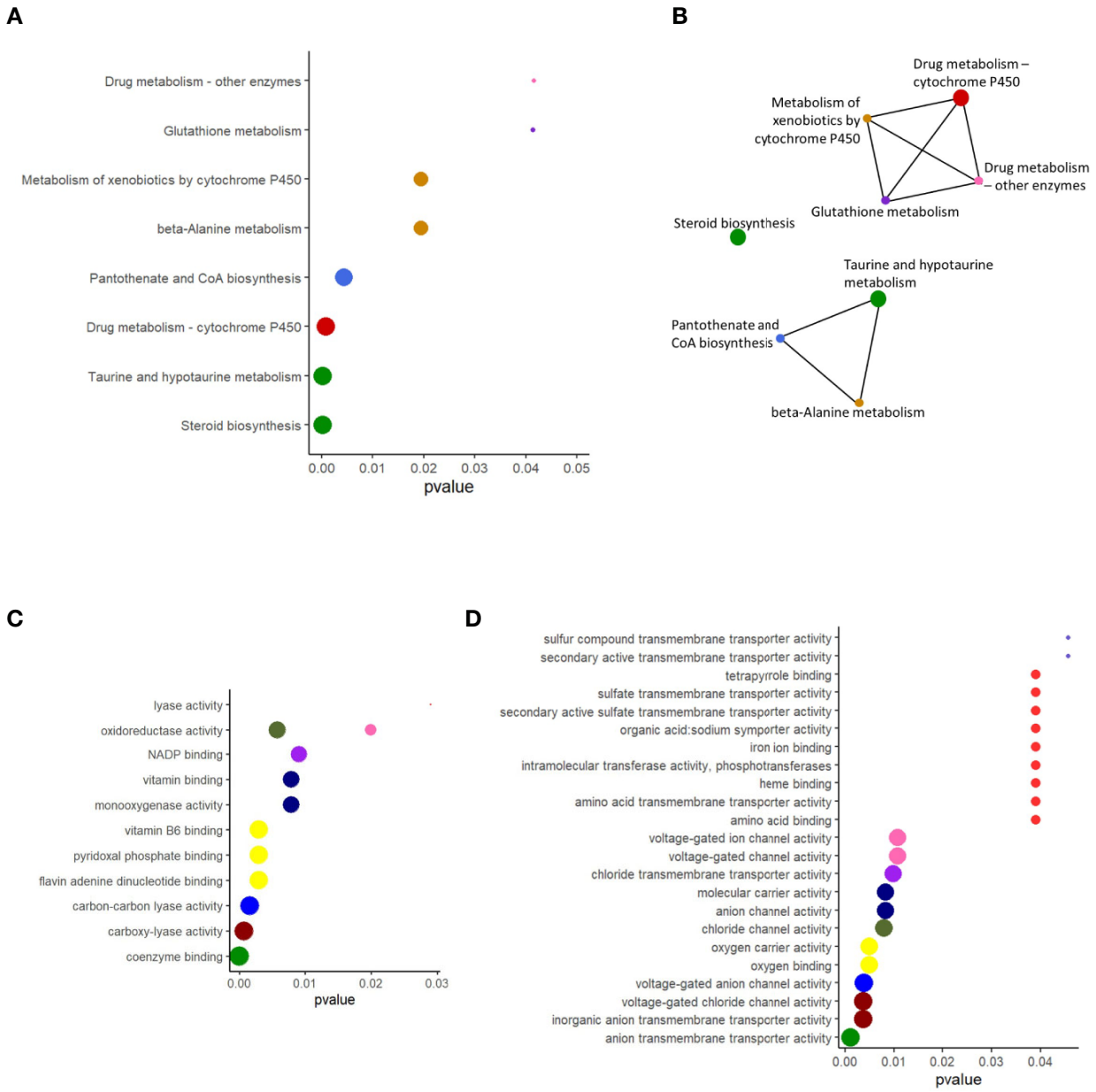


**FIGURE 4** | Enriched KEGG pathways and overrepresented GO terms for the upregulated and downregulated genes in the distal intestine of Atlantic salmon. **(A)** The biologically relevant pathways for the upregulated genes were extracted at a p value cutoff of 0.05 for the enrichment tests. **(B)** Network showing the connections between enriched pathways that have overlapping gene sets. **(C)** The biologically relevant GO terms for the upregulated genes were extracted at a p value cutoff of 0.05 for the enrichment tests. **(D)** The biologically relevant GO terms for the downregulated genes were extracted at a p value cutoff of 0.05 for the enrichment tests. X-axis shows the adjusted p values associated with the pathways/GO terms. The pathways shown in panels A and B are color coded similarly. In each figure, the sizes of the dots decrease with the p value, and the colors for dots with same p value are kept the same.

benign in terms of inflammatory signs (12). In the present study, 36 days of feeding soy products (meal, full fat, and soy saponin) led to the development of inflammation in the DI of salmon. The inflammation characteristics were similar to that described previously by others (4, 12, 30) but not as intense as reported earlier in a chemically-induced inflammation model that employed a direct application method (16).

## Distinct Effects of Soy Products in the Intestine Transcriptome

In this study, in addition to local responses to soybean products in the DI, we anticipated that changes may occur in the HK, a key immune organ. Most transcriptome studies focusing on HK have registered responses to bacterial/viral pathogens or parasites, while some studies have shown that functional feeds could

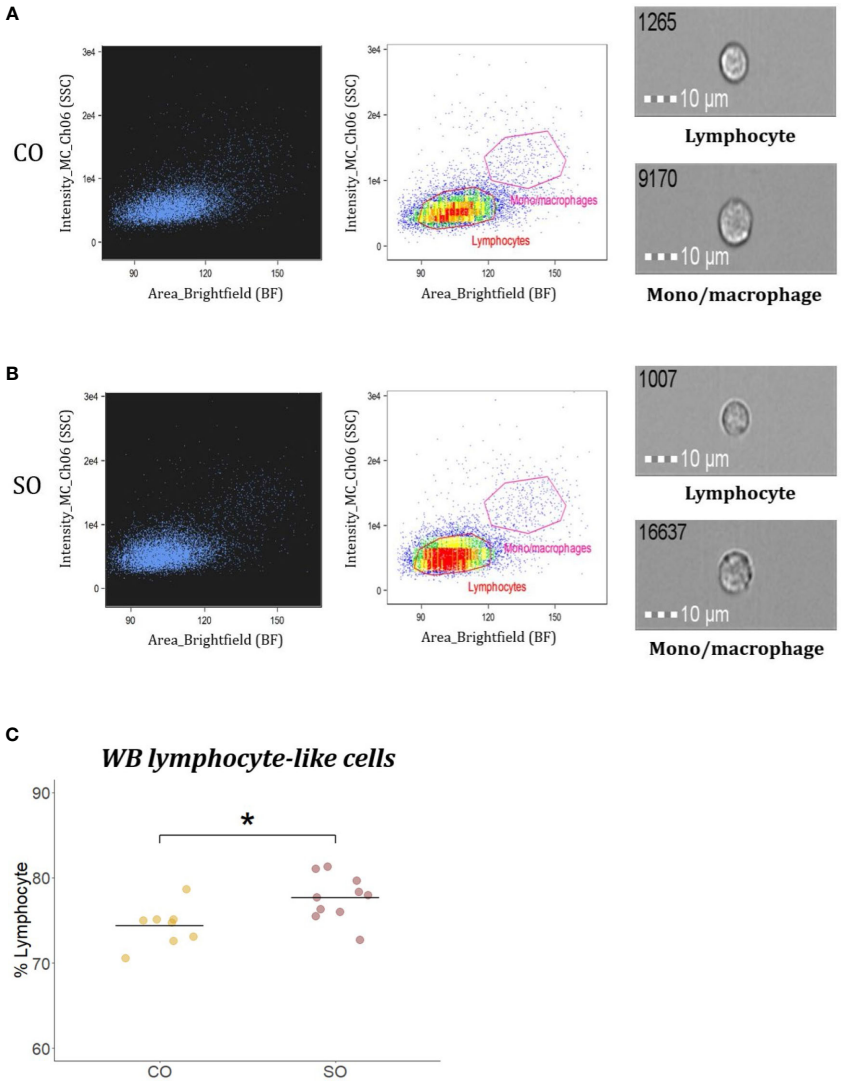


**FIGURE 5** | Flow cytometric analysis of WB lymphocyte-like cells from Atlantic salmon. Brightfield (BF) area (x axis; cell size) *vs* side scatter (SSC) intensity (y axis; cell complexity) plot shows WB leukocyte population from fish (n = 10) fed **(A)** CO or **(B)** SO feeds. Representative images of cells captured with 40× objective from each gate are shown. Scale bar = 10 µm. **(C)** Plot showing the percentage of WB lymphocyte-like cells from fish (n = 10) from the two groups. The 10 dots are values from the 10 fish. The differences were considered significant at $p < 0.05$, indicated with an asterisk.

alter expression of genes in the organ, as described in a review article (31). In the present study, we did not detect any DEGs in the head kidney similar to the transcriptome investigation by Tacchi et al. (32) that compared marine protein- and plant protein-based diets; no common genes were expressed in the intestine, muscle, and liver. Diet-induced inflammation may affect systemic response as reported for salmon fed soybean based on 44 common genes expressed in the intestine and liver (33). Furthermore, diets did not alter the HK transcripts in fish, but the responses became evident 24 h after injection with the viral mimic polyriboinosinic polyribocytidylic acid (34). In the present study, we did not find a significant impact of the soy products on the HK transcriptome. The lack of response in HK seems to indicate that it is not the optimal organ to check the diet-induced changes in transcriptome. However, future studies should consider the changes in the liver transcriptome, a metabolically active organ.

## Soy Products Evoked Inflammation-Associated Signals in the Intestine

Bacterial entry through a breach in the epithelial barrier due to defective functions and aberrant innate immune responses are accountable for evoking intestinal inflammation in humans (35). Such an inflammation triggers the transcriptional activation of selected immune-related genes (36).

Cathelicidin genes, *cathl1* and *cathl2*, are known to be expressed in the DI of salmon and were stimulated by pathogenic bacteria; in our study they were upregulated in the

DI of fish from the SO group (**Supplementary Figure 6**). Human cathelicidin, LL-37 mRNA, was increased significantly in the inflamed mucosa of ulcerative colitis and Crohn's disease (37). In addition, it is interesting to note that both *lysozyme CII* and *tumor necrosis factor receptor superfamily member 1B-like* were upregulated. Based on mammalian studies, it is known that pathogen associated molecular patterns are recognized by toll-like receptors that activate the MyD88-independent pathway including the TNF (Tumor necrosis factor) receptor associated factor 6 (TRAF6), which is associated with TNF receptor superfamily (38). Tafalla and Granja (39) have reviewed the involvement of mammalian TNF receptor superfamily 1B (TNFRSF1B) in human T cell activation, and they have suggested the same function in fishes. Another pro-inflammatory mediator, Galectin 3 (40), was altered in inflamed tissues of humans (41), as reported here. A study on striped murrel *Channa striatus* revealed the ability of a galectin, CsGal-1, to agglutinate Gram-negative bacteria (42). Galectin-3 in mammals is known to recognize 'self' glycans generally but can interact with the lipopolysaccharide (LPS) of bacteria (43). Galectin-3 is secreted by inflammatory macrophages, and its induced secretion is perceived as a danger signal by the innate immune system (44, 45). The intestinal epithelial breach in the SO group, probably resulting from the unwanted reaction, may have possibly facilitated the entry of bacteria through the mucosal barriers and altered the expression of *gal3*.

Metallothionein is an anti-inflammatory mediator. After LPS treatment, metallothionein knock-out mice showed inflammatory responses in the lung epithelial cells suggesting that metallothionein is involved in cytoprotection during LPS-related inflammation (46). In the present study, metallothionein A was downregulated in the SO group, indicating a possible connection between metallothionein A and intestinal inflammation.

Retinol-binding protein transports vitamin A from the liver to other tissues like the intestine (47). It has been reported that tissue injury during inflammation causes a reduction in the synthesis of retinol-binding protein (48). In our study, the mRNA level of retinol binding protein II in the SO group was significantly downregulated. Notably, a study on humans reported that its concentration in serum decreases during the acute-phase stage of inflammation (49).

As observed in the salmon intestine, the mRNA levels of Annexin A2 were higher in the inflamed mucosa of patients with Crohn's disease (50). Intestinal epithelial cell turnover prevents pathogen colonization (51), and the actin-binding protein, Annexin A2, is necessary for the movement of intestinal epithelial cells during wound resealing (52). A link between *anxa1* and gastroprotection was suggested in an earlier study on Atlantic salmon (16).

## Soy Products Also Impaired the Transport Mechanisms and Metabolism in the Intestine

Intestinal junctional molecules play key roles in sustaining epithelial integrity (35). Dysregulation of epithelial transport or entry of opportunistic microbes through the breaches in epithelial barrier can cause intestinal inflammation (51). The characteristic selective permeability of the epithelial barrier to ions, through gating of ion channels, enables directional transport of ions (53). Chloride channel proteins form gated pores for the passage of anions, and this process is dependent on transmembrane voltage, pH, cell-swelling and phosphorylation (54). The $Cl^-$ exits basolaterally, among other means, *via* $K^+/Cl^-$ cotransport, $Cl^-$ channel (55), and genes associated with chloride channel proteins were downregulated in the fish fed the soy products. In addition, solute carrier families are involved in ion transport across the apical membrane of fish intestine (55). *Slc6a6* is a sodium and chloride-ion dependent transporter that transports taurine and beta-alanine *via* intestinal brush border (56), and this gene was upregulated in the SO group, and the associated pathways that were enriched were taurine and beta-alanine pathways. Furthermore, $Cl^-/HCO3^-$ exchange and active transport of most neutral amino acids at the apical membrane of the fish intestine are performed by *slc26a6* and *slc6a19*, respectively (55). These solute carrier families were downregulated in salmon that were prone to the unwanted reaction. Furthermore, the enriched GO terms included chloride channel activity, voltage-gated channel activity, voltage-gated anion activity, anion channel activity *etc*. We also observed a dysregulation in other activities, *viz*. transmembrane transporter activity and symporter activity in the SO group. In addition, *slc5a1*, the key mediator of glucose and galactose uptake from the lumen, and *slc25a48*, mitochondrial amino acid transporter were upregulated, and *kcnab2* (*Potassium voltage-gated channel subfamily A regulatory beta subunit 2*), which has a role in electrolyte transport, was downregulated in the SO group. Such aberrations in humans can lead to irregular nutrient absorption (57) and disturbances in the luminal fluid microenvironment (53). The alterations in iron ion, oxygen, heme, and amino acid binding GO terms, based on the downregulated genes, and NADP, vitamins, and coenzyme binding, based on upregulated genes, also point to the impaired transport mechanisms across the epithelial layer in the SO group. Other studies have also reported the effect of soybean feeding on transporter proteins, which eventually may have a bearing on the transport of nutrients *via* epithelia. In one of them, the soybean meal–wheat gluten combination affected the expression of aquaporins, ion transporters, tight junction, and adherens junction proteins in the DI of Atlantic salmon, although the genes associated with chloride channels remained unchanged (10). Furthermore, Atlantic salmon fed soy saponins alone and soy saponin in combination with soybean meal had aberrations in intestinal permeability (12). The transcriptional changes of the genes linked to the transporter proteins may be indicating disturbances in the transport of essential nutrients and the associated pathways.

Although we identified some enriched pathways linked to the upregulated genes, there was not much overlap in the pathways we obtained and those reported previously. Based on current as well as earlier studies, steroid biosynthesis and xenobiotic metabolism (13, 33) can be highlighted as the two metabolic pathways altered by dietary soybean products. Downregulation of hepatic cytochrome P450s and other drug-metabolizing enzymes are linked to inflammation (58). Furthermore, CYP1A1, an enzyme in the phase I of the reactions which helps in the excretion of endogenous (*e.g.* steroids) and exogenous (*e.g.* drugs) substances

(59), was lower in the colonic enterocytes of patients suffering from Crohn's disease and ulcerative colitis (60). Our observation on Atlantic salmon also corroborates with this finding. The biosynthesis of steroids was enriched in the SO group, and the enrichment of two cytochrome P450-associated pathways could be indicating the need to alleviate the toxicity of steroids and soy saponin.

Hypotaurine is essential for the biosynthesis of the abundant free amino acid taurine, which has roles in innate immunity of mammals (61). High levels of this semi-essential amino acid reduce oxidative stress due to its antioxidant properties (62). In humans, taurine and $\beta$-alanine transport in the intestine takes place with the help of transporters like $Na^+$- and $Cl^-$-dependent TauT (SLC6A6) (56). Taurine is linked to growth and health of fish (63). A gene that is related to biosynthesis of taurine, *csad*, was upregulated in the distal intestine of fish from the SO group. It seems that *slc6a6*, *csad*, taurine, and hypotaurine metabolism pathways are associated with the inflammatory condition.

### Dietary Soy Components Affect Blood Lymphocyte Counts

The head kidney is the major hematopoietic organ in teleost fish, having roles similar to those of the mammalian bone marrow. Hematopoietic stem cells in the organ are capable of self-renewal and differentiating into cells of erythroid, myeloid, and lymphoid lineages (64). Injuries during inflammation or metabolic changes are known to influence the size and fate of hematopoietic stem cells (65). It has also been reported that systemic response during inflammation increased the number of granulocytes and monocytes in mice bone marrow (66). In the present study, we observed a significant increase in blood lymphocyte-like cell counts in fish fed the inflammation-causing soybean products compared to those of control. It is reported that in humans, the patrolling naive lymphocytes enter the gut and undergo activation and priming based on the condition in the intestine (67). The increase in blood lymphocyte counts of fish that developed inflammation is possibly indicative of the cell recruitment to quell the localised intestinal inflammation.

## CONCLUSIONS

The soybean–soy saponin combination induced DI inflammation in Atlantic salmon. The transcriptional changes associated with inflammation could be linked to disturbances in transport mechanisms as well as drug and taurine and hypotaurine metabolisms and steroid biosynthesis in the DI of the fish. The HK transcriptome was largely unaffected during intestinal injury. However, this needs to be verified as the increased lymphocyte numbers in the peripheral blood of the fish with intestinal inflammation may in fact be suggesting otherwise. Further investigations on the dysregulated intestinal barrier functions, reported here, will help to broaden our understanding of the intestinal inflammation in fish. The key genes involved in solute transport across the epithelial barrier such as *clcn1*, *clcn2*, *slc26a6*, *slc6a19* and immune genes such as *cath1*, *cath2*, *gal3*, *rbp2*, *mta* could serve as possible biomarkers of diet-associated intestinal inflammation and be used in further comparative studies on inflammation in mammalian models.

## DATA AVAILABILITY STATEMENT

The datasets presented in this study can be found in online repositories. Additional data and figures are presented in **Supplementary Material**.

## ETHICS STATEMENT

The animal study was reviewed and approved by the Norwegian Animal Research Authority, FDU (Forsøksdyrutvalget ID-10050). We adhered to the rules and regulations of animal welfare and followed the standard biosecurity and safety procedures at the Research Station of Nord University, Bodø, Norway.

## AUTHOR CONTRIBUTIONS

VK, VVT, JF, MS, and JD designed the research. JD and VVT were responsible for feed formulation and development. GV supervised the feeding experiments and gene expression study. YP and PS performed the RNA-Seq studies and analyses of data. YP performed the flow cytometry studies. DD performed the histology study. VK wrote the first version of the manuscript, along with YP and PS. All authors contributed to the article and approved the submitted version.

## FUNDING

This study was undertaken as part of a collaborative project "Molecular studies on the intestine of Atlantic salmon" between Nord University and DSM Nutritional Products, Switzerland, funded by the latter.

## ACKNOWLEDGMENTS

The authors acknowledge the support from the staff at the Research Station, Nord University, Bodø. The authors are grateful to Bisa Saraswathy for her help in data analysis, preparation of figures and manuscript.

## SUPPLEMENTARY MATERIAL

The Supplementary Material for this article can be found online at: https://www.frontiersin.org/articles/10.3389/fimmu.2020.596514/full#supplementary-material

**SUPPLEMENTARY FIGURE 1 |** Photomicrographs of the distal intestine of Atlantic salmon from CO and SO groups. **(A)** Inflammatory symptoms are not visible

in the SO group on day 4 after the start of the feeding trial. **(B)** Saponin-induced inflammatory characteristics become visible at day 36 after the start of the feeding. Control group—CO, and soy-derivatives fed group—SO. Scale bar: 100 µm.

**SUPPLEMENTARY FIGURE 2 |** Overview of the bioinformatics workflow adopted in this study. RNA-Seq data were first quality filtered, after which the reads were aligned to salmon genome. Next, the read counts were extracted, and then upregulated/downregulated genes were identified for the downstream analysis. KEGG pathway and GO term enrichment analysis were then performed employing the differentially expressed genes.

**SUPPLEMENTARY FIGURE 3 |** Dispersion estimates and minus over average expression plots of the data from the distal intestine. **(A)** Plots showing the shrinkage of the gene-wise dispersions—the maximum-likelihood estimates obtained from the gene data (black) are shrunk towards the fitted red curve to get the final values (blue) of dispersion. **(B)** Shrinkage of the logarithmic fold-change—the differentially expressed genes with adjusted $p < 0.05$ are shown as red dots.

**SUPPLEMENTARY FIGURE 4 |** Dispersion estimates and minus over average expression plots based on the data from the head kidney. **(A)** Plots showing the shrinkage of the gene-wise dispersions—the maximum-likelihood estimates obtained from the gene data (black) are shrunk towards the fitted red curve to get the final values (blue) of dispersion. **(B)** Shrinkage of the logarithmic fold-change—the differentially expressed genes with adjusted $p < 0.05$ are shown as red dots.

**SUPPLEMENTARY FIGURE 5 |** Heatmap showing the 53 upregulated and 38 downregulated genes in the distal intestine of Atlantic salmon. Normalized gene count was input into the pheatmap function, and the values were centered and scaled in the row direction. The column names at the bottom of the heatmap indicate the control (prefix CO) and the soybean-derivative (saponin group with prefix SO) fed groups.

**SUPPLEMENTARY FIGURE 6 |** Relative mRNA levels of the selected 15 genes in the distal intestine of Atlantic salmon from the CO and SO groups at day 36. The gene expression of control (CO) and soybean fed groups (SO) ($n = 6$) is shown. Asterisks indicate $^{**}p < 0.01$ and $^{***}p < 0.001$.

**SUPPLEMENTARY FIGURE 7 |** Correlation between the relative mRNA levels and read counts of the selected differentially expressed genes. The bar on the right side indicates the correlation coefficient; darker shades of red and blue indicate negative and positive correlations, respectively. X indicates non-significant differences based on Spearman correlation test. If the correlation coefficient is + or –0.75, $3/4^{th}$ of the circles will be shaded.

**SUPPLEMENTARY TABLE 1 |** Details of ingredients in the experimental feeds.

**SUPPLEMENTARY TABLE 2 |** Details of raw reads, cleaned reads and mapped reads from different samples.

**SUPPLEMENTARY TABLE 3 |** Details of differentially upregulated genes in the SO group compared to the CO group.

**SUPPLEMENTARY TABLE 4 |** Details of differentially downregulated genes in the SO group compared to the CO group.

**SUPPLEMENTARY TABLE 5 |** Details of differentially regulated genes in the SO group compared to the CO group.

# REFERENCES


1. Ytrestøyl T, Aas TS, Åsgård T. Utilisation of feed resources in production of Atlantic salmon (*Salmo salar*) in Norway. *Aquaculture* (2015) 448:365–74. doi: 10.1016/j.aquaculture.2015.06.023
2. Buttle LG, Burrells AC, Good JE, Williams PD, Southgate PJ, Burrells C. The binding of soybean agglutinin (SBA) to the intestinal epithelium of Atlantic salmon, *Salmo salar* and rainbow trout, *Oncorhynchus mykiss*, fed high levels of soybean meal. *Vet Immunol Immunopathol* (2001) 80(3):237–44. doi: 10.1016/S0165-2427(01)00269-0
3. Zhang J-X, Guo L-Y, Feng L, Jiang W-D, Kuang S-Y, Liu Y, et al. Soybean β-conglycinin induces inflammation and oxidation and causes dysfunction of intestinal digestion and absorption in fish. *PLoS One* (2013) 8(3):e58115. doi: 10.1371/journal.pone.0058115
4. Bakke A. "Pathophysiological and immunological characteristics of soybean meal-induced enteropathy in salmon: Contribution of recent molecular investigations". In: LE Cruz-Suárez, D Ricque-Marie, M Tapia-Salazar, MG Nieto-López, DA Villarreal-Cavazos, J Gamboa-Delgado, L Hernández-Hernández, editors. *Avances en Nutrición Acuícola XI - Memorias del Décimo Primer Simposio Internacional de Nutrición Acuícola*. Universidad Autónoma de Nuevo León, Monterrey, México: San Nicolás de los Garza, N. L., México (2011). p. 345–72.
5. Desai AR, Links MG, Collins SA, Mansfield GS, Drew MD, Van Kessel AG, et al. Effects of plant-based diets on the distal gut microbiome of rainbow trout (*Oncorhynchus mykiss*). *Aquaculture* (2012) 350–353:134–42. doi: 10.1016/j.aquaculture.2012.04.005
6. Green TJ, Smullen R, Barnes AC. Dietary soybean protein concentrate-induced intestinal disorder in marine farmed Atlantic salmon, *Salmo salar* is associated with alterations in gut microbiota. *Vet Microbiol* (2013) 166 (1):286–92. doi: 10.1016/j.vetmic.2013.05.009
7. Nayak SK. Role of gastrointestinal microbiota in fish. *Aquac Res* (2010) 41 (11):1553–73. doi: 10.1111/j.1365-2109.2010.02546.x
8. Sørensen M, Penn M, El-Mowafi A, Storebakken T, Chunfang C, Øverland M, et al. Effect of stachyose, raffinose and soya-saponins supplementation on nutrient digestibility, digestive enzymes, gut morphology and growth performance in Atlantic salmon (*Salmo salar*, L). *Aquaculture* (2011) 314 (1):145–52. doi: 10.1016/j.aquaculture.2011.02.013
9. Refstie S, Korsøen ØJ, Storebakken T, Baeverfjord G, Lein I, Roem AJ. Differing nutritional responses to dietary soybean meal in rainbow trout (*Oncorhynchus mykiss*) and Atlantic salmon (*Salmo salar*). *Aquaculture* (2000) 190(1):49–63. doi: 10.1016/S0044-8486(00)00382-3
10. Hu H, Kortner TM, Gajardo K, Chikwati E, Tinsley J, Krogdahl Å. Intestinal fluid permeability in Atlantic salmon (*Salmo salar* L.) is affected by dietary protein source. *PLoS One* (2016) 11(12):e0167515. doi: 10.1371/journal.pone.0167515
11. Sahlmann C, Sutherland BJG, Kortner TM, Koop BF, Krogdahl Å, Bakke AM. Early response of gene expression in the distal intestine of Atlantic salmon (*Salmo salar* L.) during the development of soybean meal induced enteritis. *Fish Shellfish Immunol* (2013) 34(2):599–609. doi: 10.1016/j.fsi.2012.11.031
12. Knudsen D, Jutfelt F, Sundh H, Sundell K, Koppe W, Frøkiær H. Dietary soya saponins increase gut permeability and play a key role in the onset of soyabean-induced enteritis in Atlantic salmon (*Salmo salar* L.). *Br J Nutr* (2008) 100(1):120–9. doi: 10.1017/S0007114507886338
13. Kortner TM, Skugor S, Penn MH, Mydland LT, Djordjevic B, Hillestad M, et al. Dietary soyasaponin supplementation to pea protein concentrate reveals nutrigenomic interactions underlying enteropathy in Atlantic salmon (*Salmo salar*). *BMC Vet Res* (2012) 8(1):101. doi: 10.1186/1746-6148-8-101
14. Gu M, Jia Q, Zhang Z, Bai N, Xu X, Xu B. Soya-saponins induce intestinal inflammation and barrier dysfunction in juvenile turbot (*Scophthalmus maximus*). *Fish Shellfish Immunol* (2018) 77:264–72. doi: 10.1016/j.fsi.2018.04.004
15. Zhang C, Rahimnejad S, Wang Y-r, Lu K, Song K, Wang L, et al. Substituting fish meal with soybean meal in diets for Japanese seabass (*Lateolabrax japonicus*): Effects on growth, digestive enzymes activity, gut histology, and expression of gut inflammatory and transporter genes. *Aquaculture* (2018) 483:173–82. doi: 10.1016/j.aquaculture.2017.10.029
16. Vasanth G, Kiron V, Kulkarni A, Dahle D, Lokesh J, Kitani Y. A microbial feed additive abates intestinal inflammation in Atlantic salmon. *Front Immunol* (2015) 6:409. doi: 10.3389/fimmu.2015.00409
17. Bancroft J, Gamble M. *Theory and practice of histological techniques*. London, UK: Churchill Livingstone (2007). p. 125–38.
18. Siriyappagouder P, Galindo-Villegas J, Dhanasiri AK, Zhang Q, Mulero V, Kiron V, et al. *Pseudozyma* priming influences expression of genes involved in

metabolic pathways and immunity in zebrafish larvae. *Front Immunol* (2020) 11:978. doi: 10.3389/fimmu.2020.00978
19. Martin M. Cutadapt removes adapter sequences from high-throughput sequencing reads. *EMBnet J* (2011) 17(1):10–12. doi: 10.14806/ej.17.1.200
20. Love MI, Huber W, Anders S. Moderated estimation of fold change and dispersion for RNA-seq data with DESeq2. *Genome Biol* (2014) 15(12):550–0. doi: 10.1186/s13059-014-0550-8
21. Morgan M. *AnnotationHub: Client to access AnnotationHub resources*. *Bioconductor* (2019), R package version 2.16.0.
22. Yu G, Wang L-G, Han Y, He Q-Y. clusterProfiler: An R package for comparing biological themes among gene clusters. *OMICS* (2012) 16 (5):284–7. doi: 10.1089/omi.2011.0118
23. Hong G, Zhang W, Li H, Shen X, Guo Z. Separate enrichment analysis of pathways for up-and downregulated genes. *J R Soc Interface* (2014) 11 (92):20130950. doi: 10.1098/rsif.2013.0950
24. Wickham H. *ggplot2: Elegant Graphics for Data Analysis (Use R!)*. Houston, USA: Springer (2016).
25. Pedersen TL. *Package "ggraph"*. *Bioconductor* (2018), R package Version 1.0.2.
26. Vandesompele J, De Preter K, Pattyn F, Poppe B, Van Roy N, De Paepe A, et al. Accurate normalization of real-time quantitative RT-PCR data by geometric averaging of multiple internal control genes. *Genome Biol* (2002) 3(7):research0034.1. doi: 10.1186/gb-2002-3-7-research0034
27. Park Y, Abihssira-García IS, Thalmann S, Wiegertjes GF, Barreda DR, Olsvik PA, et al. Imaging flow cytometry protocols for examining phagocytosis of microplastics and bioparticles by immune cells of aquatic animals. *Front Immunol* (2020) 11:203. doi: 10.3389/fimmu.2020.00203
28. Wehkamp J, Götz M, Herrlinger K, Steurer W, Stange EF. Inflammatory bowel disease. *Dtsch Arztebl Int* (2016) 113(5):72–82. doi: 10.3238/arztebl.2016.0072
29. Krogdahl Å, Bakke-McKellep AM, Baeverfjord G. Effects of graded levels of standard soybean meal on intestinal structure, mucosal enzyme activities, and pancreatic response in Atlantic salmon (*Salmo salar* L.). *Aquac Nutr* (2003) 9 (6):361–71. doi: 10.1046/j.1365-2095.2003.00264.x
30. Krogdahl Å, Gajardo K, Kortner TM, Penn M, Gu M, Berge GM, et al. Soya saponins induce enteritis in Atlantic salmon (*Salmo salar* L.). *J Agric Food Chem* (2015) 63(15):3887–902. doi: 10.1021/jf506242t
31. Martin SAM, Król E. Nutrigenomics and immune function in fish: New insights from omics technologies. *Dev Comp Immunol* (2017) 75:86–98. doi: 10.1016/j.dci.2017.02.024
32. Tacchi L, Secombes CJ, Bickerdike R, Adler MA, Venegas C, Takle H, et al. Transcriptomic and physiological responses to fishmeal substitution with plant proteins in formulated feed in farmed Atlantic salmon (*Salmo salar*). *BMC Genomics* (2012) 13(1):363. doi: 10.1186/1471-2164-13-363
33. De Santis C, Bartie KL, Olsen RE, Taggart JB, Tocher DR. Nutrigenomic profiling of transcriptional processes affected in liver and distal intestine in response to a soybean meal-induced nutritional stress in Atlantic salmon (*Salmo salar*). *Comp Biochem Physiol Part D Genomics Proteomics* (2015) 15:1–11. doi: 10.1016/j.cbd.2015.04.001
34. Caballero-Solares A, Hall JR, Xue X, Eslamloo K, Taylor RG, Parrish CC, et al. The dietary replacement of marine ingredients by terrestrial animal and plant alternatives modulates the antiviral immune response of Atlantic salmon (*Salmo salar*). *Fish Shellfish Immunol* (2017) 64:24–38. doi: 10.1016/j.fsi.2017.02.040
35. Geremia A, Biancheri P, Allan P, Corazza GR, Di Sabatino A. Innate and adaptive immunity in inflammatory bowel disease. *Autoimmun Rev* (2014) 13 (1):3–10. doi: 10.1016/j.autrev.2013.06.004
36. Ahmed AU, Williams BRG, Hannigan GE. Transcriptional activation of inflammatory genes: Mechanistic insight into selectivity and diversity. *Biomolecules* (2015) 5(4):3087–111. doi: 10.3390/biom5043087
37. Kusaka S, Nishida A, Takahashi K, Bamba S, Yasui H, Kawahara M, et al. Expression of human cathelicidin peptide LL-37 in inflammatory bowel disease. *Clin Exp Immunol* (2018) 191(1):96–106. doi: 10.1111/cei.13047
38. Akira S, Uematsu S, Takeuchi O. Pathogen recognition and innate immunity. *Cell* (2006) 124(4):783–801. doi: 10.1016/j.cell.2006.02.015
39. Tafalla C, Granja AG. Novel Insights on the regulation of B cell functionality by members of the tumor necrosis factor superfamily in jawed fish. *Front Immunol* (2018) 9:1285. doi: 10.3389/fimmu.2018.01285
40. Sundblad V, Quintar AA, Morosi LG, Niveloni SI, Cabanne A, Smecuol E, et al. Galectins in intestinal inflammation: Galectin-1 expression delineates response to treatment in celiac disease patients. *Front Immunol* (2018) 9:379. doi: 10.3389/fimmu.2018.00379
41. Papa Gobbi R, De Francesco N, Bondar C, Muglia C, Chirdo F, Rumbo M, et al. A galectin-specific signature in the gut delineates Crohn's disease and ulcerative colitis from other human inflammatory intestinal disorders. *BioFactors* (2016) 42(1):93–105. doi: 10.1002/biof.1252
42. Arasu A, Kumaresan V, Sathyamoorthi A, Chaurasia MK, Bhatt P, Gnanam AJ, et al. Molecular characterization of a novel proto-type antimicrobial protein galectin-1 from striped murrel. *Microbiol Res* (2014) 169(11):824–34. doi: 10.1016/j.micres.2014.03.005
43. Mey A, Leffler H, Hmama Z, Normier G, Revillard JP. The animal lectin galectin-3 interacts with bacterial lipopolysaccharides via two independent sites. *J Immunol* (1996) 156(4):1572–7.
44. Sato S, Nieminen J. Seeing strangers or announcing "danger": Galectin-3 in two models of innate immunity. *Glycoconj J* (2002) 19(7):583–91. doi: 10.1023/B:GLYC.0000014089.17121.cc
45. Sato S. Galectins as molecules of danger signal, which could evoke an immune response to infection. *Trends Glycosci Glycotechnol* (2002) 14(79):285–301. doi: 10.4052/tigg.14.285
46. Inoue K-i, Takano H, Shimada A, Satoh M. Metallothionein as an anti-inflammatory mediator. *Mediators Inflamm* (2009) 2009:7. doi: 10.1155/2009/101659
47. Hebiguchi T, Mezaki Y, Morii M, Watanabe R, Yoshikawa K, Miura M, et al. Massive bowel resection upregulates the intestinal mRNA expression levels of cellular retinol-binding protein II and apolipoprotein A-IV and alters the intestinal vitamin A status in rats. *Int J Mol Med* (2015) 35(3):724–30. doi: 10.3892/ijmm.2015.2066
48. Rosales FJ, Ritter SJ, Zolfaghari R, Smith JE, Ross AC. Effects of acute inflammation on plasma retinol, retinol-binding protein, and its mRNA in the liver and kidneys of vitamin A-sufficient rats. *J Lipid Res* (1996) 37(5):962–71.
49. Larson LM, Namaste SM, Williams AM, Engle-Stone R, Addo OY, Suchdev PS, et al. Adjusting retinol-binding protein concentrations for inflammation: Biomarkers Reflecting Inflammation and Nutritional Determinants of Anemia (BRINDA) project. *Am J Clin Nutr* (2017) 106(suppl_1):390S–401S. doi: 10.3945/ajcn.116.142166
50. Zhang Z, Zhao X, Lv C, Li C, Zhi F. Annexin A2 expression in intestinal mucosa of patients with inflammatory bowel disease and its clinical implications. *Nan Fang Yi Ke Da Xue Xue Bao* (2012) 32(11):1548–52.
51. Ramanan D, Cadwell K. Intrinsic defense mechanisms of the intestinal epithelium. *Cell Host Microbe* (2016) 19(4):434–41. doi: 10.1016/j.chom.2016.03.003
52. Rankin CR, Hilgarth RS, Leoni G, Kwon M, Den Beste KA, Parkos CA, et al. Annexin A2 regulates β1 integrin internalization and intestinal epithelial cell migration. *J Biol Chem* (2013) 288(21):15229–39. doi: 10.1074/jbc.M112.440909
53. Chan HC, Chen H, Ruan Y, Sun T. Physiology and pathophysiology of the epithelial barrier of the female reproductive tract: Role of ion channels. *Adv Exp Med Biol* (2012) 763:193–217. doi: 10.1007/978-1-4614-4711-5_10
54. Mindell JA, Maduke M. ClC chloride channels. *Genome Biol* (2001) 2(2): REVIEWS3003. doi: 10.1186/gb-2001-2-2-reviews3003
55. Grosell M. Chapter 4 - The role of the gastrointestinal tract in salt and water balance. In: M Grosell, AP Farrell, CJ Brauner, editors. *Fish Physiology: The Multifunctional Gut of Fish*. Cambridge, Massachusetts, United States: Academic Press (2010). p. 135–64.
56. Anderson CMH, Howard A, Walters JRF, Ganapathy V, Thwaites DT. Taurine uptake across the human intestinal brush-border membrane is via two transporters: H+-coupled PAT1 (SLC36A1) and Na+- and Cl (-)-dependent TauT (SLC6A6). *J Physiol* (2009) 587(Pt 4):731–44. doi: 10.1113/jphysiol.2008.164228
57. Perez-Torras S, Iglesias I, Llopis M, Lozano JJ, Antolin M, Guarner F, et al. Transportome profiling identifies profound alterations in Crohn's disease partially restored by commensal bacteria. *J Crohns Colitis* (2016) 10(7):850–9. doi: 10.1093/ecco-jcc/jjw042
58. Morgan E. Impact of infectious and inflammatory disease on cytochrome P450–mediated drug metabolism and pharmacokinetics. *Clin Pharmacol* (2009) 85(4):434–8. doi: 10.1038/clpt.2008.302

59. Sen A, Stark H. Role of cytochrome P450 polymorphisms and functions in development of ulcerative colitis. *World J Gastroenterol* (2019) 25(23):2846–62. doi: 10.3748/wjg.v25.i23.2846
60. Plewka D, Plewka A, Szczepanik T, Morek M, Bogunia E, Wittek P, et al. Expression of selected cytochrome P450 isoforms and of cooperating enzymes in colorectal tissues in selected pathological conditions. *Pathol Res Pract* (2014) 210(4):242–9. doi: 10.1016/j.prp.2013.12.010
61. Schuller-Levis GB, Park E. Taurine and its chloramine: Modulators of immunity. *Neurochem Res* (2004) 29(1):117–26. doi: 10.1023/B:NERE.0000010440.37629.17
62. Oliveira MW, Minotto JB, de Oliveira MR, Zanotto-Filho A, Behr GA, Rocha RF, et al. Scavenging and antioxidant potential of physiological taurine concentrations against different reactive oxygen/nitrogen species. *Pharmacol Rep* (2010) 62(1):185–93. doi: 10.1016/s1734-1140(10)70256-5
63. Wei Y, Liang M, Xu H, Zheng K. Taurine alone or in combination with fish protein hydrolysate affects growth performance, taurine transport and metabolism in juvenile turbot (*Scophthalmus maximus* L.). *Aquac Nutr* (2019) 25(2):396–405. doi: 10.1111/anu.12865
64. Kobayashi I, Katakura F, Moritomo T. Isolation and characterization of hematopoietic stem cells in teleost fish. *Dev Comp Immunol* (2016) 58:86–94. doi: 10.1016/j.dci.2016.01.003
65. Xia S, X-p L, Cheng L, Han M-T, Zhang M-M, Shao Q-X, et al. Fish oil-rich diet promotes hematopoiesis and alters hematopoietic niche. *J Endocrinol* (2015) 156(8):2821–30. doi: 10.1210/en.2015-1258
66. Ueda Y, Kondo M, Kelsoe G. Inflammation and the reciprocal production of granulocytes and lymphocytes in bone marrow. *J Exp Med* (2005) 201(11):1771–80. doi: 10.1084/jem.20041419
67. Habtezion A, Nguyen LP, Hadeiba H, Butcher EC. Leukocyte trafficking to the small intestine and colon. *Gastroenterology* (2016) 150(2):340–54. doi: 10.1053/j.gastro.2015.10.046

**Conflict of Interest:** JD is employed by the company SPAROS Lda. Olhão, Portugal. VVT was employed by the company DSM Nutritional Products, Global Innovations, Kaiseraugst, Switzerland.

The remaining authors declare that the research was conducted in the absence of any commercial or financial relationships that could be construed as a potential conflict of interest.

The authors declare that this study received funding from DSM Nutritional Products. The funder had the following involvement in the study: research design and feed formulation.

frontiers in Immunology

ORIGINAL RESEARCH
published: 23 December 2020
doi: 10.3389/fimmu.2020.615536

# Short-Chain Fatty Acids Promote Intracellular Bactericidal Activity in Head Kidney Macrophages From Turbot (*Scophthalmus maximus* L.) *via* Hypoxia Inducible Factor-1α

*Jinjin Zhang*[1], *Hui Zhang*[1], *Miao Liu*[1], *Yawen Lan*[1], *Huiyuan Sun*[1], *Kangsen Mai*[1,2] *and Min Wan*[1,2*]

[1] Key Laboratory of Aquaculture Nutrition and Feed, Ministry of Agriculture & Key Laboratory of Mariculture, Ministry of Education, College of Fisheries, Ocean University of China, Qingdao, China, [2] Pilot National Laboratory of Marine Science and Technology, Qingdao, China

OPEN ACCESS

**Edited by:**
Jun Li,
Lake Superior State University, United States

**Reviewed by:**
Zhi Luo,
Huazhong Agricultural University, China
Yong-hua Hu,
Chinese Academy of Tropical Agricultural Sciences, China

***Correspondence:**
Min Wan
wanmin@ouc.edu.cn

**Specialty section:**
This article was submitted to Comparative Immunology, a section of the journal Frontiers in Immunology

**Received:** 09 October 2020
**Accepted:** 18 November 2020
**Published:** 23 December 2020

**Citation:**
Zhang J, Zhang H, Liu M, Lan Y, Sun H, Mai K and Wan M (2020) Short-Chain Fatty Acids Promote Intracellular Bactericidal Activity in Head Kidney Macrophages From Turbot (Scophthalmus maximus L.) via Hypoxia Inducible Factor-1α. Front. Immunol. 11:615536. doi: 10.3389/fimmu.2020.615536

Short-chain fatty acids (SCFAs) are mainly produced by microbiota through the fermentation of carbohydrates in the intestine. Acetate, propionate, and butyrate are the most abundant SCFA metabolites and have been shown to be important in the maintenance of host health. In this study, head kidney macrophages (HKMs) were isolated and cultured from turbots. We found that the antibacterial activity of HKMs was increased after these cells were incubated with sodium butyrate, sodium propionate or sodium acetate. Interestingly, our results showed that all three SCFAs enhanced the expression of hypoxia inducible factor-1 α (HIF-1α) in HKMs, and further study confirmed that butyrate augmented the oxygen consumption of these cells. Moreover, HIF-1α inhibition diminished the butyrate-promoted intracellular bacterial killing activity of macrophages, and SCFAs also raised the gene expression and activity of lysozymes in HKMs *via* HIF-1α signaling. In addition, our results suggested that butyrate induced HIF-1α expression and the bactericidal activity of HKMs through histone deacetylase inhibition, while G protein-coupled receptors did not contribute to this effect. Finally, we demonstrated that butyrate induced a similar response in the murine macrophage cell line RAW264.7. In conclusion, our results demonstrated that SCFAs promoted HIF-1α expression *via* histone deacetylase inhibition, leading to the enhanced production of antibacterial effectors and increased bacterial killing of macrophages.

**Keywords: butyrate, propionate, acetate, lysozyme, histone deacetylase, reactive oxygen species**

## INTRODUCTION

Butyrate, propionate, and acetate, which are collectively called short-chain fatty acids (SCFAs), are products of the microbial fermentation of dietary fiber in the gut. It is well-known that SCFAs are important energy and signaling molecules, displaying beneficial effects on various physiological processes (1). In aquaculture, SCFAs have been used as growth promoters (2). Recently, the effects of SCFAs and their salts have been highlighted as immune stimulators on the health of aquatic organisms (2, 3). For example, Tian et al. demonstrated that the growth and intestinal immune functions of grass carp (*Ctenopharyngodon idella*) were improved when fish were fed a butyrate-supplemented diet, and fish receiving butyrate in their diet were protected from *Aeromonas hydrophila* infection (4). Moreover, a recent study from our research group reported that butyrate supplementation in turbot diet significantly alleviated high-soybean meal-induced enteritis (5).

In mammals, it has been demonstrated that SCFAs exert physiological functions either through the inhibition of histone deacetylases (HDACs) or the activation of G-protein-coupled receptors (GPCRs) (6). Histone deacetylation is mediated by HDACs, while HDAC inhibition induces histone hyperacetylation and reactivates suppressed genes (7). SCFAs are well-known HDAC inhibitors that have been shown to regulate the expression of numerous genes (8). Additionally, four GPCRs, GPR41, GPR43, GPR109A and Olfactory receptor 78 have been reported to mediate the different functions of SCFAs in higher animals. However, these receptors are still unknown in aquatic animals (3).

The head kidney of teleosts has been considered as a haemopoietic organ similar to the bone marrow of higher vertebrates, and it has been found that erythrocytes and leukocytes, such as macrophages, granulocytes and B lymphocytes, develop and differentiate in the teleost head kidney (9, 10). It is well-known that macrophages play a significant role in non-specific defense mechanisms in all vertebrates against invading pathogens. They have the capacity to kill pathogens through phagocytosis, production of reactive oxygen and nitrogen intermediates, and some antibacterial components, including lysozyme and antibacterial peptides (11). Therefore, head kidney macrophages (HKMs) of turbots have been isolated and utilized in our study to investigate the mechanism how SCFAs regulate the bactericidal activity of fish macrophages.

It is well-known that, hypoxia-inducible factors are the major signaling molecules that coordinate transcriptional responses to low-$O_2$ environments (12). Previous studies have shown that HIF-1$\alpha$ is essential for myeloid cell function and inflammatory responses (13), and Kelly et al. also emphasized the importance of HIF-1$\alpha$ stabilization by SCFAs in intestine homeostasis (14). Moreover, commensal bacteria induce HIF-1$\alpha$ expression, resulting in the activation of innate immune effectors to prevent *Candida albican*s colonization (15). In this study, we have affirmed that butyrate causes increased oxygen consumption and HIF-1$\alpha$ expression in HKMs. Furthermore, we provided evidence that SCFAs promote HIF-1$\alpha$ expression *via* HDAC inhibition in HKMs, leading to the elevated production of antimicrobial effectors and the suppression of bacterial survival in macrophages. Our study, for the first time, depicts a molecular mechanism describing how SCFAs promote bacterial clearance by macrophages in fish.

## MATERIALS AND METHODS

### Fish

Turbots (*Scophthalmus maximus* L.) of about 400–600 g in size were obtained from a commercial fish farm in Shandong Province, China. The fish were acclimatized in a seawater circulation system located in the Fisheries College of Ocean University of China for two weeks before the experiments. The fish were maintained in tanks (200 L) supplied with filtered, well-oxygenated and thermo-regulated seawater (salinity 35‰, temperature 17 ± 1°C), and were fed twice daily with commercial diets. No illness signs in these fish were observed during experiments. Husbandry and handling of the fish in the present study were performed strictly according to the Management Rule of Laboratory Animals (Chinese order no. 676 of the State Council, revised 1 March, 2017).

### Reagents

L-15 leibovitz cell culture medium and Dulbecco's modified eagle medium (DMEM) with high glucose were from HyClone (Logan, Utah, USA); FBS was obtained from Invitrogen (Carlsbad, CA, USA); antibiotics (penicillin, streptomycin, and amphotericin B), PBS, Percoll and trypan blue were from Solarbio (Beijing, China); sodium acetate, sodium propionate, sodium butyrate, and trichostatin A were purchased from Sigma (St. Louis, MO, USA); antibody against HIF-1$\alpha$, dimethyl-bisphenol A and chrysin were from Santa Cruz (Santa Cruz, CA, USA); BBoxiProbe™ R01 kit was from BestBio (Shanghai, China); RNAeasy™ animal RNA isolation kit, reactive oxygen species assay kit and DAF-FM DA were purchased from Beyotime (Shanghai, China); HiScript® III RT SuperMix for qPCR was from Vazyme (Nanjing, China); SYBR green qPCR kit was from Accurate Biology (Hunan, China); Pertussis toxin was obtained from APE×BIO (Houston, Texas, USA); Lysozyme assay kit was from Jiancheng (Nanjing, China).

### HKM Isolation

Macrophages were isolated according to the method described by Chung and Secombes (16). Briefly, the head kidney of the turbot was removed and immediately washed twice with L-15 medium supplemented with penicillin (100 KU/ml), streptomycin (10 mg/ml), and amphotericin B (25 μg/ml), before being cut into small pieces. Next, the small pieces were passed through a 100 μm nylon mesh, and the obtained cell suspension was washed twice in L-15 cell culture medium with antibiotics (penicillin, streptomycin, and amphotericin B) and 2% FBS, and centrifuged at 200 g for 5 min between washes. After that, the cell suspension was separated on a 34/51% Percoll density gradient by centrifugation at 400 g. After 30 min, the cells at the interface were collected and washed twice by centrifugation at 200 g for 5 min. The cell pellets were re-suspended in L-15 medium supplemented with antibiotics, and the viability of the cells was measured by trypan blue exclusion, indicating

that over 90% of the total number of cells were viable (data not shown). The cells were dispensed and cultured on different cell culture plates at 24°C. After 2 h, the non-adherent cells were washed off, and the adherent macrophages were kept in complete medium for further use.

The quality and purity of the adherent monolayers were further examined by Giemsa staining (**Supplementary Figure 1A**). When these adherent cells were analyzed by FACS (FC500, Beckman, USA), only one cell population was detected (**Supplementary Figure 1B**). Further analysis confirmed that the gene expression of macrophage colony-stimulating factor receptor (M-CSFR), a specific marker of macrophages (17), was much higher in adherent cells than in non-adherent cells (**Supplementary Figure 1C**).

## Bacterial Killing Assay

HKMs were incubated with SCFAs or additional reagents for 24 h, followed by washing three times with PBS. Afterwards, cells were incubated with equal numbers of *Edwardsiella tarda* (*E. tarda*) at 24°C under shaking. After 2 h, the cells were lysed in ice-cold water and then vortexed for 30 s. Thereafter, the cell lysates were serially diluted and plated on agar plates overnight at 28°C. The following day, viable bacteria were counted, and the bacterial survival rate was calculated.

## RNA Isolation and cDNA Transcription

RNA was extracted with the RNAeasy™ Animal RNA isolation kit according to the manufacturers' instructions. The quantity of total RNA was determined by using a NanoDrop spectrophotometer (NanoDrop Technologies), and the quality of the extracted RNA was determined by agarose gel electrophoresis. cDNA was synthesized from total RNA using HiScript III reverse transcriptase.

## Real-Time Quantitative PCR

The sequences of all primers used in this study are listed in **Table 1**. Real-time qPCR was performed using a thermo-cycler CFX96 instrument (BioRad). The expression of target genes was normalized to $\beta$-actin.

## Real-Time $O_2$ Consumption

The real-time $O_2$ consumption in these cells was measured using a BBoxiProbe™ R01 kit according to the manufacturers' instructions. Briefly, HKMs were cultured in a 96-well plate with a transparent bottom and black sides for 24 h. Next, 150 µl of complete medium containing sodium butyrate (NaB, 10 mM), and 10 µl of oxygen fluorescent probe was added. Meanwhile, 100 µl of blocking buffer was immediately added to each well to prevent external oxygen generation. After that, the plate was put in a microplate reader (FLUOstar Omega, BMG, Germany), and fluorescence was detected over 2 h at 2-min intervals. As the fluorescence of this oxygen probe can be quenched by $O_2$, the value of the fluorescence signal was inversely proportional to the amount of $O_2$ in each sample. The rate of oxygen consumption was calculated based on the changes of fluorescence signal over 2 h as follows: oxygen consumption rate (%) = (final fluorescence in NaB-treated cells − initial fluorescence in NaB-treated cells)/(final fluorescence in control cells − initial fluorescence in control cells) × 100%.

## Reactive Oxygen Species Assay

Reactive oxygen species (ROS) content was measured by using a ROS assay kit according to the manufacturer's instructions. Briefly, HKMs were cultured in a 96-well plate with a transparent bottom and black sides for 24 h. Thereafter, the cells were treated with NaB (10 mM) or control buffer for another 24 h. After the cells were washed with PBS three times, they were co-incubated with *E. tarda* (1:1) or control buffer for 2 h. After washing with PBS, the fluorescent probe DCFH-DA was added and incubated with cells for 30 min in the dark. After washing off redundant fluorescent probe, the fluorescence values in the cells were determined using a microplate reader (FLUOstar Omega, BMG, Germany). The wells without a fluorescent probe were set as a baseline control, while the wells containing cells treated with only control buffer were set as a negative control. ROS (%) = (fluorescence in the experimental well − fluorescence in the baseline control well)/(fluorescence in the negative control well − fluorescence in the baseline control well) × 100%.

## Nitric Oxide Assay

Nitric oxide (NO) production in HKMs was analyzed using a DAF-FM DA kit according to the manufacturer's instructions. HKMs were cultured in a 96-well plate and incubated with NaB (10 Mm) for 24 h. After washing with PBS three times, the cells were co-incubated with *E. tarda* (1:1) or control buffer for 2 h. The cells were washed again and then incubated with the fluorescent probe DAF-FM DA for 30 min in the dark. After the redundant fluorescent probe was removed, the fluorescence value of each well was determined using a microplate reader (FLUOstar Omega, BMG,

**TABLE 1** | Primer sequences used for gene expression analysis.

| Target genes | Forward primers (5′–3′) | Reverse primers (5′–3′) |
|---|---|---|
| Turbot *M-SCFR* | CTCCAATCAGAGGGCACCCAT | TCGGAACTGTCTCCCGTCCTT |
| Turbot *β-actin* | GCGTGACATCAAGGAGAAGC | TGGAAGGTGGACAGGGAAGC |
| Turbot *HIF-1α* | CCACCACCACTGACGATTCA | GCTGGGGTAGCTGTTGACAT |
| Turbot *g-type lysozyme* | GAGACTGGAACCCACACAGGAACG | CTGCTCTCCGCTCC AATCAGGAA |
| Murine *β-actin* | CATTGTTACCAACTGGGACGACA | GTCATCTTTTCACGGTTGGCCTT |
| Murine *HIF-1α* | GTGAACCCATTCCTCATCCGTCA | TGGCAAGCATCCTGTACTGTCC |
| Murine *lysozyme* | CTGGGACTCCTCCTGCTTTCT | GGGATCTCTCACCACCCTCTT |
| Murine *CAMP* | ACGAGGATCCAGATACTCCCAAGT | TTCCTTGAAGGCACATTGCTCAGG |

Germany). The wells without the addition of a fluorescent probe were set as a baseline control, while wells containing cells treated with only control buffer were set as a negative control. NO (%) = (fluorescence in the experimental well – fluorescence in the baseline control well)/(fluorescence in the negative control well – fluorescence in the baseline control well) × 100%.

## Measurement of Lysozyme Activity

Lysozyme activity was measured with a lysozyme assay kit according to the manufacturers' instructions. Briefly, HKMs or RAW264.7 cells were cultured in a 96-well plate overnight. After that, HKMs or RAW264.7 cells were treated with different reagents for 24 h at 24°C or 37°C, followed by three PBS washes. Next, 100 μl of cold micrococcus (100 μg/ml) was added in each well, and incubated for another 5 min. Finally, the absorbance was measured at 530 nm twice at a 2-min interval. The lysozyme activity was calculated as follows:

$$\begin{aligned}&\text{Lysozyme activity (U/ml)}\\&= \text{standard activity}(200\text{U/ml}) \times \text{dilution ratio}\\&\quad \times (\text{final transparence in the experimental well-initial transparence in the experimental well})\\&\quad /(\text{final transparence in the standard well-initial transparence in the standard well});\ \text{Transparence}\\&= 1/10^{\text{absorbance}}\end{aligned}$$

## Statistical Analysis

Results are presented as the mean ± SEM. Differences between the means were evaluated using one-way ANOVA or Tukey's t-test. $P < 0.05$ was considered statistically significant.

# RESULTS

## SCFAs Enhanced the Bactericidal Activity of Turbot HKMs

To assess the influence of SCFAs on the bacterial killing ability of turbot HKMs, isolated macrophages were incubated with control buffer, sodium butyrate (NaB), sodium propionate (NaP) or sodium acetate (NaA) at different concentrations (1, 5, 10 mM) for 24 h. Thereafter, macrophages were subjected to *E. tarda* for 2 h, and the number of viable bacteria in the macrophages were counted. As the results showed, the survival rates of *E. tarda* in HKMs pretreated with NaB (**Figure 1A**), NaP (**Figure 1B**) or NaA (**Figure 1C**) were significantly lower than those in macrophages treated with control buffer. These findings suggest that all three SCFAs promote the bactericidal activity of turbot HKMs.

## SCFAs Augmented Oxygen Consumption and HIF-1α Expression in Turbot HKMs

To test whether SCFAs treatment affected the oxygen consumption by these cells, the oxygen content in turbot HKMs was monitored. Our results showed that when HKMs

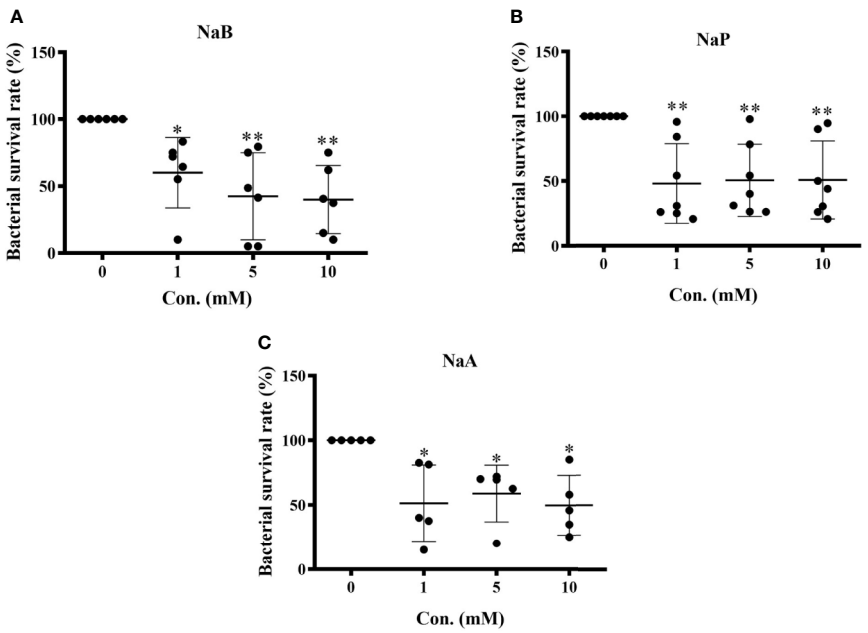


**FIGURE 1** | Short chain fatty acids (SCFAs) restrained bacterial growth in turbot head kidney macrophages (HKMs). HKMs were incubated with **(A)** sodium butyrate (NaB, n = 6), **(B)** sodium propionate (NaP, n = 7) and **(C)** sodium acetate (NaA, n = 5) in different concentrations (0, 1, 5, 10 mM) for 24 h. Thereafter, macrophages were subjected to *Edwarsiella tarda* (1:1) for 2 h, and the survival rate of ingested bacteria in SCFAs-treated macrophages was measured as described in Methods. The results were from at least three independent experiments. Error bars are presented as mean ± SD; $^{*}p < 0.05$, $^{**}p < 0.01$.

were subjected to NaB, more fluorescent $O_2$ sensor was detected in these cells than in control buffer-treated cells, since $O_2$ could quench the fluorescence of $O_2$ sensor (**Figure 2A**). Our results also suggest that NaB induces a rapid oxygen consumption in macrophages. Around 50% more oxygen consumption was detected after HKMs were treated with NaB for 2 h (**Figure 2B**).

Since HIF-1$\alpha$ expression and stability is strictly regulated by oxygen stress, the gene expression of HIF-1$\alpha$ was analyzed in SCFA-treated HKMs. When macrophages were exposed to NaB for different times up to 24 h, the results showed that the gene expression of HIF-1$\alpha$ increased steadily from 0 to 24 h (**Figure 2C**). Moreover, HIF-1$\alpha$ gene expression in HKMs treated with NaB, NaP or NaA for 24 h was elevated significantly compared to the control group (**Figure 2D**).

## SCFAs Regulated the Production of Antibacterial Effectors in Turbot HKMs

To identify which effectors could contribute to SCFA-boosted intracellular bacterial killing of HKMs, the gene expression of lysozyme and enzyme activity was analyzed. As our results showed, all three SCFAs significantly raised the gene expression of lysozyme (**Figure 3A**) as well as lysozyme enzyme activity (**Figure 3B**). In addition, the production of ROS and NO in NaB-treated HKMs was also measured. The results showed that NaB incubation alone promoted ROS production, while no effect on NO production was observed in HKMs (**Figures 3C, D**). As expected, *E. tarda* infection induced the production of ROS and NO in HKMs, and NaB pretreatment further elevated *E. tarda*-induced ROS content in HKMs (**Figure 3C**). However, NaB repressed the NO production caused by *E. tarda* infection (**Figure 3D**).

## HIF-1α Mediated Butyrate-Induced Lysozyme Expression and Bactericidal Activity in Macrophages

Next, HKMs were pre-incubated with two specific HIF-1$\alpha$ inhibitors, dimethyl-bisphenol A (DBA) or chrysin, to confirm whether HIF-1$\alpha$ was associated with SCFA-induced antibacterial activity. As our results showed, butyrate almost ablated the ability to lower bacterial survival in HKMs, when HIF-1$\alpha$ activity was inhibited by DBA (**Figure 4A**) or chrysin (**Figure 4B**). Similarly, the butyrate-promoted gene expression of lysozyme (**Figures 4C, D**) and lysozyme enzyme activity (**Figures 4E, F**) was diminished in HKMs, when macrophages were pre-incubated with HIF-1$\alpha$ inhibitors. These results indicate that HIF-1$\alpha$ signaling plays a vital role in butyrate-induced intracellular bacterial killing of macrophages.

## SCFAs Activated HIF-1α Signaling and Antibacterial Mechanisms in HKMs Through HDAC Inhibition

In the following experiments, we attempted to clarify if butyrate activates HIF-1$\alpha$ either through HDAC inhibition or *via* GPCRs. First, we tested the effects of trichostatin A (TSA), a well-known

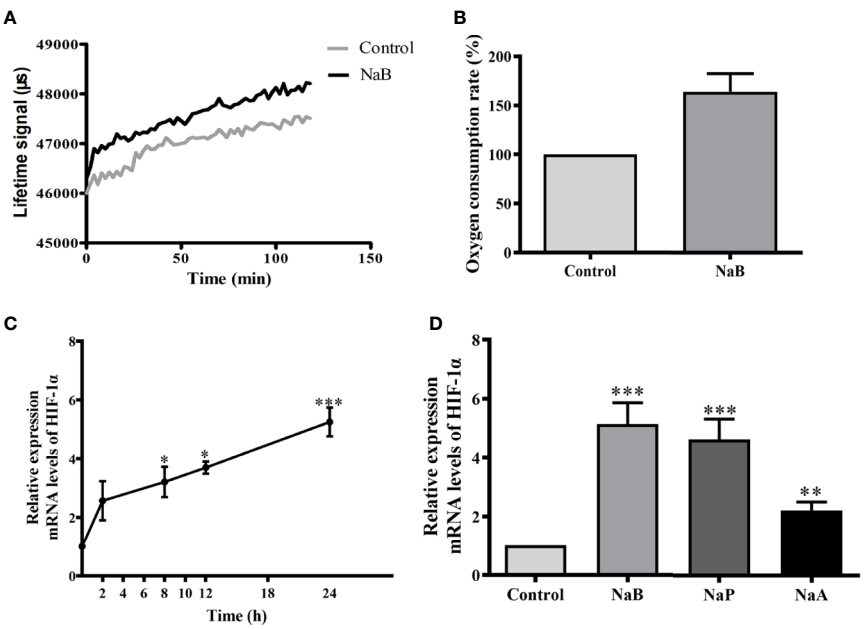


**FIGURE 2** | SCFAs elevated oxygen consumption and HIF-1$\alpha$ gene expression in HKMs. **(A, B)** When HKMs were treated with NaB (10 mM), fluorescence of the oxygen probe in the cells was monitored within 2 h **(A),** and the rate of oxygen consumption at 2 h in HKMs was analyzed (**B**, n = 3). **(C)** Isolated macrophages were incubated with NaB (10 mM) for different time courses (0, 2, 8, 12, and 24 h), and HIF-1$\alpha$ gene expression in macrophages was detected (n = 3). **(D)** After HKMs were stimulated with 10 mM of NaB (n = 11), NaP (n = 6) or NaA (n = 6) for 24 h, the gene expression of HIF-1$\alpha$ in macrophages was measured. The results were representative of at least three independent experiments, and data were normalized by comparing to the control group. Error bars represent mean ± SEM. $^*p < 0.05$, $^{**}p < 0.01$, $^{***}p < 0.001$.

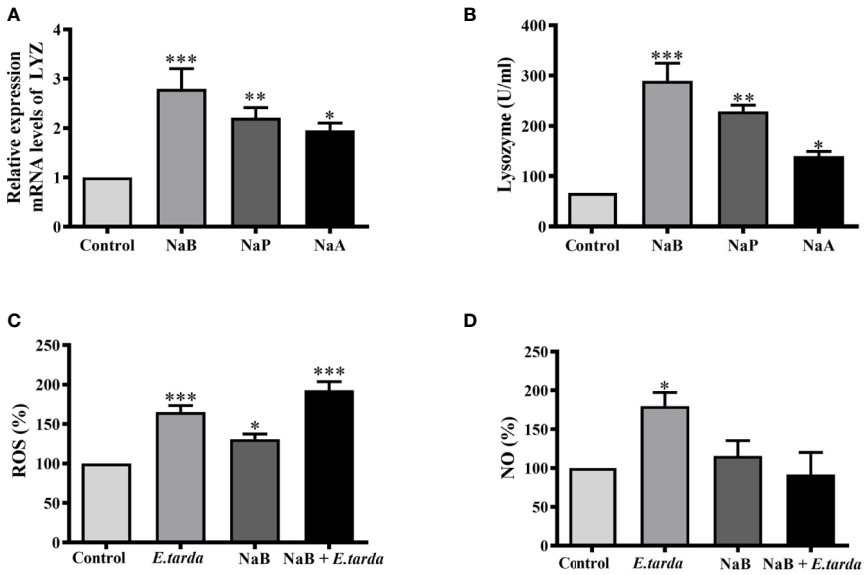


**FIGURE 3** | SCFAs promoted the gene expression and enzyme activity of lysozyme. **(A, B)** HKMs were stimulated with SCFAs (10 mM) for 24 h to analyze the gene expression of lysozyme (**A**, n = 7) and enzyme activity (**B**, n = 4). **(C, D)** HKMs were treated with NaB (10 mM) for 24 h. Thereafter, *Edwarsiella tarda* was added (cells: bacteria = 1:1) and co-incubated for 2 h, and the contents of ROS (**C,** n = 8) or NO (**D,** n = 8) in the cells were measured. The results were calculated from at least three independent experiments; error bars were presented as mean ± SEM. $^{*}p < 0.05$, $^{**}p < 0.01$, $^{***}p < 0.001$.

HDAC inhibitor. Consistently, the bacterial survival rate in HKMs was significantly lower in TSA or NaB-treated macrophages than in control cells (**Figure 5A**). In addition, TSA also significantly enhanced the gene expression of HIF-1$\alpha$ in HKMs, as NaB did (**Figure 5B**). Moreover, lysozyme gene expression, as well as lysozyme enzyme activity, increased in TSA-treated HKMs (**Figures 5C, D**).

In contrast, the effects of pertussis toxin (PT), a specific inhibitor of GPCR signaling, were assessed. When HKMs were co-treated with NaB and PT, PT displayed no effects on NaB-induced HIF-1$\alpha$ expression compared to the cells treated with butyrate alone (**Figure 5E**), confirming that GPCRs were not involved in this response.

## Butyrate Enhanced Antibacterial Activity in Murine RAW264.7 Cells

We further examined whether butyrate induced the same effects on macrophages from other species. Therefore, the murine macrophage cell line RAW264.7 was cultured and incubated with NaB for 24 h. In agreement with our results from HKMs, the bacterial survival rate in butyrate-treated RAW264.7 cells also significantly declined compared to control cells (**Figure 6A**). Meanwhile, butyrate elevated the gene and protein expression of HIF-1$\alpha$ (**Figures 6B, C**), and promoted lysozyme production in RAW264.7 cells (**Figures 6D, E**). As shown in **Figure 6F**, butyrate also elevated the gene expression of murine cathelicidin. Thus, the butyrate-activated antibacterial signaling pathway in macrophages seems to be conserved across evolution from teleosts to mammals.

# DISCUSSION

In this study, we isolated and cultured HKMs from turbots, and demonstrated that SCFAs enhanced HIF-1$\alpha$ expression and the production of antimicrobial components *via* HDAC inhibition, leading to an enhanced bactericidal activity in turbot HKMs. SCFAs have been shown to promote immune responses and infectious disease resistance in fish (18, 19). Our study provides the evidence to explain on a cellular level how SCFAs contributed to the bacterial clearance by immune cells in fish.

Host microbial cross-talk has attracted a great deal of interest in recent years, and accumulating evidence has demonstrated that gut microbiota is essential to maintain intestinal homeostasis and the regulation of host health (20). SCFAs are bacterial fermentation products from dietary fibers and include mainly acetate (C2), propionate (C3) and butyrate (C4) in higher animals, as well as in aquatic animals (3). It is well-known that SCFAs are major mediators of host–microbe interaction in the intestine (1), and SCFAs, especially butyrate, promote intestinal epithelial barrier function and regulate the host mucosal immune system (1, 6).

In fish, the concentrations of SCFAs increase towards the distal intestine (3), and it has been reported that the total SCFAs in the hindguts of herbivorous freshwater grass carp (*Ctenopharyngodon idellus*) is approximately 5.04 mM (21), while SCFAs in the hindgut of two herbivorous marine fish, *K. sydneyanus* and *O. pullus*, were found to be higher than 37 mM (22). In addition to the gastrointestinal tract, the presence of SCFAs in the oral cavity and female genital tract of humans has

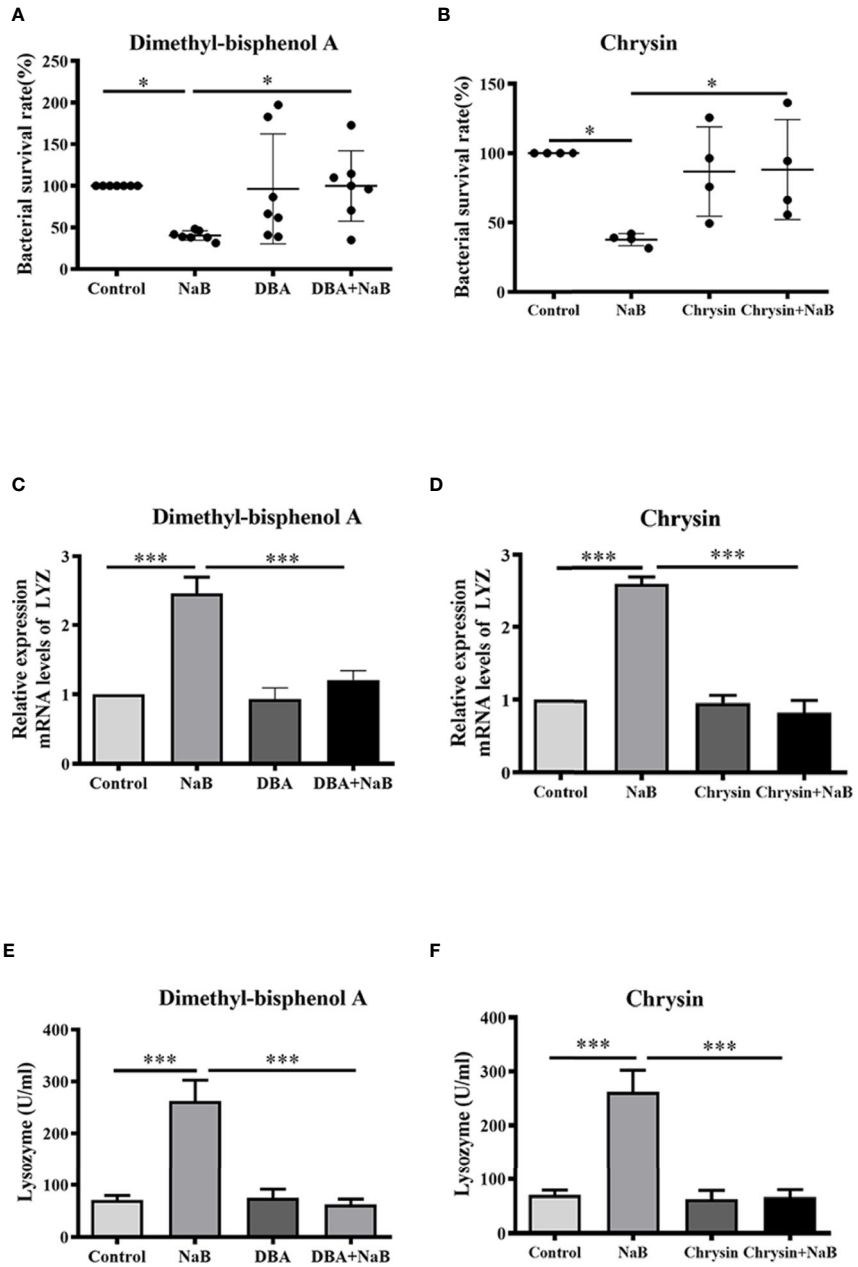


**FIGURE 4** | Butyrate increased bactericidal activity of macrophages through activation of HIF-1$\alpha$. **(A, B)** HKMs were exposed to NaB (1 mM) as well as specific HIF-1α inhibitor, dimethyl-bisphenol A (DBA, 25 μM) (**A**, n = 7) or chrysin (25 μM) (**B**, n = 4) for 24 h, followed by the assessment of bacterial killing activity of treated macrophages. Error bars are presented as mean ± SD. **(C, D)** HKMs were treated with NaB (1 mM) plus DBA (**C,** n = 6) or chrysin (**D**, n = 3) for 24 h, and the gene expression of lysozyme was detected. **(E, F)** HKMs were incubated with NaB (1 mM) plus DBA (**E,** n = 7) or chrysin (**F**, n = 7) for 24 h, and lysozyme activity was assessed. Data were calculated from at least three independent experiments. * $p < 0.05$, ***$p < 0.001$.

been detected in the millimolar range (23, 24). Interestingly, it has also been reported that gut-microbiota-derived SCFAs can exert their influence in peripheral tissues. As an example, it was shown that gut microbiota-derived SCFAs promoted the expression of the antimicrobial peptide CRAMP in pancreatic $\beta$-cells to prevent the development of diabetes (25). Moreover, Trompette et al. demonstrated convincingly that mice fed with a high-fiber diet exhibited increased circulating levels of SCFAs, and these mice were protected against allergic inflammation in the lung (26). Although the plasma concentrations of SCFAs in higher animals have been reported to be in the micromolar range (26, 27), there is little information regarding the threshold levels of SCFAs needed for beneficial responses within the peripheral tissues. Nevertheless, our results show that SCFAs ranging from

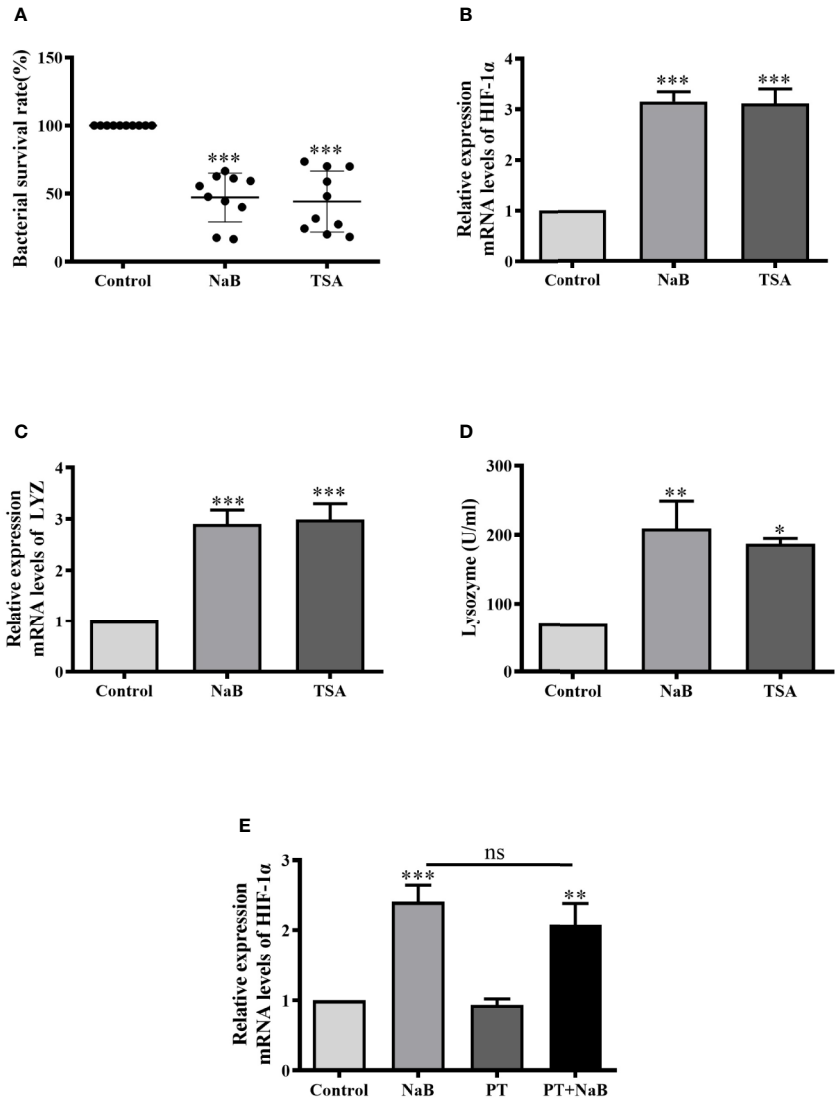


**FIGURE 5** | SCFAs augmented HIF-1$\alpha$ expression, lysozyme activity and bacterial killing of HKMs *via* HDAC Inhibition. **(A–D)** HKMs were treated with NaB (10 mM) or TSA (1 μM). After 24 h, the bacterial survival rate in HKMs (**A**, n = 10), the gene expression of HIF-1$\alpha$ (**B**, n = 8) or lysozyme (**C**, n = 7), and lysozyme activity (**D**, n = 4) were analyzed. **(E)** HKMs were treated with control buffer, NaB (1 mM), pertussis toxin (PT, 1 μg/ml) or NaB plus PT for 24 h, and the gene expression of HIF-1$\alpha$ in HKMs was assessed (n = 14). The results were calculated from at least three independent experiments. $^{*}p < 0.05$, $^{**}p < 0.01$, $^{***}p < 0.001$, ns: non significance.

1 to 10 mM promoted bacterial killing of macrophages *in vitro*. Additionally, we tested concentrations of butyrate as low as 10 μM, which also augmented the bactericidal activity of turbot HKMs (data not shown). Considering the gastrointestinal tract and other peripheral tissues harbor a large reservoir of tissue macrophages, protecting the mucosal tissues against harmful pathogens (28), it would be reasonable to speculate that microbiota-derived SCFAs could promote pathogen clearance by intestinal and other peripheral macrophages in fish and also in higher animals, since butyrate exhibited similar effects on murine macrophages (**Figure 6**).

SCFAs exert their functions *via* either GPCRs or HDAC inhibition. It is widely known that SCFAs inhibit HDAC activity in many cell types, and previous studies have shown that butyrate, and to a lesser extent, propionate acts as an HDAC inhibitor, exerting effects on the inflammatory process by downregulating the expression of pro-inflammatory genes (29–31). In addition, acetate can also act as an HDAC inhibitor (32, 33). In our study, we demonstrated that SCFAs induced HIF-1$\alpha$ expression in HKMs *via* the inhibition of HDACs. To date, the mechanism by which SCFAs inhibit HDACs is still unclear. It appears that SCFAs may directly act on HDACs *via* different transporters on the cells, or indirectly

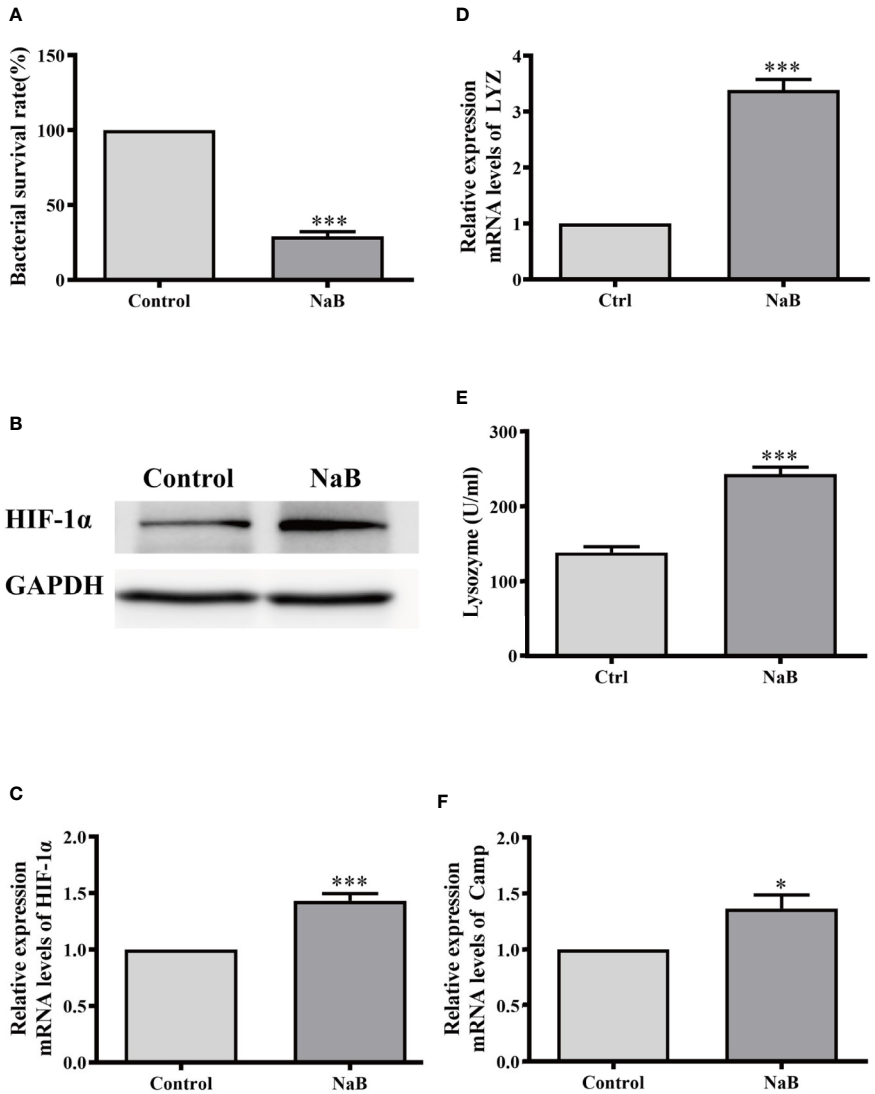


**FIGURE 6** | Sodium butyrate elevated antibacterial activity of RAW264.7 cells. RAW264.7 cells were cultured and stimulated with control buffer or NaB (1 mM) for 24 h. Afterwards, **(A)** the bacterial survival rate in RAW264.7 cells was analyzed (n = 8); **(B, C)** the protein level of HIF-1α in HKMs was assessed **(B)** and HIF-1α gene expression was also detected (**C**, n = 7); **(D, E)** The gene expression of lysozyme (**D**, n = 10) and lysozyme activity (**E**, n = 6) was measured. **(F)** The *CAMP* gene expression was analyzed (n = 8). The results were calculated from at least three independent experiments. Error bars represent mean ± SEM. *p < 0.05, ***p < 0.001.

through GPCR activation (34). Our results, however, have indicated that SCFAs enter into target cells and act inside these cells, since we demonstrated that GPCRs were not involved in SCFA-induced responses (**Figure 5E**). Although diffusion is a route for SCFAs to enter cells, studies in higher animals have revealed that carrier-mediated mechanisms constitute the major route for the entry of SCFAs in their anionic form into target cells, especially in the colonic epithelium (35). So far, several transport systems responsible for the cellular uptake of SCFAs have been identified in higher animals, including $H^+$-coupled and $Na^+$-coupled transport system (35). However, little is known about SCFA transporters in fish. Thus, it would be very interesting to further clarify how SCFAs are transported into macrophages in teleosts.

Hypoxia-inducible factors are the major cellular mechanisms that coordinate the transcriptional responses to low-$O_2$ environments (12). It was previously demonstrated that SCFAs depleted oxygen and induced the stabilization of HIF-1$\alpha$ in intestinal epithelial cells (14), which increased epithelial barrier function and reduced intestinal inflammation and bacterial translocation (36). Interestingly, it was reported that acute HDAC inhibition resulted in rapid increased oxygen consumption in the head tissue of the fruitfly (37) and in diabetic mice (38). Consistently, our study confirmed that oxygen consumption was increased significantly in butyrate-incubated macrophages, which led to enhanced HIF-1α expression in turbot HKMs (**Figure 2**).

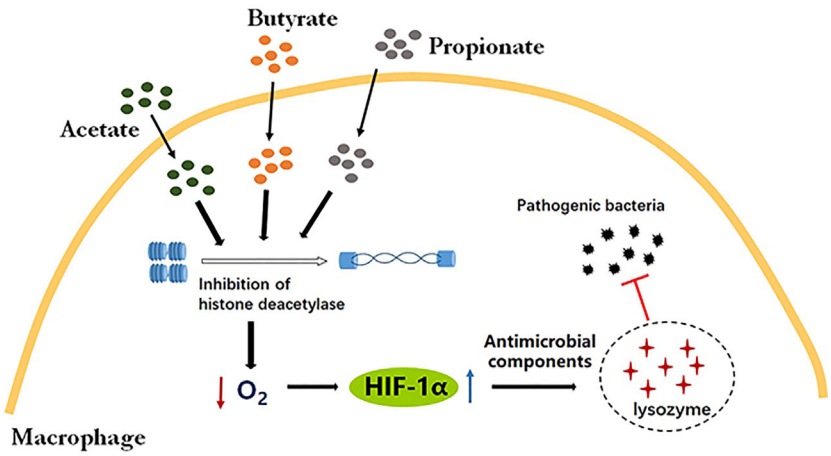


**FIGURE 7** | SCFAs promoted intracellular bactericidal activity of macrophages *via* HIF-1$\alpha$. SCFAs, including butyrate, propionate and acetate, induce hypoxia and HIF-1$\alpha$ expression *via* HDAC inhibition in macrophages. The activation of HIF-1$\alpha$ signaling enhances the production of antibacterial components, such as lysozymes, leading to the efficient clearance of pathogenic bacteria in macrophages.

More importantly, HIF-1$\alpha$ is a critical hub that integrates hypoxic and immunogenic signals during infection and/or inflammation (39). Previously it was reported that HIF-1$\alpha$ expression in murine macrophages and neutrophils is essential for effective bacterial killing *via* promoting the production of key immune effector molecules, such as antimicrobial components, NO and TNF-α (40). Lysozyme is considered to be a key component of the innate immune response to pathogen infections and has strong antibacterial activity. It is well documented that fish lysozyme possesses lytic activity against both Gram-positive bacteria and Gram-negative bacteria (41). The g-type lysozyme in turbot has been shown to play an important role in the defense against most bacterial infections (42), in particular, g-type lysozyme increased the disease resistance in the mucosal surfaces of fish (43). Therefore, the expression and activity of turbot g-type lysozyme in HKMs were analyzed in our study. Our results showed that the expression and activity of g-type lysozymes in butyrate-treated turbot HKMs was elevated in a HIF-1$\alpha$-dependent manner, which potentially contributes to the SCFA-promoted bacterial killing of macrophages.

It is well-known that ROS have potent antimicrobial activity against bacteria, fungi and viruses (44). The primary sources of ROS in phagocytes come from "respiratory burst" by conversion of $O_2$ to $O_2^-$ *via* oxidases and subsequent dismutation to $H_2O_2$ (45). Previous report has exhibited a dependence of ROS production on oxygen consumption in cells (46). Thus, our results indicate that butyrate increases oxygen consumption in macrophages, resulting in the enhanced ROS generation, as well as the upregulation of HIF-1$\alpha$-dependent lysozyme production. Consequently, butyrate-promoted antimicrobial effectors, including ROS and lysozymes, contribute to eliminate intracellular bacteria in macrophages. In addition, NO is a small messenger that regulates a variety of physiological functions, including phagocytic defense mechanisms (47). In fact, NO has been recognized as one of the most versatile players in the immune system (48). Previous reports have demonstrated that butyrate inhibits bacteria-induced NO production in murine macrophages (29, 49), and our result provides the evidence that butyrate causes a similar response in HKMs (**Figure 3D**).

Antimicrobial peptides (AMPs) are another important set of factors in host defense against pathogenic microbes. In fish, cationic AMPs are mainly divided into five families, including piscidins, cathelicidins, defensins, hepcidins and high-density lipoproteins (50). Previous study has illustrated that the activation of HIF-1$\alpha$ resulted in the elevated expression of cathelicidins in order to inhibit gastrointestinal colonization of fungi (15). Recently, it was reported that the activation of intestinal HIF-1$\alpha$ boosted local AMP expression to facilitate microbial homeostasis in zebrafish (51). Nevertheless, our result showed that the gene expression of turbot hepcidin in HKMs was not increased by SCFA treatment (data not shown). Although cathelicidins and $\beta$-defensins, two important AMP families, have not been identified in turbot, and the result from murine macrophages showed that butyrate significantly upregulated the gene expression of cathelicidin antimicrobial peptide (**Figure 6F**), which might be beneficial to butyrate-promoted bactericidal activity of macrophages.

## CONCLUSION

For the first time, our study has demonstrated that SCFAs augmented oxygen consumption and activated HIF-1$\alpha$ signaling *via* HDAC inhibition in macrophages. Moreover, SCFA-induced HIF-1$\alpha$ resulted in the elevated production of antimicrobial effectors and bacterial clearance by macrophages, revealing potential novel mechanisms whereby SCFAs contribute to bacterial clearance by macrophages (**Figure 7**).

## DATA AVAILABILITY STATEMENT

The raw data supporting the conclusions of this article will be made available by the authors, without undue reservation.

## ETHICS STATEMENT

The animal study was reviewed and approved by the Institutional Animal Care and Use Committee of the Ocean University of China. The present study was conducted in strict accordance with the recommendations in the Guide for the Use of Experimental Animals of Ocean University of China. All efforts had been dedicated to minimize suffering of the animals.

## AUTHOR CONTRIBUTIONS

JZ designed and performed experiments, analyzed data and wrote the manuscript. HZ, ML, YL, and HS performed experiments. KM supervised the project. MW supervised the project, designed experiments, analyzed data, and wrote the manuscript. All authors contributed to the article and approved the submitted version.

## FUNDING

This study was supported by National Key R&D Program of China (Grant No. 2018YFD0900400); the National Natural Science Foundation of China (Grant No. 31972802); Natural Science Foundation of Shandong Province (Grant No. ZR2019MC041); Youth Talent Program Supported by Laboratory for Marine Fisheries Science and Food Production Processes, Pilot National Laboratory for Marine Science Technology (Qingdao) (Grant No. 2018-MFS-T11).

## ACKNOWLEDGMENTS

We are grateful to Prof. Birgitta Agerberth in Karolinska Institutet, Sweden for her revision on this manuscript.

## SUPPLEMENTARY MATERIAL

The Supplementary Material for this article can be found online at: https://www.frontiersin.org/articles/10.3389/fimmu.2020.615536/full#supplementary-material

## REFERENCES

1. Koh A, De Vadder F, Kovatcheva-Datchary P, Bäckhed F. From Dietary Fiber to Host Physiology: Short-Chain Fatty Acids as Key Bacterial Metabolites. *Cell* (2016) 165:1332–45. doi: 10.1016/j.cell.2016.05.041
2. Hoseinifar SH, Sun Y-Z, Caipang CM. Short-chain fatty acids as feed supplements for sustainable aquaculture: an updated view. *Aquacult Res* (2017) 48:1380–91. doi: 10.1111/are.13239
3. Tran NT, Li Z, Wang S, Zheng H, Aweya JJ, Wen X, et al. Progress and perspectives of short-chain fatty acids in aquaculture. *Rev Aquacult* (2020) 12:283–98. doi: 10.1111/raq.12317
4. Tian L, Zhou XQ, Jiang WD, Liu Y, Wu P, Jiang J, et al. Sodium butyrate improved intestinal immune function associated with NF-κB and p38MAPK signalling pathways in young grass carp (Ctenopharyngodon idella). *Fish shellfish Immunol* (2017) 66:548–63. doi: 10.1016/j.fsi.2017.05.049
5. Liu Y, Chen Z, Dai J, Yang P, Xu W, Ai Q, et al. Sodium butyrate supplementation in high-soybean meal diets for turbot (Scophthalmus maximus L.): Effects on inflammatory status, mucosal barriers and microbiota in the intestine. *Fish shellfish Immunol* (2019) 88:65–75. doi: 10.1016/j.fsi.2019.02.064
6. Parada Venegas D, De la Fuente MK, Landskron G, González MJ, Quera R, Dijkstra G, et al. Short Chain Fatty Acids (SCFAs)-Mediated Gut Epithelial and Immune Regulation and Its Relevance for Inflammatory Bowel Diseases. *Front Immunol* (2019) 10:277. doi: 10.3389/fimmu.2019.00277
7. Zhao LM, Zhang JH. Histone Deacetylase Inhibitors in Tumor Immunotherapy. *Curr med Chem* (2019) 26:2990–3008. doi: 10.2174/0929867324666170801102124
8. Lin MY, de Zoete MR, van Putten JP, Strijbis K. Redirection of Epithelial Immune Responses by Short-Chain Fatty Acids through Inhibition of Histone Deacetylases. *Front Immunol* (2015) 6:554. doi: 10.3389/fimmu.2015.00554
9. Abdel-Aziz EH, Abdu SBS, Ali TE, Fouad HF. Haemopoiesis in the head kidney of tilapia, Oreochromis niloticus (Teleostei: Cichlidae): a morphological (optical and ultrastructural) study. *Fish Physiol Biochem* (2010) 36:323–36. doi: 10.1007/s10695-008-9297-z
10. Kondera E. Haematopoiesis in the head kidney of common carp (Cyprinus carpio L.): a morphological study. *Fish Physiol Biochem* (2011) 37:355–62. doi: 10.1007/s10695-010-9432-5
11. Van den Bossche J, O'Neill LA, Menon D. Macrophage Immunometabolism: Where Are We (Going)? *Trends Immunol* (2017) 38:395–406. doi: 10.1016/j.it.2017.03.001
12. Choudhry H, Harris AL. Advances in Hypoxia-Inducible Factor Biology. *Cell Metab* (2018) 27:281–98. doi: 10.1016/j.cmet.2017.10.005
13. Kim YE, Lee M. HIF-1α activation in myeloid cells accelerates dextran sodium sulfate-induced colitis progression in mice. *Dis Models Mech* (2018) 11: dmm033241. doi: 10.1242/dmm.033241
14. Kelly CJ, Zheng L, Campbell EL, Saeedi B, Scholz CC, Bayless AJ, et al. Crosstalk between Microbiota-Derived Short-Chain Fatty Acids and Intestinal Epithelial HIF Augments Tissue Barrier Function. *Cell host Microbe* (2015) 17:662–71. doi: 10.1016/j.chom.2015.03.005
15. Fan D, Coughlin LA, Neubauer MM, Kim J, Kim MS, Zhan X, et al. Activation of HIF-1α and LL-37 by commensal bacteria inhibits Candida albicans colonization. *Nat Med* (2015) 21:808–14. doi: 10.1038/nm.3871
16. Chung S, Secombes CJ. Analysis of events occurring within teleost macrophages during the respiratory burst. *Comp Biochem Physiol Part B: Comp Biochem* (1988) 89:539–44. doi: 10.1016/0305-0491(88)90171-X
17. Grayfer L, Kerimoglu B, Yaparla A, Hodgkinson JW, Xie J, Belosevic M. Mechanisms of Fish Macrophage Antimicrobial Immunity. *Front Immunol* (2018) 9:1105. doi: 10.3389/fimmu.2018.01105
18. Safari R, Hoseinifar SH. Modulation of antioxidant defense and immune response in zebra fish (Danio rerio) using dietary sodium propionate. *Fish Physiol Biochem* (2016) 42:1733–9. doi: 10.1007/s10695-016-0253-z
19. Hoseinifar SH, Zoheiri F, Caipang CM. Dietary sodium propionate improved performance, mucosal and humoral immune responses in Caspian white fish (Rutilus frisii kutum) fry. *Fish shellfish Immunol* (2016) 55:523–8. doi: 10.1016/j.fsi.2016.06.027
20. Tilg H, Zmora N, Adolph TE, Elinav E. The intestinal microbiota fuelling metabolic inflammation. *Nat Rev Immunol* (2020) 20:40–54. doi: 10.1038/s41577-019-0198-4
21. Hao YT, Wu SG, Jakovlić I, Zou H, Li WX, Wang GT. Impacts of diet on hindgut microbiota and short-chain fatty acids in grass carp (Ctenopharyngodon idellus). *Aquacult Res* (2017) 48:5595–605. doi: 10.1111/are.13381
22. Mountfort DO, Campbell J, Clements KD. Hindgut fermentation in three species of marine herbivorous fish. *Appl Environ Microbiol* (2002) 68:1374–80. doi: 10.1128/aem.68.3.1374-1380.2002

23. Huang CB, Alimova Y, Myers TM, Ebersole JL. Short- and medium-chain fatty acids exhibit antimicrobial activity for oral microorganisms. *Arch Oral Biol* (2011) 56:650–4. doi: 10.1016/j.archoralbio.2011.01.011
24. Mirmonsef P, Gilbert D, Zariffard MR, Hamaker BR, Kaur A, Landay AL, et al. The effects of commensal bacteria on innate immune responses in the female genital tract. *Am J Reprod Immunol* (2011) 65:190–5. doi: 10.1111/j.1600-0897.2010.00943.x
25. Sun J, Furio L, Mecheri R, van der Does AM, Lundeberg E, Saveanu L, et al. Pancreatic β-Cells Limit Autoimmune Diabetes via an Immunoregulatory Antimicrobial Peptide Expressed under the Influence of the Gut Microbiota. *Immunity* (2015) 43:304–17. doi: 10.1016/j.immuni.2015.07.013
26. Trompette A, Gollwitzer ES, Yadava K, Sichelstiel AK, Sprenger N, Ngom-Bru C, et al. Gut microbiota metabolism of dietary fiber influences allergic airway disease and hematopoiesis. *Nat Med* (2014) 20:159–66. doi: 10.1038/nm.3444
27. Topping DL, Clifton PM. Short-chain fatty acids and human colonic function: roles of resistant starch and nonstarch polysaccharides. *Physiol Rev* (2001) 81:1031–64. doi: 10.1152/physrev.2001.81.3.1031
28. Muller PA, Matheis F, Mucida D. Gut macrophages: key players in intestinal immunity and tissue physiology. *Curr Opin Immunol* (2020) 62:54–61. doi: 10.1016/j.coi.2019.11.011
29. Chang PV, Hao L, Offermanns S, Medzhitov R. The microbial metabolite butyrate regulates intestinal macrophage function via histone deacetylase inhibition. *Proc Natl Acad Sci USA* (2014) 111:2247–52. doi: 10.1073/pnas.1322269111
30. Wang J, Wei Z, Zhang X, Wang Y, Yang Z, Fu Y. Propionate Protects against Lipopolysaccharide-Induced Mastitis in Mice by Restoring Blood-Milk Barrier Disruption and Suppressing Inflammatory Response. *Front Immunol* (2017) 8:1108. doi: 10.3389/fimmu.2017.01108
31. Silva LG, Ferguson BS, Avila AS, Faciola AP. Sodium propionate and sodium butyrate effects on histone deacetylase (HDAC) activity, histone acetylation, and inflammatory gene expression in bovine mammary epithelial cells. *J Anim Sci* (2018) 96:5244–52. doi: 10.1093/jas/sky373
32. Soliman ML, Rosenberger TA. Acetate supplementation increases brain histone acetylation and inhibits histone deacetylase activity and expression. *Mol Cell Biochem* (2011) 352:173–80. doi: 10.1007/s11010-011-0751-3
33. Olaniyi KS, Amusa OA. Sodium acetate-mediated inhibition of histone deacetylase alleviates hepatic lipid dysregulation and its accompanied injury in streptozotocin-nicotinamide-induced diabetic rats. *Biomed pharmacother = Biomedecine pharmacotherapie* (2020) 128:110226. doi: 10.1016/j.biopha.2020.110226
34. He J, Zhang P, Shen L. Short-Chain Fatty Acids and Their Association with Signalling Pathways in Inflammation, Glucose and Lipid Metabolism. *Int J Mol Sci* (2020) 21:E6356. doi: 10.3390/ijms21176356
35. Sivaprakasam S, Bhutia YD, Yang S, Ganapathy V. Short-Chain Fatty Acid Transporters: Role in Colonic Homeostasis. *Compr Physiol* (2017) 8:299–314. doi: 10.1002/cphy.c170014
36. Fachi JL, Felipe JS, Pral LP, da Silva BK, Corrêa RO, de Andrade MCP, et al. Butyrate Protects Mice from Clostridium difficile-Induced Colitis through an HIF-1-Dependent Mechanism. *Cell Rep* (2019) 27:750–61.e7. doi: 10.1016/j.celrep.2019.03.054
37. Becker L, Nogueira MS, Klima C, de Angelis MH. Rapid and transient oxygen consumption increase following acute HDAC/KDAC inhibition in Drosophila tissue. *Sci Rep* (2018) 8:4199. doi: 10.1038/s41598-018-22674-2
38. Galmozzi A, Mitro N, Ferrari A, Gers E, Gilardi F, Godio C, et al. Inhibition of class I histone deacetylases unveils a mitochondrial signature and enhances oxidative metabolism in skeletal muscle and adipose tissue. *Diabetes* (2013) 62:732–42. doi: 10.2337/db12-0548
39. Stothers CL, Luan L, Fensterheim BA, Bohannon JK. Hypoxia-inducible factor-1α regulation of myeloid cells. *J Mol Med (Berlin Germany)* (2018) 96:1293–306. doi: 10.1007/s00109-018-1710-1
40. Peyssonnaux C, Datta V, Cramer T, Doedens A, Theodorakis EA, Gallo RL, et al. HIF-1alpha expression regulates the bactericidal capacity of phagocytes. *J Clin Invest* (2005) 115:1806–15. doi: 10.1172/jci23865
41. Saurabh S, Sahoo PK. Lysozyme: an important defence molecule of fish innate immune system. *Aquacult Res* (2008) 39:223–39. doi: 10.1111/j.1365-2109.2007.01883.x
42. Zhao L, Sun JS, Sun L. The g-type lysozyme of Scophthalmus maximus has a broad substrate spectrum and is involved in the immune response against bacterial infection. *Fish shellfish Immunol* (2011) 30:630–7. doi: 10.1016/j.fsi.2010.12.012
43. Gao C, Fu Q, Zhou S, Song L, Ren Y, Dong X, et al. The mucosal expression signatures of g-type lysozyme in turbot (Scophthalmus maximus) following bacterial challenge. *Fish shellfish Immunol* (2016) 54:612–9. doi: 10.1016/j.fsi.2016.05.015
44. Dryden M. Reactive oxygen species: a novel antimicrobial. *Int J antimicrob Agents* (2018) 51:299–303. doi: 10.1016/j.ijantimicag.2017.08.029
45. Dupré-Crochet S, Erard M, Nüβe O. ROS production in phagocytes: why, when, and where? *J leukocyte Biol* (2013) 94:657–70. doi: 10.1189/jlb.1012544
46. Grivennikova VG, Kareyeva AV, Vinogradov AD. Oxygen-dependence of mitochondrial ROS production as detected by Amplex Red assay. *Redox Biol* (2018) 17:192–9. doi: 10.1016/j.redox.2018.04.014
47. Wink DA, Hines HB, Cheng RY, Switzer CH, Flores-Santana W, Vitek MP, et al. Nitric oxide and redox mechanisms in the immune response. *J leukocyte Biol* (2011) 89:873–91. doi: 10.1189/jlb.1010550
48. Bogdan C. Nitric oxide and the immune response. *Nat Immunol* (2001) 2:907–16. doi: 10.1038/ni1001-907
49. Park JW, Kim HY, Kim MG, Jeong S, Yun CH. Short-chain Fatty Acids Inhibit Staphylococcal Lipoprotein-induced Nitric Oxide Production in Murine Macrophages. *Immune network* (2019) 19:e9. doi: 10.4110/in.2019.19.e9
50. Valero Y, Saraiva-Fraga M, Costas B, Guardiola FA. Antimicrobial peptides from fish: beyond the fight against pathogens. *Rev Aquacult* (2020) 12:224–53. doi: 10.1111/raq.12314
51. Zhang Z, Ran C, Ding QW, Liu HL, Xie MX, Yang YL, et al. Ability of prebiotic polysaccharides to activate a HIF1α-antimicrobial peptide axis determines liver injury risk in zebrafish. *Commun Biol* (2019) 2:274. doi: 10.1038/s42003-019-0526-z


**Conflict of Interest:** The authors declare that the research was conducted in the absence of any commercial or financial relationships that could be construed as a potential conflict of interest.

frontiers in Immunology

ORIGINAL RESEARCH
published: 18 January 2021
doi: 10.3389/fimmu.2020.615980

# MHC II-PI$_3$K/Akt/mTOR Signaling Pathway Regulates Intestinal Immune Response Induced by Soy Glycinin in Hybrid Grouper: Protective Effects of Sodium Butyrate

*Bin Yin*[1,2,3†], *Hongyu Liu*[1,2,3†], *Beiping Tan*[1,2,3*], *Xiaohui Dong*[1,2,3], *Shuyan Chi*[1,2,3], *Qihui Yang*[1,2,3] *and Shuang Zhang*[1,2,3]

[1] Laboratory of Aquatic Animal Nutrition and Feed, Fisheries College, Guangdong Ocean University, Zhanjiang, China, [2] Aquatic Animals Precision Nutrition and High Efficiency Feed Engineering Research Centre of Guangdong Province, Zhanjiang, China, [3] Key Laboratory of Aquatic, Livestock and Poultry Feed Science and Technology in South China, Ministry of Agriculture, Zhanjiang, China

OPEN ACCESS

**Edited by:**
Nan Wu,
Institute of Hydrobiology (CAS), China

**Reviewed by:**
Lu Dan-Qi,
Sun Yat-sen University, China
Chaoxia Ye,
South China Normal University, China

***Correspondence:**
Beiping Tan
bptan@126.com

†These authors have contributed equally to this work and share first authorship

**Specialty section:**
This article was submitted to Comparative Immunology, a section of the journal Frontiers in Immunology

**Received:** 10 October 2020
**Accepted:** 30 November 2020
**Published:** 18 January 2021

**Citation:**
Yin B, Liu H, Tan B, Dong X, Chi S, Yang Q and Zhang S (2021) MHC II-PI$_3$K/Akt/mTOR Signaling Pathway Regulates Intestinal Immune Response Induced by Soy Glycinin in Hybrid Grouper: Protective Effects of Sodium Butyrate. Front. Immunol. 11:615980. doi: 10.3389/fimmu.2020.615980

Soy glycinin (11S) is involved in immune regulation. As an additive, sodium butyrate (SB) can relieve inflammation caused by 11S. To further delve into the mechanisms. A diet containing 50% fishmeal was the control group (FM group), and the experimental groups consisted of the FM group baseline plus 2% glycinin (GL group), 8% glycinin (GH group), and 8% glycinin + 0.13% sodium butyrate (GH-SB group). The specific growth ratio (SGR), feed utilization, and density of distal intestinal (DI) type II mucous cells were increased in the GL group. In the serum, IFN-γ was significantly upregulated in the GL group, and IgG and IL-1β were upregulated in the GH group. IgG, IL-1β, and TNF-α in the GH-SB group were significantly downregulated compared to those in the GH group. The mRNA levels of mTOR C1, mTOR C2, and Deptor were upregulated in the GL, GH, and GH-SB groups in the DI compared with those in the FM group, while the mRNA levels of mTOR C1 and Deptor in the GH group were higher than those in the GL and GH-SB groups. 4E-BP1, RICTOR, PRR5, MHC II, and CD4 were upregulated in the GH group. TSC1, mLST8, and NFY mRNA levels in the GL and GH-SB groups were upregulated compared with those in the FM and GH groups. Western blotting showed P-PI$_3$K$^{Ser294}$/T-PI$_3$K, P-Akt$^{Ser473}$/T-Akt, and P-mTOR$^{Ser2448}$/T-mTOR were upregulated in the GH group. Collectively, our results demonstrate that low-dose 11S could improve serum immune by secreting IFN-γ. The overexpression of IgG and IL-1β is the reason that high-dose 11S reduces serum immune function, and supplementing SB can suppress this overexpression. Low-dose 11S can block the relationship between PI$_3$K and mTOR C2. It can also inhibit the expression of 4E-BP1 through mTOR C1. High-dose 11S upregulates 4E-BP2 through mTOR C1, aggravating intestinal inflammation. SB could relieve inflammation by blocking PI$_3$K/mTOR C2 and inhibiting 4E-BP2. Generally speaking, the hybrid grouper obtained different serum and DI immune responses under different doses of 11S, and these responses were ultimately manifested in growth performance.

SB can effectively enhance serum immunity and relieve intestinal inflammation caused by high dose 11S.

**Keywords: hybrid grouper (*Epinephelus fuscoguttatus*♀×*E. lanceolatus*♂), soy glycinin, sodium butyrate, intestinal inflammation, MHC II-PI$_3$K/Akt/mTOR signaling pathway**

## INTRODUCTION

Hybrid grouper (*Epinephelus fuscoguttatus*♀×*E. lanceolatus*♂) is a type of broad salt tolerant fish in warm coastal waters. It is widely cultivated in southern China. Characteristics of hybrid groupers include fast growth and strong disease resistance. In 2017, the Chinese Ministry of Agriculture included groupers into the national marine fish industry technology system. As a carnivorous marine fish, hybrid grouper feed typically is up to 50% protein, with a content of fish meal also as high as 50%. The addition of a large amount of fish meal to the feed during the breeding period is the main cause of high phosphorus and nitrogen pollution in aquaculture water. Nitrogen and phosphorus are the two main pollutants in aquatic environments (1). Fish meal usually contains 51.1–73.0% crude protein and 1.67–4.21% phosphorus, whereas plant-based protein, such as soybean meal, usually contains 44.8–50% crude protein and only 0.6–0.7% phosphorus (2). Therefore, the use of plant-based protein to replace some of the fish meal in fish feed can reduce the feed's crude protein and phosphorus content, thereby reducing nitrogen and phosphorus pollution in the breeding water. To avoid excessive pollution, scholars have long committed to using plant proteins to replace fish meal. Soybean meal, a common source of plant protein, is widely available at low prices. However, it contains a large amount of anti-nutritional factors such as glycinin and β-conglycinin, which cause groupers to have a very low tolerance for it.

Glycinin (11S) is one of the most immunogenic factors in soybean antigen protein, accounting for about 40% of the total protein content in soybeans. Its thermal stability leads to its weak inactivation ability under normal heating treatment. Too much glycinin may cause intestinal allergies and disrupt the intestinal barrier, which could cause a large amount of nutrients in the feed to be excreted and enter the water instead of being absorbed by the intestine. Unlike in mammals, the antigen-binding epitopes of fish intestines are mainly concentrated in the distal intestine (DI) (3). Differentiated DI epithelial cells are the most susceptible to antigen binding, causing the allergic response to be most pronounced in the DI (4). However, in some experiments in which soybean meal replaced fish meal, the rate of weight gain was improved with low substitution levels (5). We suspect that this phenomenon is related to low-dose 11S immune enhancement. Nevertheless, the hybrid grouper has poor tolerance to soybean meal (6), largely because of its high 11S content (7). Poor growth is mainly due to inflammation in the intestinal tract, which leads to a decrease in the efficiency of nutrient absorption (8). Studies have shown that glycinin causes intestinal allergies in animals and induces intestinal cellular oxidative damage by decreasing antioxidant enzyme activities in juvenile turbot (*Scophthalmus maximus* L.) (9).

The antigen protein 11S enters the body and becomes an allergen with antigenic activity, stimulating allergic reactions in the intestinal mucosal immune system. This causes intestinal damage, intestinal permeability changes, digestion issues, and malabsorption. There are four types of allergic reactions: Type I is an acute allergic reaction mediated by the specific antibody IgE; Type II is cytotoxic response. Cytolysis or tissue damage due to complement involvement when an antigenic antibody reaction with the corresponding antigen occurs. Type III is a delayed reaction mediated by a specific antigen-antibody complex; and Type IV is a delayed allergic reaction mediated by specific T lymphocytes (10). However, the exact mechanisms of intestinal allergy type and inflammatory response induced by 11S in carnivorous marine fish have not been reported.

Sodium butyrate (SB) has been widely used in livestock and poultry as an alternative to antibiotics. It has also been applied to aquatic animals in recent years and has achieved good results (11). Its active ingredient, butyric acid, provides energy directly to intestinal epithelial cells without being absorbed by the hepatobiliary system or entering the tricarboxylate transport system. It maintains the normal state of intestinal mucosal epithelial cells and promotes digestion and absorption of the small intestine (12). SB may increase the antioxidant capacity of grass carp by inhibiting apoptosis-related products and improving the integrity of intestinal cell structure by upregulating intestinal zonula occludens-1 (ZO-1), zonula occludens-2 (ZO-2), and claudin-b protein (13). In addition, SB can relieve inflammation by anti-oxidation. It can reduce xanthine oxidase activity in the intestinal mucosa of rats with ulcerative colitis, as well as reduce glutathione content, oxygen free radicals, and lipid peroxidation of unsaturated fatty acids in cells. However, no systematic study has been conducted on the repair effect of SB on intestinal abnormalities caused by antigen protein 11S in hybrid groupers. Presently, there are no studies on the application of SB to hybrid groupers. In this experiment, the immune regulatory effect of 11S on the hybrid grouper was investigated. To provide a theoretical reference for improving the tolerance of hybrid grouper to soybean meal protein sources, supplementation with SB was used to repair the intestinal inflammation caused by the high level of antigenic protein 11S.

In this study, the hybrid grouper, an economic fish widely farmed in southern China, was chosen as the subject of our experiment. We were interested in comparing the differences between different levels of glycinin and SB repair effects. We wanted to test the effects of glycinin and SB on growth performance, serum biochemical indices, distal intestinal morphology, and inflammation.

## MATERIAL AND METHODS

### Animals

The fish used in this experiment were purchased from a commercial hatchery in East Island (Zhanjiang, China),

temporarily cultured in a cement pond at the Biological Research Base of Guangdong Ocean University, and domesticated with commercial feed for 7 days. The animal protocol was approved by the ethics review board of Guangdong Ocean University. All procedures were performed according to the standards of the National Institutes of Health Guide for the Care and Use of Laboratory Animals (NIH Publication No. 8023, revised 1978) and relevant Chinese policies.

## Feeding Trial and Challenge Test

After they were stable, 480 healthy experimental fish of the same weight were randomly selected and allocated to 16 plastic barrels reinforced with glass fiber, with 30 fish per barrel. The fish were cultured for 8 weeks. The fish were separated into four treatment groups. Every day, each treatment was repeated 4 times, full feeding was performed at 8:00 and 17:00, and 70% of the water was replaced. During the experiment, the water temperature was 29.00 ± 1.30°C, salinity was 34.00 ± 2.00 ‰, dissolved oxygen concentration was ≥7.00 mg/L, pH was 7.80–8.10, and ammonia nitrogen concentration was ≤0.09 mg/L. At the end of the 8-week feeding trial, 40 fish were randomly selected from each group (10 fish per replicate). Following the methodology by Yin et al. (5), each fish was intraperitoneally injected with 200 μl of *Vibrio parahaemolyticus* at a concentration of $7.41 \times 10^8$ CFU/ml and observed for a week until stabilized. The cumulative mortality of each group was counted.

## Diet Formulations

The control groups (FM group) were fed with a control diet (0% glycinin, 0% SB). The experimental groups (named GL, GH, and GH-SB, respectively) were fed with diet GL (2% glycinin, 0% SB), diet GH (8% glycinin, 0% SB), and diet GH-SB (8% glycinin, 1.33% SB). Methionine and lysine were supplemented in GL, GH, and GH-SB diets. Nutrient composition and amino acid profiles are shown in **Tables S1** and **S2**, respectively. Purified glycinin (from soybean meal) was purchased from China Agricultural University (patent no. 200410029589.4, China). Water was added to adjust the pH of the 11S suspension to 7.2. The suspension was freeze dried for 72 h to make the 11S solid, and a small pulverizer was used to crush it. Microencapsulated SB (30%) was kindly provided by Shanghai Menon Animal Nutrition Technology Co., Ltd. All feed ingredients were crushed into powder through a 380 μm mesh. After all the ingredients were combined, fish oil, soy lecithin, and water were added and mixed thoroughly. After being pelletized and air dried for 2–3 days at room temperature, all the feed was kept in a refrigerator (-20°C) until use.

## Sample Collection and Analysis

After 8 weeks of the feeding trial, the fish were starved for 24 h before being weighed and counted. Three fish from each tank were randomly selected to have their blood drawn using a 1 mL needle tube. The blood samples were placed in a 1.5-ml centrifuge tube on ice for temporary storage and then put in a 4°C refrigerator to rest. The samples were centrifuged at 3500 rpm for 15 min. The supernatant was carefully separated and stored at -80°C to be later used for measuring enzyme activity and testing related biochemical indicators. Three new fish were randomly selected, and the DI from each fish, from the anus to the first corner of the intestine, was removed. After removing it, it was quickly washed in PBS, and water was absorbed on qualitative filter paper. One of the DIs was stored in a 10-ml centrifuge tube containing 5 ml of 4% paraformaldehyde for AB-PAS section preparation. The other two DIs were temporarily stored in liquid nitrogen and placed in a -80 °C refrigerator to be used for determination of gene and protein expression.

## Distal Intestinal Alcian Blue-Periodic Acid Schiff (AB-PAS) Section

For histopathological analyses, tissues were first embedded in paraffin, cut into 3–4 μm thick sections, and AB-PAS stained as described by Bergström et al. (14). A Leica DM 6000 optical microscope was used to observe 10 randomly selected plicas and muscle thicknesses in each section. The number of type II mucous cells on each plica was measured using the cellSens Standard 1.8 software, and the number of type II cells per millimeter was calculated.

## Total RNA Extraction and cDNA Synthesis

Total RNA extraction was performed on 100–150 mg of the distal intestine using 1 ml of Trizol (TRI Reagent solution, Invitrogen, Carlsbad, CA, USA) according to the instructions previously described by Orriss et al. (15). The RNA quality and quantity were assessed by electrophoresis on 1% agarose gels and spectrophotometric analysis with NanoDrop 2000 (A260:280 nm ratio), respectively. The PrimerScript™ RT-PCR Kit (TaKaRa, Kusatsu, Japan) was used to reverse-transcribe RNA into cDNA according to the manufacturer's instructions. Specific primers (**Table S3**) were designed according to the full-length sequences from transcriptome sequencing (not published) of the hybrid grouper. An Applied Biosystems 7500 Real-Time PCR System (Life Technologies, Carlsbad, CA, USA) was used to perform all the real-time PCR reactions using a SYBR ® Premix Ex Taq™ Kit (Takara). Relative gene expression was analyzed using the $2^{-\Delta\Delta CT}$ method according to Livak et al. (16).

## Total Protein Extraction and Sodium Dodecyl Sulfate-Polyacrylamide Gel Electrophoresis (SDS-PAGE)

PBS (1x), cell lysate, protease inhibitors, phosphorylase inhibitors, and PMSF were added to intestinal tissues for low-temperature fragmentation and centrifuged at 12,000 rpm for 20 min. Then, the intermediate layer was collected, and the protein concentration was determined using the Beyotime BCA kit using bovine serum as a standard, as described by Xing et al. (17). According to the experimental requirements of the Western Blot, loading buffer and PBS were added to the protein sample to make the final concentration 2 μg/μl. The EP tube containing the sample was then placed in boiling water for 10 min, quickly put on ice, and then moved to a -80°C refrigerator until use. SDS-PAGE was used to separate the protein samples (20 μg total protein per glue hole). The gel was run with a 90 V electrophoresis instrument for about 30 min, transferred to a 0.45 μm PVDF membrane (Millipore), and run under 110 V for approximately 80 min. The membrane was blocked with 5% skim milk powder in TBST buffer (band) for 1 h at room

temperature. TBST buffer was used to wash the membrane three times for 10 min each time. The primary antibody was incubated at room temperature for 2 h, washed three times with TBST for 10 min each time, and then incubated with the secondary antibody at room temperature for 1 h. ECL reagents (Millipore) were then used to visualize the membrane (band). The following antibodies were used in this study: antibodies against $PI_3$ kinase p85 (4292), phospho-$PI_3$ kinase class III ($Ser^{249}$, 13857S), Akt (9272S), phospho-Akt ($Ser^{473}$, 9271S), mTOR (2972S), phospho-mTOR ($Ser^{2448}$, 2971S), and GAPDH (2118S). All antibodies were purchased from Cell Signaling Technology. Since mammalian antibodies were used, amino acid sequences of the studied protein from hybrid grouper were aligned in the NCBI database (https://blast.ncbi.nlm.nih.gov/Blast.cgi) to check the identity of the antibodies. Western bands were quantified using NIH Image 1.63 software.

## Calculations and Statistical Analysis

WGR (weight gain rate, %) = 100 × (final weight - initial weight)/initial weight

SGR (specific growth rate, %/day) = 100 × (ln(final weight) - ln(initial weight))/days of experiment

SR (survival rate, %) = 100 × final fish number/initial fish number

FCR (feed coefficient ratio) = feed consumed/weight gain

Id/Ph = intestinal diameter/plica height

All statistical evaluations were subjected to one-way analysis of variance followed by Tukey's multiple range tests to determine significant differences among treatment groups. Analyses were done using Social Sciences version 22 (SPSS Inc., Chicago, IL, USA) at a level of $P < 0.05$, as described by Guo et al. (18). The results are presented as the mean ± SE.

# RESULTS

## Growth Performance and Challenge Test

The growth parameters and feed utilization are listed in **Table 1**. The initial body weight of fish in each group was 7.71 ± 0.04 g. After an 8-week feeding trial, fish fed the GL diet gained more SGR than those fed the FM, GH, and GH-SB diets ($P < 0.05$), and no significant difference was observed between the FM and GH-SB groups ($P > 0.05$). Compared with the FM group, the GH group had decreased FCR ($P < 0.05$). After a 7-day challenge test, the cumulative mortality (CM) in the GH and GH-SB groups increased ($P < 0.05$). No significant difference was found for SR ($P < 0.05$).

## Serum Biochemical Indexes

The serum biochemical indexes are shown in **Figure 1**. The IFN-γ content in the GL, GH, and GH-SB groups was significantly higher than that in the FM group ($P < 0.05$). IgG levels in the GH and GH-SB groups were significantly higher than those in the FM group ($P < 0.05$). The IL-1β content decreased and increased in the GL and GH groups, respectively, compared with that in the FM group ($P < 0.05$). The TNF-α content in the GH group was significantly higher than that in the GH-SB group ($P < 0.05$), and there was no significant difference among the FM, GL, and GH-SB groups ($P > 0.05$).

## Distal Intestinal Morphological Development

The distal intestinal morphological development is shown in **Figure 2**. The plica height, plica width, and muscle thickness (**Figure 3**) in the FM, GL, and GH-SB groups were higher than those in the GH group ($P < 0.05$). The plica height in the GL group was higher than that in the FM group ($P < 0.05$). Id/Ph decreased in the GL group ($P > 0.05$) and increased in the GH group ($P < 0.05$) compared with that in the FM group; there was no difference between the FM group and GH-SB group ($P > 0.05$). The number of type II mucous cells in the GL group was significantly higher than that in the FM and GH-SB groups ($P < 0.05$); this number was significantly lower in the GH group than in the FM, GL, and GH-SB groups ($P < 0.05$).

## Distal Intestinal Immune-Related Genes Expression

The distal intestinal antigen processing and presentation-related signaling molecule gene expression in the DI are presented in **Figure 4**. The mRNA levels of RICTOR, PRR5, MHC II, and CD4 were upregulated in the GH group ($P < 0.05$). The mRNA levels of mTOR, mTOR C1, and Deptor were upregulated in the GL, GH, and GH-SB groups compared with those in the FM group ($P < 0.05$). Meanwhile, the mRNA levels of mTOR, mTOR C1, and Deptor in the GH group were higher than those in the GL and GH-SB groups ($P < 0.05$). RhoA, PKC, GILT, and CTSB mRNA levels were downregulated in the GL, GH, and GH-SB groups ($P < 0.05$). The mRNA levels of $PI_3K$ RS5, IKKα, RAPTOR, PRAS40, mTOR C2, TEL2, p70 S6K, AEP, SGK1, CIITA, RFX5, CREB1, and 4EBP1 were upregulated in the GH

**TABLE 1** | Growth parameters and feed utilization of juvenile hybrid grouper (*Epinephelus fuscoguttatus*♀×*E. lanceolatus*♂) fed the experimental diets for 8 weeks.

| | FM | GL | GH | GH-SB |
|---|---|---|---|---|
| IBW (g) | 7.70±0.05 | 7.71±0.03 | 7.70±0.03 | 7.72±0.04 |
| FBW (g) | 50.60±0.26$^{b}$ | 58.80±0.54$^{c}$ | 45.09±0.70$^{a}$ | 52.29±1.31$^{b}$ |
| WGR (%) | 557.22±3.33$^{b}$ | 663.60±6.95$^{c}$ | 485.57±9.15$^{a}$ | 579.14±17.06$^{b}$ |
| SGR (%/day) | 3.36±0.01$^{b}$ | 3.63±0.02$^{c}$ | 3.15±0.05$^{a}$ | 3.42±0.08$^{b}$ |
| SR (%) | 100.00±0.00 | 95.83±1.60 | 99.17±0.83 | 97.78±2.22 |
| FCR | 0.81±0.05$^{ab}$ | 0.65±0.11$^{a}$ | 1.35±0.17$^{c}$ | 0.99±0.06$^{b}$ |

*Value show means ± SE (n = 4); Significance was evaluated by one-way ANOVA followed by Tukey's multiple range tests. FM, control diet; GL, containing 2% 11S diet, GH, containing 8% 11S diet, GH-SB, containing 8% 11S and 0.13% SB diet. IBW, initial body weight; FBW, final body weight; WGR, weight gain rate; SGR, specific growth rate; SR, survival rate; FCR, feed coefficient ratio.* $^{a, b, c}$*Mean values among all treatments with different letters were significantly different when the interaction was significant (P < 0.05).*

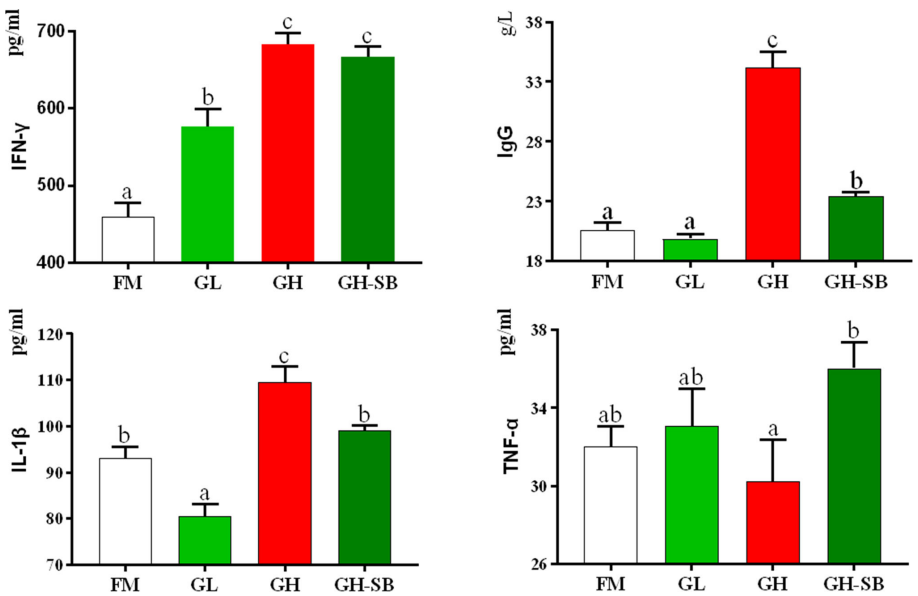


**FIGURE 1** | Serum biochemical indexes of juvenile hybrid grouper (*Epinephelus fuscoguttatus*♀×*E. lanceolatus*♂) fed the experimental diets for 8 weeks. Value show means ± SE (n = 4); Significance was evaluated by one-way ANOVA followed by Tukey's multiple range tests. FM, control diet; GL, containing 2% 11S diet, GH, containing 8% 11S diet, GH-SB, containing 8% 11S and 0.13% SB diet. IFN-γ, interferon-gamma; IgG, immunoglobulin G; IL-1β, interleukin-1 beta; TNF-α, tumor necrosis factor-alpha. [a,b,c]Mean values among all treatments with different letters were significantly different when the interaction was significant ($P < 0.05$).

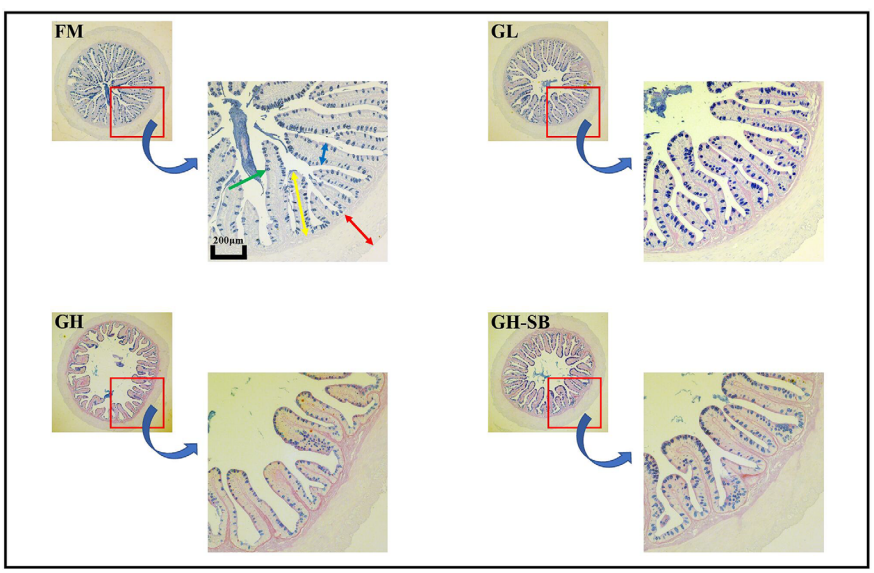


**FIGURE 2** | Distal intestinal AB-PAS staining section of juvenile hybrid grouper (*Epinephelus fuscoguttatus*♀×*E. lanceolatus*♂) fed the experimental diets for 8 weeks. Green arrow: type II mucous cell; red arrow: muscle thickness; yellow arrow: plica height: blue arrow: plica width.

group compared with those in the FM group ($P < 0.05$), and SGK1, CIITA, RFX5, CREB1, and 4EBP1 were downregulated in the GH-SB group ($P < 0.05$). TSC1, mLST8, and NFY mRNA levels in the GL and GH-SB groups were upregulated compared with those in the FM and GH groups ($P < 0.05$). The mRNA levels of TSC2 and Rheb in the GH-SB group were upregulated compared with those in the GH group ($P < 0.05$). The mRNA levels of S6 in the GL and GH-SB groups were downregulated compared with those in the FM group ($P < 0.05$). However, there were no significant differences in the mRNA levels of 3-PDK1, Akt, 4EBP1, EIF4E, EIF4B, Sin1, MHC I, and TCR mRNA in the FM, GL, GH, and GH-SB groups ($P > 0.05$).

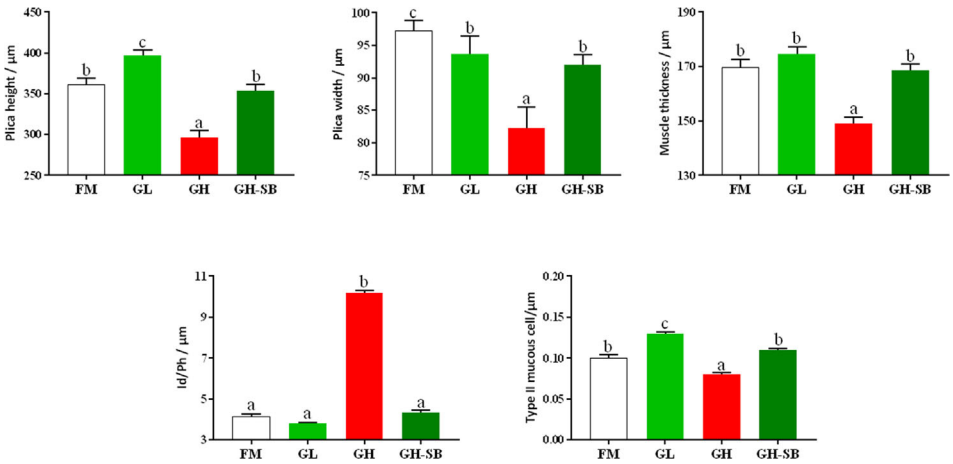


**FIGURE 3** | Distal intestinal morphological development of juvenile hybrid grouper (*Epinephelus fuscoguttatus*♀×*E. lanceolatus*♂) fed the experimental diets for 8 weeks. Value show means ± SE (n = 4); Significance was evaluated by one-way ANOVA followed by Tukey's multiple range tests. FM, control diet; GL, containing 2% 11S diet, GH, containing 8% 11S diet, GH-SB, containing 8% 11S and 0.13% SB diet. [a,b,c]Mean values among all treatments with different letters were significantly different when the interaction was significant ($P < 0.05$).

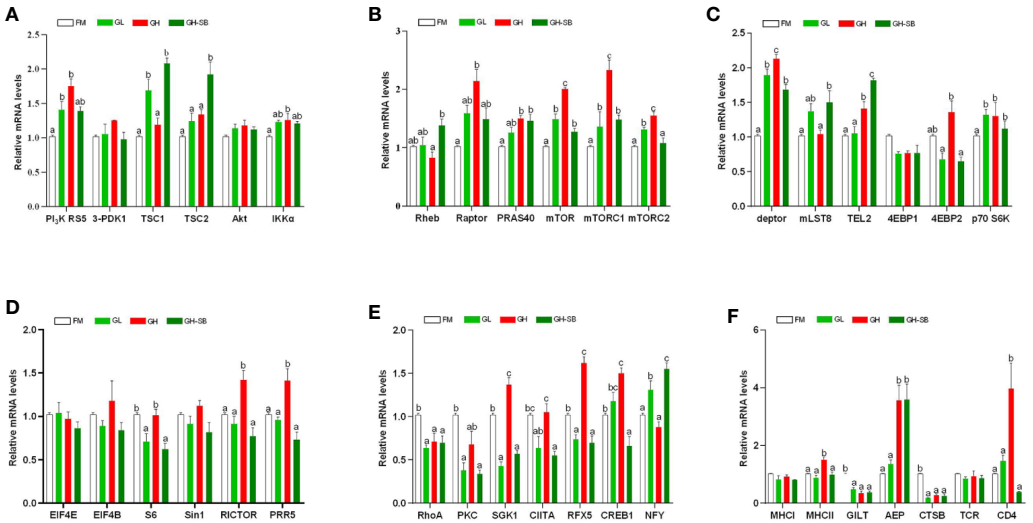


**FIGURE 4** | Distal intestinal antigen processing and presentation-related genes expression of juvenile hybrid grouper (*Epinephelus fuscoguttatus*♀×*E. lanceolatus*♂) fed the experimental diets for 8 weeks. Results are represented as mean ± SE (n = 4). **(A)** $PI_3K$ RS5, phosphatidylinositol 3-kinase regulatory subunit 5; 3-PDK1, 3-phosphoinositide dependent kinase-1; TSC1, tuberous 1; TSC2, tuberous 2; Akt, serine/threonine-protein kinase; IKKα, inhibitor of nuclear factor kappa-B kinase subunit α; **(B)** Rheb, Ras homolog enriched in brain; Raptor, regulatory associated protein of mTOR; PRAS40, proline-rich Akt1 substrate 1; mTOR, mammalian target of rapamycin; mTOR C1, mammalian target of rapamycin complex 1; mTOR C2, mammalian target of rapamycin complex 2; **(C)** deptor, DEP domain-containing mTOR-interacting protein; mLST8, target of rapamycin complex subunit lst8; TEL2, telomere length regulation protein; 4EBP1, eukaryotic translation initiation factor 4E binding protein 1; 4EBP2, eukaryotic translation initiation factor 4E binding protein 2; p70 S6K, ribosomal protein S6 kinase β1; **(D)** EIF4E, translation initiation factor 4E; EIF4B, translation initiation factor 4B; S6, small subunit ribosomal protein S6; Sin1, target of rapamycin complex 2 subunit; RICTOR, rapamycin-insensitive companion of mTOR; PRR5, proline-rich protein 5; **(E)** RhoA, Ras homolog gene family, member A; PKCα, protein kinase C α; SGK1, serum/glucocorticoid-regulated kinase 1; CIITA, major histocompatibility complex class II trans-activator; RFX5, regulatory factor X5; CREB1, cyclic AMP-responsive element-binding protein 1; NFY, nuclear transcription factor Y subunit α; **(F)** MHC I, major histocompatibility complex class I antigen; MHC II, major histocompatibility complex class II antigen; GILT, gamma-interferon-inducible-lysosomal thiol reductase; AEP, asparaginyl endopeptidase; CTSB, cathepsin B; TCR, T cell receptor; CD4, T-cell surface glycoprotein. Significance was evaluated by one-way ANOVA followed by Tukey's multiple range tests. FM, control diet; GL, containing 2% 11S diet, GH, containing 8% 11S diet, GH-SB, containing 8% 11S and 0.13% SB diet. [a,b,c]Mean values among all treatments with different letters were significantly different when the interaction was significant ($P < 0.05$).

## Distal Intestinal $PI_3K$-Akt-mTOR Protein Expression

The distal intestinal $PI_3K$/Akt/mTOR protein expression in DI is presented in **Figure 5**. The P-$PI_3K$ and P-$PI_3K$/T-$PI_3K$ in the GH group showed a significant increase compared with those in the FM group ($P < 0.05$) but a significant decrease in the GH-SB group compared with those in the GH group ($P < 0.05$). By contrast, for T-$PI_3K$, P-$PI_3K$, and P-$PI_3K$/T-$PI_3K$, no significant differences were noted between the FM and GL groups. In addition, T-Akt and P-Akt levels in the GL and GH groups and P-Akt/T-Akt in the GH group were significantly increased compared with those in the FM group ($P < 0.05$). As for the GH-SB group, T-$PI_3K$, P-$PI_3K$, and P-$PI_3K$/T-$PI_3K$ showed a significant decrease compared to those in the GL, GH, and GH groups, respectively ($P < 0.05$). T-mTOR and P-mTOR showed a significant decrease in the GL group as well as a significant decrease in the GH-SB group. P-mTOR and P-mTOR/T-mTOR increased significantly in the GH group ($P < 0.05$).

# DISCUSSION

## Growth Performance and Challenge Test

11S is one of the antigen proteins with high content and strong antigenicity in soybean meal and its processed products. According to the protein structure, 11S generally accounts for about 40% of the total protein content of soybean meal (19). High-dose 11S destroys the morphological structure, reduces nutrient absorption, and reduces immunity of the intestine; however, low-dose 11S intake usually has an immune-enhancing effect. Li et al. showed that supplementing the feed with 3% of 11S increased the final weight and SGR of juvenile turbot, while 12% decreased weight and SGR (9). This outcome matches our results. In this experiment, growth performance in the GH group was significantly decreased by 8% 11S. This corresponds to trends found for SGR, feed intake (FI), and feed efficiency (FE) in grass carp (*Ctenopharyngodon idella*) and FE in Jian carp (*Cyprinus carpio* var Jian) (7), which were all also decreased by 8% 11S.

After adding sodium butyrate to the GH group to create group GH-SB, the WGR and SGR were significantly increased. The FCR was also significantly decreased compared with the GH group. Similar results were found in turbot (11) and rice field eel (*Monopterus albus*) (20). This indicates that sodium butyrate could alleviate growth inhibition caused by high levels of soybean meal or 11S in the feed. As an additive, SB can be absorbed in the intestinal lumen, and it can quickly provide energy for intestinal epithelial cells through oxidation (21). It is also an activator that improves intestinal villi proliferation and crypt deepening (22), and it enhances intestinal absorption capacity (13). Its special smell is very attractive to piglets, so it can be used as an attractant, SB also strengthens its immunity and digestion (23).

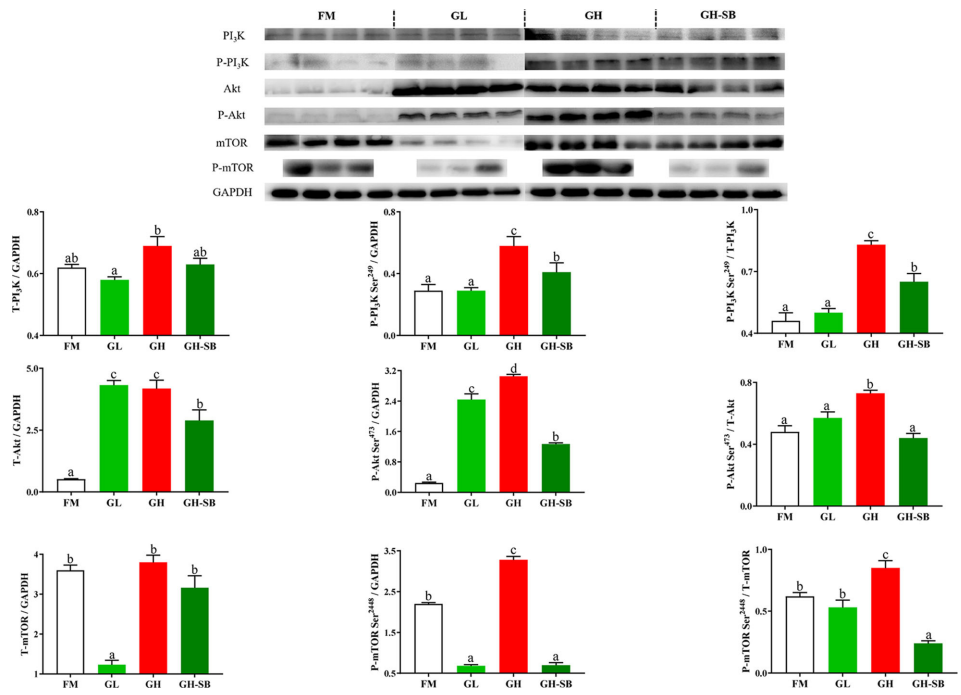


**FIGURE 5** | Dietary modulations of distal intestinal responses in the target of $PI_3K$/Akt/mTOR signaling pathway. Results are represented as mean ± SE (n = 4). Significance was evaluated by one-way ANOVA followed by Tukey's multiple range tests. FM, control diet; GL, containing 2% 11S diet, GH, containing 8% 11S diet, GH-SB, containing 8% 11S and 0.13% SB diet. [a,b,c]Mean values among all treatments with different letters were significantly different when the interaction was significant ($P < 0.05$).

These may be the reasons for the improved growth performance of the hybrid grouper.

To explore the effects of different doses of 11S and SB supplementation on the disease resistance of the hybrid grouper, we conducted a one-week challenge test experiment after the end of the 8-week breeding experiment. As a gram-negative bacterium, *Vibrio parahaemolyticus* has a wide distribution, mainly living in seawater, fish, shrimp, shells, and crustaceans (24). It usually causes gastrointestinal infections and extra-intestinal infections in aquatic animals. In addition, it can also cause symptoms such as diarrhea and fever if people eat raw or uncooked seafood with *Vibrio parahaemolyticus* (25). In gilthead sea bream (*Sparus aurata*) (26% replacement level) (26), the SGR was increased in the low soybean substitution level group, and similar results were found in Atlantic salmon (25% and 33% replacement levels) (27), white snook (*Centropomus viridis*) (30% replacement level) (28), and Russian sturgeon (*Acipenser gueldenstaedtii*) (20% replacement level) (29). This trend might be related to increased immunity. For this reason, we used *Vibrio parahaemolyticus* to conduct a challenge experiment to observe the change in cumulative mortality after the breeding experiment (**Figure S1**). We found that the CM in the FM and GL groups were not significantly different. In addition, no significant difference in CM was found between the GH and GH-SB groups. We speculated that a low dose of 11S and the addition of SB does not seem to be associated with disease resistance for the growth improvement of the hybrid grouper.

## Serum Immunity

IFN-γ is produced by Th1 and NK cells. Its main function is immune regulation, and it is an activator of phagocytes and neutrophils. It can promote the differentiation of T and B cells and enable various types of cells to express MHC class II antigens. In an inflammatory environment, iNKT cells are stimulated to produce IFN-γ. In this study, serum IFN-γ levels increased in the GL group and the GH group. This indicates that low-dose 11S could properly enhance immunity by increasing IFN-γ. When the amount of 11S increases, the secretion of IFN-γ will increase abnormally. Based on the results, this abnormal increase cannot be alleviated by supplementing with SB. IgG is the main antibody component in serum and extracellular fluid. It plays an important role in immunity against infections, especially in the secondary immune response (30). It is the main antibody of toxins, viruses, and bacteria, which can react with the corresponding antigen to eliminate the damage of the antigen to the body. In this experiment, after adding high-dose 11S, serum IgG showed a significant increase. This indicates that IgG is also involved in the 11S-mediated allergic reaction of the hybrid grouper, which is similar to the results of a study on piglets (31). After supplementing with SB, IgG was reduced to a certain extent, indicating that SB can alleviate the allergic reaction caused by 11S by lowering the serum IgG content. However, in nursery pigs, the content of IgG was upregulated by SB (32). Combined with the results of this experiment, we speculate that the role of SB mainly enhances serum immunity by modulating the secretion of host immune-enhancing cytokines in the hybrid grouper. This regulation could be closely related to the supplying of energy for intestinal epithelial cells and regulation of the expression of intestinal epithelial inflammatory factors (33).

IL-1β is mainly produced by mononuclear macrophages after being stimulated by external antigens which can activate T lymphocytes and B lymphocytes, thereby upregulating immune function (34). IL-1β is also an important indicator for measuring the severity of inflammatory bowel disease. The occurrence of enteritis is usually accompanied by an abnormal increase in serum IL-1β (35–37). In this experiment, supplementation with 11S at low and high levels reduced and increased the serum IL-1β content, respectively. After further supplementation with SB, the IL-1β content returned to the level of the control group. IL-1β is a pro-inflammatory cytokine with multiple biological activities. The reason for the increase of IL-1β in the GH group may be that when a high dose of 11S destroys small intestinal epithelial cells, a large number of monocytes in the intestinal mucosa propria are infiltrated, Th1 lymphoid immune cells are activated, and the pro-inflammatory factor IL is produced (38). In addition, IL-1β can stimulate T-type immune cells to differentiate and produce IFN-γ. In mice, SB may inhibit pro-inflammatory response by downregulating IL-1β (39). IL-1β may be decreased by SB for ischemic stroke in middle-aged female rats (40). These results are similar to the results of this experiment on hybrid grouper. Our results suggest that SB can also alleviate intestinal inflammation caused by high levels of 11S by inhibiting the secretion of IL-1β.

The massive production of TNF-α as a typical pro-inflammatory cytokine in humans is an important link in the pathogenesis of intestinal inflammation (41, 42). TNF-α is mainly produced by specific cells such as macrophages and monocytes, and it has a variety of biological activities. By mediating phosphorylation and ubiquitination of IkB, the nuclear localization sequence of NF-κB is exposed, and NF-kB is immediately transferred. It is located in the nucleus and binds to the NF-κB site to initiate gene transcription, leading to the release of large amounts of cytokines including TNF-α. The released cytokines can further activate NF-κB and intensify further inflammation (43). We found that high levels of 11S increased the serum TNF-α level of the hybrid grouper, indicating that 11S can induce intestinal inflammation by increasing TNF-α, which is similar to the results of studies on pigs (44) and Chinese mitten crabs (*Eriocheir sinensis*) (45). However, the aggravation caused by 11S in the hybrid grouper can be alleviated by supplementing with SB. We speculate that this may be related to the inhibitory effect of SB on NF-kB (46).

## Distal Intestinal Morphological Development (AB-PAS)

The fish intestine is the most important place for fish to absorb nutrients and is also an important immune organ. Whether the intestine is healthy and structurally intact directly determines the growth and immune performance of the fish (47). Compared with mammals, fish have thin intestinal walls and fragile intestines (only one-twentieth the thickness of the mammalian intestinal wall), which are extremely vulnerable to damage, destruction, and

changes in external factors, especially feed ingredients. Therefore, repair and protection of fish intestines has always been one of the hot spots in fish nutrition and immunology research. The height of fish intestinal plica usually determines the fish's immunity levels. Generally, the higher the fold, the stronger the immunity and absorption capacity; however, the fold height cannot accurately measure intestinal development. Therefore, we used the diameter of the intestine divided by the height of the plica to evaluate the histology of the intestine. Although there was no statistically significant difference between the Id/Ph of the GL group and the FM group in the distal intestine, there was still a certain degree of reduction. The GH group showed a significant increase, indicating that high doses of 11S can significantly inhibit intestinal development. This can be observed in the intestinal AB-PAS section (**Figure 2**). Adding 8% of 11S to the feed can significantly inhibit the plica height of the proximal, mid, and distal intestines of grass carp (7), which is a similar result to this experiment. In mice, the intestinal inflammation induced by SB also showed a decrease in plica height (48).

Furthermore, the muscle thickness of the distal intestine was also affected by 11S. The thickness of the intestinal muscle layer can reflect the peristaltic ability of the intestine, thereby preventing the occurrence of intestinal diseases to a certain extent (49). This shows that after adding a high dose of 11S to the feed, the peristalsis of the distal intestine is inhibited, while a low dose of 11S could promote peristalsis of the distal intestine. In the GH-SB group, we found that plica height, muscle thickness, and Id/Ph were all significantly improved compared with the GH group, indicating that SB can effectively alleviate the inhibition of development caused by high-dose 11S in the distal intestine of the hybrid grouper. SB can regulate the tight junction of the intestine (50) and enhance intestinal epithelial barrier function (51). We speculate that this positive protective effect on the intestines also exists in hybrid groupers. As previously mentioned, fish intestines have a strong immune function because they have a large number of mucous cells. They can produce acidic mucus, which plays an important role in protein digestion, bacterial capture, and immune stimulation (52). Studying the source of stimulation causing mucous cell differentiation, increased number and density, and improved immunity of fish is a valuable area of research.

From **Figure 2**, it can be found that type II mucous cells are mainly present in the distal intestine of the hybrid grouper (AB-PAS dyed blue). Interestingly, the density of mucous cells in the GL group increased significantly, suggesting that low doses of 11S can act as a source of stimulation to promote the differentiation of type II mucosal cells. This would cause secretion of acidic mucopolysaccharides and immunoglobulins with antibacterial and bactericidal effects, and enhancement of non-specific immunity in fish. The density of type II mucous cells in the GH group was significantly reduced, indicating that the high dose of 11S inhibited the differentiation of type II mucous cells. Type II mucosal cell density increased again after the addition of SB at high doses of 11S. This indicates that SB relieved the inhibition of type II mucosal cell differentiation caused by high doses of 11S, promoted differentiation, and performed normal physiological functions. This may be related to the ability of SB to induce cell differentiation (53) and promote anti-apoptosis (54).

## Distal Intestinal Immune Response

Changes in intestinal immune function are usually accompanied by the regulation of related immune pathways and the activation and inhibition of key components, which are finally manifested in growth and tissue morphology. Low-dose 11S has a certain immune enhancement effect on hybrid grouper, while high-dose 11S produces immunosuppression and induces enteritis. At the same time, the addition of sodium butyrate can act on the hindgut to make hybrid groupers exhibit better growth and immunity. However, it is currently unclear how this difference is regulated. A previous study showed that the uptake of soybean antigens by the intestine of aquatic animals mainly occurs in the latter half of the intestine of fish (55); therefore, we selected the distal intestine near the cloaca for a targeted study. To further explore how low and high doses of 11S and sodium butyrate regulate the distal intestine of the hybrid grouper, we performed the following quantitative research.

The weight of glycinin molecules is 350 kDa. After the hybrid grouper ingests glycinin, most of the glycinin is degraded into peptides and amino acids. A small portion passes through the intestinal epithelium in the form of macromolecular proteins, completely enters the blood and lymph, and stimulates the intestinal mucosal immune tissue to produce related allergic reactions (56, 57). The major histocompatibility complex (MHC) is a highly polymorphic group of genes in vertebrate coding that is directly related to the immune response (58). Fish MHC molecules have abundant polymorphisms. The classic MHC I and MHC II molecules of bony fish belong to different linkage groups and play an important role in antigen presentation in the immune system (59). In this experiment, the addition of 11S at a low level (**Figure 6A**) showed no significant regulation in the expression of MHC I and MHC II, indicating that the normal immune recognition was not disturbed. The CTSB and AEP involved in the formation of endosomes were downregulated, which slowed the inhibition of intestinal cell differentiation by CTSB. Thus, AEP does not seem to be involved in this process. The $PI_3K$ protein family is involved in the regulation of cell proliferation, differentiation, apoptosis, and other cell functions. The activation of $PI_3K$ can produce the second messenger PIP3 on the plasma membrane (60). It can also act as a second messenger to bind to the PH domain of Akt, and make Akt Thr308 and Ser473 phosphoric acid under the catalysis of PDK1 and PDK2, respectively. As a highly conserved serine/threonine-protein kinase, mTOR usually forms two different complexes in the body, mTOR C1 and mTOR C2, which play an important role in regulating the intestinal immune response (61). $PI_3K$ RS5 was significantly upregulated, while Sin1, RICTOR, PRR5, and 3-PDK1, the four key components that act on the Akt pathway, did not change significantly, indicating that $PI_3K$ did not directly act on Akt or through mTOR C2. mTOR C2 was upregulated, and according to the results of the Western blot (**Figure 5**), Akt was phosphorylated at Ser473, indicating that mTOR C2 is involved in Akt activation. We found that both mTOR C1 and mTOR C2

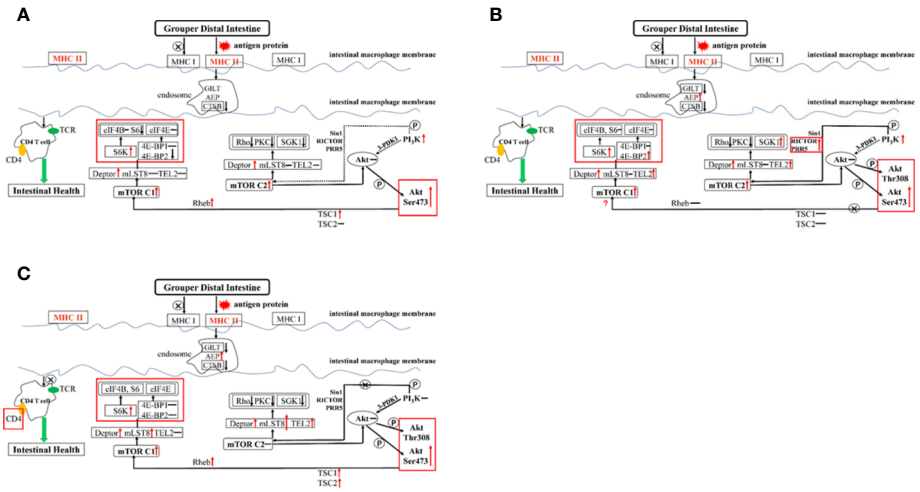


**FIGURE 6** | Summary of the potential pathways about exogenous antigen 11S processing and presentation in the distal intestine. Letter P in a circle, phosphorylation; ↓, down-regulated; ↑, up-regulated; –, constant; →, through; –⊗→, not through; ···, might through. **(A)** GL group; **(B)** BH group; **(C)** GSH-SB group.

were the Deptor parts which played a major regulatory role in the distal intestine of the hybrid grouper rather than mLST8 and TEL2. Deptor promoted the differentiation of intestinal cells by inhibiting the activity of Rho, PKC, and SGK1. Previous studies have found that Rho is highly expressed in the intestine of Crohn's disease with intestinal inflammation (62). PKC induces keratinocyte apoptosis and intradermal inflammation through independent signaling pathways (63), and inflammation signals stimulate the expression of SGK1 in macrophages (64), indicating that low-dose 11S can inhibit inflammation by downregulating Rho, PKC, and SGK1. Similar to how Akt is phosphorylated at Ser473, TSC1 and TSC2 can also be phosphorylated to enrich Rheb, thereby activating mTOR C1, upregulating downstream S6K, and downregulating 4E-BP2 instead of 4E-BP1 through Deptor. 4E-BP2 can limit the anti-inflammatory response of macrophages by inhibiting IL-10 and cyclooxygenase-2 (65), and the activation of p70 S6K can reduce skin inflammation in atopic dermatitis (66). Therefore, in the hybrid grouper, low-dose 11S has a certain immune-enhancing effect, which may be closely related to inhibition of 4E-BP2 and promotion of the expression of p70 S6K.

When high-dose 11S was supplemented (**Figure 6B**), MHC I did not participate in regulation, but MHC II did, similar to the results of low-level addition. MHC II was activated, inhibiting CTSB and GILT. The key gene AEP in the process of CD4 T cell activation (67) was sharply upregulated, and the regulation of CD4 T cells was completely opened. From the results of CD4 glycoprotein and TCR, it is mainly the CD4 glycoprotein acting on the cell surface. $PI_3K$ was significantly upregulated, while Sin1 and 3-PDK1 still had no significant regulation. RICTOR and PRR5 were upregulated, indicating that $PI_3K$ does not directly act on Akt, but can activate mTOR C2 through RICTOR and PRR5 to further act on Akt. In contrast to the low dose, mTOR C2 also upregulates TEL2 while acting on Deptor. Deptor promotes the differentiation of intestinal cells by inhibiting the activity of Rho and PKC kinases, but not SGK1. At the same time, TEL2 activation leads to the activation of SGK1, leading to intensified intestinal inflammation. We found that in the step from Akt Ser473 phosphorylation to mTOR C1, TSC1 and TSC2 remained unchanged, and Rheb was not enriched. This result indicated that the path from Akt to mTOR C1 was blocked; however, mTOR C1 still showed high expression, indicating that there may be some other regulations. In a mouse intestinal gastric cancer model, mTOR C1 was overactivated, and the activation of the $PI_3K$/mTOR C1 pathway was necessary for the occurrence of inflammation-related gastrointestinal tumors (68). Combined with the results of this experiment, the small molecule protein downstream of mTOR C1 seems to be more suitable as a marker to detect hybrid grouper enteritis. The two key assembly factors, Deptor and TEL2, were simultaneously activated, and they both upregulated S6K and 4E-BP2, reducing distal intestine anti-inflammatory ability.

SB has a positive effect on hybrid groupers when considering growth, serum indexes, and distal intestinal development. To explore how SB protects the distal intestine, thereby alleviating the intestinal damage caused by high doses of 11S, we further supplemented SB to the GH group. After high-dose 11S supplementation with SB (**Figure 6C**), we found that MHC I and MHC II were similar to the GL group. Neither were significantly upregulated and both were in a normal state. Compared with the GH group, MHC II was significantly downregulated. Similar to the high-dose 11S group, CTSB and GITL were inhibited, AEP was still sharply upregulated, and the regulation of CD4 T cells was activated. The difference is that, from the expression of CD4, the glycoprotein on the surface of CD4 T cells seems to stop receiving signals from the endosomes. $PI_3K$ phosphorylation increased in the GH-SB group compared with that in the FM group (**Figure 5**). Sin1, RICTOR, PRR5, and 3-PDK1 did not cause significant regulation and mTOR C2 was not activated, indicating that this pathway was blocked to a certain extent. Further research found that, compared

with the high-dose group, mLST8 was upregulated and SGK1 was thereby inhibited, which protected the distal intestine. After Akt Ser473 is phosphorylated to mTOR C1, both TSC1 and TSC2 are activated, which causes Rheb enrichment and activation of mTOR C1. mTOR C1 upregulates S6K and acts on Deptor and mLST8 simultaneously, but 4E-BP1 and 4E-BP2 remain unchanged to protect CD4 T cells from normal differentiation and function.

## CONCLUSIONS

In the current study, low-dose 11S increased the SGR, feed utilization rate, and density of distal intestinal-type II mucous cells of the hybrid grouper. The serum immune function was enhanced by the secretion of IFN-γ. High-dose 11S hurt SGR, feed utilization, and distal intestinal development. The serum immune function was weakened due to the abnormal increase in IgG and IL-1β. After supplementation with sodium butyrate, IgG, IL-1β, and TNF-α can be adjusted to normal levels, causing enhancement to immunity in the distal intestine. Hybrid groupers present foreign antigen proteins through MHC II. $PI_3K$ is not associated with mTOR C2. mTOR C1 improves intestinal immunity by inhibiting 4E-BP2 under low-dose 11S. $PI_3K$ associated with mTOR C2 upregulates SGK1 through RICTOR and PRR5, while mTOR C1 upregulates 4E-BP2 through TEL2, aggravating intestinal inflammation. After supplementing with SB, $PI_3K$/mTOR C2 is blocked, and mLST8 inhibits SGK1. At the same time, mTOR C1 inhibits the expression of 4E-BP2 through mLST8 and relieves the inflammation caused by the high dose of 11S in the intestine. In summary, the hybrid grouper obtained different serum and intestinal immune responses under the conditions of different doses of 11S, and these responses were ultimately manifested in growth performance. Sodium butyrate can effectively improve serum immunity and relieve intestinal inflammation caused by high dose 11S.

## DATA AVAILABILITY STATEMENT

The raw data supporting the conclusions of this article will be made available by the authors, without undue reservation.

## ETHICS STATEMENT

The animal protocol was approved by the ethics review board of Guangdong Ocean University. All procedures were performed according to the standards of the National Institutes of Health Guide for the Care and Use of Laboratory Animals (NIH Publication No. 8023, revised 1978) and relevant Chinese policies.

## AUTHOR CONTRIBUTIONS

All authors have actively contributed to this study. The author's contributions are as follows: HL and BT designed the study. BY conducted the study and analyzed the data. XD participated in the interpretation of the results. BY wrote the manuscript. QY, SC, and SZ purchased the reagent supplies. HL revised the manuscript. All authors contributed to the article and approved the submitted version.

## FUNDING

This work was supported by the National Key R&D Program of China (2019YFD0900200), the National Natural Science Foundation of China (no. 31772864), and the Natural Science Foundation of Guangdong Province (2018A030313154&2020A1515011129).

## ACKNOWLEDGMENTS

We would like to thank the Key Laboratory of Control for Disease of Aquatic Economic Animals of Guangdong Higher Education Institutes (Zhanjiang, China) for kindly providing the *Vibrio parahaemolyticus* strain in this experiment.

## SUPPLEMENTARY MATERIAL

The Supplementary Material for this article can be found online at: https://www.frontiersin.org/articles/10.3389/fimmu.2020.615980/full#supplementary-material

## REFERENCES

1. Porrello S, Lenzi M, Tomassetti P, Persia E, Finoia MG, Mercatali I. Reduction of aquaculture wastewater eutrophication by phytotreatment ponds system II. Nitrogen and phosphorus content in macroalgae and sediment. *Aquaculture* (2003) 219:531–44. doi: 10.1016/S0044-8486(03)00013-9
2. Resources N. *Nutrient Requirements of Fish and Shrimp*. Washington, DC: National Academy Press (2011).
3. Baeverfjord GT, Krogdahl A. Development and regression of soybean meal induced enteritis in Atlantic salmon, *Salmo salar* L., distal intestine: a comparison with the intestines of fasted fish. *J Fish Dis* (2010) 19:375–87. doi: 10.1046/j.1365-2761.1996.d01-92.x
4. Bakke-Mckellep AM, Sperstad S, Penn MH, Salas PM, Refstie S, Landsverk T, et al. Effects of dietary soybean meal, inulin and oxytetracycline on gastrointestinal histological characteristics, distal intestine cell proliferation and intestinal microbiota in Atlantic salmon (*Salmo salar L.*). *Br J Nutr* (2007) 97:699–713. doi: 10.1017/S0007114507381397
5. Yin B, Liu HY, Tan BP, Dong XH, Chi SY, Yang QH, et al. Cottonseed protein concentrate (CPC) suppresses immune function in different intestinal segments of hybrid grouper ♀*Epinephelusfuscoguttatus* × ♂*Epinephelus. lanceolatu* via TLR-2/MyD88 signaling pathways. *Fish Shellfish Immunol* (2018) 81:318–28. doi: 10.1016/j.fsi.2018.07.038
6. Zhang W, Tan BP, Ye GL, Wang JX, Zhang HT. Identification of potential biomarkers for soybean meal-induced enteritis in juvenile pearl gentian grouper, *Epinephelus lanceolatus*♂ × *Epinephelus fuscoguttatus*♀. *Aquaculture* (2019) 512:734337. doi: 10.1016/j.aquaculture.2019.734337
7. Jiang WD, Hu K, Zhang JX, Liu Y, Jiang J, Wu P, et al. Soyabean glycinin depresses intestinal growth and function in juvenile Jian carp (*Cyprinus carpio* var Jian): protective effects of glutamine. *Br J Nutr* (2015) 114:1569–83. doi: 10.1017/S0007114515003219

8. Venold FF, Penn MH, Krogdahl S, Overturf K. Severity of soybean meal induced distal intestinal inflammation, enterocyte proliferation rate, and fatty acid binding protein (Fabp2) level differ between strains of rainbow trout (*Oncorhynchus mykiss*). *Aquaculture* (2012) 364-365:281–92. doi: 10.1016/j.aquaculture.2012.08.035
9. Li YX, Yang P, Zhang YJ, Ai QH, Xu W, Zhang WB, et al. Effects of dietary glycinin on the growth performance, digestion, intestinal morphology and bacterial community of juvenile turbot, *Scophthalmus maximus* L. *Aquaculture* (2017) 479:125–33. doi: 10.1016/j.aquaculture.2017.05.008
10. Dua S, Dowey J, Foley L, Islam S, Clark AT. Diagnostic value of tryptase in food allergic reactions: a prospective study of 160 adult peanut challenges. *J Aller Cl Imm-Pract* (2018) 6:1692–8. doi: 10.1016/j.jaip.2018.01.006
11. Liu Y, Chen ZC, Dai JH, Yang P, Xu WQ, Ai QH, et al. Sodium butyrate supplementation in high-soybean meal diets for turbot (*Scophthalmus maximus* L.): Effects on inflammatory status, mucosal barriers and microbiota in the intestine. *Fish Shellfish Immunol* (2019) 88:65–75. doi: 10.1016/j.fsi.2019.02.064
12. Wang CC, Wu H, Lin FH, Gong R, Hu CH. Sodium butyrate enhances intestinal integrity, inhibits mast cell activation, inflammatory mediator production and JNK signaling pathway in weaned pigs. *Innate Immun* (2018) 24:40–6. doi: 10.1177/1753425917741970
13. Wu P, Tian L, Zhou XQ, Jiang WD, Liu Y, Jiang J, et al. Sodium butyrate enhanced physical barrier function referring to Nrf2, JNK and MLCK signaling pathways in the intestine of young grass carp (*Ctenopharyngodon idella*). *Fish Shellfish Immunol* (2018) 73:121–32. doi: 10.1016/J.FSI.2017.12.009
14. Bergstrom HJ, Birchenough G, Johansson MEV, Hansson GC. Gram-positive bacteria are held at a distance in the colon mucus by the lectin-like Protein ZG16. *Proc Natl Acad Sci U S A* (2017) 113:13833–8. doi: 10.1016/S0016-5085(17)33402-9
15. Orriss IR, Key ML, Brandao-Burch A, Patel JJ, Burnstock G, Arnett TR. The regulation of osteoblast function and bone mineralisation by extracellular nucleotides: The role of p2x receptor. *Bone* (2012) 51:389–400. doi: 10.1016/j.bone.2012.06.013
16. Livak KJ, Schmittgen TD. Analysis of relative gene expression data using real-time quantitative PCR and the 2(-Delta Delta C(T)) method. *Methods* (2001) 25:402–8. doi: 10.1006/meth.2001
17. Xing FZ, Zhao YG, Zhang YY, He L, Zhao JK, Liu MY, et al. Nuclear and membrane estrogen receptor antagonists induce similar mTORC2 activation-reversible changes in synaptic protein expression and actin polymerization in the mouse hippocampus. *CNS Neurosci Ther* (2018) 24:495–507. doi: 10.1111/CNS.12806
18. Guo XZ, Ran C, Zhang Z, He SX, Jin M, Zhou ZG. The growth-promoting effect of dietary nucleotides in fish is associated with an intestinal microbiota-mediated reduction in energy expenditure. *J Nutr* (2017) 147:781–8. doi: 10.3945/jn.116.245506
19. Utsumi S, Matsumura Y, Mori T. Structure-function relationship of soy proteins. In: *Food proteins and their applications*. New York: Marcel Dekker Inc. (1997). pp. 257-91.
20. Zhang JZ, Zhong L, Chi SY, Chu WY, Liu YL, Hu Y. Sodium butyrate supplementation in high-soybean meal diets for juvenile rice field eel (*Monopterus albus*): Effects on growth, immune response and intestinal health. *Aquaculture* (2020) 520:734952. doi: 10.1016/j.aquaculture.2020.734952
21. Yaku K, Enami Y, Kurajyo C, Matsui-Yuasa I, Konishi Y, Kojima-Yuasa A. The enhancement of phase 2 enzyme activities by sodium butyrate in normal intestinal epithelial cells is associated with Nrf2 and p53. *Mol Cell Biochem* (2012) 370:7–14. doi: 10.1007/s11010-012-1392-x
22. Liu WS, Yang YO, Zhang JL, Gatlin DM, Ringø E, Zhou ZG. Effects of dietary microencapsulated sodium butyrate on growth, intestinal mucosal morphology, immune response and adhesive bacteria in juvenile common carp (*Cyprinus carpio*) pre-fed with or without oxidised oil. *Br J Nutr* (2014) 112:15–29. doi: 10.1017/S0007114514000610
23. Mazzoni M, Gall ML, De Filippi S, Minieri L, Trevisi P, Wolinski J, et al. Supplemental sodium butyrate stimulates different gastric cells in weaned pigs. *J Nutr* (2008) 138:1426–31. doi: 10.1111/j.1365-277X.2008.00867.x
24. Gulati A, Kumar R, Mukhopadhaya A. Differential recognition of *Vibrio parahaemolyticus* OmpU by toll-like receptors in monocytes and macrophages for the induction of proinflammatory responses. *Infect Immun* (2019) 87:e00809–18. doi: 10.1128/IAI.00809-18
25. Baumeister L, Hochman ME, Schwarz JR, Brinkmeyer R. Occurrence of *Vibrio vulnificus* and toxigenic *Vibrio parahaemolyticus* on sea catfishes from Galveston Bay, Texas. *J Food Prot* (2014) 77:1784–6. doi: 10.4315/0362-028X.JFP-14-175
26. Martínez-Llorens S, Vidal AT, Garcia IJ, Torres MP, Cerd MJ. Optimum dietary soybean meal level for maximizing growth and nutrient utilization of on-growing gilthead sea bream (*Sparus aurata*). *Aquac Nutr* (2010) 15:320–8. doi: 10.1111/j.1365-2095.2008.00597.x
27. Carter CG, Hauler RC. Fish meal replacement by plant meals in extruded feeds for Atlantic salmon, *Salmo salar* L. *Aquaculture* (2000) 185:299–311. doi: 10.1016/S0044-8486(99)00353-1
28. Arriaga-Hernández D, Hernández C, Martínez-Montaño E, Ibarra-Castro L, Lizárraga-Velázquez E, Leyva-López N, et al. Fish meal replacement by soybean products in aquaculture feeds for white snook, *Centropomus viridis*: Effect on growth, diet digestibility, and digestive capacity. *Aquaculture* (2020) 530:735823. doi: 10.1016/J.aquaculture.2020.735823
29. Emre N, Güroy D, Yalim FB, Emre Y, Güroy B, Mantoğlu S, et al. Growth performance, body composition, haematological and serum parameters to fish meal replacement by soybean meal and cottonseed meal in Russian Sturgeon (*Acipenser gueldenstaedtii*). *J Limnol Freshw Fish Res* (2018) 4:169–76. doi: 10.17216/LIMNOFISH.460773
30. Arnold JN, Dwek RA, Rudd PM, Sim RB. Mannan binding lectin and its interaction with immunoglobulins in health and in disease. *Immunol Lett* (2006) 106:103–10. doi: 10.1016/j.imlet.2006.05.007
31. Taliercio E, Kim SW. Epitopes from two soybean glycinin subunits are antigenic in pigs. *J Sci Food Agric* (2013) 93:2927–32. doi: 10.1002/jsfa.6113
32. Jang YD, Lindemann MD, Monegue HJ, Monegue JS. The effect of coated sodium butyrate supplementation in sow and nursery diets on lactation performance and nursery pig growth performance. *Livest Sci* (2017) 195:13–20. doi: 10.1016/j.livsci.2016.11.005
33. Melo ADB, Silveira H, Bortoluzzi C, Lara LJ, Garbossa CAP. Intestinal alkaline phosphatase and sodium butyrate may be beneficial in attenuating LPS-induced intestinal inflammation. *Genet Mol Res GMR* (2016) 15:1–9. doi: 10.4238/gmr15048875
34. Kallapur S G, Presicce P, Senthamaraikannan P, Alvarez M, Tarantal A,F, Miller LM. Intra-amniotic IL-1β induces fetal inflammation in Rhesus Monkeys and alters the regulatory T Cell/IL-17 balance. *J Immunol* (2013) 191:1102–9. doi: 10.4049/jimmunol.1300270
35. Coccia M, Harrison OJ, Schiering C, Asquith MJ, Becher B, Powrie F, et al. IL-1β mediates chronic intestinal inflammation by promoting the accumulation of IL-17A secreting innate lymphoid cells and CD4+ Th17 cells. *J Exp Med* (2012) 209:1595–609. doi: 10.1084/JEM.20111453
36. Bersudsky M, Luski L, Fishman D, White RM, Ziv-Sokolovskaya N, Dotan S, et al. Non-redundant properties of IL-1α and IL-1β during acute colon inflammation in mice. *Gut* (2012) 63:598–609. doi: 10.1136/gutjnl-2012-303329
37. Yan L, Liu MF, Zuo ZY, Jing L, Zhang C. TLR9 regulates the NF-κB-NLRP3-IL-1β pathway negatively in *Salmonella*-induced NKG2D-mediated intestinal inflammation. *J Immunol* (2017) 199:761–73. doi: 10.4049/jimmunol.1601416
38. Sun H, Liu X, Wang YZ, Liu JX, Feng J. Soybean glycinin- and β-conglycinin-induced intestinal immune responses in a murine model of allergy. *Food Agric Immunol* (2013) 24:357–69. doi: 10.1080/09540105.2012.704507
39. Guo Y, Xiao Z, Wang YN, Yao WH, Liao S, Yu B, et al. Sodium butyrate ameliorates Streptozotocin-Induced Type 1 diabetes in mice by inhibiting the HMGB1 expression. *Front Endocrinol* (2018) 9:630. doi: 10.3389/fendo.2018.00630
40. Park MJ, Sohrabji F. The histone deacetylase inhibitor, sodium butyrate, exhibits neuroprotective effects for ischemic stroke in middle-aged female rats. *J Neuroinflamm* (2016) 13:300–0. doi: 10.1186/s12974-016-0765-6
41. Ohama T, Hori M, Momotani E, Iwakura Y, Guo F, Kishi H, et al. Intestinal inflammation downregulates smooth muscle CPI-17 through induction of TNF-α and causes motility disorders. *Am J Physiol Gastrointest Liver Physiol* (2007) 292:G1429–38. doi: 10.1152/AJPGI.00315.2006
42. Lanfranchi GA, Tragnone A. Serum and faecal tumour necrosis factor-α as marker of intestinal inflammation. *Lancet* (1992) 339:1053. doi: 10.1016/0140-6736(92)90573-L
43. Subbiah P, Yuji Z, Ron B, Gregory M, Hemachandra R. Induction of an inflammatory loop by interleukin-1β and tumor necrosis factor-α involves NF-kB and STAT-1 in differentiated human neuroprogenitor cells. *PloS One* (2013) 8:e69585. doi: 10.1371/journal.pone.0069585

44. Peng CL, Cao CM, He MC, Shu YS, Tang XB. Soybean glycinin- and β-conglycinin-induced intestinal damage in piglets via the p38/JNK/NF-κB signaling pathway. *J Agr Food Chem* (2018) 66:9534–41. doi: 10.1021/acs.jafc.8b03641
45. Han FL, Wang XD, Guo JL, Qi CL, Xu C. Effects of glycinin and β-conglycinin on growth performance and intestinal health in juvenile Chinese mitten crabs (*Eriocheir sinensis*). *Fish Shellfish Immunol* (2018) 84:269–79. doi: 10.1016/j.fsi.2018.10.013
46. Albino MR, Souza CLD, Damiani TC, Alberto RH, Silva VF, Fontana VM, et al. Sodium butyrate decreases the activation of NF-κB reducing inflammation and oxidative damage in the kidney of rats subjected to contrast-induced nephropathy. *Nephrol Dial Transplant* (2012) 27:3136–40. doi: 10.1093/ndt/gfr807
47. Salinas I, Parra D. Fish mucosal immunity: intestine. *Mucosal Health Aquacult* (2015) 135–70. doi: 10.1016/b978-0-12-417186-2.00006-6
48. Ma X, He PL, Sun P, Han PF. Lipoic acid: an immunomodulator that attenuates glycinin-induced anaphylactic reactions in a rat model. *J Agr Food Chem* (2010) 58:5086–92. doi: 10.1021/jf904403u
49. Che J, Su B, Tang B, Bu X, Li J, Lin Y, et al. Apparent digestibility coefficients of animal and plant feed ingredients for juvenile *Pseudobagrus ussuriensis*. *Aquac Nutr* (2017) 23:1128–35. doi: 10.1111/ANU.12481
50. Wu JL, Zou JY, Hu ED, Chen DZ, Chen L, Lu FB, et al. Sodium butyrate ameliorates S100/FCA-induced autoimmune hepatitis through regulation of intestinal tight junction and toll-like receptor 4 signaling pathway. *Immunol Lett* (2017) 190:169–76. doi: 10.1016/j.imlet.2017.08.005
51. Wang HB, Wang PY, Wang X, Wan YL, Liu YC. Butyrate enhances intestinal epithelial barrier function via up-regulation of tight junction protein claudin-1 transcription. *Dig Dis Sci* (2012) 57:3126–35. doi: 10.1007/s10620-012-2259-4
52. Bosi G, Giari L, Depasquale JA, Carosi A, Lorenzoni M, Dezfuli BS. Protective responses of intestinal mucous cells in a range of fish–helminth systems. *J Fish Dis* (2017) 40:1001–14. doi: 10.1111/jfd.12576
53. Buommino E, Pasquali D, Sinisi A, Bellastella A, Morelli F, Metafora S. Sodium butyrate/retinoic acid costimulation induces apoptosis-independent growth arrest and cell differentiation in normal and ras-transformed seminal vesicle epithelial cells unresponsive to retinoic acid. *J Mol Endocrinol* (2000) 24:83–94. doi: 10.1677/jme.0.0240083
54. Chitikova ZV, Aksenov ND, Pospelov VA, Pospelova TV. Sodium butyrate induces cell senescence in transformed rodent cells resistant to apoptosis. *Cell Tissue Biol* (2011) 5:277–84. doi: 10.1134/S1990519X11030114
55. Dalmo RA, Bogwald J. Distribution of intravenously and perorally administered Aeromonas salmonicida lipopolysaccharide in Atlantic salmon, *Salmo salar* L. *Fish Shellfish Immunol* (1996) 6:427–41. doi: 10.1006/fsim.1996.0041
56. Huang Q, Xu HB, Yu Z, Gao P, Liu S. Inbred Chinese Wuzhishan (WZS) minipig model for soybean glycinin and β-conglycinin allergy. *J Agr Food Chem* (2010) 58:5194–8. doi: 10.1021/jf904536v
57. Swoboda I, Bugajska-Schretter A, Verdino P, Keller W, Sperr WR, Valent P, et al. Recombinant carp parvalbumin, the major cross-reactive fish allergen: a tool for diagnosis and therapy of fish allergy. *J Immunol* (2002) 168:4576–84. doi: 10.4049/JIMMUNOL.168.9.4576
58. Dijkstra JM, Grimholt U, Leong J, Koop BF, Hashimoto K. Comprehensive analysis of MHC class II genes in teleost fish genomes reveals dispensability of the peptide-loading DM system in a large part of vertebrates. *BMC Evol Biol* (2013) 13:260. doi: 10.1186/1471-2148-13-260
59. Bingulac-Popovic J, Figueroa F, Sato A, Talbot WS, Johnson SL, Gates M, et al. Mapping of *Mhc* class I and class II regions to different linkage groups in the zebrafish, *Danio rerio*. *Immunogenetics* (1997) 46:129–34. doi: 10.1007/s002510050251
60. Gamper CJ, Powell JD. All PI3Kinase signaling is not mTOR: dissecting mTOR-dependent and independent signaling pathways in T cells. *Front Immunol* (2012) 3:312. doi: 10.3389/fimmu.2012.00312
61. Ren WK, Jie Y, Hao X, Shuai C, Gang L, Bie T, et al. Intestinal microbiota-derived GABA mediates interleukin-17 expression during enterotoxigenic *Escherichia coli* Infection. *Front Immunol* (2016) 7:685. doi: 10.3389/FIMMU.2016.00685
62. Segain JP, Blétière D, Sauzeau V, Bourreille A, Loirand G. Rho kinase blockade prevents inflammation via nuclear factor κB inhibition: evidence in Crohn's disease and experimental colitis. *Gastroenterology* (2003) 124:1180–7. doi: 10.1016/S0016-5085(03)00283-X
63. Cataisson C, Joseloff E, Murillas R, Wang A, Atwell C, Torgerson S, et al. Activation of cutaneous protein kinase C alpha induces keratinocyte apoptosis and intraepidermal inflammation by independent signaling pathways. *J Immunol* (2003) 171:2703–13. doi: 10.1016/S0016-5085(03)00283-X
64. Schernthaner-Reiter MH, Kiefer F, Zeyda M, Stulnig TM, Luger A, Vila G. Strong association of serum- and glucocorticoid-regulated kinase 1 with peripheral and adipose tissue inflammation in obesity. *Int J Obes* (2015) 39:1143–50. doi: 10.1038/IJO.2015.41
65. William M, Leroux LP, Chaparro V, Lorent J, Graber TE, M'Boutchou, et al. eIF4E-binding proteins 1 and 2 limit macrophage anti-inflammatory responses through translational repression of IL-10 and cyclooxygenase-2. *J Immunol* (2018) 200:4102–16. doi: 10.4049/JIMMUNOL.1701670
66. Osada-Oka M, Hirai S, Izumi Y, Misumi K, Iwao H. Red ginseng extracts attenuate skin inflammation in atopic dermatitis through p70 ribosomal protein S6 kinase activation. *J Pharmacol Sci* (2018) 136:9–15. doi: 10.1016/J.JPHS.2017.11.002
67. Freeley S, Cardone J, Günther SC, West EE, Reinheckel T, Watts C, et al. Asparaginyl endopeptidase (Legumain) supports human Th1 induction via cathepsin L-mediated intracellular C3 activation. *Front Immunol* (2018) 9:2449. doi: 10.3389/FIMMU.2018.02449
68. Thiem S, Pierce TP, Palmieri M, Putoczki TL, Buchert M, Preaudet A, et al. mTORC1 inhibition restricts inflammation-associated gastrointestinal tumorigenesis in mice. *J Clin Invest* (2013) 123:767–81. doi: 10.1172/JCI65086


**Conflict of Interest:** The authors declare that the research was conducted in the absence of any commercial or financial relationships that could be construed as a potential conflict of interest.

frontiers in Immunology

ORIGINAL RESEARCH
published: 20 January 2021
doi: 10.3389/fimmu.2020.618687

# Integrated Analysis of circRNA-miRNA-mRNA Regulatory Networks in the Intestine of *Sebastes schlegelii* Following *Edwardsiella tarda* Challenge

*Min Cao[1], Xu Yan[2], Baofeng Su[3], Ning Yang[1], Qiang Fu[1], Ting Xue[1], Lin Song[2], Qi Li[1] and Chao Li[1]**

*[1] School of Marine Science and Engineering, Qingdao Agricultural University, Qingdao, China, [2] College of Marine Science and Biological Engineering, Qingdao University of Science & Technology, Qingdao, China, [3] School of Fisheries, Aquaculture and Aquatic Sciences, Auburn University, Auburn, AL, United States*

*Sebastes schlegelii*, an important aquaculture species, has been widely cultured in East Asian countries. With the increase in the cultivation scale, various diseases have become major threats to the industry. Evidence has shown that non-coding RNAs (ncRNAs) have remarkable functions in the interactions between pathogens and their hosts. However, little is known about the mechanisms of circular RNAs (circRNAs) and coding RNAs in the process of preventing pathogen infection in the intestine in teleosts. In this study, we aimed to uncover the global landscape of mRNAs, circRNAs, and microRNAs (miRNAs) in response to *Edwardsiella tarda* infection at different time points (0, 2, 6, 12, and 24 h) and to construct regulatory networks for exploring the immune regulatory mechanism in the intestine of *S. schlegelii.* In total, 1,794 mRNAs, 87 circRNAs, and 79 miRNAs were differentially expressed. The differentially expressed RNAs were quantitatively validated using qRT-PCR. Kyoto Encyclopedia of Genes and Genomes (KEGG) enrichment analysis showed that most of the differentially expressed mRNA genes and the target genes of ncRNAs were related to immune signaling pathways, such as the NF-κB signal pathway, pathogen recognition receptors related to signaling pathways (Toll-like receptors and Nod-like receptors), and the chemokine signaling pathway. Based on these differentially expressed genes, 624 circRNA-miRNA pairs and 2,694 miRNA-mRNA pairs were predicted using the miRanda software. Integrated analyses generated 25 circRNA-miRNA-mRNA interaction networks. In a novel_circ_0004195/novel-530/*IκB* interaction network, novel_530 was upregulated, while its two targets, novel_circ_0004195 and *IκB*, were downregulated after *E. tarda* infection. In addition, two circRNA-miRNA-mRNA networks related to apoptosis (novel_circ_0003210/novel_152/apoptosis-stimulating of p53 protein 1) and interleukin (novel_circ_0001907/novel_127/interleukin-1 receptor type 2) were also identified in our study. We thus speculated that the downstream NF-κB signaling pathway, p53 signaling pathway, and apoptosis pathway might play vital roles in the immune response in the intestine of

OPEN ACCESS

**Edited by:**
*Nan Wu,*
*Institute of Hydrobiology (CAS), China*

**Reviewed by:**
*Lixing Huang,*
*Jimei University, China*
*Bo Peng,*
*Sun Yat-sen University, China*

***Correspondence:**
*Chao Li*
*chaoli@qau.edu.cn*

**Specialty section:**
*This article was submitted to Comparative Immunology, a section of the journal Frontiers in Immunology*

**Received:** *18 October 2020*
**Accepted:** *26 November 2020*
**Published:** *20 January 2021*

**Citation:**
*Cao M, Yan X, Su B, Yang N, Fu Q, Xue T, Song L, Li Q and Li C (2021) Integrated Analysis of circRNA-miRNA-mRNA Regulatory Networks in the Intestine of Sebastes schlegelii Following Edwardsiella tarda Challenge. Front. Immunol. 11:618687. doi: 10.3389/fimmu.2020.618687*

*S. schlegelii.* This study revealed a landscape of RNAs in the intestine of *S. schlegelii* during *E. tarda* infection and provided clues for further study on the immune mechanisms and signaling networks based on the *circRNA-miRNA-mRNA axis* in *S. schlegelii*.

**Keywords: *Sebastes schlegelii*, *Edwardsiella tarda*, intestine, circRNA-miRNA-mRNA network, immune response**

## INTRODUCTION

The immune system of vertebrates is a complex network that consists of different types of molecules, cells, and organs and plays key roles in recognizing foreign "invaders," such as bacteria and viruses, thus resisting pathogen invasion and maintaining homeostasis (1). Distinct from other invertebrates, fish live in aquatic environments enriched with microorganisms. The mucosal surfaces, including the intestine, skin, and gills, serve as the first line of host defense, forming an immune barrier once the organism is invaded by pathogens (2). As an important part of the mucosal immune system, the intestinal mucosa faces great challenges by being constantly exposed to a large microbial community (3). In recent years, more and more studies have proved that the intestinal mucosa plays an important role in protecting the host against pathogen infection. For instance, Li et al (2012). characterized the role of the intestinal epithelial barrier in *Ictalurus punctatus* following *Edwardsiella ictaluri* challenge and identified 1,633 differentially expressed genes associated with immune activation and inflammatory responses (4). Moreover, TLR5 and the downstream MyD88-dependent signaling pathway were triggered in the intestine of *Danio rerio* after injection with a live attenuated *Vibrio anguillarum* vaccine (5). In addition, the major histocompatibility complex (MHC) was induced in the intestine of *Paralichthys olivaceus* after *E. tarda* infection (6). The above studies proved that the intestinal mucosal immune system plays a vital role in the immune responses against infection in teleost fishes. The exploration of the key immune genes and signaling pathways is needed to further characterize its molecular regulatory mechanism.

Increasing evidences have demonstrated that non-coding RNAs (ncRNAs), including long non-coding RNA (lncRNAs), microRNAs (miRNAs), and circular RNAs (circRNAs), are involved in the interactions between pathogens and their hosts (7–10). For example, large intergenic noncoding RNA (lincRNA) in *Oncorhynchus mykiss* was associated with immune response, which coexpressed with immune related genes such as integrin, Rab20, MHC class I genes, genes in PI3K or mTOR pathway, and genes in T cell receptor signaling pathway (11). A very recent report identified a novel lncRNA (*SETD3-OT*) in turbot with potential functions in regulating cell cycle and cell apoptosis, immune cell development, and immune response against infections (12). Most of the ncRNA studies have been focused on miRNAs in teleost. MiRNAs are small ncRNAs that play important roles in gene regulation at the posttranscriptional level by inhibiting mRNA translation or inducing mRNA degradation (13). Challenge studies performed in teleost fish have identified differentially expressed miRNAs that are associated with immune response genes and signaling pathways (14–22). For example, high-throughput sequencing and microarray analyses were used by Gong et al. (2015) to investigate the roles of miRNA such as miR-142-5p, miR-223, and miR-181a of *Cynoglossus semilaevis* in response to *V. anguillarum* infection (14). Similarly, high-throughput sequencing was also used to identify miRNAs that related with air-breathing organs in fish (15), with immune genes and associated signaling pathways after lipopolysaccharide (LPS) stimulation (16). Meanwhile, target genes of DE-miRNAs in common carp were enriched in focal adhesion, extracellular matrix (ECM)-receptor interaction, erythroblastic leukemia viral oncogene homolog (ErbB) signaling pathway, regulation of actin cytoskeleton, and adherent junction signal pathways (17). Based on the expression profiles of miRNAs, Liao et al. (2017) found regulationary functions of miRNAs in digestive and immune-related organs: gill, intestine, and hepatic caecum (18). Meanwhile, IL-1 receptor-associated kinase 4 (IRAK4) was identified and validated, which can be targeted by miR-203, thus inhibiting the activation of nuclear factor κB (NF-κB) signaling pathway (19). Besides, research found that miRNAs can regulate the toll-like receptor signaling pathways in teleost fish (20).

In addition to lncRNAs and miRNAs, circRNAs are a new category of ncRNA, which can be used as miRNA molecular sponges to influence the expression of miRNA, thereby affecting the synthesis of downstream target genes and signaling pathways (23). Because of their stable closed-loop structures, circRNAs could be perfect molecular markers for studying many diseases (24, 25). More importantly, recent studies have demonstrated that circRNAs have substantial effects on host-pathogen interactions in teleost fish. For example, the expression profiles of circRNAs in grass carp (*Ctenopharyngodon idella*) in response to grass carp reovirus infection were investigated, and 41 differentially expressed circRNAs were identified, which can bind to 72 miRNAs that may be associated with immune responses, blood coagulation, hemostasis, and complement and coagulation cascades (26). Moreover, 62 differentially expressed circRNAs were found in *E. tarda* infected intestinal tissues in *P. olivaceus*, which may be correlated with the herpes simplex infection pathway and IgA production pathway (6). However, only a few studies have been performed on the mechanism of interactions between ncRNAs and coding RNAs in teleost fishes, especially in the process of preventing pathogen infection in the intestine (6, 27). Moreover, there were no systematic study of the circRNAs, miRNAs, and mRNAs and the regulatory networks of competing endogenous RNAs (ceRNA) in *S. schlegelii* after pathogen infections.

*S. schlegelii* (black rockfish), one of the most popular and economically important aquaculture species, has a long-standing culture history in East Asian countries such as Japan, Korea, and

China (28). With the expansion of the cultivation scale, numerous large outbreaks of bacterial and viral diseases have become major bottlenecks restricting its industry (29–31). Therefore, studies on black rockfish immune-related genes can expand our understanding of ncRNA that related to immune response and regulatory mechanisms, and are also helpful to guide the prevention and control of its diseases. Previous studies have investigated several immune-related genes, such as high mobility group box 1, c-type lectin, galectin-8, cathepsin K, chemokine ligand 25, and melanocortin-4, in black rockfish in response to pathogen stimulation (32–37). However, no systematic report on the interactions of ncRNAs and coding RNAs in *S. schlegelii* during infection has been performed.

In this study, we aimed to uncover the global landscape of mRNAs, circRNAs, and miRNAs in response to *E. tarda* infection at different time points (0, 2, 6, 12, and 24 h) to construct their regulatory networks. This study would not only provide novel insights into the roles of circRNAs, miRNAs, mRNAs, and relevant regulatory networks during pathogen infections but also broaden our understanding of the immune responses and regulatory mechanisms in the intestine of *S. schlegelii*.

# MATERIALS AND METHODS

## Sample Collection and Bacterial Infection

The experimental adult *S. schlegelii* were obtained from a local fish farm in Qingdao, Shandong Province. And the experimental protocols were approved by the Committee on the Ethics of Animal Experiments of Qingdao Agricultural University IACUC (Institutional Animal Care and Use Committee). In this study, healthy black rockfish with an average length of 15 ± 2 cm were selected for following experiments. Then, these fish were acclimatized in the laboratory in a flow-through system filtered with seawater at 22 ± 1°C for a week before conducting bacterial infection experiments. Thereafter, a pre-challenge for *S. schlegelii* was performed, and *E. tarda* was isolated from the symptomatic fish. Subsequently, the isolated and confirmed *E. tarda* was cultured in LB medium at 28°C overnight at 180 rpm/min. The fish immersed in sterilized media were defined as the control (CON). At the same time, the fish in the experimental groups were immersed in *E. tarda* at a final concentration of $1 \times 10^7$ CFU/ml for 4 h and then transferred into culture conditions. Subsequently, intestinal tissues from the *E. tarda*–infected groups were separately collected at different time points (2, 6, 12, and 24 h), and designated as EI2H, EI6H, EI12H, and EI24H, respectively. Each group had three replicates, and each replicate included 6 random individuals.

## Histopathological Examination

To observe the histopathological changes in intestinal tissues between control and *E. tarda*–infected *S. schlegelii*, intestines from 15 fish were isolated and fixed in 4% paraformaldehyde, dehydrated, and embedded in paraffin. Then, the embedded tissues were sectioned and stained with hematoxylin and eosin (H&E) according to a standard protocol reported by De Vico et al. for histological analysis (38).

## Total RNA Extraction and Quality Control

Total RNA from 15 samples was extracted using TRIzol Reagent (Invitrogen, Carlsbad, CA, USA) and were further treated with RNase-free DNase I to remove DNA (TIANGEN, Beijing, China). The concentration, purity, and integrity of the RNA samples were assessed using a NanoPhotometer spectrophotometer (IMPLEN, CA, USA) and Bioanalyzer 2100 system (Agilent Technologies, CA, USA). High-quality RNAs were used for the construction of the sequencing libraries.

## RNAs Libraries Construction, Sequencing, and Data Processing

For both mRNA and circRNA library construction, 5 μg of RNA per sample was used as the input. For mRNA library construction, ribosomal RNA (rRNA) was removed from the total RNA using an Epicenter Ribo-Zero rRNA Removal Kit (Illumina, USA). For circRNA library construction, 40 U RNase R was added to the rRNA removal system and incubated at 37°C for 3 h to remove linear RNA. Subsequently, the purified RNAs were fragmented to 150–200 bp and used to construct the sequencing library using Illumina TruSeq RNA Sample Preparation Kit (Illumina, San Diego, USA) according to the manufacturer's recommendations with different indices. Before sequencing, the quality of the mRNA library was detected using the Agilent Bioanalyzer 2100 system. After sequencing on an Illumina Hiseq 2500 platform, the raw data generated were filtered to remove low-quality reads, adapter sequences, and reads containing Ns. Then, the clean data were aligned to the assembled genome of *S. schlegelii* using TopHat v2.0.12 (39). For circRNA identification, we used the following criteria for circRNA identification: 1) both ends of splice sites must be GU/AG; 2) mismatch ≤ 2; and 3) back-spliced junction reads ≥ 1. The two splice sites must not be more than 100 kb apart on the genome according to the structural characteristics of circRNA. To explore expression patterns, mRNA or circRNA expression was calculated as reads per kilobase per million reads (RPKM). The differential expression analysis of mRNAs or circRNAs was performed using the DESeq2 R package (1.10.1) (40). The criterion of adjusted $P$-value < 0.05 was used to identify differentially expressed RNAs. Data are available from Dryad at: https://doi.org/10.5061/dryad.7pvmcvdrp.

For miRNA library construction, a total of 5 μg of total RNA per sample was used as input to construct a small RNA library using the NEBNext® Multiplex Small RNA Library Prep Set for Illumina® (NEB, USA) according to the manufacturer's recommendations, and index codes were added to each sample. Briefly, the 5' ends and 3' adapters were specifically ligated to the 5 and 3' ends of miRNA, siRNA, and piRNA, respectively. After ligation, the first-strand cDNA was synthesized using M-MuLV Reverse Transcriptase (RNase H) and then amplified using LongAmp Taq 2X Master Mix, SR Primer for Illumina, and index primer. Subsequently, the PCR products ranged from 140 to 160 bp were recovered from an 8%

polyacrylamide gel for the final miRNA library construction. Similarly, library quality was detected on the Agilent Bioanalyzer 2100 system using DNA High Sensitivity Chips. After sequencing and filtration of raw data, clean reads were obtained. Then, small RNA tags were mapped onto the assembled genome of *S. schlegelii* using Bowtie (41). The mapped small RNA tags were screened in the miRBase 20.0 database to identify known miRNAs. In addition, mirdeep2 and srna-tools-cli were used to obtain potential miRNA and draw secondary structures (42). For novel miRNA prediction, miREvo (43) and mirdeep2 (42) were integrated to predict the novel miRNAs based on the characteristics of the hairpin structure of the miRNA precursor. The counts and base bias at the first position of all known and novel miRNAs were calculated using perl scripts. Two databases, miFam.dat (http://www.mirbase.org/ftp.shtml) and Rfam (http://rfam.sanger.ac.uk/search/) were explored for the occurrence of miRNA families. For function analysis of miRNAs, miRanda was used to predict their target genes (44). MiRNA expression was estimated using TPM (transcript per million) (45). Significantly, differentially expressed miRNAs were identified using the threshold: *P*-value < 0.05. To further understand the functions of these significantly differentially expressed (DE) circRNA, mRNA, and miRNAs, Gene Ontology (GO) and Kyoto Encyclopedia of Genes and Genomes (KEGG) enrichment analyses were performed using the GOseq R package and KOBAS, respectively (46, 47).

## Co-Expression Network Analysis

The circRNA-miRNA, miRNA-mRNA, and circRNA-miRNA-mRNA networks were developed based on possible functional relationships between DE-circRNAs, DE-miRNAs, and DE-mRNAs. The candidate miRNA-circRNA relationships were predicted using miRanda (44) by thresholds: total sore ≥ 140; total energy < 17 kmol). Similarly, miRanda (44) was used to predict the target DE-mRNAs of DE-miRNAs. Then, a miRNA-mRNA regulation network was constructed. In the constructed miRNA-mRNA network, these confirmed miRNAs were selected as candidates to predict the corresponding circRNA-miRNA pairs. Finally, the co-expression relationships among circRNAs, mRNAs, and miRNAs were selected to establish the regulatory network using Cytoscape (v3.4.0) (48).

## Validation of the Differential Expression of circRNAs, miRNAs, and mRNAs

To validate the differential expression of circRNAs, miRNAs, and mRNAs, the samples were prepared using the same method mentioned in the RNA library construction and sequencing section. To validate the expression patterns of the differentially expressed circRNAs and mRNAs, total RNAs of the *E. tarda* infected *S. schlegelii* and control groups were extracted using TRIzol reagent (Invitrogen, Carlsbad, CA, USA), and then reverse transcribed into cDNA using a PrimeScript™ RT reagent Kit (Takara, Otsu, Japan) according to the manufacturer's instructions. Hereafter, ribosomal protein L17 *(RPL17)* was used as an internal control for the normalization of gene expression (49). Primers for the 6 DE-mRNAs and 6 DE-circRNAs for qRT-PCR analysis were designed using PrimerQuest (https://sg.idtdna.com/PrimerQuest/Home). For circRNA primers, the primers were designed according to the sequences that span the circRNA backsplice junctions. For miRNA primers, we designed the forward primers according to the standards mentioned in the miRcute miRNA isolation kit (Tiangen Biotech). Subsequently, the expression levels of these genes were analyzed using a CFX96 real-time PCR detection system (Bio-Rad Laboratories, Hercules, CA, USA). The reaction systems contained 0.4 μl of the diluted template cDNA, 0.2 μl of each primer, 4.2 μl of SYBR® Premix Ex TaqTM II (TliRNaseH Plus), and 5.0 μl of RNA-free water. The reaction mixtures were pre-denatured for 5 min at 95°C, followed by 35 cycles of 95°C for 5 s, 56°C for 30 s, and 72°C for 30 s, and then up to 95°C at a rate of 0.1°C/s increments for melting curve analysis. The differentially expressed miRNAs were also confirmed using qRT-PCR. First, small RNAs (<200 nt) were extracted with the miRcute miRNA isolation kit (Tiangen Biotech) and amplified using the miRcute miRNA qPCR detection kit (Tiangen Biotech) under the following PCR conditions: 95°C for 15 min, followed by 40 cycles of two steps (95°C for 5 s and 60°C for 30 s). Next, 5S rRNA was selected to normalize the relative expression levels of 6 DE-miRNAs. Finally, the $2^{-\Delta\Delta Ct}$ method was used to calculate the relative fold changes (50). The data are shown as the mean ± SE of three replicates. All the primers used in this study are listed in Supporting **Table S1**.

# RESULTS

## Histopathological Analysis

To understand the histopathological changes in intestinal tissues when exposed to pathogenic bacteria, *E. tarda* was used to infect *S. schlegelii* and the infected intestinal tissues were dissected for histopathological analysis. The intestinal tissues from the control group and different infection time points (2, 6, 12, and 24 h) were observed for morphological structures. Light microscopic examination of the normal intestine showed that the mucosal folds, submucosa, circular muscular layer (muscularis), serosa, lamina propria, goblet cells, and epithelium were visible and well arranged (**Figure 1A**). As the infection time progressed, the integrity of the intestinal mucosa structure changed and further microscopic examination showed hyperplasia of the mucosa, thickening of the lamina propria, epithelial cell shedding, mucosal fold breakage, increase in goblet cells, and changes in autolysis and necrosis. At 2 h post-infection, the structure of the intestinal tissue was complete, goblet cells increased in number, and some wandering cells and a few vacuoles interlined the epithelium (**Figure 1B**). After 6 h of infection, the goblet cells continued to increase, the width of the mucosa and lamina propria increased, and some epithelium structure started to disassemble, and more apical opening of the goblet cells was observed. In addition, more lymphocytes were detected in the vacuoles close to the submucosa (**Figure 1C**). Distinct autolysis was observed on the surface of the mucosa and epithelial cells. Autolytic changes also included intestinal necrosis. Some of the

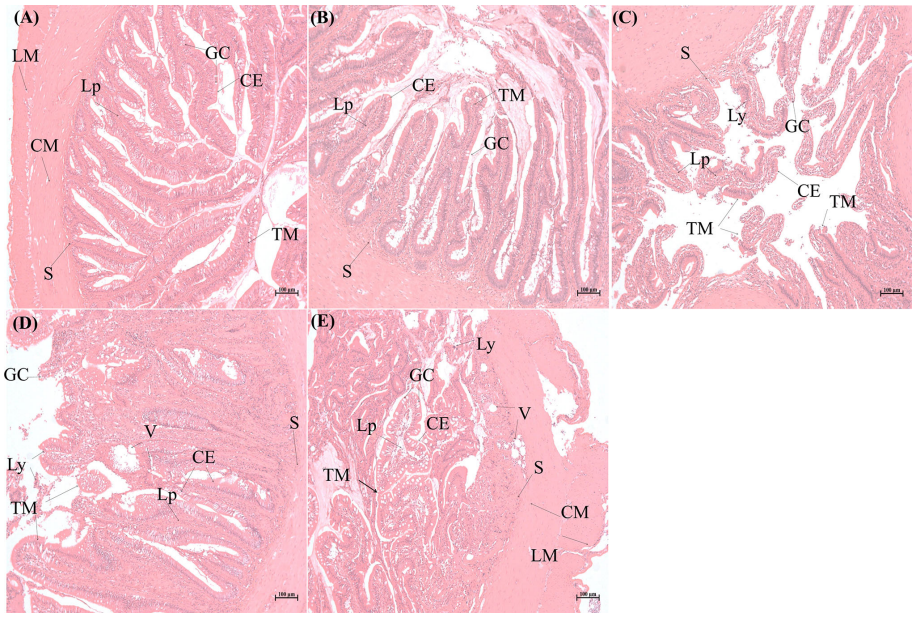


**FIGURE 1** | Histopathological analysis of intestinal tissues of *Sebates schlegelii* following *Edwardsiella tarda* challenge. **(A)** is the representative microstructure of healthy intestine of the control. **(B–E)** represent the microstructures of intestines 2, 6, 12, and 24 h after *E. tarda* infection, respectively. CE, columnar epithelial cell; CM, circular muscularis; GC, goblet cell; LM, longitudinal muscularis; Lp, lamina propria; Ly, lymphocytes; S, submucosa; TM, tunica mucosa; V, vacuole.

lamina epithelial cells were pinched off, clustered, and packed. Significantly large vacuoles were observed, which might be entangled with pinocytotic vesicles, and the intestinal structures are destroyed (**Figure 1D**). When dissecting the intestinal tissues, we found that it had lost its elasticity and broke easily when pulled in some portions (data not shown). More goblet cells were seen, some budded off, and the lamina propria structure was further loosened. Numerous lymphoid cells were scattered in the lamina propria and the vacuole of the cytoplasm (**Figure 1E**). The intestinal villi was deformed and shed, and the folded mucosa was destroyed (**Figure 1E**). Our results indicated that the destruction of *E. tarda* to intestinal tissues of *S. schlegelii* is a time-dependent manner.

## Identification, Quantification, and Differential Expression Analysis of circRNAs, miRNAs, and mRNAs

### Identification of circRNAs in Response to *E. tarda* Infection in *S. schlegelii*

To understand the roles of circRNAs in response to *E. tarda* infection in the intestine of *S. schlegelii*, we performed circRNA sequencing using the rRNA-depleted samples of non-infected (CON) and infected samples at different time points (2, 6, 12, and 24 h). The results showed that RNA purity, concentration, and the amount of RNA met the requirements for circRNA database construction. As shown in **Table S2**, there were approximately 47.72, 56.82, 50.35, 42.12, and 42.48 million clean reads in the CON, EI2H, EI6H, EI12H, and EI24H groups, respectively. The Q20 values of these data were higher than 97%, and the average GC content was 54.17%. Among them, 74.08% of the reads were aligned to the genome. Then, the clean reads were used for circRNA identification. In total, we identified 2,629 circRNAs in *S. schlegelii*, which were widely distributed on 20 chromosomes (**Figure 2A** and Dataset 1). Exon cyclized RNA is formed by a splice donor downstream of the exon that is ligated to a splice acceptor upstream of the exon. Since the order of the exons has been rearranged, the normal linear alignment cannot obtain the ring-spliced reads. Therefore, we obtained backspliced junction reads. The valid data can be aligned to the reference genome and defined as exons, introns, and intergenic regions. The results showed that 68.01% of circRNAs were composed of exons, while 6.69% and 25.30% were located in the intronic and intergenic regions, respectively (**Figure 2B**). In addition, we found that the size of most circRNAs ranged from 200 to 400 bp (**Figure 2C**). To explore the expression patterns of these circRNAs, a hierarchical cluster analysis of 87 differentially expressed circRNAs (DE-circRNAs) was performed among the CON, EI2H, EI6H, EI12H, and EI24H groups, which classified the expression patterns of the uninfected and *E. tarda* infected samples into different clusters (**Figure 2D**). There were two, three, one, and four clusters that showed upregulation in the *E. tarda* infected groups at 2, 6, 12, and 24 h post-infection when compared with control group, respectively. Furthermore, the differences in circRNA expression patterns among different time points and controls were analyzed (**Figure 2E**). A total of 26 DE-circRNAs were observed at early infection time points when compared to the control. Among them, half were upregulated and half were downregulated. At 6 h post-infection, 14 and 13

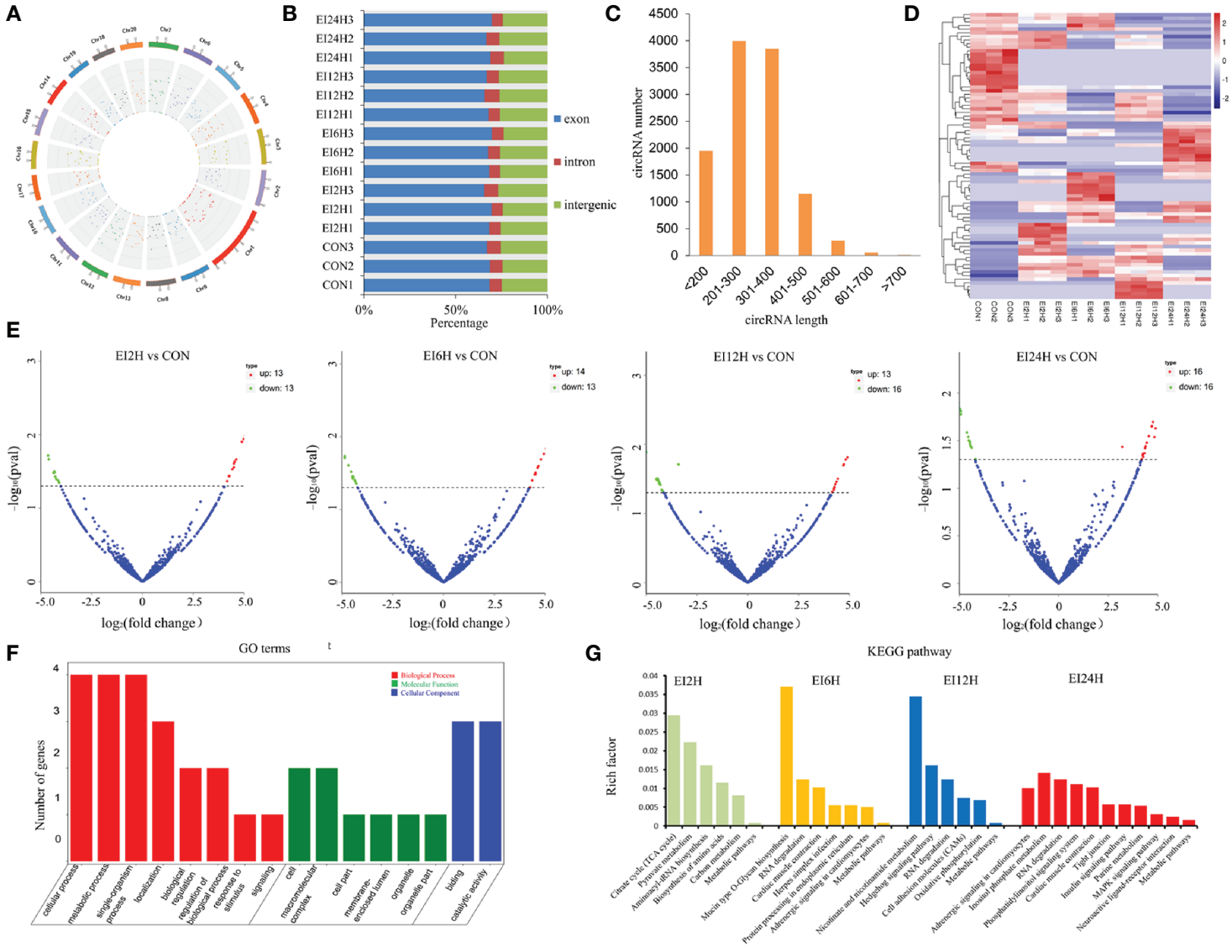


**FIGURE 2** | circRNA expression overview in the intestinal of *Sebates schlegelii* following *E. tarda* challenge. **(A, B)** Genome location of circRNAs. **(C)** circRNAs length distribution. **(D)** Heatmap of DE circRNAs among control and infected groups. **(E)** Volcano Plots of DE circRNAs among control and infected groups. Red blocks represent up-regulated circRNAs and green blocks represent down-regulated circRNAs. **(F)** Go term analysis of DE circRNAs. **(G)** KEGG analysis of DE circRNAs.

circRNAs were found to be upregulated during *E. tarda* infection. Moreover, 13 circRNAs were found to be significantly upregulated and 16 circRNAs were significantly downregulated at 12 h post-infection relative to the control groups. In addition, 32 DE-circRNAs were detected in the 24 h post-infection groups with half upregulated and the other half downregulated.

To elucidate the biological function of circRNAs in *S. schlegelii* after *E. tarda* infection, we performed GO and KEGG functional analysis of these DE-circRNAs. GO is an internationally standardized gene function classification system that provides a dynamically controlled vocabulary to fully describe the properties of genes and gene products in an organism. The 125 core GO terms of four time points post-infection were extracted (**Figure 2F** and **Figure S1**), which can be classified into biological processes, cellular components, and molecular functions. Regarding molecular function, GO terms such as cellular process, metabolic process, single-organism process, localization, biological regulation, regulation of the biological process, and response to stimulus were enriched. In the cellular component, GO terms such as cell, macromolecular complex, cell part, organelle, and organelle part were functionally enriched. Meanwhile, binding and catalytic activity were the most important molecular functions. To further focus on the function of these DE-circRNAs, KEGG pathways were analyzed and enriched. The results showed 6, 7, 6, and 11 circRNAs in the four groups (EI2H, EI6H, EI12H, and EI24H), which were involved in 23 KEGG metabolic pathways, such as tight junction and MAPK signaling pathways (**Figure 2G**).

### Identification of DE miRNAs Between *E. tarda*–Infected and Control Groups

To explore which miRNAs showed differential expression patterns in response to *E. tarda* infection, we identified miRNAs in *S. schlegelii* and investigated the expression patterns of these miRNAs at different time points (0, 2, 6, 12, and 24 h). After removing the low-quality raw reads and mRNA, Rfam, and Repbase mappable reads, the average bases of CON, EI2H, EI6H, EI12H, and EI24H samples were 0.59, 0.58, 0.60, 0.56, and 0.54 Gb, respectively (**Table S3**). These reads were used for further miRNA identification and function analysis. We found that 68.78%, 66.40%, 63.86%, 67.39%, and 67.40% of small RNA reads were mapped onto the *S. schlegelii* genome (**Table S4**). As shown in **Figure 3A**, the length of these sRNAs ranged from 18 to 35 nt, with 22 nt as the dominant one, followed by 21 and 23 nt, respectively (**Figure 3A**). The first nucleotide bias analysis of miRNAs in *S. schlegelii* showed that the first residues of the 21, 22, and 23 nt miRNAs were predominantly uridine (U) (**Figure S2**).

A total of 736 miRNAs were identified, including 289 conserved miRNAs and 447 novel miRNAs (**Figure 3B** and Dataset 2). Sequencing analysis revealed that 177 miRNAs exhibited significant variation after *E. tarda* infection. Their transcriptional patterns along the time course of infection showed expression patterns at 2 and 12 h, which were similar to those of the control group. Moreover, we found that the miRNAs were most responsive at 6 h post-infection. Besides, some miRNAs were induced after a long period of infection (**Figure 3C**). To further clarify the miRNA response mechanism, we compared the differences between the miRNAs at different time points after infection and the miRNA in the control group. The results showed that 6, 72, 9, and 82 DE-miRNAs exhibited significant variation in H2 vs. H0, H6 vs. H0, H12 vs. H0, and H24 vs. H0 comparisons, respectively (**Figure 3D**). To further explore the function of these DE-miRNAs, their target genes and functions were statistically analyzed. The results showed that these DE-miRNAs target 3,750 genes. GO analysis showed that these target genes were mainly enriched in the 3,245 GO term process (**Figure 3E**). Analysis of the KEGG metabolic pathway showed that these genes were involved in metabolic pathways (158), MAPK signaling pathway (47), calcium signaling pathway (35), protein processing in the endoplasmic reticulum (28), focal adhesion (28), tight junction (24), and apoptosis (25) (**Figure 3F**).

### Identification of DE mRNAs Between *E. tarda*–Infected and Control Groups

To identify the different expression levels of mRNAs in the *E. tarda* infected groups and control group, 15 mRNA libraries were constructed. Finally, 702, 740, 497, and 609 genes were identified as DEGs in EI2H, EI6H, EI12H, and EI24H libraries, respectively, compared with CON (**Figures 4A–D**). A total of core 97 genes showed different expression levels at all the infected time points (**Figure 4E**). Furthermore, GO analysis and KEGG pathway analysis were used to examine the functions of these DE mRNAs. GO analysis was conducted with the DE mRNAs in *S. schlegelii* using the Blast2GO program to classify their biological functions. In detail, 2,011 DE mRNAs were successfully assigned to GO terms with 1,070 functional terms (**Figure 4F**). Among them, 57.03%, 24.05%, and 18.92% DE miRNAs were assigned to the biological process, molecular function, and cellular component categories, respectively. To further elucidate the physiological implications and interactions of the DE mRNAs identified in our sequencing analysis, we BLASTed the DE mRNAs against referenced canonical pathways in the KEGG database using BLASTx with an E-value cutoff of 1e-5. KEGG analysis showed that the enriched pathways were mainly involved in metabolic pathways, biosynthesis of amino acids, and carbon metabolism (**Figure 4G**).

## Co-Expression Network Construction

### Construction of the Potential circRNA-miRNA Co-Expression Network

CircRNA molecules are rich in miRNA binding sites and acting as miRNA sponges in cells, thereby abolishing the inhibition of miRNAs on their target genes and increasing the expression levels of target genes, which was defined as a competitive endogenous RNA (ceRNA) mechanism (51). Therefore, an integrative analysis of the interplay between circRNAs and their target miRNAs was performed to elucidate their functional connections. Taken together, we identified 148 miRNAs that

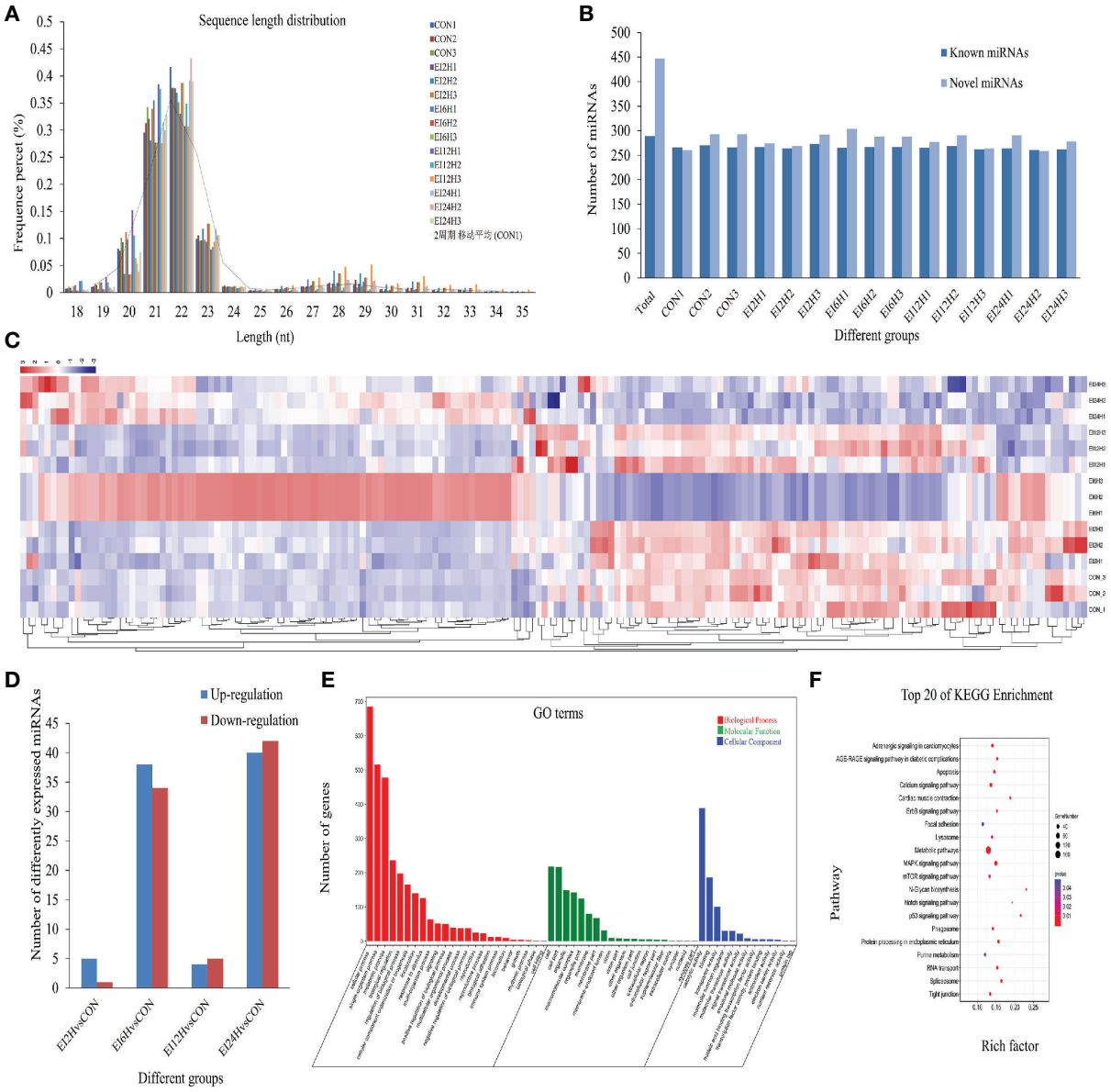


**FIGURE 3** | The miRNA expression overview in the intestine of *Sebates schlegelii* following *E. tarda* challenge. **(A)** The length distribution of identified miRNAs. **(B)** Number of known and novel miRNAs. **(C)** Heatmap of DE miRNAs among control and infected groups. **(D)** DE miRNAs among control and infected groups. **(E)** Go term analysis of DE miRNAs. **(F)** KEGG analysis of DE miRNAs.

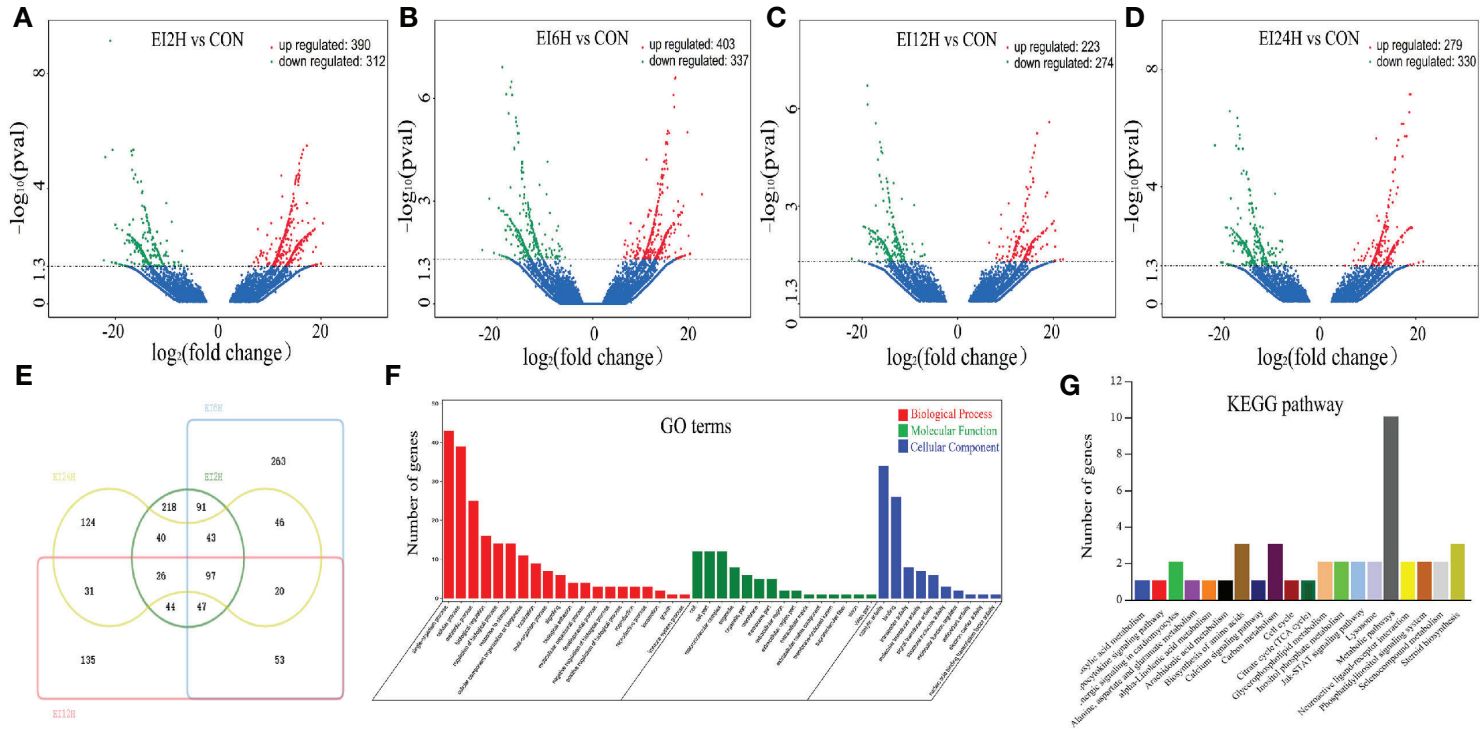


**FIGURE 4** | Analysis of mRNA sequencing data in the intestine of *Sebates schlegelii* following *E. tarda* challenge. **(A–D)** Volcano plots were drawn to visualize the standardized expression of mRNAs between the infected and control groups. The red and green points represent differentially expressed mRNAs with statistical significance ($P < 0.05$). **(E)** Veen diagram of mRNAs. **(F)** Go term analysis of DE mRNAs. **(G)** KEGG analysis of DE mRNAs.

were bound to 156 circRNAs with different expression levels and generated 624 circRNA and miRNA pairs (**Table S5**). In detail, novel_circ_0004195 may function as ceRNAs and sequester novel_530 to relieve its binding and targeting of 124 mRNAs (including cytokine receptor-like factor, the inhibitor of kappa B (*IκB*), cohesin, and transcription factor) (**Table S6**). We also found that five circRNAs (novel_circ_0001019, novel_circ_0002395, novel_circ_0003142, novel_circ_0003744, and novel_circ_0003853) have binding sites for novel_663, which targets the G-protein coupled receptor, E3 ubiquitin-protein ligase, and myomaker. In addition, the relationship between dre-miR-203a-3p and novel_circ_0001819, dre-miR-150, novel_circ_0003210, and novel_circ_0003372 were also predicted. The target genes of the two miRNAs are related to transmembrane protein 65, MAP kinase-activated protein kinase, and tetraspanin. Taken together, these circRNAs/miRNAs could play important roles in host defense when organisms are infected by pathogenic bacteria.

## Construction of the Potential miRNA-mRNA Co-Expression Network

In the present study, the regulatory networks of DE-miRNAs and their corresponding target mRNAs were constructed and investigated using the MiRanda software. In total, 4,545 mRNAs were found to be targeted by 79 DE-miRNAs (**Table S6**). Among them, 7 (8.86%) miRNAs were found to target only one mRNA, such as dre-miR-203a-3p, ccr-miR-142-3p, dre-miR-454b, and novel_264. However, most miRNAs could target more than one mRNA. For instance, novel_277, dre-miR-23b-5p, dre-miR-24b-3p, and novel_10 had 488, 484, 329, and 264 target mRNAs, respectively. In addition, many mRNAs were associated with more than one miRNA; for example, the immunoglobulin superfamily DCC subclass member 3 was targeted by ccr-miR-128 and dre-miR-128-3p. Methyltransferase-like protein 24 was targeted by ccr-miR-10d, dre-miR-10d-5p, and novel_49. The results indicate that complex miRNA-mRNA regulatory networks existed in the process of pathogen invasion and host defense.

## Construction of the Potential circRNA-miRNA-mRNA Network

To further explore the potential network of circRNAs, miRNAs, and mRNAs, we constructed circRNA-miRNA-mRNA co-expression networks based on the circRNA-miRNA and miRNA-mRNA results (**Figure 5**). The DEcircRNA-miRNA-mRNA networks suggested that 17 downregulated circRNAs bound to 22 miRNAs and 26 miRNA-targeted mRNAs, while 19 upregulated circRNAs were linked to 30 miRNAs and 37 miRNA-targeted mRNAs. In the network of circRNA-miRNA-

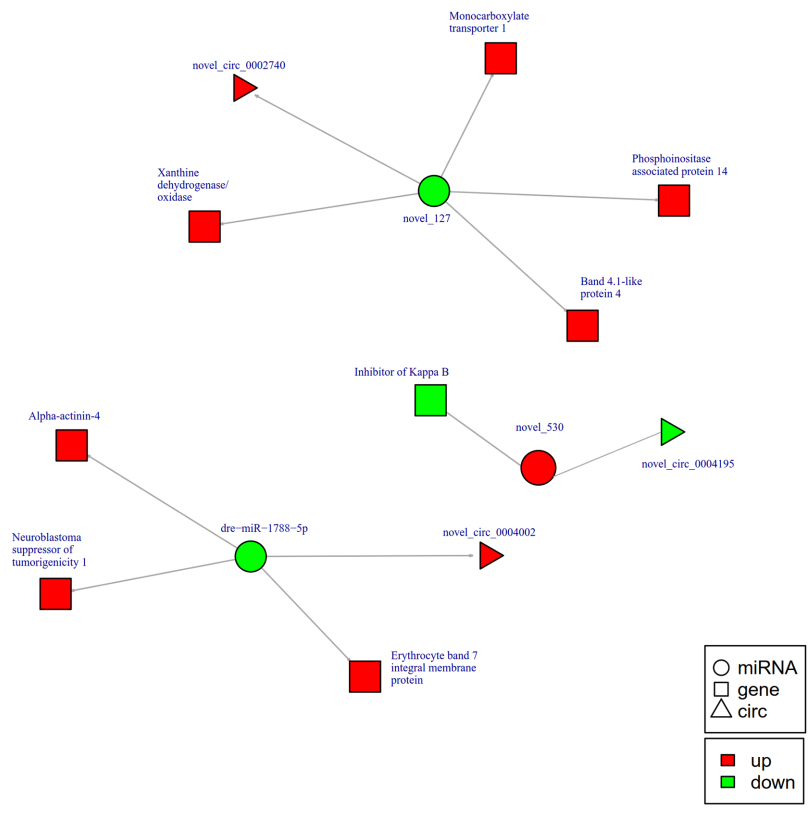


**FIGURE 5** | The circRNA-miRNA-mRNA interaction networks in the intestine of *Sebates schlegelii* fowllowing *E. tarda* infection at 2 h. Circles represent miRNA, triangles represent circRNA, and squares represent mRNA. Red and green shaded represent up-regulated and down-regulated RNAs, respectively.

mRNA 2 h post-infection, two upregulated circRNAs (novel_circ_0002740 and novel_circ_0004002) related to miRNA novel_127 and dre-miR-1788-5p, and the two miRNAs radiated to their target genes such as Interleukin-1 receptor type 2, a neuroblastoma suppressor of tumorigenicity 1. In contrast, the downregulated novel_circ_00004195 was connected to novel_530 and *IκB* (**Figure 5**). When constructing the potential circRNA-miRNA-mRNA network at 6 h post-infection, we found that at the center of the network, novel_circ_0001907 and novel_circ_0003210 were upregulated. We also found a network containing novel_circ_00004195 that was downregulated. The three circRNAs radiated to their respective predicted miRNAs, novel_127, dre-miR-152, and novel_530. Meanwhile, their related miRNAs were connected to their respective target mRNAs such as xanthine dehydrogenase/oxidase, interleukin-1 receptor type 2, cytochrome P450, apoptosis-stimulating of p53 protein 1, neuroendocrine convertase 1, inhibitor of kappa B (*IkB*), and anillin (**Figure 6**). According to our results, miRNAs including novel_530, dre-miR-101, and dre-miR-1966, radiated three circRNAs (novel_circ_00004195, novel_circ_00000741, and novel_circ_0002744) and their target genes (*IkB*, short transient receptor potential channel 6 and ras association domain-containing protein 2 and others) at 12 h (**Figure 7**). Furthermore, five co-expression networks for circRNAs regulating targeted miRNAs and miRNAs regulating targeted mRNAs were formed after 24 h of infection. In detail, miRNA_38 was linked by anlsin and was linked by novel_circ_0003372 and novel_circ_0003247. MiRNA novel_781 radiated to acyl-CoA synthetase family member 3, novel_circ_0000348, and novel_circ_0002180. MiRNA novel-530 radiated to novel_circ_0004195 and *IkB*. In addition, a network containing novel_circ_0002455/dre-miR-20a-5p/lymphoid-restricted membrane protein was also found at this time point (**Figure 8**). These circRNA-miRNA-mRNA networks can be selected as candidates for the following functional analysis.

## GO and KEGG Analysis of circRNA Co-Expression Genes

To better understand the mechanisms that responded to *E. tarda* infection, GO and KEGG enrichment analysis was performed to explore the function of circRNA co-expression genes. GO enrichment analysis revealed 23 terms, which are presented in **Figure 9A**. The results showed that the most enriched GO terms were strongly associated with single-organism process (GO: 0044699), cellular process (GO: 0009987), metabolic process (GO: 0008152), cell part (GO: 0044464), and cell (GO: 0005623). KEGG pathway analysis was conducted to characterize the targeted genes (**Figure 9B**), which were

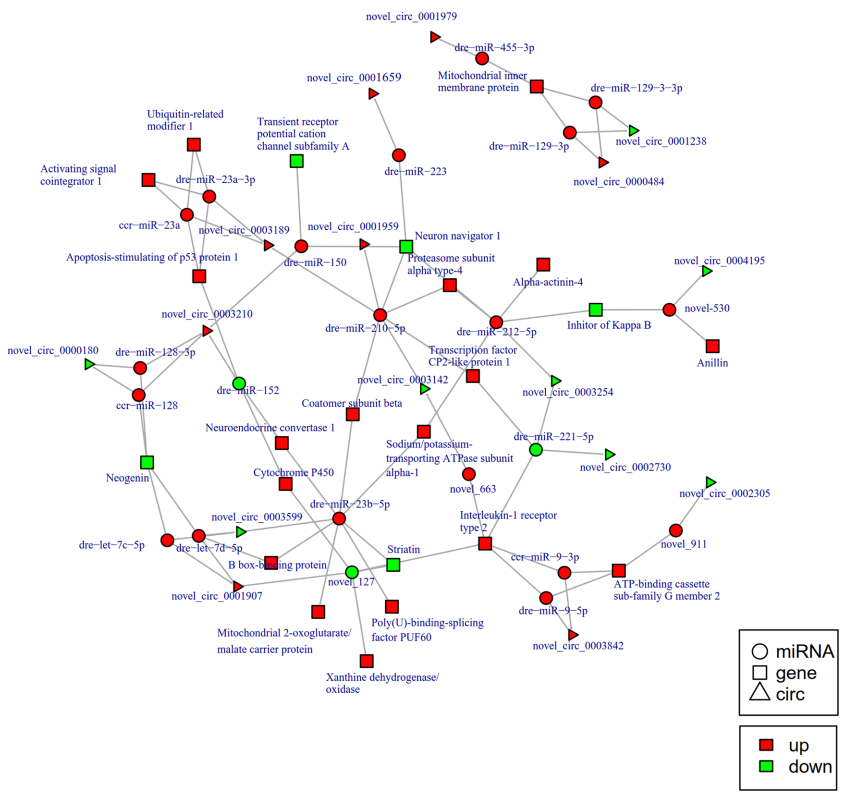


**FIGURE 6** | The circRNA-miRNA-mRNA interaction networks in the intestine of *Sebates schlegelii* fowllowing *E. tarda* infection at 6 h. Circles represent miRNA, triangles represent circRNA, and squares represent mRNA. Red and green shaded represent up-regulated and down-regulated RNAs, respectively.

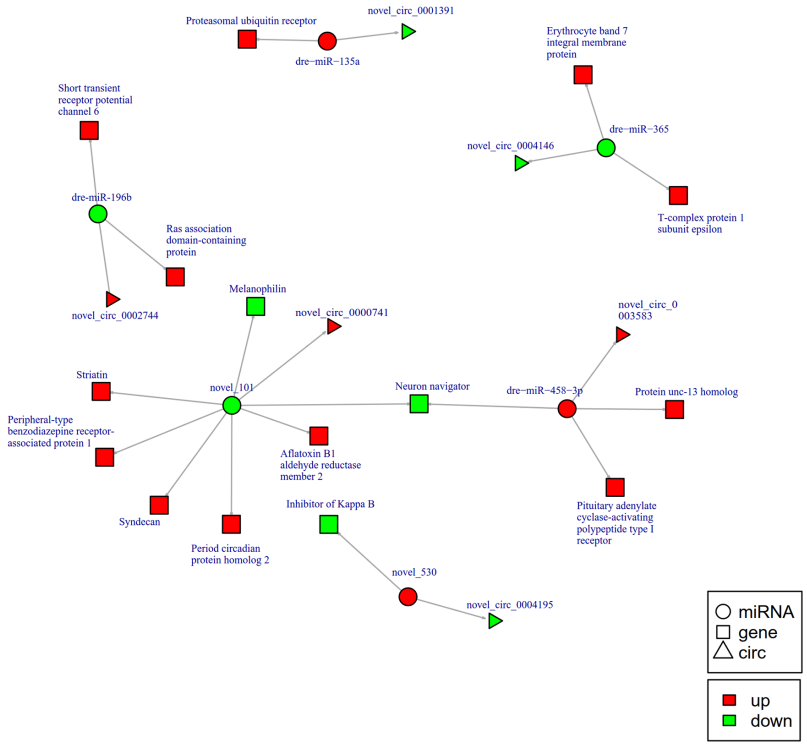


**FIGURE 7** | The circRNA-miRNA-mRNA interaction networks in the intestine of *Sebates schlegelii* fowllowing *E. tarda* infection at 12 h. Circles represent miRNA, triangles represent circRNA, and squares represent mRNA. Red and green shaded represent up-regulated and down-regulated RNAs, respectively.

predicted to be related to herpes simplex infection, cell adhesion molecules (CAMs), focal adhesion, and tight junctions.

## Validation of the Differentially Expressed circRNAs, miRNAs, and mRNAs *via* qRT-PCR

To validate the expression levels of circRNAs, miRNAs, and mRNAs obtained by sequencing, we randomly selected six circRNAs (circRNA_729, circRNA_2647, circRNA_2943, circRNA_3141, circRNA_3199, and circRNA_4195), six miRNAs (novel_530, novel_186, novel_663, dre-miR-150, dre-miR-210-5p, and dre-miR-455-3p), and six mRNAs [insulin receptor, dachshund homolog, protein Mpv17, aquaporin, NLRC3, and inhibitor of kappa B (*IkB*)] and measured their expression levels after *E. tarda* infection using RT-qPCR (**Figures 10–12**). For example, two genes (insulin receptor and aquaporin) were upregulated when *S. schlegelii* was infected with *E. tarda*. CircRNA_4195 showed downregulated expression in response to *E. tarda* infection. Meanwhile, we found that the relative expression of circRNA_2943 was inversely related to the expression from the sequencing result, with upregulated expression in response to *E. tarda* infection at 12 and 24 h. The qRT-PCR results of dre-miR-210-5p showed different expression patterns at the 12 h infection point when compared with that from the Illumina platform. The results showed that the expression trends of most genes in qRT-PCR were in agreement with the sequencing data.

# DISCUSSION

The mucosal immune system is the first barrier to defend against the invasion of external pathogens (52). The intestinal mucosa, an important part of the mucosal immune system, plays an important role in the immune response to pathogenic bacteria (53). In our study, *E. tarda* can affect the structure and integrity of the intestinal tissues of *S. schlegelii* in a time-dependent manner. Similar to the histopathological study by Xiu et al. (6), the integrity of the intestinal mucosa structure showed pathological changes such as cell swelling, thickening of the lamina propria, shedding and fragmentation of epithelial cells, and mucosal folds when *P. olivaceus* was infected with *E. tarda*. Furthermore, we found the formation of numerous goblet cells and vacuoles as the infection progressed, which indicated secretion of mucin/mucus, stimulation of immune response, the activity of secondary lysosomes and enzymatic degradation of organelles, and further destruction of the intestine. These histopathological structures demonstrated that *E. tarda* infection changed the physical and integrity barriers of the intestine and stimulated immune responses.

Studies have shown that ncRNAs participate in the interactions between pathogenic microorganisms and teleosts (7, 9, 10, 54, 55). However, studies on the mechanisms of ncRNA regulatory networks in the intestinal mucosal immune response of teleosts are still in infancy. In this study, *S. schlegelii* was used as the research object, *E. tarda* was used as the pathogen to

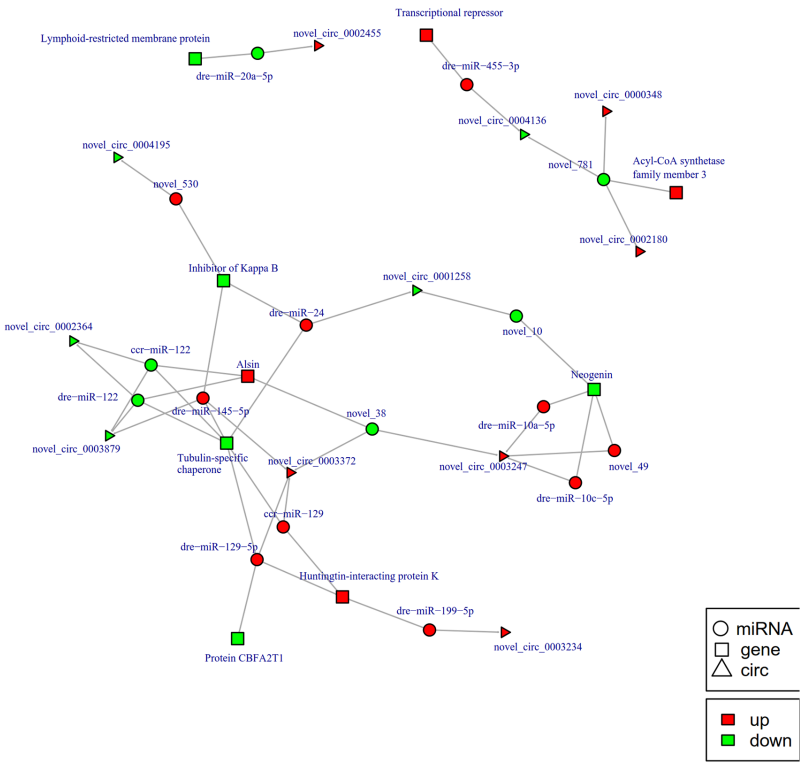


**FIGURE 8** | The circRNA-miRNA-mRNA interaction networks in the intestine of *Sebastes schlegelii* fowllowing *E. tarda* infection at 24 h. Circles represent miRNA, triangles represent circRNA, and squares represent mRNA. Red and green shaded represent up-regulated and down-regulated RNAs, respectively.

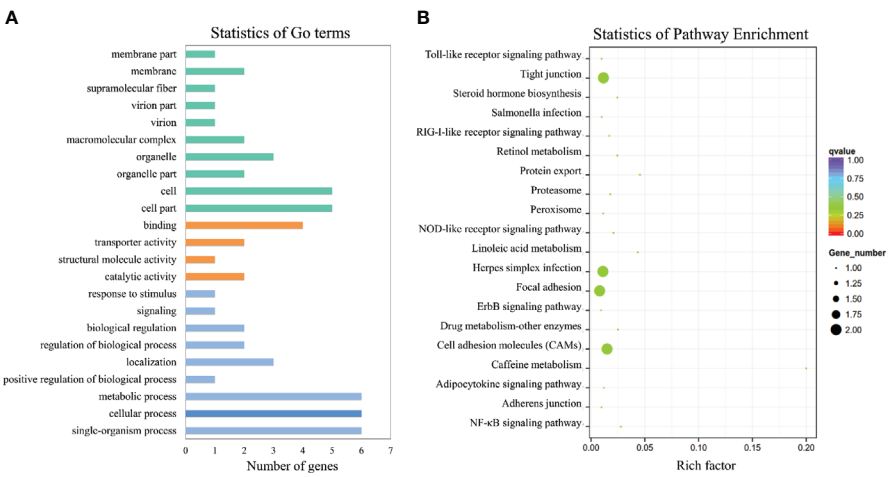


**FIGURE 9** | GO and KEGG analysis of the circRNA co-expression genes. **(A)** GO analysis of circRNA co-expression genes. **(B)** Statistics of KEGG pathways enrichment of circRNA co-expression genes. The colorful bar refers to the q-value of the respective signaling pathway. Size of the point refers to the number of genes within each pathway.

construct an infection model, and the dynamic changes in the transcription level (mRNA) and transcription regulation level (circRNA and miRNA) in the intestine were monitored to explore the circrNA-mirNA-mRNA regulatory network in response to infection. CircRNA is a novel group of ncRNAs with covalently linked closed-loop structures that are generated by reverse splicing events, which are widely expressed in tissues and inhibit the degradation of RNase R enzymes (56). Previous

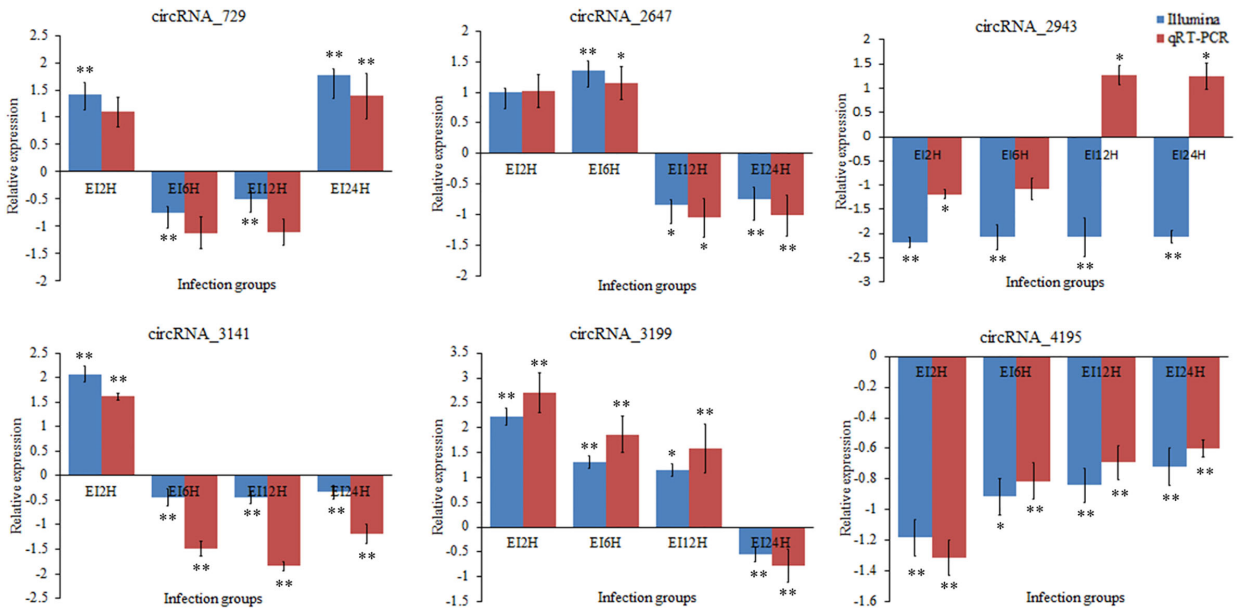


**FIGURE 10** | Validation of circRNAs by qRT-PCR analysis. The expression patterns of qRT-PCR were presented between control and, 2, 6, 12, and 24 h infection groups. The results showed the relative fold change and their mean ± standard error (SE) from triplicate experiments. ** indicates significance at the 0.01 level, * indicates significance at the 0.05 level.

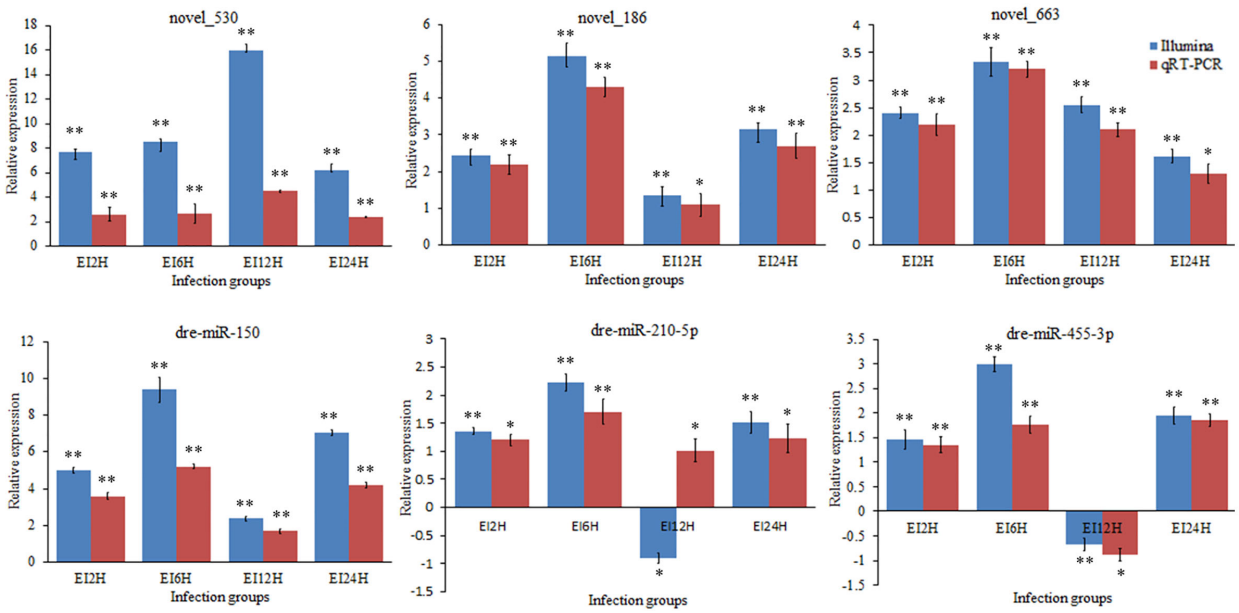


**FIGURE 11** | Validation of miRNAs by qRT-PCR analysis. The expression patterns of qRT-PCR were presented between control and, 2, 6, 12, and 24 h infection groups. The results showed the relative fold change and their mean ± standard error (SE) from triplicate experiments. ** indicates significance at the 0.01 level, * indicates significance at the 0.05 level.

studies have demonstrated that circRNAs can function as miRNA sponges, bind to RNA-binding proteins, and regulate the transcription of target genes and alternative splicing (57). With the development of high-throughput sequencing and bioinformatics techniques, massive amounts of circRNA data from different cells and tissues have been acquired. Most studies on circRNAs are currently about human disease-related genes and in some model species. For example, Memczak et al (2013).

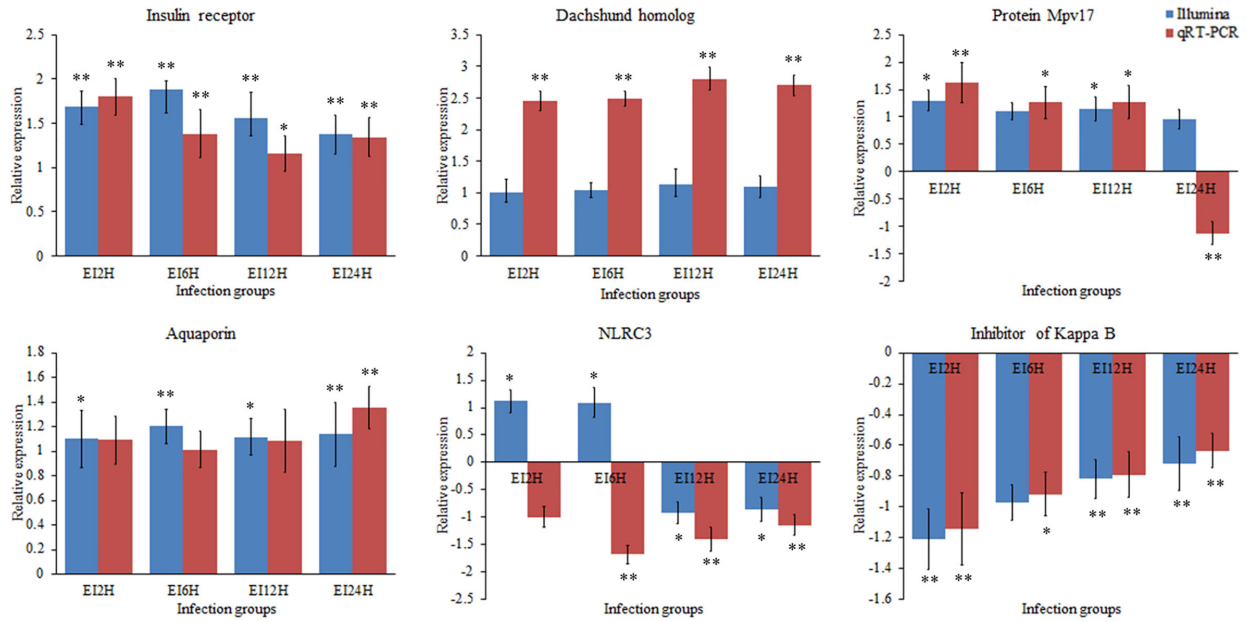


**FIGURE 12** | Validation of mRNAs by qRT-PCR analysis. The expression patterns of qRT-PCR were presented between control and, 2, 6, 12, and 24 h infection groups. The results showed the relative fold change and their mean ± standard error (SE) from triplicate experiments. ** indicates significance at the 0.01 level, * indicates significance at the 0.05 level.

proved that the overexpression of ciRS-7/CDR1 could influence the development of the brain by inhibiting the expression of miR-7 (58). Recently, studies have shown that circRNAs are involved in host immune response to pathogenic bacteria in teleost as well as in the developmental process. These studies confirm the existence of circRNA in several species, such as large yellow croaker (*Larimichthys crocea*), *C.semilaevis*, *Oreochromis niloticus*, *Carassius auratus* gibelio, grass carp, and *P. olivaceus* (6, 27, 59–62). However, studies on circRNAs in teleost, especially in intestinal mucosal immune response, are still limited when compared with those in mammals.

In our study, 87 DE-circRNAs were captured at four infection time points in *S. schlegelii* exposed to *E. tarda* infection. Some of these circRNAs were induced once *S. schlegelii* were infected with *E. tarda.* Function analysis showed that the regulated circRNAs were involved in important pathways, such as tight junctions and MAPK signaling pathways, which implied that these circRNAs play vital roles in preventing *S. schlegelii* from *E. tarda* infection. Besides circRNA, miRNAs can regulate the host immune response to various pathogens at the post-transcriptional level by inhibiting mRNA translation or inducing mRNA degradation (13). For example, miRNAs in snout bream, half-smooth tongue sole, and common carp showed different expression patterns when stimulated by pathogenic bacteria or lipopolysaccharides (14, 16, 17). In addition, miRNAs can regulate related signaling pathways by targeting multiple molecules (such as TLR-associated signaling proteins and TLR-induced cytokines) (20). In the present study, we investigated the expression patterns of 79 miRNAs identified at different time points and analyzed their function through their target genes. Analysis of the KEGG metabolic pathway showed that these genes were involved in the metabolic pathway, MAPK signaling pathway, calcium-signaling pathway, protein processing in the endoplasmic reticulum, focal adhesion, tight junction, and apoptosis. These processes also presented a close relationship with immunity. In addition, we found the matching information of mRNA and miRNA, which provided basic data for further research on their regulatory relationships.

In the present study, we systematically analyzed circRNA, miRNA, and mRNA expression profiles in *S. schlegelii* following infection with *E. tarda.* We found that *E. tarda* infection could affect circRNA, miRNA, and mRNA expression profiles. Integrated analyses generated 25 circRNA-miRNA-mRNA interaction networks. Similarly, the potential circRNA-miRNA-mRNA regulatory networks of nectin2, MHC II α-chain, and MHC II β-chains were constructed in the intestine of *P. olivaceus* (6). Fan et al (2019). predicted 2,136 circRNAs in tilapia and analyzed their potential functions by linking them with miRNAs and mRNAs. Meanwhile, we found that the targeted genes in the circRNA-miRNA-mRNA network were involved in immunity-related signaling pathways, such as herpes simplex infection, cell adhesion molecules (CAMs), focal adhesion, tight junction, NOD-like receptor signaling pathway, Toll-like receptor signaling pathway, and NF-κB signaling pathways (61). Interestingly, the novel_circ_0004195/novel_530/*IkB* interaction network was found at all four time points. It has been demonstrated that mammalian nuclear transcription factor NF-κB (nuclear factor of kappa B) family proteins play an important role in the immune system and participate in immune response, tumor formation, and apoptosis by

regulating the expression of genes related to lymphocyte development and survival (63). *IκB* is an inhibitor of NF-κB, which keeps NF-κB inactive at rest. Once *IκB* is phosphorylated, it loses its inhibitory effect on NF-κB when cells are triggered by an external signal, and thus can enter the nucleus and regulate gene expression (64). Subsequently, many downstream cytokines and inflammatory factors can be activated to form immune protection for organisms when NF-κB is activated (65). In our study, we found that the expression level of novel_530 increased along the infection time. Thus, it can inhibit the expression of its target gene *IκB*, thereby activating the NF-κB signaling pathway. Therefore, we speculated that novel_circ_0004195/novel_530 might inhibit the expression of *IκB*. Subsequently, the downstream NF-κB signaling pathway was activated. Thus, it can exert the immune barrier function of the intestinal mucosa. In addition, we found networks (novel_circ_0003210/novel_152/apoptosis-stimulating of p53 protein 1 and novel_circ_0001907/novel_127/interleukin-1 receptor type 2) related to apoptosis and interleukin. For this novel_circ_0003210/novel_152/apoptosis-stimulating of p53 protein 1 network, we found that apoptosis-stimulating of p53 protein 1 was upregulated after 6 h of infection. It has been reported that apoptosis-stimulating of p53 protein 1 is an apoptosis-stimulating protein of the p53 (ASPP) family, which contains four ankyrin repeats and an SH3 domain that is involved in protein-protein interactions through the promotion of DNA binding and transactivation of p53-family proteins (66). This implies that the p53 signaling pathway may respond to this infection. Previous studies have reported that the apoptosis and p53 signaling pathways play important roles in immunity (67, 68). Similarly, the induction of interleukin-1 receptor type 2 in the network of novel_circ_0001907/novel_127/interleukin-1 receptor type 2 was observed after infection. We speculate that this network is involved in the immune response in the intestine of *S. schlegelii* because the interleukin 1 receptor family has been demonstrated to play a crucial role in immune responses in the human lung (69). As mentioned in our study, the integrities and morphologies of intestinal tissues of *S. schlegelii* changed with the increasing of infection time. So, what are the associations between histopathological changes and these predicted regulatory networks? Previously, we speculated that novel_530 can relieve the inhibition of *IκB* from the NF-κB signaling pathway by up-regulating its expression. It has been demonstrated that the activation of the NF-κB signaling pathway can active downstream inflammatory factors to cause local inflammation in organism (65). The inflammatory response not only plays a key role in resisting the invasion of pathogens but also induces changes in cell morphologies in organisms (70, 71). Meanwhile, we found that novel_circ_0003210 in the network novel_circ_0003210/novel_152/apoptosis-stimulating of p53 protein 1 is also up-regulated after *E. tarda* infection. Novel_circ_0003210 is a regulator of p53 signaling pathway, which is involved in inducing cell cycle arrest and promoting apoptosis (72). Moreover, numberous reports indicated that the apoptosis present abnormal morphological characteristics, such as karyopyknosis, shrinking cytomembrane, vacuolation, etc (73, 74). Therefore, we speculated that the observation of cell morphologies and even cell death might be related to the regulatory networks of these circRNAs. However, further investigations are still required to determine the targeting relationships of these identified circRNA-miRNA-mRNA networks to understand the immune response and regulatory mechanism of *S. schlegelii*.

## CONCLUSION

We systematically analyzed circRNAs, miRNAs, and mRNAs in the intestine of *S. schlegelii* after infection with *E. tarda* at different time points (2, 6, 12, and 24 h). Additionally, the corresponding networks of circRNA-miRNA-mRNA were further constructed to investigate their potential roles during *E. tarda* infection. In particular, our results imply that circRNAs play important roles in response to pathogen infection by regulating their related pathways. In total, the integrated analyses generated 25 circRNA-miRNA-mRNA interaction networks, including a novel_circ_0004195/novel_530/*IkB* interaction network, which may exert the immune barrier function by activating the NF-κB signaling pathway in the intestine of *S. schlegelii*. In addition, the circRNA-miRNA-mRNA networks, related to apoptosis (novel_circ_0003210/novel_152/apoptosis-stimulating of p53 protein 1) and interleukin (novel_circ_0001907/novel_127/interleukin-1 receptor type 2), were also identified in our study. Our study indicated that the intestinal immune response of *S. schlegelii* was regulated by circRNAs and miRNAs. However, further studies are needed to explore the mechanism between ncRNAs and mRNAs to better understand the intestinal mucosal immune response in *S. schlegelii*, to better provide theoretical guidance for *S. schlegelii* disease prevention and control.

## DATA AVAILABILITY STATEMENT

Data are available from Dryad at: https://doi.org/10.5061/dryad.7pvmcvdrp.

## ETHICS STATEMENT

The animal study was reviewed and approved by Qingdao Agricultural University.

## AUTHOR CONTRIBUTIONS

MC: analyzed the results and wrote this paper. XY and NY: collected materials and performed the bacteria challenge experiment. QF, TX, and LS: analyzed the sequencing results of circRNA, miRNA, and mRNA. BS: performed the histopathological analysis on the intestine tissues and revised the manuscript. CL and BS: conceived, designed the research,

and revised the manuscript. All authors contributed to the article and approved the submitted version.

## FUNDING

This study was supported by Scientific and Technological Innovation of Blue Granary (2018YFD0900503), Young Experts of Taishan Scholars (NO.tsqn201909130), Science and Technology Support Plan for Youth Innovation of Colleges and Universities in Shandong Province (2019KJF003), the "First Class Fishery Discipline" Programme in Shandong Province, a special talent programme "One Thing One Decision (Yishi Yiyi)" Programme in Shandong Province, China, Breeding Plan of Shandong Provincial Qingchuang Research Team (2019), and Breeding Plan of Shandong Provincial Qingchuang Research Team (2019).

## SUPPLEMENTARY MATERIAL

The Supplementary Material for this article can be found online at: https://www.frontiersin.org/articles/10.3389/fimmu.2020.618687/full#supplementary-material

**SUPPLEMENTARY FIGURE 1 |** Venn diagram of core GO terms at four post-infections.

**SUPPLEMENTARY FIGURE 2 |** Mapping reads of small RNAs on the *S. schlegelii* genome.

## REFERENCES

1. Zimmerman LMVogel LABowden RM. Understanding the vertebrate immune system: insights from the reptilian perspective. *J Exp Biol* (2010) 213(5):661–71. doi: 10.1242/jeb.038315
2. Xu ZParra DGómez DSalinas IZhang YAvon Gersdorff Jørgensen L, et al. Teleost skin, an ancient mucosal surface that elicits gut-like immune responses. *Proc Natl Acad Sci U S A* (2013) 110(32):13097–102. doi: 10.1073/pnas.1304319110
3. Hooper LVLittman DRMacpherson AJ. Interactions between the microbiota and the immune system. *Science* (2012) 36(6086):1268–73. doi: 10.1126/science.1223490
4. Li CZhang YWang RLu JNandi SMohanty S, et al. RNA-seq analysis of mucosal immune responses reveals signatures of intestinal barrier disruption and pathogen entry following *Edwardsiella ictaluri* infection in channel catfish, *Ictalurus punctatus*. *Fish Shellfish Immunol* (2012) 2(5):816–27. doi: 10.1016/j.fsi.2012.02.004
5. Liu XWu HChang XTang YLiu QZhang Y. Notable mucosal immune responses induced in the intestine of zebrafish (*Danio rerio*) bath–vaccinated with a live attenuated *Vibrio anguillarum* vaccine. *Fish Shellfish Immunol* (2014) 40(1):99–108. doi: 10.1016/j.fsi.2012.02.004
6. Xiu YJiang GZhou SDiao JLiu HSu B, et al. Identification of potential immune–related circRNA-miRNA-mRNA regulatory network in intestine of *Paralichthys olivaceus* during *Edwardsiella tarda* infection. *Front Genet* (2019) 10:731. doi: 10.3389/fgene.2019.00731
7. Andreassen RHøyheim B. miRNAs associated with immune response in teleost fish. *Dev Comp Immunol* (2017) 75:77–85. doi: 10.1016/j.dci.2017.02.023
8. Gorski SAVogel JDoudna JA. RNA-based recognition and targeting: sowing the seeds of specificity. *Nat Rev Mol Cell Biol* (2017) 18(4):215–28. doi: 10.1038/nrm.2016.174
9. Li XLiu CXue WZhang YJiang SYin Q, et al. Coordinated circRNA biogenesis and function with NF90/NF110 in viral infection. *Mol Cell* (2017) 67(2):214–27. doi: 10.1016/j.molcel.2017.05.023
10. Valenzuela-Muñoz VValenzuela-Miranda DGallardo-Escárate C. Comparative analysis of long non–coding RNAs in Atlantic and Coho salmon reveals divergent transcriptome responses associated with immunity and tissue repair during sea lice infestation. *Dev Comp Immunol* (2018) 87:36–50. doi: 10.1016/j.dci.2018.05.016
11. Wang JFu LKoganti PPWang LHand JMMa H, et al. Identification and functional prediction of large intergenic noncoding RNAs (lincRNAs) in rainbow trout (*Oncorhynchus mykiss*). *Mar Biotechnol* (2016) 18(2):271–82. doi: 10.1007/s10126-016-9689-5
12. Yang NWang BYu ZLiu XFu QCao M, et al. Characterization of a novel lncRNA (SETD3-OT) in turbot (*Scophthalmus maximus* L.). *Fish Shellfish Immunol* (2020) 102:145–51. doi: 10.1016/j.fsi.2020.04.010
13. Bushati NCohen SM. microRNA functions. *Annu Rev Cell Dev Biol* (2007) 23(1):175–205. doi: 10.1146/annurev.cellbio.23.090506.123406
14. Gong GSha ZChen SLi CYan HChen Y, et al. Expression profiling analysis of the microRNA response of *Cynoglossus semilaevis* to *Vibrio anguillarum and* other stimuli. *Mar Biotechnol* (2015) 17(3):338–52. doi: 10.1007/s10126-015-9623-2
15. Huang SCao XTian XWang W. High-throughput sequencing identifies micrornas from posterior intestine of loach (*Misgurnus anguillicaudatus*) and their response to intestinal air-breathing inhibition. *PLoS One* (2016) 11(2):e0149123. doi: 10.1371/journal.pone.0149123
16. Jiang YHTang LLZhang FYJiang HYLiu XWYang LY, et al. Identification and characterization of immune-related micro RNAs in blunt snout bream, *Megalobrama amblycephala*. *Fish Shellfish Immunol* (2016) 49:470–92. doi: 10.1016/j.fsi.2015.12.013
17. Zhao LLu HMeng QWang JWang WYang L, et al. Profilings of microRNAs in the liver of common Carp (*Cyprinus carpio*) infected with *Flavobacterium columnare*. *Int J Mol Sci* (2016) 17(4):566. doi: 10.3390/ijms17040566
18. Liao XYang LChen XChen J. Identification of microRNA expression profiles in the gill, intestine and hepatic caecum of *Branchiostoma belcheri*. *Protein Cell* (2017) 8(4):302–7. doi: 10.1007/s13238-016-0365-3
19. Xu TChu QCui JZhao X. The inducible microRNA-203 in fish represses the inflammatory responses to Gram–negative bacteria by targeting IL–1 receptor-associated kinase 4. *J Biol Chem* (2018) 293(4):1386–96. doi: 10.1074/jbc.RA117.000158
20. Zhou ZLin ZPang XShan PWang J. MicroRNA regulation of Toll–like receptor signaling pathways in teleost fish. *Fish Shellfish Immunol* (2018) 75:32–40. doi: 10.1016/j.fsi.2018.01.036
21. Gao CCai XFu QYang NSong LSu B, et al. Dynamics of miRNA transcriptome in turbot (*Scophthalmus maximus* L.) intestine following *Vibrio anguillarum* infection. *Mar Biotechnol* (2019a) 21(4):550–64. doi: 10.1007/s10126-019-09903-z
22. Gao CFu QYang NSong LTan FZhu J, et al. Identification and expression profiling analysis of microRNAs in Nile tilapia (*Oreochromis niloticus*) in response to *Streptococcus agalactiae* infection. *Fish Shellfish Immunol* (2019b) 87:333–45. doi: 10.1016/j.fsi.2019.01.018
23. Wang MYu FWu WZhang YChang WPonnusamy M, et al. Circular RNAs: A novel type of non–coding RNA and their potential implications in antiviral immunity. *Int J Biol Sci* (2017) 13(12):1497. doi: 10.7150/ijbs.22531
24. Mao WHuang XWang LZhang ZLiu MLi Y, et al. Circular RNA hsa_circ_0068871 regulates FGFR3 expression and activates STAT3 by targeting miR-181a-5p to promote bladder cancer progression. *J Exp Clin Canc Res* (2019) 38(1):1–14. doi: 10.1186/s13046-019-1136-9
25. Rong XGao WYang XGuo J. Downregulation of hsa_circ_0007534 restricts the proliferation and invasion of cervical cancer through regulating miR-498/BMI-1 signaling. *Life Sci* (2019) 235:116785. doi: 10.1016/j.lfs.2019.116785
26. He LZhang AXiong LLi YHuang RLiao L, et al. Deep circular RNA sequencing provides insights into the mechanism underlying grass carp reovirus infection. *Int J Mol Sci* (2017) 18(9):1977. doi: 10.3390/ijms18091977
27. Liu BYuan RLiang ZZhang TZhu MZhang X, et al. Comprehensive analysis of circRNA expression pattern and circRNA-mRNA-miRNA network in

*Ctenopharyngodon idellus* kidney (CIK) cells after grass carp reovirus (GCRV) infection. *Aquaculture* (2019) 512:734349. doi: 10.1016/j.aquacutlure.2019.734349
28. Kim KHHwang YJKwon SR. Influence of daily water temperature changes on the chemiluminescent response and mortality of cultured rockfish (*Sebastes schlegeli*). *Aquaculture* (2001) 192(2–4):93–9. doi: 10.1016/S0044-8486(00)00460-9
29. Kang SHShin GWShin YSPalaksha KJKim YRYang HH, et al. Experimental evaluation of pathogenicity of *Lactococcus garvieae* in black rockfish (*Sebastes schlegeli*). *J Vet Sci* (2004) 5(4):387–90. doi: 10.4142/jvs.2004.5.4.387
30. Kitamura SIJung SJKim WSNishizawa TYoshimizu MOh MJ. A new genotype of lymphocystivirus, LCDV-RF, from lymphocystis diseased rockfish. *Arch Virol* (2006) 151(3):607–15. doi: 10.1007/s00705-005-0661-3
31. Han HJKim DYKim WSKim CSJung SJOh MJ, et al. Atypical Aeromonas salmonicida infection in the black rockfish, *Sebastes schlegeli* Hilgendorf, in Korea. *J Fish Dis* (2011) 34(1):47–55. doi: 10.1111/j.1365-2761.2010.01217.x
32. Zhang XPHu YHLi YWang JJWang GHWang RJ, et al. A high-mobility group box 1 that binds to DNA, enhances pro-inflammatory activity, and acts as an anti–infection molecule in black rockfish, *Sebastes schlegelii*. *Fish Shellfish Immunol* (2016) 56:402–9. doi: 10.1016/j.fsi.2016.07.034
33. Du XWang GHSu YLZhang MHu YH. Black rockfish C-type lectin, SsCTL4: a pattern recognition receptor that promotes bactericidal activity and virus escape from host immune defense. *Fish Shellfish Immunol* (2018) 79:340–50. doi: 10.1016/j.fsi.2018.05.033
34. Madusanka RKPriyathilaka TTJanson NDKasthuriarachchi TDWJung STharuka MN, et al. Molecular, transcriptional and functional delineation of Galectin–8 from black rockfish (*Sebastes schlegelii*) and its potential immunological role. *Fish Shellfish Immunol* (2019) 93:449–62. doi: 10.1016/j.fsi.2019.07.072
35. He SWDu XWang GHWang JJXie BGu QQ, et al. Identification and characterization of a cathepsin K homologue that interacts with pathogen bacteria in black rockfish, *Sebastes schlegelii*. *Fish Shellfish Immunol* (2020) 98:499–507. doi: 10.1016/j.fsi.2020.01.050
36. Wang JMeng ZWang GFu QZhang M. A CCL25 chemokine functions as a chemoattractant and an immunomodulator in black rockfish, *Sebastes schlegelii*. *Fish Shellfish Immunol* (2020) 100:161–70. doi: 10.1016/j.fsi.2020.02.063
37. Zhang YWen HSLi YLyu LKZhang ZXWang XJ, et al. Melanocortin-4 receptor regulation of reproductive function in black rockfish (*Sebastes schlegelii*). *Gene* (2020) 741:144541. doi: 10.1016/j.gene.2020.144541
38. De Vico GCataldi MCarella FMarino FPassantino A. Histological, histochemical and morphometric changes of splenic melanomacrophage centers (SMMCs) in Sparicotyle-infected cultured sea breams (*Sparus aurata*). *Immunopharm Immunot* (2008) 30(1):27–35. doi: 10.1080/08923970701812290
39. Trapnell CWilliams BAPertea GMortazavi AKwan GVan Baren MJ, et al. Transcript assembly and quantification by RNA-Seq reveals unannotated transcripts and isoform switching during cell differentiation. *Nat Biotechnol* (2010) 28(5):511–5. doi: 10.1038/nbt.1621
40. Love MIHuber WAnders S. Moderated estimation of fold change and dispersion for RNA-seq data with DESeq2. *Genome Biol* (2014) 15(12):550. doi: 10.1186/s13059-014-0550-8
41. Langmead BTrapnell CPop MSalzberg SL. Ultrafast and memory–efficient alignment of short DNA sequences to the human genome. *Genome Biol* (2009) 10(3):R25. doi: 10.1186/gb-2009-10-3-r25
42. Friedländer MRMackowiak SDLi NChen WRajewsky N. miRDeep2 accurately identifies known and hundreds of novel microRNA genes in seven animal clades. *Nucleic Acids Res* (2012) 40(1):37–52. doi: 10.1093/nar/gkr688
43. Wen MShen YShi STang T. miREvo: An integrative microRNA evolutionary analysis platform for next-generation sequencing experiments. *BMC Bioinf* (2012) 13:140. doi: 10.1186/1471-2105-13-140
44. Enright AJJohn BGaul UTuschl TSander CMarks DS. MicroRNA targets in *Drosophila*. *Genome Biol* (2003) 5(1):R1. doi: 10.1186/gb-2003-5-1-r1
45. Zhou LChen JLi ZLi XHu XHuang Y, et al. Integrated profiling of microRNAs and mRNAs: microRNAs located on Xq27. 3 associate with clear cell renal cell carcinoma. *PLoS One* (2010) 5(12):e15224. doi: 10.1371/journal.pone.0015224
46. Xie CMao XHuang JDing YWu JDong S, et al. KOBAS 2.0: a web server for annotation and identification of enriched pathways and diseases. *Nucleic Acids Res* (2011) 39(suppl_2):W316–22. doi: 10.1093/nar/gkr483
47. Young MDWakefield MJSmyth GKOshlack A. goseq: Gene Ontology testing for RNA–seq datasets. *R Bioconductor* (2012) 8:1–25.
48. Su GMorris JHDemchak BBader GD. Biological network exploration with Cytoscape 3. *Curr Protoc Bioinf* (2014) 47(1):8–13. doi: 10.1002/0471250953.bi0813s47
49. Ma LMWang WJLiu CHYu HYWang ZGWang XB, et al. Selection of reference genes for reverse transcription quantitative real-time PCR normalization in black rockfish (*Sebastes schlegeli*). *Mar Genomics* (2013) 11:67–73. doi: 10.1016/j.margen.2013.08.002
50. Livak KJSchmittgen TD. Analysis of relative gene expression data using real-time quantitative PCR and the $2^{-\Delta\Delta CT}$ method. *Methods* (2001) 25(4):402–8. doi: 10.1006/meth.2001
51. Hansen TBJensen TIClausen BHBramsen JBFinsen BDamgaard CK, et al. Natural RNA circles function as efficient microRNA sponges. *Nature* (2013) 495(7441):384–8. doi: 10.1038/nature11993
52. Salinas I. The mucosal immune system of teleost fish. *Biology* (2015) 4(3):525–39. doi: 10.3390/biology4030525
53. Hart SWrathmell ABHarris JEGrayson TH. Gut immunology in fish: a review. *Dev Comp Immunol* (1988) 12(3):453–80. doi: 10.1016/0145-305X(88)90065-1
54. Sun YLuo GZhao LHuang LQin YSu Y, et al. Integration of RNAi and RNA-seq Reveals the Immune Responses of *Epinephelus coioides* to *sigX* Gene of *Pseudomonas plecoglossicida*. *Front Immunol* (2018) 16(9):1624. doi: 10.3389/fimmu.2018.01624
55. Zhang PCao SZou THan DLiu HJin J, et al. Effects of dietary yeast culture on growth performance, immune response and disease resistance of gibel carp (*Carassius auratus gibelio* CAS III). *Fish Shellfish Immunol* (2018) 82:400–7. doi: 10.1016/j.fsi.2018.08.044
56. Chen LLYang L. Regulation of circRNA biogenesis. *RNA Biol* (2015) 12(4):381–8. doi: 10.1080/15476286.2015.1020271
57. Qu SYang XLi XWang JGao YShang R, et al. Circular RNA: a new star of noncoding RNAs. *Cancer Lett* (2015) 365(2):141–8. doi: 10.1016/j.canlet.2015.06.003
58. Memczak SJens MElefsinioti ATorti FKrueger JRybak A, et al. Circular RNAs are a large class of animal RNAs with regulatory potency. *Nature* (2013) 495(7441):333–8. doi: 10.1038/nature11928
59. Xu SXiao SQiu CWang Z. Transcriptome-wide identification and functional investigation of circular RNA in the teleost large yellow croaker (*Larimichthys crocea*). *Mar Genomics* (2017) 32:71–8. doi: 10.1016/j.margen.2016.12.004
60. Li JLv YLiu RYu YShan CBian W, et al. Identification and characterization of a conservative W chromosome-linked circRNA in half–smooth tongue sole (*Cynoglossus semilaevis*) reveal its female–biased expression in immune organs. *Fish Shellfish Immunol* (2018) 82:531–5. doi: 10.1016/j.fsi.2018.08.063
61. Fan BChen FLi YWang ZWang ZLu Y, et al. A comprehensive profile of the tilapia (*Oreochromis niloticus*) circular RNA and circRNA-miRNA network in the pathogenesis of meningoencephalitis of teleosts. *Mol Omics* (2019) 15(3):233–46. doi: 10.1039/C9MO00025A
62. Hu XDai YZhang XDai KLiu BYuan R, et al. Identification and characterization of novel type of RNAs, circRNAs in crucian carp *Carassius auratus* gibelio. *Fish Shellfish Immunol* (2019) 94:50–7. doi: 10.1016/j.fsi.2019.08.070
63. Li QVerma IM. NF–κB regulation in the immune system. *Nat Rev Immunol* (2002) 2(10):725–34. doi: 10.1038/nri910
64. Karin MGreten FR. NF-κB: linking inflammation and immunity to cancer development and progression. *Nat Rev Immunol* (2005) 5(10):749–59. doi: 10.1038/nri1703
65. Bauernfeind FGHorvath GStutz AAlnemri ESMacDonald KSpeert D, et al. Cutting edge: NF-κB activating pattern recognition and cytokine receptors license NLRP3 inflammasome activation by regulating NLRP3 expression. *J Immunol* (2009) 183(2):787–91. doi: 10.4049/jimmunol.0901363
66. Wang CGao CChen YYin JWang PLv X. Expression pattern of the apoptosis-stimulating protein of p53 family in $p53^{+}$ human breast cancer cell lines. *Cancer Cell Int* (2013) 13(1):116. doi: 10.1186/1475-2867-13-116
67. Cohen JJDuke RCFadok VASellins KS. Apoptosis and programmed cell death in immunity. *Annu Rev Immunol* (1992) 10(1):267–93. doi: 10.1146/annurev.iy.10.040192.001411

68. Rivas CAaronson SAMunoz-Fontela C. Dual role of p53 in innate antiviral immunity. *Viruses* (2010) 2(1):298–313. doi: 10.1084/jem.20080383
69. Coyle AJLloyd CTian JNguyen TErikkson CWang L, et al. Crucial role of the interleukin 1 receptor family member T1/ST2 in T helper cell type 2–mediated lung mucosal immune responses. *J Exp Med* (1999) 190(7):895–902. doi: 10.1084/jem.190.7.895
70. Nadiri AWolinski MKSaleh M. The inflammatory caspases: key players in the host response to pathogenic invasion and sepsis. *J Immunol* (2006) 177 (7):4239–45. doi: 10.4049/jimmunol.177.7.4239
71. Sheng WZong YMohammad AAjit DCui JHan D, et al. Pro-inflammatory cytokines and lipopolysaccharide induce changes in cell morphology, and upregulation of ERK1/2, iNOS and $sPLA_2$-IIA expression in astrocytes and microglia. *J Neuroinflamm* (2011) 8:121. doi: 10.1186/1742-2094-8-121
72. Kuo PLChiang LCLin CC. Resveratrol- induced apoptosis is mediated by p53-dependent pathway in Hep G2 cells. *Life Sci* (2002) 72(1):23–34. doi: 10.1016/s0024-3205(02)02177-x
73. Kalinichenko SGMatveeva NY. Morphological characteristics of apoptosis and its significance in neurogenesis. *Neurosci Behav Physiol* (2008) 38(4):333–44. doi: 10.1007/s11055-008-0046-7
74. Houwerzijl EJBlom NRvan der. Want JJEsselink MTKoornstra JJSmit JW, et al. Ultrastructural study shows morphologic features of apoptosis and para-apoptosis in megakaryocytes from patients with idiopathic thrombocytopenic purpura. *Blood* (2004) 103(2):500–6. doi: 10.1182/blood-2003-01-0275

**Conflict of Interest:** The authors declare that the research was conducted in the absence of any commercial or financial relationships that could be construed as a potential conflict of interest.

frontiers in Immunology

ORIGINAL RESEARCH
published: 22 January 2021
doi: 10.3389/fimmu.2020.609890

# Protein Phosphatase PP1 Negatively Regulates IRF3 in Response to GCRV Infection in Grass Carp (*Ctenopharyngodon idella*)

*Xudong Hu*[1,2], *Bing Wang*[1,2], *Haohao Feng*[1,2], *Man Zhou*[1,2], *Yusheng Lin*[1,2] *and Hong Cao*[1,2*]

[1] Institute of Hydrobiology, Chinese Academy of Sciences, Wuhan, China, [2] University of Chinese Academy of Sciences, Beijing, China

Protein phosphatase-1 (PP1) has an important role in many cell functions, such as cell differentiation, development, immune response and tumorigenesis. However, the specific role of PP1 in the antiviral response in fish remains to be elucidated. In this study, the *PPP1R3G* homolog was identified in the grass carp (*Ctenopharyngodon idella*) and its role in defence against the GCRV infection was investigated. Phylogenetic analysis demonstrated that CiPPP1R3G clustered with homologues from other teleosts. Temporal expression analysis *in vivo* revealed that the expression level of *CiPPP1R3G* was significantly up-regulated in response to GCRV infection in grass carps, especially in the intestine and head-kidney. Cellular distribution analysis revealed that CiPPP1R3G was located in the nucleus and cytoplasm. Overexpression of *CiPPP1R3G* significantly negatively regulated the expression of CiIRF3, thus inhibiting its activation. In summary, we systematically analyzed the *PPP1R3G* gene in grass carp and illustrated its function as a negative regulator in the anti-GCRV immune responses.

**Keywords: *PPP1R3G*, GCRV, antiviral, grass carp, intestine**

OPEN ACCESS

***Edited by:***
*Wei-Dan Jiang,*
*Sichuan Agricultural University, China*
***Reviewed by:***
*Javier Santander,*
*Memorial University of Newfoundland, Canada*
*Liu Zhen,*
*Changsha University, China*

***Correspondence:**
*Hong Cao*
*regancao@ihb.ac.cn*

***Specialty section:***
*This article was submitted to Comparative Immunology, a section of the journal Frontiers in Immunology*

***Received:*** *24 September 2020*
***Accepted:*** *07 December 2020*
***Published:*** *22 January 2021*

***Citation:***
*Hu X, Wang B, Feng H, Zhou M, Lin Y and Cao H (2021) Protein Phosphatase PP1 Negatively Regulates IRF3 in Response to GCRV Infection in Grass Carp (Ctenopharyngodon idella). Front. Immunol. 11:609890. doi: 10.3389/fimmu.2020.609890*

## HIGHLIGHTS

- CiPPP1R3G negatively regulates IRF3 and inhibits its activation.
- CiPPP1R3G inhibits grass carp IFN1 transcription.
- CiPPP1R3G is a negative regulator in the anti-GCRV immune responses.

## INTRODUCTION

Protein phosphatase 1 (PP1), a serine (Ser)/threonine (Thr) phosphatase, is a member of the phosphoprotein phosphatase (PPP) superfamily (1–3). It is one of the most conserved proteins in eukaryotic cells (4). PP1 plays crucial roles in many biological processes including cell division and meiosis, metabolism, cell cycle arrest and apoptosis. It exerts these functions through the

nucleophilic attack to catalyse the hydrolysis of serine/threonine-linked phosphate monoesters, and then dephosphorylates the substrate (4, 5). PP1 is composed of a glycogen-targeting regulatory (G) subunit and a catalytic subunit (PP1c) (4). These regulatory subunits are very important for the function of PP1, and seven genes that encode different G subunits have been recognised so far: PPP1R3A to PPP1R3G (4).

PPP1R3G, as a regulatory subunit of PP1, was demonstrated to be involved in the regulation of glucose homeostasis and hepatic glycogenesis in mice (6). Another study reported that the AKT (serine-threonine protein kinase) directly phosphorylated the PPP1R3G in response to insulin or feeding in hepatocytes, and the phosphorylation of PPP1R3G accelerates postprandial glucose clearance and glycogenesis (7).

However, the function of PPP1R3G in the innate immunity still remains to be elucidated. Innate immunity is the fundamental defence system to protect animals from the infection of invading pathogens (8). In the antiviral immune response process, viral nucleic acids can be recognized by some pattern recognition receptors (PRRs), such as the NOD-like receptors (NLRs), retinoic acid-inducible gene (RIG)-I-like receptors (RLRs), and Toll-like receptors (TLRs) (9–14).

Grass carp is an economically important fish widely cultured in more than 40 countries (15). Its annual production reached 5.53 million tons in 2019, accounting for 18.36% of the harvest of all freshwater Chinese fisheries in that year (16). Nevertheless, its cultivation industry is often plagued by frequent outbreaks of hemorrhagic disease (17–19), caused by the grass carp reovirus (GCRV), a double-stranded RNA (dsRNA) virus belonging to the family Reoviridae, genus *Aquareovirus* (20).

In this study, we identified and investigated the *PPP1R3G* gene in grass carp (*CiPPP1R3G*). Our data revealed that PPP1R3G was up-regulated at the mRNA level after the GCRV infection in grass carp and demonstrated that it is a negative regulator in the anti-GCRV immune responses.

# MATERIALS AND METHODS

## Experimental Fish

Healthy full-sib 3-months grass carps weighing ∼30 g were used in the study. The fish were obtained from the Institute of Hydrobiology, Chinese Academy of Sciences and maintained in aerated freshwater at 26-28°C. All animal experiments were approved by the Animal Research and Ethics Committee of the Institute of Hydrobiology, Chinese Academy of Sciences.

## Cells and Viruses

Grass carp kidney (CIK) cells were maintained at 28°C in the medium 199 (Invitrogen) supplemented with 15% foetal bovine serum (FBS, Invitrogen). Human embryonic kidney (HEK) 293T cells were grown at 37°C and 5% $CO_2$ in a DMEM medium (Invitrogen) supplemented with 15% FBS. Type I grass carp reovirus (GCRV-0901, $10^6$ TCID50/ml) was propagated in CIK cells until cytopathic effects (CPE) were observed, and then the cultured media with cells were harvested and stored at −80°C until use. Type II grass carp reovirus (GCRV-HZ08) was diluted to the titer of $2.97\times10^3$ RNA copy/μl for use in the experiments.

**TABLE 1** | Primers used for all of the studies.

| Primers | Sequences (5'—3') | Purpose |
|---|---|---|
| CiPPP1R3G-F | GATGACCCATCCAAAACCGCTCT | cDNA cloning |
| CiPPP1R3G-R | TCACTTGGTGTCACACAACTCC | |
| CiIRF3-F | ATGACCCATCCAAAACCGCT | |
| CiIRF3-R | CTTGGTGTCACACAACTCCATC | |
| qPCR-Ci-β-actin-F | AGCCATCCTTCTTGGGTATG | qRT-PCR |
| qPCR-Ci-β-actin-R | GGTGGGGCGATGATCTTGAT | |
| qPCR-Ci-PPP1R3G-F | TTAGATCCGAGCGCTTCTGT | |
| qPCR-Ci-PPP1R3G-R | TTCACTGGATGTCGAGCTGT | |
| qPCR-Ci-IRF3-F | ACTTCAGCAGTTTAGCATTCCC | |
| qPCR-Ci-IRF3-R | GCAGCATCGTTCTTGTTGTCA | |
| qPCR-Ci-IFN1-F | AAGCAACGAGTCTTTGAGCCT | |
| qPCR-Ci-IFN1-R | GCGTCCTGGAAATGACACCT | |
| qPCR-Ci-GAPDH-F | ATGACTCCACCCATGGCAAG | |
| qPCR-Ci-GAPDH-R | CTGGGGGCAGAGATGATGAC | |
| qPCR-Ci-B2M-F | TTCCATTTCCAGCCAGTCCC | |
| qPCR-Ci-B2M-R | TTTCGAAGGCCAGGTCAGTC | |
| pCMV-Ci-PPP1R3G-F | ATGGCCATGGAGGCCCGAATTCGGATGACCCATCCAAAACCGCTCT | Plasmid Construction |
| pCMV-Ci-PPP1R3G-R | GCGGTACCTCGAGAGATCTCGGTCGACTCACTTGGTGTCACACAACTCC | |
| pCMV -Ci-IRF3-F | ATGGCCATGGAGGCCCGAATTCGATGACCCATCCAAAACCGCT | |
| pCMV -Ci-IRF3-R | GCGGTACCTCGAGAGATCTCGGTCGACCTTGGTGTCACACAACTCCATC | |
| pAc- Ci-PPP1R3G-F | AGCTCAAGCTTCGAATTCTGATGAACATAATGAATGAGGAGC | |
| pAc- Ci-PPP1R3G-R | GGGCCCGCGGTACCGTCGACTGTATCGCGTGGAAAGCTGCGGTT | |
| pAc-Ci-IRF3-F | ACTCAGATCTCGAGCTCAAGCTTCGAATTCATGACCCATCCAAAACCGCT | |
| pAc-Ci-IRF3-R | GGGCCCGCGGTACCGTCGACTGCTTGGTGTCACACAACTCCATC | |

## Identification and Sequence Analysis of CiPPP1R3G

According to the previous study of the transcriptome of the grass carp (21), the CiPPP1R3G mRNA (GenBank accession number MT833843) was obtained by PCR amplification using the primers listed in **Table 1**. The searches for similar protein sequences were performed by the BLASTP program, and conserved domain features were predicted using the SMART program (http://smart.emblheidelberg.de/). The phylogenetic tree was constructed using the Neighbour-joining method (NJ) with 1000 bootstraps in MEGA 7.0.

## Experimental Viral Infection, Sample Collection, and Histological Observation

Healthy full-sib 3-month-old grass carps were divided into two groups: the GCRV-treated group and negative control group (approximately 150 specimens per group). Each fish in the experimental group (I) was infected *via* an intraperitoneal injection of 200 μl of GCRV-HZ08 ($2.97 \times 10^3$ RNA copy/μl), while fish from the control group (II) were injected with 200 μl PBS. At 1–7 days post-injection, samples of spleen, liver, intestine, head-kidney and muscle tissues were harvested from both groups (biological replicates: $n$=4 specimens from each group). For the histological examination analyses, the intestine samples of both GCRV-treated (3-days post infection) and control groups ($n$=3, respectively) were fixed in the formalin, sectioned, stained with hematoxylin and eosin, and analyzed by two pathologists independently using light microscopy.

## Quantitative Real-Time PCR and Tissue Expression of CiPPP1R3G

The total RNA of cells and spleen, liver, intestine, muscle and head-kidney tissues were extracted from four randomly selected grass carp specimens 1–4 days post GCRV infection, whereas 5–7 days post GCRV infection specimens exhibiting typical symptoms of disease (e.g., muscle bleeding) were selected. After grinding each sample in liquid nitrogen, 1 ml of Trizol reagent was added per 50 mg of tissue. Total RNA was purified by MonScriptTM DNase, and then the cDNA was synthesized according to the protocol of the using MonScriptTM RTIII Super Mix kit (Monad, China) according to the manufacturer's protocol. Quantitative real-time PCR (qRT-PCR) was performed to reveal the mRNA expression patterns of the CiPPP1R3G gene *in vivo*. The RNA was extracted using Trizol reagent (Invitrogen). RNase-free DNase was used to remove all contaminating genomic DNA. qRT-PCR was performed with FastSYBR Green PCR Master mix (Bio-Rad) on the Applied Biosystems StepOne™ Real-Time PCR System. PCR conditions were as follows: 95°C for 5 min, then 45 cycles of 95°C for 20 s, 60°C for 20 s, and 72°C for 20 s. Primers for PCR were designed *via* an online tool IDT Real Time PCR (http://www.idtdna.com/scitools/Applications/RealTimePCR/). Primer sequences are listed in **Table 1**. We tested the suitability of three commonly used internal reference genes, including *β-actin*, *GAPDH* and *B2M*, all of which exhibited a relatively stable expression in a previous study (22). Their expression was studied by qRT-PCR, and results analysed using the NormFinder software (22). The Ct values of candidate reference genes are provided in the **Supplementary Table 1**. The M values of candidate reference genes were: *β-actin* (0.006) >*B2M* (0.015) > *GAPDH* (0.061). The gene with best expression stability is *β-actin* and it was selected as the internal reference gene. The length of PCR products was about 100–200 bp. Three replicates were included for each sample, and relative expression levels were calculated using the $2^{-\triangle\triangle Ct}$ method (23).

## Plasmid Construction

The open reading frame (ORF) of CiPPP1R3G was subcloned into pCMV-Flag vector (Clontech) and pAcGFP-N1 (Clontech). The ORF of grass carp IRF3 (KC898261) was subcloned into pCMV-Myc vector (Clontech) and pM-RFP vector (Clontech). The grass carp IFN (CiIFN) was obtained from the lab of Prof. Su (Huazhong Agriculture University, China) and cloned into pGL3-Basic luciferase reporter vector (Promega). The plasmid containing CiIFN1pro-Luc in pGL3-Basic luciferase reporter vectors were constructed as described previously (24). All recombinant plasmids were verified by DNA sequencing.

## Transient Transfection and Virus Infection

For the luciferase assay, transient cell transfections were performed in CIK cells seeded in 6-well or 24-well plates by using Lipofectamine 2000 Transfection Reagent (Invitrogen) according to the manufacturer's protocol. CIK cells were seeded in 6-well plates overnight and transfected with CiIRF3-Myc or the pCMV-Myc vector separately (2 μg/well for luciferase analysis and 1 μg/well for qRT-PCR). Next, to investigate the response of CiPPP1R3G to CiIRF3, CIK cells were seeded in 6-well plates overnight and transfected with CiPPP1R3G-Flag, CiIRF3-Myc and the pCMV-Myc vector together (1 μg/well for qRT-PCR). The virus titration (GCRV-0901) was examined in CIK cells as previously described (25).

## siRNA Mediated Knockdown

Transient knockdown of CiPPP1R3G in CIK cells was achieved by transfection of siRNA targeting CiPPP1R3G mRNA. Three siRNA sequences, si-CiPP1#1: GGAGAAGAGCCAAGUCCUUTT, si-CiPP1#2: CCGUGGACUCCGGUGACAUTT, and si-CiPP1#3: CCAUGUACACGCCUCCUUUTT (all sense5′-3′), targeting different regions of CiPPP1R3G were synthesized by GenePharma (Jiangsu, China). CIK cells were transfected with siRNA using Lipofectamine 2000 Transfection Reagent (Invitrogen). The silencing efficiencies of the siRNA candidates were then evaluated by qRT-PCR, by comparing them to the negative control siRNA (si-NC) provided by the supplier. A preliminary experiment indicated that si-CiPP1#3 possessed the best silencing efficiency at a final concentration of 100 pmol. The subsequent knockdown experiments were performed with si-CiPP1#3. CIK cells were transfected with si-CiPP1#3 for 24 h and infected with GCRV for another 24 h post-infection.

## Reporter Gene Analysis

To investigate the interferon promoter activity evoked by the CiPPP1R3G, pGL3-basic luciferase reporter vector and CiIFN1-Luc

(obtained from the lab of Prof. Su) were co-transfected in CIK cells as described previously (26). The pRL-CMV (Promega) plasmid was co-transfected to normalize the transfection efficiencies. CIK cells were seeded into 24-well plates, and 24 h later co-transfected with: 1) 300 ng CiIFN1-pro-Luc plasmid, 300 ng pCMV-Myc plasmid and 300 ng pCMV-Flag plasmid; 2) 300 ng CiIFN1pro-Luc plasmid, 300 ng pCMV-Myc plasmid and 300 ng CiPPP1R3G-Flag plasmid; 3) 300 ng CiIFN1pro-Luc plasmid, 300 ng CiIRF3-Myc plasmid and 300 ng pCMV-Flag plasmid; 4) 300 ng CiIFN1pro-Luc plasmid, 300 ng CiIRF3-Myc plasmid and 300 ng CiPPP1R3G-Flag plasmid. Renilla luciferase internal control vector (30 ng, pRL-CMV, Promega) was added in each group. At 24 h post-transfection, the cells were washed in PBS and lysed to measure the luciferase activity by Dual-Luciferase Reporter Assay System, according to the manufacturer's protocol (Promega). Firefly luciferase activities were normalized on the basis of Renilla luciferase activity. The final results were calculated as averages of more than three independent experiments, each performed in triplicate.

## Subcellular Localization Analysis

To investigate the subcellular localization of CiPPP1R3G and CiIRF3, GFP-fused CiPPP1R3G (pAcGFP-N1-CiPPP1R3G) vector plasmids and RFP-fused CiIRF3 (pAcRFP-N1-CiIRF3) vector plasmids were transfected into CIK cells. CIK cells were plated onto coverslips in confocal dishes and transfected with the above plasmids for 24h. Then the cells were washed twice with PBS and fixed with 4% PFA for 1h. Finally, the samples were visualized using a laser scanning confocal microscope (Carl Zeiss).

## Western Blotting Analysis

HEK293T cells were transfected with different combinations of CiPPP1R3G-Flag and the pCMV-Flag vectors (5 μg each). Then the cells were lysed in radioimmunoprecipitation (RIPA) lysis buffer [1% NP-40, 50 mM Tris-HCl (pH 7.5), 150 mM NaCl, 1 mM EDTA, 1 mM NaF, 1 mM sodium orthovanadate, 1 mM phenylmethylsulfonyl fluoride, and 0.25% sodiumdeoxycholate] containing protease inhibitor mixture. After incubation on ice for 1 h, lysates were collected and centrifuged at 10,000 g at 4°C for 15 min. Next, Western blot analysis was performed as described previously (26).

## Co-IP Analysis

For transient-transfection and Co-IP experiments, HEK293T cells were seeded into two petri dishes (10 cm in diameter) overnight and then cotransfected with a total of 10 μg of the following plasmids: (1) CiPPP1R3G-Flag and CiIRF3-Myc (test group) and (2) pCMV-FLAG and CiIRF3-Myc (control group). After 24 h, the medium was removed carefully, and the cell monolayer was washed twice with 10 ml ice-cold PBS. Then the cells were harvested in cell lysis buffer (1% NP-40, 50 mM Tris-HCl [pH 7.5], 150 mM NaCl, 1 mM EDTA, 1 mM NaF, 1 mM sodium orthovanadate [$Na_3VO_4$], 1 mM phenylmethylsulfonyl fluoride [PMSF], 0.25% sodium deoxycholate) containing a protease inhibitor cocktail (Sigma-Aldrich) at 4°C for 0.5 h on a rocker platform. The cellular debris was removed by centrifugation at 10,000 g for 15 min at 4°C. The supernatant was transferred to a fresh tube and incubated with 20 μl anti-Flag agarose beads (Sigma-Aldrich) overnight at 4°C with constant agitation. Then the samples were further analyzed by immunoblotting (IB). Immunoprecipitated proteins were collected by centrifugation at 5,000 g for 1 min at 4°C, washed three times with lysis buffer, The immunoprecipitates and the total cell lysates were boiled with 2× SDS sample buffer. The immunoprecipitates and total cell lysates were analyzed by IB with the indicated antibodies (Abs).

## Statistical Analysis

The results of qRT-PCR data were reported as mean ± SEM of three independent experiments. Statistical analysis (unpaired t-test) was performed using GraphPad Prism 5 (GraphPad Software Inc.). A $p < 0.05$ was considered to be statistically significant.

# RESULTS

## CiPPP1R3G Sequence Analysis

The CiPPP1R3G mRNA (GenBank accession number MT833843) is 756 bp in length, and encodes 251 amino acids (aa) (**Supplementary Figure 1**). BLASTP analysis showed that CiPPP1R3G had highest similarity to *Gobiocypris rarus* PPP1R3G (92.8%) (GenBank ID., MT833844), followed by PPP1R3G of *Cyprinus carpio* (86.9%) (GenBank ID., XM_019066810) and *Carassius auratus* (84.8%) (GenBank ID., XM_026200865). In the phylogenetic analysis, CiPPP1R3G clustered with homologues from other fishes, and exhibited the closest relationship to *G. rarus* (**Figure 1**).

## Temporal Expression Pattern of CiPPP1R3G mRNA After the GCRV Infection

The distribution of CiPPP1R3G mRNA was detected in the spleen, liver, intestine, muscle and head-kidney tissues. Transcripts of CiPPP1R3G were expressed in all examined tissues, with the highest expression in the liver, and lowest in the intestine (**Figure 2A**). These data demonstrated that CiPPP1R3G is ubiquitously expressed in the tissues of grass carp.

qRT-PCR was performed to investigate the expression of CiPPP1R3G in these tissues after the GCRV infection. The expression level of CiPPP1R3G reached a peak at 2 d in the muscle (16.15-fold, $p < 0.001$), at 3 d in the liver (5.88-fold, $p < 0.001$), head-kidney (236.01, $p < 0.001$) and intestine (205.73-fold, $p < 0.01$), and at 5 d in the spleen (9.25-fold, $p < 0.001$) (**Figure 2B**).

## The Expression of CiIRF3 Was Negatively Regulated by CiPPP1R3G

It is well known that IRF3 is a pivotal signalling molecule of the innate immune response. In the present study, to confirm the association of CiPPP1R3G and CiIRF3, we transfected expression plasmids of CiIRF3-Myc and CiPPP1R3G-Flag into HEK 293T cells and performed a Co-IP assay. Our results revealed that CiPPP1R3G interacted with CiIRF3 (**Figure 3A**). In addition, compared with the control group, the expression of CiIRF3 was negatively regulated by the overexpression of CiPPP1R3G in a dose-dependent manner (**Figure 3B**).

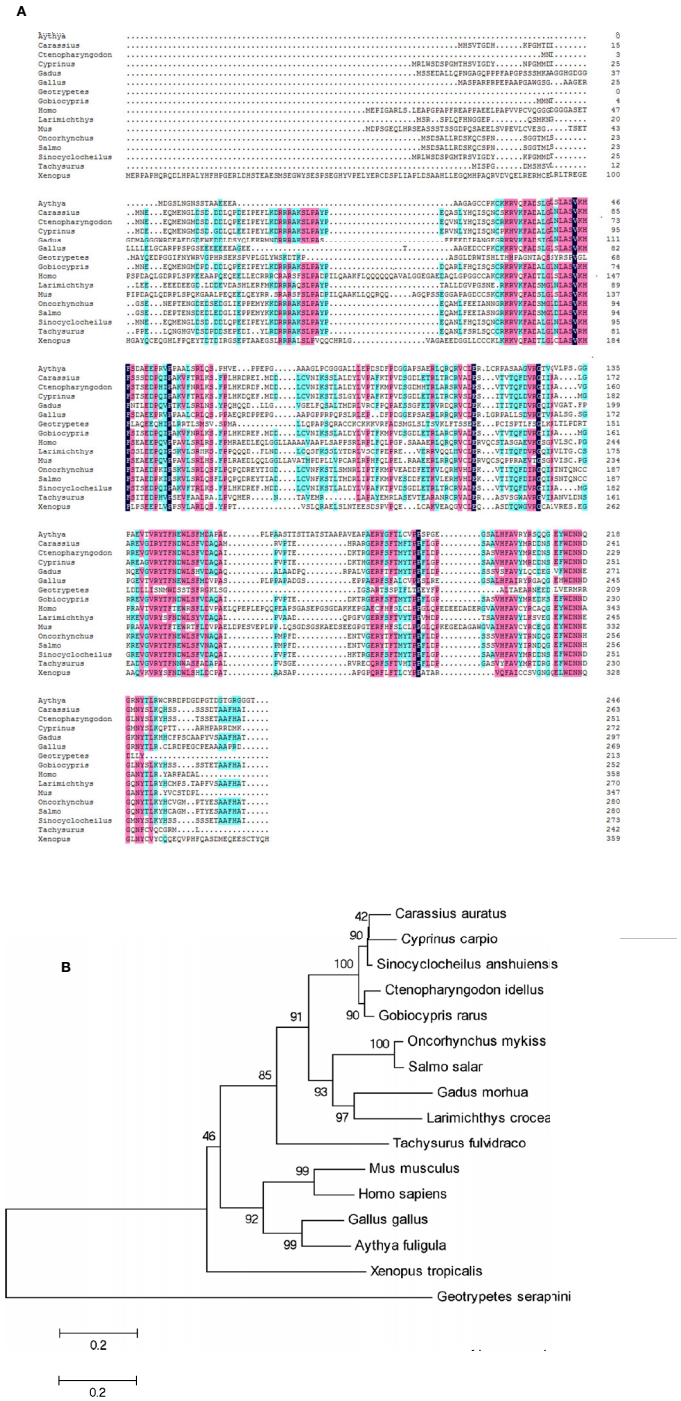


FIGURE.1B

**FIGURE 1** | Phylogenetic analysis of the CiPPP1R3G protein and multiple alignment of the amino acid sequences of PPP1R3G from different species. **(A)** Amino acid sequence alignment of CiPPP1R3G protein and species. **(B)** Phylogenetic tree was constructed by the neighbor-joining method. The scale indicates genetic distance. Accession numbers of PPP1R3G amino acid sequences are as follows: *Mus musculus*, NP_083904.1; *Oncorhynchus mykiss*, XP_021418751.1; *Gadus morhua*, XP_030204922.1; *Carassius auratus*, XP_026056650.1; *Cyprinus carpio*, XP_018922355.1; *Sinocyclocheilus anshuiensis*, XP_016296100.1; *Salmo salar*, XP_014036113.1; *Larimichthys crocea*, XP_010750048.1; *Tachysurus fulvidraco*, XP_027005035.1; *Homo sapiens*, NP_001138587.1; *Gallus gallus*, XP_004939761.2; *Aythya fuligula*, XP_032036977.1; *Xenopus tropicalis*, XP_004915359.2; *Geotrypetes seraphini*, XP_033790671.1.

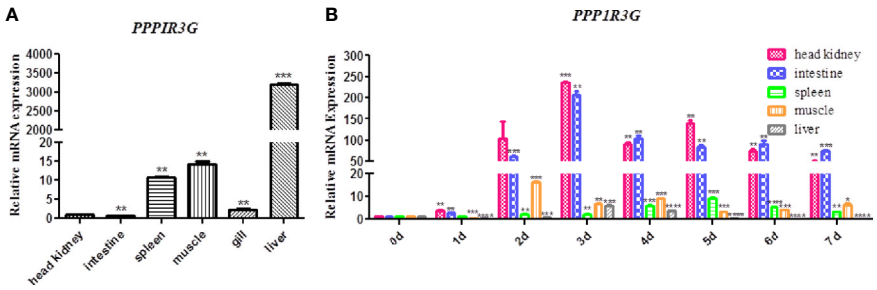


**FIGURE 2** | Tissue distribution of CiPPP1R3G in grass carp and Quantitative Real-Time PCR analysis. **(A)** Total RNAs from different tissues of grass carp were extracted to detect the transcripts of CiPPP1R3G, and *β-actin* was used as an internal control for normalization to produce relative expression. The expression levels in other tissues are shown as fold change compared with the head-kidney (which was set to 1). Error bars represent the means ± SEM (*n*=3). **(B)** The expression analysis of CiPPP1R3G in different tissues of grass carp at 0–7 d post GCRV infection. The expression level of the control group (day 0) was set to 1. *β-actin* was used as an internal control for normalization in both analyses. Error bars represent the means ± SEM of three replicates. Asterisks indicate significant differences from the control (*$p < 0.05$, **$p < 0.01$, ***$p < 0.001$, ****$p < 0.0001$).

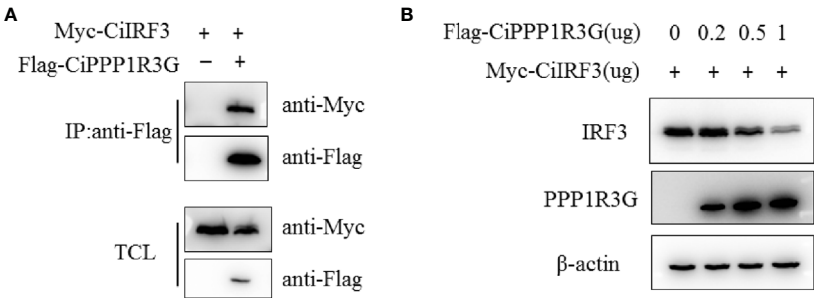


**FIGURE 3** | The expression of CiIRF3 was negatively regulated by CiPPP1R3G. **(A)** CiPPP1R3G associates with CiIRF3. HEK293T cells seeded into 10-cm$^2$ dishes were transfected with the indicated plasmids (5 μg each). After 24h, cell lysates were immunoprecipitated (IP) with anti-Flag affinity gel. The immunoprecitates and cell lysates were analysed by IB with anti-Flag, anti-Myc, and anti-β-actin Abs, respectively. TCL: total cell lysates. **(B)** Overexpression of CiPPP1R3G induces the reduction of CiIRF3 in a dose-dependent manner. HEK293T cells seeded in 6-well plates overnight were co-transfected with 1 μg CiIRF3-Myc and 1 μg pCMV-Flag, or CiPPP1R3G-Flag (0, 0.25, 0.5 and 1 μg, respectively), 24h later the cell lysates were detected by IB with the anti-Flag, anti-Myc, and anti-β-actin Abs.

## CiPPP1R3G Negatively Mediated the Activation of CiIFN1 Caused by CiIRF3

In this study, the activation of CiIFN1 caused by the CiIRF3 was investigated through a luciferase assay. As shown in **Figure 4A**, compared with the empty vector control group, CiIRF3 significantly upregulated the activation of the CiIFN1 promoter up to 34.27-fold. However, the activation of the CiIFN1 promoter was obviously reduced to 3.85-fold by the co-transfection of CiIRF3, CiPPP1R3G and the CiIFN1 promoter (**Figure 4A**). Subsequently, we performed qRT-PCR assays to examine the expression of CiIFN1 after a challenge with GCRV in CIK cells. Consistently, overexpression of the CiPPP1R3G significantly attenuated the expression of CiIFN1 induced by the GCRV (**Figure 4B**). Conversely, the effect of CiPPP1R3G knockdown on the expression of CiIFN1 was evaluated using siRNAs. As shown in **Figure 4C**, compared with cells transfected with control siRNAs (NC), the cells transfected with *CiPPP1R3G*-specific siRNAs (si-CiPP1#3) exhibited a significantly decreased level (50–60%) of *CiPPP1R3G* expression. The qRT-PCR analysis revealed that the knockdown of CiPPP1R3G increased the expression of CiIFN1 (**Figure 4D**). Taken together, our results demonstrated that PPP1R3G can negatively mediate the activation of the IFN1 caused by the IRF3 in grass carp.

## Subcellular Localization of CiPPP1R3G and CiIRF3

Subcellular localization of CiPPP1R3G was examined by transient transfection of the pAcGFP-N1-CiPPP1R3G plasmid into CIK cells. The green fluorescent signal of pAcGFP-N1-CiPPP1R3G was distributed in the cytoplasm and nucleus of the CIK cells (**Figure 5A**). Next, we co-transfected pAcGFP-N1-CiPPP1R3G with pM-RFP-CiIRF3. The red fluorescent signal of pM-RFP-CiIRF3 was mainly observed in the cytosol and almost overlapped with the green signal from CiPPP1R3G (**Figures 5B, C**). Taken together, our data indicated that CiPPP1R3G was localized in the cytoplasm and nucleus, and associated with CiIRF3.

## Histologic Observations of the Intestine of GCRV-Infected Grass Carp

HE staining was applied to the grass carp intestine tissue samples collected 3 days post GCRV-infection in order to detect

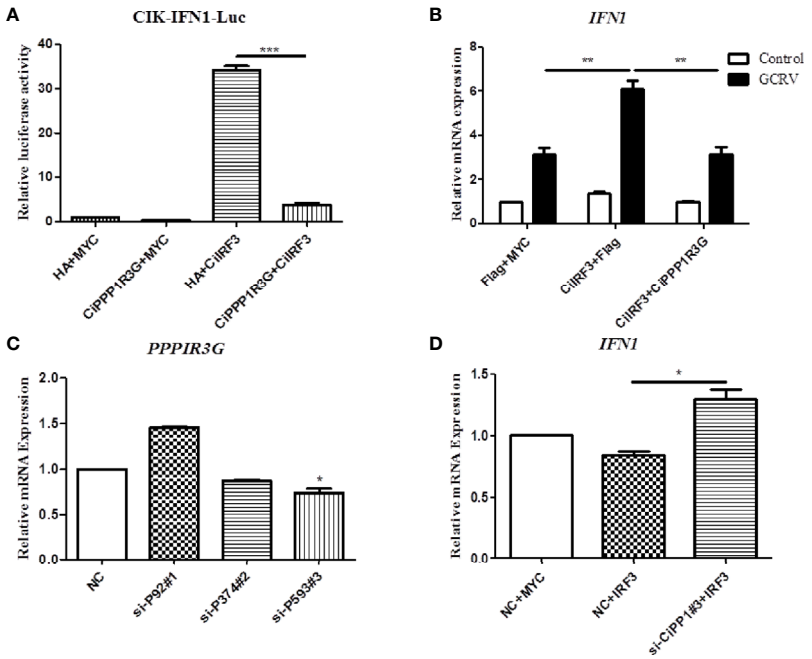


**FIGURE 4** | CiPPP1R3G Negatively Mediated the Activation of CiIFN1 Caused by CiIRF3. **(A)** Overexpression of CiIRF3 activates the CiIFN1 promoter, whereas overexpression of CiPPP1R3G suppressed the activation caused by CiIRF3. CIK cells were seeded in 6-well plates overnight and cotransfected with 1) 300 ng CiIFN1pro-Luc plasmid and 300 ng CiIRF3-Myc plasmid; or 2) 300 ng CiIFN1pro-Luc plasmid, 300 ng CiIRF3-Myc plasmid, and 300 ng CiPPP1R3G-Flag; or 3) pCMV-Flag. 30 ng of Renilla luciferase internal control vector (pRL-CMV, Promega) was added in each group. 24 hours later, the cells were washed in PBS and lysed to measure the luciferase activity by the Dual-Luciferase Reporter Assay System. **(B)** CiPPP1R3G suppresses the expression of CiIFN1 induced by GCRV infection in CIK cells. Error bars represent the means ± SEM ($n$ = 3). Asterisks indicate significant differences from the control (**$p < 0.01$, ***$p < 0.001$). **(C)** CiPPP1R3G mRNA levels were inferred using real-time PCR in negative control-siRNA (NC) or si-CiPPP1R3G treated CIK cells to confirm the knockdown efficiency of endogenous CiPPP1R3G. **(D)** Knockdown of CiPPP1R3G increased the expression of CiIFN1 in CIK cells. Error bars represent the means ± SEM ($n$ = 3). Asterisks indicate significant differences from the control (*$p < 0.05$).

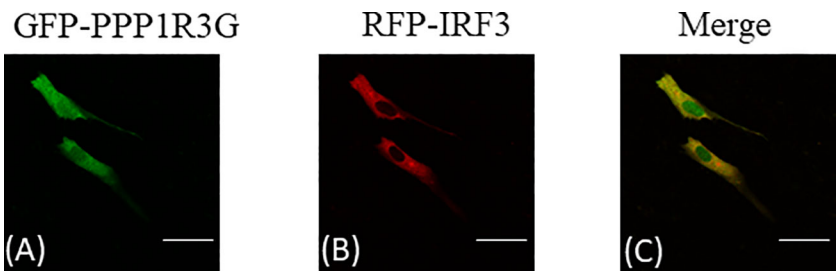


**FIGURE 5** | CiPPP1R3G locates in the cytoplasm and nucleus and interacts with the CiIRF3. CIK cells seeded in confocal dishes were co-transfected with pAcGFP-N1-CiPPP1R3G and pAcRFP-N1-CiIRF3 (2 μg each) or 2 μg of empty vector. 24h later, the cells were treated with indicated antibodies. **(A)** Green staining represents the CiPPP1R3G protein signal. **(B)** Red staining represents the CiIRF3 protein signal. **(C)** Merged signal of CiPPP1R3G and CiIRF3. Bar = 25μm. All experiments were repeated at least three times, with similar results.

morphological changes in the intestine after the GCRV-infection and high expression of CiPPPiR3G. As shown in **Figure 6A**, no pathological alterations were detected in the control group. In comparison with the control group, the intestine samples of GCRV-infected fish exhibited obvious lymphocyte infiltration into both LP (lamina propria) and IEL (intestinal epithelial layer), widened LP, narrowing of the interspace between the villi, and shortening of the height of MF (mucosal fold; $p < 0.05$; **Figure 6B**).

## DISCUSSION

As an important phosphatase, PP1 participants in the regulation of a wide range of cellular events (4, 5). Among them, it plays a pivotal role in the antiviral immune response. A previous study reported that PP1 can modulate the phosphorylation of the capsid of Venezuelan equine encephalitis virus (VEEV), and the inhibition of PP1 could slow down the viral replication in human cells

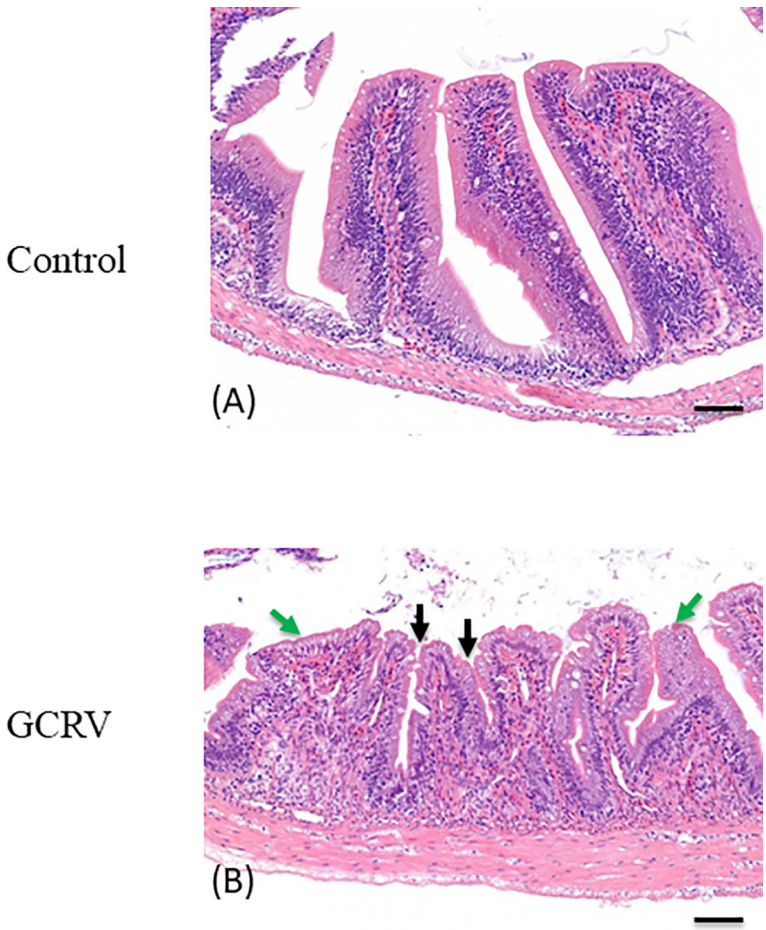


**FIGURE 6** | Histological analysis of the intestine in studied grass carp. **(A)** Normal intestine tissue was used as a negative control. **(B)** The typical intestinal folds with obvious lymphocyte infiltration into both LP (lamina propria) and IEL (intestinal epithelial layer) accompanied by widened LP and shortened MF (green arrow), and narrowing of the interspace between the villi (black arrow) were observed in the intestine tissue of GCRV-infected fish samples. Bar = 50 μm.

(U87MG astrocytoma cells, ATCC HTB-14) (27). In addition, it was revealed that PP1 can interact with the V proteins of measles virus and Nipah virus, thereby inhibiting dephosphorylation of MDA5 and eschewing the innate immune recognition of MDA5 (28).

As one of the regulatory subunits of the PP1, PPP1R3G has a major role in the regulation of postprandial glucose homeostasis during the fasting-feeding transition through its modulation of liver glycogenesis (6). PPP1R3G deletion accelerates the metabolic rate and reduces the glycogen level in adipose tissue in mice, indicating that PPP1R3G links glycogen and lipid metabolisms *in vivo* (29). In fish (silver carp *Hypophthalmichthys molitrix*), a study found that after a treatment with toxic *Microcystis aeruginosa*, PPP1R3G was down-regulated, indicating that it might play a major role in the detoxifying and antitoxic mechanisms of microcystin in fish (30).

In this study, a PPP1R3G protein was identified from grass carp and we found that it negatively regulates the function of IRF3 in the anti-GCRV immune responses. Temporal expression pattern revealed that CiPPP1R3G mRNA is highly expressed in several tissues; the highest in the liver, and relatively low in the intestine and head-kidney. As several previous studies reported, PPP1R3G plays an important role in the regulation of glycogenesis and glycogen metabolism in liver (6, 29). Interestingly, after the GCRV stimulation, the mRNA level of CiPPP1R3G increased sharply in the intestine and head-kidney, indicating that these two tissues are the frontline of CiPPP1R3G to perform its function in the innate immune response against GCRV infection.

Fish intestine is the major site of immune responses in teleost fish (31–37). The immune cells that are essential for the gut immunization are plenteously present in the intestinal mucosa of teleost species (38). A previous study reported that the intestine is the main source of T cells in adult sea bass (*Dicentrarchus labrax*) (39). This tissue is also very important for anti-viral immune responses. For example, it was reported that IPNV (Infectious Pancreatic Necrosis Virus) infection could induce a differentiated epithelial immune response in the gut of Atlantic salmon (*Salmo salar*) (40). In the olive flounder (*Paralichthys olivaceus*), after the

stimulation with VHSV (Viral Haemorrhagic Septicaemia Virus), a significant up-regulation of gene transcripts of IgT and its receptor pIgR (polymeric IgR) in the gut of the immunized fish (41). IgT is most abundant in mucosal compartments (42) and pIgR is strongly expressed in the gut enterocytes, where it recognizes the Ig molecules and transports them to the immune reaction site (31).

In the present study, we investigated the expression of PPP1R3G after the GCRV infection in grass carp. Interestingly, we found a significant up-regulation of the transcripts of PPP1R3G in the intestine compared with other tissues. An obvious histopathological alternation was detected in the intestine tissue of grass carp after GCRV infection. In conclusion, we found that the PPP1R3G play a negative role in the anti-GCRV immune responses. Further *in vivo* studies are needed to elucidate the molecular mechanisms of PPP1R3G-mediated signalling pathway in fish.

## DATA AVAILABILITY STATEMENT

The datasets presented in this study can be found in online repositories. The names of the repository/repositories and accession number(s) can be found in the article/**Supplementary Material**.

## ETHICS STATEMENT

The animal study was reviewed and approved by Animal Research and Ethics Committee of the Institute of Hydrobiology, Chinese Academy of Sciences.

## AUTHOR CONTRIBUTIONS

HC conceived and designed the experiments. XH, BW, HF, MZ, and YL performed the experiments and analyzed the data. HC wrote the manuscript. All authors reviewed the manuscript. All authors contributed to the article and approved the submitted version.

## FUNDING

This work was supported by National Natural Science Foundation of China (31972827).

## ACKNOWLEDGMENTS

We thank Prof. Jianguo Su (Huazhong Agriculture University, China) for providing the plasmid of grass carp IFN1 (CiIFN1). We thank Dr. Fang Zhou (Institute of Hydrobiology, Chinese Academy of Sciences) for assistance with confocal microscopy analysis.

## SUPPLEMENTARY MATERIAL

The Supplementary Material for this article can be found online at: https://www.frontiersin.org/articles/10.3389/fimmu.2020.609890/full#supplementary-material

**SUPPLEMENTARY FIGURE 1** | The mRNA sequence and protein sequence of CiPPP1R3G.

## REFERENCES

1. Bollen M, Peti W, Ragusa MJ, Beullens M. The extended PP1 toolkit: designed to create specificity. *Trends Biochem Sci* (2010) 35(8):450–8. doi: 10.1016/j.tibs.2010.03.002
2. Choy MS, Page R, Peti W. Regulation of protein phosphatase 1 by intrinsically disordered proteins. *Biochem Soc Trans* (2012) 40(5):969–74. doi: 10.1042/BST20120094
3. Rebelo S, Santos M, Martins F, da Cruz e Silva EF, da Cruz e Silva OA. Protein phosphatase 1 is a key player in nuclear events. *Cell Signal* (2015) 27 (12):2589–98. doi: 10.1016/j.cellsig.2015.08.007
4. Ceulemans H, Bollen M. Functional diversity of protein phosphatase-1, a cellular economizer and reset button. *Physiol Rev* (2004) 84(1):1–39. doi: 10.1152/physrev.00013.2003
5. Lad C, Williams NH, Wolfenden R. The rate of hydrolysis of phosphomonoester dianions and the exceptional catalytic proficiencies of protein and inositol phosphatases. *Proc Natl Acad Sci USA* (2003) 100:5607–10. doi: 10.1073/pnas.0631607100
6. Luo X, Zhang Y, Ruan X, Jiang X, Zhu L, Wang X, et al. Fasting-induced protein phosphatase 1 regulatory subunit contributes to postprandial blood glucose homeostasis via regulation of hepatic glycogenesis. *Diabetes* (2011) 60 (5):1435–45. doi: 10.2337/db10-1663
7. Li Q, Zhao Q, Zhang J, Zhou L, Zhang W, Chua B, et al. The Protein Phosphatase 1 Complex Is a Direct Target of AKT that Links Insulin Signaling to Hepatic Glycogen Deposition. *Cell Rep* (2019) 28(13):3406–3422.e7. doi: 10.1016/j.celrep.2019.08.066
8. Rolff J, Siva-Jothy MT. Invertebrate ecological immunology. *Science* (2003) 301(5632):472–5. doi: 10.1126/science.1080623
9. Okamoto M, Tsukamoto H, Kouwaki T, Seya T, Oshiumi H. Recognition of Viral RNA by Pattern Recognition Receptors in the Induction of Innate Immunity and Excessive Inflammation During Respiratory Viral Infections. *Viral Immunol* (2017) 30(6):408–20. doi: 10.1089/vim.2016.0178
10. Nazmi A, Dutta K, Hazra B, Basu A. Role of pattern recognition receptors in flavivirus infections. *Virus Res* (2014) 185:32–40. doi: 10.1016/j.virusres.2014.03.013
11. Blasius AL, Beutler B. Intracellular toll-like receptors. *Immunity* (2010) 32 (3):305–15. doi: 10.1016/j.immuni.2010.03.012
12. Goubau D, Deddouche S, Reis e Sousa C. Cytosolic sensing of viruses. *Immunity* (2013) 38(5):855–69. doi: 10.1016/j.immuni.2013.05.007
13. Reikine S, Nguyen JB, Modis Y. Pattern Recognition and Signaling Mechanisms of RIG-I and MDA5. *Front Immunol* (2014) 5:342. doi: 10.3389/fimmu.2014.00342
14. Margolis SR, Wilson SC, Vance RE. Evolutionary Origins of cGAS-STING Signaling. *Trends Immunol* (2017) 38(10):733–43. doi: 10.1016/j.it.2017.03.004
15. Jiang YL. Hemorrhagic disease of grass carp: status of outbreaks, diagnosis, surveillance, and research. *Isr J Aquacult-Bamid* (2009) 61:188–96. doi: 10.1093/icesjms/fsp104
16. Bureau of Fisheries. *China fisheries Statistics Yearbook*. Beijing, China: Agriculture Press (2020). p. 30.
17. Wang Q, Zeng W, Liu C, Zhang C, Wang Y, Shi C, et al. Complete genome sequence of a reovirus isolated from grass carp, indicating different genotypes of GCRV in China. *J Virol* (2012) 86(22):12466. doi: 10.1128/JVI.02333-12
18. Cheng L, Fang Q, Shah S, Atanasov IC, Zhou ZH. Subnanometer-resolution structures of the grass carp reovirus core and virion. *J Mol Biol* (2008) 382 (1):213–22. doi: 10.1016/j.jmb.2008.06.075
19. Rao Y, Su J. Insights into the antiviral immunity against grass carp (*Ctenopharyngodon idella*) reovirus (GCRV) in grass carp. *J Immunol Res* (2015) 2015:670437. doi: 10.1155/2015/670437

20. Jia R, Cao LP, Du JL, Liu YJ, Wang JH, Jeney G, et al. Grass carp reovirus induces apoptosis and oxidative stress in grass carp (*Ctenopharyngodon idellus*) kidney cell line. *Virus Res* (2014) 185:77–81. doi: 10.1016/j.virusres.2014.03.021
21. Shi M, Huang R, Du F, Pei Y, Liao L, Zhu Z, et al. RNA-seq profiles from grass carp tissues after reovirus (GCRV) infection based on singular and modular enrichment analyses. *Mol Immunol* (2014) 61(1):44–53. doi: 10.1016/j.molimm.2014.05.004
22. Andersen CL, Jensen JL, Ørntoft TF. Normalization of real-time quantitative reverse transcription-PCR data: a model-based variance estimation approach to identify genes suited for normalization, applied to bladder and colon cancer data sets. *Cancer Res* (2004) 64(15):5245–50. doi: 10.1158/0008-5472.CAN-04-0496
23. Lin Y, Wang B, Wang N, Ouyang G, Cao H. Transcriptome analysis of rare minnow (*Gobiocypris rarus*) infected by the grass carp reovirus. *Fish Shellfish Immunol* (2019) 89:337–44. doi: 10.1016/j.fsi.2019.04.013
24. Lu LF, Li S, Lu XB, LaPatra SE, Zhang N, Zhang XJ, et al. Spring Viremia of Carp Virus N Protein Suppresses Fish IFNφ1 Production by Targeting the Mitochondrial Antiviral Signaling Protein. *J Immunol* (2016) 196(9):3744–53. doi: 10.4049/jimmunol.1502038
25. Chen J, Li ZC, Lu LF, Li P, Li XY, Li S. Functional Characterization of Dark Sleeper (*Odontobutis obscura*) TBK1 on IFN Regulation. *Front Immunol* (2019) 10:985. doi: 10.3389/fimmu.2019.00985
26. Liu X, Cai X, Zhang D, Xu C, Xiao W. Zebrafish foxo3b Negatively Regulates Antiviral Response through Suppressing the Transactivity of irf3 and irf7. *J Immunol* (2016) 197(12):4736–49. doi: 10.4049/jimmunol.1601187
27. Carey BD, Ammosova T, Pinkham C, Lin X, Zhou W, Liotta LA, et al. Protein Phosphatase 1α Interacts with Venezuelan Equine Encephalitis Virus Capsid Protein and Regulates Viral Replication through Modulation of Capsid Phosphorylation. *J Virol* (2018) 92(15):e02068–17. doi: 10.1128/JVI.02068-17
28. Davis ME, Wang MK, Rennick LJ, Full F, Gableske S, Mesman AW, et al. Antagonism of the phosphatase PP1 by the measles virus V protein is required for innate immune escape of MDA5. *Cell Host Microbe* (2014) 16(1):19–30. doi: 10.1016/j.chom.2014.06.007
29. Zhang Y, Gu J, Wang L, Zhao Z, Pan Y, Chen Y. Ablation of PPP1R3G reduces glycogen deposition and mitigates high-fat diet induced obesity. *Mol Cell Endocrinol* (2017) 439:133–40. doi: 10.1016/j.mce.2016.10.036
30. Hu M, Qu X, Pan L, Fu C, Jia P, Liu Q, et al. Effects of toxic Microcystis aeruginosa on the silver carp Hypophthalmichtys molitrix revealed by hepatic RNA-seq and miRNA-seq. *Sci Rep* (2017) 7(1):10456. doi: 10.1038/s41598-017-10335-9
31. Magrone T, Russo MA, Jirillo E. Dietary Approaches to Attain Fish Health with Special Reference to their Immune System. *Curr Pharm Des* (2018) 24 (41):4921–31. doi: 10.2174/1381612825666190104121544
32. Boschi I, Randelli E, Buonocore F, Casani D, Bernini C, Fausto AM, et al. Transcription of T cell-related genes in teleost fish, and the European sea bass (*Dicentrarchus labrax*) as a model. *Fish Shellfish Immunol* (2011) 31(5):655–62. doi: 10.1016/j.fsi.2010.10.001
33. Niklasson L, Sundh H, Olsen RE, Jutfelt F, Skjødt K, Nilsen TO, et al. Effects of cortisol on the intestinal mucosal immune response during cohabitant challenge with IPNV in Atlantic salmon (*Salmo salar*). *PloS One* (2014) 9 (5):e94288. doi: 10.1371/journal.pone.0094288
34. Wu N, Wang B, Cui ZW, Zhang XY, Cheng YY, Xu X, et al. Integrative Transcriptomic and microRNAomic Profiling Reveals Immune Mechanism for the Resilience to Soybean Meal Stress in Fish Gut and Liver. *Front Physiol* (2018) 9:1154. doi: 10.3389/fphys.2018.01154
35. Wu N, Xu X, Wang B, Li XM, Cheng YY, Li M, et al. Anti-foodborne enteritis effect of galantamine potentially via acetylcholine anti-inflammatory pathway in fish. *Fish Shellfish Immunol* (2020) 97:204–15. doi: 10.1016/j.fsi.2019.12.028
36. Sun Y, Xu W, Li D, Zhou H, Qu F, Cao S, et al. p38 mitogen-activated protein kinases (MAPKs) are involved in intestinal immune response to bacterial muramyl dipeptide challenge in *Ctenopharyngodon idella*. *Mol Immunol* (2020) 118:79–90. doi: 10.1016/j.molimm.2019.12.007
37. Qu F, Tang J, Peng X, Zhang H, Shi L, Huang Z, et al. Two novel MKKs (MKK4 and MKK7) from *Ctenopharyngodon idella* are involved in the intestinal immune response to bacterial muramyl dipeptide challenge. *Dev Comp Immunol* (2019) 93:103–14. doi: 10.1016/j.dci.2019.01.001
38. Kole S, Qadiri S, Shin SM, Kim WS, Lee J, Jung SJ. Nanoencapsulation of inactivated-viral vaccine using chitosan nanoparticles: Evaluation of its protective efficacy and immune modulatory effects in olive flounder (*Paralichthys olivaceus*) against viral haemorrhagic septicaemia virus (VHSV) infection. *Fish Shellfish Immunol* (2019) 91:136–47. doi: 10.1016/j.fsi.2019.05.017
39. Munang'andu HM, Mutoloki S, Evensen Ø. A Review of the Immunological Mechanisms Following Mucosal Vaccination of Finfish. *Front Immunol* (2015) 6:427. doi: 10.3389/fimmu.2015.00427
40. Rombout JH, Abelli L, Picchietti S, Scapigliati G, Kiron V. Teleost intestinal immunology. *Fish Shellfish Immunol* (2011) 31(5):616–26. doi: 10.1016/j.fsi.2010.09.001
41. Magnadottir B. Immunological control of fish diseases. *Mar Biotechnol (New York N Y)* (2010) 12(4):361–79. doi: 10.1007/s10126-010-9279-x
42. Lapatra SE, Turner T, Lauda KA, Jones GR, Walker S. Characterization of the humoral response of rainbow trout to infectious hematopoietic necrosis virus. *J Aquat Anim Health* (1993) 5(3):165–71. doi: 10.1577/1548-8667(1993)005<0165:COTHRO>2.3.CO;2


**Conflict of Interest:** The authors declare that the research was conducted in the absence of any commercial or financial relationships that could be construed as a potential conflict of interest.

frontiers in Immunology

ORIGINAL RESEARCH
published: 09 February 2021
doi: 10.3389/fimmu.2020.622387

# Study on Immune Response of Organs of *Epinephelus coioides* and *Carassius auratus* After Immersion Vaccination With Inactivated *Vibrio harveyi* Vaccine

*Hua Gong, Qing Wang*, Yingtiao Lai, Changchen Zhao, Chenwen Sun, Zonghui Chen, Jiafa Tao* and Zhibin Huang*

*Key Lab of Aquatic Animal Immune Technology of Guangdong Province, Key Lab of Fishery Drug Development of Ministry of Agriculture and Rural Affairs, Pearl River Fisheries Research Institute of Chinese Academy of Fishery Sciences, Guangzhou, China*

OPEN ACCESS

**Edited by:**
*Nan Wu,*
*Chinese Academy of Sciences, China*

**Reviewed by:**
*Xiuzhen Sheng,*
*Ocean University of China, China*
*Jingguang Wei,*
*South China Agricultural University, China*

***Correspondence:**
*Qing Wang*
*Sunny_929@163.com*
*Jiafa Tao*
*taojiafa6418@163.com*

**Specialty section:**
*This article was submitted to Comparative Immunology, a section of the journal Frontiers in Immunology*

**Received:** *28 October 2020*
**Accepted:** *21 December 2020*
**Published:** *09 February 2021*

**Citation:**
*Gong H, Wang Q, Lai Y, Zhao C, Sun C, Chen Z, Tao J and Huang Z (2021) Study on Immune Response of Organs of Epinephelus coioides and Carassius auratus After Immersion Vaccination With Inactivated Vibrio harveyi Vaccine. Front. Immunol. 11:622387. doi: 10.3389/fimmu.2020.622387*

Immersion vaccination relies on the response of fish mucosa-associated lymphoid tissues, the Crucian carp (*Carassius auratus*) and Grouper (*Epinephelus coioides*) were researched in this paper to examine local mucosal immune responses and associated humoral system responses following immersion vaccination. We administered $1.5 \times 10^7$ CFU/ml formalin-inactivated *Vibrio harveyi* cells and measured mucus and serum antibody titers as well as IgM, MHC II mRNA levels in immune organs. The mucosal antibody response preceded the serum response indicating a role for local mucosal immunity in immersion vaccination. IgM and MHC II mRNA levels were relatively greater for the spleen and head kidney indicating the importance and central position of systemic immunity. Expression levels were also high for the gills while skin levels were the lowest. IgM and MHC II mRNA levels were altered over time following vaccination and the hindgut, liver and spleen were similar indicating a close relationship, so the absolute value of $r$ is used to analyze the correlation among different organs immunized. It can be inferred the existence of an internal immune molecular mechanism for Immune synergy hindgut-liver-spleen, from the peak time ($14^{th}$ day), the relative ratio of genes expression in the same tissues between the immunized grouper and the control group (26 times), and Pearson correlation coefficient ($0.8<|r|<1$). Injection challenges with live *V. harveyi* indicated that the relative protection rates for the crucian carp and Grouper was basically the same at 44.4% and 47.4%, respectively. It is believe that crucian carp may be used as a substitute for the valuable grouper in immunity experiment, just from aspect of the relative percent survival (RPS) and how it changes with time. But they were not consistent about the IgM mRNA expression between that of crucian carp and grouper after immersion the *Vibrio* vaccine.

**Keywords: immersion vaccination, mucosal immunity, immune mechanism, immune synergy of hindgut-liver-spleen, IgM, MHC II, Pearson correlation coefficient(*r*)**

## INTRODUCTION

Immersion vaccination has numerous advantages over traditional methods including minimal pain for the fish, lower labor costs, and time coupled with greater operator safety especially for large numbers of small fish. There are numerous commercial products used for this type of procedure that are currently in use in Europe, America, and East Asia and is the recommended immunization procedure (1, 2). However, immersion vaccination also possesses drawbacks such as the generation of weak immune responses and a large amount of vaccine is necessary that can increase costs (3). Therefore, it is of great theoretical significance and practical value to systematically study the mechanism of immersion vaccination and its influencing factors in order to develop efficient, stable, inexpensive, and practical vaccines (2, 4).

There are many aspects of fish immunology still unknown and we are far from close to understanding on which immune mechanisms the protection against many of these pathogens resides (5). Mucosal surfaces of fish, including skin, gill, and gut, contain numerous immune substances poorly studied that act as the first line of defense against a broad spectrum of pathogens (6), and these organs provide the local immune responses required for a competent immune system in fish. Among the containing immune substances, Immunoglobulin M (IgM) is the first antibody that is produced in the immune system and provides a crucial first line of defense for the immune system (7). So far, three main Ig isotypes have been identified in teleosts, including IgM, IgD, and IgT/Z (8, 9), tetrameric IgM is widely accepted as the prevalent serum and mucus Ig type in most teleosts (3, 6). And IgT/Z is thought to be specialized in mucosal immunity, but as known that there is not every teleost species possesses these isotypes Ig (3, 9). This suggested that IgM was the most important mediator in the fish specific humoral and mucosal immune responses (3, 8–10).

The genes of the MHC are recognized as an essential component of the vertebrate adaptive immune system, and are responsible for the recognition and presentation of foreign antigens (11). Classical MHC class IImolecules (MHC II) are restricted to professional antigen presenting cells, which activates B cell differentiation into plasma cells, producing antibodies specific to the invading pathogen, and memory cells, preserving a record of past infection (12, 13). MHC II-dependent immune memory is considered an essential component of the adaptive immune response (14).

In the current study, we utilized immersion vaccination of inactivated *Vibrio harveyi* cells for the Crucian carp (*Carassius auratus*) and Grouper (*Epinephelus coioides*) and measured alterations in antibody titers in skin mucus and serum and IgM mRNA levels in gill, skin, hindgut, liver, spleen, and head kidney (HK). We also challenged the fish with live *V. harveyi* by injection to determine the protective effect of vaccination over time. The mucosal and systemic immune responses that we measured will provide theoretical support for research and development as well as for the practical use of fish immersion vaccines.

## MATERIALS AND METHODS

### Materials

Crucian carp and grouper (400 each) from the Guangdong Daya Bay Fisheries Experimental Center and a farm in Nanhai, Guangdong Province that possessed average lengths of 10 ± 1.5 cm. The fish were acclimated for 7 days and randomly divided into two groups: 200 were used for immunization and 100 were retained as controls. The water temperature was maintained at 28 ± 2.0°C. The bacterial pathogen *V. harveyi* strain SpGY020601 was isolated and identified at Aquatic Diseases and Immunity Laboratory of the Pearl River Fisheries Research Institute (15–17). The bacteria were inactivated by exposure to 0.3% formalin as previously reported (18). The immersion vaccination protocol utilized 1.5 × 107 CFU/ml and a 30-min immersion time in 0.65% normal saline for crucian carp and 0.85% for grouper. Control fish received immersion in saline in the absence of the inactivated bacteria.

### Indirect ELISA

#### Serum and Skin Mucus Collection

Serum and mucosal samples were taken from 9 fish at random on days 2, 4, 7, 11, 14, 21, and 28 after immunization. The skin surfaces were lightly scraped with clean glass slides and resulting mucus of three fish per sample time and group was mixed. An equal volume of 0.85% normal saline was then added and the solution was centrifuged at 10,000 rpm for 20 min and the supernatant was collected. Blood samples (0.3 ml) was sampled from the tail vein and allowed to stand at room temperature for 1 h and then incubated overnight at 4°C. The samples were then and centrifuged at 4,500 rpm for 15 min and the serum was collected and used for analysis.

#### Determination of Antibody Titer

IgM antibody titers were determined as previously described (10, 19, 20). In brief, 96-well ELISA plates were coated with formalin-inactivated *V. harveyi* suspensions overnight at 4°C and then blocked using 5% skimmed milk at 37°C for 1.5 h. Diluted mucus samples were then added followed by incubation at 37°C for 1.5 h. The antibodies used for the ELISA were mouse anti-grouper IgM monoclonal Mab-2D3 (Institute of Animal Husbandry and Veterinary of Fujian Academy of Agricultural Sciences, China) (21) and a horseradish peroxidase-labeled sheep anti-mouse IgG (Jackson, USA).Tetramethylbenzidine was then added and the reactions were terminated with the addition of 2 M sulfuric acid after 20 min. A negative control using serum or mucus from non-immunized fish and blank controls containing only the suspending solutions were used at the same time. Absorbance was measured at 450 nm using a Multiskan Mk3 instrument (Thermo Fisher, Pittsburg, PA, USA). Samples were judged positive when the optical density of the samples was ≥ 2.1 than the blank control.

### Real-Time PCR

The primer sequences used for detection of immune gene expression are listed in **Table 1**. And the primers used for gene

**TABLE 1** | Primers used for RT-PCR.

| Fish | Gene | Primer Sequence | Product (bp) |
|---|---|---|---|
| Crucian carp (*Carassius auratus*) | IgM | F 5′- TGACCCTGACTTGCTATGTG-3′<br>R 5′-CAGAGACTGGTGGTGAACTAC-3′ | 218 |
| | β actin | F 5′-AGAGGGAAATCGTGCGTG-3′<br>R 5′-GAAGGAAGGCTGGAAGAGG-3′ | 185 |
| Grouper (*Epinephelus coioides*) | IgM | F 5′-GCCTGTATCCTGATTGTCGG-3′<br>R 5′-GCTGGGACTTCAGGTTGTTG-3′ | 115 |
| | MHC II | F 5′-GGACATCAGACCCTGGACCAA-3′<br>R 5′-ACACCGAGCAGACCGACAGT-3′ | 105 |
| | 18s DNA | F 5′-GGACACGGAAAGGATTGACAG-3′<br>R 5′– CGGAGTCTCGTTCGTTATCGG-3′ | 99 |

detection were designed using Primer Express 3.0 software (Thermo Fisher) for the grouper IgM, MHC II and internal reference 18S rDNA and for the crucian carp IgM and internal reference β-actin. Specificity of the primers was tested using NCBI BLAST (https://blast.ncbi.nlm.nih.gov/Blast). Primers were synthesized by Shanghai Bioengineering Technology (Shanghai, China).

And the PCR reaction system(25 μl) as following:

$$SYBR\ Premix\ Ex\ Taq^{™}(2\times)\ 12.5\ \mu l\quad \text{Primer F/R}\ (10\ \mu\text{mol}/L\ each)\ 0.5\ \mu l$$

$$\text{RT}\ \ 1\ \mu\text{l}\quad \text{Nuclease}-\text{free water}\quad\ 10.5\ \mu\text{l}$$

Total RNA was extracted from gill, skin, hindgut, liver, spleen and HK using Trizol reagent (Invitrogen, Carlsbad, CA, USA). RNA levels were quantified using UV spectroscopy and $OD_{260}$/$OD_{280}$ ratios between 1.8 and 2.0 were considered sufficient for analysis. Electrophoresis in 1% agarose gels was used to identify the integrity of the extracted RNA. RNA was reverse-transcribed using 1 μg RNA in a 20-μl total volume using a M-MLV reverse transcription kit according to the manufacturer's instructions (Promega, Madison, WI, USA).

Real-time qPCR analysis was performed using 2 μl cDNA template, 10.4 μl of SYBR premix ex Taq (Takara, Japan), 0.4 μl of 10 μM primers and 6.8 μl of deionized water. Amplification conditions using an Real-time fluorescence quantitative PCR instrument (ABI7500, USA) were as follows: 95°C for 4 min, followed by 35 cycles of 95°C for 20 s, 56°C for 20 s, and 72°C for 20 s and a final step of 72°C for 5 min. The integrity of the amplified products was assessed using melting curve analysis using the software supplied with the instrument.

## Demonstration of Protective Immunity

The bacterial suspension ($1.8 \times 10^9$ CFU/ml) was diluted five times continuously with sterile physiological saline, then the crucian carp and grouper were injected intraperitoneally with $5^0$ to $5^{-4}$ dilution bacterial suspension at a dose of 0.2 ml/tail. The control group was injected with the same amount of sterile saline. During the test, the water temperature was 28 ± 1°C. The fish were observed continuously for one week, the death number of experimental animals was recorded, and the median lethal dose (LD50) was calculated according to Reed&Muench method (Reed L J & Muench, 1938).

The protective function of the *V. harveyi* vaccination was examined using 20 fish from each group at 1, 2, 3, 4, and 5 weeks following vaccination. The fish were randomly selected and received 0.2 ml of $1.2 \times 10^8$ CFU/ml of *V. harveyi* by intraperitoneal injection. The fish were maintained for 2 weeks with a tank temperature of 28 ± 1°C and monitored for signs of morbidity and mortality. The relative percent survival (RPS) was calculated according to the following formula:

$$RPS = \left(1 - \frac{\text{mortality rate of immune group}}{\text{mortality rate of control group}}\right) \times 100\,\%$$

## Data Analysis

The experimental data were expressed as mean ± SD and levels of significance were assessed using one-way ANOVA using SPSS14 (IBM, Chicago, IL, USA), the LSD method for the Student's *t*-test, and the correlation analysis of different organs of grouper after immersion with inactivated *V. harveyi* vaccine was using Pearson correlation coefficient($r$), which calculated according to the following formula (22):

$$r = \frac{\Sigma(x-\overline{x})(y-\overline{y})}{\sqrt{\Sigma(x-\overline{x})^2\Sigma(y-\overline{y})^2}}$$

The absolute value of $r$ is used to analyze the correlation, the larger the value of |r|, the closer the relationship is. Among them, $|r|<0.3$, means no correlation; $0.3\leq|r|<0.5$, means low linear correlation; $0.5\leq|r|<0.8$, means moderately linear correlation; $0.8\leq|r|\leq1$, means highly linear correlation.

# RESULTS

## Dynamic Changes of Mucus and Serum Antibody Titers

We used an indirect ELISA method to follow alterations in antibody titers of mucus and blood over time. The antibody titers in carp skin mucus peaked on day 7 and then declined and returned to pre-immunization levels by week 3. The titers in the control group were not significantly altered during the whole time course. Overall, except for days 0 (the day of the vaccination) and 21, antibody titers in the immune groups were significantly higher than for the controls ($P < 0.05$). On

day 21 the serum titers peaked and then declined but remained at high level to weeks 6 where immune group titers were significantly higher than controls ($P < 0.05$) (**Figure 1**, left). The titers for the grouper showed similar changes and mucus titers peaked on day 7 while serum titers were maximal on day 21 (**Figure 1**, right).

## Alterations in IgM mRNA Expression in Different Tissues

RNA samples taken from the HK, spleen, liver, hindgut, gills and skin were initially examined by gel electrophoresis to determine RNA integrity. These samples contained sharp bands corresponding to 28S and 18S rRNA indicating the absence of degradation in the purification procedure (**Figure S1**). These samples were then used of RT-PCR analysis to measure tissue levels of IgM mRNA. The mRNA of IgM mRNA and β-actin gene were used as the standard, although there was a good similarity with the samples to be tested, problems such as the dissolution medium of the standard and the extraction method of nucleic acid would affect the stability of the standard curve (23). It can be known that when SYBR Green I fluorescent dye is used for quantitative PCR detection, the formation and interference of primer dimers can also be effectively avoided by optimizing the reaction system, and specific PCR products can be obtained.

The levels of IgM mRNA were up-regulated in all six tissues after immersion vaccination. The most significant changes for both fish were seen in the spleen that were increased 93- and 36-fold for the grouper and the crucian carp respectively. The relative abundance for IgM mRNA from the crucian carp tissues was ranked as spleen > HK> liver >gill > hindgut>skin, while grouper was spleen > HK> liver >gill > hindgut>skin. The alterations in mRNA levels over time were similar between the two fish for the gills and skin with increases at day 4 post-inoculation. Expression levels in spleen increased at days 14 and 7, and in the hindgut on days 14 and 4 for the grouper and crucian carp, respectively. The up-regulation of expression in the HK appeared later and was maximal at day 21 for both fish (**Figures 2**, **3**).

## Alterations in MHC II mRNA Expression in Different Tissues of Grouper

According to the relative expression of MHC- II of grouper different organs (**Figure 4**), Up-regulation of MHC gene expression was detected in six organs after immersion vaccination. The relative expression level of MHC II in HK is relatively high (the peak value is close to 2.0), while the relative expression level in skin is the smallest (the peak value is only 0.064), and the expression level in gill and hindgut is relatively low. But the MHC II expressions quickly reach the peak in gill and skin, which shows the important role of gill and skin in antigen presentation and transmission during immersion (3, 5, 8). The same dynamic changes were observed in hindgut, spleen, and liver, and the expression levels were obviously increased within 4 days after immunization, and reached the peak at 14 days all. The expression of MHC II was up-regulated fastest in gill, reached its peak 2 days after immunization, while peaked up-regulated later in HK, but the up-regulation lasted for a long time until the 28th day.

## Relation of Different Organs During Immunization Reaction

Among the 6 organs of immunized grouper, the expression of MHC II was up-regulated fastest in gill, reached its peak 2 days after immunization. Besides this, the expressions of gene peaked all in the 4$^{th}$ day in the gill and skin. And the gene expressions peak time of grouper hindgut, spleen and liver were all in 14$^{th}$ day after vaccination, but these in crucian carp were near the 4$^{th}$ day all, which indicated that there is difference between this two species fish in immunity protection mechanism.

The expressions of IgM and MHC II up-regulated most were all in HK, about 26 times higher than that of control group 21 days after immunization, and the level just like the IgM expression in grouper HK after *V. alginolyticus* challenge (24). The gill was next, which was 15 times higher than the control group on the second day after immunization. The skin was up-regulated by 13 times on the 4$^{th}$ day after immunization compared with the control group. After that, the expression level in hindgut, liver and spleen increased slightly, and they were about 6 times all higher than those in the control group on the

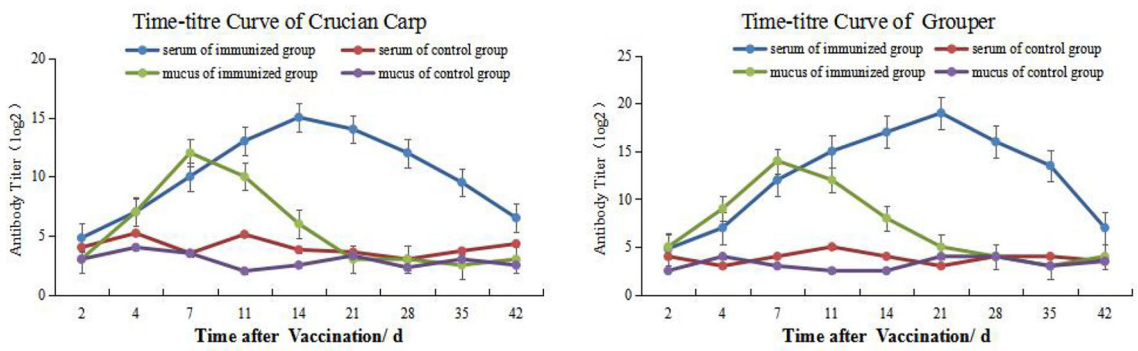


**FIGURE 1** | Time-and antibody titers of *Carassius auratus* (left) and *Epinephelus coioides* (right).

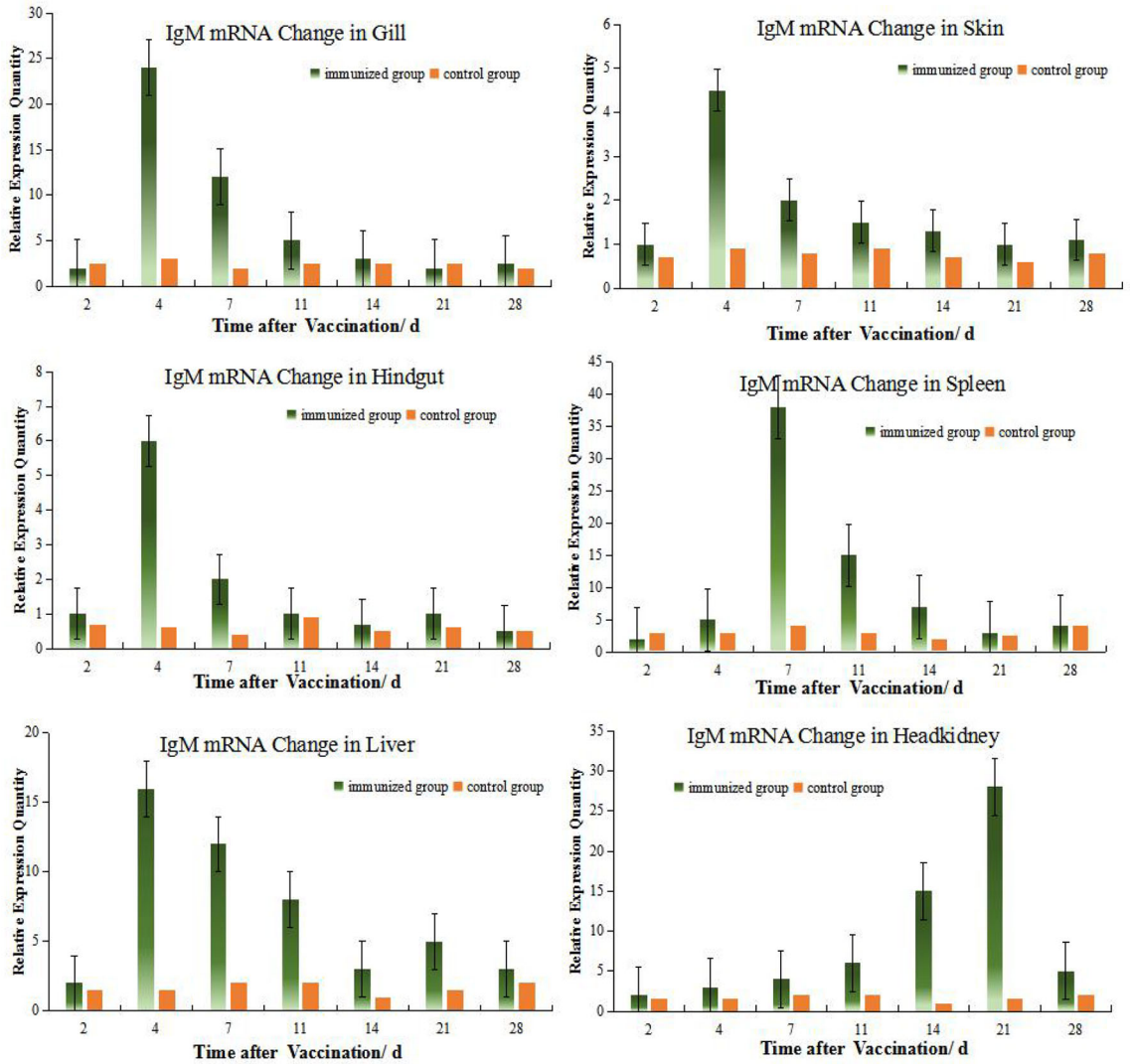


**FIGURE 2** | Relative quantification of crucian carp IgM gene mRNA in different organs. The relative abundance for IgM mRNA from the tissues was ranked as spleen > HK> gill >liver > hindgut>skin. The alterations in mRNA levels over time were similar for the gills, skin, hindgut and liver with increases at day 4 post-inoculation. And there were clear change difference between spleen and HK at this experiment, although both organs are central immune organs.

14th day after immunization (**Table 2**). And the same value occurred in immunized crucian carp hindgut, liver and spleen higher than the control, which were about 10 times.

In order to quantify the comparison results, we draw lessons from the water ecological treatment method (22), and introduce Parson correlation coefficient to study the relationship between organs in immune response. Among the six organs of immunized grouper, it was found that hindgut, spleen and liver had relatively higher *r* value each other, whether in the up-regulation expression of IgM or MHC II (**Figure 5**). And the mucosal organs, such as gill and skin, had the relatively higher correlations each other in the IgM experiment, had the relatively lower correlations in the MHC II expression, showed the difference of antigen presentation about the two organs (18).

## Protective Immunity

The Results of challenge tests (**Table 3**) showed that the strain has strong toxicity to crucian carp and grouper as the reference (15, 16), the LD50 of the strain to this two species were $6.1 \times 10^6$ CFU/ml both calculated by R-M method. So *V. harveyi* strain can be used with same concentration for two species of fish in the challenge protection test. To demonstrate the effectiveness of the immersion vaccination, we challenged the fish by injection of inactivated *V. harveyi* cells at weeks 1, 2, 3, 4, and 5 post–vaccination (**Table 4**). The protection after 1 week immunization was < 30% and maximal rates of 44.4% and 47.4% were achieved by week 4. The serum antibody titers for both fish mirrored these changes but the mucosal titers did not. In addition, the maximal protection against challenge appeared on week 4 (28 days)

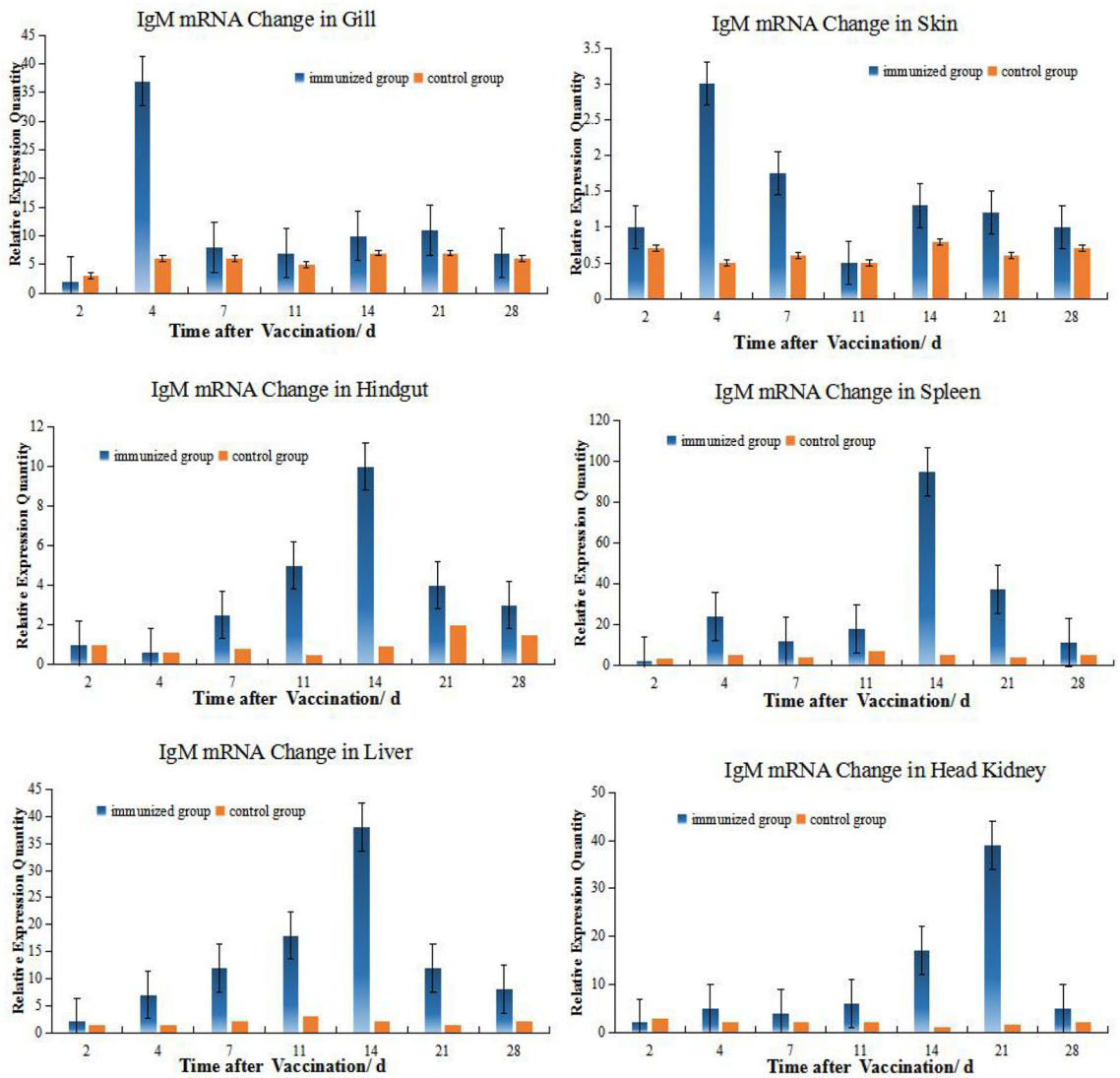


**FIGURE 3** | Relative quantification of grouper IgM gene mRNA in different organs. The relative abundance for IgM mRNA from the tissues was ranked as spleen > HK> liver>gill> hindgut>skin. The alterations in mRNA levels over time were similar for the hindgut, liver, and spleen with increases at day 14 post-inoculation. Organ IgM mRNA expression levels changed with time and the hindgut, liver and spleen followed the same temporal trend.

whereas the highest serum antibody levels were found on week 3 (21 days).

And the *r* value of RPS and antibody showed that the protect of vaccine is moderately linear correlation with antibody in mucus, while low linear correlation with antibody in serum (**Table 5**). Interestingly, the value of $r$ <0.05 between antibody in mucus and that in serum showed no correlation directly, which verified the relative independence of mucosal immunity from system immunity after immersion vaccination of grouper.

## DISCUSSION

Many studies on immersion vaccination in fish have been reported in recent years (1–3), However, injection immunization technology is still the mainstream of application in the worldwide application (2, 3, 8, 20, 25, 26), whether manual injection or mechanical injection (25, 26). because immersion vaccination has numerous advantages over the injection methods including minimal pain for fish, lower labor costs and time coupled with greater operator safety especially for large numbers of small fish (2, 3, 18). However, immersion vaccination also possesses drawbacks such as the generation of weak immune responses and a large amount of vaccine is necessary and this can increase costs (2, 26). So there has been progress in defining uptake, processing, presentation and reaction of antigens in aquatic animal mucosal immunity during immersion vaccination, just to enhance immunogenicity and promote or regulate the level or type of immune response. We found that

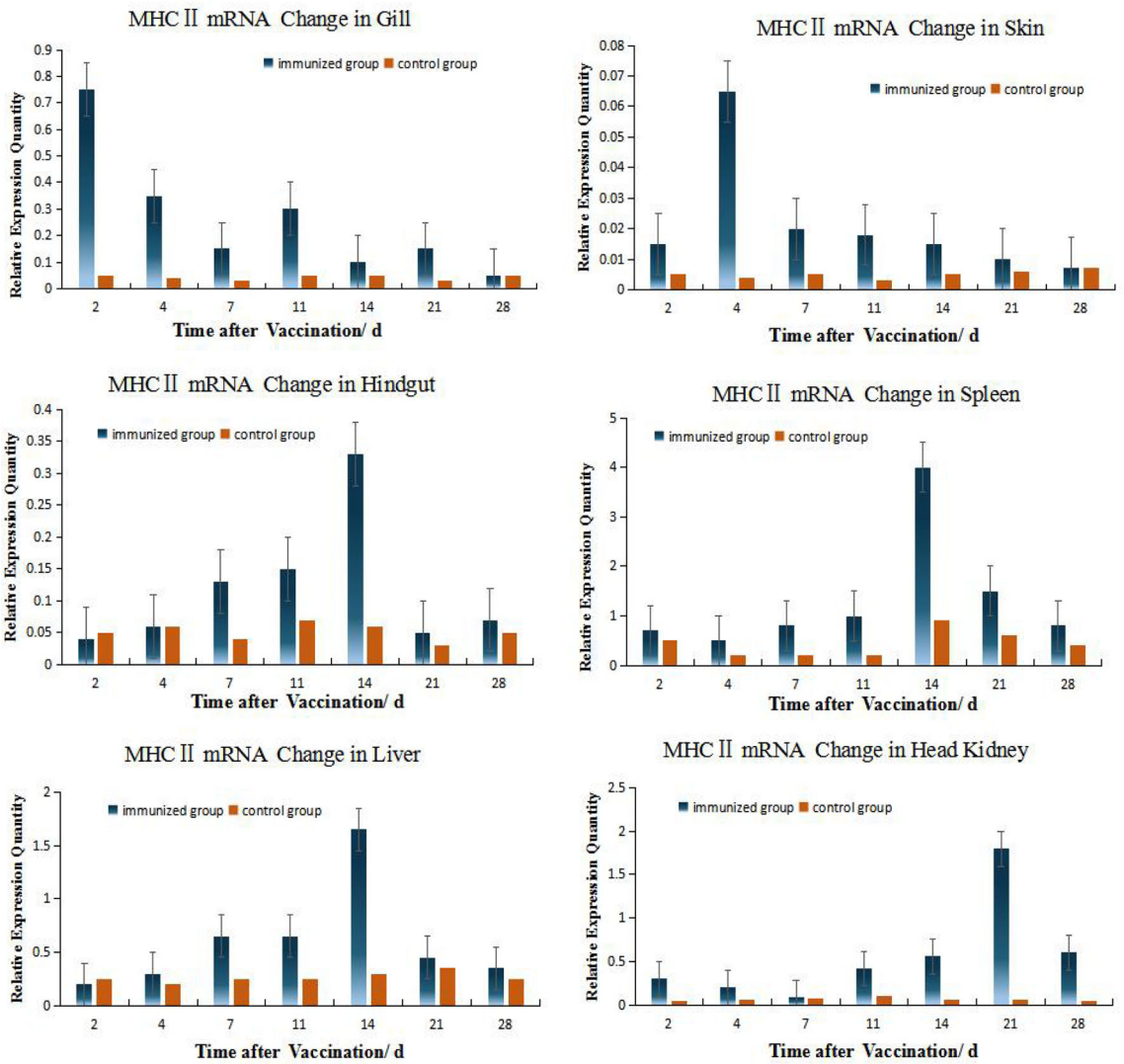


**FIGURE 4** | Relative quantification of grouper MHC II gene mRNA in different organs. The relative abundance for MHC II mRNA from the tissues was ranked as spleen > HK> liver>gill> hindgut>skin. The alterations in mRNA levels over time were similar for the hindgut, liver, and spleen with increases at day 14 post-inoculation. Organ MHC II mRNA expression levels changed with time and the hindgut, liver and spleen followed the same temporal trend.

**TABLE 2** | Statistics on the peak time and maximum value of gene expression up-regulation multiple in different tissues after immunization compared with control group.

| Tissue | Gill | | Skin | | Hindgut | | Spleen | | Liver | | HK | |
|---|---|---|---|---|---|---|---|---|---|---|---|---|
| | Peak time/d | Relative values | Peak time/d | Relative values | Peak time/d | Relative values | Peak time/d | Relative values | Peak time/d | Relative values | Peak time/d | †Relative values |
| Crucian Carp IgM | 4 | 8.0 | 4 | 5.0 | 4 | 10 | 4 | 10.7 | 7 | 9.5 | 21 | 18.7 |
| Grouper IgM | 4 | 6.2 | 4 | 6.0 | 14 | 11.1 | 14 | 19.0 | 14 | 19.0 | 21 | 26.0 |
| Grouper MHC II | 2 | 15.0 | 4 | 13.0 | 14 | 5.5 | 14 | 6.0 | 14 | 5.5 | 21 | 25.7 |

*† Relative value the ratio of gene expression in the same tissues between the immunized grouper and the control group.*

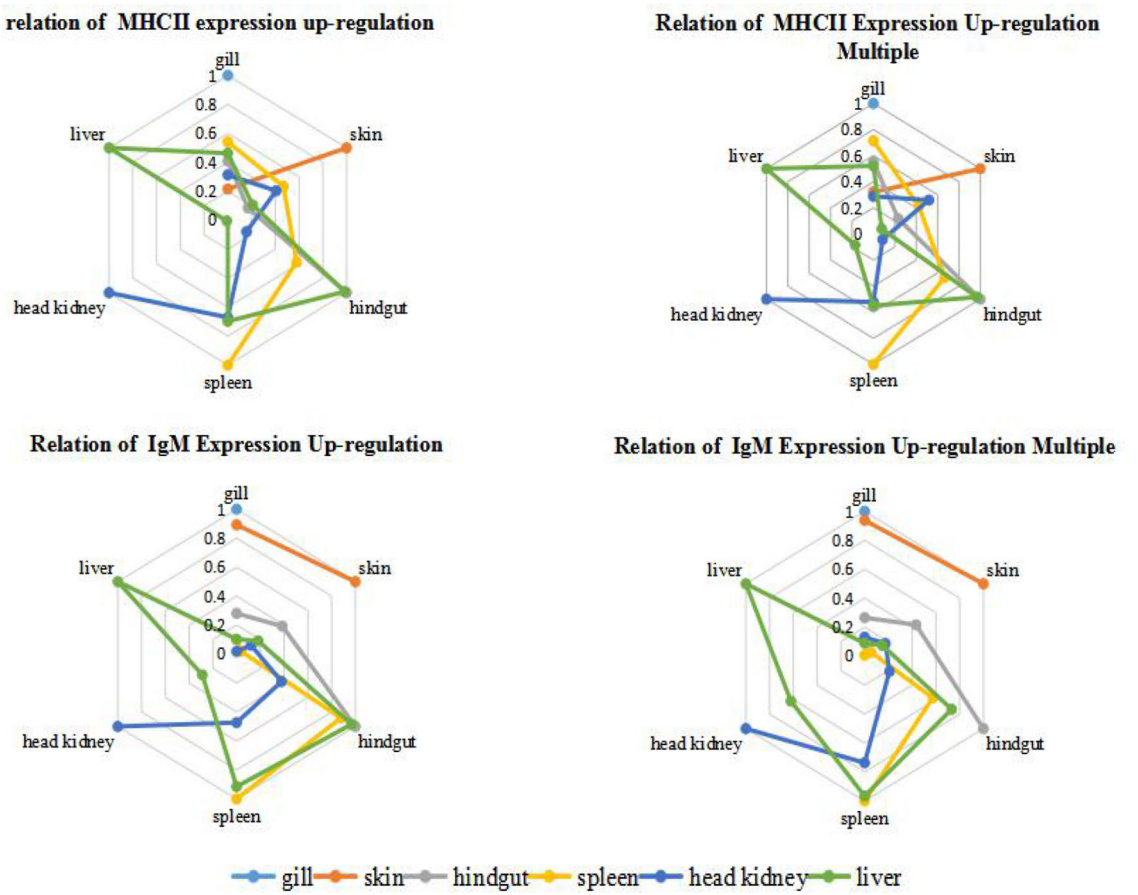


**FIGURE 5** | Correlation analysis of grouper organs after immersion with inactivated *V. harveyi* vaccine. The relation of gene expression up-regulation was analyzed by the absolute value of *r* between the quantitative changes of gene expression in different organs after immunization; while the relation of gene expression up-regulation multiple was analyzed by the absolute *r* value of between the relative ratio of gene expression in different organs after immunization is analyzed, and this relative ratio is the ratio of gene expression in the same tissues between the immunized grouper and the control group.

the inactivated *V. harveyi* vaccine induced a peak mucosal antibody titer earlier than that for serum indicating a more robust mucosal immunity in response to immersion vaccination. Consistent with these observations, tissue expression of IgM mRNA in the gill and skin mucosa peaked 4 days following vaccination and then declined. Interestingly, both fish showed similar patterns and this was consistent with the role these tissues play in the early stages of resisting pathogen invasion (19).

It was generally recognized that fish mucosal immunity exists and is relatively independent of the whole body immune system (3, 5, 8, 9, 18, 19). But most of them are discussed from the aspects of reaction process and reaction intensity. This paper introduces Parson Correlation Coefficient analysis for the first time, and verifies the relative independence of mucosal immunity objectively and mathematically. The value of *r* was so small between antibody in mucus and that in serum, which showed no correlation directly, and meant the relative independence of mucosal immunity from system immunity after immersion vaccination.

## Changes in Gills and Skins After Immersion

Mucosal-related tissues are key elements in preventing pathogen entry (8, 9). The mucosal lymphoid tissues (MALT) include

**TABLE 3** | Challenge of no-immunized fish with different concentrations of suspension *V. harveyi* administered by injection (number of deaths/number of trials).

| Concentrations of suspension (CFU/ml) | $1.8\times10^9$ | $3.6\times10^8$ | $7.2\times10^7$ | $1.44\times10^7$ | $2.88\times10^6$ | Sterile physiological saline |
|---|---|---|---|---|---|---|
| Crucian carp (*Carassius auratus*) | 9/10 | 7/10 | 6/10 | 4/10 | 2/10 | 0/10 |
| Grouper (*Epinephelus coioides*) | 9/10 | 7/10 | 6/10 | 4/10 | 2/10 | 0/10 |

**TABLE 4** | Challenge of immunized fish with *V. harveyi* administered by injection.

| Fish | Time of challenge: post-innoculation (week) | Number of experimental fish (tail) | Number of deaths (tail) | Mortality (%) | †RPS (%) |
|---|---|---|---|---|---|
| Crucian carp (*Carassius auratus*) | 1 | 20 | 16 | 80 | 11.2 |
| | 2 | 20 | 14 | 70 | 22.2 |
| | 3 | 20 | 11 | 55 | 38.8 |
| | 4 | 20 | 10 | 50 | 44.4 |
| | 5 | 20 | 13 | 65 | 37.8 |
| | 6 | 20 | 15 | 75 | 16.7 |
| | control | 20 | 18 | 90 | — — |
| Grouper (*Epinephelus coioides*) | 1 | 20 | 16 | 80 | 15.8 |
| | 2 | 20 | 14 | 70 | 26.3 |
| | 3 | 20 | 13 | 65 | 31.6 |
| | 4 | 20 | 10 | 50 | 47.4 |
| | 5 | 20 | 11 | 55 | 42.1 |
| | 6 | 20 | 14 | 70 | 26.3 |
| | control | 20 | 19 | 95 | — — |

*†Relative percent survival.*

**TABLE 5** | The Pearson correlation coefficient(*r*) of RPS and antibody titer of immunized grouper with inactive *V. harveyi* vaccine.

| | RPS (%) | Antibody in serum | Antibody in mucus |
|---|---|---|---|
| RPS (%) | 1 | | |
| Antibody in serum | 0.320028265 | 1 | |
| Antibody in mucus | 0.728643536 | 0.041561845 | 1 |

nasopharynx-associated lymphoid tissues (NALT), gill-associated lymphoid tissues (GIALT), skin-associated lymphoid tissues (SALT) and gut-associated lymphoid tissues (GALT) (3). The particular systems responsible for immunity resulting from immersion vaccination are currently unclear. There are most likely also species differences for immune responsiveness (9, 10). There are many species of fish, such as seabream (*Sparus aurata*) (6), Atlantic salmon(*Salmo salar*) (27), IgM presence in the skin mucus was signifificantly lower than in the serum, while no clear differences were detected between skin mucus and serum Ig of carp (19) and olive flounder (28). In our study, the titer level of Ig in skin mucus was same as that in serum, but IgM and MHC II expression levels in the gills were much higher than that in the skin and hindgut indicating the gills for both fish species were robust mucosal immune response organs.

Of course, immersion inoculation utilizes mucosal immunity while parenteral administration of antigen induces a systemic reaction and specific antibody production (10, 29), so gill, skin and hindgut show different immune responses after immersion vaccination. It is reported that the soluble extracellular products of pathogenic *V. harveyi* stains showed strong toxicity to crucian carp and the fibroblasts of grass carp (16), so there are soluble and insoluble antigens both in the inactivated *V. harveyi* vaccine. The skin serves as the major organ for antigen uptake and particles remain in both skin and gill tissues for at least 24 days following exposure and a minority are transported to the spleen and kidney (30). And soluble bovine serum albumin (BSA) and insoluble fluorescent latex microspheres were both phagocytosed *via* the epithelium in channel catfish and adsorption of particulates has been documented in the skin and gill tissues of rainbow trout after immersion vaccination (6, 31). Hence, there are some differences in MHC II expression between gill and skin, but the *r* of the two organs IgM expression is almost 1.

The gill mucosal and immune-related tissues contain both macrophages and cells capable of expressing MHC (25, 32, 33), This has been confirmed in ultrastructural analysis of the gills of *Oncorhynchus tschawytscha* (31) and IgM-producing cells have also been detected in gill of *Siniperca chuatsi* (34), and some cells that most likely are dendritic cells were found in Ultrastructure of gills (32), which can be considered to be the main antigen presenting cells (35). We found that IgM gene expression levels in the gills were significantly increased following immunization and were much greater than for the skin mucosa for the grouper and crucian carp. This indicated that the gills were the primary local immune response organs that mounted a local response to the immersion antigen.

## Hypothesis of the Immune Synergy of the Hindgut-Liver-Spleen

IgM mRNA levels were also higher in spleen and HK following vaccination demonstrating the importance of systemic immunity. Previous studies have demonstrated that IgM mRNA in spleen, HK, gills and hindgut of *S. chuatsi* increased after intraperitoneal injection of inactivated *Flavobacterium columniformis* (33). Rainbow trout immersion inoculation with *Yersinia rugosa* increased IgM mRNA levels in the HK but not in the rear kidney (36). The latter was consistent with higher levels of plasma cells in the front kidney and our experimental results were consistent with these studies.

The expression of IgM mRNA in the hindgut was also higher than that for the skin mucosa in the present study. IgM production in most teleost intestine has not been reported for the Peyer's plaques, M cells, sIgA, and J chains (1, 7, 8, 19, 37). In sheepshead (*Archosargus probatocephalus*), a noncovalent dimer of covalent dimeric subunits has been described associated to a 95-kDa secretory component like protein (7, 38), but this was not found in bile of the same species and also never observed in other

teleost (8). In addition, there is no evidence of specific homing of mucosal lymphocytes to the fish intestine (37). In our study, IgM mRNA expression in the intestine after immersion was generally higher than skin. This was most likely the result of antigen absorption by the digestive tract during immersion and links systemic and local mucosal immunity (3). However, organ IgM mRNA expression levels changed with time and the hindgut, liver and spleen followed the same temporal trend. Parenthetical administration induces systemic reactions and the production of specific antibodies. In fish, bile can also provide immune effector and may cooperate with the intestinal tract and liver while maintaining an internal balance and is a unique mechanism of immunity (39). For instance, molecular adaptation mechanisms involved in fish intestine-liver immunity is related to soybean meal stress (40). However, histochemical analysis has shown that the numbers of lymphocytes in liver tissues was relatively small but abundant in the vascular system (41). It is reported that the artery supplying blood to the spleen originates from the gastric arteries of the dorsal aorta in the *Chiloscyllium punctatum (*42), and 4 days after fertilization, Hox11 gene expression in a small area of the gut of the zebrafish embryo indicates the appearance of the splenic primordium (43), showed the possibility of close immunity connection between spleen and hindgut. The spleen and HK are the primary lymphoid organs of fish and are the primary sites of antigen capture (3, 26). Serum antibodies originate in HK and plasma cells of the spleen and kidney are distributed around blood vessels (32, 34). For instance, the toxic effects of microcystins to zebrafish were reflected in the spleen, intestine and gills with the up-regulation of immune-related genes that demonstrates the relationship between spleen and mucosal immunity (41).

On the contrary, the *r* value of the HK is relatively low with other organs($|r| < 0.4$, means low linear correlation), except for the slightly higher correlation with spleen ($0.5 \leq |r| < 0.8$, means moderately linear correlation). The HK and spleen are the major sites for trapping of antigens and the production of antibodies, and the predominant source of serum Ig is suggested to be plasma cells in the HK (44, 45), making this teleost tissue analogous to the bone marrow of mammals (46).As this is the case, exogenous antigen presentation in HK would be anticipated (47). In this study, the peak expression of IgM and MHCII in grouper HK were 21$^{st}$ day both, which were later than 14$^{th}$ day in spleen, showing that the response to antigen in HK is slightly later than that in spleen. And the peak of blood antibody titer is also 21$^{st}$ day, which verified that the main source of serum Ig is the plasma cells in HK (44, 45).

Together these data indicated that the immunity provided by the hindgut-liver-spleen system is profoundly important for fish but the specific mechanisms needs further tissue and molecular confirmations for a complete explanation of this cellular pathway.

### Comparison of IgM Gene Expression Changes Between the Grouper and Crucian Carp

Many studies believe that tilapia, crucian carp may be used as a substitute for the valuable mariculture animals in relevant experimental research (16, 17, 48, 49). In our experiments, *V. harveyi* strain can infect Crucian carp and grouper both, and the $LD_{50}$ of the strain to crucian carp and group are at same level calculated by R-M method. We also examined whether there were differences in the immune responses between the grouper and crucian carp by challenging with live *V. harveyi* cells. The RPS levels were basically the same for both fish. They both peaked in the 4$^{th}$ week, remained at their peak in the 5$^{th}$ week, and dropped to the level of the 2$^{nd}$ week in the 6$^{th}$ week, just the grouper RPS level is somewhat higher than the carp (47.4% vs. 44.4%).

However, they were not consistent that the internal immune response between that of crucian carp and grouper after immersion the *Vibrio* vaccine. IgM expression levels in the grouper spleen was up-regulated on day 3 following immunization and peaked on day 14$^{th}$ while in crucian carp levels were maximal on day 7$^{th}$. In spite of this, IgM expression levels for both fish were high from day 7$^{th}$ to 21$^{st}$. The expression levels in HK increased significantly later and were maximal at day 21$^{st}$ and these expression levels for the grouper and crucian carp were significant with increases of 40.6- and 28.3-fold, respectively. Therefore, IgM levels in the HKs of these fish were consistent. In contrast, IgM expression levels in the hindgut peaked for the grouper at day 14$^{th}$ but on day 4$^{th}$ in the crucian carp. Previous studies have indicated that Ig-positive cells in the sea bass, salmon and cyprinid fish are distributed in their intestinal mucosa and levels differed between species (3, 24, 45, 50). This difference may be due to differences between species, which have also been found in marine fish after both immersion and injection vaccination protocols (20).

Therefore, different species fish cannot be substituted for each other in immune evaluation, especially those with distant evolutionary relatives, whose immune protection phenomena may be similar, but their internal immune protection patterns are quite different.

## DATA AVAILABILITY STATEMENT

The original contributions presented in the study are included in the article/**Supplementary Material**. Further inquiries can be directed to the corresponding authors.

## ETHICS STATEMENT

The animal study was reviewed and approved by The Animal Experiment Committee of Pearl River Fisheries Research Institute, Chinese Academy of Fisheries Sciences.

## AUTHOR CONTRIBUTIONS

HG and ZH conceived the projects. HG, QW, YL, CZ, CS, and JT performed the experiments. HG, QW, ZC, JT and ZH did

data analysis. HG and QW wrote the manuscript. QW and JT revised the manuscript. All authors contributed to the article and approved the submitted version.

## FUNDING

The work was funded by grants from National Key Research and Development Program of China (2019YFD0900103); Central Public-interest Scientific Institution Basal Research Fund, CAFS (2020TD45); Guangzhou Science and Technology Plan Project (201904020004).

## SUPPLEMENTARY MATERIAL

The Supplementary Material for this article can be found online at: https://www.frontiersin.org/articles/10.3389/fimmu.2020.622387/full#supplementary-material

**Supplementary Figure 1 |** Agarose gel electrophoresis of total RNA isolated from fish tissues. Lanes 1 to 4. *Carassius auratus* and Lanes 5 to 8. *Epinephelus coioides* including samples from HK, spleen, gills and skin, respectively. Due to the large number of RNA samples, we only show the total RNA in several tissues extracted at a time point.

**Supplementary Figure 2 |** Melting curves of β-actin (left, Tm: 92 ± 0°C) and IgM (right, Tm: 87 ± 0°C). The fusion curve analysis showed that the PCR products of β-Actin and IgM genes showed a sharp single peak, and there are no other stray peaks.

## REFERENCES

1. Brudeseth BE, Wiulsrød R, Fredriksen BN, Lindmo K, Løkling K-E, Bordevik M, et al. Status and future perspectives of vaccines for industrialized fin-fish farming. *Fish Shellfish Immunol* (2013) 6):1–10. doi: 10.1016/j.fsi.2013.05.029
2. Wu SQ, Tao JF, Gong H, Chang OQ, Ren Y, Liu LH, et al. Situation and tendency of the fishery vaccine development. *Chin Fishery Qual Stand* (2014) 4(01):1–13.
3. Bøgwald J, Dalmo RA. Review on Immersion Vaccines for Fish: An Update 2019. *Microorganisms* (2019) 7(12):627–45. doi: 10.3390/microorganisms7120627
4. Ashry SH, Ahmad TA. The use of propolis as vaccine's adjuvant. *Vaccine* (2012) 31(1):31–9. doi: 10.1016/j.vaccine.2012.10.095
5. Christopher JS. Can Advances in Fish Immunology Change Vaccination Strategies? *Fish Pathol* (2009) 44(1):14–5. doi: 10.3147/jsfp.44.14
6. Guardiola FA, Cuesta A, Arizcun M, Meseguer J, Esteban MA. Comparative skin mucus and serum humoral defense mechanisms in the teleost gilthead seabream (*Sparus aurata*). *Fish Shellfish Immunol* (2014) 36(2):545–51. doi: 10.1016/j.fsi.2014.01.001
7. Klimovich VB, Samoilovich MP, Klimovich BV. Problem of J-chain of immunoglobulins. *J Evol Biochem Physiol* (2008) 44(2):151–66. doi: 10.1134/S0022093008020023
8. Yu YY, Wang QC, Huang ZY, Ding L, Xu Z. Immunoglobulins, Mucosal Immunity and Vaccination in Teleost Fish. *Front Immunol* (2020) 11:567941. doi: 10.3389/fimmu.2020.567941
9. Xu Z, Takizawa F, Casadei E, Shibasaki Y, Ding Y, Sauters Thomas JC, Yu Y, et al. Specialization of mucosal immunoglobulins in pathogen control and microbiota homeostasis occurred early in vertebrate evolution. *Sci Immunol* (2020) 5(44):3254. doi: 10.1126/scIImmunol.aay3254
10. Khansari AR, Balasch JC, Vallejos Vida E, Parra D, Reyes-López FE, Tort L, et al. Comparative Immune- and Stress-Related Transcript Response Induced by Air Exposure and *Vibrio anguillarum* Bacterin in Rainbow Trout (*Oncorhynchus mykiss*) and Gilthead Seabream (*Sparus aurata*) Mucosal Surfaces. *Front Immunol* (2018) 9:856. doi: 10.3389/fimmu.2018.00856
11. Monzón-Argüello C, Garcia de Leaniz C, Gajardo G, Consuegra S. Eco-immunology of fish invasions: the role of MHC variation. *Immunogenetics* (2014) 66(6):393–402. doi: 10.1007/s00251-014-0771-8
12. Wilson AB. MHC and adaptive immunity in teleost fishes. *Immunogenetics* (2017) 69(8-9):521–8. doi: 10.1007/s00251-017-1009-3
13. Dijkstra JM, Grimholt U, Leong J, Koop BF, Hashimoto K. Comprehensive analysis of MHC class II genes in teleost fish genomes reveals dispensability of the peptide-loading DM system in a large part of vertebrates. *BMC Evol Biol* (2013) 13(1):260. doi: 10.1186/1471-2148-13-260
14. Flajnik MF, Kasahara M. Origin and evolution of the adaptive immune system: genetic events and selective pressures. *Nat Rev Genet* (2010) 11(1):47–59. doi: 10.1038/nrg2703
15. Chen XG, Wu SQ, Shi CB, Li NQ. Isolation and identification of pathogenetic *Vibrio harveyi* from estuary cod (*Epinephelus coioides*). *J Fishery Sci China* (2004) 11(4):313–7.
16. Shi CB, Hu XF, Chen XG, Li KB, Wu SQ. characteristics of the extracellar products of two pathogenic *Vibro harveyi* stains. *Acta Hydrob Sin* (2007) 31(1):83–7.
17. Li H, Qian YH, Shi CB, Pan HJ, Wu SQ. Effects of two adjuvants on a conjugated vaccine made from outer membrane protein complex of *Vibrio harveyi* and lipopolysaccharide of *V.alginolyticus*. *J Fish Sci* (2007) 26(9):489–93.
18. Tao JF, Lai YT, Ren Y, Kang GH, Zhang Y, Shi CB, et al. Preliminary Study on Condition for Inactivation of *Vibrio* by Formalin. *Chin J Biologicals* (2011) 24(01):64–6.
19. Nakanishi T, Ototake M. Antigen uptake and immune responses after immersion vaccination. *Dev Biol Standardization* (1997) 90(1):59–68.
20. Gong H, Chen LL, Lai YT, Shi CB, Sun CW, Tao JF, et al. Immunization of *Epinephelus coioides* and T*rachinotus ovatus* with injection and immersion of inactivated vaccine against *Vibrio harveyi* and *Vibrio alginolyticus* in marine fish. *J Guangdong Feed* (2020) 29(04):26–30.
21. Chen HY, Xu BF, Lin NF, Liu XD, Chen Q, Lin TL, et al. Production and characterization of monoclonal antibodies against *Epinephelus akaara*. *Fujian J Agric Sci* (2011) 26(5):687–90.
22. Booth GD, Niccolucci MJ, Schuster EG. *Identifying Proxy Sets in Multiple Linear Regression [Microform]: An Aid to Better Coefficient Interpretation[M]*. Ogden, UT, USA: U.S. Dept. of Agriculture, Forest Service, Intermountain Research Station (1993).
23. Suziu N, Yoshid A, Naknor Y. Quantitative analysis of multi-species oral biofilms by TaqMan Real-Time PCR. *Clin Med Res* (2005) 3(3):176–85.
24. Cui M, Zhang QZ, Yao ZJ, Zhang Z, Zhang H, Wang Y. Immunoglobulin M gene expression analysis of orange-spotted grouper, *Epinephelus coioides*, following heat shock and *Vibrio alginolyticus* challenge. *Fish shellfish Immunol* (2010) 29(6):1060–5. doi: 10.1016/j.fsi.2010.08.018
25. Karen PP, Scott EL. Advances in fish vaccine delivery. *Dev Comp Immunol* (2011) 35(12):1256–62. doi: 10.1016/j.dci.2011.03.007
26. Sommerset I, Krossøy K, Biering E, Frost P. Vaccines for fish in aquaculture. *Expert Rev Vaccines* (2005) 4(1):89–101. doi: 10.1586/14760584.4.1.89
27. Hatten F, Fredriksen Å, Hordvik I, Endresen C, et al. Presence of IgM in cutaneous mucus, but not in gut mucus of Atlantic salmon, *Salmo salar*. Serum IgM is rapidly degraded when added to gut mucus. *Fish shellfish Immunol* (2001) 11(3):257–68. doi: 10.1006/fsim.2000.0313
28. Palaksha KJ, Shin GW, Kim YR, Jung TS. Evaluation of non-specific immune components from the skin mucus of olive flounder ( *Paralichthys olivaceus* ) [J]. *Fish Shellfish Immunol* (2008) 24(4):479–88. doi: 10.1016/j.fsi.2008.01.005
29. David P, Felipe RE, Lluis T. Mucosal Immunity and B Cells in Teleosts: Effect of Vaccination and Stress. *Front Immunol* (2015) 6:354. doi: 10.3389/fimmu.2015.00354
30. Huising MO, Guichelaar T, Hoek C, Verburg-van Kemenade BML, Flik G, Savelkoul HFJ, et al. Increased efficacy of immersion vaccination in fish with hyperosmotic pretreatment. *Vaccine* (2003) 21(3):4178–93. doi: 10.1016/S0264-410X(03)00497-3
31. Ototake M, Iwama GK, Nakanishi T. The uptake of bovine serum albumin of bath-immunized rainbow trout *Oncorbyncbus mykiss*. *Fish Shellfish Immunol* (1996) 12:321–33. doi: 10.1006/fsim.1996.0033

32. Grove S, Johansen R, Reitan LJ, McL C. Immune- and enzyme histochemical characterisation of leukocyte populations within lymphoid and mucosal tissues of Atlantic halibut (*Hippoglossus hippoglossus*). *Fish shellfish Immunol* (2006) 20(5):693–708. doi: 10.1016/j.fsi.2005.08.009
33. Wang Q, Wu GH, Gong H, Shi CB, Li H, Wu SQ. Expression of MHC class II molecules of *Epinephelus coioides* vaccinated with killed *Vibrio harveyi*. *J Guangdong Agric Sci* (2010) 37(12):136–9.
34. Jingyun T. *B lymphocyte development and cloning of T lymphocyte receptor gene in Siniperca chuatsi [D]*. Beijing, China: Graduate School of Chinese Academy of Sciences (Institute of Aquatic Biology (2007).
35. Mildner A, Jung S. Development and function of dendritic cell subsets. *Immunity* (2014) 40(5):642–56. doi: 10.1016/j.immuni.2014.04.016
36. Tian JY, Sun BJ, Luo YP, Zhang Y, Nie P. Distribution of IgM, IgD and IgZ in mandarin fish, *Siniperca chuatsi* lymphoid tissues and their transcriptional changes after *Flavobacterium columnare* stimulation. *Aquaculture* (2009) 288 (1):14–21. doi: 10.1016/j.aquaculture.2008.11.023
37. Rombout JHWM, Abelli L, Picchietti S, Scapigliati G, Viswanath K. Teleost intestinal immunology. *Fish shellfish Immunol* (2010) 31(5):616–26. doi: 10.1016/j.fsi.2010.09.001
38. Lobb CJ, Clem LW. Phylogeny of Immunoglobulin Structure and Function. XI. Secretory immunoglobulins in the cutaneous mucus of the aheepshead, *Archosargus Probatocephalus*. *Dev Comp Immunol* (1981) 5(4):587–96. doi: 10.1016/S0145-305X(81)80033-X
39. Wu N, Song YL, Wang B, Zhang XY, Zhang XJ, Wang YL, et al. Fish gut-liver immunity during homeostasis or inflammation revealed by integrative transcriptome and proteome studies. *Sci Rep* (2016) 6:36048. doi: 10.1038/srep36048
40. Wu N, Wang B, Cui ZW, Zhang XY, Cheng YY, Xu X, et al. Integrative Transcriptomic and microRNAomic Profiling Reveals Immune Mechanism for the Resilience to Soybean Meal Stress in Fish Gut and Liver. *Front Physiol* (2018) 9:1154. doi: 10.3389/fphys.2018.01154
41. Chen C, Liu W, Wang L, Jian L, Yuanyuan C, Jienan J, et al. Pathological damage and immunomodulatory effects of zebrafish exposed to microcystin-LR. *Toxicon* (2016) 118(8):13–20. doi: 10.1016/j.toxicon.2016.04.030
42. Davidson GA, Lin SH, Secombes CJ, Ellis AE. Detection of specific and 'constitutive' antibody secreting cells in the gills, head kidney and peripheral blood leucocytes of dab (*Limanda limanda*). *Vety Immunol Immunopathol* (1997) 58(3):363–74. doi: 10.1016/S0165-2427(97)00017-2
43. Randi NG, Sigrun E. Immunoglobulin producing cells in the spotted wolffish (*Anarhichas minor Olafsen*): localization in adults and during juvenile development. *Dev Comp Immunol* (2003) 27(6):569–78. doi: 10.1016/S0145-305X(03)00028-4
44. Press CM, Evensen O. The morphology of the immune system in teleost fishes. *Fish Shellfish Immunol* (1999) 9:309–18. doi: 10.1006/fsim.1998.0181
45. Semple SL, Heath G, Christie D, Braunstein M, Kales SC, Dixon B. Immune stimulation of rainbow trout reveals divergent regulation of MH class II-associated invariant chain isoforms. (2019) 71: (5-6):407–20. doi: 10.1007/s00251-019-01115-y
46. Huang N, Chen XQ. Summary of fish immune system. *Fujian J Husbandry Vety* (2005) 27(6):20–2.
47. Langenau DM, Palomero T, Kanki JP, Ferrando AA, Zhou Y, Zon LI, et al. Molecular cloning and developmental expression of Tlx (Hox11) genes in zebrafish (*Danio rerio*). *Mech Dev* (2002) 117(1):243–8. doi: 10.1016/S0925-4773(02)00187-9
48. Zheng FY, Shi CB, Pan HJ, Wu SQ. Isolation and identification of pathogen from diseased *Anguilla anguilla*. *Guangdong J Shanghai Fish Univ* (2005) 14 (03):3242–7.
49. Li YB, Zheng FY, Hu XF, Chen XG, Shi CB, Wu SQ. Cytotoxinic analysis of extracellar products from marine pathogenic *Vibrio* using PSF cell line. *Guangdong J Agric Sci* (2012) 39(01):113–5.
50. Estefanía M-A, Aquilino C, Syahputra K, Al-Jubury A, Araújo C, Skov J, et al. CK11, a Teleost Chemokine with a Potent Antimicrobial Activity. *J Immunol (Baltimore Md. 1950)* (2019) 202(3):857–70. doi: 10.4049/jimmunol.1800568


**Conflict of Interest:** The authors declare that the research was conducted in the absence of any commercial or financial relationships that could be construed as a potential conflict of interest.

frontiers in Immunology

REVIEW
published: 16 February 2021
doi: 10.3389/fimmu.2020.622377

# Systemic and Mucosal B and T Cell Responses Upon Mucosal Vaccination of Teleost Fish

*Estefanía Muñoz-Atienza*[†], *Patricia Díaz-Rosales and Carolina Tafalla*[*]

*Fish Immunology and Pathology Laboratory, Animal Health Research Centre (CISA-INIA), Madrid, Spain*

OPEN ACCESS

**Edited by:**
*Nan Wu,*
*Chinese Academy of Sciences, China*

**Reviewed by:**
*Uwe Fischer,*
*Friedrich-Loeffler-Institute, Germany*
*Chao Li,*
*Qingdao Agricultural University, China*

***Correspondence:**
*Carolina Tafalla*
*tafalla@inia.es*

[†]**Present address:**
*Estefanía Muñoz-Atienza, Grupo de Seguridad y Calidad de los Alimentos por Bacterias Lácticas, Bacteriocinas y Probióticos (Grupo SEGABALBP), Sección Departamental de Nutrición y Ciencia de los Alimentos (Nutrición, Bromatología, Higiene y Seguridad Alimentaria), Facultad de Veterinaria, Universidad Complutense de Madrid, Madrid, Spain*

**Specialty section:**
*This article was submitted to Comparative Immunology, a section of the journal Frontiers in Immunology*

**Received:** *28 October 2020*
**Accepted:** *29 December 2020*
**Published:** *16 February 2021*

**Citation:**
*Muñoz-Atienza E, Díaz-Rosales P and Tafalla C (2021) Systemic and Mucosal B and T Cell Responses Upon Mucosal Vaccination of Teleost Fish. Front. Immunol. 11:622377. doi: 10.3389/fimmu.2020.622377*

The development of mucosal vaccines against pathogens is currently a highly explored area of research in both humans and animals. This is due to the fact that mucosal vaccines have the potential to best elicit protective responses at these mucosal surfaces, which represent the frontline of host defense, thus blocking the pathogen at its initial replication sites. However, in order to provide an efficient long-lasting protection, these mucosal vaccines have to be capable of eliciting an adequate systemic immune response in addition to local responses. In aquaculture, the need for mucosal vaccines has further practical implications, as these vaccines would avoid the individual manipulation of fish out of the water, being beneficial from both an economic and animal welfare point of view. However, how B and T cells are organized in teleost fish within these mucosal sites and how they respond to mucosally delivered antigens varies greatly when compared to mammals. For this reason, it is important to establish which mucosally delivered antigens have the capacity to induce strong and long-lasting B and T cell responses. Hence, in this review, we have summarized what is currently known regarding the adaptive immune mechanisms that are induced both locally and systemically in fish after mucosal immunization through different routes of administration including oral and nasal vaccination, anal intubation and immersion vaccination. Finally, based on the data presented, we discuss how mucosal vaccination strategies could be improved to reach significant protection levels in these species.

**Keywords: teleost fish, mucosal vaccination, systemic immune responses, B cells, T cells, immunoglobulins**

## INTRODUCTION

Vaccination is a cost-efficient method to prevent the development of infectious diseases in humans and animals. Vaccine design aims to achieve long-term protection against a specific antigen by inducing an antigen-specific memory response in cells of the adaptive immune system, B and T cells, that will respond faster and with greater strength to a second encounter with this antigen. For this, antigen-presenting cells (APCs) are involved in digesting and degrading the antigen to provide antigen-specific activation of T cells, both $CD4^+$ helper T cells and $CD8^+$ cytotoxic T cells, the latter with the capacity to destroy virus-infected or tumor cells. B cells act as APCs and can also present the antigen to T cells, receiving in return activation signals from T helper cells in thymus-dependent (TD) responses or being activated by the antigen itself in the

case of thymus-independent (TI) antigens. Upon activation, B cells start a differentiation process that leads them to a plasmablast state and eventually to become plasma cells, cells with a greater capacity to secrete immunoglobulins (Igs). Secreted Igs are referred to as antibodies. Throughout this differentiation process, memory B cells are also generated, as do memory T cells, also generated during the activation of T cells. In order to rationally design effective vaccines, it is fundamental to understand how these elements implicated in generating adaptive immunity respond to different vaccine formulations (1, 2). In mammals, different subsets of memory T lymphocytes have been described, including central memory T cells that remain in lymph and blood, tissue-resident memory T cells that reside within the tissues, and effector memory T cells that circulate amongst blood and peripheral tissues (3). In this context, CD4 tissue-resident memory T cells seem to play a key role in maintaining long-term protective immunity to mucosal pathogens as demonstrated in mice mucosally immunized with intranasal live attenuated vaccines against influenza virus (4) and coronaviruses (5). Regarding memory B lymphocytes, they are mainly found in the spleen and lymph nodes in mice and human, but can be also maintained as tissue-resident memory B cells at the sites of infection (6). Interestingly, intranasal live-attenuated influenza vaccines not only induced hemagglutinin-reactive plasmablasts but also memory B cells in the mediastinal lymph nodes (7). Therefore, the capacity of antigens to induce the generation of pathogen-specific tissue-resident memory B and T cells at mucosal surfaces seems as an important point to take into account when designing novel mucosal vaccines.

Most of the commercially available vaccines for both humans and animals are delivered through injection. However, in the past years, the interest and demand for the development of mucosal vaccines has considerably grown, taking into account that most infectious agents colonize the host through mucosal surfaces and it is at these sites that the initial replication steps occur (8). In this respect, having established that mucosal immunization has a superior ability to induce mucosal immune responses than systemic immunization (9), the search for effective mucosal vaccines is not only prompted from a logistic point of view, but also to produce vaccines that can efficiently block the pathogens at these early replicating sites before they are further disseminated throughout the organism. Despite all these advantages, there are only a few commercially available mucosal vaccines for humans or animals. This highlights the many challenges that the development of effective mucosal vaccines encounter. On one side, the vaccine formulations have to be correctly absorbed at the proper mucosal surface and taken up by a mucosal cell that can efficiently present the antigen. On the other hand, a successful mucosal vaccine has to overcome the mucosal tolerance that tightly controls the mucosal immune system to avoid unwanted immune responses to commensals or food antigens (8).

Despite these difficulties, some mucosal vaccines have shown to overcome mucosal tolerance and be able to generate efficient systemic immune responses in addition to local responses, including the production of specific antibodies and cell-mediated immunity (10–12), being this the basis for their efficacy, generating high levels of protection in humans. This is the case of the attenuated oral vaccine for the prevention of typhoid fever, caused by *Salmonella enterica* serovar Typhi, which elicits cell-mediated immune responses, involving both $CD4^+$ helper T lymphocytes and $CD8^+$ cytotoxic T cells (13). It is important to mention that although $CD8^+$ T lymphocytes are mainly associated with defense against viral infections, these cells also play an important role clearing intracellular bacterial infections (14). Along the same line, the killed bivalent whole-cell *Vibrio cholerae* O1 and O139 vaccine produces a high increase of antibody titers and a strong O antigen–specific B memory response after oral immunization (15). In the case of mucosal vaccines against viruses, the intranasal administration of inactivated and live-attenuated influenza vaccines induce protective antibodies capable of inhibiting hemagglutination in serum (16). In this case, however, only the live-attenuated and not the inactivated vaccine generated influenza-specific $CD4^+$ and $CD8^+$ T cells (16). Additionally, the protective immune response to two oral live-attenuated rotavirus vaccines composed of a monovalent attenuated human rotavirus or five bovine–human rotaviruses is mostly due to rotavirus-specific immunoglobulin A (IgA) in serum (17). Oral vaccination has been also revealed successful to control infectious diseases in wildlife, including an oral vaccine against rabies used in foxes (18) and one against classical swine fever (CSF) administered to wild boar (19). Therefore, it seems that when mucosal vaccines are capable of inducing strong systemic adaptive immune effects, protection can be achieved.

In aquaculture, most commercially available vaccines are administrated by intraperitoneal injection, often providing a strong and long-lasting protection, especially in the case of antibacterial vaccines. However, this method involves fish handling which provokes a great amount of stress to the fish, which at the end results in reduced responsiveness to the vaccine and even in some unwanted mortalities. Furthermore, vaccination cannot be administered by injection at very early life stages, and it is precisely in these stages when fish are more susceptible to infectious diseases (20–22). For this reason, huge efforts are focused to find new approaches of mass vaccine administration through mucosal surfaces (*e.g.*, oral immunization and immersion) as these routes have benefits from both an economic/practical and an animal welfare point of view (20–22).

Teleost fish lack well-organized lymphoid structures in their mucosal associated lymphoid tissues (MALTs) such as Peyer's patches in the intestine or tonsils and adenoids in the nasal cavity but instead present diffuse immune cells scattered throughout the tissue. Although some authors accurately point out that this does not constitute a real MALT, for clarity, we will designate these immune cells as MALT as referred to in most fish immunology papers (23–25). In order to succeed in the development of mucosal vaccination for aquacultured fish, it is imperative that we understand how the regulatory constituents of the local immune system in teleost fish guarantee that antigens presented in MALTs produce appropriate systemic immune

responses. In addition, teleost fish B cell responses also differ in many aspects from mammalian B2 cell (conventional B cell) responses, as fish B cells retain many innate features such as a strong phagocytic capacity and microbicidal activity (26), also described in mammalian innate B1 lymphocytes (27).

Teleost fish only express three antibody isotypes (IgM, IgD, and IgT/Z). Thus, fish B cells have never been shown to undergo class switch recombination, a process through which mammals replace the constant region of IgM by that of IgA, IgE, or IgG, antibodies with higher affinity and different effector functions (28, 29). In fact, in mammalian mucosal surfaces, it is IgA that plays a predominant immune role (30). Thus, in teleost fish, the majority of naïve B cells from central immune organs co-express IgM and IgD on the cell membrane, resembling naïve B cell subsets present in mammals (31). When these cells are activated, as in mammals, IgD is lost from the cell membrane, giving the rise to activated $IgM^+$ B cells that have a plasmablast/plasma cell profile (32). However, unlike mammals, these cells do not differentiate further to IgA-secreting plasma cells. Given the lack of IgA in fish, the fish-specific IgT has been proposed as a functional equivalent of IgA based on recent findings. $IgT^+$ B cells, which represent an independent B cell lineage, are more abundant than $IgM^+$ B cells in mucosal surfaces such as the gut (33), the skin (34), and the gills (35), secreting polymeric IgT into the mucus to protect these tissues from pathogens. Finally, when fish were exposed to specific parasitic infections, IgT responses were shown to be predominant in the mucosal compartments in contrast to IgM responses that seemed restricted to systemic compartments (33–35). Despite this, systemic IgT responses have also been reported to both mucosal and systemic stimulations (36, 37), therefore the precise role of IgT in fish adaptive immunity is still largely unknown.

Interestingly, in mammals, some cells have been shown to undergo an unconventional class switch through which only IgD is produced (38, 39). These cells, that can secrete IgD, have been reported mainly in the upper respiratory tract (38, 39). Despite their identification, the precise role of IgD in mammals is still unknown. Thus far, circulating IgD has been shown to interact with basophils through a calcium-fluxing receptor inducing antimicrobial, opsonizing, inflammatory, and immunostimulating factors (39). Equivalent cells only expressing IgD on the cell membrane ($IgD^+$ B cells) have been reported in channel catfish (*Ictalurus punctatus*) blood (40) and rainbow trout (*Oncorhynchus mykiss*) gills and intestine (41, 42), and secreted IgD has been identified as well in many fish species including catfish, rainbow trout, Atlantic salmon (*Salmo salar*), Atlantic cod (*Gadus morhua*), and grass carp (*Ctenopharyngodon idella*) (40, 43). Interestingly, in rainbow trout, IgD secreted by these gut $IgD^+$ B cells, has been shown to coat the intestinal microbiota (42) as described for teleost IgM and IgT (33), suggesting that secreted IgD may play an evolutionary conserved role in mucosal homeostasis (42), as previously suggested in mice (44).

Cellular immunity also plays a key role in mucosal protection against pathogens through the generation of memory T cell subsets localized in mucosal tissues (45). For instance, in mice, an intratracheal vaccination strategy that combined Toll-like receptor (TLR) agonists with antigen-carrying lipid nanocapsules generated long-lived memory T cells not only in lungs but also in the intestinal and vaginal mucosa (45). Similarly, the pulmonary administration of a plasmid DNA vaccine induced robust systemic $CD8^+$ T-cell responses in lungs and draining lymph nodes of mice equivalent to those generated by intramuscular vaccination (46). Recently, it has been shown in mice that the protective effect exerted by the intranasal administration of a recombinant murine cytomegalovirus expressing an MHC I restricted epitope from influenza A virus H1N1 was critically mediated by antigen-specific $CD8^+$ T cells (47). In fish, a high number of T cells have been reported to be present in mucosal surfaces such as intestine and gills in several fish species and the role of $CD8^+$ T cells mediating cellular protection against intracellular bacteria or viruses has been established [reviewed by Nakanishi et al. (48)]. However, to our knowledge, information regarding how T cells locally respond to mucosal vaccination in fish is missing.

Taking all these specific features of the fish immune system into account, the characterization of how mucosal immune cells respond to antigens locally, and then deliver activation signals to systemic immune tissues has special relevance to find out which type of mucosally delivered vaccine formulations are capable of providing strong and long-lasting B and T cell memory responses in these species. Consequently, we have focused this work on reviewing the adaptive immune responses elicited in fish upon mucosal immunization through different routes of administration including oral and nasal vaccination, anal intubation, and immersion vaccination. We have also highlighted the gaps found to evaluate T and B cell responses for some specific vaccines and routes of administration. Specifically, we have considered those studies in which at least one of the following responses has been reported: antibody response in serum, transcriptomic effect in genes related to adaptive immune response (*e.g.*, IgM, IgT, IgD, MHC II, CD4, and CD8), as well as T cell-mediated immunity and B cell responses observed in mucosal and also in central tissues as thymus, peripheral blood, head kidney, and spleen. Finally, taking all this information into consideration, we discuss several strategies to improve the efficiency of mucosal vaccination in teleost fish.

## LOCAL AND SYSTEMIC EFFECTS AFTER ORAL VACCINATION

Several studies have been focused on evaluating the local and systemic effects of oral immunization against bacteria and viruses in fish since this route of administration requires less fish handling, induces minimum stress, reduces side effects, and also allows vaccination at any stage of the life cycle in fish (49). Oral immunization of antigens can be administered by a great variety of ways including non-encapsulated or encapsulated feed, gavage (considered as an experimental way of delivering vaccines) or through the use of bioencapsulation vectors such as planktonic *Crustacea* (*e.g.*, *Daphnia*), rotifers,

and *Artemia*, all of them aimed at protecting the antigen from degradation until it reaches the most posterior segments of the digestive tract where immune induction has been shown to take place (21). These include the hindgut (50, 51) as well as the pyloric caeca, characterized in rainbow trout to be one of the most responsive gut segments to immunization (52).

## Antibacterial Vaccines

Some vaccines designed against bacterial pathogens have been shown to produce high levels of serum antibodies when administrated in the fish feed (53–57). For instance, the level of protective antibodies elicited by a live attenuated *Streptococcus agalactiae* vaccine in Nile tilapia (*Oreochromis niloticus*) was significantly higher compared to the control group, reaching their maximum levels at 14–21 days after the immunization (55). In the case of the red tilapia hybrid (*Oreochromis mossambicus* x *O. niloticus*), fish vaccinated with formalin-killed *St. agalactiae* showed significantly higher IgM levels compared to controls, lasting up to 6 weeks after administration of the first booster dose (54). However, when a double booster regime was undertaken consistent higher levels of antibodies were reached until week 12, suggesting that this feed-based vaccination regime is a suitable strategy to obtain a long-lasting protection (54). Similarly, rainbow trout immunized with a non-microencapsulated live rifampicin-attenuated oral vaccine against *Flavobacterium psychrophilum* reached higher antibody titers than those obtained in fish vaccinated with the equivalent microencapsulated vaccine (53). Interestingly, a similar antibody response was observed between fish vaccinated orally and those intraperitoneally injected with the non-encapsulated vaccine (53). In the same way, oral vaccination of Atlantic salmon (*S. salar*) with live attenuated *Piscirickettsia salmonis* using a bioadhesive MicroMatrixTM cationic polysaccharide formulation produced systemic anti-*P. salmonis* IgM with a magnitude slightly higher than that of sera obtained from intraperitoneally vaccinated fish (57). In this study, specific antibodies were also detected in the intestinal mucosa of the oral vaccine-treated group at 350 degree-days post-vaccination (57).

In addition to these studies that show that some oral vaccination strategies are capable of producing systemic in addition to mucosal antibodies (57), there are very few data available on the characterization of B and T cell responses in central or mucosal tissues after oral immunization by means of transcriptional or functional analysis. In this sense, a study performed in gilthead sea bream (*Sparus aurata*) showed that the levels of specific IgM antibodies in the serum and IgT antibodies in skin mucus were significantly increased in orally vaccinated animals when challenged with *Photobacterium damselae* subsp. *piscicida* (37). In this case, challenged fish that had been orally vaccinated showed increased transcription of secreted IgT in intestine and head kidney, and much higher in spleen when compared to challenged unvaccinated fish (37). Regarding IgM, the transcription of membrane IgM was significantly upregulated in spleen, whereas the transcription of both membrane and secreted IgM forms were significantly downregulated in the intestine (37).

As an alternative to being a route for vaccination *per se*, oral vaccination has been proposed as a booster to acquire longer protection to intraperitoneally administered antigens. In this sense, the production of specific IgM antibodies was significantly increased when Atlantic salmon, rainbow trout and coho salmon (*Oncorhynchus kisutch*) were boosted orally after having been vaccinated with an injectable mono or polyvalent vaccine against salmonid rickettsial septicemia (SRS) (56). The oral boosters not only increased the magnitude of the response but also maintained the antibody response for longer, up to 2800–3200 degree-days (56).

## Antiviral Vaccines

The development of oral vaccines against viruses has been the aim of many studies in recent years (49, 50, 52, 58–63). Some of these studies have shown that oral antiviral vaccines can increase both systemic and mucosal immune responses to a previously administered intraperitoneal vaccine. Specifically, the administration of alginate-encapsulated antigens of infectious pancreatic necrosis virus (IPNV) in the feed after intraperitoneal vaccination in Atlantic salmon induced not only a significant higher antibody response following the first and the second booster, but also a significant higher CD4 and GATA3 expression in head kidney and spleen, known to be associated with T helper 2 responses that induce the secretion of Igs by B cells (61). Additionally, IgT transcription was also significantly increased in the intestine of fish orally immunized with the alginate-encapsulated vaccine (61). In some other cases, the antiviral vaccine was capable of inducing a strong immune response on its own. For example, in rainbow trout, detectable levels of anti-IPNV neutralizing antibodies were observed 90 days after administering along with the feed, for three consecutive days, 10 μg of an alginate-encapsulated DNA vaccine coding for the VP2 gene of IPNV (pcDNA-VP2) (59). Furthermore, IgM and IgT transcription was also significantly increased in response to this vaccine in kidney at day 30 post-vaccination (59). When this oral DNA vaccine was administered directly into the esophagus, neutralizing antibodies were also evident at 2, 3, 4, and 8 weeks post-vaccination (62). Additionally, IgM and IgT mRNA levels strongly increased in pyloric caeca, and to a lesser extent in head kidney (60). Accordingly, the pyloric caeca region was the area of the digestive tract in which a significant increase in the number of both $IgM^+$ and $IgT^+$ lymphocytes was more evident in response to this oral alginate-encapsulated IPNV DNA vaccine by means of immunohistochemistry analysis (52). Similarly, anti-IPNV antibodies were also detected in the sera of rainbow trout orally vaccinated with a DNA vaccine encapsulated in alginate microparticles as well as in chitosan/tripolyphosphate nanoparticles (58). In this case, the transcription levels of IgM, IgT, and CD4 (related to the presence of T helper cells) were dependent on the vaccine dose and were significantly upregulated in rainbow trout head kidney of all orally vaccinated fish groups compared to controls (58).

A significant increase in the production of antibodies against the infectious hematopoietic necrosis virus (IHNV) was detected in serum samples of rainbow trout vaccinated with an alginate

microsphere encapsulated-DNA vaccine compared to sera from unvaccinated fish (50). Remarkably, this vaccine also induced the expression of several markers of the adaptive immune response, such as CD4, CD8, IgM, and IgT in the kidney and the spleen in a dose-dependent manner, although it should be noted that the vaccine doses that had to be used to achieve these responses were much higher than those used in the case of the oral alginate-encapsulated IPNV DNA vaccine (50). In 2017, a description of mucosal and systemic immune responses to IHNV induced by an orally delivered yeast expressing the G of IHNV on the cell surface was reported (63). In this work, the oral vaccine provoked a significant upregulation of CD8, IgM, and IgT mRNA levels in the hindgut, spleen, and head kidney from rainbow trout, with stronger levels reached in the intestine than in the other tissues (63).

The capacity of orally administered antiviral vaccines to induce antibodies has also been demonstrated in several species of carp (64–68). A single oral immunization using a formalin-inactivated crucian carp hematopoietic necrosis virus (CHNV) was not sufficient to induce measurable serum antibody responses in ginbuna crucian carp (*Carassius auratus langsdorfii*) (67). However, when fish were orally boosted 7 days after the initial oral immunization, significant antibody titers were reached between 30 and 60 days post-booster (67). Remarkably, orally immunized had higher antibody titers compared to non-immunized controls, and also significant cytotoxic peripheral blood lymphocytes (PBLs) against fibroblastic target cells fish and intraperitoneally infected when challenged with the live virus (67). In another study, VP6-specific serum antibodies were detected in grass carp (*Ctenopharyngodon idella*) during 2–8 weeks after vaccination with a recombinant baculovirus containing the *vp6* gene from grass carp reovirus (GCRV) (68). Similarly, when common carp (*Cyprinus carpio*) and koi (*C. carpio koi*) were orally immunized with a recombinant *Lactobacillus plantarum* expressing the G protein of spring viremia of carp virus (SVCV) combined with the ORF81 protein of koi herpesvirus (KHV), significant levels of specific IgM were detected against the two viruses (64). Following a different approach, when common carp (*C. carpio* var. Jian) larvae were fed with *Artemia* coated with recombinant *Saccharomyces cerevisiae* expressing the cyprinid herpesvirus-3 (CyHV-3) envelope antigen pORF65 high levels of specific anti-pORF65 antibodies were induced, in addition to higher levels of IgM and CD8α transcription in the spleen (66). Similarly, the oral gavage of *S. cerevisiae* expressing CyHV-3 ORF131 evoked the production of specific serum IgM as well as the increase of the IgT1 mRNA levels in the spleen and the head kidney (65). However, no differences were observed between carps immunized with vaccine and the control yeast, attributing the increase of the IgT expression to the mucosal modulator of the yeast rather than to the expressed protein in this microorganism (65).

## LOCAL AND SYSTEMIC EFFECTS AFTER IMMERSION VACCINATION

There are two methods to immunize fish by immersion: i) dip vaccination in which fish are immersed in water containing a relatively high dose of vaccine for few seconds or minutes; and ii) bath vaccination in which fish are introduced in a more diluted vaccine solution for a longer period of time (69). Although the great advantage of immersion vaccination is that the antigen is taken up through the skin, the intestine and gills, very large amounts of antigen are required and usually the levels of protection reached are not high, possible due to the fact that only a limited amount of antigen reaches the immune effector sites in these mucosal tissues (70). Despite this, being a method suitable to vaccinate a large number of fish at the same time, it has been used to administer many commercial antibacterial vaccines for fish. Commercial immersion vaccines commonly used in aquaculture include vaccines such as that against pasteurellosis for sea bream or against vibriosis for sea bass (*Dicentrarchus labrax*) and turbot (*Scophthalmus maximus*).

### Antibacterial Vaccines

Most studies focused on establishing the local and systemic effects of immersion vaccines has been carried out with antibacterial vaccines, specifically against *Yersinia ruckeri*, *F. psychrophilum*, *Listonella* (formerly *Vibrio*) *anguillarum*, and *Edwardsiella tarda*. In most of these studies, except for those performed with *E. tarda*, the vaccines were administered by the dip methodology. Thus, dip vaccination of rainbow trout against enteric red mouth disease (ERM) using a commercial *Y. ruckeri* bacterin biotype 1 (AQUAVAC ERM vaccine, MSD Animal Health) (1:10 diluted-vaccine for 5 min) has shown to significantly increase *Y. ruckeri*-specific IgM antibody titers at 4, 8, and 26 weeks post-vaccination (71). Similarly, a booster vaccination using different dilutions (1:100 and 1:1,000) of the commercial vaccine AQUAVAC RELERA (MSD Animal Health) which combines *Y. ruckeri* biotypes 1 and 2, significantly increased antibody levels compared to fish vaccinated with only one dose (72). Interestingly, both commercial vaccines when administered by dip vaccination (1:10 diluted-vaccine for 30 s) increased the expression of adaptive immune genes in the later phase of infection, and also the occurrence of $CD8^+$ and $IgM^+$ cells in the spleen and head kidney, thus correlating the cellular changes with protection of vaccinated fish (73).

Significant levels of *F. psychrophilum*-specific antibodies were also reported in dip vaccinated rainbow trout (1:10 diluted-vaccine for 3 min) in several studies (70, 74). In addition, the administration of a polyvalent whole cell vaccine containing formalin-inactivated *F. psychrophilum* (1:10 diluted-vaccine for 30 s) elicited a low, although significant, increment of serum IgT at 6 weeks post-vaccination in rainbow trout (75). In this study, the number of $IgT^+$ cells detected in spleen and head kidney of immersion vaccinated fish was also significantly higher in vaccinated fish. Intriguingly, the expression of CD8α in the head-kidney at day 2 and the levels of CD4-1 and CD8α transcription in the spleen at day 7 were significantly downregulated in vaccinated fish, suggesting the mobilization of both helper and cytotoxic T cells from these organs. However, IgT and IgM transcription levels were significantly upregulated in the hindgut at day 2 (75).

Dip vaccination of sea bass with a whole killed *L. anguillarum* serotype O1 and O2 bivalent commercial vaccine (MICROViB,

Microtek International) also produced an increase of specific IgM antibodies (76). In zebrafish (*Danio rerio*) dip vaccinated for 8 min with attenuated *L. anguillarum*, the specific antibody levels did not rise significantly following vaccination (77). A recent study analyzed the response of Atlantic cod (*G. morhua*) to a dip vaccination against *L. anguillarum* (1:10 diluted-vaccine for 30 s), revealing changes in the levels of transcription of genes related to adaptive immunity processes as established by means of a transcriptome analysis in head kidney (78). Thus, genes related to T cell activity (CD8, TRGC1, TNFSF11, EOMES, PERF1, UNC13D), and B cell activity (IGLC2) were positively differentially expressed in vaccinated fish (78). Specifically, TRGC1 is a T cell receptor gamma and TNFSF11 is involved in the regulation of T cell-dependent immune responses. On the other hand, the increase in EOMES, PERF1, and UNC13D levels observed in vaccinated fish suggest the specific activation of cytotoxic T cells that preferentially express these genes (78).

Regarding the immune response elicited by vaccines administered by bath, the immunization of Japanese flounder (*Paralichthys olivaceus*) with a formalin-inactivated form of *E. tarda* produced a significantly higher upregulation of MHC II, TCRα, CD4-1, and IgT transcription in the skin and gills than that observed in spleen and kidney (79). On the contrary, the expression of IgM was much higher in lymphoid organs than in mucosal tissues (79).

### Antiviral Vaccines

The efficacy of antiviral vaccines administered by bath to induce B and T cell responses has been also demonstrated in fish (80–82). For instance, a significant specific antibody response was detected in carp 28 and 36 days after bath vaccination for 30 min with a KHV vaccine which consisted in inactivated *Escherichia coli* expressing glycoprotein-25 (80). In another study, carbon nanotubes were tested as vaccine carriers to enhance the efficacy of an immersion vaccine (81, 82). Specifically, functionalized single-walled carbon nanotubes (SWCNTs) used as carriers of a DNA vaccine encoding a matrix protein of SVCV and expressing a green fluorescent protein (pEGFP-M) produced a significant increase of antibody levels and an upregulation of IgM, IgZ1, CD8β, CD4, MHC I, and MHC II transcription levels in carp immunized by bath twice for 10 h after a 3 day interval (81), suggesting the activation of both cytotoxic and helper T lymphocytes upon immunization. Similarly, bath vaccination of Mandarin fish (*Siniperca chuatsi*) for 10 h with a subunit vaccine system encoding the major capsid protein (MCP) of the infectious spleen and kidney necrosis virus (ISKNV) based on SWCNTs produced higher levels of antibody as well as higher IgM mRNA levels than those obtained in groups vaccinated with the naked vaccine (82).

## LOCAL AND SYSTEMIC EFFECTS AFTER NASAL VACCINATION

After the identification of the nasal-associated lymphoid tissue (NALT), some studies have emphasized the importance of nasal immunity to both infections and intranasal immunizations (83). In this respect, the efficacy of nasal vaccines has been uniquely demonstrated in rainbow trout (25, 84, 85), and as a consequence, only a few studies have identified the mucosal and systemic mechanisms elicited by vaccines administered through this route (23, 25).

### Antibacterial Vaccines

There is only one study focused on how fish respond locally and systemically to an antibacterial vaccine administered through the nasal cavity (23). In this study, an inactivated vaccine against *Y. ruckeri* administered either nasally or intraperitoneally in rainbow trout produced an increase of the nasal IgM repertoire diversity, indicating that both local and systemic antigen exposures are capable of inducing B cell responses in the NALT (23). In the case of splenic B cells, nasal vaccination decreased both IgM and IgT clonotype diversity. On the other hand, specific serum IgM and IgT titers were significantly risen after intraperitoneal vaccination but not after nasal immunization (23).

### Antiviral Vaccines

Concerning antiviral vaccines, the administration of a live attenuated IHNV vaccine into the olfactory cup, was reported to elicit an antiviral adaptive immune response in the head kidney and the olfactory organ similar to that triggered by IHNV intramuscular vaccination (25). Moreover, the expression of IgM mRNA levels were significantly higher in the olfactory tissue at day 14 post-immunization in comparison to day 4, indicating the capacity of this vaccine to induce an adaptive immune response (25).

## LOCAL AND SYSTEMIC EFFECTS AFTER ANAL INTUBATION

Some studies have explored the effects of anal immunization. Although this immunization strategy offers many disadvantages from a practical point of view, it can be considered as a way to investigate how the intestinal mucosa directly reacts to antigens without having to protect the antigen from degradation in the upper digestive segments (86, 87). In 2000, a study addressed how rainbow trout responded to fluorescein isothiocyanate (FITC) conjugated to keyhole limpet hemocyanin (KLH) when was administered intraperitoneally or anally (88). The results showed that fish injected with FITC-KLH developed higher antibody level of mucosal and serum anti-FITC antibodies when compared to fish immunized anally (88). Recently, the anal route has been used to study specific B cell responses to two model antigens, TNP-KLH (2,4,6-trinitrophenyl KLH), a TD antigen and TNP-LPS, a TI antigen (87). This study demonstrated that, in the absence of additional adjuvants, rainbow trout preferentially responded to anally administered TNP-LPS, while the response to TNP-KLH was much weaker. Thus, TNP-LPS elicited TNP-specific serum IgM, and a significant increase in the number of total and TNP-specific IgM-secreting cells in both spleen and kidney, with the kidney being the site where most of these cells were found at later time

points. In the spleen, a proliferative response of both $IgM^+$ B and T cells was also clearly visible at early time points, while weaker proliferative responses were observed in the kidney. At transcriptional level, a significant decrease in FOXP3A, FOXP3B, CD4, and CD8 mRNA levels was detected in the intestine of TNP-LPS-immunized fish, which suggested a local downregulation of different T cell subsets (87).

### Antibacterial Vaccines

Few data is available concerning the effect of antibacterial vaccines administered anally. A *L. anguillarum* inactivated vaccine as well as the extracellular products obtained when producing the vaccine were shown to increase antibody titers in carp 21 days after anal intubation (89).

### Antiviral Vaccines

A formalin-inactivated CHNV administered by anal intubation produced a significant upregulation of TCRß mRNA levels in the kidney and the intestine of ginbuna crucian carp when compared to control unvaccinated fish (90). This result led the authors to hypothesize that this vaccine was effective at triggering systemic and local T cell responses. Additionally, an increase of the percentage of proliferating $CD8^+$ cells was detected in the posterior portion of the hindgut, pointing to this part of the intestine as an important site for generating virus-specific $CD8^+$ cytotoxic T cells upon anal vaccination (90).

## COMPARISON OF THE LOCAL AND SYSTEMIC EFFECTS AFTER IMMUNIZATION BY SEVERAL ROUTES

In some studies different routes of mucosal administration have been compared in order to identify which delivery method reached the higher adaptive immune responses at both local and systemic levels.

### Antibacterial Vaccines

In 1986, a study performed in carp showed that a formalin-killed *L. anguillarum* vaccine administered by anal immunization increased antigen-specific antibodies in serum, and after anal boosting, similar levels of serum antibodies were reached compared with two consecutive intramuscular injections (91). An enhancement of antigen-specific Ig titers in skin mucus was also detected after anal immunization (91). However, no significant antibody titers were elicited in serum after oral immunization, not even when bacteria were administered daily with the food (91). In rainbow trout, protection against *L. anguillarum* correlated positively with serum antibody levels after, but not prior to, boosting by oral, immersion or injection with a formalin-killed vaccine (92). In the case of African catfish (*Clarias gariepinus*), the analysis of serum samples after vaccination with a formalin-inactivated *L. anguillarum* O2 bacterin by four delivery routes showed that fish vaccinated by intraperitoneal injection obtained the highest antibody levels, followed by fish immunized by anal intubation, oral administration and immersion (93). However, the levels of antibodies reached in skin mucus were higher upon anal intubation, followed by immersion, oral intubation, and intraperitoneal injection (93), demonstrating that mucosal vaccines have a superior capacity to induce mucosal responses. In the case of barramundi (*Lates calcarifer*), fish injected intraperitoneally with an experimental *Vibrio harveyi* inactivated vaccine displayed significantly higher serum antibody activity than immersed and intubated fish (94). In eel (*Anguilla anguilla*), the bivalent formalin and heat-inactivated vaccine against two eel-pathogenic serovars of *Vibrio vulnificus* induced the production of significant antibody levels in plasma as well as in the skin and gut mucus despite the *via* of administration (oral, anal, immersion, or intraperitoneal vaccination) (95). Interestingly, in all cases, the production of IgM was faster in mucus while antibody titers were higher and lasted longer in plasma (95). In rainbow trout, no significant increase of IgM titers in serum, gill or skin mucus was observed 28 days after immunization of fish with live attenuated *F. psychrophilum* by anal intubation or immersion, unlike fish vaccinated intraperitoneally (96). However, the levels of secretory IgD and IgT expression were significantly upregulated in gills and intestine of fish immunized by the immersion and anal intubation route, respectively (96). In another study, the oral or anal administration of rainbow trout with a *Y. ruckeri* O1 bacterin induced protection against ERM, without affecting the levels of *Y. ruckeri* specific antibodies in plasma. The authors attributed this protection to an immune response mounted locally in the intestine (97). On the contrary, significantly higher antibody levels in serum were detected 45 days post-immunization in mrigal (*Cirrhinus mrigala*) anally or orally vaccinated against *E. tarda* in comparison to those detected in control fish or in fish vaccinated by immersion and intraperitoneal injection (98). In skin and gill mucus, significantly higher antibodies levels were obtained in the oral and immersion groups (98). In gut mucus, significantly higher values of antibodies were detected in the immersion group compared to the rest of the treatments (98). However, oral and immersion immunization routes offered better protection of mrigal compared to other antigen delivery routes (98).

### Antiviral Vaccines

No significant differences were observed in serum antibody levels in rainbow trout intraperitoneally, anally, and orally immunized with viral hemorrhagic septicemia virus (VHSV) (99). The vaccine consisted in lyophilized virus surrounded by polyethylene glycol (PEG) and then extruded under low temperature (99). In olive flounder fingerlings, specific anti-VHSV antibody titers were significantly enhanced in serum, and also in the skin and intestinal mucus following vaccination with a poly lactic-co-glycolic acid (PLGA) or chitosan encapsulated formalin-inactivated VHSV vaccine administered together with the feed or by immersion (100, 101). Additionally, a significant upregulation of IgM, IgT, pIgR, MHC I, MHC II transcripts was detected in the kidney, skin, and intestine of vaccinated fish (100, 101).

Bath and oral immunizations of grouper (*Epinephelus coioides*) larvae with a binary ethylenimine (BEI)-inactivated

nervous necrosis virus (NNV) vaccine induced the transcription of IgM, IgT, MHC I, MHC II, and CD8 not only in viscera but also in mucosal tissues at specific time points (102), suggesting the involvement of both local and systemic B and T cells.

## STRATEGIES FOR IMPROVING THE EFFICIENCY OF MUCOSAL VACCINATION IN TELEOST FISH

There are many mucosally administered vaccines that are only capable of triggering local immune responses and have been shown to be incapable of providing fish with a sufficient level of protection upon pathogen encounter [reviewed in (21)]. Thus, although in many of the studies mentioned through this work the levels of protection conferred by the vaccines have not been studied, it seems clear that those mucosal vaccines that are capable of eliciting strong systemic B and T cell responses are better suited to confer protection, and these are the ones we have focused on in this paper. However, it should be noted, that most of these studies in which adaptive immune responses to vaccines were undertaken, antibody production was measured and very few of them analyzed T cell responses, despite their relevance, especially in the case of antiviral vaccines. Additionally, all determinations of specific antibody titers focused on the identification of IgM specific antibodies, as no studies to date have reported the presence of antigen-specific IgT or IgD antibodies in fish. Therefore, the development of additional immunological tools in different fish species that would allow us to have a wider view of how B and T cell responses are activated in response to vaccine antigens seems essential to establish immunological correlates of protection. Only through a complete understanding of how antibodies and cellular responses correlate to protection, we will be able to rationally design effective mucosal vaccines in the future.

To increase the efficacy of non-optimal mucosal vaccine formulations, two aspects have to be taken into account. The formulation of the antigen has to be optimized to allow it to reach mucosal effector sites in an unaltered way in sufficient amount. For oral vaccines, this implies reaching the more distal gut segments such as hindgut (50) or pyloric caeca (52). However, knowledge on how the antigen is taken up at these mucosal sites and presented to cells of the adaptive system is still scarce. These studies are essential to understand to which cell types the antigen should be directed. For oral vaccines, encapsulation has been the most commonly used method to protect antigens from degradation and increase their uptake in the gut after oral immunization, whereas a fewer number of studies have used alternative strategies such as antigen expression in live feed (58). The other aspect that should be taken into account to increase the efficacy of mucosal vaccines, is the fact that these vaccines should circumvent mucosal tolerance, a mechanism through which the immune response in these mucosal surfaces is tightly regulated to avoid a continuous response to innocuous antigens. To this aim, inclusion of adjuvants may help to increase the immunogenicity of these antigens and bypass mucosal tolerance. However, this implies a greater knowledge of these regulatory systems as well as a search for adjuvants suited for mucosal deliver in fish. For instance, in mammals, the most commonly used mucosal adjuvants are toxin-based adjuvants (*e.g.*, enterotoxigenic *E. coli* heat-labile toxin and cholera toxin), immunostimulatory adjuvants (*e.g.*, monophosphoryl lipid, CpG, and QS21, a substance extracted from the bark of *Quillaja saponaria*), particulate adjuvants (*e.g.*, emulsions and highly immunogenic immune stimulating complex) (103), or microbiota-derived components such as flagellin (104). Very few information is available regarding the adjuvant potential of these molecules in fish. The adjuvant potential of the *E. coli* LT (R192G/L211A) toxoid (dmLT) was first tested in carp in combination with an oral DNA vaccine against SVCV showing no efficacy (105). However, taking into account that a specific adjuvant may not be suitable for one antigen, but could be effective in combination with one of a different nature, Martín-Martín et al. (106) established a simple protocol designed to initially evaluate the effects of potential oral adjuvants for two different pathogens. The results pointed to dmLT as an preferential adjuvant for oral antibacterial vaccines in rainbow trout, since the combination of the toxoid with VHSV only produced minor transcriptional effects, while the effects were much more pronounced when combined with *Aeromonas salmonicida* (106). The adjuvant effect of *Q. saponaria* saponin (QSS) has been also tested in fish, particularly on the protection of turbot fry against *L. anguillarum* (107). The results showed that turbot immersed in seawater containing QSS for 10 min and then vaccinated in a formalin-inactivated *L. anguillarum* MN suspension for 30 min produced a significant expression of IgM mRNA in skin, spleen, and kidney at 14 days post-immunization in comparison to fish vaccinated without QSS by immersion or intraperitoneal injection (107). Moreover, a higher serum antibody titer was also demonstrated after 14 days in the vaccinated fish although at levels lower than those reached in the intraperitoneally immunized fish (107). Another strategy which has been proposed for aquacultured fish is the use of proteins derived from the host rather than foreign antigens as adjuvants (108). This is the case of sea bass fed with a commercial vaccine against *L. anguillarum* and *Vibrio ordalii* (AQUAVAC Vibrio Oral, ISPAH) adjuvanted with a fish-self recombinant cytokine, such as the tumor necrosis factor α (rTNFα). The supplementation of this vaccine with rTNFα significantly enhanced disease resistance against vibriosis, enhancing the infiltration of T cells into the gut epithelium, upregulating the expression of the IgT gene in the hindgut but not raising specific IgM titers in serum (108).

Regarding microbiota-derived components, the immune-stimulating effects of β-glucans on the fish immune system when administered on their own have become evident using different administration routes (109). Recently, immersion vaccination of gilbel carp (*Carassius auratus gibelio*) with β-glucans and β-propiolactone-inactivated cyprinid herpesvirus 2 protected against a viral challenge more efficiently than fish vaccinated in the absence of β-glucans (110). In this work, the

levels of transcription of IL-2 and IFN-γ2 in head kidney and spleen as well as of IgM and IgZ in the spleen were higher when β-glucans were included (110). In rainbow trout, a recombinant flagellin from the salmonid pathogen *Y. ruckeri* induced a strong antibody response when intraperitoneally injected (111). Thus, it would be interesting to study how fish B and T cells respond to bacterial flagellin when administered as a mucosal adjuvant and whether this protein is able to promote adaptive immune responses in fish as previously observed in mice (104).

It is worthwhile to mention that, in the last years, not only microbiota-derived components but also live microorganisms, designated as immunobiotics, have been shown to modulate the mucosal immune system. Therefore, immunobiotics have been considered as a potential alternative to enhance the response to vaccination (112, 113). For example, the nasal administration of *Lactobacillus rhamnosus* CRL1505 as an adjuvant improved the humoral and cellular adaptive immune responses induced by influenza virus infection or vaccination in mice (112). Regarding this strategy, few data have been reported in fish. Yeast has been proposed as vehicle for oral antigen delivery due to its immunomodulatory properties and potential to boost local immune responses, acting as an adjuvant (49). Thus, in rainbow trout, the oral administration of *Pichia pastoris* yeast expressing a green fluorescence protein (GFP) was shown to exert a rapid local innate immune response in the intestine increasing IgT transcription in the midgut at 24 h post-treatment, and a subsequent systemic response, increasing the transcription of IgM and IgT in the spleen after 7 days (49). In this scenario, it is plausible that the use of immunobiotics can be explored in the future as adjuvants for novel fish mucosal vaccine formulations.

## CONCLUDING REMARKS

Taking into account that pathogens enter the organisms through mucosal surfaces where they initiate their replication and having established that mucosal vaccines have a superior ability to trigger mucosal immunity than systemic vaccines, mucosal vaccines seem as a great alternative to vaccines administered through injection. However, it does seem that these vaccines must be capable of eliciting robust systemic immune effects in order to provide long-lasting memory B and T cell responses. Although in fish, mucosal vaccines also provide numerous advantages from a practical point of view, almost no oral vaccines and very few immersion vaccines are available in the market for aquacultured species, many of them intended as boosters and not as vaccines on their own. The efficacy of these vaccines depends not only on the immunogenicity of the antigen itself (that may be increased by the addition of suited adjuvants) but also on the availability of this antigen for mucosal immune cells. In this sense, in mammals and also in fish, recent strategies to develop effective mucosal vaccines have been aimed at directing the antigens to specific antigen sampling cells within the mucosa (10, 114, 115). However, these strategies require a much better knowledge of how immune responses are organized in mucosal surfaces in fish, as well as a full phenotypical and functional characterization of the cells implicated in this response. Thus, the design of efficient mucosal vaccines for fish still requires investigation of many aspects. In parallel, it is also essential to develop new immunological tools that can help us evaluate the response to these vaccine formulations and establish correlates of protection. Despite all these gaps, it seems obvious that those mucosal vaccines capable of inducing not only local, but also systemic B and T cell responses are better placed to confer high protection levels. Thus, in this review we have highlighted this information, as it could be used as a starting point to continue the optimization towards economically profitable mucosal vaccines.

## AUTHOR CONTRIBUTIONS

EM-A collected all the information included in this review and wrote the manuscript with help and contributions from PD-R and CT. All authors contributed to the article and approved the submitted version.

## FUNDING

This work was supported by the European Research Council (ERC Consolidator Grant 2016 725061 TEMUBLYM), by the Spanish Ministry of Science, Innovation, and Universities (project AGL2017-85494-C2-1-R) and by the *Comunidad de Madrid* (grant 2016-T1/BIO-1672). EM-A was recipient of a Juan de la Cierva-Incorporación Postdoctoral Contract (IJC2018-035843-I) funded by the Spanish Ministry of Science, Innovation and Universities.

## REFERENCES

1. Amanna IJ, Slifka MK. Contributions of humoral and cellular immunity to vaccine-induced protection in humans. *Virology* (2011) 411(2):206–15. doi: 10.1016/j.virol.2010.12.016
2. Kang S-M, Compans RW. Host responses from innate to adaptive immunity after vaccination: molecular and cellular events. *Mol Cells* (2009) 27(1):5–14. doi: 10.1007/s10059-009-0015-1
3. Takamura S. Niches for the long-term maintenance of tissue-resident memory T cells. *Front Immunol* (2018) 9:1214. doi: 10.3389/fimmu.2018.01214
4. Zens KD, Chen JK, Farber DL. Vaccine-generated lung tissue-resident memory T cells provide heterosubtypic protection to influenza infection. *JCI Insight* (2016) 1(10):e85832. doi: 10.1172/jci.insight.85832
5. Zhao J, Zhao J, Mangalam AK, Channappanavar R, Fett C, Meyerholz DK, et al. Airway memory CD4(+) T cells mediate protective immunity against emerging respiratory coronaviruses. *Immunity* (2016) 44(6):1379–91. doi: 10.1016/j.immuni.2016.05.006
6. Palm AE, Henry C. Remembrance of things past: long-term B cell memory after infection and vaccination. *Front Immunol* (2019) 10:1787. doi: 10.3389/fimmu.2019.01787

7. Jegaskanda S, Mason RD, Andrews SF, Wheatley AK, Zhang R, Reynoso GV, et al. Intranasal live Influenza vaccine priming elicits localized B cell responses in mediastinal lymph nodes. *J Virol* (2018) 92(9):e01970-17. doi: 10.1128/jvi.01970-17
8. Chen K, Cerutti A. Vaccination strategies to promote mucosal antibody responses. *Immunity* (2010) 33(4):479–91. doi: 10.1016/j.immuni.2010.09.013
9. Neutra MR, Kozlowski PA. Mucosal vaccines: the promise and the challenge. *Nat Rev Immunol* (2006) 6(2):148–58. doi: 10.1038/nri1777
10. Fujkuyama Y, Tokuhara D, Kataoka K, Gilbert RS, McGhee JR, Yuki Y, et al. Novel vaccine development strategies for inducing mucosal immunity. *Expert Rev Vaccines* (2012) 11(3):367–79. doi: 10.1586/erv.11.196
11. Li M, Wang Y, Sun Y, Cui H, Zhu SJ, Qiu HJ. Mucosal vaccines: strategies and challenges. *Immunol Lett* (2020) 217:116–25. doi: 10.1016/j.imlet.2019.10.013
12. Lycke N. Recent progress in mucosal vaccine development: potential and limitations. *Nat Rev Immunol* (2012) 12(8):592–605. doi: 10.1038/nri3251
13. Sztein MB. Cell-mediated immunity and antibody responses elicited by attenuated *Salmonella enterica* Serovar Typhi strains used as live oral vaccines in humans. *Clin Infect Dis* (2007) 45 Suppl 1:S15–19. doi: 10.1086/518140
14. Wong P, Pamer EG. CD8 T cell responses to infectious pathogens. *Annu Rev Immunol* (2003) 21:29–70. doi: 10.1146/annurev.immunol.21.120601.141114
15. Harris JB. Cholera: immunity and prospects in vaccine development. *J Infect Dis* (2018) 218(suppl_3):S141–s146. doi: 10.1093/infdis/jiy414
16. Hoft DF, Babusis E, Worku S, Spencer CT, Lottenbach K, Truscott SM, et al. Live and inactivated influenza vaccines induce similar humoral responses, but only live vaccines induce diverse T-cell responses in young children. *J Infect Dis* (2011) 204(6):845–53. doi: 10.1093/infdis/jir436
17. Ward RL. Rotavirus vaccines: how they work or don't work. *Expert Rev Mol Med* (2008) 10:e5. doi: 10.1017/s1462399408000574
18. Freuling CM, Hampson K, Selhorst T, Schröder R, Meslin FX, Mettenleiter TC, et al. The elimination of fox rabies from Europe: determinants of success and lessons for the future. *Philos Trans R Soc Lond B Biol Sci* (2013) 368 (1623):20120142. doi: 10.1098/rstb.2012.0142
19. Rossi S, Staubach C, Blome S, Guberti V, Thulke H-H, Vos A, et al. Controlling of CSFV in European wild boar using oral vaccination: a review. *Front Microbiol* (2015) 6:1141. doi: 10.3389/fmicb.2015.01141
20. Adams A. Progress, challenges and opportunities in fish vaccine development. *Fish Shellfish Immunol* (2019) 90:210–4. doi: 10.1016/j.fsi.2019.04.066
21. Embregts CW, Forlenza M. Oral vaccination of fish: lessons from humans and veterinary species. *Dev Comp Immunol* (2016) 64:118–37. doi: 10.1016/j.dci.2016.03.024
22. Plant KP, LaPatra SE. Advances in fish vaccine delivery. *Dev Comp Immunol* (2011) 35(12):1256–62. doi: 10.1016/j.dci.2011.03.007
23. Magadán S, Jouneau L, Boudinot P, Salinas I. Nasal vaccination drives modifications of nasal and systemic antibody repertoires in rainbow trout. *J Immunol* (2019) 203(6):1480–92. doi: 10.4049/jimmunol.1900157
24. Salinas I, Zhang YA, Sunyer JO. Mucosal immunoglobulins and B cells of teleost fish. *Dev Comp Immunol* (2011) 35(12):1346–65. doi: 10.1016/j.dci.2011.11.009
25. Tacchi L, Musharrafieh R, Larragoite ET, Crossey K, Erhardt EB, Martin SAM, et al. Nasal immunity is an ancient arm of the mucosal immune system of vertebrates. *Nat Commun* (2014) 5:5205. doi: 10.1038/ncomms6205
26. Li J, Barreda DR, Zhang YA, Boshra H, Gelman AE, Lapatra S, et al. B lymphocytes from early vertebrates have potent phagocytic and microbicidal abilities. *Nat Immunol* (2006) 7(10):1116–24. doi: 10.1038/ni1389
27. Gao J, Ma X, Gu W, Fu M, An J, Xing Y, et al. Novel functions of murine B1 cells: active phagocytic and microbicidal abilities. *Eur J Immunol* (2012) 42 (4):982–92. doi: 10.1002/eji.201141519
28. Cain KD, Jones DR, Raison RL. Antibody-antigen kinetics following immunization of rainbow trout (*Oncorhynchus mykiss*) with a T-cell dependent antigen. *Dev Comp Immunol* (2002) 26(2):181–90. doi: 10.1016/s0145-305x(01)00063-5
29. Stavnezer J, Amemiya CT. Evolution of isotype switching. *Semin Immunol* (2004) 16(4):257–75. doi: 10.1016/j.smim.2004.08.005
30. Macpherson AJ, McCoy KD, Johansen FE, Brandtzaeg P. The immune geography of IgA induction and function. *Mucosal Immunol* (2008) 1(1):11–22. doi: 10.1038/mi.2007.6
31. Díaz-Rosales P, Muñoz-Atienza E, Tafalla C. Role of teleost B cells in viral immunity. *Fish Shellfish Immunol* (2019) 86:135–42. doi: 10.1016/j.fsi.2018.11.039
32. Granja AG, Tafalla C. Different IgM(+) B cell subpopulations residing within the peritoneal cavity of vaccinated rainbow trout are differently regulated by BAFF. *Fish Shellfish Immunol* (2019) 85:9–17. doi: 10.1016/j.fsi.2017.10.003
33. Zhang YA, Salinas I, Li J, Parra D, Bjork S, Xu Z, et al. IgT, a primitive immunoglobulin class specialized in mucosal immunity. *Nat Immunol* (2010) 11(9):827–35. doi: 10.1038/ni.1913
34. Xu Z, Parra D, Gómez D, Salinas I, Zhang YA, von Gersdorff Jørgensen L, et al. Teleost skin, an ancient mucosal surface that elicits gut-like immune responses. *Proc Natl Acad Sci U S A* (2013) 110(32):13097–102. doi: 10.1073/pnas.1304319110
35. Xu Z, Takizawa F, Parra D, Gómez D, von Gersdorff Jørgensen L, LaPatra SE, et al. Mucosal immunoglobulins at respiratory surfaces mark an ancient association that predates the emergence of tetrapods. *Nat Commun* (2016) 7:10728. doi: 10.1038/ncomms10728
36. Castro R, Jouneau L, Pham HP, Bouchez O, Giudicelli V, Lefranc MP, et al. Teleost fish mount complex clonal IgM and IgT responses in spleen upon systemic viral infection. *PloS Pathog* (2013) 9(1):e1003098. doi: 10.1371/journal.ppat.1003098
37. Piazzon MC, Galindo-Villegas J, Pereiro P, Estensoro I, Calduch-Giner JA, Gómez-Casado E, et al. Differential Modulation of IgT and IgM upon parasitic, bacterial, viral, and dietary challenges in a perciform fish. *Front Immunol* (2016) 7:637. doi: 10.3389/fimmu.2016.00637
38. Arpin C, de Bouteiller O, Razanajaona D, Fugier-Vivier I, Brière F, Banchereau J, et al. The normal counterpart of IgD myeloma cells in germinal center displays extensively mutated IgVH gene, Cmu-Cdelta switch, and lambda light chain expression. *J Exp Med* (1998) 187(8):1169–78. doi: 10.1084/jem.187.8.1169
39. Chen K, Xu W, Wilson M, He B, Miller NW, Bengtén E, et al. Immunoglobulin D enhances immune surveillance by activating antimicrobial, proinflammatory and B cell-stimulating programs in basophils. *Nat Immunol* (2009) 10(8):889–98. doi: 10.1038/ni.1748
40. Edholm ES, Bengtén E, Stafford JL, Sahoo M, Taylor EB, Miller NW, et al. Identification of two IgD+ B cell populations in channel catfish, *Ictalurus punctatus*. *J Immunol* (2010) 185(7):4082–94. doi: 10.4049/jimmunol.1000631
41. Castro R, Bromage E, Abós B, Pignatelli J, González Granja A, Luque A, et al. CCR7 is mainly expressed in teleost gills, where it defines an IgD+IgM- B lymphocyte subset. *J Immunol* (2014) 192(3):1257–66. doi: 10.4049/jimmunol.1302471
42. Perdiguero P, Martín-Martín A, Benedicenti O, Díaz-Rosales P, Morel E, Muñoz-Atienza E, et al. Teleost IgD+IgM– B cells mount clonally expanded and mildly mutated intestinal IgD responses in the absence of lymphoid follicles. *Cell Rep* (2019) 29(13):4223–4235.e4225. doi: 10.1016/j.celrep.2019.11.101
43. Ramírez-Gómez F, Greene W, Rego K, Hansen JD, Costa G, Kataria P, et al. Discovery and characterization of secretory IgD in rainbow trout: secretory IgD is produced through a novel splicing mechanism. *J Immunol* (2012) 188 (3):1341–9. doi: 10.4049/jimmunol.1101938
44. Choi JH, Wang KW, Zhang D, Zhan X, Wang T, Bu CH, et al. IgD class switching is initiated by microbiota and limited to mucosa-associated lymphoid tissue in mice. *Proc Natl Acad Sci U S A* (2017) 114(7):E1196–e1204. doi: 10.1073/pnas.1621258114
45. Li AV, Moon JJ, Abraham W, Suh H, Elkhader J, Seidman MA, et al. Generation of effector memory T cell-based mucosal and systemic immunity with pulmonary nanoparticle vaccination. *Sci Transl Med* (2013) 5 (204):204ra130. doi: 10.1126/scitranslmed.3006516
46. Bivas-Benita M, Bar L, Gillard GO, Kaufman DR, Simmons NL, Hovav AH, et al. Efficient generation of mucosal and systemic antigen-specific CD8+ T-cell responses following pulmonary DNA immunization. *J Virol* (2010) 84 (11):5764–74. doi: 10.1128/jvi.02202-09
47. Zheng X, Oduro JD, Boehme JD, Borkner L, Ebensen T, Heise U, et al. Mucosal CD8+ T cell responses induced by an MCMV based vaccine vector confer protection against influenza challenge. *PLoS Pathog* (2019) 15(9): e1008036. doi: 10.1371/journal.ppat.1008036
48. Nakanishi T, Shibasaki Y, Matsuura Y. T Cells in Fish. *Biology* (2015) 4 (4):640–63. doi: 10.3390/biology4040640
49. Embregts CWE, Reyes-Lopez F, Pall AC, Stratmann A, Tort L, Lorenzen N, et al. *Pichia pastoris* yeast as a vehicle for oral vaccination of larval and adult teleosts. *Fish Shellfish Immunol* (2019) 85:52–60. doi: 10.1016/j.fsi.2018.07.033

50. Ballesteros NA, Alonso M, Saint-Jean SR, Pérez-Prieto SI. An oral DNA vaccine against infectious haematopoietic necrosis virus (IHNV) encapsulated in alginate microspheres induces dose-dependent immune responses and significant protection in rainbow trout (*Oncorrhynchus mykiss*). *Fish Shellfish Immunol* (2015) 45(2):877–88. doi: 10.1016/j.fsi.2015.05.045
51. Rombout JH, Abelli L, Picchietti S, Scapigliati G, Kiron V. Teleost intestinal immunology. *Fish Shellfish Immunol* (2011) 31(5):616–26. doi: 10.1016/j.fsi.2010.09.001
52. Ballesteros NA, Castro R, Abós B, Rodríguez Saint-Jean SS, Pérez-Prieto SI, Tafalla C. The pyloric caeca area is a major site for IgM(+) and IgT(+) B cell recruitment in response to oral vaccination in rainbow trout. *PLoS One* (2013) 8(6):e66118. doi: 10.1371/journal.pone.0066118
53. Ghosh B, Bridle AR, Nowak BF, Cain KD. Assessment of immune response and protection against bacterial coldwater disease induced by a live-attenuated vaccine delivered orally or intraperitoneally to rainbow trout, *Oncorhynchus mykiss* (Walbaum). *Aquaculture* (2015) 446:242–9. doi: 10.1016/j.aquaculture.2015.04.035
54. Ismail MS, Siti-Zahrah A, Syafiq MRM, Amal MNA, Firdaus-Nawi M, Zamri-Saad M. Feed-based vaccination regime against streptococcosis in red tilapia*Oreochromis niloticus* x *Oreochromis mossambicus*. *BMC Vet Res* (2016) 12(1):194. doi: 10.1186/s12917-016-0834-1
55. Li LP, Wang R, Liang WW, Huang T, Huang Y, Luo FG, et al. Development of live attenuated *Streptococcus agalactiae* vaccine for tilapia via continuous passage *in vitro*. *Fish Shellfish Immunol* (2015) 45(2):955–63. doi: 10.1016/j.fsi.2015.06.014
56. Tobar I, Arancibia S, Torres C, Vera V, Soto P, Carrasco C, et al. Successive oral immunizations against *Piscirickettsia salmonis* and infectious salmon anemia virus are required to maintain a long-term protection in farmed salmonids. *Front Immunol* (2015) 6:244. doi: 10.3389/fimmu.2015.00244
57. Tobar JA, Jerez S, Caruffo M, Bravo C, Contreras F, Bucarey SA, et al. Oral vaccination of Atlantic salmon (*Salmo salar*) against salmonid rickettsial septicaemia. *Vaccine* (2011) 29(12):2336–40. doi: 10.1016/j.vaccine.2010.12.107
58. Ahmadivand S, Soltani M, Behdani M, Evensen Ø, Alirahimi E, Hassanzadeh R, et al. Oral DNA vaccines based on CS-TPP nanoparticles and alginate microparticles confer high protection against infectious pancreatic necrosis virus (IPNV) infection in trout. *Dev Comp Immunol* (2017) 74:178–89. doi: 10.1016/j.dci.2017.05.004
59. Ballesteros NA, Rodriguez Saint-Jean S, Perez-Prieto SI. Food pellets as an effective delivery method for a DNA vaccine against infectious pancreatic necrosis virus in rainbow trout (*Oncorhynchus mykiss*, Walbaum). *Fish Shellfish Immunol* (2014) 37(2):220–8. doi: 10.1016/j.fsi.2014.02.003
60. Ballesteros NA, Saint-Jean SSR, Encinas PA, Pérez-Prieto SI, Coll JM. Oral immunization of rainbow trout to infectious pancreatic necrosis virus (IPNV) induces different immune gene expression profiles in head kidney and pyloric ceca. *Fish Shellfish Immunol* (2012) 33(2):174–85. doi: 10.1016/j.fsi.2012.03.016
61. Chen L, Klaric G, Wadsworth S, Jayasinghe S, Kuo T-Y, Evensen Ø, et al. Augmentation of the antibody response of Atlantic salmon by oral administration of alginate-encapsulated IPNV antigens. *PLoS One* (2014) 9(10):e109337. doi: 10.1371/journal.pone.0109337
62. de las Heras AI, Rodríguez Saint-Jean S, Pérez-Prieto SI. Immunogenic and protective effects of an oral DNA vaccine against infectious pancreatic necrosis virus in fish. *Fish Shellfish Immunol* (2010) 28(4):562–70. doi: 10.1016/j.fsi.2009.12.006
63. Zhao J-Z, Xu L-M, Liu M, Cao Y-S, LaPatra SE, Yin J-S, et al. Preliminary study of an oral vaccine against infectious hematopoietic necrosis virus using improved yeast surface display technology. *Mol Immunol* (2017) 85:196–204. doi: 10.1016/j.molimm.2017.03.001
64. Cui LC, Guan XT, Liu ZM, Tian CY, Xu YG. Recombinant *Lactobacillus* expressing G protein of spring viremia of carp virus (SVCV) combined with ORF81 protein of koi herpesvirus (KHV): a promising way to induce protective immunity against SVCV and KHV infection in cyprinid fish via oral vaccination. *Vaccine* (2015) 33(27):3092–9. doi: 10.1016/j.vaccine.2015.05.002
65. Liu Z, Wu J, Ma Y, Hao L, Liang Z, Ma J, et al. Protective immunity against CyHV-3 infection via different prime-boost vaccination regimens using CyHV-3 ORF131-based DNA/protein subunit vaccines in carp *Cyprinus carpio* var. Jian. *Fish Shellfish Immunol* (2020) 98:342–53. doi: 10.1016/j.fsi.2020.01.034
66. Ma Y, Liu Z, Hao L, Wu J, Qin B, Liang Z, et al. Oral vaccination using Artemia coated with recombinant *Saccharomyces cerevisiae* expressing cyprinid herpesvirus-3 envelope antigen induces protective immunity in common carp (*Cyprinus carpio* var. Jian) larvae. *Res Vet Sci* (2020) 130:184–92. doi: 10.1016/j.rvsc.2020.03.013
67. Sato A, Okamoto N. Induction of virus-specific cell-mediated cytotoxic responses of isogeneic ginbuna crucian carp, after oral immunization with inactivated virus. *Fish Shellfish Immunol* (2010) 29(3):414–21. doi: 10.1016/j.fsi.2010.04.017
68. Xue R, Liu L, Cao G, Xu S, Li J, Zou Y, et al. Oral vaccination of BacFish-vp6 against grass carp reovirus evoking antibody response in grass carp. *Fish Shellfish Immunol* (2013) 34(1):348–55. doi: 10.1016/j.fsi.2012.11.024
69. Bøgwald J, Dalmo RA. Review on immersion vaccines for fish: an update 2019. *Microorganisms* (2019) 7(12):627. doi: 10.3390/microorganisms7120627
70. Sudheesh PS, Cain KD. Optimization of efficacy of a live attenuated *Flavobacterium psychrophilum* immersion vaccine. *Fish Shellfish Immunol* (2016) 56:169–80. doi: 10.1016/j.fsi.2016.07.004
71. Raida MK, Nylén J, Holten-Andersen L, Buchmann K. Association between plasma antibody response and protection in rainbow trout *Oncorhynchus mykiss* immersion vaccinated against *Yersinia ruckeri*. *PLoS One* (2011) 6(6):e18832. doi: 10.1371/journal.pone.0018832
72. Chettri JK, Jaafar RM, Skov J, Kania PW, Dalsgaard I, Buchmann K. Booster immersion vaccination using diluted *Yersinia ruckeri* bacterin confers protection against ERM in rainbow trout. *Aquaculture* (2015) 440:1–5. doi: 10.1016/j.aquaculture.2015.01.027
73. Deshmukh S, Kania PW, Chettri JK, Skov J, Bojesen AM, Dalsgaard I, et al. Insight from molecular, pathological, and immunohistochemical studies on cellular and humoral mechanisms responsible for vaccine-induced protection of rainbow trout against *Yersinia ruckeri*. *Clin Vaccine Immunol* (2013) 20(10):1623–41. doi: 10.1128/CVI.00404-13
74. Ma J, Bruce TJ, Sudheesh PS, Knupp C, Loch TP, Faisal M, et al. Assessment of cross-protection to heterologous strains of *Flavobacterium psychrophilum* following vaccination with a live-attenuated coldwater disease immersion vaccine. *J Fish Dis* (2019) 42(1):75–84. doi: 10.1111/jfd.12902
75. Hoare R, Ngo TPH, Bartie KL, Adams A. Efficacy of a polyvalent immersion vaccine against *Flavobacterium psychrophilum* and evaluation of immune response to vaccination in rainbow trout fry (*Onchorynchus mykiss* L.). *Vet Res* (2017) 48(1):43. doi: 10.1186/s13567-017-0448-z
76. Angelidis P, Karagiannis D, Crump EM. Efficacy of a *Listonella anguillarum* (syn. *Vibrio anguillarum*) vaccine for juvenile sea bass *Dicentrarchus labrax*. *Dis Aquat Organ* (2006) 71(1):19–24. doi: 10.3354/dao071019
77. Zhang Z, Wu H, Xiao J, Wang Q, Liu Q, Zhang Y. Immune responses evoked by infection with *Vibrio anguillarum* in zebrafish bath-vaccinated with a live attenuated strain. *Vet Immunol Immunopathol* (2013) 154(3-4):138–44. doi: 10.1016/j.vetimm.2013.05.012
78. Solbakken MH, Jentoft S, Reitan T, Mikkelsen H, Jakobsen KS, Seppola M. Whole transcriptome analysis of the Atlantic cod vaccine response reveals subtle changes in adaptive immunity. *Comp Biochem Phys D* (2019) 31:100597. doi: 10.1016/j.cbd.2019.100597
79. Du Y, Tang X, Sheng X, Xing J, Zhan W. The influence of concentration of inactivated *Edwardsiella tarda* bacterin and immersion time on antigen uptake and expression of immune-related genes in Japanese flounder (*Paralichthys olivaceus*). *Microb Pathog* (2017) 103:19–28. doi: 10.1016/j.micpath.2016.12.011
80. Aonullah AA, Nuryati S, Alimuddin, Murtini S. Efficacy of koi herpesvirus DNA vaccine administration by immersion method on *Cyprinus carpio* field scale culture. *Aquac Res* (2017) 48(6):2655–62. doi: 10.1111/are.13097
81. Zhang C, Zheng Y-Y, Gong Y-M, Zhao Z, Guo Z-R, Jia Y-J, et al. Evaluation of immune response and protection against spring viremia of carp virus induced by a single-walled carbon nanotubes-based immersion DNA vaccine. *Virology* (2019) 537:216–25. doi: 10.1016/j.virol.2019.09.002
82. Zhao Z, Zhang C, Jia YJ, Qiu DK, Lin Q, Li NQ, et al. Immersion vaccination of Mandarin fish *Siniperca chuatsi* against infectious spleen and kidney necrosis virus with a SWCNTs-based subunit vaccine. *Fish Shellfish Immunol* (2019) 92:133–40. doi: 10.1016/j.fsi.2019.06.001
83. Das PK, Salinas I. Fish nasal immunity: From mucosal vaccines to neuroimmunology. *Fish Shellfish Immunol* (2020) 104:165–71. doi: 10.1016/j.fsi.2020.05.076

84. LaPatra S, Kao S, Erhardt EB, Salinas I. Evaluation of dual nasal delivery of infectious hematopoietic necrosis virus and enteric red mouth vaccines in rainbow trout (*Oncorhynchus mykiss*). *Vaccine* (2015) 33(6):771–6. doi: 10.1016/j.vaccine.2014.12.055
85. Salinas I, LaPatra SE, Erhardt EB. Nasal vaccination of young rainbow trout (*Oncorhynchus mykiss*) against infectious hematopoietic necrosis and enteric red mouth disease. *Dev Comp Immunol* (2015) 53(1):105–11. doi: 10.1016/j.dci.2015.05.015
86. Chen L, Evensen Ø, Mutoloki S. IPNV antigen uptake and distribution in Atlantic salmon following oral administration. *Viruses* (2015) 7(5):2507–17. doi: 10.3390/v7052507
87. Martín-Martín A, Simón R, Abós B, Díaz-Rosales P, Tafalla C. Rainbow trout mount a robust specific immune response upon anal administration of thymus-independent antigens. *Dev Comp Immunol* (2020) 109:103715. doi: 10.1016/j.dci.2020.103715
88. Cain KD, Jones DR, Raison RL. Characterisation of mucosal and systemic immune responses in rainbow trout (*Oncorhynchus mykiss*) using surface plasmon resonance. *Fish Shellfish Immunol* (2000) 10(8):651–66. doi: 10.1006/fsim.2000.0280
89. Joosten PHM, Kruijer WJ, Rombout JHWM. Anal immunisation of carp and rainbow trout with different fractions of a *Vibrio anguillarum* bacterin. *Fish Shellfish Immunol* (1996) 6(8):541–51. doi: 10.1006/fsim.1996.0051
90. Tajimi S, Kondo M, Nakanishi T, Nagasawa T, Nakao M, Somamoto T. Generation of virus-specific CD8(+) T cells by vaccination with inactivated virus in the intestine of ginbuna crucian carp. *Dev Comp Immunol* (2019) 93:37–44. doi: 10.1016/j.dci.2018.12.009
91. Rombout JW, Blok LJ, Lamers CH, Egberts E. Immunization of carp (*Cyprinus carpio*) with a *Vibrio anguillarum* bacterin: indications for a common mucosal immune system. *Dev Comp Immunol* (1986) 10(3):341–51. doi: 10.1016/0145-305x(86)90024-8
92. Palm RCJr., Landolt ML, Busch RA. Route of vaccine administration: effects on the specific humoral response in rainbow trout *Oncorhynchus mykiss*. *Dis Aquat Organ* (1998) 33(3):157–66. doi: 10.3354/dao033157
93. Vervarcke S, Ollevier F, Kinget R, Michoel A. Mucosal response in African catfish after administration of *Vibrio anguillarum* O2 antigens via different routes. *Fish Shellfish Immunol* (2005) 18(2):125–33. doi: 10.1016/j.fsi.2004.06.004
94. Crosbie PB, Nowak BF. Immune responses of barramundi, *Lates calcarifer* (Bloch), after administration of an experimental *Vibrio harveyi* bacterin by intraperitoneal injection, anal intubation and immersion. *J Fish Dis* (2004) 27(11):623–32. doi: 10.1111/j.1365-2761.2004.00575.x
95. Esteve-Gassent MD, Fouz B, Amaro C. Efficacy of a bivalent vaccine against eel diseases caused by *Vibrio vulnificus* after its administration by four different routes. *Fish Shellfish Immunol* (2004) 16(2):93–105. doi: 10.1016/s1050-4648(03)00036-6
96. Makesh M, Sudheesh PS, Cain KD. Systemic and mucosal immune response of rainbow trout to immunization with an attenuated *Flavobacterium psychrophilum* vaccine strain by different routes. *Fish Shellfish Immunol* (2015) 44(1):156–63. doi: 10.1016/j.fsi.2015.02.003
97. Villumsen KR, Neumann L, Ohtani M, Strøm HK, Raida MK. Oral and anal vaccination confers full protection against enteric redmouth disease (ERM) in rainbow trout. *PLoS One* (2014) 9(4):e93845. doi: 10.1371/journal.pone.0093845
98. Qadiri SSN, Makesh M, Rajendran KV, Rathore G, Purushothaman CS. Specific immune response in mucosal and systemic compartments of *Cirrhinus mrigala* vaccinated against *Edwardsiella tarda: in vivo* kinetics using different antigen delivery routes. *J World Aquac Soc* (2019) 50(4):856–65. doi: 10.1111/jwas.12584
99. Adelmann M, Köllner B, Bergmann SM, Fischer U, Lange B, Weitschies W, et al. Development of an oral vaccine for immunisation of rainbow trout (*Oncorhynchus mykiss*) against viral haemorrhagic septicaemia. *Vaccine* (2008) 26(6):837–44. doi: 10.1016/j.vaccine.2007.11.065
100. Kole S, Qadiri SSN, Shin SM, Kim WS, Lee J, Jung SJ. PLGA encapsulated inactivated-viral vaccine: formulation and evaluation of its protective efficacy against viral haemorrhagic septicaemia virus (VHSV) infection in olive flounder (*Paralichthys olivaceus*) vaccinated by mucosal delivery routes. *Vaccine* (2019) 37(7):973–83. doi: 10.1016/j.vaccine.2018.12.063
101. Kole S, Qadiri SSN, Shin SM, Kim WS, Lee J, Jung SJ. Nanoencapsulation of inactivated-viral vaccine using chitosan nanoparticles: evaluation of its protective efficacy and immune modulatory effects in olive flounder (*Paralichthys olivaceus*) against viral haemorrhagic septicaemia virus (VHSV) infection. *Fish Shellfish Immunol* (2019) 91:136–47. doi: 10.1016/j.fsi.2019.05.017
102. Kai YH, Wu YC, Chi SC. Immune gene expressions in grouper larvae (*Epinephelus coioides*) induced by bath and oral vaccinations with inactivated betanodavirus. *Fish Shellfish Immunol* (2014) 40(2):563–9. doi: 10.1016/j.fsi.2014.08.005
103. Savelkoul HF, Ferro VA, Strioga MM, Schijns VE. Choice and design of adjuvants for parenteral and mucosal vaccines. *Vaccines (Basel)* (2015) 3 (1):148–71. doi: 10.3390/vaccines3010148
104. Lee SE, Kim SY, Jeong BC, Kim YR, Bae SJ, Ahn OS, et al. A bacterial flagellin, *Vibrio vulnificus* FlaB, has a strong mucosal adjuvant activity to induce protective immunity. *Infect Immun* (2006) 74(1):694–702. doi: 10.1128/iai.74.1.694-702.2006
105. Embregts CWE, Rigaudeau D, Tacchi L, Pijlman GP, Kampers L, Veselý T, et al. Vaccination of carp against SVCV with an oral DNA vaccine or an insect cells-based subunit vaccine. *Fish Shellfish Immunol* (2019) 85:66–77. doi: 10.1016/j.fsi.2018.03.028
106. Martín-Martín A, Tejedor L, Tafalla C, Díaz-Rosales P. Potential of the *Escherichia coli* LT(R192G/L211A) toxoid as a mucosal adjuvant for rainbow trout (*Oncorhynchus mykiss*). *Fish Shellfish Immunol* (2020) 105:310–8. doi: 10.1016/j.fsi.2020.07.016
107. Wang Y, Wang X, Huang J, Li J. Adjuvant effect of *Quillaja saponaria* saponin (QSS) on protective efficacy and IgM generation in turbot (*Scophthalmus maximus*) upon immersion vaccination. *Int J Mol Sci* (2016) 17(3):325. doi: 10.3390/ijms17030325
108. Galindo-Villegas J, Mulero I, García-Alcazar A, Muñoz I, Peñalver-Mellado M, Streitenberger S, et al. Recombinant TNFα as oral vaccine adjuvant protects European sea bass against vibriosis: insights into the role of the CCL25/CCR9 axis. *Fish Shellfish Immunol* (2013) 35(4):1260–71. doi: 10.1016/j.fsi.2013.07.046
109. Petit J, Wiegertjes GF. Long-lived effects of administering β-glucans: indications for trained immunity in fish. *Dev Comp Immunol* (2016) 64:93–102. doi: 10.1016/j.dci.2016.03.003
110. Yan Y, Huo X, Ai T, Su J. β-glucan and anisodamine can enhance the immersion immune efficacy of inactivated cyprinid herpesvirus 2 vaccine in *Carassius auratus gibelio*. *Fish Shellfish Immunol* (2020) 98:285–95. doi: 10.1016/j.fsi.2020.01.025
111. Wangkahart E, Secombes CJ, Wang T. Studies on the use of flagellin as an immunostimulant and vaccine adjuvant in fish aquaculture. *Front Immunol* (2018) 9:3054. doi: 10.3389/fimmu.2018.03054
112. Tonetti FR, Islam MA, Vizoso-Pinto MG, Takahashi H, Kitazawa H, Villena J. Nasal priming with immunobiotic lactobacilli improves the adaptive immune response against influenza virus. *Int Immunopharmacol* (2020) 78:106115. doi: 10.1016/j.intimp.2019.106115
113. Zelaya H, Álvarez S, Kitazawa H, Villena J. Respiratory antiviral immunity and immunobiotics: beneficial effects on inflammation-coagulation interaction during influenza virus infection. *Front Immunol* (2016) 7:633. doi: 10.3389/fimmu.2016.00633
114. Fuglem B, Jirillo E, Bjerkås I, Kiyono H, Nochi T, Yuki Y, et al. Antigen-sampling cells in the salmonid intestinal epithelium. *Dev Comp Immunol* (2010) 34(7):768–74. doi: 10.1016/j.dci.2010.02.007
115. Kato G, Miyazawa H, Nakayama Y, Ikari Y, Kondo H, Yamaguchi T, et al. A Novel antigen-sampling cell in the teleost gill epithelium with the potential for direct antigen presentation in mucosal tissue. *Front Immunol* (2018) 9:2116. doi: 10.3389/fimmu.2018.02116


**Conflict of Interest:** The authors declare that the research was conducted in the absence of any commercial or financial relationships that could be construed as a potential conflict of interest.

frontiers in Immunology

ORIGINAL RESEARCH
published: 19 February 2021
doi: 10.3389/fimmu.2020.623726

# Nutrient Digestibility, Growth, Mucosal Barrier Status, and Activity of Leucocytes From Head Kidney of Atlantic Salmon Fed Marine- or Plant-Derived Protein and Lipid Sources

*Solveig L. Sørensen[1], Youngjin Park[1], Yangyang Gong[1,2†], Ghana K. Vasanth[1†], Dalia Dahle[1], Kjetil Korsnes[1,3], Tran Ha Phuong[1], Viswanath Kiron[1], Sjur Øyen[4], Karin Pittman[4,5] and Mette Sørensen[1*]*

[1] Faculty of Biosciences and Aquaculture, Nord University, Bodø, Norway, [2] Key Laboratory of East China Sea Fishery Resources Exploitation, Ministry of Agriculture, East China Sea Fisheries Research Institute, Chinese Academy of Fishery Sciences, Shanghai, China, [3] BioVivo Technologies AS, Bodø, Norway, [4] Department of Biosciences, University of Bergen, Bergen, Norway, [5] Quantidoc AS, Bergen, Norway

OPEN ACCESS

**Edited by:**
*Min Wan,*
*Ocean University of China, China*

**Reviewed by:**
*Kim Dawn Thompson,*
*Moredun Research Institute, United Kingdom*
*Zhigang Zhou,*
*Feed Research Institute (CAAS), China*

***Correspondence:**
*Mette Sørensen*
*mette.sorensen@nord.no*

**†Present addresses:**
*Yangyang Gong,*
*Zhejiang NHU Co., Ltd, Xinchang, China*
*Ghana K. Vasanth,*
*Cermaq Norway AS, Nordfold, Norway*

**Specialty section:**
*This article was submitted to Comparative Immunology, a section of the journal Frontiers in Immunology*

**Received:** *30 October 2020*
**Accepted:** *31 December 2020*
**Published:** *19 February 2021*

**Citation:**
*Sørensen SL, Park Y, Gong Y, Vasanth GK, Dahle D, Korsnes K, Phuong TH, Kiron V, Øyen S, Pittman K and Sørensen M (2021) Nutrient Digestibility, Growth, Mucosal Barrier Status, and Activity of Leucocytes From Head Kidney of Atlantic Salmon Fed Marine- or Plant-Derived Protein and Lipid Sources. Front. Immunol. 11:623726. doi: 10.3389/fimmu.2020.623726*

Nutrient digestibility, growth, and mucosal barrier status of fish skin, gills, and distal intestine were studied in Atlantic salmon fed feeds based on marine or plant-derived ingredients. The barrier status was assessed by considering the expression of four mucin genes, five genes that encode antimicrobial proteins, distal intestine micromorphology, and design-based stereology of the midgut epithelium. In addition, the head kidney leukocytes were examined using flow cytometry; to understand the differences in their counts and function. Five experimental feeds containing the main components i) fishmeal and fish oil (BG1), ii) soybean meal (BG2; to induce enteritis), iii) fishmeal as the main protein source and rapeseed oil as the main lipid source (BG3), iv) a mix of plant protein concentrates as the protein sources and fish oil as the lipid source (BG4), and v) plant and marine ingredients in the ratio 70:30 (BG5) were produced for the study. Atlantic salmon with initial weight 72.7 ± 1.2 g was offered the experimental feeds for 65 days. The results revealed that the weights of all fish groups doubled, except for fish fed BG2. Fish fed the BG2 diet had lower blood cholesterol concentration, developed enteritis, had lower expression of *muc2* in the distal intestine, and had a compromised barrier status in the intestine. Expression of both the mucin genes and genes that encode antimicrobial peptides were tissue-specific and some were significantly affected by diet. The fish fed BG1 and BG3 had more head kidney lymphocyte-like cells compared to BG5-fed fish, and the phagocytic activity of macrophage-like cells from the head kidney was the highest in fish fed BG1. The intestinal micromorphology and the mucosal mapping suggest two different ways by which plant-based diets can alter the gut barrier status; by either reducing the mucous cell sizes, volumetric densities and barrier status (as noted for BG2)

or increasing volumetric density of mucous cells (as observed for BG4 and BG5). The results of the compromised intestinal barrier in fish fed plant ingredients should be further confirmed through transcriptomic and immunohistochemical studies to refine ingredient composition for sustainable and acceptable healthy diets.

**Keywords: Atlantic salmon, enteritis, mucosal barrier status, plant ingredients, mucin gene, antimicrobial genes, stereology, distal intestine**

## INTRODUCTION

Mucosal surfaces of fishes, the skin, gills, and gastrointestinal tract, are important barriers that protect the host from pathogens and infections. The barriers include a mucosal epithelium which is covered by mucus and a wide range of components such as antimicrobial peptides that inhibit the entry of pathogens (1, 2). Mucus contains O-glycosylated proteins called mucins, and the expression of mucin genes in fish is altered by parasite infection (3) and fish density- and handling-related stress (4). The mucin glycosylation itself plays a key role in disease resistance in fish (5) and is affected both by the origin and size of Atlantic salmon (6). Antimicrobial peptides (AMPs) are also important components of the innate immune system in fish (2). The AMPs are classified into different families which show broad-spectrum antimicrobial activity to overcome the different resistance mechanisms activated by microbial organisms (2, 7, 8). The innate immune system plays a key role in keeping fish healthy in intensive aquaculture systems, especially the components at the semipermeable mucosal epithelia in the gut (9–11). Dietary interventions are known to strengthen the intestinal barrier in mice and humans, thereby allowing the organ to carry out its intended functions (12). However, little information is available as to how the intensive production systems and use of modern diets affect the gut barrier function of fishes.

Modern diets are formulated on the presumption that fish do not have a need for specific ingredients, but combinations of different ingredients can help meet the nutrient requirements of the farmed species. Fishmeal (FM) and fish oil (FO) are still considered to be the gold standard feed ingredients. However, their use in commercial fish feeds is reduced to a minimum because of static supply, increasing demand resulting in increasing prices and debates about sustainability when fish is used to feed fish. Commercial feeds used in Norwegian salmon farming are based on plant-derived products, which constitute 71% of the feed ingredients, while the marine feed ingredients is reduced to approximately ~25% (13). Soy protein concentrate has become the key protein source and rapeseed oil the primary oil source in present-day salmon feeds (13, 14). However, these ingredients have certain drawbacks. Feeding rapeseed oil is known to affect the n-3/n-6 ratio in the fillets of farmed salmon. Use of plant products with unfavourable n-6/n-3 ratio or diets without eicosapentaenoic acid (EPA) may bring about histomorphological changes in the intestine and can reduce fish growth (15, 16). Many studies have shown that the intestinal structure, microbiota and ion and water transport of Atlantic salmon are affected by the feed ingredients (17–19). However, further research is needed to understand the effect of feed ingredients on the immune defense of the fish, especially at the intestinal level.

Most studies have employed fishmeal-based diets to evaluate the impact of plant ingredients on salmon; the researchers have replaced either fishmeal with plant protein or fish oil with plant oil. Few studies have investigated the effect of different combinations of protein and oil derived from marine and plant origin on the growth and health of the fish. The aim of this study was to investigate the combined effect of replacing marine proteins and lipids with a mixture of plant-derived protein concentrates and oil on growth, nutrient digestibility, mucosal barrier status and systemic immune responses. The barrier status was assessed based on the expression of mucin genes in the skin, gills, and distal intestine, the expression of genes that encode antimicrobial proteins in the skin and distal intestine, histological changes in the distal intestine and information from design-based stereology of the midgut epithelium. Stereology was used to evaluate the mucosal barrier function because this type of mucosal mapping is more sensitive and independent of section orientation (11, 20). Furthermore, to understand the systemic effect, head kidney leukocytes were examined using flow cytometry.

## MATERIAL AND METHODS

### Experimental Design and Feeds

The study used five experimental diets: a control diet (BG1) based on fishmeal and fish oil; a diet containing 20% soybean meal and 30% fishmeal and fish oil (BG2); a diet with fishmeal and rapeseed oil (BG3); a diet based on a mix of plant protein concentrates as the main protein source (soy protein concentrate, pea protein concentrate and corn gluten meal) and fish oil (BG4); and one diet resembling a commercial diet with the same protein ingredients as in BG4 and a mix of rapeseed oil and fish oil (BG5; **Table 1**). All diets were supplemented with crystalline amino acids (lysine, histidine, methionine and threonine) and inorganic phosphate (**Table 1** and **Supplementary Table 1**). Diets also contained 0.01% yttrium oxide as an inert marker for digestibility measurements.

The five feed mixes were prepared and homogenized (30 min) using a horizontal ribbon mixer. The feed mixes were conditioned with steam and water in an atmospheric double differential preconditioner (DDC) prior to extrusion in a TX-52 co-rotating, fully intermeshing twin-screw extruder (Wenger Manufacturing Inc., Sabetha, KS, USA). The temperature of

**TABLE 1** | Ingredient composition (%) of the experimental feeds.

| | BG1 | BG2 | BG3 | BG4 | BG5 |
|---|---|---|---|---|---|
| Fishmeal | 50 | 30 | 50 | 10 | 10 |
| Wheat meal | 13.85 | 6.55 | 13.85 | 6.05 | 6.05 |
| Wheat gluten | 5 | 10 | 5 | 10 | 10 |
| Soy protein concentrate | 0 | 0 | 0 | 20 | 20 |
| Soybean meal | 0 | 20 | 0 | 0 | 0 |
| Corn Gluten | 0 | 0 | 0 | 9 | 9 |
| Pea protein concentrate | 0 | 0 | 0 | 9 | 9 |
| Fish oil | 25 | 26.4 | 3.8 | 27.5 | 7.7 |
| Rapeseed oil | 0 | 0 | 21.2 | 0 | 19.8 |
| Mineral premix | 0.59 | 0.59 | 0.59 | 0.59 | 0.59 |
| Vitamin premix | 2 | 2 | 2 | 2 | 2 |
| Monosodium Phosphate | 2.5 | 2.5 | 2.5 | 2.5 | 2.5 |
| Carop. Pink (10% Astax) | 0.05 | 0.05 | 0.05 | 0.05 | 0.05 |
| Yttrium oxide | 0.01 | 0.01 | 0.01 | 0.01 | 0.01 |
| Choline | 0.5 | 0.5 | 0.5 | 0.5 | 0.5 |
| Methionine | 0.3 | 0.6 | 0.3 | 0.9 | 0.9 |
| Lysine | 0 | 0.5 | 0 | 1.2 | 1.2 |
| Threonine | 0 | 0.1 | 0 | 0.4 | 0.4 |
| Histidine | 0.2 | 0.2 | 0.2 | 0.3 | 0.3 |

the feed mash entering the extruder was 86–88°C. Temperature at the extruder outlet were 120°C for BG1 and BG3, 128°C for BG2 and 137°C for BG4 and BG5. Three of the diets, BG2, BG4, and BG5 had lower wheat content in the recipe, and hence more moisture was added as heat into the DDC to ensure expansion. The extruder outlet had 24 circular 2.5 mm die holes. The wet extrudates were cut at the die surface with a rotating knife. To ensure the pellet quality, pellet samples were visually inspected after achievement of steady state conditions in the preconditioner and extruder. The extrudate was dried in a hot air dual layer carousel dryer (Paul Klockner, Nistertal, Germany) at a constant air temperature (77°C) to obtain final products of approximately 7–8% moisture. Then each of the diets were coated with oil in an experimental vacuum coater (Pegasus PG-10VC LAB, Dinnissen B.V., Netherlands). Immediately after coating, diets were packed in sealed plastic buckets and shipped to the research site.

## Fish and Feeding

Atlantic salmon (*Salmo salar*) post-smolts were obtained from Cermaq, Hopen, Bodø, Norway (Aquagen strain, Aquagen AS, Trondheim, Norway) and maintained at the Research Station, Nord University, Bodø, Norway. At the start of the experiment, a total of 1100 fish (initial weight 72.7 ± 1.4 g) (mean ± SD) were randomly allocated to 20 experimental units (n = 4 tanks per treatment group).

The feeding experiment was carried out in a flow-through system. In total, 20 circular fiberglass tanks (1100 L) were used for the study. Each tank was supplied with water pumped from a depth of 250 m from Saltenfjorden. During the experiment, water flow rate was maintained at 1000 L per hour, and the average temperature and salinity of the rearing water were 7.6°C and 35‰, respectively. Oxygen saturation was always above 85% measured at the water outlet. A 24-h photoperiod was maintained throughout the experimental period. The fish were fed *ad libitum* using automatic feeders (Arvo Tech, Finland) for 12 h per day from 08:00–20:00 (divided into eight feedings: 08:00–10:00, 10:00–12:00, 12:00–14:00, 14:00–16:00, 16:00–18:00, 18:00–19:00, and 19:00–20:00) during the 65-day feeding trial.

## Fish Sampling and Data Collection

At the beginning and end of the experiment, all fish (1100) were individually weighed, and their total lengths recorded. Before handling, fish were anesthetized using tricainemethanesulfonate (MS 222, 140 mg/L). Feces for digestibility determination was obtained by stripping individual fish. Feces from all individuals from a tank were pooled into one sample to obtain a value from a particular tank. The fecal samples that were immediately transferred to -20°C were used for further analyses.

For the histology and design-based stereology studies, distal intestine and mid intestine samples, respectively were collected as described in our previous publications (20–24). In addition, skin, gill and distal intestine samples were obtained for the gene expression analysis, and our standard protocols (21–23) were used in the present study also. For the cell study, the head kidney (HK) was collected at the end of experiment. These tissues were immediately transferred to 15 ml tubes to make a total volume of 4 ml in ice-cold Leibovitz's L-15 Medium (L-15; Sigma-Aldrich, Oslo, Norway), supplemented with 100 µg/ml gentamicin sulphate (Sigma), 2 mM L-glutamine (Sigma), and 15mM HEPES (Sigma).

## Biochemical and Cholesterol Analyses

Frozen fecal samples were freeze dried (VirTis benchtop, U.S.A.) for 72 h at -76°C and at a pressure of 20 bar. The moisture, protein, lipid, ash, energy and yttrium contents of the feed and freeze-dried feces were determined as described in Sørensen et al. (22). Blood was drawn from the caudal vein of 12 fish/feed, into lithium heparin vacutainers and immediately spun at 703.2 x *g* for 10 min at 4°C. Cholesterol level in the plasma was measured by application of 115 µl plasma to a T4/Cholesterol rotor cassette (Profile #500-0037, Abaxis, CA, US), and analyzed by a VETSCAN Chemistry Analyzer (VETSCAN VS2, Abaxis, CA, US). Cholesterol was only analyzed in fish from BG1-BG4 due to lack of cassettes to analyze fish from BG5.

## Mucosal Mapping

Samples for mucosal mapping with design-based stereology were collected at the end of the feeding experiment (day 65). Approximately 2 cm of the anterior part of the mid intestine from four fish (three tanks per diet group) were collected for this study—in total 12 samples per diet group. Luminal contents were first rinsed out with 10% neutral buffered formalin, and then the tissues were fixed in 10% formalin for 48 h. The fixed samples were dehydrated in an alcohol gradient, equilibrated in xylene and embedded in paraffin blocks. Approximately, 5 µm thick longitudinal sections were cut using a microtome and mounted onto a glass slide. The sections were stained with Alcian Blue pH 2.5—Periodic Acid Schiff's reagent (25) and mounted with Pertex medium.

All slides were scanned in batches using a Hamamatsu NanoZoomer S60 with a source lens; at 40x magnification and saved as high-resolution digital images in NDPI-format. The digital files were examined using NDP.view 2.6.8 (Free edition, Hamamatsu Photonics K.K. 2016). Mucosal mapping of the digitized slides was performed using the MucoMaster2 (Quantidoc AS, 2019) software according to Pittman et al. (26, 27). Blinded stereological analysis was done, maintaining the anonymity of the diet groups until the completion of the analysis. Regions of interest were manually drawn over the mucosal folds and lamina propria of each fish midgut. An unbiased selection of about 100 mucosal cells was performed to carry out the measurements for each slide as described in Pittman et al. (26) Epithelial area and mucous cell area were measured using stereological probes, followed by counting of mucous cells. Mean area of the mucous cells and percentage of epithelial with mucous cells were exported to Microsoft Excel for Office 20 365 MSO version 1908 (Microsoft Corporation, 2019). The barrier status as described in Dang et al. (20) was calculated using the mean mucous area, mucous number and epithelial area.

## Distal Intestinal Micromorphology

Sections of the distal intestine were prepared as described under *Mucosal Mapping*. Slides were examined using microscope Olympus BX51 at 100x total magnification and photomicrographs were captured employing Camera SC180 (Olympus Europa GmbH, Hamburg, Germany) and processed using the imaging software CellEntry (Soft Imaging System GmbH, Munster, Germany).

## Gene Expression Analysis

Tissues for gene expression analysis were sampled from the second gill arch (left side of the fish), skin (below dorsal fin), and distal intestine of 16 fish per diet group (four fish per tank). These tissues were immediately placed in tubes filled with RNA later® (Ambion Inc., Austin, Texas, United States), and stored at -20°C until further analysis.

The relative mRNA levels of mucin genes (*muc2*, *muc5ac1*, *muc5ac2*, and *muc5b*) in the distal intestine, skin and gills and antimicrobial protein genes (*defensin 1 - def1; defensin 2 - def2, defensin 3 - def3, defensin 4 - def4;cathelicidin 1 - cathl1*) in the distal intestine and skin were examined in this study. The primer sequences for all target and reference genes are presented in **Supplementary Table 2**. Primers were purchased from Eurofins Genomics (Luxembourg, Luxembourg).

RNA was extracted from the samples using E-Z 96 Total RNA Kit (Omega Bio-Tek, USA). Roughly 100 mg of the tissue sample was removed from RNA later® and homogenized using Zirconium oxide beads (1.4 mm; Percellys, Tarnos, France) and TRK lysis buffer in a capped free standing tube (VWR International, Oslo, Norway) at 6000 rpm. The resulting mixture was centrifuged (18,000 × g, 20°C) to obtain a clear supernatant. Briefly, 300 µl supernatant was added to 300 µl of 70% ethanol and mixed, before this mixture was added to the E-Z 96 RNA plate which contains an RNA HiBind® matrix in each well. Centrifugation (3000 rpm, 15 min) was used to draw the sample through the well, followed by several steps of buffer washes according to the kit instructions. Finally, the purified RNA was obtained by adding 65–75 µl of RNase-free water (5 Prime GmbH, Hilden, Germany) to each well and a final centrifugation.

Extracted RNA was quantified by Qubit™ RNA broad-range assay kit (Life Technologies, Carlsbad, USA) on a Qubit 3.0 Fluorometer (Life Technologies, Carlsbad, USA) and diluted with RNase-free water if necessary. cDNA synthesis was done with QuantiTect™ Reverse Transcription Kit (Quiagen GmbH, Hilden, Germany) employing 1000 ng of RNA and a reaction volume of 20 µl per sample, according to the manufacturer's instructions. The cDNA samples were diluted with nuclease free water by a factor of 10 before continuing with qPCR.

The qPCR was performed on a LightCycler® 96 (Roche Life Science) using Fast SYBR® Green Real-Time PCR Master Mix (Applied Biosystems, Carlsbad, USA). Each reaction contained 5 µl of Fast SYBR® Green PCR Master Mix, 1 µl primer mix (200 nM), and 4 µl cDNA (0.5 ng/µl). Reactions (n = 16 per diet) were performed in duplicate. Thermal cycling conditions were: initial holding at 95°C for 20 s, 40 cycles of denaturation at 95°C (3 s), and annealing/extension at 60°C (30 s).

A standard curve with known concentrations was prepared for each primer in order to calculate the gene expression. This was done by pooling RNA from every sample, reverse transcribing the pooled RNA as described above, and using the resulting cDNA to create a 6-point threefold dilution series. The equation E = (10^(−1/m)− 1) *100 was used to calculate the efficiency of the primers; E, efficiency and m, slope of the standard curve (**Supplementary Table 2**). Using geNorm (28) a normalization factor was computed for each sample based on the relative quantities of the two most stable genes from among the set of four reference genes, namely elongation factor 1AB (*ef1ab*), ribosomal protein L13 (*rpl13*), ribosomal protein S29 (*rps29*), and ubiquitin (*ubi*). The expression levels of all the target genes were calculated relative to the normalization factor.

## Head Kidney Leucocytes

Head kidney (HK) cells (six fish/group) were harvested employing the protocols described for Atlantic salmon HK cells (29). The leucocyte fraction was employed for analysis of the lymphocyte counts. The monocyte/macrophage fraction was allowed to adhere on a petri dish for 3 days at 12°C. The adherent cells were detached by washing three times with 1.5 ml ice-cold phosphate-buffered saline (PBS) supplemented with 5mM EDTA (Sigma), and centrifuged at 500 × g for 5 min at 4°C. The cells were counted using a portable cell counter (Scepter™ 2.0 cell counter, EMD Millipore, Darmstadt, Germany). The flow cytometric analyses were performed as described by Park et al. (29), employing ImageStream®X Mk II Imaging Flow Cytometer (Luminex Corporation, Austin, TX, USA). Cell analyses were performed on 20,000 cells; lymphocyte-like cell population was determined based on the positivity of cells to salmon IgM while other cell populations (monocyte/macrophages) were identified based on morphological characteristics (29). Phagocytosis was studied using fluorescent bio-particles designed for flow cytometry, as detailed in our previous publication (29). Phagocytic ability and phagocytic capacity are presented to indicate phagocytosis; the former parameter is the percent of phagocytic cells, and the latter one is calculated as the mean number of particles per phagocytic cell.

## Calculations and Statistical Analysis

Fish growth performance was analyzed using the following equations.

$$\text{Weight gain}(\%) = \left(\frac{W_f - W_i}{W_i}\right) \times 100$$

Where Wf = final body weight of fish (g/fish) and Wi = initial body weight of fish (g/fish)

$$\text{Specific Growth Rate } (\%\ day^{-1}) = \left(\frac{\text{Ln } (W_f) - \text{Ln } (W_i)}{\text{No.of feeding days}}\right) \times 100$$

$$\text{Thermal growth coefficient (TGC)} = \frac{(W_f)^{1/3} - (W_i)^{1/3}}{(T \times d)} \times 1000$$

where T is the temperature in °C and d is time in days.

Apparent Digestibility Coefficient (ADC) of nutrients and dry matter were calculated according to following equations:

$$ADC_{nutrient} = \left[1 - \left(\frac{Marker_{feed} \times Nutrient_{feces}}{Marker_{feces} \times Nutritent_{feed}}\right)\right] \times 100$$

$$ADC_{\ dry\ matter} = \left[1 - \left(\frac{Marker_{feed}}{Marker_{feces}}\right)\right] \times 100$$

where $Marker_{feed}$ and $Marker_{feces}$ represent the marker content (% dry matter) of the feed and feces, respectively, and $Nutrient_{feed}$ and $Nutrient_{feces}$ represent the nutrient contents (% dry matter) in the feed and feces, respectively. Tank was used as the experimental unit.

The mucous cell-based barrier status was calculated using the following formula:

$$\left[\frac{1}{Mucous\ cell\ area \Big/ \left[Mucous\ cell\ area\ x\ mucous\ number \Big/ Epithelial\ area \times 100\right]}\right] \times 1000$$

Statistical analyses were performed using SPSS 22.0 software and R packages for Windows. The data were tested for normality (Shapiro–Wilk normality test) and equality of variance (Levene's test). For parametric data, one way analysis of variance (ANOVA) was performed after checking for equal variance. Tukey's multiple comparison test was used to identify the significant differences among the means of the dietary groups. For non-parametric data, Kruskal-Wallis test, followed by Dunn's multiple comparison test, was performed to decipher the significant differences between the groups. A significance level of $p < 0.05$ was chosen to indicate the differences.

# RESULTS

## Apparent Digestibility Coefficients

The dry matter content in feces was significantly higher in BG1- and BG3-fed fish (14%–15%) compared with BG2-, BG4-, and BG5-fed fish (10%–11%). We observed significant differences for the digestibility values of dry matter (DM), protein, lipid, ash and energy of the five feeds (**Table 2**). The DM digestibility was significantly lower in BG4-fed (59%) fish compared to BG2 (66%) and BG3 (68%), while no differences were noted among fish fed BG1, BG2, BG3, and BG5. Protein digestibility was lowest (significantly) in fish fed the BG1 (81%) compared to the other groups (85%–88%). Lipid digestibility was the highest in fish fed BG3 (96%) and BG5 (95%), and the lowest in fish fed BG2 (87%). Digestibility value of ash in BG2-fed fish was positive (1%), while those of fish fed other diets were negative (9%–33%). Energy digestibility was significantly higher in fish fed the BG3 (84%) compared to the other groups (73%–78%).

## Growth Performance

The weight gain and growth rate are given in **Table 3**. The fish grew from an initial average weight of 70 g to a final average body weight of 150 g during the experimental period of 65 days. Significantly lower final body weight (138 g), weight gain (94%), thermal growth coefficient (2.1) was noted in fish fed the BG2 compared to the fish fed BG3 (158 g, 117%, 2.5, respectively). No differences in final body weight, weight gain, specific growth rate and thermal growth coefficient were noted for fish belonging to the different dietary treatments. Five fish died during the experiment, but mortality was not related to feed groups.

## Cholesterol

Cholesterol concentration in blood ranged from 7 to 10 Mmol/L, and certain values were significantly differences (**Figure 1**). Cholesterol level was the highest in fish fed fishmeal-based

**TABLE 2** | Dry matter content in feces and apparent digestibility coefficients (ADC %) of dry matter (DM), lipid, protein, ash, and energy in Atlantic salmon fed the experimental diets.

| | BG1 | BG2 | BG3 | BG4 | BG5 | p value |
|---|---|---|---|---|---|---|
| DM | 14.5 ± 0.5$^{a}$ | 10.4 ± 0.4$^{b}$ | 13.8 ± 0.8$^{a}$ | 11.2 ± 0.4$^{b}$ | 11.4 ± 0.4$^{b}$ | <0.001 |
| ADC % | | | | | | |
| DM | 62.1 ± 3.1$^{ab}$ | 66.1 ± 0.6$^{a}$ | 68.4 ± 1.2$^{a}$ | 59.0 ± 3.4$^{b}$ | 63.6 ± 5.4$^{ab}$ | 0.007 |
| Protein | 81.3 ± 1.7$^{b}$ | 86.1 ± 0.3$^{a}$ | 85.5 ± 0.6$^{a}$ | 86.6 ± 1.4$^{a}$ | 88.1 ± 2.2$^{a}$ | <0.001 |
| Lipid | 90.6 ± 1.3$^{b}$ | 87.4 ± 0.2$^{c}$ | 96.4 ± 0.2$^{a}$ | 92.0 ± 0.9$^{b}$ | 95.4 ± 2.4$^{a}$ | <0.001 |
| Ash | -14.1 ± 10.7$^{ab}$ | 0.9 ± 4.6$^{a}$ | -8.6 ± 1.8$^{a}$ | -33.2 ± 10.6$^{b}$ | -21.0 ± 17.5$^{ab}$ | 0.005 |
| Energy | 77.6 ± 1.7$^{b}$ | 77.3 ± 0.6$^{b}$ | 83.8 ± 0.8$^{a}$ | 73.1 ± 2.4$^{b}$ | 77.0 ± 3.6$^{b}$ | <0.001 |

*BG1: Fishmeal + Fish oil diet; BG2: Soybean meal diet; BG3: Fishmeal + Plant oil diet; BG4: Plant ingredients + Fish oil diet; BG5: Plant ingredients + Plant oil diet.*
*Values are expressed as mean ± SD (n=4 replicates). Values in the same row with different superscript letters indicate significant differences (p <.05).*

**TABLE 3** | Growth performance of Atlantic salmon for the experimental period.

| | BG1 | BG2 | BG3 | BG4 | BG5 | p value |
|---|---|---|---|---|---|---|
| IBW | 72.4 ± 1.2 | 71.3 ± 1.0 | 72.9 ± 1.7 | 73.5 ± 1.4 | 73.5 ± 0.9 | 0.15 |
| FBW | 152.3 ± 4.5$^{a}$ | 138.3 ± 5.3$^{b}$ | 158.4 ± 5.9$^{a}$ | 150.7 ± 9.4$^{ab}$ | 150.3 ± 4.9$^{ab}$ | 0.01 |
| WG | 110.2 ± 7.9$^{ab}$ | 93.8 ± 7.0$^{b}$ | 117.2 ± 3.3$^{a}$ | 105.1 ± 16.3$^{ab}$ | 104.7 ± 8.2$^{ab}$ | 0.04 |
| SGR | 1.1 ± 0.1 | 1.0 ± 0.1 | 1.2 ± 0.1 | 1.1 ± 0.1 | 1.0 ± 0.1 | 0.11 |
| TGC | 2.4 ± 0.1$^{ab}$ | 2.1 ± 0.1$^{b}$ | 2.5 ± 0.1$^{a}$ | 2.3 ± 0.3$^{ab}$ | 2.3 ± 0.1$^{ab}$ | 0.05 |

*BG1: Fishmeal + Fish oil diet; BG2: Soybean meal diet; BG3: Fishmeal + Plant oil diet; BG4: Plant ingredients + Fish oil diet; BG5: Plant ingredients + Plant oil diet.*
*IBW, Initial body weight (g); FBW, Final body weight (g); WG, Weight gain (%); SGR, Specific growth rate (% day$^{-1}$); TGC, Thermal growth coefficient.*
*Values are expressed as mean ± SD (n=4 replicates). Values in the same row with different superscript letters show significant differences (p <.05).*

diets, BG1 and BG3, and the lowest in those fed BG2. Fish fed the BG4 had lower cholesterol than those fed BG1, but not significantly different from BG3-fed fish.

## Histology of the Distal Intestine

Micromorphology of the distal intestine samples is shown in **Figure 2**. Inflammatory response in BG2-fed group was evident from the aberrant lamina propria, widened villi, villi fusion and infiltration of inflammatory cells into lamina propria from base of intestinal mucosa. In addition, nuclei of intestinal absorptive cells were displaced and supranuclear vacuoles were also absent in the distal intestine of BG2-fed fish.

Fish fed the BG1 and BG3 had distal intestine with normal features. Enterocytes had a columnar shape, with nuclei situated near the lamina propria. Supranuclear vacuoles were present and the tissue had a normal distribution of goblet cells. Lamina propria had a slender and delicate core, and normal intraepithelial leucocyte infiltration was observed in BG1- and BG3-fed fish. Fish fed BG4 and BG5 also had normally positioned cell nuclei, and the typical distribution of goblet cells. However, the supranuclear vacuoles were smaller in size compared to BG1.

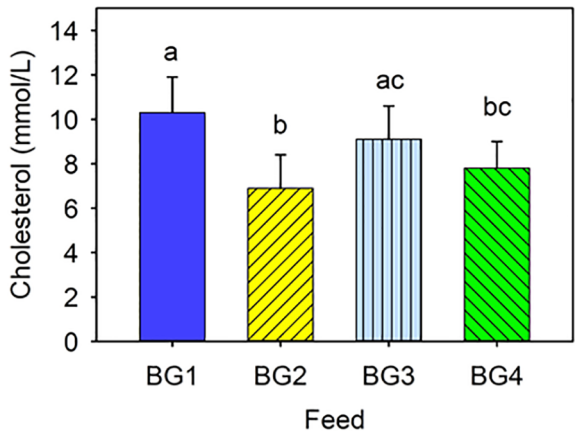


**FIGURE 1** | Cholesterol level in the blood of Atlantic salmon fed different experimental diets. BG1: Fishmeal + Fish oil diet; BG2: Soybean meal diet; BG3: Fishmeal + Plant oil diet; BG4: Plant ingredients + Fish oil diet. Values are expressed as mean ± SD (n=12 fish per diet group). Different letters above the bars indicate significant differences (p < .05).

## Mucosal Mapping

The mean area of intestinal mucous cells for the 60 fish sampled was around 155.3 ± 3,6 μm$^2$, for the five diet groups. The mucous cells' mean area per diet group was not significantly different (**Figure 3A**).

Average intestinal mucous cell density ranged from about 6% to about 11% and density of the mucous cells differed among diet groups ($p < 0.05$; **Figure 3B**). Fish fed BG2 and BG3 had mucous cell volumetric densities that was significantly lower than fish fed diets BG4 and BG5 ($p < 0.001$). Interestingly the marine diet BG1 also had a volumetric density of mucous cells in the epithelium that was significantly lower than BG4 ($p < 0.05$), and the values indicated a strong tendency towards a lower volumetric density than fish fed BG5 ($p = 0.057$).

The mucous cell-based barrier status values of the different fish groups also indicated a strong tendency to differ ($p = 0.062$). Fish fed BG2 had the lowest average barrier status (0.440 ± 0.055) and those fed BG1, BG2 and BG3 had a significantly lower barrier status than fish fed diets BG4 and BG5 (**Figure 3C**, $p < 0.01$).

## Expression of Mucin Genes and Antimicrobial Protein-Encoding Genes

The relative expression of mucin genes in Atlantic salmon skin, gills, and distal intestine is shown in **Figure 4**, respectively. Expression of all four mucin genes were analyzed for all three tissues, and the expressional pattern was found to be tissue-specific.

The skin expressed *muc5ac1, muc5ac2*, and *muc5b* (**Figure 4A**). The expression of *muc5ac1* was relatively higher than those of the other two genes, and significant differences were observed only for the *muc5ac1* gene. The fish fed BG5 diet had the highest relative expression of the *muc5ac1* gene; approximately 3-fold higher compared to other groups. On the other hand, fish fed BG4 tended to have higher expression (2-fold) than those fed BG1-BG3 but lower (-1.5-fold) than BG5-fed fish.

The gills expressed the two genes *muc5ac2* and *muc5b*, and these genes showed an overall higher relative expression (**Figure 4B**). A similar relative expression pattern was noted for both the genes; the highest value (2.1-fold) for fish fed BG2 and lowest in fish fed BG4.

The distal intestine expressed *muc2* (**Figure 4C**). Fish fed BG2 had a significantly reduced (-3.2-fold compared to BG1) expression compared to all the other fish groups. The BG1 group had the highest relative expression (1.3-fold) and was significantly different compared to BG2, BG3 and BG4.

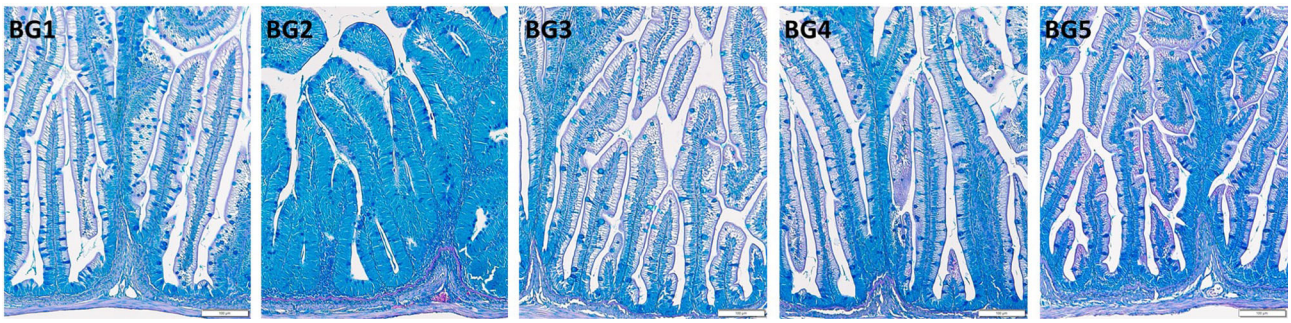


**FIGURE 2** | Histomorphology of the distal intestine of Atlantic salmon fed diets BG1-5. BG1: Fishmeal + Fish oil diet; BG2: Soybean meal diet; BG3: Fishmeal + Plant oil diet; BG4: Plant ingredients + Fish oil diet; BG5: Plant ingredients + Plant oil diet.

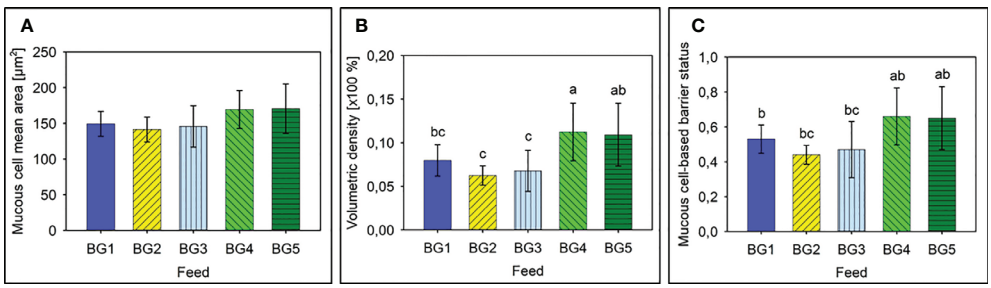


**FIGURE 3** | Mucus cell-based analysis to assess the barrier status in the mid intestine of Atlantic salmon. **(A)** Mean area of mucus cells present in the mid intestinal epithelium of Atlantic salmon. **(B)** Mean volumetric density of mucous cells present in the mid intestine of Atlantic salmon. **(C)** Barrier status of the mid intestine of Atlantic salmon. BG1: Fishmeal + Fish oil diet BG1: Fishmeal + Fish oil diet; BG2: Soybean meal diet; BG3: Fishmeal + Plant oil diet; BG4: Plant ingredients + Fish oil diet; BG5: Plant ingredients + Plant oil diet. Values are expressed as mean ± SD (n=12 fish per diet group). Different letters above the bars indicate significant differences among diet groups.

As for the relative expression of AMPs in Atlantic salmon skin (**Figure 5A**) and distal intestine (**Figure 5B**), the relative expression of *cathl1* and *def1* in the skin of Atlantic salmon was relatively high and the expression of *cathl1* was significantly higher in fish fed BG2 (2.5-fold compared to BG1 and BG3-4) and BG5 (2-fold, **Figure 5A**). We did not observe any differences in the expression of *def1* in the different fish groups. In the distal intestine, *def3* had higher relative expression than *cathl1* (**Figure 5B**). Expression of both genes in the diet groups differed significantly. The expression of *cathl1* was significantly higher in fish fed BG3 compared to those fed BG1 and BG4. The *def3* had the highest expression (3.7-fold) in fish fed BG1 and lowest for those fed BG2 and BG4.

## Salmon Head Kidney Lymphocyte-Like Cell Population and Phagocytic Activity of Macrophage-Like Cells

The percentages of lymphocyte-like cells in the head kidney from fish fed BG1 (39%) and BG3 (41%) were significantly higher than that of fish fed BG5 (24%; **Figure 6**; $p < 0.05$). However, there was no significant difference between the counts of fish fed BG1 and BG3 (41%; $p > 0.05$) or those fed BG2 (30%) and BG4 (32%).

Phagocytic ability (**Figure 7A**) and capacity (**Figures 7B, C**) of HK macrophage-like cells from fish fed BG1 were significantly higher than those fed the other diets ($p < 0.001$). There were no significant differences among the fish fed BG2-5 ($p > 0.05$).

# DISCUSSION

The experimental diets were formulated to investigate nutrient digestibility, growth, mucosal barrier status, and activity of leucocytes from head kidney of the fish fed marine- or plant-derived protein and lipid sources. Plant protein concentrates were chosen to evade the negative effect of carbohydrate and antinutritional factors in plant ingredients on fish health, as noted by other researchers (30–33). Furthermore, feeding studies with Atlantic salmon have shown good growth performance with fishmeal incorporation at 3% or even without the finite ingredient; in such cases amino acids in the feed should be well balanced (32) and the feed should contain attractants derived from marine ingredients (31, 32). Hence, we included the essential amino acids in all the feeds. Rapeseed oil was chosen as the plant oil because it is commonly used to replace fish oil in

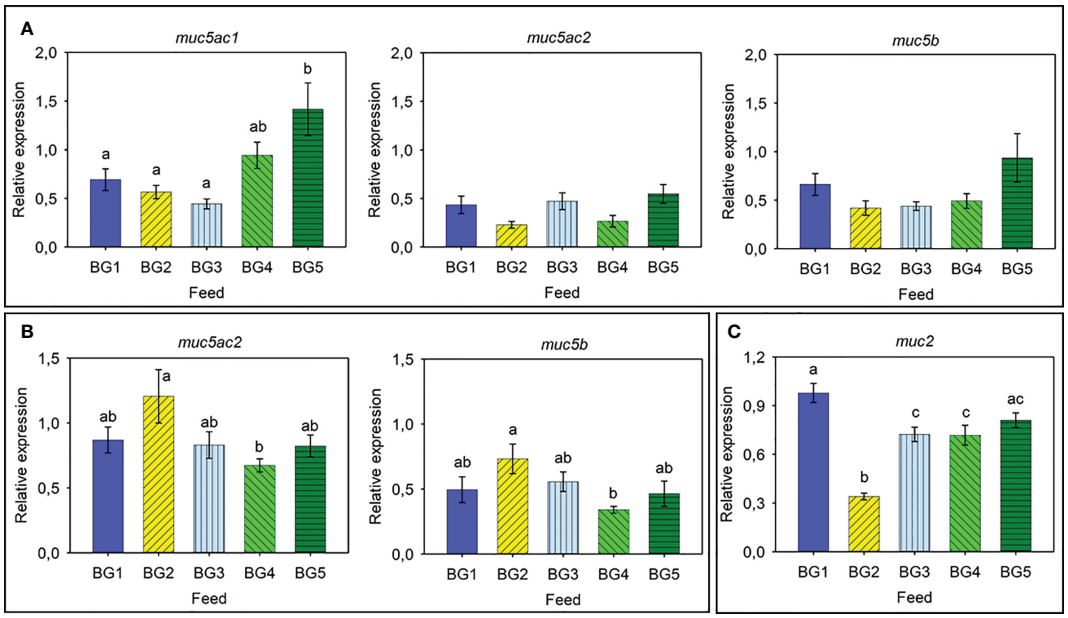


**FIGURE 4** | Relative expression of mucin-related genes in Atlantic salmon. **(A)** Skin: *muc5ac1*, *muc5ac2*, and *muc5b*. **(B)** Gills: *muc5ac2* and *muc5b*. **(C)** Distal intestine: *muc2*. BG1: Fishmeal + Fish oil diet; BG2: Soybean meal diet; BG3: Fishmeal + Plant oil diet; BG4: Plant ingredients + Fish oil diet; BG5: Plant ingredients + Plant oil diet. Values are expressed as mean ± SD (n=12 fish per diet group). Different letters above the bars indicate significant differences ($p < .05$). Expression of *muc2* was too low to be quantified in the skin. Expression of *muc5ac1* and *muc2* was too low to be quantified in the gills. Expression of *muc5ac1*, *muc5ac2*, and *muc5b* was too low to be quantified in the distal intestine.

modern aqua diets (14). The soybean meal diet (SBM; BG2) was deliberately designed to study enteritis; based on earlier reports (34–37). Soybean meal-induced inflammation model is often used to study effects of the ingredient on gut health as well as bile acid levels and hypocholesterolaemia (36–38).

This experiment was not designed as a typical growth performance trial with feed intake measurements. Nevertheless, the results showed that except for the fish fed soybean meal (BG2), all diet groups doubled their weights during the 65 days feeding trial; this result indicates that the diets generally performed well. The lower weight gain of fish fed BG2 is not an unexpected finding because previous studies have already reported such a consequence of soybean meal feeding. Fish fed BG3 diet that contains 50% fishmeal and 21% rapeseed oil had the best growth; the good growth is likely to be due to the high protein and lipid digestibility of this diet.

The lowest protein digestibility was observed for the fish fed the fishmeal and fish oil diet (BG1). Protein digestibility of fishmeal-based diet can vary between 82% to almost 90% (39, 40). However, the difference in protein digestibility between BG1 and BG3 was unexpected because both diets contained the same amount and source of fishmeal. Lipid digestibility was lower in the diets containing fish oil (BG1, BG2 and BG4). The result may be explained by the higher content of saturated fatty acids in fish oil compared to rapeseed oil (41). The lowest lipid digestibility was noted for the fish fed the SBM diet, and the finding corroborates with those of earlier studies (36–38). The highest energy digestibility was observed in fish fed fishmeal and plant oil (BG3), reflecting the high protein and lipid digestibility. Reduced DM content in feces from Atlantic salmon fed SBM or SPC is in line with other studies on salmonids (17, 36, 42, 43), and could likely to be an effect of altered expression of genes encoding aquaporins, ion transporters, tight junction and adherence junction proteins (17), leading to a loss of junction barrier integrity.

The morphological changes observed in the distal intestine of the fish fed the SBM diet were consistent with soybean meal-induced enteritis and in line with several other studies that employed 20% SBM in diets for salmonids. For the other diet groups, there were no severe signs of enteritis. Saponin is the antinutritional factor responsible for inducing enteritis in soybean meal fed Atlantic salmon (44), but severity is potentiated by other bioactive components of the plant ingredients (34). Soy protein concentrate is devoid of saponins (45) and incorporation up to 45% into marine based diets do not cause severe gut inflammatory and immune responses in Atlantic salmon (46, 47). Fish fed the fishmeal-based diets (BG1 and BG3) had normal distal intestine features and the only dietary difference between these two groups was the inclusion of rapeseed oil (BG3). The reduction of supranuclear vacuoles noted for fish fed BG4 and BG5 compared to BG1 indicated subtle plant-based diet-induced aberrations as reported in other studies. Loss of absorptive vacuoles was also reported by Katerina et al. (48); they evaluated the effect of replacement of fish oil with the alga *Schizochytrium limacinum* throughout the entire life cycle of Atlantic salmon by feeding the fish with diets low in marine ingredients. The final grow-out diets in the latter experiment contained either 10% fishmeal and 4.3% fish, or 10% fishmeal and 6.25% alga. Irrespective of the diet, the authors

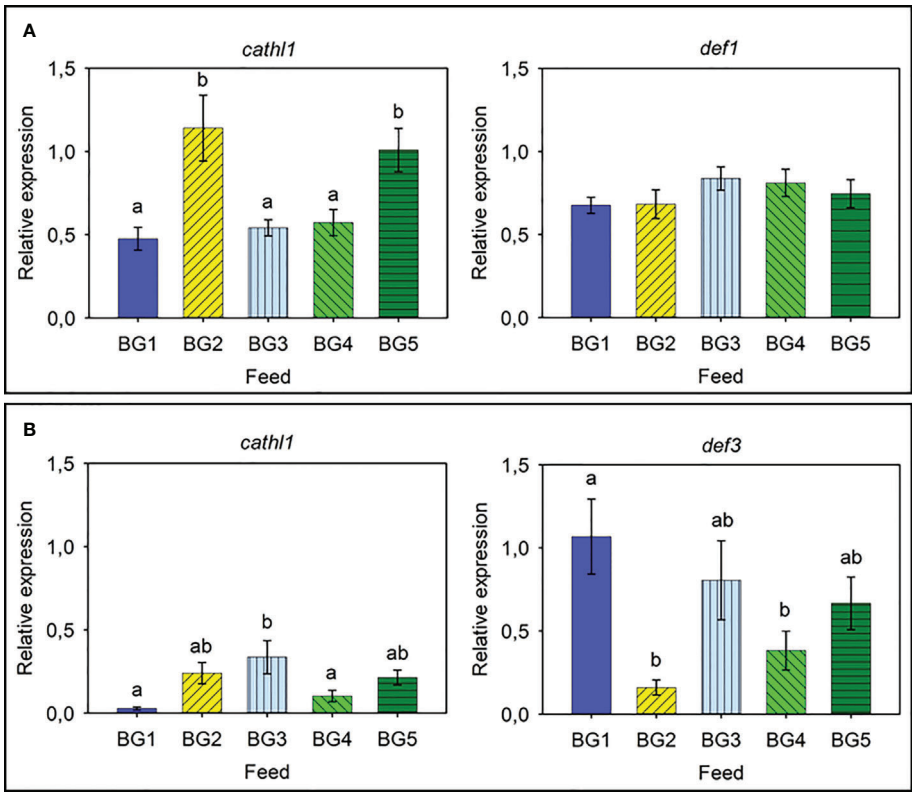


**FIGURE 5** | Relative expression of antimicrobial protein genes in the skin and distal intestine of Atlantic salmon. **(A)** Skin *cathl1* and *def1*. **(B)** Distal intestine *cathl1* and *def3*. BG1: Fishmeal + Fish oil diet; BG2: Soybean meal diet; BG3: Fishmeal + Plant oil diet; BG4: Plant ingredients + Fish oil diet; BG5: Plant ingredients + Plant oil diet. Values are expressed as mean ± SD (n=12 fish per diet group). Different letters indicate significant differences ($p < .05$). Expression of *def2*, *def3*, and *def4* was too low to be quantified in the skin. Likewise, the expression of *def1*, *def2*, and *def4* was too low to be quantified in the distal intestine.

observed abnormal histomorphology in the distal intestine of the fish, characterized by enterocytes lacking vacuoles, abnormally tall folds with extensively developed branches and infiltration of inflammatory cells into the connective tissue. Taken together these two studies suggest that salmon compensate the lack of absorptive vacuoles by hypertrophy of the primary and secondary folds in the distal intestine. Based on the histology results from the present study we state that plant protein concentrates (not rapeseed oil) can also induce mild enteritis similar to the micromorphological changes that were noted in BG4 and BG5 that contained a mix of plant protein concentrates. It should be noted that all the diets in the present study were optimized to contain at least 1.7% EPA and docosahexaenoic acid (DHA) in the diets. The EPA+DHA content was also higher than the levels used by Katerina et al. (48). Other studies have pointed out the importance of fish oil to maintain a healthy barrier status and to maintain a good host disease resistance status. European seabass fed low levels of fish oil was not able to resist the invasive pathogens; an infection with *Vibrio anguillarum* resulted in increased translocation of the bacteria and increased fish mortality (49).

The lower cholesterol level in the fish fed the SBM diet is in line with other experiments that noticed hypocholesterolaemia as well as changes in the expression of genes involved in cholesterol biosynthetic pathways in fish fed soybean meal and lupin meal (36, 38, 50–52). The reduction in cholesterol level in the plasma of SBM fed fish is associated with saponins in SBM (34, 44, 51, 53). Fish fed the fishmeal and rapeseed oil diet (BG3) also had a numerically lower cholesterol level than BG1 but slightly higher than in fish fed plant protein mix and rapeseed oil (BG4). Sissener et al. (54) found a correlation between cholesterol level in the feed and its concentration in plasma, bile and whole fish. Therefore, the lower cholesterol in fish fed BG3 and BG4 can be partly explained by the lower content of cholesterol in these diets.

The mucosal mapping of the five diet groups revealed a consistent relationship with the growth data; the soybean meal diet group (BG2) had the smallest mean area, lowest volumetric density and an ensuing poor mucous cell-based barrier status compared to the other groups. Mucosal mapping results agree with more traditional analyses of gut health and with the overall growth performance. In contrast, both feeds containing a mix of plant protein concentrates (BG4 and BG5) had the largest mean mucous cell area, highest volumetric density and aberrant barrier status. These results suggest that the plant proteins cause enteritis in two ways; either by reducing (BG2) or increasing (BG4 and BG5) the mucous cell sizes and volumetric densities.

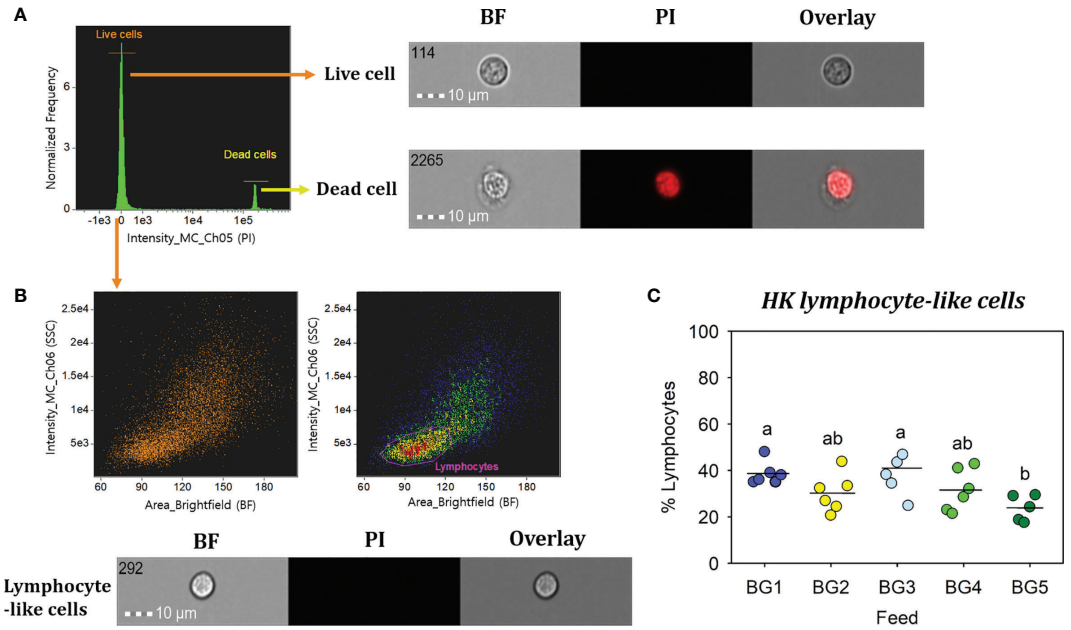


**FIGURE 6** | Percentage of head kidney lymphocyte-like cells from Atlantic salmon fed different experimental diets. BG1: Fishmeal + Fish oil diet; BG2: Soybean meal diet; BG3: Fishmeal + Plant oil diet; BG4: Plant ingredients + Fish oil diet; BG5: Plant ingredients + Plant oil diet. **(A)** Live cells (orange) were separated by excluding the dead cells (yellow); by staining with propidium iodide (PI). **(B)** Brightfield (BF) area (cell size) vs. side scatter (SSC) intensity (cell internal complexity) plot showing the HK leucocyte population. **(C)** Percentage of HK lymphocyte-like cells from fish (n=6) fed different experimental diets. Statistically significant differences ($p < 0.05$) between dietary groups are indicated by different letters. All cell images were captured with 40× objective. Scale bar = 10 µm. BF, brightfield; PI, propidium iodide.

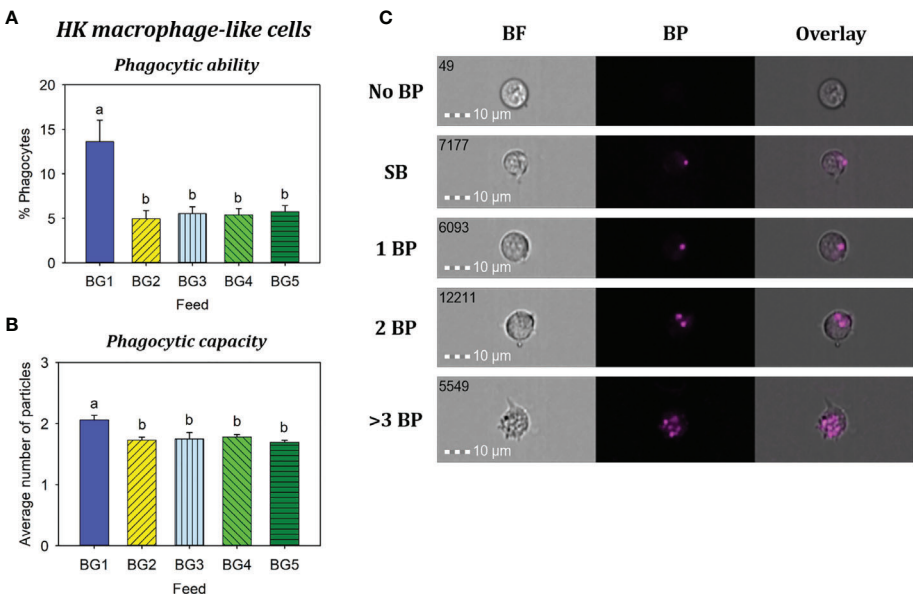


**FIGURE 7** | Phagocytosis of head kidney macrophage-like cells from Atlantic salmon fed different experimental diets. BG1: Fishmeal + Fish oil diet; BG2: Soybean meal diet; BG3: Fishmeal + Plant oil diet; BG4: Plant ingredients + Fish oil diet; BG5: Plant ingredients + Plant oil diet. **(A)** Percent of phagocytic cells. **(B)** mean number of particles ingested per phagocytic cell. **(C)** Representative cell images indicate cells with no BP, SB, and 1BP, 2BP, and >3BP. Statistically significant differences ($p < 0.05$) between dietary groups are indicated by different letters. Bar plots show mean ± SD, n = 6. All cell images were captured with 40× objective. Scale bar = 10 µm. SB, surface-binding particles; 1 BP, 2 BP, and > 3 BP, one to three internalized bio-particles; BF, brightfield.

The present study focused on the secreted mucin genes that are expressed on certain mucosal tissues of salmon (4). Earlier studies have mainly investigated the expression of mucin genes in relation to stress (4), or as markers of parasite infestation (3, 55). Mucin genes are diagnostic markers of severe human diseases; e.g. airway disorders, inflammatory diseases, cancers (56–58). Tissue-specific expression of mucin genes–*muc2*-like genes in the distal intestine and *muc5*-like genes in the skin and gills–is consistent with previous research on Atlantic salmon (4). Sveen et al. (4) reported high expression of *muc5ac1* and *muc5b* in the skin and *muc5ac2* in the gills. In the present experiment only the expression of *muc5ac1* in the skin of fish fed the experimental diets differed significantly. Fish fed diets with high levels of plant protein concentrates had the highest expression of *muc5ac1*, but only the group fed diet with the highest incorporation of plant ingredients (BG5) had significantly higher *muc5ac1*. In the gills, the relative expression of *muc5ac2* was slightly higher than *muc5b* and the expression of both genes was significantly higher in fish fed soybean meal in the diet (BG2) and lowest in those fed the combination of plant protein ingredients and fish oil (BG4). Higher expression of *muc2* in the distal intestine of fish fed the marine ingredient-based diet (BG1) and down regulation in fish fed soybean meal (BG2) clearly indicate that this gene is correlated to intestinal health. The *muc2* has an anti-inflammatory and tumor suppressive role, and experiments with *muc2* knockout mice have shown abnormal goblet cells followed by development of colitis and colorectal cancer (59, 60). Mucus layer and microbiota structure are interdependent on each other, and the major and minor forms of O-glycosylated entities of *Muc2* in mice colon are known to have key roles in host-microbiota symbiosis (61). Diet is an important determinant of gut microbiota, and it is known that these microorganisms enhance the expression of e.g. *Muc2* and *Fut2* (galactoside 2-alpha-L-fucosyltransferase 2) to strengthen the mucus barrier and mucin glycan structure, thereby preventing the entry of microbes into the intestinal epithelium (62). The lower expression of *muc2* in fish fed BG3 compared to BG1 can only be explained by the different oil sources since both contained fishmeal. The difference between BG1 and BG4 could be due to the replacement of fishmeal with plant protein concentrates. The lower expression of *muc2* for fish fed the soybean meal diet (BG2) suggests that this gene may be used as a marker for severe intestinal inflammation.

Antimicrobial peptides are defense molecules that have key roles in disease prevention in fishes (63). The expression of both cathelicidins and defensins has been induced in salmonids subjected to bacterial challenge (64, 65). In the present study, *cathl1* was expressed in both the skin and distal intestine, but the expression was the highest in the skin of Atlantic salmon. The observation corroborates with that of Chang et al. (65); they also observed differential expression of the two cathelicidin genes in different tissues. After a bacterial challenge the expression of *cathl1* increased in some tissues but not in all (65). In the present experiment, the relative expression in the skin and distal intestine was affected by the feeds. As for the defensin genes, the gene *def1* was only expressed in the skin and it was unaffected by the feeds. On the other hand, *def3* was expressed in the distal intestine and was affected by the feeds. Similar to the *muc2* expression in the distal intestine, the expression of *def3* was the highest for fish fed BG1 and the lowest for fish fed BG2. Increased production of AMPs can be considered as a strategy of the fish to stimulate its immune system, and could serve as an alternate approach to reduce disease outbreaks in fish farms (2, 8).

In the present study, percentages of lymphocyte-like cells from the major hematopoietic organ (HK) of fish fed more plant ingredients (BG5) was significantly lower compared to those fed fishmeal-based diets (BG1 and BG3). The low content of fishmeal and fish oil in the BG5 diet may have influenced the counts of HK lymphocyte-like cells. In a study on European sea bass (66), the total number of circulating leucocytes in fish fed 100% fish oil diet was significantly higher than in fish fed plant oil diets. A study on mice has reported that a diet rich in fish oil promotes hematopoiesis (67); mice fed fish oil diet had significantly higher hematopoietic stem cells and hematopoietic progenitors in the spleen compared to mice fed low or high-fat diets. Increased phagocytic activity by macrophages is indicative of increased disease resistance competence (68). The significantly increased phagocytic ability and capacity of HK macrophage-like cells observed in the fish fed BG1 compared to those of other diets could be linked to increased dietary n-3 fatty acid, as reported previously (69–72).

Plant protein concentrates was used in the present experiment to reduce the effect of antinutritional factors. However, fish fed the plant protein concentrates (BG4 and BG5) in the present experiment also had altered histology and mucosal barrier status–loss of absorptive vacuoles, increased mucous cell volumetric densities and barrier status– compared to those fed the fishmeal as protein source (BG1 and BG3). There seems to be a close connection between nutritional status, modulations of the immune cell populations and their functions (73). We assume that higher *muc2* expression in the distal intestine of fish fed BG1 could contribute to the enhanced intestinal barrier protection as well as increase in immune cell counts and their function in head kidney indicating the importance of fishmeal and fish oil for the health of the fish.

In conclusion, the ADC values were within the normal ranges and the fish grew well on all diets, except the fish fed SBM. Fish fed the plant protein ingredients (BG4 and BG5) had lower DM content in the feces and had mild enteritis. Decreased mucous cell size and low barrier status were hallmarks of fish fed soybean meal, but increased cell size and abnormal barrier status were the features of fish fed plant protein mixes irrespective of lipid source. These results suggest two types of impact on gut health over the long term; either reduce mucosal protection or over-activate it. The four mucin genes in Atlantic salmon skin, gills, and distal intestine were affected by the ingredient composition. The expression of the antimicrobial peptide genes, *cathl1* and *def3* were also affected by the ingredients in the diets. Furthermore, higher numbers of lymphocyte-like cells, increased phagocytic ability and capacity of macrophage-like cells in head kidney as well as higher *muc2* expression in the distal intestine of fish fed the marine based diet (BG1) points to the compromised intestinal barrier in fish fed plant ingredients. These data can be combined with marker

gene information to further refine dietary compositions for sustainable and acceptable healthy diets.

## DATA AVAILABILITY STATEMENT

The original contributions presented in the study are included in the article/**Supplementary Material**, further inquiries can be directed to the corresponding author.

## ETHICS STATEMENT

The animal study was reviewed and approved by National Animal Research Authority (FDU: Forsøksdyrutvalget ID-5887) in Norway.

## AUTHOR CONTRIBUTIONS

KK and MS designed the study and feed formulation. Feeding trials were supervised by MS, YG, and SS. GV helped SS in conducting the qPCR study. YP performed the cell study. TP, SØ, and KP were responsible for the stereology part of the manuscript. DD performed the histology study. SS wrote the first version of the manuscript. VK and MS edited the manuscript. All authors contributed to the article and approved the submitted version.

## FUNDING

This study was part of the project "*Blodanalyser av laks som metode for vurdering av tarmhelse*" funded by MABIT, project number AF0082.

## SUPPLEMENTARY MATERIAL

The Supplementary Material for this article can be found online at: https://www.frontiersin.org/articles/10.3389/fimmu.2020.623726/full#supplementary-material

## REFERENCES

1. Kiron V. Fish immune system and its nutritional modulation for preventive health care. *Anim Feed Sci Technol* (2012) 173:111–33. doi: 10.1016/j.anifeedsci.2011.12.015
2. Masso-Silva JA, Diamond G. Antimicrobial peptides from fish. *Pharm (Basel)* (2014) 7:265–310. doi: 10.3390/ph7030265
3. Pérez-Sánchez J, Estensoro I, Redondo MJ, Calduch-Giner JA, Kaushik S, Sitjà-Bobadilla A. Mucins as diagnostic and prognostic biomarkers in a fish-parasite model: Transcriptional and functional analysis. *PloS One* (2013) 8:e65457. doi: 10.1371/journal.pone.0065457
4. Sveen LR, Grammes FT, Ytteborg E, Takle H, Jørgensen SM. Genome-wide analysis of Atlantic salmon (*Salmo salar*) mucin genes and their role as biomarkers. *PloS One* (2017) 12:e0189103. doi: 10.1371/journal.pone.0189103
5. Venkatakrishnan V, Padra JT, Sundh H, Sundell K, Jin C, Langeland M, et al. Exploring the Arctic charr intestinal glycome: Evidence of increased n-glycolylneuraminic acid levels and changed host–pathogen interactions in response to inflammation. *J Proteome Res* (2019) 18:1760–73. doi: 10.1021/acs.jproteome.8b00973
6. Benktander J, Venkatakrishnan V, Padra JT, Sundh H, Sundell K, Murugan AVM, et al. Effects of size and geographical origin on Atlantic salmon, *Salmo salar*, mucin *O*-glycan repertoire. *Mol Cell Proteomics* (2019) 18:1183–96. doi: 10.1074/mcp.RA119.001319
7. Joo H-S, Fu C-I, Otto M. Bacterial strategies of resistance to antimicrobial peptides. *Philos Trans R Soc Lond Ser B: Biol Sci* (2016) 371:20150292. doi: 10.1098/rstb.2015.0292
8. Kościuczuk EM, Lisowski P, Jarczak J, Strzałkowska N, Jóźwik A, Horbańczuk J, et al. Cathelicidins: family of antimicrobial peptides. A review. *Mol Biol Rep* (2012) 39:10957–70. doi: 10.1007/s11033-012-1997-x
9. Gomez D, Sunyer JO, Salinas I. The mucosal immune system of fish: The evolution of tolerating commensals while fighting pathogens. *Fish Shellfish Immunol* (2013) 35:1729–39. doi: 10.1016/j.fsi.2013.09.032
10. Jutfelt F. Barrier function of the gut. In: AP Farrell, editor. *Encyclopedia of fish physiology: from genome to environment. Volume 2*. Amsterdam: Academic press (2011). p. 1322–31.
11. Torrecillas S, Montero D, Caballero MJ, Pittman KA, Custódio M, Campo A, et al. Dietary mannan oligosaccharides: counteracting the side effects of soybean meal oil inclusion on European sea bass (*Dicentrarchus labrax*) gut health and skin mucosa mucus production? *Front Immunol* (2015) 6:397. doi: 10.3389/fimmu.2015.00397
12. Camilleri M, Lyle BJ, Madsen KL, Sonnenburg J, Verbeke K, Wu GD. Role for diet in normal gut barrier function: developing guidance within the framework of food-labeling regulations. *Am J Physiol Gastrointest Liver Physiol* (2019) 317:G17–39. doi: 10.1152/ajpgi.00063.2019
13. Aas TS, Ytrestøyl T, Åsgård T. Utilization of feed resources in the production of Atlantic salmon (*Salmo salar*) in Norway: An update for 2016. *Aquac Rep* (2019) 15:100216. doi: 10.1016/j.aqrep.2019.100216
14. Ytrestøyl T, Aas TS, Åsgård T. Utilisation of feed resources in production of Atlantic salmon (*Salmo salar*) in Norway. *Aquaculture* (2015) 448:365–74. doi: 10.1016/j.aquaculture.2015.06.023
15. Bou M, Berge GM, Baeverfjord G, Sigholt T, Østbye T-K, Romarheim OH, et al. Requirements of n-3 very long-chain PUFA in Atlantic salmon (*Salmo salar* L): effects of different dietary levels of EPA and DHA on fish performance and tissue composition and integrity. *Br J Nutr* (2017) 117:30–47. doi: 10.1017/S0007114516004396
16. Moldal T, Løkka G, Wiik-Nielsen J, Austbø L, Torstensen BE, Rosenlund G, et al. Substitution of dietary fish oil with plant oils is associated with shortened mid intestinal folds in Atlantic salmon (*Salmo salar*). *BMC Vet Res* (2014) 10:60. doi: 10.1186/1746-6148-10-60
17. Hu H, Kortner TM, Gajardo K, Chikwati E, Tinsley J, Krogdahl Å. Intestinal fluid permeability in Atlantic salmon (*Salmo salar* L.) is affected by dietary protein source. *PloS One* (2016) 11:e0167515–e0167515. doi: 10.1371/journal.pone.0167515
18. Kiron V, Park Y, Siriyappagouder P, Dahle D, Vasanth G, Dias J, et al. Intestinal transcriptome reveals soy derivatives-linked changes in Atlantic salmon. *Front Immunol* (2020) 11:3013. doi: 10.3389/fimmu.2020.596514. In press.
19. Ringø E, Zhou Z, Vecino JLG, Wadsworth S, Romero J, Krogdahl Å, et al. Effect of dietary components on the gut microbiota of aquatic animals. A never-ending story? *Aquac Nutr* (2016) 22:219–82. doi: 10.1111/anu.12346
20. Dang M, Pittman K, Sonne C, Hansson S, Bach L, Søndergaard J, et al. Histological mucous cell quantification and mucosal mapping reveal different aspects of mucous cell responses in gills and skin of shorthorn sculpins (*Myoxocephalus scorpius*). *Fish Shellfish Immunol* (2020) 100:334–44. doi: 10.1016/j.fsi.2020.03.020
21. Kiron V, Sørensen M, Huntley M, Vasanth GK, Gong Y, Dahle D, et al. Defatted biomass of the microalga, *Desmodesmus* sp., can replace fishmeal in the feeds for Atlantic salmon. *Front Mar Sci* (2016) 3:67. doi: 10.3389/fmars.2016.00067
22. Sørensen M, Gong Y, Bjarnason F, Vasanth GK, Dahle D, Huntley M, et al. *Nannochloropsis oceania*-derived defatted meal as an alternative to fishmeal in Atlantic salmon feeds. *PloS One* (2017) 12:e0179907. doi: 10.1371/journal.pone.0179907

23. Vasanth G, Kiron V, Kulkarni A, Dahle D, Lokesh J, Kitani Y. A microbial feed additive abates intestinal inflammation in Atlantic salmon. *Front Immunol* (2015) 6:409. doi: 10.3389/fimmu.2015.00409
24. Gong Y, Sørensen SL, Dahle D, Nadanasabesan N, Dias J, Valente LMP, et al. Approaches to improve utilization of *Nannochloropsis oceanica* in plant-based feeds for Atlantic salmon. *Aquaculture* (2020) 522:735122. doi: 10.1016/j.aquaculture.2020.735122
25. Bancroft JD, Gamble M. *Theory and practice of histological techniques. 6th edn*. Churchill Livingstone: Elsevier (2008).
26. Pittman K, Pittman A, Karlson S, Cieplinska T, Sourd P, Redmond K, et al. Body site matters: an evaluation and application of a novel histological methodology on the quantification of mucous cells in the skin of Atlantic salmon, *Salmo salar* L. *J Fish Dis* (2013) 36:115–27. doi: 10.1111/jfd.12002
27. Pittman K, Sourd P, Ravnøy B, Espeland Ø, Fiksdal IU, Oen T, et al. Novel method for quantifying salmonid mucous cells. *J Fish Dis* (2011) 34:931–6. doi: 10.1111/j.1365-2761.2011.01308.x
28. Vandesompele J, De Preter K, Pattyn F, Poppe B, Van Roy N, De Paepe A, et al. Accurate normalization of real-time quantitative RT-PCR data by geometric averaging of multiple internal control genes. *Genome Biol* (2002) 3:research0034.0031. doi: 10.1186/gb-2002-3-7-research0034
29. Park Y, Abihssira-García IS, Thalmann S, Wiegertjes GF, Barreda DR, Olsvik PA, et al. Imaging flow cytometry protocols for examining phagocytosis of microplastics and bioparticles by immune cells of aquatic animals. *Front Immunol* (2020) 11:203. doi: 10.3389/fimmu.2020.00203
30. De Santis C, Crampton VO, Bicskei B, Tocher DR. Replacement of dietary soy- with air classified faba bean protein concentrate alters the hepatic transcriptome in Atlantic salmon (*Salmo salar*) parr. *Comp Biochem Physiol D: Genomics Proteomics* (2015) 16:48–58. doi: 10.1016/j.cbd.2015.07.005
31. Kousoulaki K, Rønnestad I, Rathore R, Sixten HJ, Campbell P, Nordrum S, et al. Physiological responses of Atlantic salmon (*Salmo salar* L.) fed very low (3%) fishmeal diets supplemented with feeding-modulating crystalline amino acid mixes as identified in krill hydrolysate. *Aquaculture* (2018) 486:184–96. doi: 10.1016/j.aquaculture.2017.12.011
32. Zhang Y, Øverland M, Shearer KD, Sørensen M, Mydland LT, Storebakken T. Optimizing plant protein combinations in fish meal-free diets for rainbow trout (*Oncorhynchus mykiss*) by a mixture model. *Aquaculture* (2012) 360-361:25–36. doi: 10.1016/j.aquaculture.2012.07.003
33. Collins SA, Øverland M, Skrede A, Drew MD. Effect of plant protein sources on growth rate in salmonids: Meta-analysis of dietary inclusion of soybean, pea and canola/rapeseed meals and protein concentrates. *Aquaculture* (2013) 400-401:85–100. doi: 10.1016/j.aquaculture.2013.03.006
34. Krogdahl Å, Gajardo K, Kortner TM, Penn M, Gu M, Berge GM, et al. Soya saponins induce enteritis in Atlantic salmon (*Salmo salar* L.). *J Agric Food Chem* (2015) 63:3887–902. doi: 10.1021/jf506242t
35. Øverland M, Sørensen M, Storebakken T, Penn M, Krogdahl Å, Skrede A. Pea protein concentrate substituting fish meal or soybean meal in diets for Atlantic salmon (*Salmo salar*)—Effect on growth performance, nutrient digestibility, carcass composition, gut health, and physical feed quality. *Aquaculture* (2009) 288:305–11. doi: 10.1016/j.aquaculture.2008.12.012
36. Sørensen M, Penn M, El-Mowafi A, Storebakken T, Chunfang C, Øverland M, et al. Effect of stachyose, raffinose and soya-saponins supplementation on nutrient digestibility, digestive enzymes, gut morphology and growth performance in Atlantic salmon (*Salmo salar*, L). *Aquaculture* (2011) 314:145–52. doi: 10.1016/j.aquaculture.2011.02.013
37. Baeverfjord G, Krogdahl A. Development and regression of soybean meal induced enteritis in Atlantic salmon, *Salmo salar* L., distal intestine: a comparison with the intestines of fasted fish. *J Fish Dis* (1996) 19:375–87. doi: 10.1046/j.1365-2761.1996.d01-92.x
38. Kortner TM, Gu J, Krogdahl Å, Bakke AM. Transcriptional regulation of cholesterol and bile acid metabolism after dietary soyabean meal treatment in Atlantic salmon (*Salmo salar* L.). *Br J Nutr* (2013) 109:593–604. doi: 10.1017/S0007114512002024
39. Gong Y, Bandara T, Huntley M, Johnson ZI, Dias J, Dahle D, et al. Microalgae *Scenedesmus* sp. as a potential ingredient in low fishmeal diets for Atlantic salmon (*Salmo salar* L.). *Aquaculture* (2019) 501:455–64. doi: 10.1016/j.aquaculture.2018.11.049
40. Sørensen M, Berge GM, Reitan KI, Ruyter B. Microalga *Phaeodactylum tricornutum* in feed for Atlantic salmon (*Salmo salar*)—Effect on nutrient digestibility, growth and utilization of feed. *Aquaculture* (2016) 460:116–23. doi: 10.1016/j.aquaculture.2016.04.010
41. Turchini G, Mailer RJ. Rapeseed (canola) oil and other monounsaturated fatty acid-rich vegetable oils. In: GM Turchini, W-K Ng, DR Tocher, editors. *Fish oil replacement and alternative lipid sources in aquaculture feeds*. Florida, USA: CRC Press (2011). p. 161–208.
42. Refstie S, Korsøen ØJ, Storebakken T, Baeverfjord G, Lein I, Roem AJ. Differing nutritional responses to dietary soybean meal in rainbow trout (*Oncorhynchus mykiss*) and Atlantic salmon (*Salmo salar*). *Aquaculture* (2000) 190:49–63. doi: 10.1016/S0044-8486(00)00382-3
43. Refstie S, Storebakken T, Roem AJ. Feed consumption and conversion in Atlantic salmon (*Salmo salar*) fed diets with fish meal, extracted soybean meal or soybean meal with reduced content of oligosaccharides, trypsin inhibitors, lectins and soya antigens. *Aquaculture* (1998) 162:301–12. doi: 10.1016/S0044-8486(98)00222-1
44. Knudsen D, Jutfelt F, Sundh H, Sundell K, Koppe W, Frøkiær H. Dietary soya saponins increase gut permeability and play a key role in the onset of soyabean-induced enteritis in Atlantic salmon (*Salmo salar* L.). *Br J Nutr* (2008) 100:120–9. doi: 10.1017/S0007114507886338
45. Ireland PA, Dziedzic SZ, Kearsley MW. Saponin content of soya and some commercial soya products by means of high-performance liquid chromatography of the sapogenins. *J Sci Food Agric* (1986) 37:694–8. doi: 10.1002/jsfa.2740370715
46. Król E, Douglas A, Tocher DR, Crampton VO, Speakman JR, Secombes CJ, et al. Differential responses of the gut transcriptome to plant protein diets in farmed Atlantic salmon. *BMC Genomics* (2016) 17:156. doi: 10.1186/s12864-016-2473-0
47. De Santis C, Ruohonen K, Tocher DR, Martin SAM, Król E, Secombes CJ, et al. Atlantic salmon (*Salmo salar*) parr as a model to predict the optimum inclusion of air classified faba bean protein concentrate in feeds for seawater salmon. *Aquaculture* (2015) 444:70–8. doi: 10.1016/j.aquaculture.2015.03.024
48. Katerina K, Berge GM, Turid M, Aleksei K, Grete B, Trine Y, et al. Microalgal *Schizochytrium limacinum* biomass improves growth and filet quality when used long-term as a replacement for fish oil, in modern salmon diets. *Front Mar Sci* (2020) 7:57. doi: 10.3389/fmars.2020.00057
49. Torrecillas S, Caballero MJ, Mompel D, Montero D, Zamorano MJ, Robaina L, et al. Disease resistance and response against *Vibrio anguillarum* intestinal infection in European seabass (*Dicentrarchus labrax*) fed low fish meal and fish oil diets. *Fish Shellfish Immunol* (2017) 67:302–11. doi: 10.1016/j.fsi.2017.06.022
50. Geay F, Ferraresso S, Zambonino-Infante JL, Bargelloni L, Quentel C, Vandeputte M, et al. Effects of the total replacement of fish-based diet with plant-based diet on the hepatic transcriptome of two European sea bass (*Dicentrarchus labrax*) half-sibfamilies showing different growth rates with the plant-based diet. *BMC Genomics* (2011) 12:522. doi: 10.1186/1471-2164-12-522
51. Gu M, Kortner TM, Penn M, Hansen AK, Krogdahl Å. Effects of dietary plant meal and soya-saponin supplementation on intestinal and hepatic lipid droplet accumulation and lipoprotein and sterol metabolism in Atlantic salmon (*Salmo salar* L.). *Br J Nutr* (2014) 111:432–44. doi: 10.1017/S0007114513002717
52. Romarheim OH, Skrede A, Penn M, Mydland LT, Krogdahl Å, Storebakken T. Lipid digestibility, bile drainage and development of morphological intestinal changes in rainbow trout (*Oncorhynchus mykiss*) fed diets containing defatted soybean meal. *Aquaculture* (2008) 274:329–38. doi: 10.1016/j.aquaculture.2007.11.035
53. Chikwati EM, Venold FF, Penn MH, Rohloff J, Refstie S, Guttvik A, et al. Interaction of soyasaponins with plant ingredients in diets for Atlantic salmon, *Salmo salar* L. *Br J Nutr* (2012) 107:1570–90. doi: 10.1017/S0007114511004892
54. Sissener NH, Rosenlund G, Stubhaug I, Liland NS. Tissue sterol composition in Atlantic salmon (*Salmo salar* L.) depends on the dietary cholesterol content and on the dietary phytosterol:cholesterol ratio, but not on the dietary phytosterol content. *Br J Nutr* (2018) 119:599–609. doi: 10.1017/S0007114517003853
55. Marcos-López M, Calduch-Giner JA, Mirimin L, MacCarthy E, Rodger HD, O'Connor I, et al. Gene expression analysis of Atlantic salmon gills reveals mucin 5 and interleukin 4/13 as key molecules during amoebic gill disease. *Sci Rep* (2018) 8:13689. doi: 10.1038/s41598-018-32019-8
56. Janssen WJ, Stefanski AL, Bochner BS, Evans CM. Control of lung defence by mucins and macrophages: ancient defence mechanisms with modern functions. *Eur Respir J* (2016) 48:1201–14. doi: 10.1183/13993003.00120-2015

57. Sheng YH, Hasnain SZ, Florin THJ, McGuckin MA. Mucins in inflammatory bowel diseases and colorectal cancer. *J Gastroenterol Hepatol* (2012) 27:28–38. doi: 10.1111/j.1440-1746.2011.06909.x
58. Yonezawa S, Higashi M, Yamada N, Yokoyama S, Kitamoto S, Kitajima S, et al. Mucins in human neoplasms: Clinical pathology, gene expression and diagnostic application. *Pathol Int* (2011) 61:697–716. doi: 10.1111/j.1440-1827.2011.02734.x
59. Velcich A, Yang W, Heyer J, Fragale A, Nicholas C, Viani S, et al. Colorectal cancer in mice genetically deficient in the mucin Muc2. *Science* (2002) 295:1726–9. doi: 10.1126/science.1069094
60. Van der Sluis M, De Koning BA, De Bruijn AC, Velcich A, Meijerink JP, Van Goudoever JB, et al. Muc2-deficient mice spontaneously develop colitis, indicating that MUC2 is critical for colonic protection. *Gastroenterology* (2006) 131:117–29. doi: 10.1053/j.gastro.2006.04.020
61. Bergstrom K, Shan X, Casero D, Batushansky A, Lagishetty V, Jacobs JP, et al. Proximal colon–derived O-glycosylated mucus encapsulates and modulates the microbiota. *Science* (2020) 370:467–72. doi: 10.1126/science.aay7367
62. Schroeder BO. Fight them or feed them: how the intestinal mucus layer manages the gut microbiota. *Gastroenterol Rep* (2019) 7:3–12. doi: 10.1093/gastro/goy052
63. van der Marel M, Adamek M, Gonzalez SF, Frost P, Rombout JHWM, Wiegertjes GF, et al. Molecular cloning and expression of two β-defensin and two mucin genes in common carp (*Cyprinus carpio* L.) and their up-regulation after β-glucan feeding. *Fish Shellfish Immunol* (2012) 32:494–501. doi: 10.1016/j.fsi.2011.12.008
64. Casadei E, Wang T, Zou J, González Vecino JL, Wadsworth S, Secombes CJ. Characterization of three novel β-defensin antimicrobial peptides in rainbow trout (*Oncorhynchus mykiss*). *Mol Immunol* (2009) 46:3358–66. doi: 10.1016/j.molimm.2009.07.018
65. Chang C-I, Zhang Y-A, Zou J, Nie P, Secombes CJ. Two cathelicidin genes are present in both rainbow trout (*Oncorhynchus mykiss*) and Atlantic salmon (*Salmo salar*). *Antimicrob Agents Chemother* (2006) 50:185–95. doi: 10.1128/aac.50.1.185-195.2006
66. Mourente G, Good JE. Bell JG. Partial substitution of fish oil with rapeseed, linseed and olive oils in diets for European sea bass (*Dicentrarchus labrax* L.): effects on flesh fatty acid composition, plasma prostaglandins E2 and F2α, immune function and effectiveness of a fish oil finishing diet. *Aquac Nutr* (2005) 11:25–40. doi: 10.1111/j.1365-2095.2004.00320.x
67. Xia S, Li X-p, Cheng L, Han M-t, Zhang M-m, Shao Q-x, et al. Fish oil-rich diet promotes hematopoiesis and alters hematopoietic niche. *Endocrinology* (2015) 156:2821–30. doi: 10.1210/en.2015-1258
68. Magnadóttir B. Innate immunity of fish (overview). *Fish Shellfish Immunol* (2006) 20:137–51. doi: 10.1016/j.fsi.2004.09.006
69. Blazer VS. Piscine macrophage function and nutritional influences: A review. *J Aquat Anim Health* (1991) 3:77–86. doi: 10.1577/1548-8667(1991)003<0077:PMFANI>2.3.CO;2
70. Kiron V, Fukuda H, Takeuchi T, Watanabe T. Essential fatty acid nutrition and defence mechanisms in rainbow trout *Oncorhynchus mykiss*. *Comp Biochem Physiol A: Physiol* (1995) 111:361–7. doi: 10.1016/0300-9629(95)00042-6
71. Sheldon WM, Blazer VS. Influence of dietary lipid and temperature on bactericidal activity of channel catfish macrophages. *J Aquat Anim Health* (1991) 3:87–93. doi: 10.1577/1548-8667(1991)003<0087:IODLAT>2.3.CO;2
72. Thompson KD, Tatner MF, Henderson RJ. Effects of dietary (n-3) and (n-6) polyunsaturated fatty acid ratio on the immune response of Atlantic salmon, *Salmo salar* L. *Aquac Nutr* (1996) 2:21–31. doi: 10.1111/j.1365-2095.1996.tb00004.x
73. Alwarawrah Y, Kiernan K, MacIver NJ. Changes in nutritional status impact immune cell metabolism and function. *Front Immunol* (2018) 9:1055. doi: 10.3389/fimmu.2018.01055


**Conflict of Interest:** KK is employed by BioVivo Technologies AS, Bodø, Norway. KP is employed by Quantidoc AS, Bergen, Norway.

The remaining authors declare that the research was conducted in the absence of any commercial or financial relationships that could be construed as a potential conflict of interest.

frontiers in Immunology

ORIGINAL RESEARCH
published: 31 March 2021
doi: 10.3389/fimmu.2021.623764

# Identification and Characterization of Long Non-coding RNAs in the Intestine of Olive Flounder (*Paralichthys olivaceus*) During *Edwardsiella tarda* Infection

*Yunji Xiu*[1], *Yingrui Li*[1,2], *Xiaofei Liu*[1,2], *Lin Su*[1], *Shun Zhou*[1] *and Chao Li*[1]*

[1] School of Marine Science and Engineering, Qingdao Agricultural University, Qingdao, China, [2] College of Marine Science and Engineering, Nanjing Normal University, Nanjing, China

OPEN ACCESS

**Edited by:**
*Min Wan,*
*Ocean University of China, China*

**Reviewed by:**
*Carlo C. Lazado,*
*Norwegian Institute of Food, Fisheries and Aquaculture Research (Nofima), Norway*
*Lei Wang,*
*Chinese Academy of Fishery Sciences (CAFS), China*

***Correspondence:**
*Chao Li*
*chaoli@qau.edu.cn*

**Specialty section:**
*This article was submitted to Comparative Immunology, a section of the journal Frontiers in Immunology*

**Received:** *30 October 2020*
**Accepted:** *23 February 2021*
**Published:** *31 March 2021*

**Citation:**
*Xiu Y, Li Y, Liu X, Su L, Zhou S and Li C (2021) Identification and Characterization of Long Non-coding RNAs in the Intestine of Olive Flounder (Paralichthys olivaceus) During Edwardsiella tarda Infection. Front. Immunol. 12:623764. doi: 10.3389/fimmu.2021.623764*

Long non-coding RNAs (lncRNAs) play widespread roles in fundamental biological processes, including immune responses. The olive flounder (*Paralichthys olivaceus*), an important economical flatfish widely cultured in Japan, Korea, and China, is threatened by infectious pathogens, including bacteria, viruses, and parasites. However, the role of lncRNAs in the immune responses of this species against pathogen infections is not well-understood. Therefore, in this study, we aimed to identify lncRNAs in the intestine of olive flounder and evaluate their differential expression profiles during *Edwardsiella tarda* infection, which is an important zoonotic and intestinal pathogen. A total of 4,445 putative lncRNAs were identified, including 3,975 novel lncRNAs and 470 annotated lncRNAs. These lncRNAs had shorter lengths and fewer exons compared with mRNAs. In total, 115 differentially expressed lncRNAs (DE-lncRNAs) were identified during *E. tarda* infection. To validate the expression pattern of lncRNAs, six DE-lncRNAs were randomly selected for quantitative real-time PCR. The co-located and co-expressed mRNAs of DE-lncRNAs were predicted, which were used to conduct the Gene Ontology (GO) and Kyoto Encyclopedia of Genes and Genomes (KEGG) enrichment analyses. The target genes of DE-lncRNAs enriched numerous immune-related processes and exhibited a strong correlation with immune-related signaling pathways. To better understand the extensive regulatory functions of lncRNAs, the lncRNA–miRNA–mRNA regulatory networks were constructed, and two potential competing endogenous RNA (ceRNA) networks, LNC_001979-novel_171-Potusc2 and LNC_001979-novel_171-Podad1, were preliminarily identified from the intestine of olive flounders for the first time. In conclusion, this study provides an invaluable annotation and expression profile of lncRNAs in the intestine of olive flounder infected with *E. tarda*; this forms a basis for further studies on the regulatory function of lncRNAs in the intestinal mucosal immune responses of olive flounder.

**Keywords: long non-coding RNA, *Paralichthys olivaceus*, *Edwardsiella tarda*, intestinal mucosal immune response, lncRNA-miRNA-mRNA**

## INTRODUCTION

Long non-coding RNAs (lncRNAs) are a group of non-coding RNAs (ncRNAs) that are longer than 200 nucleotides (1). Although a few lncRNAs have been reported to encode small peptides (2, 3), most lncRNAs cannot translate into proteins. Compared with coding genes, lncRNAs have fewer and longer exons, and exhibit more tissue-specific expression and lower expression (1). LncRNAs have been divided into different categories based on their length, transcript properties, genomic location, regulatory elements, and function, in which three classes of lncRNAs (intergenic lncRNAs, antisense lncRNAs, and intronic lncRNAs) are known based on their genomic location (4). Lacking sequence conservation across different species, lncRNAs were initially considered as transcriptional noise and their biological importance was doubted (1). However, studies have shown that lncRNAs play important roles in the regulation of immune responses and host defense against pathogens (5). Several lncRNAs have been shown to be differentially expressed during microbial component stimulation or pathogen infection (5). Upon microbial component stimulation, the lncRNAs might regulate the transcription of immune genes by interacting with other complexes. In addition, these lncRNAs might play an important role in controlling host–pathogen interactions via regulating the growth and replication of pathogens, or via cell-autonomous anti-microbial defense mechanisms. In conclusion, lncRNAs can regulate a variety of biological processes at transcriptional and post-transcriptional levels, such as DNA methylation, histone modification, splicing, transcription, and translation, by interacting with genomic DNA, RNA, proteins, or a combination of these (1). Recently, several novel findings suggested that lncRNAs can act as miRNA sponges to bind miRNAs competitively to modulate the expression of mRNAs.

LncRNAs have been extensively studied in teleosts and emerging evidence suggests that lncRNAs may also serve as important regulators in the immune responses of teleosts (2). In teleosts, a number of lncRNAs have been shown to be differentially expressed during pathogen infections. Through comparative transcriptome data analysis, lncRNAs from rainbow trout (*Oncorhynchus mykiss*) (6), Atlantic salmon (*Salmo salar*) (7–10), Coho salmon (*Oncorhynchus kisutch*) (10), large yellow croakers (*Larimichthys crocea*) (11), zebrafish (*Danio rerio*) (12), European sea bass (*Dicentrarchus labrax*) (13), and Nile tilapia (*Oreochromis niloticus*) (3) were widely modulated after viruses, bacteria, or parasite infections. Enrichment analysis revealed that the modulated lncRNAs were localized near immune- and stress-related genes (10, 13). Previous studies have confirmed that lncRNAs might be implicated in teleost immune responses to pathogen infections. However, further analyses are required to fully characterize their detailed functions and mechanisms.

Despite the evidence for the immune-related regulatory functions of lncRNAs, few studies have been conducted on olive flounder (*Paralichthys olivaceus*). Olive flounder, which is an important economical flatfish, has been widely cultured in Japan, Korea, and China (14). However, the olive flounder industry is threatened by infectious pathogens, including bacteria, viruses, and parasites (15), which cause mixed infectious diseases, numerous deaths, and huge economic losses (16). Acting as a critical zoonotic and intestinal pathogen, *Edwardsiella tarda* could also result in substantial economic losses to the olive flounder aquaculture industry (16). A previous study identified 10,270 lncRNAs from mixed immune-related tissues (gill, intestine, liver, and kidney) in olive flounder with the PacBio Sequel platform, which consists of 38.18% antisense, 32.62% sense intronic, 20.58% lincRNA, and 8.62% sense overlapping lncRNA (17). In addition, the expression pattern and function of lncRNAs in the skeletal muscle of olive flounder have been characterized, which indicated that lncRNAs may participate in the development of skeletal muscle through cis- or trans-acting mechanisms (18). In summary, previous studies have provided a scientific basis for further studies on the biological function of lncRNAs in olive flounder, and these lncRNAs are greatly in need of further investigation. Considering that lncRNAs play important roles in modulating the immune responses of teleosts, it is necessary to further characterize the regulatory function and mechanism of lncRNAs in olive flounder.

In this study, lncRNAs were identified and characterized from the intestine of olive flounder. Besides serving as the prime site for nutrient absorption, the intestine represent one of the first lines of defense (19). Moreover, the expression patterns of lncRNAs at different time points post *E. tarda* infection were characterized. Additionally, co-localization and co-expression analyses were performed to predict the potential lncRNA–mRNA interactions in response to bacterial infections. GO and KEGG enrichment analyses were carried out with the targeted mRNA of lncRNAs. Moreover, the competing endogenous RNA (ceRNA) network, lncRNA–miRNA–mRNA, was constructed with differentially expressed lncRNAs, miRNAs, and mRNAs that had been reported previously (14). In conclusion, this study provides the expression and function analysis of newly identified lncRNAs from the intestine of olive flounder, which is one of the main mucosa-associated lymphoid tissues of teleosts. Our study provides insights into intestinal immune responses of lncRNAs during host–pathogen interactions and lays the foundation for further functional studies on lncRNAs during pathogen infections.

## METHODS AND MATERIALS

### Experimental Fish, Bacteria Challenge, and Sample Collection

The experimental fish, bacteria challenge, and sample collection have been described in a previous study (14). Briefly, a total of 50 olive flounders (body weight 120 ± 10 g, body length 22 ± 3 cm) were purchased from Huanghai Aquaculture Company, Shandong, China and raised at 20 ± 1°C in a recirculating water system for 1 week before the experiments, during which they were fed twice a day with a commercial diet. The health of the experimental fish was confirmed by randomly sampling for bacteriological, parasitological, and virological examinations. In the challenge experiment, a total of 27 olive

flounders were immersed in the *E. tarda* solution with a final concentration of $6 \times 10^7$ CFU/ml for 2 h and then returned to the recirculating water system. Then, the posterior intestine from nine fish were collected at 2, 8, and 12 h post-immersion, which was designated as H2, H8, and H12, respectively. In the control group, the *E. tarda* solution was replaced with aseptic seawater, and the posterior intestine from nine fish were collected and designated as H0. Overall, this experiment included four time points (H0, H2, H8, and H12), and each time point contained three biological replicates that consisted of three fish for each one. The posterior intestine was quickly isolated and frozen immediately in liquid nitrogen until RNA isolation.

## RNA Isolation and Library Preparation for lncRNA Sequencing

Total RNA from the posterior intestine was isolated using the Trizol reagent (Invitrogen, USA) following the manufacturer's protocol. RNA degradation and contamination were assessed on a 1% agarose gel. RNA purity was monitored using the NanoPhotometer® spectrophotometer (IMPLEN, CA, USA). RNA concentration was assessed using the RNA Assay Kit in Qubit® 2.0 Flurometer (Life Technologies, CA, USA). RNA integrity was measured using the RNA Nano 6000 Assay Kit of the Bioanalyzer 2100 system (Agilent Technologies, CA, USA). The library sequencing was performed by Novogene Corporation (Tianjin, China). A total amount of 3 μg of RNA per sample was used as the input material for the RNA sample preparations and sequencing. First, ribosomal RNA (rRNA) was removed using the Ribo-zero™ rRNA Removal Kit (Epicentre, USA), and rRNA-free residue was cleaned up by ethanol precipitation. Subsequently, sequencing libraries were generated using the rRNA-depleted RNA using the Ultra™ Directional RNA Library Prep Kit for Illumina® (NEB, USA) following the manufacturer's instructions. Briefly, fragmentation was conducted using divalent cations under elevated temperatures in the NEBNext First Strand Synthesis Reaction Buffer (5X). The first strand of cDNA was synthesized using a random hexamer primer and M-MuLV Reverse Transcriptase (RNaseH-), while the second strand of cDNA was synthesized using DNA Polymerase I and RNase H. In order to select cDNA fragments that were ∼150–200 bp in length, the library fragments were purified with the AMPure XP system (Beckman Coulter, Beverly, USA). Then, 3 μL of USER Enzyme (NEB, USA) was used with size-selected, adaptor-ligated cDNA at 37°C for 15 min followed by 5 min at 95°C before PCR. Thereafter, PCR was performed with Phusion High-Fidelity DNA polymerase, universal PCR primers, and index (X) primers. Next, the products were purified (AMPure XP system) and their library quality was assessed on the Agilent Bioanalyzer 2100 system. Following the manufacturer's instructions, the clustering of the index-coded samples was then performed on a cBot Cluster Generation System using TruSeq PE Cluster Kit v3-cBot-HS (Illumia). Finally, after the cluster generation, the libraries were sequenced on an Illumina Hiseq 4000 platform and 150 bp paired-end reads were generated.

## Transcriptome Assembly and lncRNA Identification

Raw reads were first processed through in-house Perl scripts, in which clean reads were acquired by removing low-quality reads that contained adapter sequences and ploy-N from the raw data. At the same time, the Q20, Q30, and GC content of the clean data were calculated. The high-quality clean data were used for the subsequent downstream analyses. Then, the reference genome and gene model annotation files were downloaded from the genome website directly (ftp://ftp.ncbi.nlm.nih.gov/genomes/all/GCF/001/970/005/GCF_001970005.1_Flounder_ref_guided_V1.0/). The reference genome index was built using bowtie2 v2.2.8 and paired-end clean reads were aligned to the reference genome using HISAT2 v2.0.4 (20). Next, the mapped reads of each sample were assembled using StringTie v1.3.1 (21) in a reference-based approach. StringTie uses a novel network flow algorithm as well as an optional *de novo* assembly step to assemble and quantitate full-length transcripts that represent multiple splice variants for each gene locus.

Based on the transcriptase splicing results, we set a series of strict screening conditions based on the structural characteristics of lncRNAs and the functional characteristics of non-coding proteins. We followed the five basic principles below to filter lncRNAs: (1) exon number $\geq$ 2; (2) transcript length $>$ 200 bp; (3) filter annotated transcripts and lncRNAs; (4) expression level (Cuffquant software, FPKM $\geq$ 0.5); (5) transcripts with coding potential predicted by CNCI (Coding-Non-Coding-Index), CPC (Coding Potential Calculator), Pfam Scan, and PhyloCSF (phylogenetic codon substitution frequency) were filtered out, and those without coding potential were our candidate set of lncRNAs.

## Different Expression Analysis of lncRNAs and qRT-PCR Verification

Gene expression was normalized using the fragments per kilobase of exon per million reads mapped (FPKM), which was calculated using Cuffdiff (v2.1.1) (22). Cuffdiff provides statistical routines for determining differential expression in the gene expression data using a model based on the contrary binomial distribution (22). Subsequently, differentially expressed lncRNAs at H2, H8, and H12 compared with H0 were filtered, and lncRNAs with a $p$-value $< 0.05$ were assigned as differentially expressed.

To validate the Illumina sequencing data, a total of six differentially expressed lncRNA were randomly selected for the qRT-PCR analysis. First, cDNA was synthetized using the PrimeScript 1st strand cDNA Synthesis Kit (Takara, Japan). Then, specific primers were designed based on their sequences and EF1α was used as the internal control. The qRT-PCR was performed with the CFX96 Real-time Fluorescent quantitative PCR system (Bio-Rad, USA) using TB Green™ Premix Ex Taq™ II (TaKaRa, Japan). The amplification cycle was as follows: 95°C for 30 s, 40 cycles at 95°C for 5 s, and 60°C for 1 min, followed by a melting curve from 60 to 95°C. Data are shown as means ± SE for three replicates, and statistical analysis was performed using SPSS19.0.

**TABLE 1 |** Information of lncRNAs sequencing data.

| Sample Name | Raw Reads | Clean Reads | Clean Bases | Error Rate | Q20 (%) | Q30 (%) | GC Content |
|---|---|---|---|---|---|---|---|
| HO_1 | 91,001,552 | 85,570,680 | 12.84 G | 0.02 | 97.16 | 92.72 | 47.40 |
| HO_2 | 98,086,488 | 92,224,408 | 13.83 G | 0.02 | 97.18 | 92.72 | 48.90 |
| HO_3 | 116,471,068 | 109,413,634 | 16.41 G | 0.02 | 96.99 | 92.32 | 48.85 |
| H2_1 | 133,971,546 | 125,928,236 | 18.89 G | 0.02 | 97.10 | 92.55 | 49.09 |
| H2_2 | 91,713,816 | 86,756,860 | 13.01 G | 0.02 | 97.19 | 92.72 | 49.33 |
| H2_3 | 83,268,176 | 81,661,360 | 12.25 G | 0.02 | 97.29 | 92.87 | 49.59 |
| H8_1 | 84,134,060 | 82,485,038 | 12.37 G | 0.02 | 97.33 | 92.97 | 49.47 |
| H8_2 | 89,841,602 | 88,149,192 | 13.22 G | 0.02 | 97.33 | 92.98 | 49.26 |
| H8_3 | 85,281,542 | 83,698,290 | 12.55 G | 0.01 | 97.39 | 93.10 | 49.37 |
| H12_1 | 123,787,190 | 121,500,194 | 18.23 G | 0.01 | 97.39 | 93.09 | 49.28 |
| H12_2 | 99,739,544 | 97,782,904 | 14.67 G | 0.02 | 97.33 | 92.96 | 49.00 |
| H12_3 | 112,061,808 | 109,856,848 | 16.48 G | 0.01 | 97.37 | 93.09 | 47.94 |

## Target Gene Prediction and Enrichment Analysis

The target genes of the DE-lncRNAs were predicted using *cis*/*trans*-regulatory algorithms. The *cis* and *trans* regulatory roles refer to the influence of lncRNAs on neighboring target genes and other genes at the expression level, respectively. We searched coding genes that were 10/100 k upstream and downstream of lncRNA, which were considered to be co-located target genes. Co-expressed target genes were predicted using the expressed Pearson correlation coefficient between the lncRNAs and corresponding coding genes using custom scripts ($p < 0.05$ and $|R| > 0.95$). Finally, regulatory networks were constructed and visualized by Cytoscape v3.6.1. In this case, the coding genes used for target gene prediction have been previously reported based on the immune responses of *P. olivaceus* against an *E. tarda* challenge (14).

The Gene Ontology (GO) enrichment analysis of lncRNA target genes was performed using the GOseq package in R, in which gene length bias was corrected (23). GO terms with $p < 0.05$ were considered significantly enriched by differentially expressed genes. KEGG is a database that contains large-scale molecular datasets generated by genome sequencing and other high-throughput experimental technologies (http://www.genome.jp/kegg/) that can be used to elucidate the high-level functions and utilities of biological systems (24), such as cells, organisms, and ecosystems, from molecular-level information. We used the KOBAS software to test the statistical enrichment of the lncRNA target genes in KEGG pathways (25).

## Construction of the lncRNA–miRNA–mRNA Regulatory Network

To better understand the extensive regulatory functions of lncRNAs, the lncRNA mediated ceRNA network was constructed with differentially expressed miRNAs and mRNAs that have been reported previously (14). The lncRNA–miRNA and miRNA–mRNA interaction analysis was conducted with the microRNA target prediction tool miRanda, and the lncRNA–miRNA–mRNA network was generated using a combination of the lncRNA–miRNA network and miRNA–mRNA network with the Cytoscape 3.6.1 software.

## Luciferase Assay

To test the interaction between LNC_001979 or mRNA (Potusc2, Podad1) and novel_171, luciferase reporter assays were conducted using the dual-luciferase reporter system. The wild-type target sequences of LNC_001979, Potusc2, and Podad1 were cloned into the pmirGLO reporter luciferase vector and named pmirGLO-LNC_001979-WT, pmirGLO-Potusc2-WT, and pmirGLO-Podad1-WT, respectively. Then, the wild-type recombinant plasmids were mutated into pmirGLO-LNC_001979-Mut, pmirGLO-Potusc2-Mut, and pmirGLO-Podad1-Mut with mutant primers and the In-fusion HD Cloning Kit (Takara, Japan) following the manufacturer's instructions. HEK293T cells were co-transfected with wild-type or mutant-type recombinant plasmid and novel_171 mimics or negative control mimics (NC) using Lipofectamine 2000 (Invitrogen, USA). The cells were collected at 48 h after transfection and the luciferase activity was detected using the Luciferase Assay Systems kit (Promega, USA) following the manufacturer's instructions.

# RESULTS

## Genome-Wide Identification of lncRNAs

Twelve cDNA libraries were constructed to perform Illumina sequencing. The data has been deposited in NCBI database, with the BioProject number of PRJNA510440. The raw reads, clean reads, clean bases, error rate, Q20, Q30, and GC contents for each library are shown in **Table 1**. A total of 305,559,108, 308,953,538, 259,257,204, and 335,588,542 raw reads were acquired from the H0, H2, H8, and H12 group, respectively. All the libraries were of good quality, with clean base values $\geq$12.25 G, error rates $\leq$0.02, Q20 $\geq$ 96.99%, and Q30 $\geq$ 92.32%. Therefore, all the libraries were verified in be appropriate for further study. Then, the clean reads from all the libraries were used to discern the lncRNAs. As shown in **Figure 1A**, the lncRNAs were obtained following

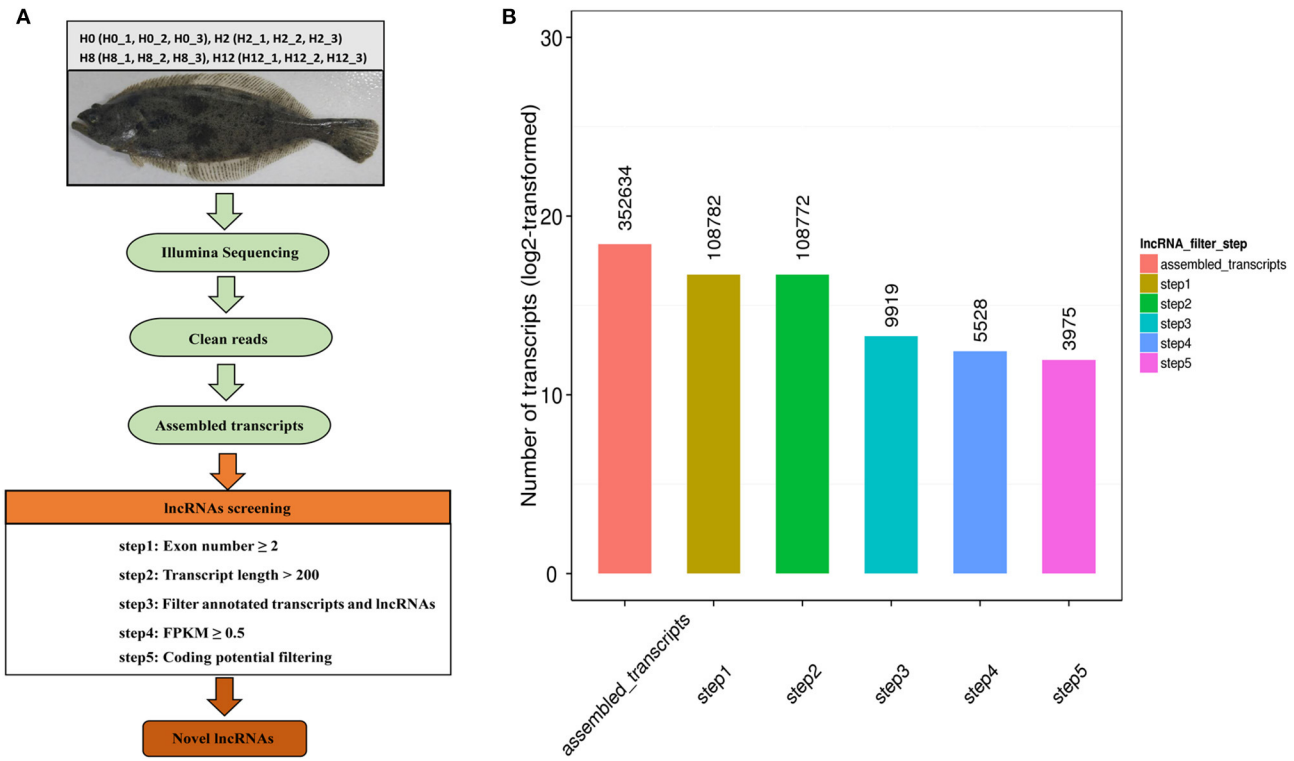


**FIGURE 1 | (A)** Identification pipeline for lncRNAs in olive flounders. **(B)** The numbers of candidate transcripts at five filtering stages.

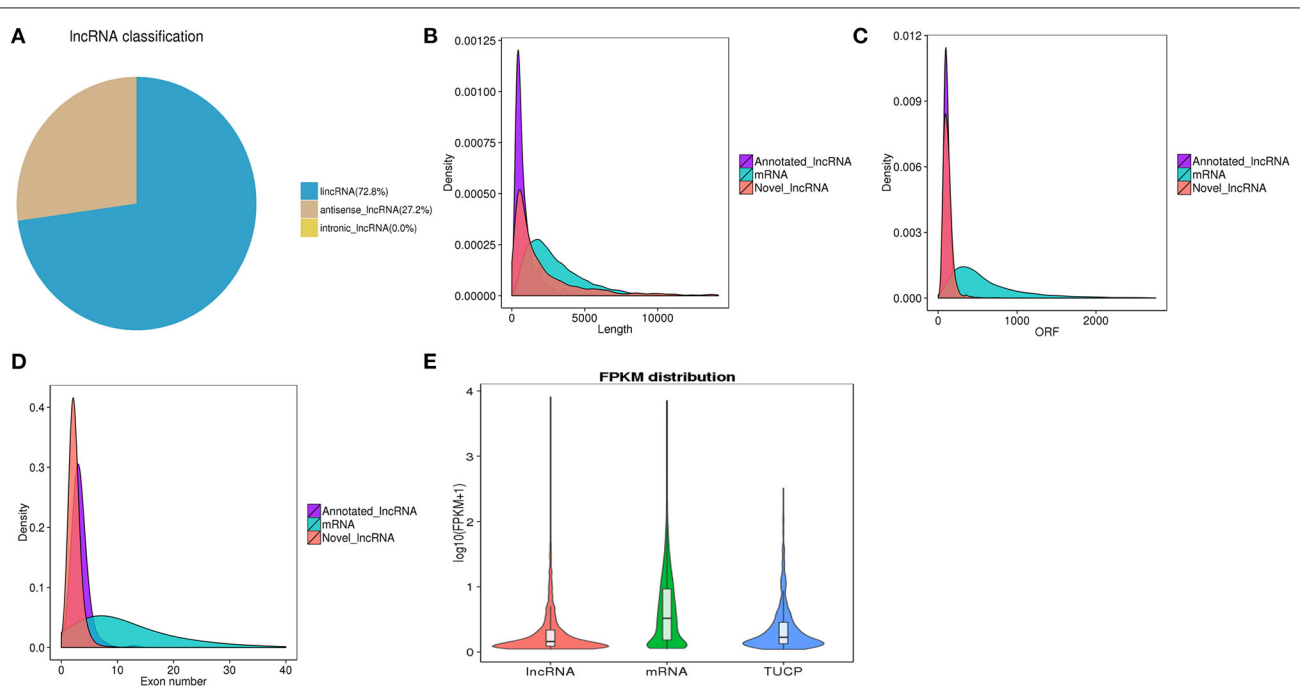


**FIGURE 2 | (A)** Classification of lncRNAs in three classes. **(B)** Comparison of transcript lengths in annotated lncRNAs, mRNAs, and novel lncRNAs. **(C)** Comparison of ORF lengths in annotated lncRNAs, mRNAs, and novel lncRNAs. **(D)** Comparison of exon numbers in annotated lncRNAs, mRNAs, and novel lncRNAs. **(E)** Expression levels of lncRNAs, mRNAs, and TUCP from all samples.

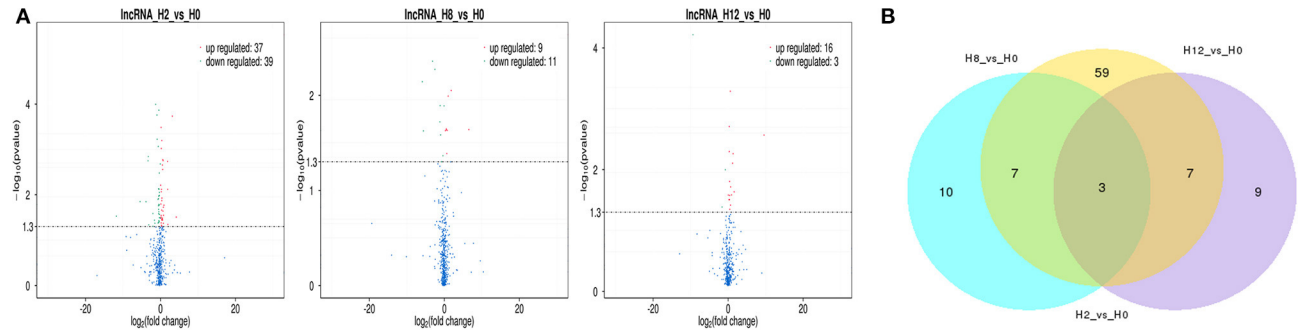


**FIGURE 3 | (A)** Volcano plots of differentially expressed lncRNAs in the H2 vs. H0, H8 vs. H0, and H12 vs. H0 comparisons. The red and blue blots represent the significantly upregulated and downregulated DE-lncRNAs. **(B)** Venn diagram of the DE-lncRNAs in the three comparisons.

the five basic filtering steps, and a total of 108,782, 108,772, 9,919, 5,528, and 3,975 transcripts were identified from step 1 to step 5, respectively (**Figure 1B**). Finally, a total of 4,445 putative lncRNAs were identified, including 3,975 novel lncRNAs and 470 annotated lncRNAs (**Supplementary Table 1**).

## Characteristics of lncRNAs

LncRNAs were classified based on their genomic location, and the 4,445 lncRNAs consisted of 72.8% lincRNA (long intergenic non-coding RNA) and 27.2% antisense lncRNA but no intronic lncRNA (**Figure 2A**). We then compared the full length, ORF length, and exon number between the lncRNAs and mRNAs. We found that both novel and annotated lncRNAs were shorter in full length and ORF length than the mRNAs (**Figures 2B,C**). The ORF length of the lncRNAs ranged from 24 to 1,066 nucleotides, which was shorter than most of the mRNA ORF lengths. As shown in **Figure 2D**, the lncRNAs had fewer exons than the mRNAs. All the lncRNAs had 2–13 exons, while the mRNAs had a much wider distribution range of exon numbers. Otherwise, the average expression level of lncRNAs was much lower than that of mRNAs (**Figure 2E**).

## Different Expression Levels of lncRNAs Under *E. tarda* Infection

In comparison with H0, a total of 115 lncRNAs showed significantly different expression levels ($p$-value $< 0.05$), including 76, 20, and 19 DE-lncRNAs in the H2, H8, and H12 groups, respectively (**Figure 3A**). The most significant dfferences existed in the H2 group, in which 37 lncRNAs were significantly upregulated and 39 lncRNAs were significantly downregulated ($p$-value $< 0.05$). As shown in the Venn diagram, some DE-lncRNAs were differentially expressed at two or three comparisons. Moreover, despite the large number of DE-lncRNAs between the experimental and control groups, only three DE-lncRNAs (∼2.6%) overlapped among three inter-group comparisons, and 14 DE-lncRNAs (∼12.2%) overlapped among two inter-group comparisons (**Figure 3B**).

To validate the RNA-seq data, six DE-lncRNAs (LNC_001979, XR_002202604.1, LNC_003414, LNC_003963, XR_002202677.1, and XR_002203466.1) were randomly selected for the qRT-PCR analysis (**Figure 4**). Although individual lncRNAs differed from the RNA-seq data at some time points, most of the qRT-PCR results were in high accordance with the transcriptomic results, which confirmed the reliability and accuracy of the RNA-seq data.

## Prediction of DE-lncRNA Targeted Genes

Co-localization and co-expression analyses were conducted between DE-lncRNAs and mRNAs to predict the potential lncRNA–mRNA interactions in response to bacterial infections and establish the potential roles of the lncRNAs in immunoreactions. A total of 33,531 co-location lncRNA–mRNA pairs were observed, including 3,326 lncRNAs and 18,168 mRNAs (**Supplementary Table 2**). We found that LNC_001129 and XR_002202865.1 exhibited the highest degree (degree = 48), followed by LNC_000228, LNC_000803, LNC_000768, LNC_000769, LNC_000774, LNC_000773, LNC_000772, LNC_000771, and LNC_000770 (degree = 45). Meanwhile, in the co-expression analysis, we observed a total of 91,501 lncRNA–mRNA pairs that contained 2,412 lncRNAs and 7,264 mRNAs (**Supplementary Table 3**). Of these pairs, a total of 91,221 (99.69%) were positively correlated and 280 (0.31%) were negatively correlated. We found that LNC_001467 (degree = 355) and LNC_000543 (degree = 338) indicated higher degrees. These results highlighted that lncRNAs exhibited significant expression correlations with protein-coding genes on *P. olivaceus* in response to bacterial infections.

## Function Analysis of DE-lncRNA Target Genes

To further analyze the potential function of 18,168 co-located and 7,264 co-expressed mRNAs, we analyzed their associated function using the GO enrichment and KEGG pathway analyses.

The GO enrichment analysis results are represented in **Supplementary Tables 4**, **5** for co-located and co-expressed mRNAs, respectively. In this study, numerous immune-related processes were enriched in biological processes, such as the intracellular transport of viral proteins in host cells (GO:0019060), regulation of viral protein levels in host cells by viruses (GO:0046719), bacteriocin immunity (GO:0030153), humoral immune response (GO:0006959), innate immune response (GO:0045087), evasion or tolerance

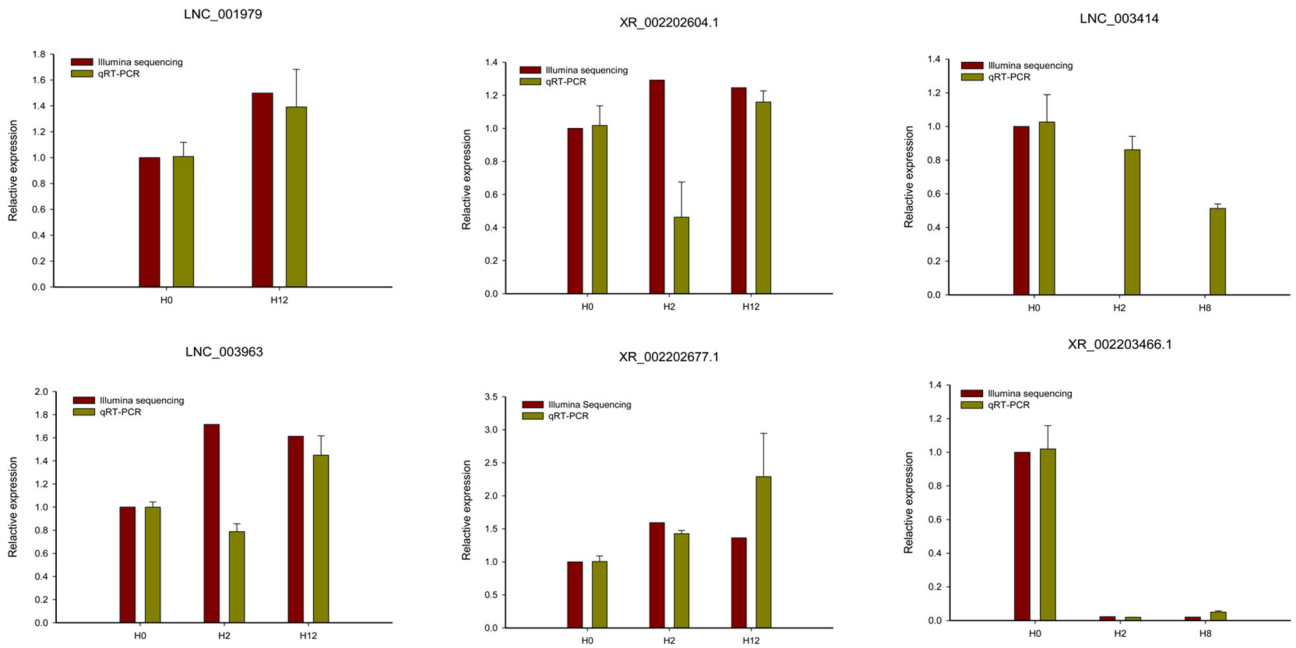


**FIGURE 4 |** qRT-PCR analysis of six randomly selected DE-lncRNAs (LNC_001979, XR_002202604.1, LNC_003414, LNC_003963, XR_002202677.1, and XR_002203466.1). The qRT-PCR analysis results were compared with data obtained from Illumina sequencing.

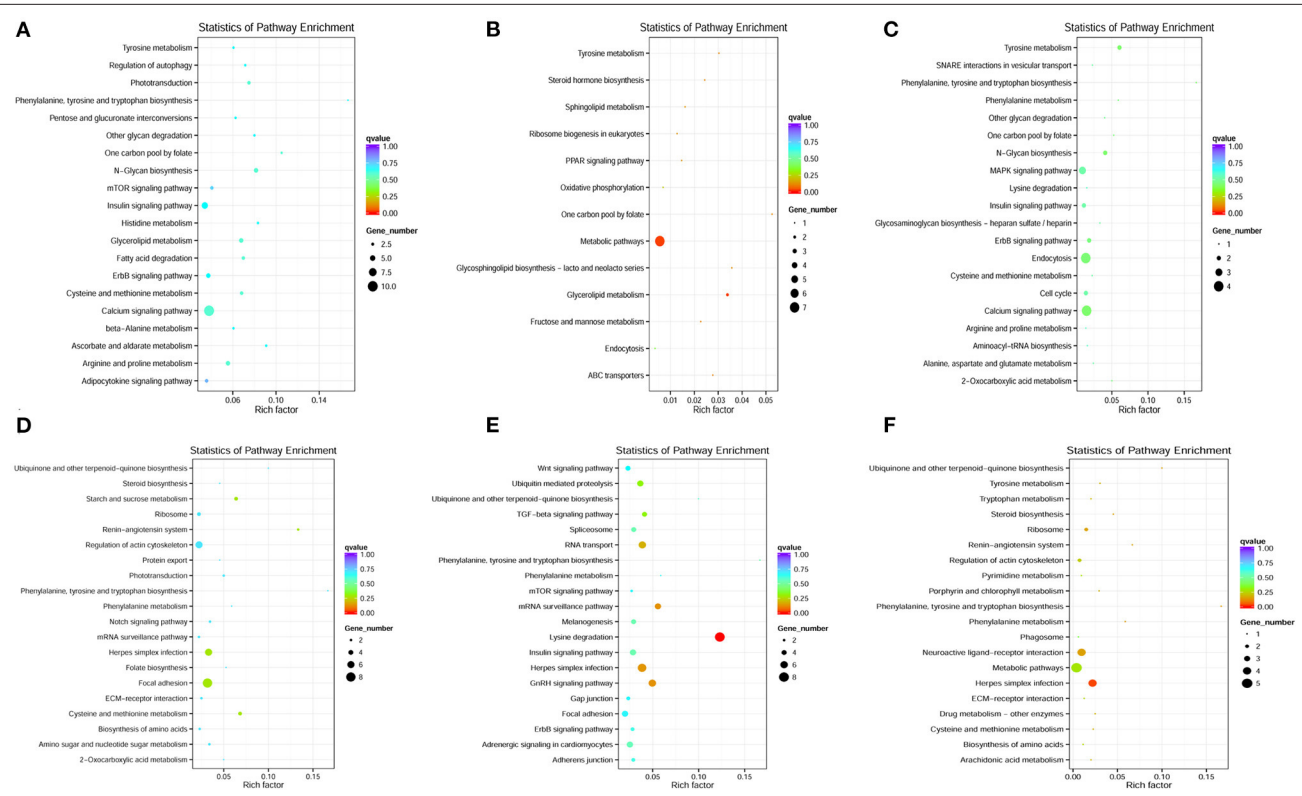


**FIGURE 5 |** KEGG pathway enrichment of co-located and co-expressed mRNAs. **(A–C)** The most significantly enriched top 20 pathways of co-located mRNAs in the H2 vs. H0, H8 vs. H0, and H12 vs. H0 comparisons, respectively. **(D–F)** The most significantly enriched top 20 pathways of co-expressed mRNAs in the H2 vs. H0, H8 vs. H0, and H12 vs. H0 comparisons, respectively.

of the host defense response (GO:0030682), avoidance of host defenses (GO:0044413).

Otherwise, the most significantly enriched top 20 pathways were selected to represent the KEGG pathway enrichment results. As shown in **Figure 5**, the KEGG pathway enrichment results shown that the target genes of DE-lncRNAs exhibited a strong correlation with immune-related signaling pathways, including the regulation of autophagy, the PPAR signaling pathway, endocytosis, the MAPK signaling pathway, the Notch signaling pathway, herpes simplex infections, ECM–receptor interactions, and phagosomes. This suggested that lncRNAs may play essential roles in modulating mRNA expression levels and subsequently trigger downstream immune signaling pathways to regulate the immune response to pathogen infections in fish.

## Bioinformatics Analysis of lncRNA–miRNA–mRNA Networks

To better comprehend the role of differentially expressed lncRNAs, lncRNA–miRNA–mRNA ceRNA triple regulatory networks were constructed. The lncRNA–miRNA–mRNA networks were generated using a combination of lncRNA–miRNA pairs and miRNA–mRNA pairs, which were predicted using the MiRanda software based on their differentially expressed results (**Figure 6**). This network contained 169 lncRNA–miRNA pairs and 3,682 miRNA–mRNA pairs, including 64 lncRNAs, 31 miRNAs, and 1,766 mRNAs (**Supplementary Table 6**).

Among the 169 lncRNA–miRNA pairs, a few circRNA-miRNA pairs existed in multiple comparison groups; for example, XR_002202301.1-novel_171 existed in all three comparisons, LNC_003414-novel_561, LNC_003415-novel_561, and LNC_000378-novel_561 existed in both H2 vs. H0 and H8 vs. H0 comparisons, XR_002202604.1-novel_144, LNC_002022-novel_144, LNC_000378-novel_144, LNC_002022-novel_171, LNC_002022-novel_51, XR_002202350.1-novel_51, LNC_002022-pol-miR-144-3p, LNC_000378-pol-miR-144-3p, and LNC_003631-pol-miR-144-3p existed in both H2 vs. H0 and H12 vs. H0 comparisons. Among the 3,682 miRNA–mRNA pairs, 179 miRNA–mRNA pairs existed in multiple comparison groups; for example, novel_171-109627566, novel_171-109625534, novel_171-109646742, novel_171-109646311, novel_171-109644261, novel_171-109632613, novel_171-109639130, novel_171-109641813, novel_171-109624060, novel_171-109639395, novel_171-109634146, and novel_171-109631850 pairs existed in all of the three comparisons.

## Potential LNC_001979-Novel_171-mRNA (Potusc2 and Podad1) ceRNA Network

Bioinformatics analyses revealed that LNC_001979, Potusc2, and Podad1 harbor a common standard target sequence for novel_171 (**Figures 7A–C**). To investigate whether LNC_001979, Potusc2, and Podad1 are direct targets of novel_171, a dual-luciferase reporter assay was performed. As shown in **Figures 7D–F**, novel_171 mimics the markedly decreased luciferase activity of cells transfected with pmirGLO-LNC_001979-WT, pmirGLO-Potusc2-WT, or pmirGLO-Podad1-WT, but no effect on luciferase activity was observed in cells transfected with pmirGLO-LNC_001979-Mut, pmirGLO-Potusc2-Mut, or pmirGLO-Podad1-Mut. The novel_171 negative control was also subjected to HEK293 cells for luciferase activity, there was no effect on luciferase activity in cells transfected with wild or mutant plasmids. These results revealed that novel_171 can directly target LNC_001979, Potusc2, and Podad1.

# DISCUSSION

## Transcriptome Assembly

Recently, an increasing number of lncRNAs have been identified and characterized from different immune-related tissues of teleosts using high-throughput sequencing, some of which have been proven to play important roles in immune responses against pathogen infections (26). In this study, the Illumina platform was used to investigate the lncRNA profile of olive flounder. More complete and unbiased transcriptome datasets were developed, which will help elucidating the function of lncRNAs related to immune responses under pathogen infections in teleosts.

In this study, each library produced more than 83 million raw reads. After filtering the low-quality reads, a total of 287,208,722, 294,346,456, 254,332,520, and 329,139,946 clean reads were acquired from the H0, H2, H8, and H12 group, respectively, which accounted for more than 93% of the raw reads. Furthermore, at least 84% of the clean reads from each library were mapped on to the genome of the olive flounder, which is higher than what has been previously reported. Previous reports have shown that the mapping rates were only 67.32, 74, and 79.13% (18, 27), which are relatively low. It has been speculated that the low mapping rates of olive flounders may be due to their imperfect reference genome (18). In conclusion, we obtained good clean reads and mapping rates, which is of great significant for further studies on screening and verifying the roles of lncRNAs.

A total of 4,445 putative lncRNAs were identified, including 3,975 novel lncRNAs and 470 annotated lncRNAs, which tremendously enriched the pool of lncRNAs in fish intestine. The intestine, which is one of the main mucosa-associated lymphoid tissues in teleosts (28), was likely the main route of *E. tarda* entry (29, 30). Despite evidence for the immune functions of teleost intestines, no study on lncRNAs has exclusively focused on intestinal tissue; most of the studies have just been conducted on the head kidney, spleen, and liver. Otherwise, we found that olive flounder lncRNAs share several more common characteristics of lncRNAs than mRNAs, including shorter full lengths and ORF lengths, fewer exons, sequence length, lower expression levels, and sequence conservation (31).

## DE-lncRNAs and Annotation of Target Genes

Recently, a growing body of literature identified that lncRNAs acting as positive or negative regulators in immunity against bacterial infection (32). On the one hand, the host lncRNAs play important roles in protecting host from pathogen invasion by regulating immune-related genes at epigenetic,

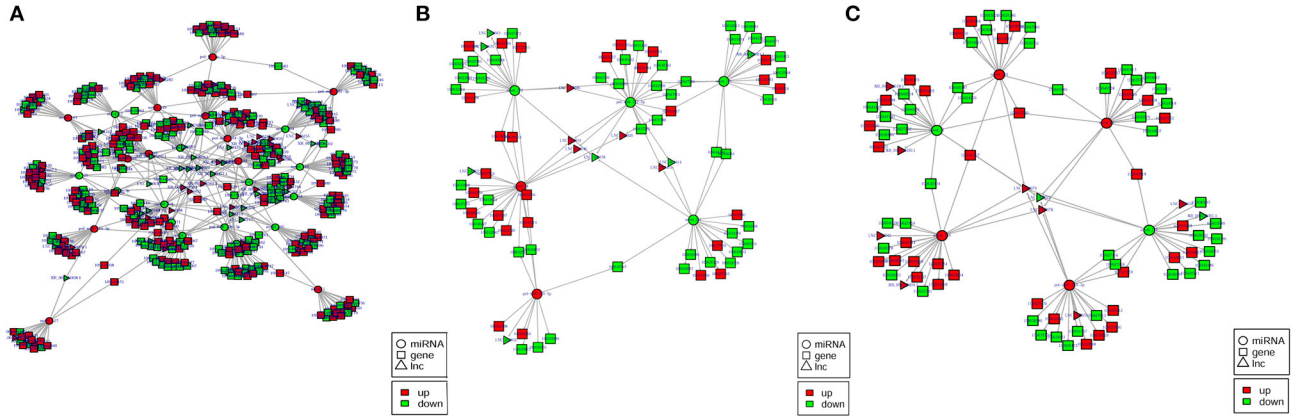


**FIGURE 6 | (A–C)** The predicted lncRNA–miRNA–mRNA networks in the H2 vs. H0, H8 vs. H0, and H12 vs. H0 comparisons, respectively. LncRNA, miRNA, and mRNA are represented by triangles, circles, and squares, respectively. The red color represents upregulated, and the green color represents downregulated.

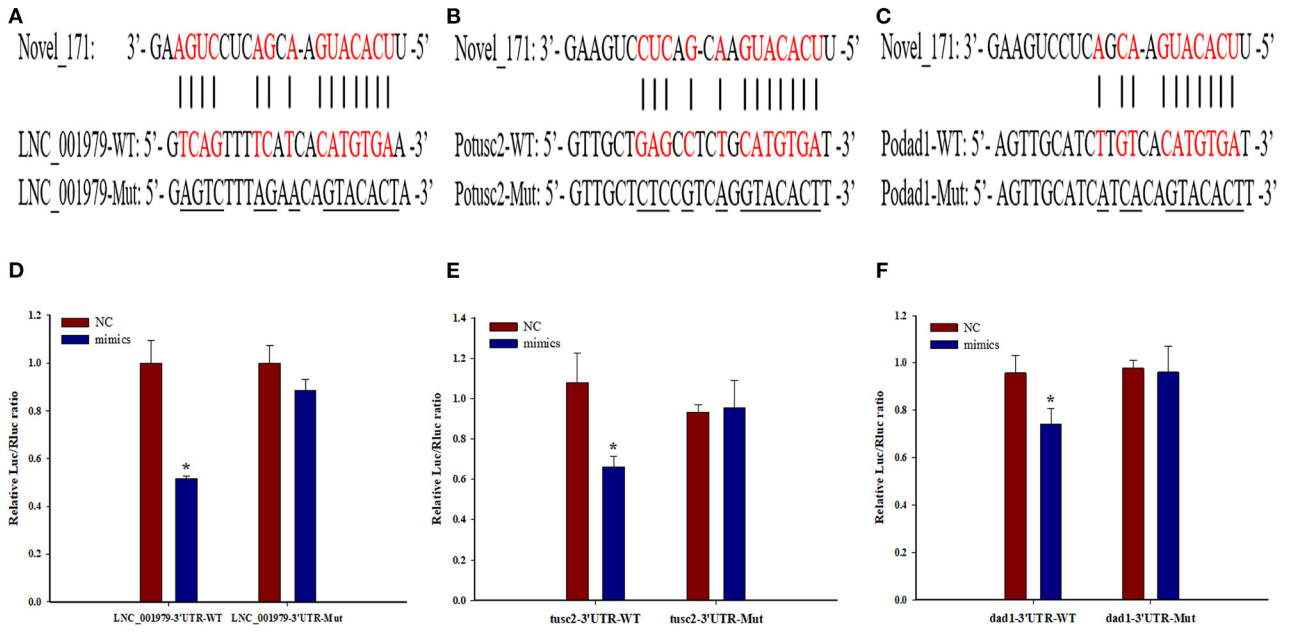


**FIGURE 7 |** The potential LNC_001979-novel_171-mRNA (Potusc2 and Podad1) ceRNA network. Sequence alignment of novel_171 and its binding sites in the LNC_001979 **(A)**, Potusc2 **(B)**, and Podad1 **(C)**. HEK293 cells were transfected with wild-type or mutant LNC_001979 **(D)**, Potusc2 **(E)**, and Podad1 **(F)**, together with novel_171 mimics, or NC. The asterisks (*) indicate significant differences ($P < 0.05$) between the NC and mimics group.

transcriptional, and post-transcriptional levels (32). In the epigenetic modification, lncRNAs regulate DNA methylation and histone modification to change the state of chromatin, thereby leading to transcriptional activation or silencing (32). At the transcriptional level, lncRNAs can directly affect the transcription of downstream genes by physically interacting with transcription factors, structural proteins, and RNA binding proteins (33). At the post-transcriptional level, lncRNAs affect gene expression by regulating translation efficiency, mRNA stability, and splicing (5). On the other hand, bacteria can manipulate the host signaling pathways by regulating the host lncRNAs to escape immune clearance (32), for example, two lncRNAs, SSR42 and RNA III, participated in alpha-toxin production and *Staphylococcus aureus* hemolysis induced by antibiotics (34, 35).

In the last few years, the modulation of lncRNAs has been described in teleosts after infected with viruses, bacteria, or parasites (3, 6–13). In order to identify the lncRNAs that are involved in the defense of olive flounder against *E. tarda* infections, the expression levels of lncRNAs were calculated and the DE-lncRNAs between the experimental and control groups were filtered. A total of 115 DE-lncRNAs were identified,

which consisted of 76, 20, and 19 DE-lncRNAs in the H2 vs. H0, H8 vs. H0, and H12 vs. H0 comparisons, respectively. We discovered that lncRNAs were expressed in a time-dependent manner post *E. tarda* infection, which indicated that DE-lncRNAs may exert a different regulatory role in the intestine of olive flounder. Moreover, our results indicate that lncRNAs might mainly participate in the early stage of host immune responses. Similarly, in the European sea bass, the number of DE-lncRNAs substantially reduced as time progressed; for example, a total of 204 and 931 lncRNAs were significantly modulated in the head kidney and brain of European sea bass 24 h after nodavirus infection, but only 93 lncRNAs and 342 lncRNAs were significantly modulated at 72 h (13). In the last few years, DE-lncRNAs have been linked to the fluctuations in typical immune-related genes. Furthermore, the described modulatory functions of DE-lncRNAs have mainly been related to their impact on the co-located and co-expressed protein-coding target genes. In this study, a total of 18,168 co-located and 7,264 co-expressed target genes were discovered, which were then annotated with GO and KEGG function databases.

The GO analysis identified that the target genes of DE-lncRNAs participated in diverse biological processes under the infectious agent. Furthermore, several target genes of DE-lncRNAs were enriched in several immune-related processes, which suggested that lncRNAs serve as intermediaries and play a significant role in regulating immune responses. A similar discovery was reported on the European sea bass, in which the GO analysis showed that numerous biological process terms directly involved in immunity were found to be enriched at 24 h post-challenge (13).

The KEGG analysis enables a better understanding of the complex network in regulatory mechanisms (17). Our results identified that the target genes of DE-lncRNAs were strongly enriched in immune-related signaling pathways, including the regulation of autophagy, the PPAR signaling pathway, endocytosis, the MAPK signaling pathway, the Notch signaling pathway, herpes simplex infection, ECM-receptor interactions, and phagosomes. Immune-related signaling pathways that are enriched by lncRNA target genes have been found in other teleosts. For example, the KEGG analysis of zebrafish showed a large number of processes linked to viral infections, such as endocytosis, the MAPK signaling pathway, herpes simplex infection, the Toll-like receptor signaling pathway, the RIG-I-like receptor signaling pathway, and the NOD-like receptor signaling pathway (12). Paneru et al. (6) reported that a total of 290 neighboring gene of DE-lncRNAs in rainbow trout had hits to KEGG pathways, in which 51 different genes were related to immunity pathways, including chemokine signaling, platelet activation, complement system, TNF signaling, T-cell receptor signaling, Fc gamma R-mediated phagocytosis, Toll-like receptor signaling, phagosomes, cytokine-cytokine receptor interactions, NOD-like receptor signaling, leukocyte trans-endothelial migration, and others. In addition, 49 different genes were involved in microbial infection processes and 28 different genes were common in both sets of these pathways. Otherwise, lncRNAs stimulated the TLR signaling pathway to elicit host antiviral responses in yellow croaker post *Vibrio anguillarum* infection (36). Therefore, lncRNAs may play central and diverse roles in controlling host immune responses against pathogen infections via triggering downstream immune signaling pathways.

## lncRNA–miRNA–mRNA Networks in Olive Flounder

An increasing number of studies have confirmed that lncRNAs can act as targets of miRNAs and then suppress the interaction between miRNAs and coding genes (6, 13). In recent years, ceRNA regulatory networks have been widely investigated in types of diseases (11, 37). Moreover, Chu et al. (27, 38) confirmed the hypothesis that ceRNA regulatory networks also exist in teleosts. In this study, the lncRNA–miRNA–mRNA networks were constructed by using a combination of lncRNA–miRNA and miRNA–mRNA pairs. KEGG analysis revealed that mRNAs in the lncRNA–miRNA–mRNA networks were significantly ($p < 0.05$) enriched in Herpes simplex infection. A total of 32 mRNAs were involved in herpes simplex infection signaling pathway, including 109,626,283, 109,623,691, 109,627,599, 109,644,197, 109,647,155, 109,641,940, 109,625,845, 109,637,327, 109,624,406, 109,633,274, 109,643,961, 109,636,767, 109,628,267, 109,643,520, 109,639,858, 109,644,261, 109,625,570, 109,634,833, 109,633,363, 109,643,253, 109,643,252, 109,637,639, 109,626,354, 109,631,327, 109,642,261, 109,641,879, 109,629,246, 109,641,908, 109,629,344, 109,646,115, 109,645,569 and 109,633,948. Herpes simplex virus (HSV) is a common human pathogen, which initially infects orofacial mucosal surfaces and replicates in epithelial cells at these sites, causing clinically overt disease characterized by vesicular lesions (39). On one hand, HSV invasion is normally followed by activation of both the innate and adaptive immune systems (40). On the other hand, HSV develops different mechanisms, including inhibition of autophagy and apoptosis to avoid the immune system and maintain itself in latency (40). This research revealed that Herpes simplex infection signaling pathway is also important in the regulation of *E. tarda* infection, and the constructed lncRNA–miRNA–mRNA networks shed new light on understanding the interplay of *E. tarda* infection and the intestinal mucosal immune responses of *P. olivaceus*.

Recently, it has been proven that lncRNAs serve as novel regulators for innate antiviral responses in teleost fish. The lncRNA MARL functions as a ceRNA for miR-122 to control the abundance of mitochondrial antiviral signaling proteins (MAVS), thereby inhibiting *Siniperca chuatsi rhabdovirus* (SCRV) replication and promoting antiviral responses (38). In addition, the lncRNA AANCR functions as a ceRNA for miR-210 to control the protein abundance of MITA, thereby inhibiting SCRV replication and promoting antiviral responses (27). To the best of our knowledge, the present study is the first to identify two potential ceRNA regulatory networks, LNC_001979-novel_171-Potusc2 and LNC_001979-novel_171-Podad1, from the intestine of olive flounder. Both the dad1 (defender against cell death 1) and tusc2 (tumor suppressor

candidate 2) encode multifunctional protein that play an important role in regulating a wide range of cellular processes. The dad1, highly conserved from yeast to mammals, act as regulatory protein to inhibit the programmed cell death which restricts the pathogens multiply and spreading in host tissue by killing pathogen-infected cells (41, 42). Several plant dad1 orthologs have been proved to play a critical role in defense against Phytophthora pathogens and might participate in the ER stress signaling pathway (43). Besides, dad1 is required for proper processing of N-linked glycoproteins and for certain cell survival in the mouse (44), and functional loss of dad1 in Drosophila would lead to a reduction of tissue growth due to increased apoptosis and lack of cell proliferation (45). The tusc2, a known tumor suppressor gene, is downregulated in non-small cell lung carcinomas, small cell lung carcinomas, mesothelioma, esophageal carcinoma, thyroid carcinoma, glioblastoma and sarcomas (46). The TUSC2 protein plays an important role in regulating a wide range of cellular processes, such as cell cycle arrest and apoptosis, in modulating the function of several kinases and affecting gene expression (47, 48). These two potential ceRNA regulatory networks were constructed based on the target prediction of novel_171, dual-luciferase reporter assays, and their relative expression levels during *E. tarda* infection. However, further studies should be conducted to confirm these two ceRNA regulatory networks and elucidate their roles in the immune responses of olive flounder intestine.

## DATA AVAILABILITY STATEMENT

The original contributions presented in the study are included in the article/**Supplementary Material**, further inquiries can be directed to the corresponding author/s.

## ETHICS STATEMENT

The animal study was reviewed and approved by Qingdao Agricultural University.

## AUTHOR CONTRIBUTIONS

YX: conduct lncRNA sequencing and wrote this paper. YL: analyze lncRNA data. XL: raise the experimental fish. LS: conduct the bacteria challenge experiment. SZ: revised the manuscript. CL: conceived and designed the research, and revised the manuscript. All authors: contributed to the article and approved the submitted version.

## FUNDING

This study was supported by Scientific and Technological Innovation of Blue Granary (2018YFD0900503), Young Experts of Taishan Scholars (NO. tsqn201909130), Science and Technology Support Plan for Youth Innovation of Colleges and Universities in Shandong Province (2019KJF003), National Natural Science Foundation of China (No. 32002421), the Advanced Talents Foundation of QAU (Grant No. 6651118016), the First Class Fishery Discipline Programme in Shandong Province, and a special talent programme One Thing One Decision (Yishi Yiyi) Programme in Shandong Province, China.

## SUPPLEMENTARY MATERIAL

The Supplementary Material for this article can be found online at: https://www.frontiersin.org/articles/10.3389/fimmu.2021.623764/full#supplementary-material

## REFERENCES

1. Robinson EK, Covarrubias S, Carpenter S. The how and why of lncRNA function: an innate immune perspective. *Biochim Biophys Acta Gene Regul Mech*. (2020) 1863:194419–36. doi: 10.1016/j.bbagrm.2019.194419
2. Wang M, Jiang S, Wu W, Yu F, Chang W, Li P, et al. Non-coding RNAs function as immune regulators in teleost fish. *Front Immunol*. (2018) 9:2801–16. doi: 10.3389/fimmu.2018.02801
3. Shen Y, Liang W, Lin Y, Yang H, Chen X, Feng P, et al. Single molecule real-time sequencing and RNA-seq unravel the role of long non-coding and circular RNA in the regulatory network during Nile tilapia (*Oreochromis niloticus*) infection with *Streptococcus agalactiae*. *Fish Shellfish Immunol*. (2020) 104:640–53. doi: 10.1016/j.fsi.2020.06.015
4. Jarroux J, Morillon A, Pinskaya M. History, discovery, and classification of lncRNAs. *Adv Exp Med Biol*. (2017) 1008:1–46. doi: 10.1007/978-981-10-5203-3_1
5. Agliano F, Rathinam VA, Medvedev AE, Vanaja SK, Vella AT. Long noncoding RNAs in host-pathogen interactions. *Trends Immunol*. (2019) 40:492–510. doi: 10.1016/j.it.2019.04.001
6. Paneru B, Altobasei R, Palti Y, Wiens GD, Salem M. Differential expression of long non-coding RNAs in three genetic lines of rainbow trout in response to infection with *Flavobacterium psychrophilum*. *Sci Rep*. (2016) 6:36032–46. doi: 10.1038/srep36032
7. Sebastian B, Diego VM, Andrea A, Simon M, Cristian GE. Long noncoding RNAs. (lncRNAs) dynamics evidence immunomodulation during ISAV-Infected Atlantic salmon (*Salmo salar*). *Sci Rep*. (2016) 6:22698–701. doi: 10.1038/srep22698
8. Valenzuela-Miranda D, Gallardo-Escárate C. Novel insights into the response of Atlantic salmon (*Salmo salar* ) to *Piscirickettsia salmonis* : Interplay of coding genes and lncRNAs during bacterial infection. *Fish Shellfish Immunol*. (2016) 59:427–38. doi: 10.1016/j.fsi.2016.11.001
9. Tarifeñosaldivia E, Valenzuelamiranda D, Gallardoescárate C. In the shadow: the emerging role of long non-coding RNAs in the immune response of Atlantic salmon. *Dev Comp Immunol*. (2017) 73:193. doi: 10.1016/j.dci.2017.03.024
10. Valenzuela-Munoz V, Valenzuela-Miranda D, Gallardo-Escarate C. Comparative analysis of long non-coding RNAs in Atlantic and Coho salmon reveals divergent transcriptome responses associated with immunity and tissue repair during sea lice infestation. *Dev Comp Immunol*. (2018) 87:36–50. doi: 10.1016/j.dci.2018.05.016
11. Liu X, Li W, Jiang L, Lü Z, Liu M, Gong L, et al. Immunity-associated long non-coding RNA and expression in response to bacterial infection in large yellow croaker (*Larimichthys crocea*). *Fish Shellfish Immunol*. (2019) 94:634–42. doi: 10.1016/j.fsi.2019.09.015
12. Valenzuela-Muñoz V, Pereiro P, lvarez-Rodríguez M, Gallardo-Escárate C, Figueras A, Novoa B. Comparative modulation of lncRNAs in wild-type

and rag1-heterozygous mutant zebrafish exposed to immune challenge with spring viraemia of carp virus. (SVCV). *Sci Rep*. (2019) 9:14174. doi: 10.1038/s41598-019-50766-0
13. Pereiro P, Lama R. Potential involvement of lncRNAs in the modulation of the transcriptome response to nodavirus challenge in European Sea Bass (*Dicentrarchus labrax* L.). *Biology*. (2020) 9:165–86. doi: 10.3390/biology9070165
14. Xiu Y, Jiang G, Zhou S, Diao J, Liu H, Su B, et al. Identification of potential immune-related circRNA-miRNA-mRNA regulatory network in intestine of *Paralichthys olivaceus* during *Edwardsiella tarda* infection. *Front Genet*. (2019) 10:731–47. doi: 10.3389/fgene.2019.00731
15. Kim JS, Harikrishnan R, Kim MC, Balasundaram C, Heo MS. Dietary administration of Zooshikella sp. enhance the innate immune response and disease resistance of *Paralichthys olivaceus* against *Sreptococcus iniae*. *Fish Shellfish Immunol*. (2010) 29:104–10. doi: 10.1016/j.fsi.2010.02.022
16. Xu TT, Zhang XH. *Edwardsiella tarda*: an intriguing problem in aquaculture. *Aquaculture*. (2014) 431:129–35. doi: 10.1016/j.aquaculture.2013.12.001
17. Xiu Y, Li Y, Liu X, Li C. Full-length transcriptome sequencing from multiple immune-related tissues of *Paralichthys olivaceus*. *Fish Shellfish Immunol*. (2020) 106:930–7. doi: 10.1016/j.fsi.2020.09.013
18. Wu S, Zhang J, Liu B, Huang Y, Li S, Wen H, et al. Identification and characterization of lncRNAs related to the muscle growth and development of Japanese Flounder (*Paralichthys olivaceus*). *Front Genet*. (2020) 11:1034–49. doi: 10.3389/fgene.2020.01034
19. Lauriano ER, Pergolizzi S, Aragona M, Montalbano G, Guerrera MC, Crupi R, et al. Intestinal immunity of dogfish *Scyliorhinus canicula* spiral valve: a histochemical, immunohistochemical and confocal study. *Fish Shellfish Immunol*. (2019) 87:490–8. doi: 10.1016/j.fsi.2019.01.049
20. Langmead B, Salzberg SL. Fast gapped-read alignment with Bowtie 2. *Nat Methods*. (2012) 9:357–9. doi: 10.1038/nmeth.1923
21. Pertea M, Kim D, Pertea GM, Leek JT, Salzberg SL. Transcript-level expression analysis of RNA-seq experiments with HISAT, StringTie and Ballgown. *Nat Protoc*. (2016) 11:1650–67. doi: 10.1038/nprot.2016.095
22. Trapnell C, Williams BA, Pertea G, Mortazavi A, Kwan G, Van Baren MJ, et al. Transcript assembly and quantification by RNA-Seq reveals unannotated transcripts and isoform switching during cell differentiation. *Nat Biotechnol*. (2010) 28:511–5. doi: 10.1038/nbt.1621
23. Young MD, Wakefield MJ, Smyth GK, Oshlack A. Gene ontology analysis for RNA-seq: accounting for selection bias. *Genome Biol*. (2010) 11:R14–26. doi: 10.1186/gb-2010-11-2-r14
24. Kanehisa M, Araki M, Goto S, Hattori M, Hirakawa M, Itoh M, et al. KEGG for linking genomes to life and the environment. *Nucleic Acids Res*. (2008) 36:D480–4. doi: 10.1093/nar/gkm882
25. Mao X, Cai T, Olyarchuk JG, Wei L. Automated genome annotation and pathway identification using the KEGG Orthology (KO) as a controlled vocabulary. *Bioinformatics*. (2005) 21:3787–93. doi: 10.1093/bioinformatics/bti430
26. Geng H, Tan XD. Functional diversity of long non-coding RNAs in immune regulation. *Genes Dis*. (2016) 3:72–81. doi: 10.1016/j.gendis.2016.01.004
27. Wang N, Wang R, Wang R, Tian Y, Shao C, Jia X, et al. The integrated analysis of RNA-seq and microRNA-seq depicts miRNA-mRNA networks involved in Japanese flounder (*Paralichthys olivaceus*) albinism. *PLoS ONE*. (2017) 12:17–41. doi: 10.1371/journal.pone.0181761
28. Salinas I. The mucosal immune system of teleost fish. *Biology*. (2015) 4:525–39. doi: 10.3390/biology4030525
29. Li C, Zhang Y, Wang R, Lu J, Nandi S, Mohanty S, et al. RNA-seq analysis of mucosal immune responses reveals signatures of intestinal barrier disruption and pathogen entry following *Edwardsiella ictaluri* infection in channel catfish, *Ictalurus punctatus*. *Fish Shellfish Immunol*. (2012) 32:816–27. doi: 10.1016/j.fsi.2012.02.004
30. Wang XP, Yan MC, Hu WL, Chen SB, Zhang SL, Xie QL. Visualization of *Sparus macrocephalus* infection by GFP-labeled *Edwardsiella tardal*. *Isr J Aquacult-Bamid*. (2012) 64:1–7.
31. Cai J, Li L, Song L, Xie L, Luo F, Sun S, et al. Effects of long term antiprogestine mifepristone (RU486) exposure on sexually dimorphic lncRNA expression and gonadal masculinization in Nile tilapia (*Oreochromis niloticus*). *Aquat Toxicol*. (2019) 215:105289–301. doi: 10.1016/j.aquatox.2019.105289
32. Wen Y, Chen H, Luo F, Zhou H, Li Z. Roles of long noncoding RNAs in bacterial infection. *Life Sci*. (2020) 263:118579. doi: 10.1016/j.lfs.2020.118579
33. Turner M, Galloway A, Vigorito E. Noncoding RNA and its associated proteins as regulatory elements of the immune system. *Nat Immunol*. (2014) 15:484–91. doi: 10.1038/ni.2887
34. Bronesky D, Wu Z, Marzi S, Walter P, Geissmann T, Moreau K, et al. Staphylococcus aureus RNAIII and its regulon link quorum sensing, stress responses, metabolic adaptation, and regulation of virulence gene expression. *Annu Rev Microbiol*. (2016) 70:299–316. doi: 10.1146/annurev-micro-102215-095708
35. Horn J, Klepsch M, Manger M, Wolz C, Rudel T, Fraunholz M. Long noncoding RNA SSR42 controls *Staphylococcus aureus* alpha-toxin transcription in response to environmental stimuli. *J Bacteriol*. (2018) 200:e00252–18. doi: 10.1128/JB.00252-18
36. Jiang L, Liu W, Zhu A, Zhang J, Zhou J, Wu C. Transcriptome analysis demonstrate widespread differential expression of long noncoding RNAs involve in *Larimichthys crocea* immune response. *Fish Shellfish Immunol*. (2016) 51:1–8. doi: 10.1016/j.fsi.2016.02.001
37. Matsumoto A, Clohessy JG, Pandolfi PP. SPAR, a lncRNA encoded mTORC1 inhibitor. *Cell Cycle*. (2017) 16:815–6. doi: 10.1080/15384101.2017.1304735
38. Anderson DM, Anderson KM, Chang CL, Makarewich CA, Nelson BR, Mcanally JR, et al. A micropeptide encoded by a putative long noncoding RNA regulates muscle performance. *Cell*. (2015) 160:595–606. doi: 10.1016/j.cell.2015.01.009
39. Yan C, Luo Z, Li W, Li X, Dallmann R, Kurihara H, et al. Disturbed Yin-Yang balance: stress increases the susceptibility to primary and recurrent infections of herpes simplex virus type 1. *Acta Pharm Sin B*. (2020) 10:383–98. doi: 10.1016/j.apsb.2019.06.005
40. Ike AC, Onu CJ, Ononugbo CM, Reward EE, Muo SO. Immune response to herpes simplex virus infection and vaccine development. *Vaccines*. (2020) 8:302. doi: 10.3390/vaccines8020302
41. Nakashima T, Sekiguchi T, Kuraoka A, Fukushima K, Shibata Y, Komiyama S, et al. Molecular cloning of a human cDNA encoding a novel protein, DAD1, whose defect causes apoptotic cell death in hamster BHK21 cells. *Mol Cell Biol*. (1993) 13:6367–74. doi: 10.1128/MCB.13.10.6367
42. Nagata S, Tanaka M. Programmed cell death and the immune system. *Nat Rev Immunol*. (2017) 17:333–40. doi: 10.1038/nri.2016.153
43. Yan Q, Si J, Cui X, Peng H, Jing M, Chen X, et al. GmDAD1, a conserved defender against cell death 1 (DAD1) from soybean, positively regulates plant resistance against phytophthora pathogens. *Front Plant Sci*. (2019) 10:107. doi: 10.3389/fpls.2019.00107
44. Hong NA, Flannery M, Hsieh SN, Cado D, Pedersen R, Winoto A. Mice lacking Dad1, the defender against apoptotic death-1, express abnormal N-linked glycoproteins and undergo increased embryonic apoptosis. *Dev Biol*. (2000) 220:76–84. doi: 10.1006/dbio.2000.9615
45. Zhang Y, Cui C, Lai ZC. The defender against apoptotic cell death 1 gene is required for tissue growth and efficient N-glycosylation in *Drosophila melanogaster*. *Dev Biol*. (2016) 420:186–95. doi: 10.1016/j.ydbio.2016.09.021
46. Mariniello RM, Orlandella FM, Stefano AE, Iervolino PLC, Smaldone G, Luciano N, et al. The TUSC2 tumour suppressor inhibits the malignant phenotype of human thyroid cancer cells via SMAC/DIABLO protein. *Int J Mol Sci*. (2020) 21:702. doi: 10.3390/ijms21030702
47. Ji L, Roth JA. Tumor suppressor FUS1 signaling pathway. *J Thorac Oncol*. (2008) 3:327–30. doi: 10.1097/JTO.0b013e31816bce65
48. Rimkus T, Sirkisoon S, Harrison A, Lo HW. Tumor suppressor candidate 2 (TUSC2, FUS-1) and human cancers. *Discov Med*. (2017) 23:325–30.

**Conflict of Interest:** The authors declare that the research was conducted in the absence of any commercial or financial relationships that could be construed as a potential conflict of interest.

# Advantages of publishing in Frontiers

**OPEN ACCESS**
Articles are free to read for greatest visibility and readership

**FAST PUBLICATION**
Around 90 days from submission to decision

**HIGH QUALITY PEER-REVIEW**
Rigorous, collaborative, and constructive peer-review

**TRANSPARENT PEER-REVIEW**
Editors and reviewers acknowledged by name on published articles

**Frontiers**
Avenue du Tribunal-Fédéral 34
1005 Lausanne | Switzerland

**Visit us:** www.frontiersin.org
**Contact us:** frontiersin.org/about/contact

**REPRODUCIBILITY OF RESEARCH**
Support open data and methods to enhance research reproducibility

**DIGITAL PUBLISHING**
Articles designed for optimal readership across devices

**FOLLOW US**
@frontiersin

**IMPACT METRICS**
Advanced article metrics track visibility across digital media

**EXTENSIVE PROMOTION**
Marketing and promotion of impactful research

**LOOP RESEARCH NETWORK**
Our network increases your article's readership